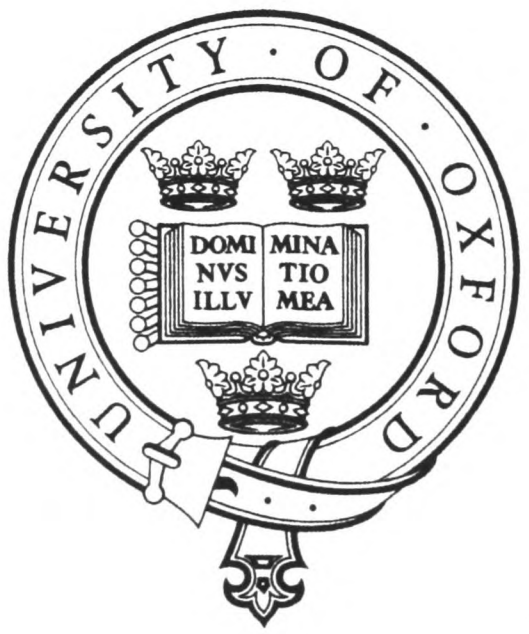
MICROBIAL MEDIATION OF DOLOMITE FORMATION: GEOCHEMICAL AND MICROBIAL INVESTIGATIONS IN THE COORONG REGION OF SOUTH AUSTRALIA

Thesis submitted for the degree of Doctor of Philosophy to the University of Oxford



by

David Wacey B.A. (Oxon)

The Department of Earth Sciences

& Worcester College

RADCLIFFE SCIENCE LIBRARY OXFORD
14 APR 2003

Trinity Term

September 2002

MICROBIAL MEDIATION OF DOLOMITE FORMATION: GEOCHEMICAL AND MICROBIAL INVESTIGATIONS IN THE COORONG REGION OF SOUTH AUSTRALIA

Thesis submitted for the degree of Doctor of Philosophy to the University of Oxford

by

David Wacey B.A. (Oxon)

Department of Earth Sciences & Worcester College

Trinity Term, 2002

ABSTRACT

Dolomite is shown to precipitate in laboratory experiments that simulate the microbiogeochemical conditions prevailing during the later stages of evaporation in the ephemeral, hypersaline, dolomitic lakes of the Coorong region, South Australia, where microbially-dominated ecosystems support intensive bacterial sulphate reduction.

Analyses of numerous lake- and pore-water samples from Coorong lakes document rapid geochemical changes with depth and time. Extremely high sulphate and magnesium ion concentrations occur in lake waters and decline rapidly with depth in pore waters through the sulphate reduction zone. Ultimately sulphate ions are totally consumed but magnesium ions are replenished, presumably from desiccated cyanobacterial sheaths. Carbonate concentrations in pore waters reach levels up to 100 times those of normal seawater.

Most-probable-number counts show that large populations of sulphate-reducing bacteria are present in sediment cores, while sulphur isotope analysis of residual lakewater sulphate indicates that microbial fractionation takes place in all the study lakes. Microbes from the lakes were cultured in the laboratory under anoxic conditions and viable populations were injected into vials containing a sterilised granular substrate immersed in a simulated lakewater solution. Falls in the levels of sulphate ion concentration and rising pH in selected vials were interpreted as due to active bacterial sulphate reduction accompanied by increased concentrations of carbonate. After 1 month, subspherical nano-grains of dolomite were precipitated. This study proposes that bacterial sulphate reduction overcomes kinetic constraints on dolomite formation by removing the sulphate ions and releasing magnesium and calcium ions from neutral ion pairs, and by generating elevated carbonate concentrations in a hypersaline and strongly electrolytic solution.

Microbiogeochemical and isotopic data therefore demonstrates that bacterial sulphate reduction controls dolomite precipitation in both the laboratory experiments and the lake sediments. It is proposed that dolomite formation through bacterial sulphate reduction provides a process analogue that is applicable to thick platformal dolostones of the past, where benthic microbial communities were the dominant colonisers of the shallow marine environment.

EXTENDED ABSTRACT

Dolomite is widespread in the geological record and yet modern occurrences are rare. From a purely thermodynamic viewpoint, modern seawater is supersaturated with respect to dolomite and so not only should it precipitate, but all $CaCO_3$ in seawater should be spontaneously dolomitized. Kinetic factors prevent this from occurring in nature, and dolomite has never been precipitated in physico-chemical experiments under sedimentary conditions. The research presented here records the quest to successfully solve this enigma by adopting microbiogeochemical and isotopic approaches to understanding modern dolomite formation.

The chain of ephemeral lakes near Salt Creek in the Coorong region of South Australia provide a natural laboratory for the study of the origin of modern sedimentary dolomite. Five lakes considered in this study have a modern infill of primary dolomite while three others, in close proximity, contain aragonite, Mg-calcite and hydromagnesite. Previous hydrologically-driven models of dolomite formation for these lake sediments lack empirical support and encounter kinetic problems related to ion complexing, in particular low CO_3^{2-} ion activity and low metal cation activities due to the presence of the sulphate ion. This study focuses upon geomicrobiological processes, in particular the role of sulphate-reducing bacteria (SRB), in dolomite formation. A microbial dolomite model, first proposed for these sediments by Wright (1999) and invoked for similar sediments in Lagoa Vermelha, Brazil by Vasconcelos *et al.* (1995) and Vasconcelos & McKenzie (1997), is critically investigated in this study. SRB are shown to enhance dolomite precipitation by modifying the chemistry of the lake- and pore-waters. Microbial degradation of cyanobacterial matter, together with reduced sulphate concentrations, may bring about an increase in dehydrated Mg^{2+} ions which are then available for incorporation into the dolomite lattice. SRB metabolism can also increase pH through a release of ammonia from organic proteins. An increase in pH, together with the hypersaline nature of the lakes, raises carbonate ion activity so that it becomes the dominant inorganic carbon phase in the lake- and pore-waters. The likelihood of carbonate precipitation is thus greatly enhanced.

Dolomite occurs in the uppermost sediments of Milne, Dolomite, Pellet, Mini Dolomite and McFaiden lakes. The dolomitic sediment is grey with a yoghurt-like consistency when wet but dries to a pale yellow colour, exhibiting polygonal cracking. In all

of the lakes except Pellet Lake, *Ruppia maritima* grass is common, resulting in a plentiful supply of organic matter to the bacterial communities. Microbial mats with cyanobacteria are also conspicuous components of the lakes late in their evaporative cycles.

The dolomite occurs as sub-micron sized grains which are often spherical to oval in morphology. Amalgamation of these grains is common, forming irregular aggregates that are seen to neomorphose into ordered structures having crystal faces and rhombohedral morphology. All of the dolomites show at least one X-ray diffraction ordering peak and are therefore true dolomites. The degree of ordering, however, calculated by comparing the (201)/(101) XRD peak height intensity, is relatively poor, ranging from weakly ordered dolomite in Pellet and McFaiden Lakes to around 75% ordered dolomite in Milne Lake. In general, the morphology of the dolomite at depth shows little change from the surface nor is there an increase in the degree of ordering. Only in Mini Dolomite Lake is there an increase in ordering with depth.

Elemental analysis of the dolomite samples from the lakes was performed on polished powder sections, mounted in resin and carbon coated to obtain mineral stoichiometry. Samples were viewed and analysed on the SEM, using a cobalt standard. The dolomite in Milne Lake (average 70% $MgCO_3$) and Pellet Lake (52%-68% $MgCO_3$) is magnesium-rich and, in the former, approaches the composition of huntite ($CaMg_3(CO_3)_4$). McFaiden Lake (45%-55% $MgCO_3$) and Dolomite Lake (47%-53% $MgCO_3$) have compositions close to ideal dolomite, whilst Mini Dolomite Lake contains a small calcium excess (average 45% $MgCO_3$). The sediments of the 'non-dolomitic' Halite Lake, North Stromatolite Lake and South Stromatolite Lake are somewhat different. Coarser, pale brown carbonate sand dominates here and evidence for bioturbation is widespread. *Ruppia* grass is largely absent as is the yoghurt-like mud, except for occasional patches in South Stromatolite Lake. The sediment in North and South Stromatolite Lakes is dominated by needles of aragonite and by plates of hydro-magnesite, mostly 5-15μm in length, with well-formed crystal faces. Occasional sub-micron precipitates do occur but these are mostly of Mg-calcite. Halite Lake is rather anomalous in being dominated by halite, Mg-calcite and aragonite.

Samples of lake- and pore-waters of unlithified shallow sediment cores were taken at different times in the late evaporative cycle of both the dolomitic and non-dolomitic lakes

during two successive field seasons in 1999 and 2000. Both lake- and pore-waters revealed high Mg/Ca ratios. The Mg/Ca ratio of a fluid has been suggested as a key variable in dolomite formation (e.g. Folk and Land, 1975). It was found, however, that the highest Mg/Ca ratios were not necessarily found in the dolomitic lakes, suggesting that this is not the only essential component of dolomite precipitation. High initial sulphate concentrations, high pH, high carbonate concentrations and high salinities were characteristic of the majority of lakewater samples, although rapid geochemical changes were recorded with depth and time. Sulphate ion concentration declined rapidly with depth in the pore-waters, coupled with an increase in pH, and a less substantial decrease in magnesium ion concentration. Carbonate ion concentrations in pore-waters reached levels up to 100 times those of normal seawater. It is proposed that the degradation of abundant organic matter by sulphate-reducers modifies the lake- and pore-water chemistries and creates the observed geochemical gradients, significantly overprinting an evaporative signal of increased ionic concentrations. Extrapolation of convergent trends between magnesium and sulphate ion concentrations predicts a cross-over at about 5cm depth, below which sulphate ions are rapidly consumed and dolomite precipitation is kinetically favoured. The depth at which dolomite precipitation is kinetically favoured may migrate towards the surface during the dynamically changing cycles of the lakes.

Total bacterial counts (acridine orange direct counts) from the sediment cores show large numbers (up to $3x10^9$) of bacteria, of which a significantly large percentage are shown to be sulphate-reducers by 'most probable number' counts. The dolomitic lakes are shown to contain substantially more SRB (up to $3.7 \times 10^6/cm^3$) than the non-dolomitic lakes (c. 1-$300 \times 10^3/cm^3$). This large difference in SRB numbers may therefore be a key factor in the precipitation of dolomite over other carbonate phases. Differential interference contrast (DIC) microscopy was used to image bacteria from the lake sediments. These images strongly resemble the morphology of the dolomite precipitate. Both these bacterial images and SEM images of the dolomitic sediment have striking similarities to microbial sediments documented by other authors (e.g. Folk, 1993a; Vasconcelos *et al.*, 1995; Vasconcelos & McKenzie, 1997; Wright, 1999; Wartmann *et al.* 2000). Subsequently, SRB closely related to *Desulfostipes* sp., *Desulfosarcina* sp. and *Desulfotomaculum* sp. were identified from the study lakes using 16S rRNA sequencing.

Sulphur isotope data shows significant ^{34}S enrichment of the residual lakewater sulphate in all of the lakes, as expected if bacterial sulphate reduction was in operation. Little variation in the isotopic signal with depth in each lake is observed, perhaps owing to a combination of species-specific effects with sporadic open system behaviour. Sulphur isotope fractionations during oxidation and disproportionation reactions in the uppermost sediments and water column can account for relatively small total enrichments and minimal variation of signal between the dolomitic and non-dolomitic lakes.

Oxygen isotope data are presented for residual sulphate ions, lakewater and the carbonate sediments. Sulphate $\delta^{18}O$ data are not easy to interpret, having received very little attention in the scientific literature. A covariant correlation was found between sulphate $\delta^{18}O$ and $\delta^{34}S$ in the dolomitic lakes. No such correlation was found in the non-dolomitic lakes, suggesting that bacterial sulphate reduction may be a controlling factor on the isotopic signals of the dolomitic lakes alone. In addition, a correlation was observed between sulphate and lakewater $\delta^{18}O$ data, suggesting that recycling of sulphate takes place within each lake so that the sulphate inherits the isotopic signal of the lakewater rather than of its original seawater source. Oxygen isotopic data from the carbonates lie towards the 'heavy' end of the spectrum shown by normal sedimentary rocks, with no distinguishable differences between the dolomitic and non-dolomitic lakes. Combining $\delta^{18}O$ data from the carbonates and the lakewaters allows a temperature of precipitation to be calculated for each of the minerals in each of the lakes. Except for Halite Lake, estimated temperatures of precipitation are in excess of those observed in the field, if it is assumed that the minerals were precipitated in equilibrium with the November lakewaters. The minerals (especially the dolomite for which the greatest discrepancy occurs) must therefore have precipitated either at a shallow depth in the sediment where temperatures are higher and/or the $\delta^{18}O$ of the water was lower or at a different (and unsampled) time in the evaporative cycle. Due to the 'hook effect' interpreted in the lakewater $\delta^{18}O$ patterns, the minerals observed could have precipitated either earlier or later than the sampled interval within the evaporative cycle. Of these, later precipitation at a shallow depth in the sediment is the preferred alternative since bacterial action is likely to have been more intense, sulphate ion concentrations lower and free Mg^{2+} ion concentrations would be higher.

Carbon isotope analysis of the carbonate sediments reveals widely spaced values for the dolomitic lakes ($\delta^{13}C$ = -1.19 to +3.22‰) whilst those for the non-dolomitic lakes are

more closely spaced ($\delta^{13}C$ = +1.12 to +3.07‰). This contrasts with previous interpretations (e.g. Rosen *et al.*, 1989) in which more ordered dolomite has lower $\delta^{13}C$ values whereas dolomite forming from dolomitization of aragonite has higher $\delta^{13}C$ values. Combined plots of carbon and oxygen isotopic data emphasize the difference between the two sets of lakes, with the dolomitic lakes generally plotting in the lower $\delta^{13}C$ and higher $\delta^{18}O$ area of the graph (Fig. 5.18). Several authors (e.g. Botz & Von der Borch, 1984; Rosen *et al.*, 1988) have rejected the possibility that an organogenic dolomite model can be applied to dolomites that lack a strongly negative $\delta^{13}C$ signal. Geochemical modelling performed here, however, suggests that the source of the carbonate ions in dolomite is inorganic carbon from bicarbonate ions already present in the lakewater. Bacterial sulphate reduction results in pH elevation and a shift of the equilibrium between inorganic bicarbonate and carbonate ions, favouring the carbonate ion. Thus, SRB are inferred to act as catalysts, making this carbonate available for incorporation into dolomite. Some contribution to the carbon reservoir by organic carbon is, however, indicated by negative $\delta^{13}C$ from two of the dolomite containing lakes. It is proposed that the carbon isotopic signature is unique to each lake, resulting from the precipitation of carbonate minerals at different times in the annual cycle of each lake, allowing varying amounts of mixing between isotopically heavy carbon from the inorganic reservoir and isotopically light carbon from the organic reservoir.

Experiments were undertaken to simulate the anoxic bio-depositional environment of the lakes. These revealed the precipitation of nano-grains of dolomite on mineral seeds of aragonite and quartz grains, using natural populations of bacteria cultured from the Coorong lakes. A series of parallel experimental vials were innoculated with Postgate B culture medium plus Coorong SRB and a sterilised granular mineral seed and observed over a period of two months. Control vials were also established with no SRB. Additional components were injected into selected vials to replicate, as closely as possible, the conditions encountered in the Coorong lakes. These components included brine, extra $MgSO_4$ and organic matter. Measurements of pH and sulphate ion concentrations revealed geochemical signals consistent with bacterial metabolism, rapidly declining sulphate ion concentrations and rising pH levels. Nano-grains of dolomite were found to have precipitated in two vials within a month of the addition of extra components while, at the same time, 80%-90% of the sulphate was consumed. Dolomite precipitated only in those vials which contained culture medium, SRB, extra $MgSO_4$ and a quantity of organic matter. Where one or more of these components was omitted, precipitates of different mineralogy

were found. This demonstrates that laboratory conditions can be established and maintained that replicate those found in the Coorong lakes and that SRB plus organic matter can indeed be key components in overcoming the kinetic inhibitors to dolomite formation. The implications for this organogenic model for sedimentary dolomite formation throughout geological history may be profound.

ACKNOWLEDGEMENTS

During my time in Oxford many people have been a source of help, inspiration and entertainment and have made my time here both enjoyable and rewarding and here is the time to recognise a few of them.

First off, a special thanks must go to my two supervisors, Dave Wright and Martin Brasier, who, by selecting me for this project, have enabled me to meet some great people whilst completing some valuable research. Thanks go to them for their guidance and encouragement and to Dave for Thursday evening beer induced discussions at the pub.

I am indebted to many members of the department for their technical expertise. Particular thanks goes to Steve Wyatt for help with any number of problems in the chemistry lab, not least for finding a safe home for my bacteria for many months and also for snippets of department gossip over a drink or two in the Kings Arms. Thanks to Owen Green and Jeremy Hyde for assistance in preparing stubs and polished sections and thanks to Norman Charnley for familiarizing me with the SEM. Thanks to Rich McAvoy and Steve Baker for slide preparation and other photographic needs.

Outside of the department thanks must go to Adrian Boyce, Tony, Julie and Paul at the isotope lab in East Kilbride; to Kevin Sharkey and Leicester University; to Barry Cragg and John Parks at Geomicrobiology in Bristol; to Chris Schofield for use of anaerobic facilities at Dyson Perrins in Oxford; to Judy Armitage and Angela Martin at biochemistry in Oxford and to Matthew Lloyd for his expertise with chemical equations.

Two field trips to the Coorong National Park in South Australia were immensely enjoyable and I would like to thank Chris von der Borch and his partner Kate for their hospitality during my time in Adelaide and to Marlene Broomfield and her family for looking after me during my many weeks of near isolation in Salt Creek. Thanks also goes to Nick McLure and the technical staff at Flinders University for assistance with equipment.

Away from the rigours of work many thanks must go to the succession of people that made the last four years so memorable. Thanks to the five-some that are Drs. Lovegrove, Walker,

Gardiner, Hobson and Jones for the occasionally inspired but usually ridiculous conversation and selection of drinks. A special thanks to Kate for instigating the now legendary Friday afternoon Happy Hour and to Dan for cycle pub crawls, notebooks and red lines! Thanks to Drs. Haddad and Simpson for belonging to the fine institution which is St. Cross bar and to Laura for her purpleness.

I'd like to thank Conall for the invitation to go on the 'jolly' that was the 2001 Castellane field trip. This turned out to be the best two weeks of 'work' in my time here and for that I would like to thank the whole of the current 4th year undergraduate class, in particular the decorative duo of Cat and Katrina. Above all I'd like to say a special thank-you to Jenny, Simon and Lisa - not only my fellow demonstrators on this trip but three of my very best friends, with whom I've shared many of the best moments of the last few years.

Away from geology a special mention must go to Sharon Moughtin for being an excellent housemate, to the Worcester MCR football team and to the members of the 1998/99 'Grad Pad', especially Alex, Dion and Effrosini. Weekend distractions and 'jollies' abroad were most welcome and for these Ed, Graham, Rich, Tom, Luke and Claire are thanked.

The research was supported by NERC grant GT04/98/222/ES and topped up when necessary by the Burdett Coutts Fund, Worcester College and the International Studies Office. To all of whom I am immensely grateful.

Finally, this section could not be complete without a mention for the support and encouragement provided by my Mum and Dad despite the fact that they continually pester me about getting a proper job.

Contents

Short Abstract i

Extended Abstract ii

Acknowledgements viii

Contents x

Chapter 1: Introduction 1

1.1. Overview 1

1.1.1. Aims 1

1.2. The Dolomite Problem 2

1.2.1. Background 2

1.2.2. Thermodynamics of dolomite precipitation 3

1.2.3. Inorganic models for dolomite formation 9

1.2.4. Experimental evidence 14

1.2.5. Other avenues of approach – sulphate inhibition 15

1.2.6. Microbial processes 15

1.3. Study Area 21

1.4. Geological setting 23

1.4.1. Quaternary history 26

1.5. Climate 26

1.6. Regional Hydrology 28

1.7. Coorong Dolomite 31

1.7.1. Previous interpretations 31

1.7.2. Source of ions for dolomite precipitation in the Coorong 33

1.7.3. Coorong dolomite – a new approach 34

1.8. Summary 36

Chapter 2: The sulphate-reducing bacteria **37**

2.1. Introduction 38

2.2. Morphology and classification 38

2.2.1. 16S rRNA sequencing 42

2.3. Dissimilatory sulphate reduction 44

2.3.1. The sulphur cycle 47

2.4. Environmental impact of SRB 47

2.5. Evolution of the SRB 49

2.6. Growth / cultivation 53

2.7. Summary 54

Chapter 3: Physiography, sedimentology and mineralogy of the distal ephemeral lakes in the Coorong Region, South Australia **55**

3.1. Introduction 56

3.1.1. General characteristics 56

3.2. Physiography and sedimentology 61

3.2.1. Milne Lake 61

3.2.2. Pellet Lake 64

3.2.3. Mini Dolomite Lake 66

3.2.4. McFaiden Lake 69

3.2.5. Dolomite Lake 71

3.2.6. Halite Lake 71

3.2.7. North Stromatolite Lake 74

3.2.8. South Stromatolite Lake 79

3.2.9. Summary of lake characteristics 82

3.3. Mineralogy / Petrology 84

3.3.1. Methodology 84

3.3.2. Milne Lake 85

3.3.3. Pellet Lake 87

3.3.4. Mini Dolomite Lake 89

3.3.5. McFaiden Lake 92

3.3.6. Dolomite Lake 95

3.3.7. Halite Lake 97

3.3.8. North Stromatolite Lake 99

3.3.9. South Stromatolite Lake 99

3.4. Evidence for bacterial mineralisation 102
3.5. Summary of observations 107

Chapter 4: Lakewater and porewater geochemistry **109**

4.1. Introduction 110
4.2. Salinity 110
4.2.1. Field measurements 111
4.2.2. Conversion to salinity 111
4.2.3. Results 114
4.3. Oxygenation 114
4.4. Carbonate chemistry 115
4.4.1. Theory 115
4.4.2. Method for calculation of carbonate ion concentration 117
4.4.3. pH measurement 117
4.4.4. pH data 118
4.4.5. The carbonate system 123
4.4.6. Derivation of the Henderson-Hasselbach equation 124
4.4.7. Sample collection and titration processing 125
4.4.8. Titration curves (example) 126
4.4.9. Calculation of carbonate ion concentration (example) 127
4.4.10. Results 129
4.5. Sulphate chemistry 133
4.5.1. Field collection and preparation 133
4.5.2. Sediment dilution 134
4.5.3. Determination of sulphate as barium sulphate 135
4.5.4. Data collection and presentation 137
4.5.5. Data analysis 140
4.5.6. The magnesium-sulphate relationship 144
4.5.7. Magnesium to calcium ratios 146
4.6. Total organic carbon 149
4.7. Summary 151

Chapter 5: Isotopic analysis **152**

5.1. Introduction 153
5.2. Sulphur isotopes 154

5.2.1. Distribution of sulphur isotopes 155
5.2.2. Biogenic fractionation of sulphur isotopes 156
5.2.3. Sulphur isotope methodology 162
5.2.3.1. Precipitation of barite sample for isotope analysis 162
5.2.3.2. Data reproducibility 162
5.2.4. Results 164
5.2.5. Discussion 166
5.3. Oxygen isotopes 172
5.3.1. Distribution of oxygen isotopes 173
5.3.2. Oxygen isotopes from SO_4^{2-} 175
5.3.2.1. Methodology 175
5.3.2.2. Data reproducibility 176
5.3.2.3. Results 177
5.3.2.4. Discussion 178
5.3.3. $\delta^{18}O$ of the carbonates 181
5.3.3.1. Methodology 181
5.3.3.2. Data reproducibility 182
5.3.3.3. Results 182
5.3.4. Lakewater $\delta^{18}O$ 183
5.3.5. Mineral-water interactions 186
5.4. Carbon isotopes 191
5.4.1. Distribution of carbon isotopes 191
5.4.2. Results 194
5.4.3. Discussion 195
5.5. Summary of isotopic data 199

Chapter 6: Bacterial enumeration, identification and precipitation experiments 201
6.1. Introduction 202
6.2. SRB enumeration 202
6.2.1. Collection and storage of SRB containing sediment 203
6.2.2. Culturing method for SRB from Coorong lakes 203
6.2.3. Numbers of positive vials 207
6.2.4. Most probable numbers 209
6.3. Acridine orange direct counts 213
6.3.1. Sampling 213

6.3.2. Analytical procedure 213
6.3.3. Spreadsheet calculations 216
6.3.4. Results 219
6.3.5. Bacterial clustering 220
6.4. Comparison of AODC and MPN values 221
6.5. Discussion 222
6.6. Bacterial identification 225
6.6.1. Results 226
6.7. Bacterial precipitation experiments 228
6.7.1. Initial components of the vials 228
6.7.2. Chemical analyses of the vials 230
6.7.3. Vial precipitates 233
6.7.3.1. Vial 1 234
6.7.3.2. Vial 6 236
6.7.3.3. Vial 7 240
6.7.3.4. Vial 8 240
6.7.3.5. Vial 10 244
6.7.3.6. Vial 15 244
6.7.3.7. Vial 21 247
6.8. Summary 250

Chapter 7: Conclusions **253**

Bibliography **262**

Appendix 1: Sediment X-ray diffractometry

Appendix 2: Mineral analyses

Appendix 3: Carbonate data

Appendix 4: Titration curves

Appendix 5: Stable isotope data sets

Appendix 6: 16S rRNA sequencing data

Appendix 7: XRD and atomic spectra for the experimental vials

CHAPTER 1



Track leading to the Bunyeroo Gorge in the vicinity of Wilpena Pound, South Australia.

Chapter 1

Introduction

1.1. OVERVIEW

The mineral dolomite, $CaMg(CO_3)_2$ is a common constituent of the rock record, yet a comprehensive understanding of its formation mechanisms has yet to be achieved. The so called 'dolomite problem' has resulted from the inability of researchers to precipitate dolomite in the laboratory under earth surface temperatures and pressures, together with the enigma of the relative scarcity of modern occurrences of the mineral despite seawater being supersaturated with respect to dolomite. This study aims to address this problem by approaching it from a kinetic rather than purely thermodynamic viewpoint, in particular focusing on the role of sulphate-reducing bacteria (SRB) in modifying ambient water chemistry. This study critically reviews previous models of dolomite formation, aims to test whether an organogenic model for dolomite precipitation is falsifiable or valid and to ascertain if it could be significantly more important in dolomite genesis than previously thought. The study does this through an integrated approach using sedimentology, geochemistry, stable isotopes and microbiology, as outlined below.

1.1.1. Aims

The research has been organised into five main areas each with specific aims:-

(1) Sedimentology - to describe the mineralogy, fabrics, textures and associations of the sediment in each of the study lakes and to relate this to a possible mode of formation.

(2) Geochemistry - to measure geochemical parameters, on both a large scale (lakewater) and small scale (top 50mm of the porewaters) and to relate these to measurements of both inorganic and biological processes.

(3) Stable isotope studies - to understand the geochemical signals and to assess the extent to which biogenic fractionation can be observed in carbon, oxygen and sulphur isotope ratios.

(4) Microbiological studies - to determine the abundance and relative importance of sulphate-reducing bacteria in the microbial community, to understand the relationship between microbial communities and ambient water chemistry, and to attempt to identify the taxa responsible for the effects observed in (1), (2) and (3).

(5) Laboratory experiments - to precipitate dolomite in the laboratory under earth surface temperatures and pressures by simulating, as closely as possible, the various parameters observed in the study of the lakes.

1.2. THE DOLOMITE PROBLEM

1.2.1. Background

The scientific background to this project lies in one of geology's ongoing problem areas, the so called 'dolomite problem'. Thermodynamics predicts that dolomite, in the marine environment, should precipitate preferentially over other carbonate phases, and moreover, all marine calcium carbonate should be immediately dolomitized (Lippman, 1973). This is not found in nature nor, until very recently, had dolomite been synthesised in the laboratory under natural temperature and pressure conditions. In addition to this, confusion has resulted from the relative scarcity of modern dolomite compared with the vast accumulations seen in the ancient rock record.

The causes of this major geological problem have been attributed to the following kinetic inhibitors:

a) the high hydration energy of the magnesium ion (e.g. Lippmann, 1973);
b) the low activity of the carbonate ion (e.g. Garrels & Thompson, 1962);
c) the presence of sulphate ions, which form complexes with e.g. magnesium ions (e.g. Baker & Kastner, 1981).

Many 'inorganic' models have been proposed to account for dolomite formation, the most popular of which are the Dorag or mixing zone model (Badiozamani, 1973) and its variations (Adams & Rhodes, 1960; Folk & Land, 1975), the evaporitic sabkha model (Hsu & Siegenthaler, 1969) and the tidal pumping model (Carballo *et al.*, 1987; Land, 1991). These will be reviewed in the following pages and it will be argued that none of these models satisfactorily explain how the kinetic inhibitors are overcome, nor do empirical data support them.

1.2.2. Thermodynamics of dolomite precipitation

The laws of thermodynamics appear to be at odds with the observations that dolomite does not precipitate in seawater, nor can it be precipitated in normal physico-chemical laboratory experiments at earth surface conditions.

Using the laws of thermodynamics it can be proven that
a) Seawater is supersaturated with respect to dolomite (e.g. Garrels and Thompson, 1962);
b) The formation of dolomite from calcite or aragonite is favoured in seawater (e.g. Garrels *et al.*, 1960);

Reasoning.

a) The degree of saturation of a mineral in seawater is assessed by comparing its solubility product to its ionic activity product.

The solubility of dolomite is represented by the solubility product, K_{sDol}.

$$[Ca^{2+}] \cdot [Mg^{2+}] \cdot [CO_3^{2-}]^2 = K_{sDol}$$

which is derived from the ionic equation of dolomite formation

$$Ca^{2+} + Mg^{2+} + 2CO_3^{2-} \longrightarrow CaMg(CO_3)_{2\ (solid)}$$

This solubility product has been determined experimentally by several authors. Halla and Ritter (1935) obtained a value of $K_{sD} = 10^{-17}$, whilst several later authors obtained values close to, and just in excess of this (see Hsu, 1967). The smallest value obtained was $10^{-19.33}$ by Garrels *et al.* (1960), whilst the value used in Figure 1.1. is $10^{-18.22}$ (Horn, 1962). This value was taken because it lies roughly in the middle of the field of published values and because the same author also determined values of K_s for magnesite and brucite using an identical method.

To assess the stability of dolomite in seawater, this solubility product must be compared to the activity product. Garrels and Thompson (1962) determined the activities of the most important species in seawater (Table 1.1); activity products for common minerals may then be calculated from these values.

Ion	**Molality**	**% Free ion**	**Activity coefficient**	**Activity**
Ca^{2+}	0.0104	91	0.28	0.00264
Mg^{2+}	0.0540	87	0.36	0.0169
Na^{+}	0.4752	99	0.76	0.356
K^{+}	0.0100	99	0.64	0.0063
Cl^{-}	0.56	100	0.64	0.3584
SO_4^{2-}	0.0284	54	0.12	1.8×10^{-3}
HCO_3^{-}	0.00238	69	0.68	9.75×10^{-4}
CO_3^{2-}	0.000269	9	0.20	4.7×10^{-6}

Resulting ionic activity products	Solubility products for comparison
$[Ca^{2+}] \cdot [CO_3^{2-}] = 10^{-7.91}$	$K_{sArag} = 10^{-8.22}$
$[Mg^{2+}] \cdot [CO_3^{2-}] = 10^{-7.10}$	$K_{sMagn} = 10^{-8.14}$
$[Ca^{2+}] \cdot [Mg^{2+}] \cdot [CO_3^{2-}]^2 = 10^{-15.01}$	$K_{sDolo} = 10^{-17}$

Table 1.1. A chemical model for seawater at 25°C, 19% chlorinity and pH 8.1 (Garrels & Thompson, 1962).

The activity product for dolomite is:

$$[Ca^{2+}] \cdot [Mg^{2+}] \cdot [CO_3^{2-}]^2 = 10^{-15.01} \quad \text{(Lippmann, 1973)}$$

The degree of saturation is thus calculated as follows:

$$\text{Saturation} = \frac{\text{Ion activity product}}{\text{Thermodynamic solubility product}}$$

Substituting the values for dolomite gives:

$$\frac{10^{-15.01}}{10^{-17}} = 97.7$$

A minimum saturation of 97.7 (anything over 1 is saturated) is obtained showing that seawater is considerably supersaturated with regard to dolomite, even using the largest calculated solubility product of $K_{sD} = 10^{-17}$.

b) Reactions in chemical or geological systems arise from the differences in free energy (G) between products and reactants. The reaction will proceed in the direction that leads to a net reduction in free energy according to the Second Law of Thermodynamics. If one assumes that dolomite forms from the replacement of calcite or aragonite, then the free energies of formation of these reactions can be used to predict which phase is thermodynamically most stable in seawater.

The reaction of the conversion of calcite to dolomite proceeds according to Equation 1.1.

$$2\,CaCO_{3(Cal)} + Mg^{2+} \longrightarrow CaMg(CO_3)_{2(dol)} + Ca^{2+} \qquad (1.1)$$

Using the standard free energy of formation values given in Table 1.2 together with the Gibbs Free Energy Equation:

$$\Delta G^\circ_{reaction} = \Sigma\, \Delta G^\circ_{products} - \Sigma\, \Delta G^\circ_{reactants}$$

$$\Delta G^\circ_{reaction} = \Delta G^\circ\ (\text{dolomite}) + \Delta G^\circ\ (Ca^{2+}) - [\,2\,\Delta G^\circ\ (\text{calcite}) + \Delta G^\circ\ (Mg^{2+})]$$

$\Delta G^\circ_{reaction}$ = -2,318 calories.

similarly, for aragonite $\Delta G^\circ_{reaction}$ = -2,778 calories.

	ΔG°_f
Dolomite	-518,734
Calcite	-269,908
Aragonite	-269,678
Ca^{2+}	-132,200
Mg^{2+}	-108,800

Table 1.2. Standard free energy values for important components during the transformation of calcite or aragonite to dolomite (at 25°C and 1atm). Data sources, Krauskopf, 1995; Robie & Waldbaum, 1968.

The equilibrium constant for Equation 1.1.

$$K = \frac{[Ca^{2+}][CaMg(CO_3)_2]}{[Mg^{2+}][CaCO_3]^2}$$

can be reduced to:

$$K = \frac{[Ca^{2+}]}{[Mg^{2+}]}$$

taking the solid phases as unity (Carpenter, 1980).

Also $\Delta G°_{reaction} = -RT \ln K$

where R = gas constant (1.987 cal/deg/mol)

T = temperature (Kelvins)

K = equilibrium constant

For the conversion of calcite to dolomite $\Delta G°_{reaction}$ = –2,318 calories.

So $-2{,}318 = -RT \ln K$

$$K = e^{\frac{-2{,}318}{-1.987(298)}}$$

$$K = 50$$

The reaction will thus go to the right ($CaCO_3$ will be dolomitized) in solutions where the $[Ca^{2+}]/[Mg^{2+}]$ activity ratio is lower than K=50. Using the activities for Ca^{2+} and Mg^{2+} given in Table 1.1, the activity ratio is calculated as only 0.156, clearly showing that $CaCO_3$ should be dolomitised in sea water.

This is shown graphically in a stability diagram (Fig. 1.1.) where the projection point for log $[Ca^{2+}]/[Mg^{2+}]$ in seawater falls into the dolomite stability field. This means that, not only should dolomite precipitate spontaneously from seawater, any immersed calcium carbonate should be converted to dolomite.

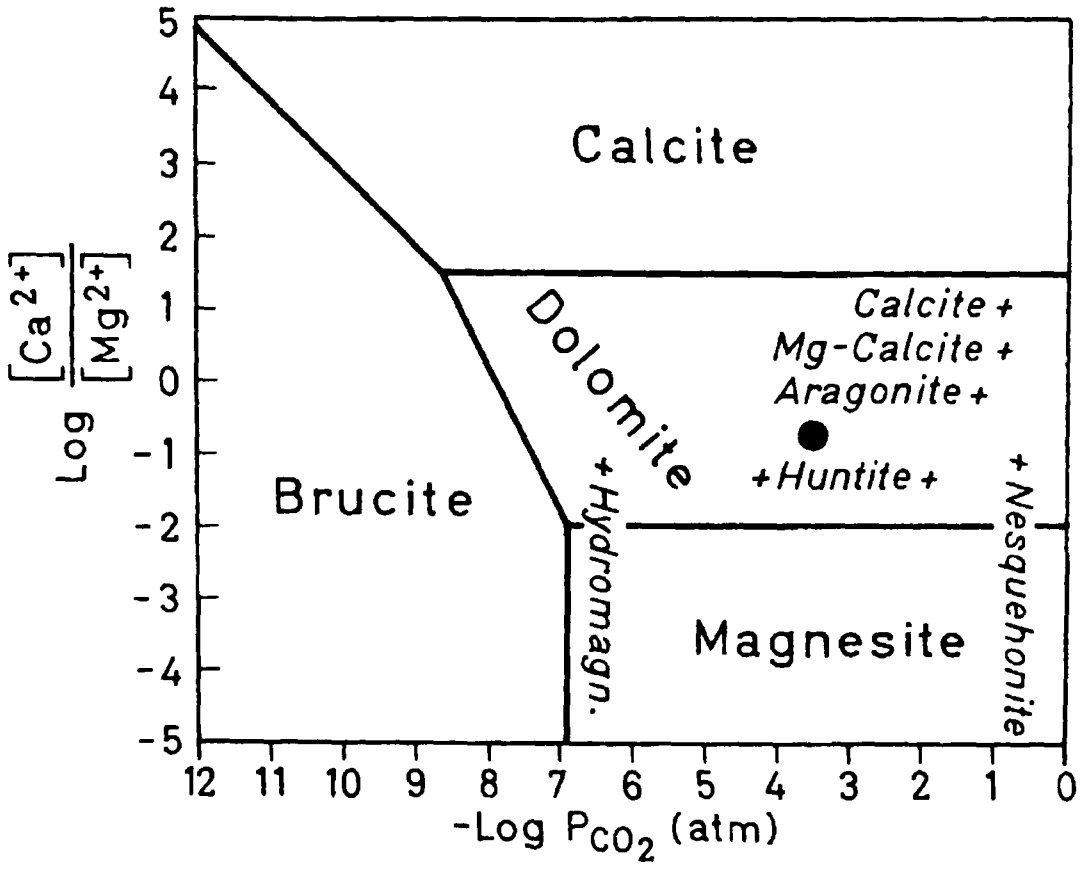


Figure 1.1. Phase diagram of the system $CaCO_3$ - $MgCO_3$ - H_2O at 25°C based on the solubility products determined by Horn (1969) for zero ionic strength. $k_{s\ Brucite} = 10^{-11.07}$, $k_{s\ Magnesite} = 10^{-8.14}$ $k_{s\ Dolomite} = 10^{-18.22}$, ($k_{s\ Calcite} = 10^{-8.35}$ after Garrels et al., 1960). Phase boundaries are shown for these stable phases only. The metastable phases occurring in the system are indicated in italics in those regions of the diagram which approximately correspond to their conditions of formation.

● shows the composition of seawater

Why does this not happen in nature?

One factor that prevents this from being so in nature is the disproportionate concentration in seawater of the component ions of dolomite (Table 1.1). The anion CO_3^{2-} concentration is extremely low compared to the cation concentration. From the kinetic model of Lippmann (1973) high concentrations of CO_3^{2-} are said to help dehydrate those magnesium ions that are adsorbed onto a crystal surface. Thus, low relative concentrations of CO_3^{2-} will tend to inhibit dolomite formation due to the dehydration barrier, even though, as far as the solubility product is concerned, high Mg^{2+} and Ca^{2+} concentrations should more than compensate for this lack of CO_3^{2-}. The problem is accentuated by the fact that it is the *activity* (a thermodynamic measurement representing energy available due to free and reactive ions in solution) of the carbonate ion rather than its concentration that governs its precipitation behaviour. The activity of CO_3^{2-} is much lower than its concentration because it has a marked affinity to form ion pairs with various cations, and especially with Na^+, Ca^{2+} and Mg^{2+},

thereby enhancing solubility and inhibiting precipitation. This becomes even more important when evaporated brines are considered because the amounts of Mg^{2+} and Na^{+} increase significantly and will therefore bond with more CO_3^{2-} in ion pairs. This is contrary to the belief that evaporation leads to dolomitisation (e.g. Butler, 1969).

A further problem in forming dolomite is the hydration of Mg^{2+} ions. The Mg^{2+}-H_2O bond is very strong owing to the Mg^{2+} ion having a relatively high charge/size ratio (3.3). This results in magnesium having a large hydration energy (-1891 KJ/mol). Compare this to Ca^{2+}, having a charge/size ratio of 1.8 and hydration energy of only -1562 KJ/mol. In addition to this, a significant amount of magnesium is held in ion pairs with sulphate. In seawater, this combination of hydration energy, $MgSO_4^0$ complexing and other ion pair inhibitions described above, results in an inability of natural seawater to precipitate dolomite, despite high super-saturations.

1.2.3. Inorganic models for dolomite formation

Emphasis upon the search for a 'special' fluid capable of bringing about dolomitization has arguably resulted in a rather limited approach to dolomite formation. Fundamental chemical constraints have generally been overlooked in favour of elaborate mixtures of water from several sources which may or may not favour dolomitization.

The earliest model of this kind came from Adams and Rhodes (1960) who suggested that the close association of dolomite, evaporites and marine limestone requires a restricted lagoon - open ocean couple for dolomite formation. They used observations from Permian dolomites to advocate a model whereby metastable limestones were altered to dolomite by hypersaline brines refluxing from evaporite lagoons (Fig. 1.2a). Adams and Rhodes (1960) claimed that these brines would have been hot, dense, alkaline and supercharged with Mg^{2+} resulting from evaporative concentration of seawater trapped behind a reef barrier. Precipitation of gypsum would lower Ca^{2+} concentrations so that Mg^{2+}/Ca^{2+} ratios would be many times that of seawater. When the brine became dense enough, it would seep down through the underlying calcium carbonates, dolomitizing them as it passed through. Adams and Rhodes (1960) used the disproportionate lack of late stage evaporites in the sequence, together with the presence of anhydrite and halite in the pores of the dolomite, as evidence

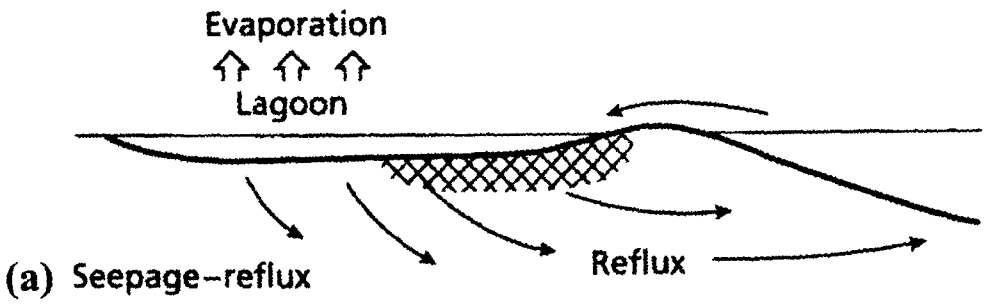
for the reflux process. Adams and Rhodes (1960) do however state that the downward extent of dolomitization by this method is theoretically limited because the brine will lose heat, alkalinity and Mg^{2+} with increased flow through the limestones. Three models using many of the ideas invoked above have since dominated the literature and are critically reviewed in the following pages.

(a) Hypersaline/ Sabkha Model

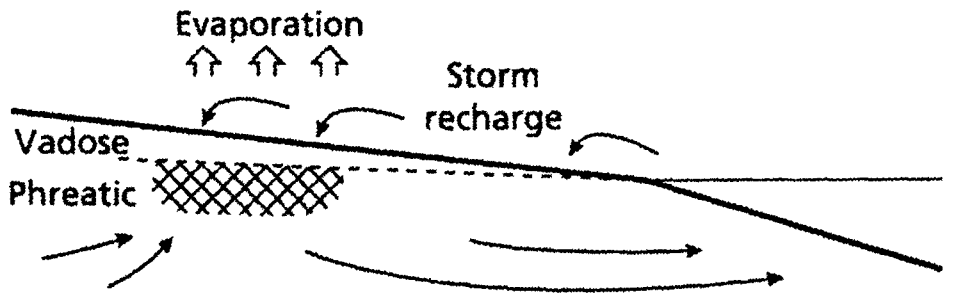
Many modern occurrences of dolomite are associated with evaporites in hypersaline settings, e.g., the Persian Gulf (e.g. Curtis *et al.*, 1963). Under strongly evaporatic conditions, where rates of evaporation greatly exceed rates of rainwater precipitation and seawater recharge, seawater beneath supratidal sabkhas becomes highly concentrated by evaporation (Fig. 1.2b). Eventually mineral phases, such as gypsum and aragonite, will precipitate from the hypersaline brine, thereby removing calcium from the water body and increasing the Mg^{2+}/Ca^{2+} ratio (Butler, 1969). It is thought that these Mg^{2+} rich brines become the dolomitizing fluid (Butler, 1969 fig. 8).

Only small amounts of dolomite have been observed in such locations and the exact mechanism by which it forms is still not understood. An important question here is whether dolomite is forming as a primary precipitate which becomes more ordered with age or whether it is forming as a replacement of precursor calcium carbonate. Replacement is favoured by the majority of authors because of mass balance equations which show that the amount of calcian dolomite increases as aragonite decreases (McKenzie, 1981). Petrographic studies, however, have shown both euhedral aragonite crystals encrusting dolomite and vice versa, which has been used as evidence for direct precipitation (Hardie, 1987, after McKenzie, 1981). Evolution of the brines in terms of Mg^{2+}, Ca^{2+} and SO_4^{2-} ions has been used as evidence for the replacement hypothesis but these calculations are based on an inferred coupled formation of dolomite and gypsum which has never been observed. In addition, it can be shown that very similar trends can be observed in brines with or without the occurrence of dolomitization (Hardie, 1987).

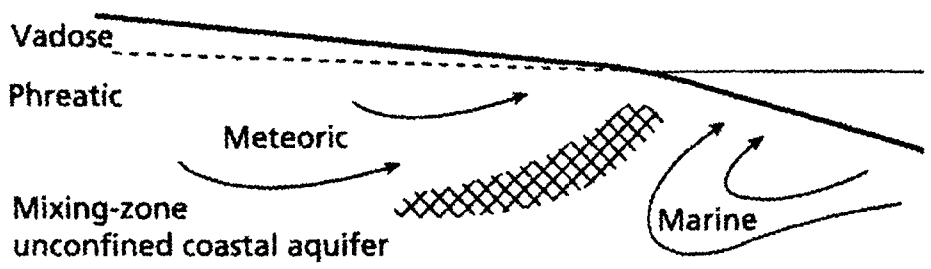
A major kinetic problem with this replacement model was first put forward by Lippmann (1973). He pointed out that evaporation leading to high Mg^{2+}/Ca^{2+} ratios would not favour dolomite formation because of the accompanying decrease in activity of the CO_3^{2-}



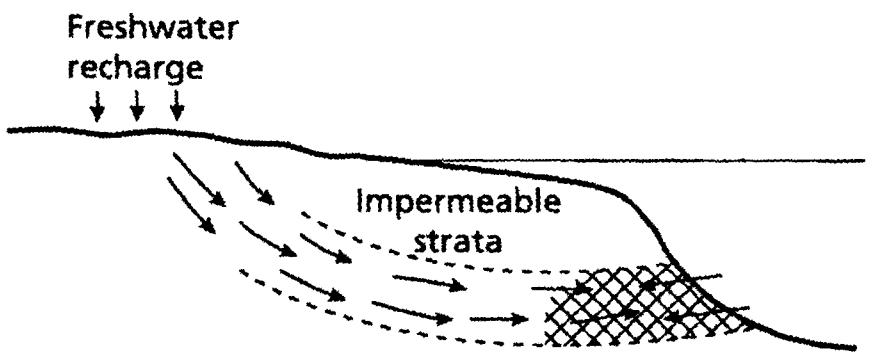
(a) Seepage–reflux



(b) Sabkha/evaporation



(c) Mixing-zone unconfined coastal aquifer



(d) Mixing-zone deep confined aquifer

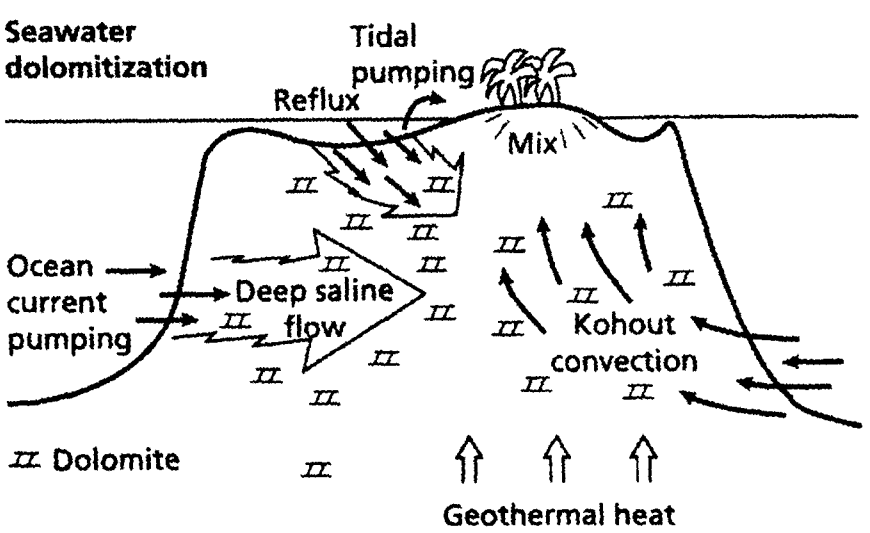


Figure 1.2. Models of inorganic dolomitization, illustrating the variety of mechanisms for moving dolomitizing fluids through the sediments, (from Tucker, 2001). See text for details.

ion. Complexing to form neutral $MgCO_3^0$ ion pairs severely reduces the activity of the carbonate ion. Mg^{2+} ions would also form neutral ion pairs with available sulphate ions, as $MgSO_4^0$. Both these ionic interactions mean that the requisite increased activities of Mg^{2+} and CO_3^{2-} ions remain problematical. Borchert and Muir (1964) further supported this sceptical view when they showed in experiments that aragonite will be the favoured carbonate for precipitation from evaporatic solutions, even where the laws of thermodynamics would predict that dolomite should be the preferred phase.

(b) Mixing zone model

Several studies (e.g. Hanshaw *et al.*, 1971; Badiozamani, 1973; Folk & Land, 1975) have suggested that brackish groundwaters produced by mixing of seawater with meteoric water (Figs 1.2 c-d) can become saturated with respect to dolomite at Mg^{2+}/Ca^{2+} concentrations which are much lower than found in hypersaline environments (close to seawater values of 3:1 or even as low as 1:1). This has been explained by reduced competition for Mg^{2+} ions from other anions in a dilute solution. The most widely quoted of these is the 'Dorag' model of Badiozamani (1973). He assumed that the replacement of calcite by dolomite will proceed in those pore-waters which are supersaturated with respect to dolomite and undersaturated with respect to calcite. Using thermodynamic arguments he suggested that although neither seawater nor freshwater meet these criteria, a mixture of the two may do so.

Although numerous authors embraced this model initially, there has been much subsequent criticism (e.g. Hardie, 1987; Machel & Mountjoy, 1986). A major stumbling block is the lack of dolomite in modern mixing zone environments, even where a mixing zone is shown to be supersaturated with respect to dolomite e.g. Barbados (Steinen *et al.*, 1978). This was attributed to kinetic difficulties by Wagner (1983). There has also been a lack of natural or experimental evidence to show that dolomite has ever formed in dilute solutions or in solutions with low Mg^{2+}/Ca^{2+} ratios. There are, furthermore, flaws in Badiozamani's original calculations for his model. Badiozamani used solubility values for ordered dolomite, whereas today it is the Ca^{2+} rich, less-ordered dolomite that is mostly seen to be forming. In addition to this, pH and pCO_2 variations were not taken into account, nor were order-disorder energies associated with dolomite. When allowances are made for these factors, one finds a very narrow range of possible fluid compositions that still fulfil the thermodynamic

criteria. Yet further evidence against this model is the observation that some dolomites formerly interpreted as mixing zone dolomites show no evidence for the replacement of calcite that this model demands. Indeed, dolomite cement phases can be shown to sharply overlie euhedral calcite cement phases that show no signs of dissolution (Sibley, 1980). Hence, the precipitating medium cannot have been undersaturated with respect to calcite as claimed. Isotopic data offers little support to the mixing zone model, because isotopic fractionation factors for dolomite remain largely unresolved and the isotopic compositions for dolomites supposedly formed in different settings are seen to actually overlap (Hardie, 1987).

A variation on the mixing zone model was proposed by Folk and Land (1975). Their schizohaline model postulates that, at low salinities and low crystallisation rates, dolomite can form readily. In an environment where high Mg^{2+}/Ca^{2+} saline waters (e.g., evaporated brine) can be diluted by mixing with freshwater, a high Mg^{2+}/Ca^{2+} ratio will be maintained but the salinity will be diluted and these 'special' waters, where competition from other ions is greatly diminished, are capable of forming ordered dolomite. With low crystallisation rates, however, large euhedral crystals of ordered dolomite should form, whereas the majority of modern dolomites are unordered and the crystal size is on the sub-micron scale (e.g. Vasconcelos & McKenzie, 1997; *this study*). In addition it can be shown (see Chapter 4) that high Mg^{2+}/Ca^{2+} ratios are not the crucial factor in forming dolomite. The schizohaline model is also falsifiable when kinetic inhibitors (Section 1.2.1.) are considered and no dolomite has been synthesised in the laboratory in this way.

(c) Seawater pumping model

Several authors (e.g., Land, 1991; Carballo *et al.*, 1987) have maintained that dolomitization can take place in a normal seawater environment (Fig. 1.2e). They maintain that this could be possible if a sufficient amount of fluid is forced through the sediment, so that the porewaters are being continuously replenished with new Mg^{2+} ions while Ca^{2+} ions can be flushed out at the same time. One example given is that from Sugarloaf Key in Florida (Carballo *et al.*, 1987), where seawater is pumped up and down through the sediment in relation to spring tides. Both precipitation of a dolomite cement and replacement of existing carbonate grains have been observed. Seawater pumping brought about by 'Kohout Convection' has also been

invoked as a possible mechanism for widespread dolomitization in the rock record (e.g. Simms, 1984). Here, the high geothermal gradient beneath some carbonate platforms is thought to generate a large scale convection system, which draws cold seawater into the platform, although little confirmatory evidence has been presented.

Seawater pumping does not explain the kinetics of dolomite formation from seawater. It fails to explain how the high enthalpy of hydration of the magnesium ion is overcome and the presence of large amounts of sulphate ions - both of which are inhibitors of dolomite formation (Lippmann, 1973; Baker & Kastner, 1981). Lippmann (1973) observed that the initiation of dolomitization in calcite needs a significant increase in carbonate alkalinity and the removal of all calcium ions by precipitation. It does not appear to be possible to maintain such conditions in normal seawater.

1.2.4. Experimental evidence

Dolomite has not been precipitated by physico-chemical means at normal temperatures and pressures in the laboratory. Lippmann (1973) reported the results of Usdowski's (1967) experiments in which dolomite was synthesised at 120°C by reacting $MgCl_2$ with solid calcium carbonate.

$$2CaCO_3 + MgCl_2 \longrightarrow CaMg(CO_3)_2 + CaCl_2 \qquad (1.2)$$

However a hydrothermal origin for normal sedimentary dolomite can be discounted from observations on the depths and temperatures at which modern dolomite is forming. Lippmann also stated that dolomite could not form from a solution alone; the only way it could form in significant quantities was by the dolomitization of pre-existing solid calcium carbonate. He maintained that a starting material must first dissolve into Ca^{2+} and CO_3^{2-} ions before reacting with Mg^{2+} ions.

$$CaCO_3(solid) + Mg^{2+} + CO_3^{2-} \longrightarrow CaMg(CO_3)_2\ (solid) \qquad (1.3)$$

He still failed, however, to precipitate dolomite in this way at temperatures below 100°C.

1.2.5. Other avenues of approach - sulphate inhibition

Although the majority of research into dolomite formation has centred around the three models described above which focus on the Mg:Ca ratio, one other pathway that has been explored recently is the influence that the sulphate ion has on dolomite formation. The discovery, during DSDP Legs 63 and 64, of extensive early diagenetic dolomites in anoxic muds along the continental margin of California and the Gulf of California (Pisciotto and Mahoney, 1981; Kelts and McKenzie, 1982) led to the consideration that reducing, organic rich, sulphate poor environments may be important in dolomite formation. Elevated Mg/Ca ratios were found not to be a limiting requirement and primary precipitates of dolomite cement in the deep sea environment were mostly associated with zones of low sulphate concentration, high alkalinity and high ammonia content (Kelts and McKenzie, 1982).

These discoveries led Baker and Kastner (1981) to demonstrate experimentally that the presence of dissolved sulphate, even at concentrations well below those found in seawater, inhibits the formation of dolomite, owing to its ability to complex with Mg^{2+} ions. Slaughter and Hill (1991) argued that sulphate inhibits carbonate precipitation due to its ability to adsorb onto active crystallisation sites in place of the carbonate ion. The former suggested that any process that would reduce sulphate concentrations would make dolomite precipitation more likely, not only by removing the SO_4^{2-} but also by the production of NH_4^+ and alkalinity. Bacterial sulphate reduction was invoked as the process to do this, though Hardie (1987) used the presence of sulphate in lake-waters where dolomite is found as an argument against this theory. The latter overlooks, however, the potential importance of the associated effects of bacterial sulphate reduction. The increase in activity of the carbonate ion, the release of magnesium from metabolised organic matter and the removal of large percentages of sulphate are more important than the actual amount of sulphate present in controlling dolomite precipitation. In addition to this, the dynamic nature and seasonality of modern lakes where dolomite is precipitating means that sulphate may be present in large amounts at the time of measurement, but a short time later may be substantially depleted or removed totally. The presence of sulphate in dolomite-containing lakes cannot therefore be taken as evidence against its inhibitory effects.

1.2.6. Microbial processes

Recently, Wright (1993, 1997, 1999, 2000), Vasconcelos *et al.* (1995), Vasconcelos and McKenzie (1997), Burns *et al.* (2000) and Wartmann *et al.* (2000), have focussed on the influence that microbes may have on the precipitation of dolomite. Wright (1993, 1997) presented petrographic evidence of biogenic fabrics preserved in very early diagenetic cherts within host dolomites of the Cambrian Eilean Dubh Formation in Northwest Scotland, first described by Brasier (1977). These suggested a link between dolomite formation and bacterial degradation. A progressive decrease in organic preservation (increased degradation) was seen to be accompanied by the appearance of dolomite rhombehedra (< 5μm - 50μm) within the nucleus and/or cortex of ooids. No rhombehedra were observed where preservation of the organic matter appears to be good. The unvarying location of the dolomite rhombehedra within the ooids was taken to show that they were intragranular precipitates formed with increasing degradation of bacterial matter and this gives a strong case for a taphanomic link. Subsequent dissolution of ooids could then result in a liberation of dolomite crystals to the sediment which would give no clue to their original mode of formation. It is silicification of these fabrics which preserves the association of dolomite and organic degradation. Many of the silica pseudomorphs of dolomite have relict dolomite cores showing that dolomite preceded diagenetic silicification. The dolomite, analysed by XRD and microprobe, is well ordered, almost stoichiometric with an average composition of Mg_{50}: Ca_{50} (Wright, 1997).

Vasconcelos and McKenzie (1997) and Vasconcelos *et al.* (1995) used the recent discovery of modern dolomite in Lagoa Vermelha, a shallow-water isolated coastal lagoon east of Rio de Janeiro, to investigate the factors important in dolomite formation in recent, low temperature, earth surface environments. Lagoa Vermelha (Fig. 1.3) has many of the same characteristics as the distal ephemeral lakes of the Coorong region. It is 2.4km^2 in area but only has a maximum depth of 1.7m, and its margins are bordered by a well developed algal mat. A barrier dune separates it from the South Atlantic Ocean and it is bordered by Pleistocene dunes on its continental side. Recharge comes in the form of both meteoric water and seawater seeping into the groundwater. Very little clastic material is brought into the lagoon so the sediment is essentially a chemical/biological precipitate. Its salinity fluctuates between brackish and hypersaline depending on the season. The major difference between Lagoa Vermelha and the Coorong is the latitude at which they are found. The Coorong is at

36°S and falls within the semi-humid climatic zone whereas Lagoa Vermelha is at 23°S and has a semi arid microclimate. Even so, Lagoa Vermelha never dries out completely and evaporite minerals are only found around its margins, in stark contrast to the ephemeral nature of the Coorong lakes. Vasconcelos and McKenzie (1997) found that a poorly ordered calcium rich dolomite was forming under anoxic conditions in a sludge at the sediment-water interface, and argued that the formation of this dolomite was mediated by microbial processes, in particular the action of sulphate-reducing bacteria (SRB). They also stated, using evidence from oxygen isotopes and from the hydrology of the area, that this precipitate was forming under extreme hypersaline conditions during the dry season. Close examination of the precipitate revealed aggregates made up of spherical and elliptical bodies < 1μm in size which were interpreted as lithified nannobacteria (Folk, 1993a; 1993b). Within the upper 0.15m of the sediment they noted early diagenetic alteration of this poorly crystalised sludge to a more stoichiometric dolomite with substantially better defined crystal faces, concluding that once nucleated, the crystals may continue to grow by inorganic processes, filling in the gaps between the spherical bodies.

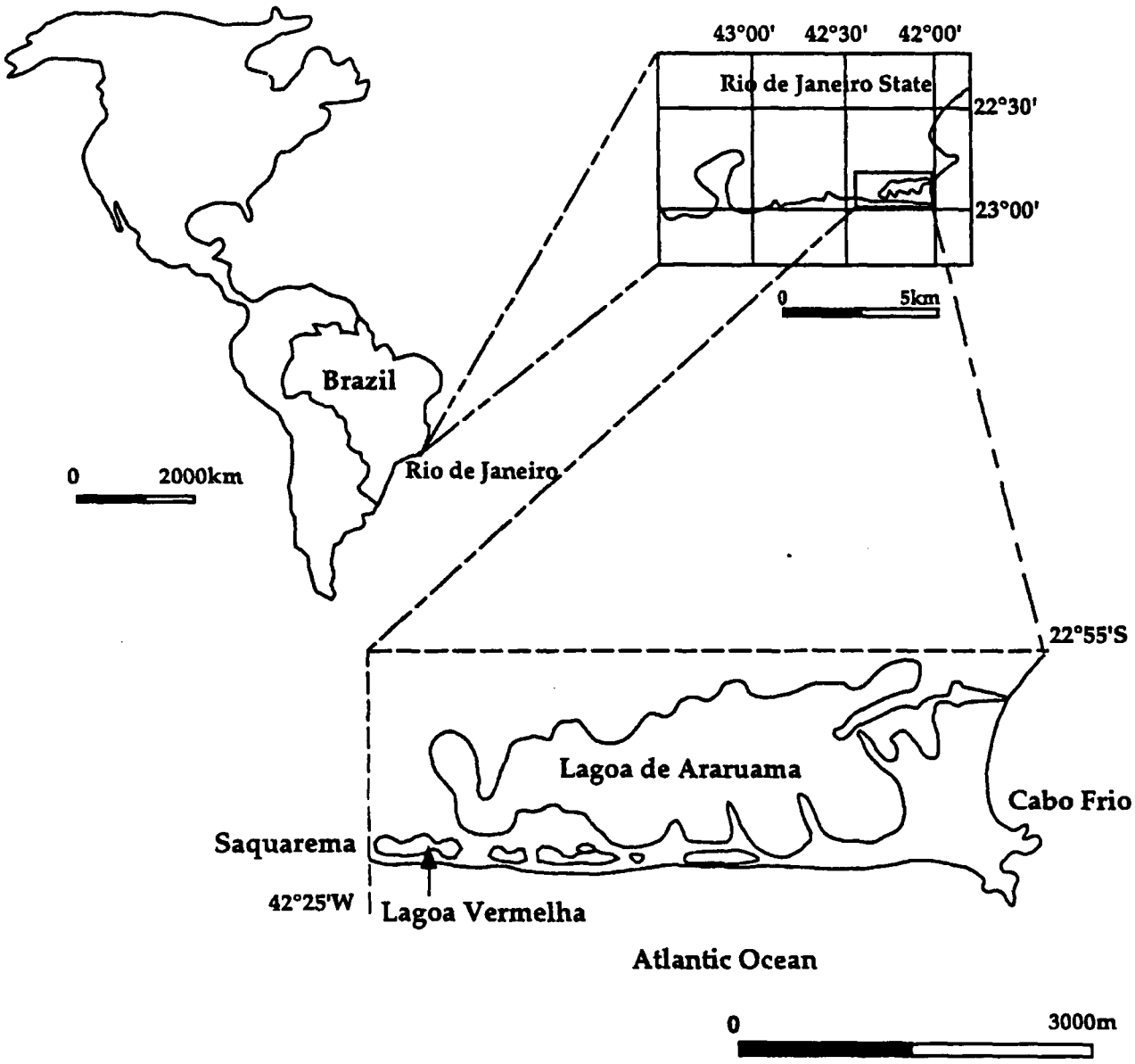


Figure 1.3. Map showing the location of Lagoa Vermelha on the coastline 90km east of Rio de Janeiro, Brazil. (Vasconcelos and McKenzie, 1997)

Further evidence to support the microbial mediation theory came from their laboratory experiments (Vasconcelos *et al.*, 1995), in which a dolomite was precipitated in anoxic conditions at low temperatures using SRB of the *Desulfovibrio* group cultured from the Lagoa Vermelha sediments. In these experiments, a Postgate B (a general media for the cultivation of *Desulfovibrio* and *Desulfotomacula*; Postgate, 1984) medium was used, modified so that salinity and pH matched those of Lagoa Vermelha; a quartz sand mineral seed was added together with 1ml of supernatant liquid from a positive culture vial. These samples were incubated for over one year at 4°C and after this time it was found that the quartz grains were weakly cemented by a carbonate, identified using X-ray diffraction (Fig. 1.4) and transmission electron microscopy as a ferroan dolomite. In addition, the morphology of the experimentally produced precipitate (Fig. 1.5) closely resembled that found naturally in Lagoa Vermelha.

Further work by the same research group (Warthmann *et al.*, 2000) refined the microbial experiments. They were able to isolate a particular strain of SRB (LV form6) from Lagoa Vermelha sediment; this strain was then used in laboratory mineral-precipitation experiments. A culture medium simulating Lagoa Vermelha conditions was created and the above bacterial strain was added, before incubating at 30°C. A partially ordered, non-stoichiometric dolomite precipitate formed with distinctive dumb-bell morphology in a little over three weeks which, with continued growth, merged together to form semi-spherical and cauliflower shapes (Fig. 1.6). The sulphate in the culture medium was consumed at the same time. It has been suggested that the morphology of the precipitate is strongly influenced by the amount of Mg in the crystal lattice (e.g. Fernandez-Diaz *et al.*, 1996). Warthmann *et al.* (2000) also concluded that specific bacteria were not only necessary for mediating the chemistry of the micro-environment but were also necessary to provide the physical nucleation sites of dolomite crystals.

This study builds upon previous work using the Coorong area of South Australia, where modern occurrences of dolomite have been reported (e.g. Von der Borch, 1976; Wright, 1999) as a natural laboratory for the investigation of microbial dolomite formation.

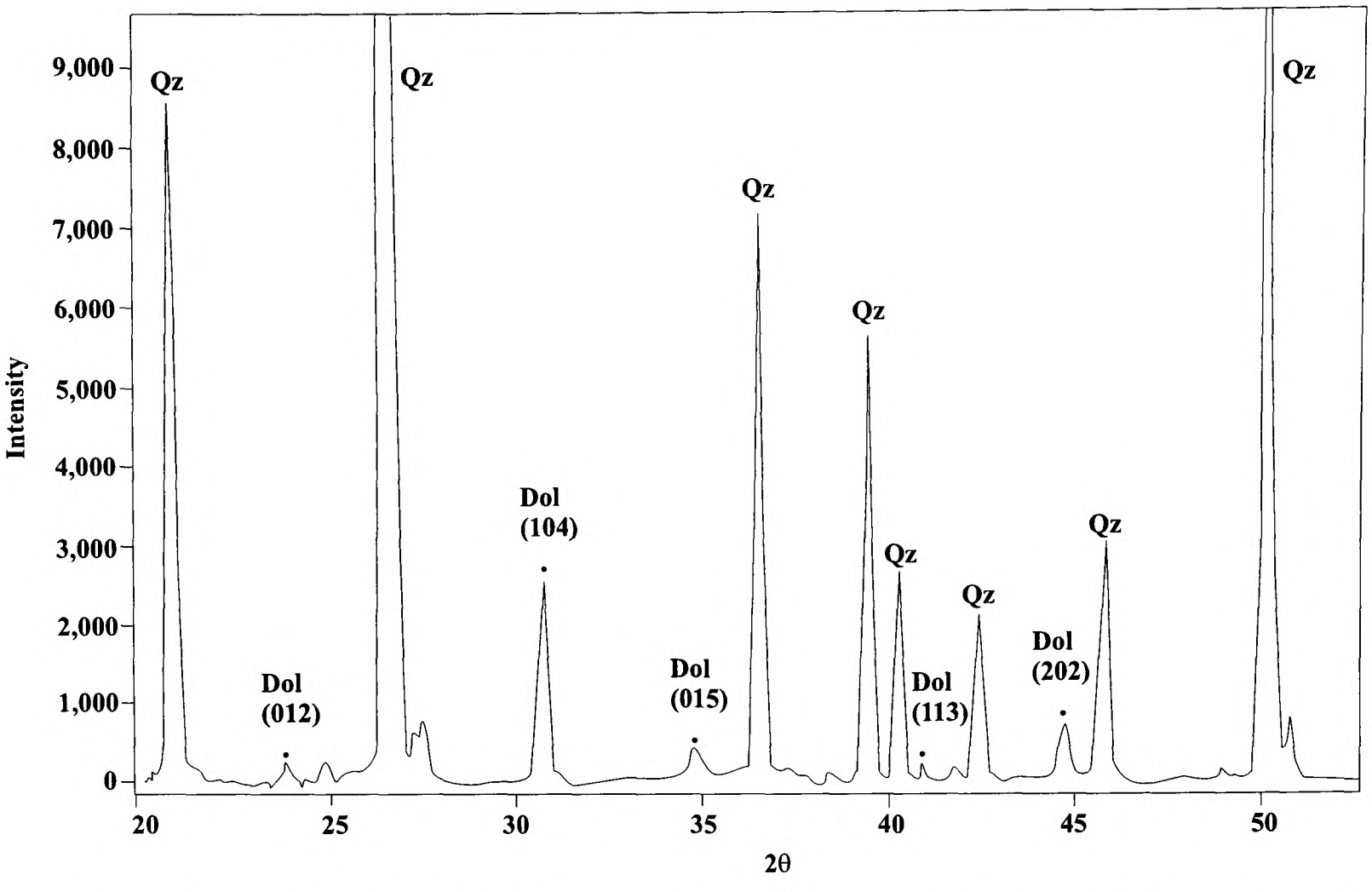


Figure 1.4. X-ray diffractogram of the bulk powdered sample recovered from the bacterial experiment of Vasconcelos *et al.*, (1995). The presence of the "ordering reflection" 015 peak indicates the mineral is a fully ordered dolomite.

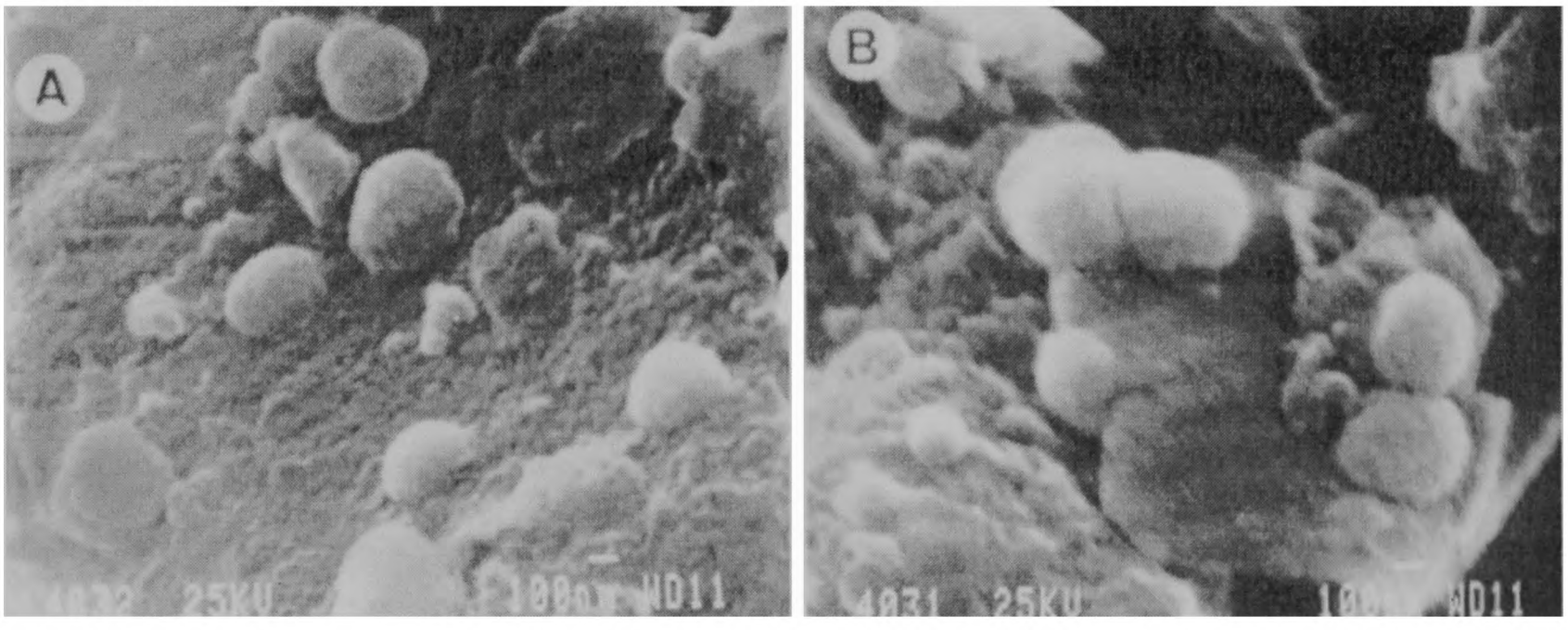


Figure 1.5. SEM photomicrographs showing the ferroan dolomite coating on the surface of the quartz substrate from bacterial experiments. (after Vasconcelos and McKenzie, 1997).

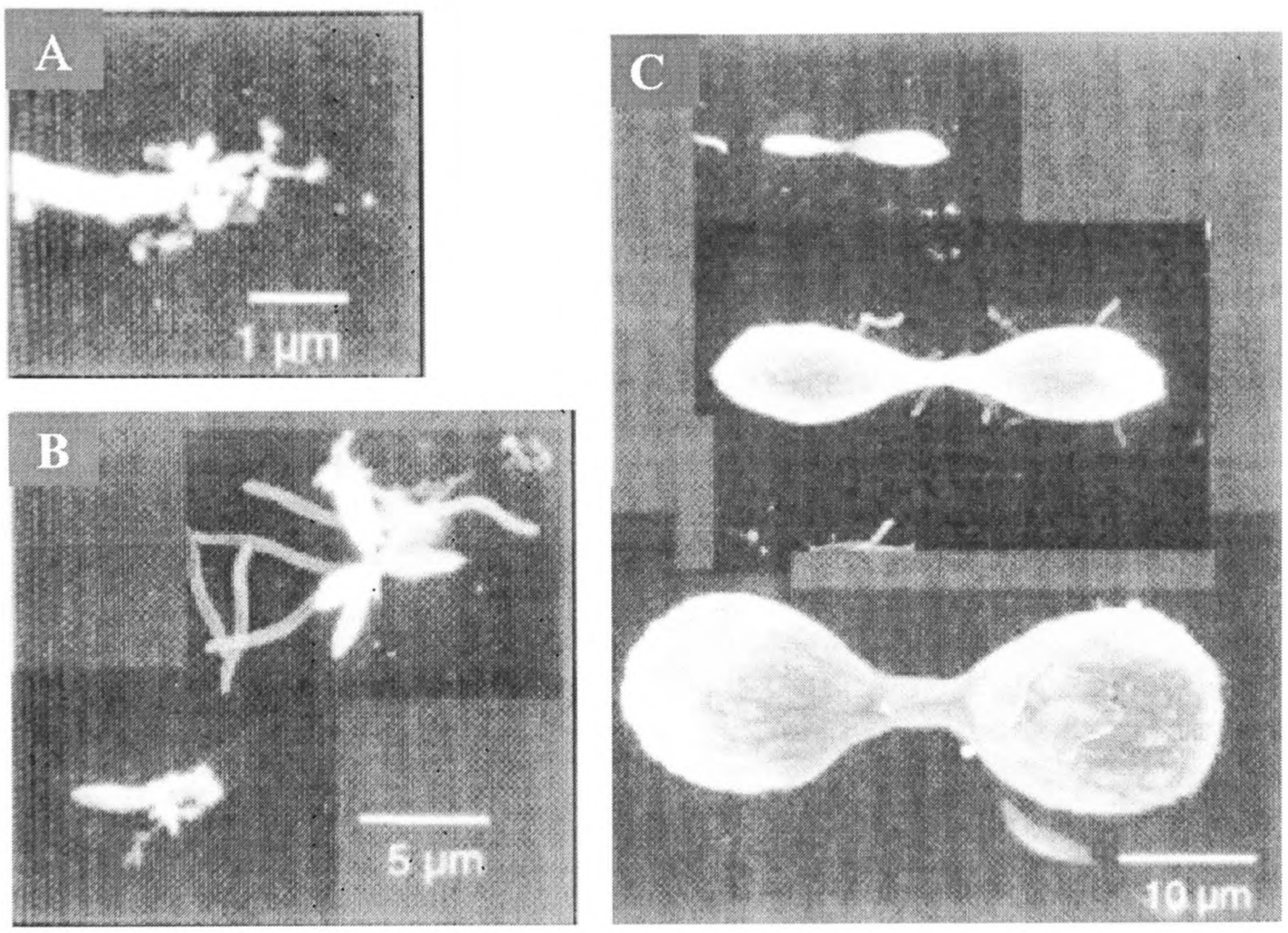


Figure 1.6. Scanning electron microscope photographs of sulphate-reducing bacteria (strain Lvform6) associated with precipitation of dolomite with dumbbell morphology. A: Possible initial stage of crystal growth at polar end of bacterial cell. B: Crystal growth appears to begin with close spatial relationship to bacterial cells, mainly inside larger aggregates of bacteria. C: Growth of dolomite dumbbells showing drastic mass increase within first 2-3 weeks after initiation. Size of bacteria (4-8 µm in length) can be used as comparative scale. D: Later stage of mineral precipitation after ~4-6 weeks, when dumbbell shape is transformed into cauliflower like structure. (After Wartmann *et al.*, 2000)

1.3. STUDY AREA

The study area (Fig. 1.7) is one of the few locations where dolomite is forming at the present day. It is located in the Coorong Region of South Australia approximately 200km south east of Adelaide, where a series of distal ephemeral, alkaline lakes lie a few hundred metres inland from the Coorong Lagoon, an offshoot of the Southern Ocean. The lakes are located next to the settlement of Salt Creek and run in a southerly direction for approximately 19km, being situated in an interdune corridor that is only c.1m above sea level, flanked on one side by Holocene dunes, and on the other by Pleistocene coast parallel dunes. The lakes studied are labelled in Figure 1.7 from which it can be seen that there is a northern chain of five lakes, the southerly four of which, in the early Holocene, were connected both to each other and to the Coorong Lagoon by a series of interlake corridors. A subsequent drop in sea level has left each one isolated. The remaining four lakes had no such connection in the Holocene.

The distal ephemeral lakes provide a perfect natural laboratory for the study of dolomite precipitation. Lakes with a modern infill of dolomite lie in close proximity to those lacking modern dolomite, and all are contained within the same hydrological and geological setting.

The lakes were visited during two field seasons in early summer, from late October to late November in 1998 and then from early November to mid December in 1999. The field seasons were timed to coincide with a time of intense evaporation and thus the latter stages of lake desiccation where it was deduced that there would be the greatest physical and chemical changes in the lakes. This was the stage in the annual cycle where, from previous work (Vasconcelos and McKenzie, 1997; Wright, 1999), it was proposed dolomite formation would most readily occur.

Eight lakes were studied; five lakes were chosen as sites of active dolomite formation, namely Milne, Pellet, Mini Dolomite, McFaiden and Dolomite Lakes. Three lakes where modern dolomite had not been observed were chosen for comparison, namely Halite, North Stromatolite and South Stromatolite Lakes.

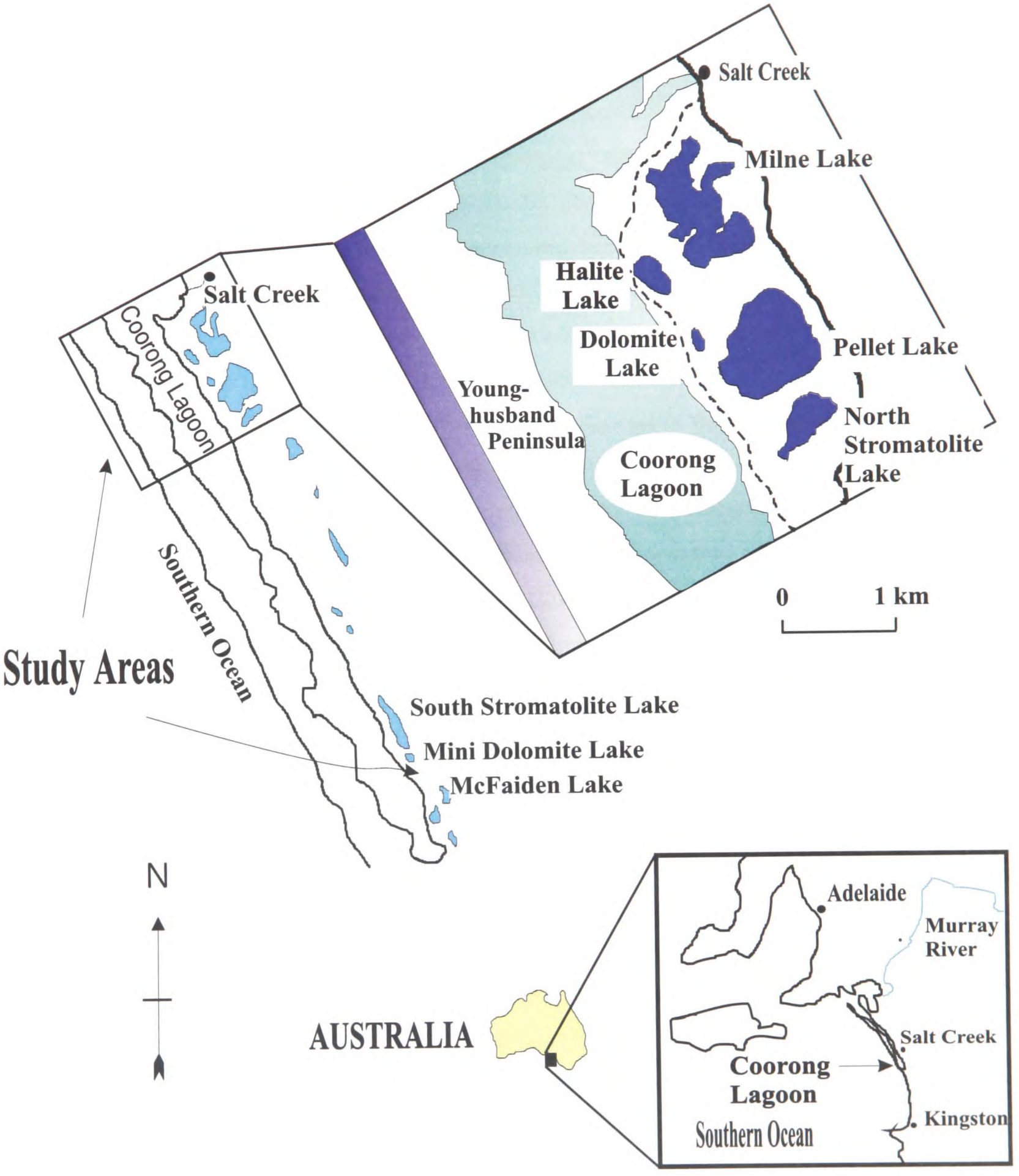


Figure 1.7. Location of field area, Coorong Region, South Australia

1.4. GEOLOGICAL SETTING

The Coorong region of South Australia lies in the Murray Basin, which is a Tertiary basin underlain by Early Palaeozoic rocks (Figs 1.8 & 1.9). It is bordered to the north by the Adelaide Geosyncline containing sediments of Late Precambrian and Cambrian age, which were subsequently uplifted and folded to form the Mount Lofty and Flinders Ranges; and to the south by another Tertiary basin, the Otway Basin. The Murray Basin is a large Tertiary Basin extending from South Australia into Victoria and New South Wales. In the northern part of the basin Permian and Cretaceous sediments underlie Tertiary sediments in troughs such as the Renmark Trough. The latter is essentially a broad fairly shallow basin separated from the Otway basin by the Padthaway Ridge, which for most of the Tertiary was a series of granite islands some of which still outcrop today just southwest of Bordertown and around Tintinara (Ludbrook, 1980). The most common sediments are of Miocene age laid down during the maximum marine incursion, which began in the Late Oligocene and persisted through to the Middle Miocene. These are limestones, sandy limestones and clays which are rich in fossils, in particular bryozoa and echinoids (Ludbrook, 1961). Early Miocene sandy limestones lie directly on top of Early Palaeozoic sediments or granites in many parts of the Murray Bridge area. Around the islands of the Padthaway Ridge, a group of fossiliferous marine sands and limestones mark an invasion by the sea in late Eocene times (Ludbrook, 1980).

This Tertiary sedimentation was a direct consequence of the final separation of Australia from Antarctica. Ocean crust began to form between the two and the Murray Basin began to subside in the Late Palaeocene to early Eocene. At this time most sedimentation was marginal marine and carbonaceous with few marine fossils. It was followed by continuous marine sedimentation during the Oligocene, a general retreat of the sea during the Middle Miocene and then limited marine incursions into the basin in the Pliocene, marked by plentiful oyster beds (Ludbrook, 1980).

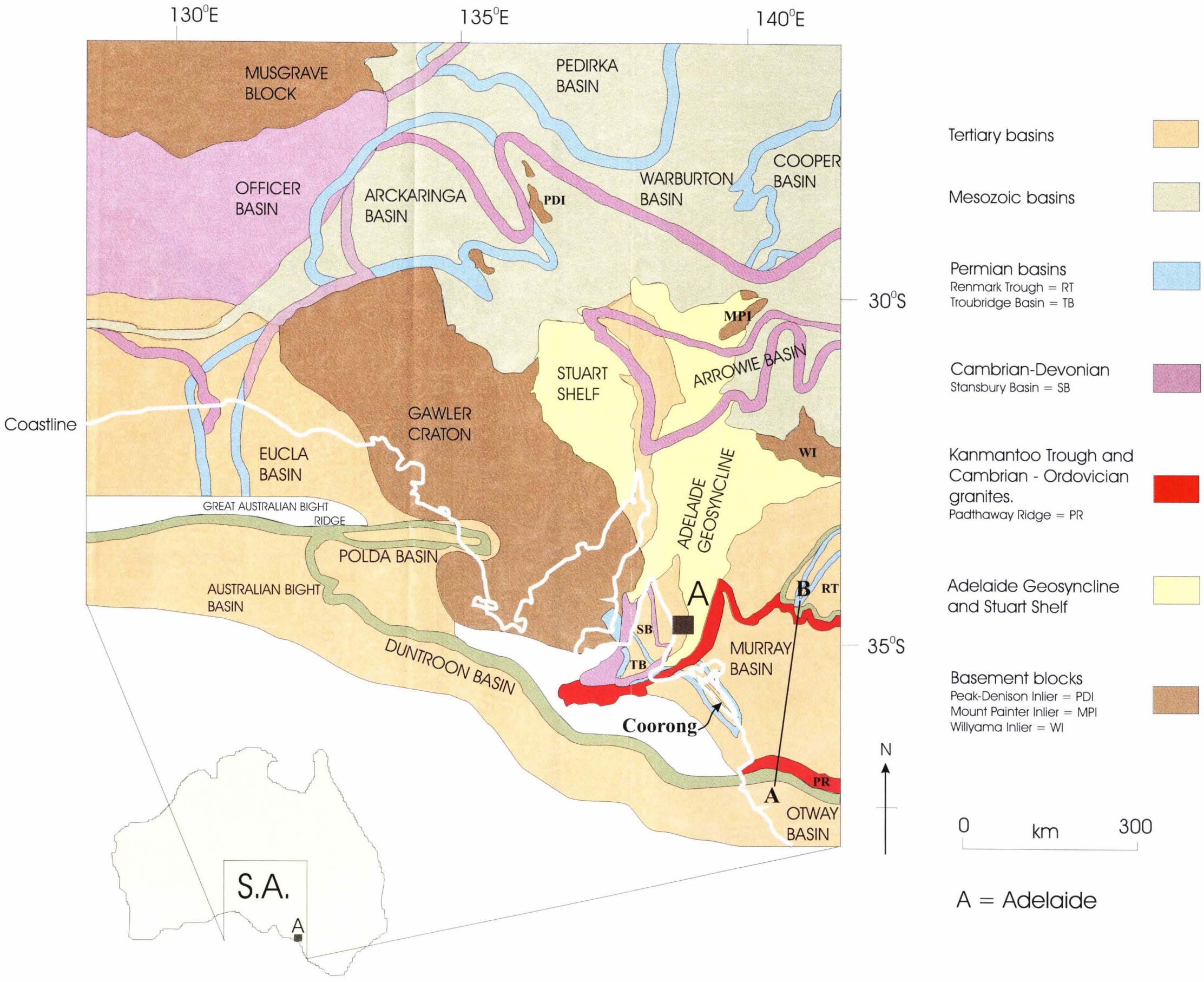


Figure 1.8 Geological Setting of South Australia (S.A. Department of Mines and Energy)

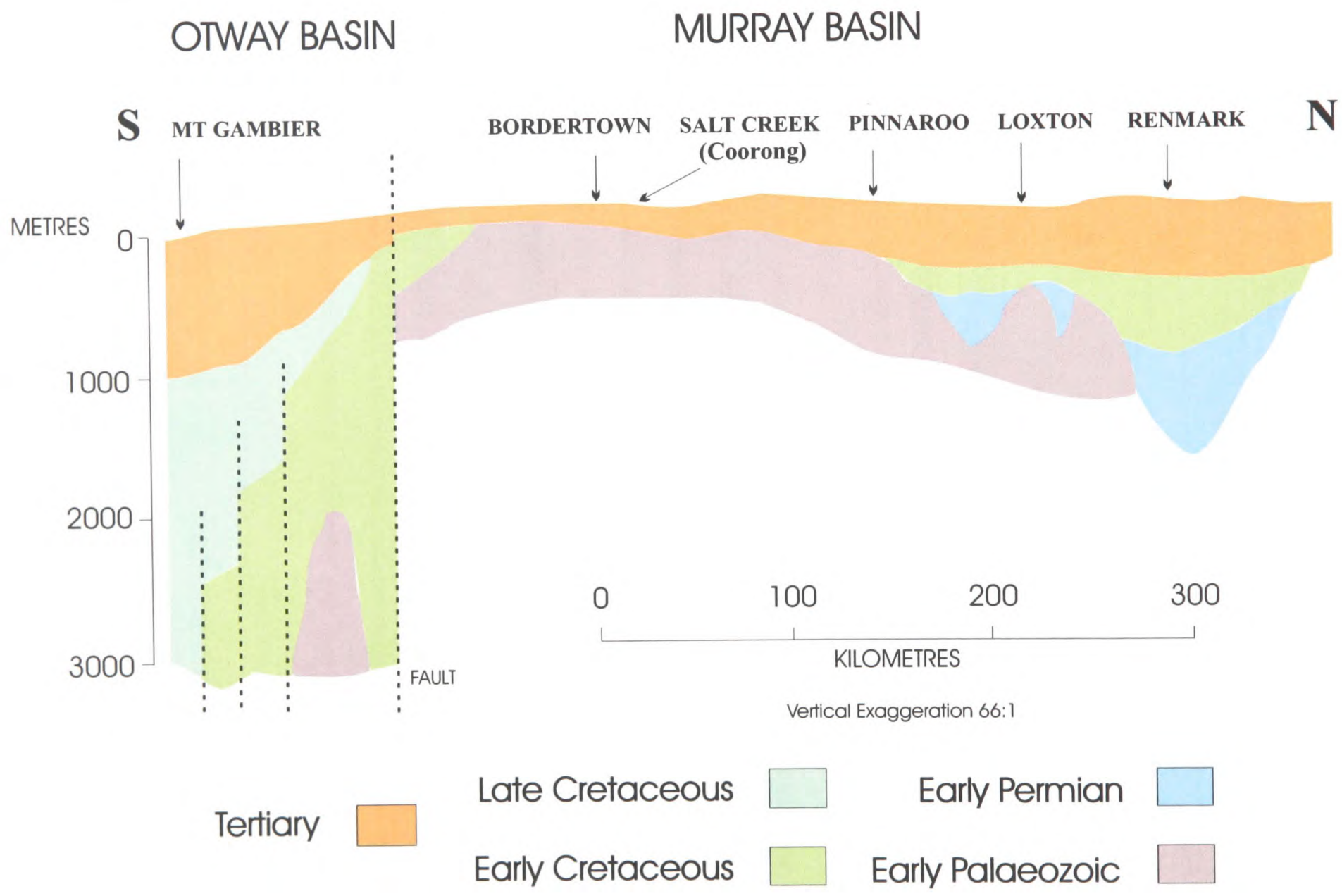


Figure 1.9. Geological cross section from Mt Gambier to the Renmark Trough (A---B on Fig. 1.8). (After Ludbrook, 1980).

1.4.1. Quaternary History

This period of time was dominated by glaciations and although Australia itself did not experience glaciation it was affected by climatic and glacio-eustatic sea level changes. For large periods of time, erosion and terrestrial deposition dominated but extensive shell beds were deposited during highstands. The Coorong Region shows the most outstanding example of sea level change, indicated by a series of semi-consolidated calcrete-encrusted sand barriers with crests up to 30m above the present interdune flats (Von der Borch, 1976). The trend of the ridges is more or less parallel to the present coastline and they increase in age away from the coast (Sprigg, 1952).

Each barrier-interdune flat couplet was probably formed in the same way as the present coastal set. Here, the lagoon (Coorong Lagoon) was formed by Holocene inundation of the eroded remnants of a Pleistocene barrier. There followed accretion of shelf-derived skeletal sands, causing barrier-building and lagoon restriction, with cut off from a marine influence followed by isolation to form distal ephemeral lakes (Fig. 1.10) (Von der Borch, 1976). The present Coorong Lagoon is at an intermediate stage of restriction from marine influence, while the next interdune corridor (which contains the ephemeral lakes in which dolomite is found) is isolated from marine influence. The lakes are inundated in winter by meteoric water accompanied by the elevation of the water table, and dry up in summer due to evaporation (Ahmad, 1996). The level of the interdune corridor, where the lacustrine dolomite is found, lies at a height close to coastal sea level, increasing to around 50m above sea level some 90km inland where they die out (Von der Borch, 1976). This rise in height is due to regional uplift associated with a widespread Quaternary volcanic province of which Mt Gambier represents the western extremity (Sprigg, 1952; Von der Borch, 1976).

1.5. CLIMATE

The Coorong region lies at a latitude of 36° South and falls within the sub-tropical, semi-humid climatic zone. This zone is characterised by a mean precipitation rate of 660mm per annum, although significant variations from this exist across the region. Annual precipitation increases from northwest to southeast, being around 500mm in the northwest and around 800mm near Mt Gambier in the southeast (Floegel, 1972). Most of the dolomite precipitation

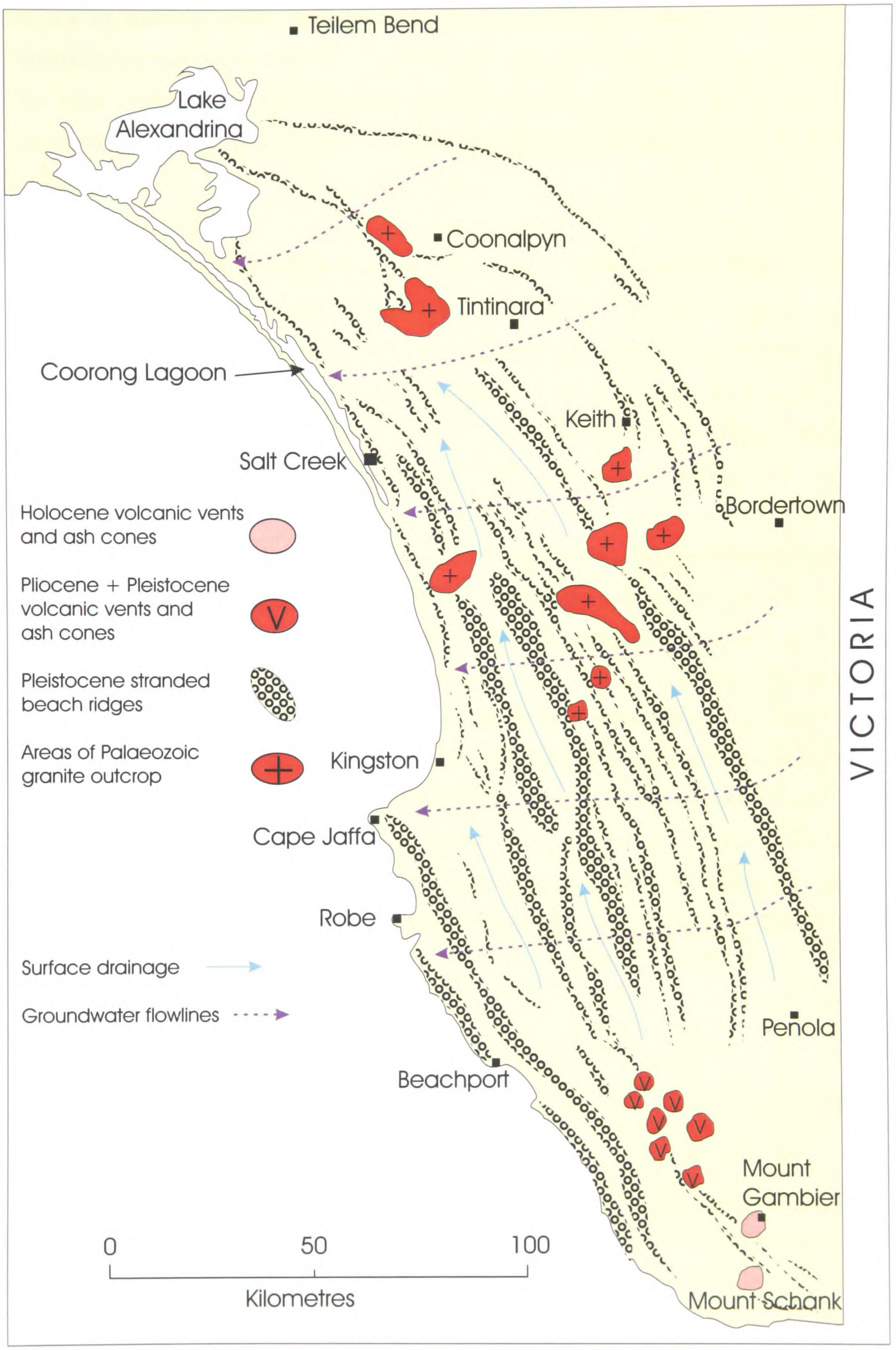


Figure 1.10. Physiography and hydrological regime of S.E. South Australia. (Adapted from Ludbrook, 1980 and Von der Borch, 1976).

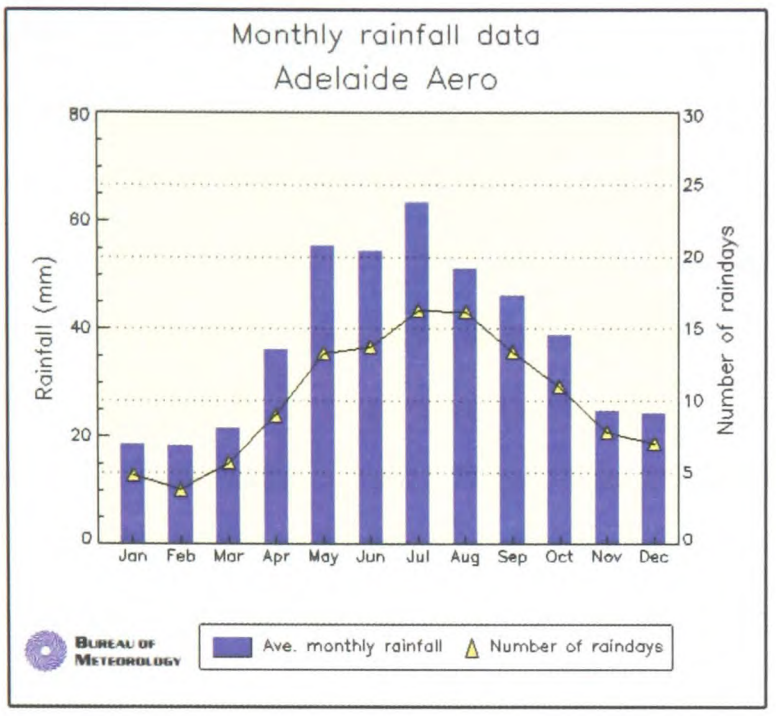
occurs in lakes in which the rainfall lies between 500 and 700mm per annum. Primary dolomite has not been observed in lakes where rainfall exceeds 700mm per annum, nor in the most arid areas where magnesite is observed (Von der Borch, 1976). In some years, precipitation at Salt Creek (my field base) has been as low as 400mm per annum (Warren, 1990).

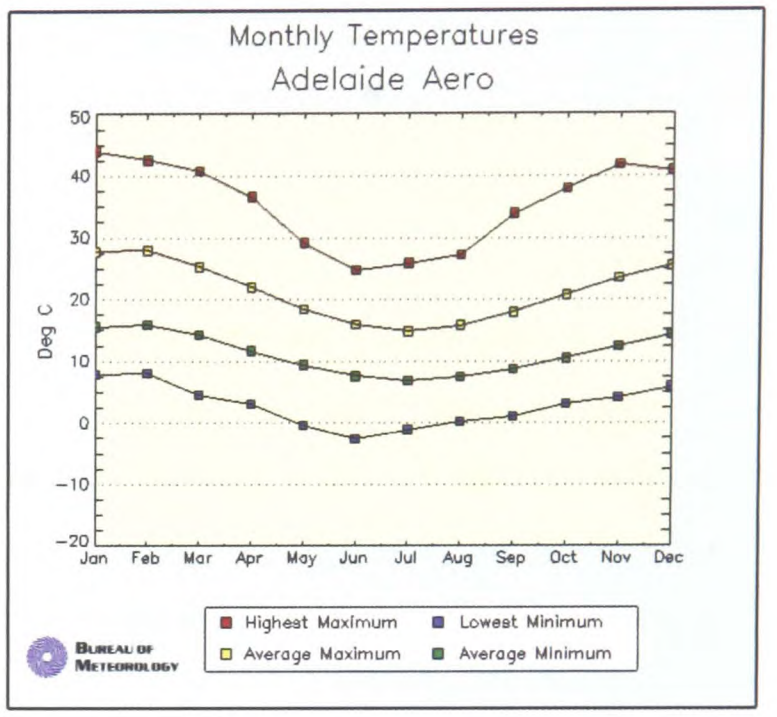
The mean annual temperature for the region is 13.5°C (see Fig. 1.11), although there are extremes ranging from 0°C during winter frosts to over 35°C on hot summer days (Von der Borch, 1976). During my stay in the Coorong (October - December), midday temperatures varied between about 18°C, when the wind direction was off the ocean, to 40°C, when the wind direction was northerly, coming from the desert interior. Temperatures often dropped to single figures during the night due to lack of cloud cover.

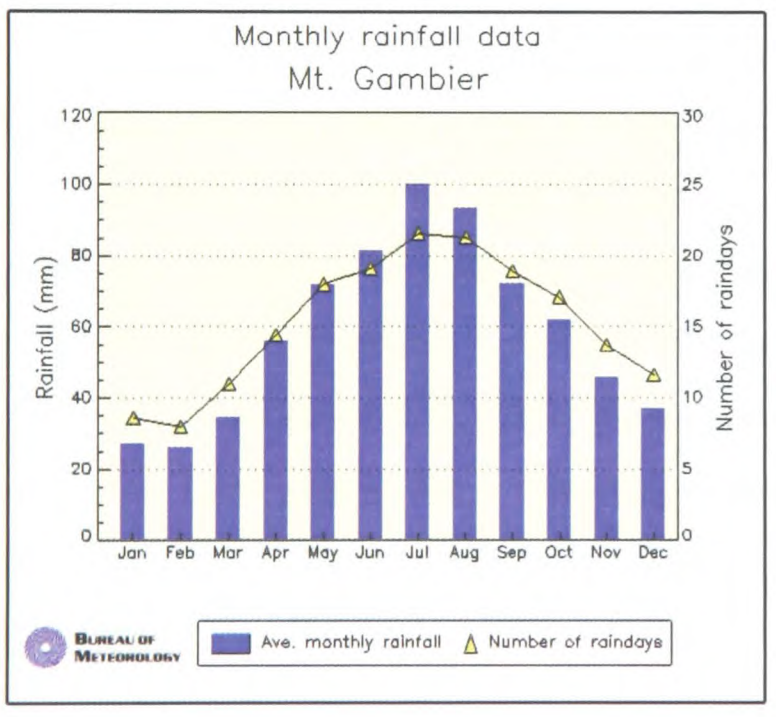
The month of July receives both the rain maximum and temperature minimum of 85mm and 9°C respectively, whilst February records the rain minimum and temperature maximum of 25mm and 18°C respectively (Fig. 1.11). Both the maximum and minimum evaporation rates occur a month earlier, i.e. in June and January (Von der Borch, 1976). My visit coincided with the transition from semihumid to semiarid intervals, when lakes were drying out rapidly. This was the time when maximal mineral precipitation was predicted to occur, in relation to the increase in activity of sulphate reducing bacteria (Wright, 1999) as discussed in Chapters 3 and 6. By the end of the various field seasons many of the lakes were completely desiccated. Although water temperatures are quoted as varying between 10 and 28°C (Rosen *et al.*, 1988), the water temperatures often reached 30°C and above during my field work.

1.6. REGIONAL HYDROLOGY

Much of the coastal plain spans a zone of shallow and partially outcropping lower Paleozoic basement rocks known as the Padthaway Ridge (Fig. 1.8) (Von der Borch, 1976). Two major aquifers underlie the main zone of primary dolomite formation; an upper unconfined aquifer made up of late Tertiary and Quaternary bryozoan limestones and calcareous sands, and a deeper, confined aquifer comprised of Eocene siliceous sand of the Knight Group







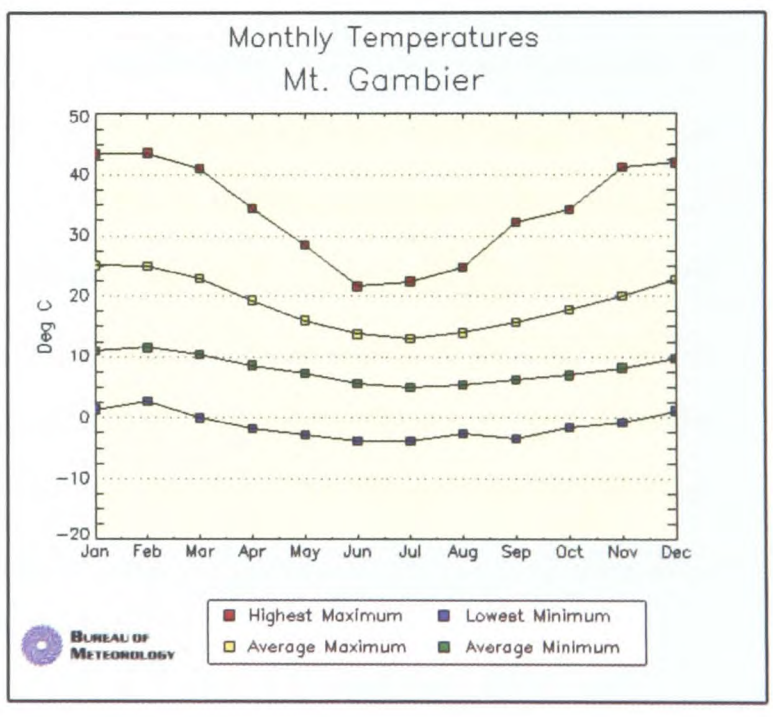


Figure 1.11. Average monthly rainfall and temperature data for two stations in South Australia, Adelaide Airport (34.96°South, 138.53°East) and Mt Gambier (37.75°South, 140.79°East), showing average rainfall maximum and temperature minimum in the month of July, and average rainfall minimum and temperature maximum in the months January/February.

Note: The Coorong Region lies approximately midway between these two weather stations at 36°South,139°East. (Australian Bureau of Meteorology, 2001)

(Floegel, 1972). These two units are separated by an aquiclude comprising the Buccleuch Group, dominantly made up of clays and lignites (O'Driscoll, 1960).

The upper unconfined aquifer is fed not only by local rainfall recharge but also by significant infiltration from freshwater swamps. The source of the latter coincides with the region of greatest rainfall in the area and also with the western margin of a region of basic lavas and ashes around Mt Gambier (O'Driscoll, 1960). Flow direction of these swamps is towards the lower rainfall area in which prolific dolomite formation occurs (Fig. 1.10). When swamp water seeps into the unconfined aquifer, a coastward flow is initiated down the hydraulic gradient. This flow rate was estimated by O'Driscoll to be fairly low (c.10mm per day) and even less near the coast where the gradient is almost flat. The water of the underlying confined aquifer originates in a widespread freshwater swamp recharge area just north of Mt Gambier and has been shown to leak through the aquiclude into the upper aquifer (Floegel, 1972).

Groundwater within the unconfined aquifer approaches the coastal discharge zone as freshwater lenses; as they reach the coastal zone they must override denser interstitial waters of oceanic and lagoonal origin (Von der Borch *et al.*, 1975). A diffuse and complex zone of mixing of continental and marine waters therefore results along the coast in the vicinity of the lakes in which primary modern dolomite is forming. This is similar to the model proposed by Hanshaw *et al.* (1971) for secondary dolomitization of limestones in the Florida region, by Land (1973) for a similar process in Jamaica and by Badiozamani (1973) for dolomitization of Ordovician carbonates in Wisconsin (see Section 1.2.3). One important difference in the Coorong, however, is that dolomite is forming by primary precipitation.

The distal ephemeral lakes themselves are filled during winter months by groundwater seepage so that they become a surface water body of the unconfined groundwater aquifer (Von der Borch *et al.*, 1975). Groundwater levels fall during the arid summer months and the distal lakes may then become perched above the water, table with their waters subsequently being concentrated by evaporation and replenished by direct rainfall and runoff.

1.7. COORONG DOLOMITE

The dolomite found in several ephemeral lakes in the Coorong Region is fine grained (<1μm to ~20μm) and often spherulitic when young, ageing to more rhombic forms (see Chapter 3). It forms layers of structureless aphanitic micrite with no associated saline or sulphate evaporite minerals. The meagre biota associated with the dolomite is of lacustrine rather than marine character. Carbonate phases include ordered dolomite plus a Ca:Mg carbonate identical to dolomite but with weak ordering reflections, with stoichiometries ranging from Ca-rich through Ca_{50}:Mg_{50} to Mg-rich. Radiocarbon studies (Von der Borch *et al.*, 1964) show the age of surface deposits to be 300 ± 250 years, increasing to 2030 ± 250 years at 33cm depth. Its primary origin is not questioned (Skinner, 1963; Von der Borch, 1965a) and it shows no evidence for replacement of a pre-existing carbonate phase. It is difficult, therefore, to attribute this dolomite to the various replacive mechanisms discussed in Section 1.2.3.

1.7.1. Coorong dolomite – previous interpretations

Coorong dolomite has been studied by a number of authors (Alderman and Skinner, 1957; Skinner, 1963; Von der Borch *et al.*, 1964; Von der Borch, 1965a+b, 1976; Alderman, 1965; Von der Borch *et al.*, 1975; Von der Borch and Jones, 1976; Vonder Borch and Lock, 1979; Botz and Von der Borch, 1984; Rosen *et al.*, 1988, 1989; Warren, 1990). The majority of interpretations have favoured an evaporative mechanism of formation although a mixing zone origin has also been proposed. A satisfactory mechanism has, however, remained elusive.

The first description of dolomitic sediments in this area comes from Kingston Lake, a little to the south of the Coorong (Alderman and Skinner, 1957). They attributed the precipitation of dolomite to elevated pH (up to 9.2) in saline waters as a result of plant growth, with *Ruppia maritima* (a source of Mg^{2+}) being the dominant species. They reported that precipitation occurred in early summer when plant growth was most vigorous and also noted that the precipitate was most plentiful where plant masses were most plentiful. This was reinforced by more work from Skinner (1963) where a similar association was noted in a second lagoon where the precipitate was a very fine grained (1-20μm) poorly ordered dolomite, precipitating directly from shallow lakewaters with an ionic composition close to

normal seawater. It was also noted that each lake acted as a single system and precipitated minerals according to specific conditions prevailing in the lake at that particular time (i.e. the lakes cannot be all lumped together as one when applying a particular model).

Von der Borch (1965a) interpreted the dolomite as forming through a mechanism of extremely slow crystal nucleation and growth, which because of the slow rate, is analogous to early diagenesis before burial. He states that dolomite is favoured by high pH and a high Mg/Ca ratio which are in turn favoured by an increased time of isolation of the lake from the main lagoon.

This hypothesis was expanded upon by Alderman (1965) who suggested that the nature of the calcium and magnesium carbonates, which form the sediments in the Coorong and its associated isolated lakes, was largely controlled by the Mg:Ca ratio in the parent water; the suite of minerals thus formed would be: aragonite then magnesian calcite, calcian dolomite, ordered dolomite and finally magnesite.

A ten year gap in the literature followed before further work. Von der Borch *et al.* (1975) and Von der Borch (1976) then favoured the formation of dolomite by evaporation of groundwaters on the landward side of a seawater-groundwater mixing zone, citing as evidence, dolomite forming as much as 90 km inland from the coast and dolomite found beneath many of the inland interdune flats. Von der Borch proposed that aragonite, Mg-calcite and poorly ordered dolomite were formed by a marine or a mixed sea-water-ground-water reservoir, whereas the ordered dolomite formed from ions provided by groundwater. He thereby explained the succession of minerals observed in an isolated lake core (basal aragonite and Mg-calcite, approximately 6500 yrs old, passing upwards into ephemeral lake facies with poorly ordered then ordered dolomite) as the result of seaward migration of the seawater-groundwater mixing zone. This hypothesis envisaged that magnesium and bicarbonate-rich groundwaters from the unconfined regional aquifer, discharge into the Coorong region and are then subjected to intense evaporation and associated chemical modification so that dolomite can form anywhere where such groundwaters are emerging.

Major problems have since become evident with this hypothesis. Firstly, it does not easily explain why dolomite is so rare elsewhere in the world at present. This anomaly has been somewhat resolved by Von der Borch through the unusual combination of an

abundant, renewable source of magnesium (basic volcanics; see next section) supplying the seaward flowing groundwaters, together with an active groundwater regime and a climate which varies from humid to semiarid. Even so, this does not explain why lakes that are only 100m apart, in the same hydrological setting, exhibit vastly different mineralogies. Nor does it explain why evaporation of the ephemeral Coorong lakewaters in the laboratory result not in dolomite precipitation but in aragonite. Von der Borch suggests that, after emergence and evaporation, these groundwaters are subjected to "as yet undefined conditions which result in dolomite formation". The realisation that evaporation alone is not enough was evident even in the early stages of his work. Evaporite minerals, which would necessarily precipitate after dolomite under these conditions are not seen in sediment cores. This absence is explained by Von der Borch *et al.* (1975) by blowing away by frequent strong winds, by recycling through later runoff and by flushing out of the system by groundwaters.

The spherulitic nature of much of the Coorong Dolomite was first noted by Von der Borch and Jones (1976) but physico-chemical controls were invoked, involving the contraction of a Ca-Mg carbonate gel and the flocculation of spherules with the aid of silica prior to aggregation and settling, which was intermittently disturbed by agitation and wetting/drying cycles. This morphological form gave further evidence that the dolomite was a direct precipitate rather than a dolomitization product from a pre-existing carbonate phase.

Rosen *et al.* (1988, 1989) used the somewhat unusual crystal chemistry (4 ± 2 mole percent excess Mg, together with expanded lattice in *c* direction and contraction in *a* direction) of the upper dolomite from Pellet Lake to propose that it was formed by rapid precipitation from solutions with greatly elevated Mg^{2+}/Ca^{2+} ratios. This was reinforced with TEM studies showing heterogenous microstructure. Carbon and oxygen isotopes show three upwardly negative cycles which were interpreted as the influence of rainwater dilution of the brine at various times.

1.7.2. Source of ions for dolomite precipitation in the Coorong

The source of ions for dolomite formation in this area is still debatable. The ocean must be considered the most likely source since the prevailing wind is off the ocean and the ephemeral lakes are well within the distance that sea spray could travel. Skinner (1963) states that a very high proportion of the dissolved salts in the lakes are believed to come from the

nearby sea as windblown cyclic salts, and to be effectively collected by runoff. Calcium, magnesium and bicarbonate ions may be made available through dissolution of skeletal components (coralline algae and echinoids which are metastable Mg-calcite) from within the shallow aquifer. Karst topography may support this. A large supply of calcium would be available from the surrounding carbonate dunes, leached out by runoff after heavy rainfall. However, calcium levels are low throughout the lake cycle and constant throughout the study period so that local leaching appears to be negligible.

A significant source of magnesium ions may come from the leaching of Tertiary and Quaternary basic volcanic rocks (Von der Borch, 1976; Von der Borch *et al.*, 1975). Ash layers are intercalated with coastal-plain sediments over a wide area in the east of the province where much of the northwest flowing surface water originates (Fig. 1.10). This ash has lost 60-80% of its original Ca^{2+}, Mg^{2+} and Na^{+}, this being leached into groundwaters and contributed to runoff waters (Hutton, 1974). Eventually this will recharge the shallow aquifer that provides the groundwater for the dolomitic lakes. Major element chemistry analysis of the groundwaters has not been able to prove whether or not there is a significant volcanic input (O'Driscoll, 1960). Within the lakes themselves, sources of magnesium include cyanobacteria. These are common in the algal mats and stromatolites, and concentrate magnesium (to levels up to four times that of normal seawater) in their sheaths and mucilage by organic complexing (Gebelein & Hoffman, 1973). When degraded, the magnesium is released into the lake or porewaters. *Ruppia* grass and *Samphire* also utilise magnesium in chlorophyll and will likewise release it once desiccated and degraded.

The physico-chemical mechanisms outlined thus far do not provide a satisfactory explanation for the primary precipitation of dolomite in the Coorong Region. The spherular nature of the dolomite precipitate, the association of plant growth and high pH with dolomite precipitation and the necessity for a supply of Mg^{2+} ions have all been recognised by previous workers. They have failed, however, to equate this with a microbial influence. A new approach to dolomite formation in the Coorong is thus required.

1.7.3. Coorong Dolomite – A new approach

An organogenic model accounting for the primary precipitation of dolomite in the distal ephemeral lakes of the Coorong Region is tested here, moving away from physico-chemical

models and instead focusing on the role of biological processes, in particular the role of sulphate-reducing bacteria (SRB). Can SRB modify chemical conditions to such an extent that they become favourable for dolomite formation?

Sulphate-reducing bacteria use sulphate as a terminal electron acceptor during anaerobic oxidation of organic compounds (Berner, 1980) (Eq. 1.4).

$$2\,CH_2O + MgSO_4^0 \longrightarrow H_2S + 2HCO_3^- + Mg^{2+} \qquad (1.4)$$

As noted in Section 1.2.2, it is the ability of sulphate ions to complex with magnesium ions and form neutral ion pairs and thus effectively remove Mg^{2+} from the ionic pool which makes sulphate an inhibitor to dolomite formation. Bacterial sulphate reduction (Eq. 1.4) results in a net release of free magnesium ions. When the SO_4^{2-} ions are used as an electron acceptor by SRB, they may also utilise the accompanying Mg^{2+} ions to aid various physiological functions within their cells (Stanier *et al.*, 1986). Even so, excess Mg^{2+} ions are likely to be released, together with other by-products of sulphate reduction, into the surrounding micro-environment. Here they are suddenly freed from their complex and are able to combine with Ca^{2+} and CO_3^{2-} to form dolomite if other kinetic inhibitors are also removed.

The low activity of CO_3^{2-} has also been demonstrated to be a kinetic inhibitor to dolomite formation (e.g. Garrels & Thompson, 1962); the activity of this ion can be increased during BSR. The microbes consume cyanobacterial and other organic matter to help support their metabolism, thus liberating ammonia from proteins and amino acids (Berner, 1980). The reaction of ammonia with water (Eq. 1.5) results in elevated pH and an excess of OH^- ions; bicarbonate must then buffer the solution (Eq. 1.6) leading to increased carbonate ion concentrations and activities (Slaughter & Hill, 1991).

$$NH_3 + H_2O \longrightarrow NH_4^+ + OH^- \qquad (1.5)$$

$$OH^- + HCO_3^- \longrightarrow H_2O + CO_3^{2-} \qquad (1.6)$$

In the hypothesis to be tested here, it is proposed that the action of sulphate-reducing bacteria in an organic rich environment can remove the kinetic inhibitors that prevent dolomite precipitation under normal temperatures and pressures.

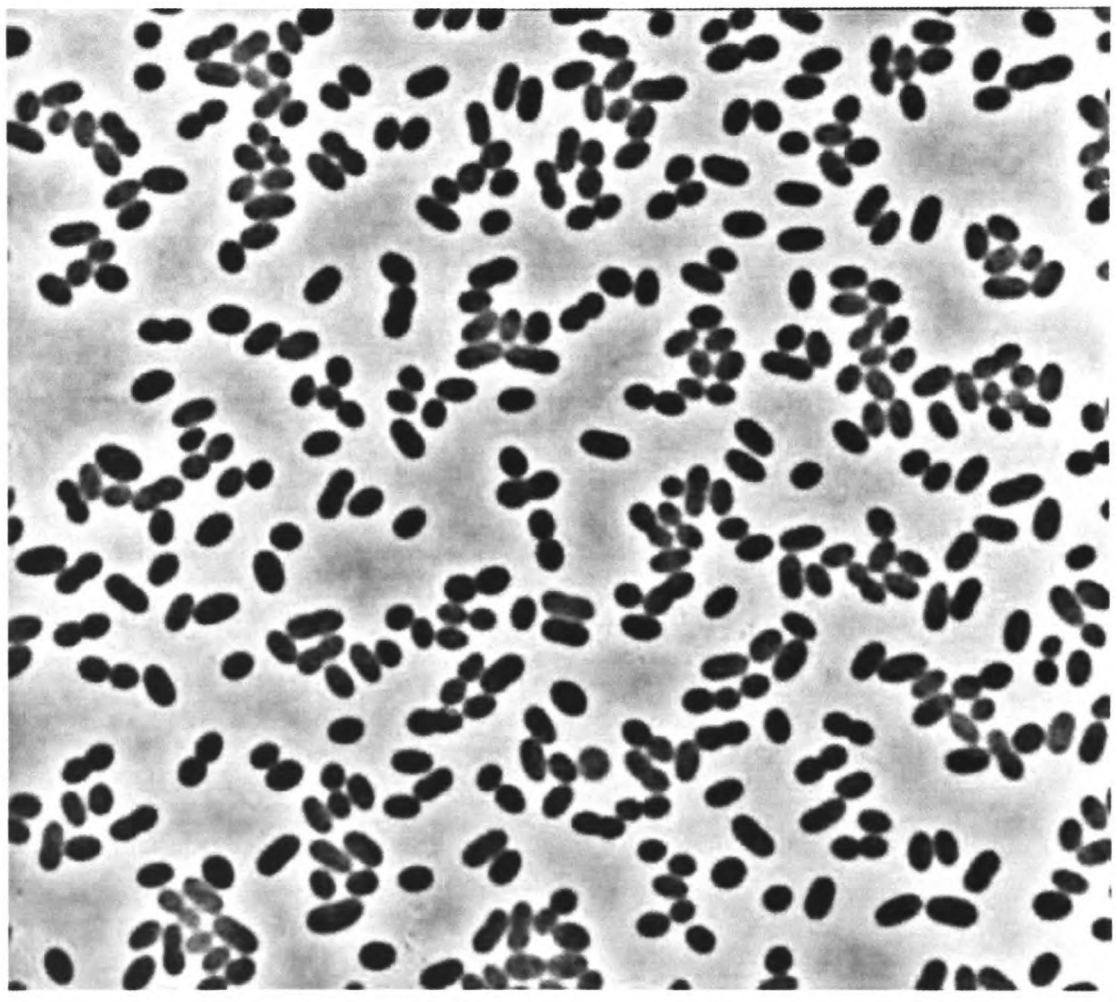
This project tests this model using a variety of approaches including:-

- Sampling and chemical analysis of lake and porewaters in the study area.
- Culturing of bacteria from cores of Coorong lake sediments followed by analysis and identification.
- Laboratory experiments using cultured Coorong bacteria to precipitate mineral phases.
- Isotope studies to examine the fractionation effects of sulphate reduction.

1.8. SUMMARY

- Thermodynamically dolomite should precipitate from normal seawater; kinetic inhibitors prevent this from occurring.
- Inorganic models for dolomite formation do not adequately explain how these kinetic inhibitors are overcome, nor can physico-chemical experiments precipitate dolomite in the laboratory.
- The distal ephemeral lakes of the Coorong Region of South Australia, one of the few locations where dolomite is precipitating at the present day were chosen as the study area for this project.
- Coorong dolomite is primary, occurring as sub-micron spherular grains exhibiting no evidence of replacing a pre-existing carbonate phase.
- Whilst the climate, hydrology and geological setting of the Coorong lakes appear to favour dolomite formation, not all of the study lakes precipitate dolomite. Other factors must be investigated in this study, not least kinetics.
- This study adopts a new approach for dolomite precipitation in the Coorong, focusing on the role of biological processes, in particular the role of sulphate-reducing bacteria.
- The multi-disciplinary investigation encompasses Sedimentological Studies (Chapter 3), Geochemical Analysis (Chapter 4), Stable Isotope Studies (Chapter 5), Microbiological Studies and Bacterial Experiments (Chapter 6).

CHAPTER 2



***Desulfobacterium autotrophicum* – a common sulphate reducing bacteria.**

Chapter 2

The sulphate-reducing bacteria

2.1. INTRODUCTION

The sulphate-reducing bacteria (SRB) are a phylogenetically diverse group of micro-organisms first discovered by the Dutch microbiologist, M.W. Beijerinck in 1895. At present around 30 genera have been identified, the most widespread and important being *Desulfovibrio* and *Desulfotomaculum* (Castro *et al.*, 2000). The SRB are mostly strictly anaerobic heterotrophs, their growth being inhibited by the presence of oxygen. Recently, however, it has been shown that sulphate reduction can take place under aerobic conditions in cyanobacterial mats (Frund & Cohen, 1992) and that some sulphate reducers may be aerobic respirers under micro-aerobic conditions (Dilling & Cypionka, 1990; Canfield & Des Marais, 1991). Even strictly anaerobic SRB can lay dormant in the presence of oxygen (Postgate, 1984). SRB are an ancient group of organisms dating back to the Neoarchaean although the exact date of their emergence is widely debated (see Section 2.5). Mesophilic species have an optimum temperature range of around 25-40°C and are found in large numbers in anoxic sediments, as well as in bottom waters of freshwater, marine and hypersaline aquatic environments. Thermophilic species prosper at 60-70°C, occurring in hot springs and submarine hydrothermal vents. Hyperthermophilic species have recently been discovered by Jorgensen *et al.* (1992), that reduce sulphate most efficiently at 103-106°C. Barophilic species have also been identified e.g. *Desulfovibrio profundus*, (Bale *et al.*, 1997) active at depths of at least 500m in marine sediments and, experimentally, still functioning at pressures of up to 400atm. Hence, SRB are broadly distributed over the earth, playing an important part in the biosphere owing to their potential for numerous geochemical, biological and environmental interactions.

2.2. MORPHOLOGY AND CLASSIFICATION

The sulphate-reducing bacteria are morphologically diverse single celled prokaryotes. Apart from their ability to reduce sulphate, the different subgroups of SRB appear not to be biologically closely related. Their basic cell structure is shown in Figure 2.1 and resembles that of many other bacterial forms.

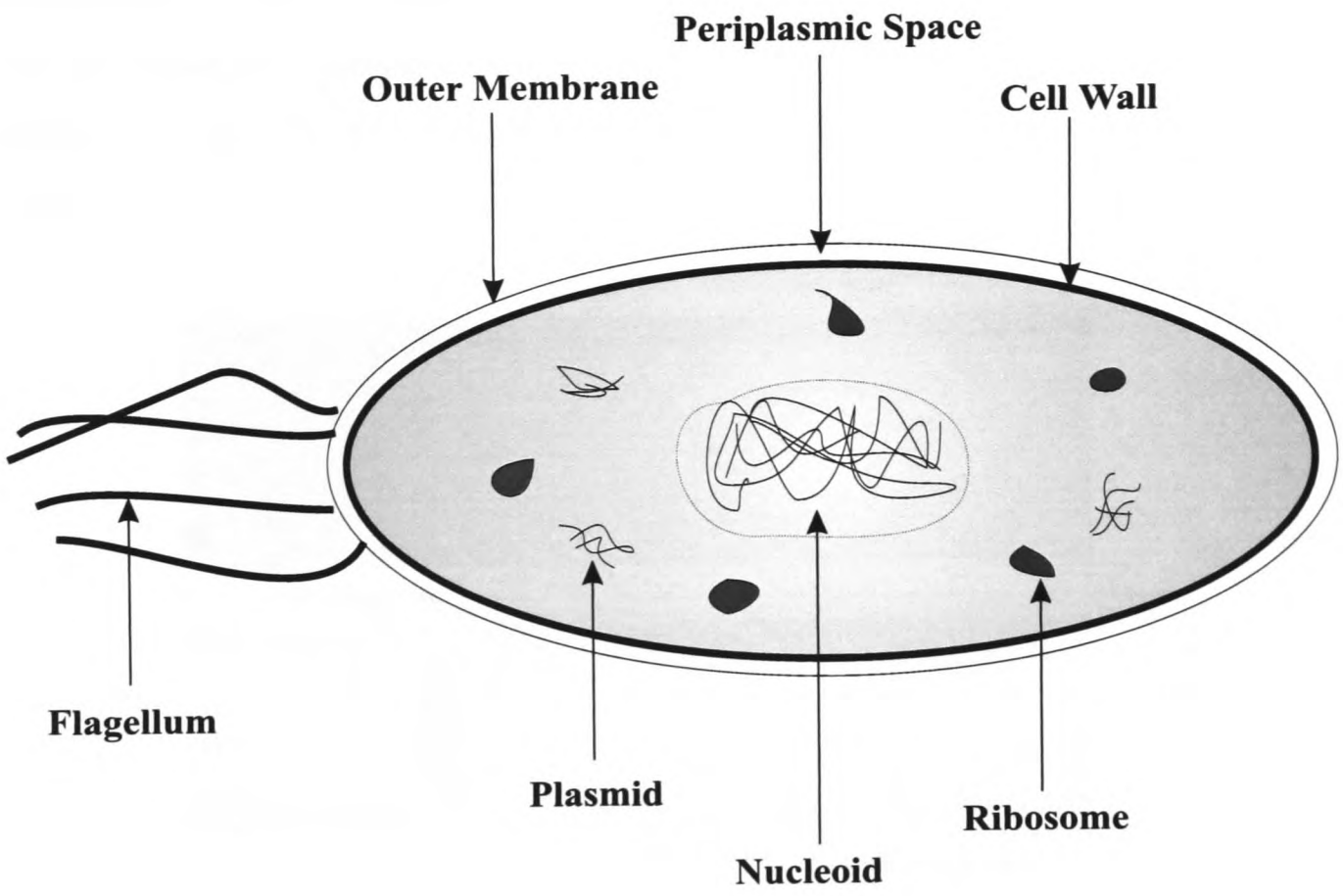


Figure 2.1. Basic bacterial cell structure (modified from Singleton, 1997)

The vast majority of SRB (all genera except *Desulfotomaculum* and *Desulfosporosinus*; Castro *et al.*, 2000) belong to that branch of bacteria that stain negative when the 'Gram Stain' is applied to them. The staining procedure, developed by the Dane, Hans Christian Gram, involves the application of a solution of iodine to cells already stained with crystal violet, producing purple coloured iodine-dye complexes in the cytoplasm of the bacteria. The cells are then treated with a decolourising agent (e.g. 95% ethanol). The difference between Gram-positive bacteria and Gram-negative bacteria is a function of the permeability of their cell wall to the iodine complexes after treatment with the decolourising agent. The cell walls of Gram-positive bacteria have an affinity for the complexes and retain the purple stain, whereas the Gram-negative bacteria are decolourised. Gram-negative bacteria can then be visualised using a pink counter stain of safranin. The cell wall of a Gram-positive bacterium

visualised using a pink counter stain of safranin. The cell wall of a Gram-positive bacterium (Figure 2.2a) consists of a thick layer (20-80nm) of peptidoglycan (a mixture of sugars and amino acids) occurring as a multi-layered mesh linked together by teichoic and muramic acids, surrounding the cell membrane. The cell wall of Gram-negative bacterium (Figure 2.2b) is much thinner (10nm) but also much more complicated. The cell membrane itself is surrounded by a thin layer of peptidoglycan which, in turn, is surrounded by a thin outer membrane composed of lipids, proteins and lipopolysaccharide (LPS) which reaches out into the environment. This outer membrane has porins (a type of protein) which allow most small hydrophilic molecules passage into the cell. The region between the cell membrane and the peptidoglycan, termed the periplasmic space, contains enzymes and nutrient-carrier proteins.

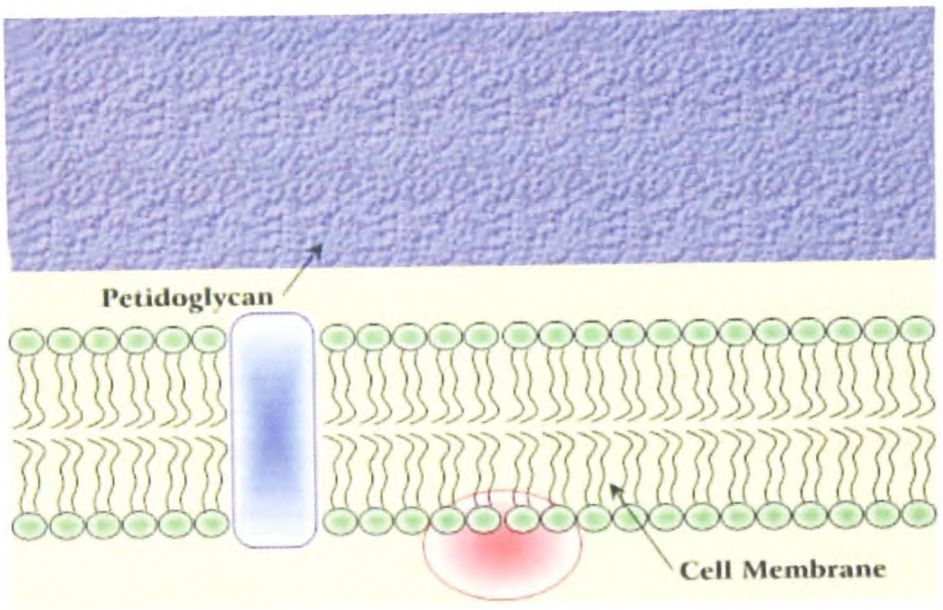


Figure 2.2a. Cell wall structure in Gram-positive bacteria (after Paustian, 2002).

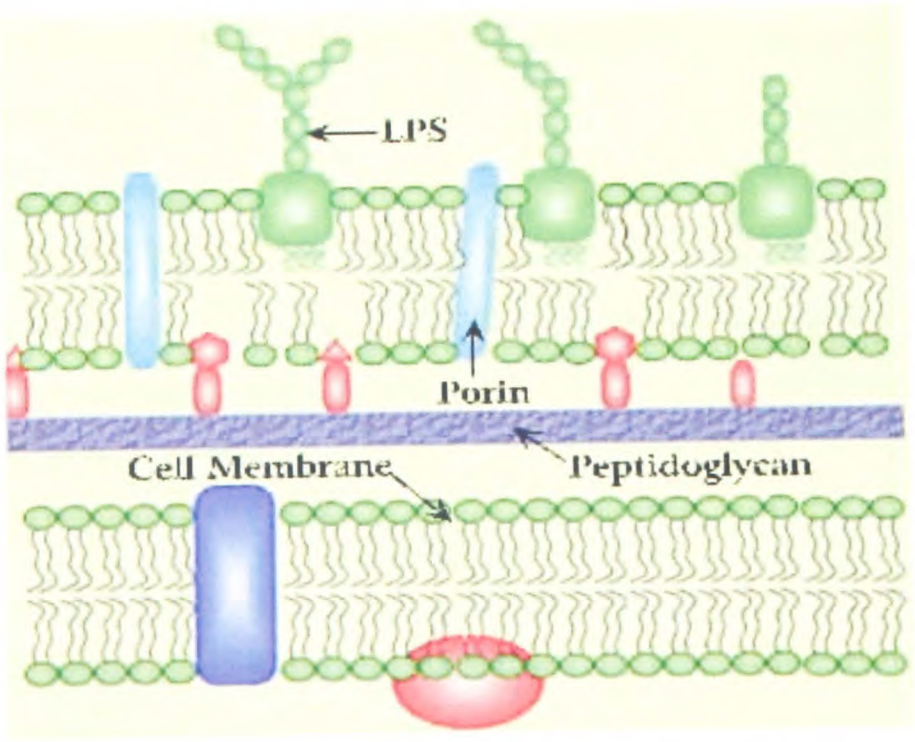


Figure 2.2b. Cell wall structure in Gram-negative bacteria (after Paustian, 2002).

Unlike eukaryotes, bacteria lack a membrane-bound nucleus. Instead their DNA forms an irregular tangle known as the nucleoid. In addition they have plasmids, small loops of DNA within the cytoplasm, that can be easily transmitted from one cell to another. This ability to trade genes allows the bacteria to be extremely adaptable.

SRB cells may be spherical, ovoid, rod-shaped, spiral or vibrioid shaped, occurring singularly, in pairs or in aggregates. Cells range in size from 0.4-3.0μm in diameter, with multicellular filamentous forms also occurring. Cells may be non-motile or motile, the latter being due to one or more flagella, whilst filamentous forms exhibit gliding motility. Because of this diverse morphology, classification was traditionally based not only on morphology but also on the type of substrate required for growth and on spore forming ability. The taxonomic classification used prior to recent advances in 16S rRNA gene sequencing was based upon Bergey's Manual of Determinative Bacteriology (9 editions up to 1994, edited by Holt *et al.*) which divides SRB into three subgroups.

Subgroup 1. Spore forming. *Desulfotomaculum* and *Desulfosporosinus* are the only genera in this subgroup. Spores are very resistant to adverse environmental factors, and once these adverse conditions are removed, the spores germinate to create a new population. Some species oxidise organic substrates completely to CO_2, whilst others are incomplete oxidisers, ceasing at acetate.

Subgroup 2. Non-spore-forming. SRB with no citric acid cycle. These can only oxidise organic substrates incompletely to acetate. *Desulfovibrio* is one such genus, using mainly H_2 and lactate as substrates.

Subgroup 3. Non-spore-forming. SRB with a citric acid cycle. These oxidise organic substrates completely to CO_2. *Desulfobacter* is one such genus, using a wide array of substrates such as acetate, formate and the higher monocarboxylic acids, fumarate and succinate, as well as lactate and H_2.

Genera within subgroups, and indeed species within genera, are then classified according to cell shape, cell size, motility and specific substrate utilization. This type of taxonomic classification is difficult due to the scarcity of defining characteristics and the problems associated with obtaining pure cultures from suitable media.

2.2.1. 16S rRNA Sequencing

With the advent of DNA nano-technology, 16S rRNA sequence similarity is now the generally accepted way to measure phylogenetic relationships between the different bacterial genera and, as such, new genera and species are constantly being discovered. It is probable that only a very small percentage of SRB have so far been characterised. Figures 2.3a-c show phylogenetic trees of the SRB constructed by Castro *et al.* (2000) using sequences obtained directly from GenBank (http://www.ncbi.nlm.nih.gov). This review compiled data obtained from several laboratories and divides the SRB into four groups: Gram-negative mesophilic SRB; Gram-positive spore forming SRB; thermophilic bacterial SRB; and thermophilic archaeal SRB. Only the first two groups may be encountered in this study as temperatures required for thermophilic SRB to prosper are not observed in the Coorong region. The majority of genera fall into the Gram-negative mesophilic SRB which is subdivided into two families; the Desulfovibrionaceae, containing the genera *Desulfovibrio* and *Desulfomicrobium*; and the Desulfobacteriaceae containing a broad range of up to 19 genera (Castro *et al.*, 2000).

Some genera reveal more disparity than others. For example, Devereux *et al.* (1989) showed that *Desulfobacter* has a minimum of 95% similarity between species, whereas species within the genus *Desulfovibrio,* such as *D. vulgaris* and *D. africanus*, only share 87% similarity. In addition, DNA within the *Desulfovibrio* genus shows widely different GC* mole percentages (49-66%) (Devereux *et al.*, 1990). This disparity can be seen on the phylogenetic tree of Devereux *et al.* (Fig. 1, 1989) where a species such as *Desulfovibrio baarsi* plots a long distance away from other *Desulfovibrio* species. This may point to the fact that the taxonomy of some SRB is in need of revision. The phylogenetic trees given in Figures 2.3a-c are by no means comprehensive with new species identification and reclassification progressing as we speak. It is, however, the most comprehensive tree found in current accessible literature and it does show the close association between SRB and other bacterial groups such as *Bacillus* and *Clostridium.* Indeed, the spore forming *Desulfotomaculum* group clusters with the *Clostridium* branch of the Gram-positive eubacteria, showing a closer relationship to these than to the other SRB. For a description of the bacteria identified from the Coorong study area, see Section 6.6 and Appendix 6.

* GC% = (guanine + cystosine) / (guanine + cystosine + adenine + thymine)

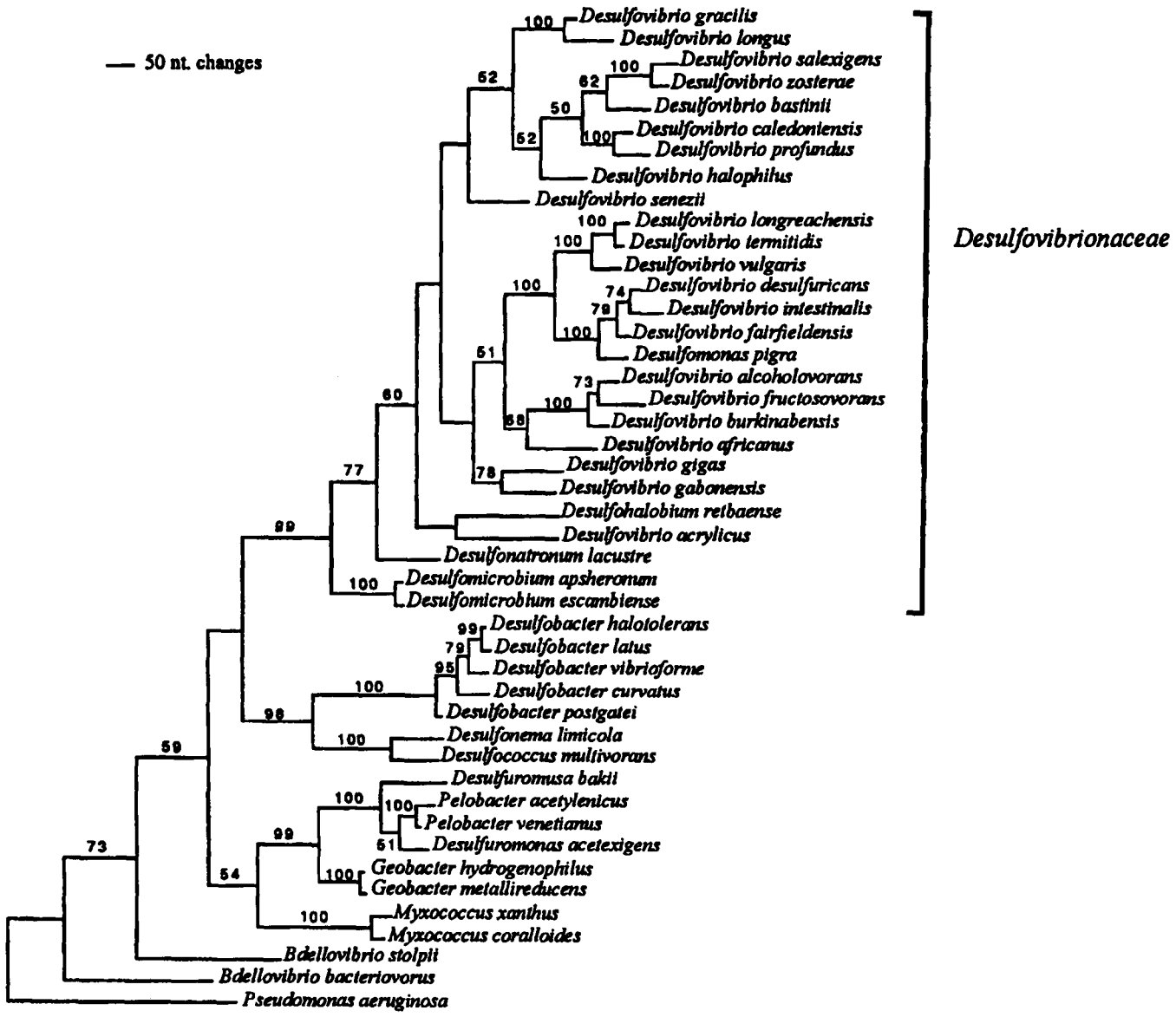


Figure 2.3a. Phylogenetic tree for the Gram-negative mesophilic SRB, with emphasis on the family Desulfovibrionaceae (Castro *et al.*, 2000).

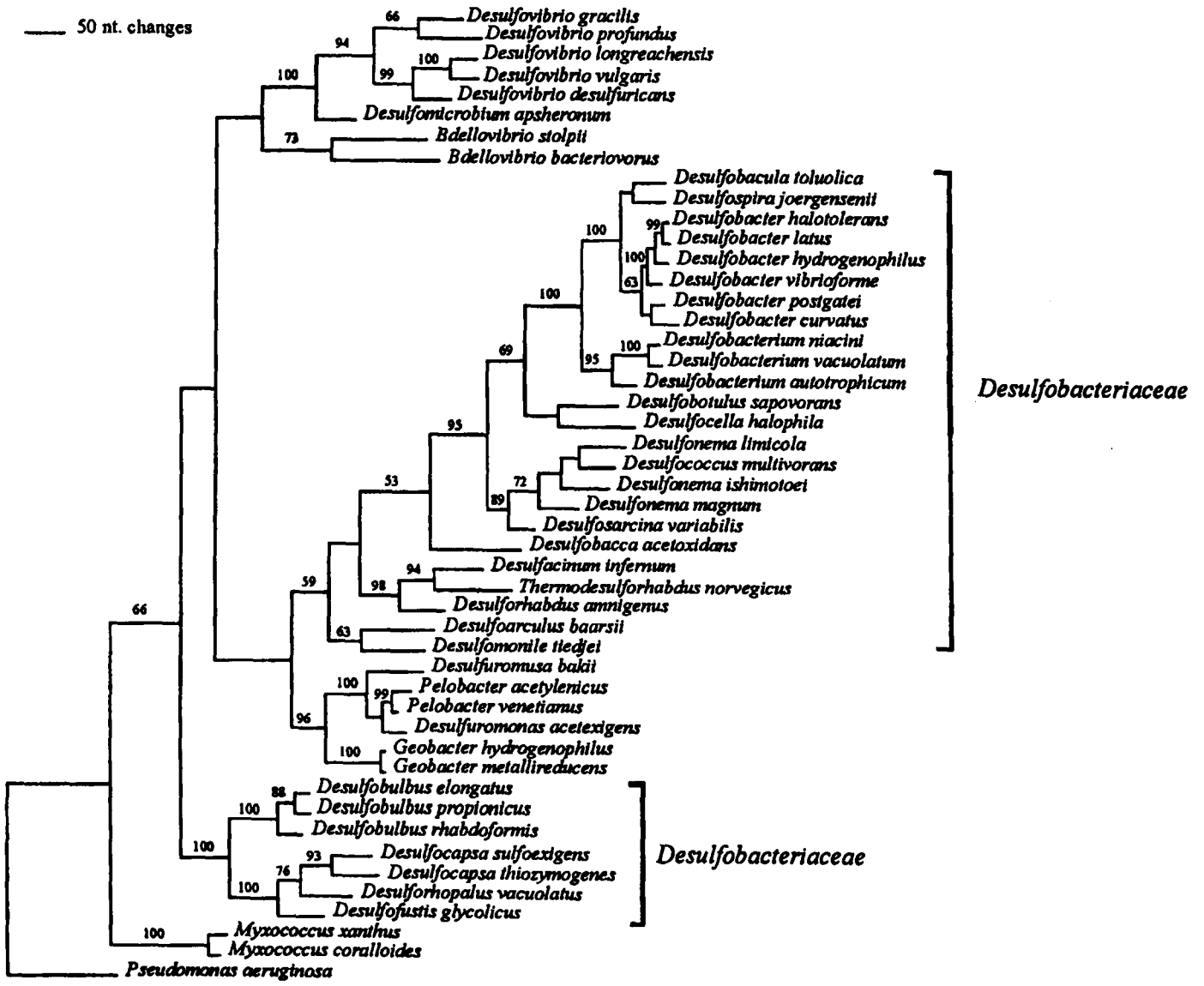


Figure 2.3b. Phylogenetic tree for the Gram-negative mesophilic SRB, with emphasis on the family Desulfobacteriaceae (Castro *et al.*, 2000).

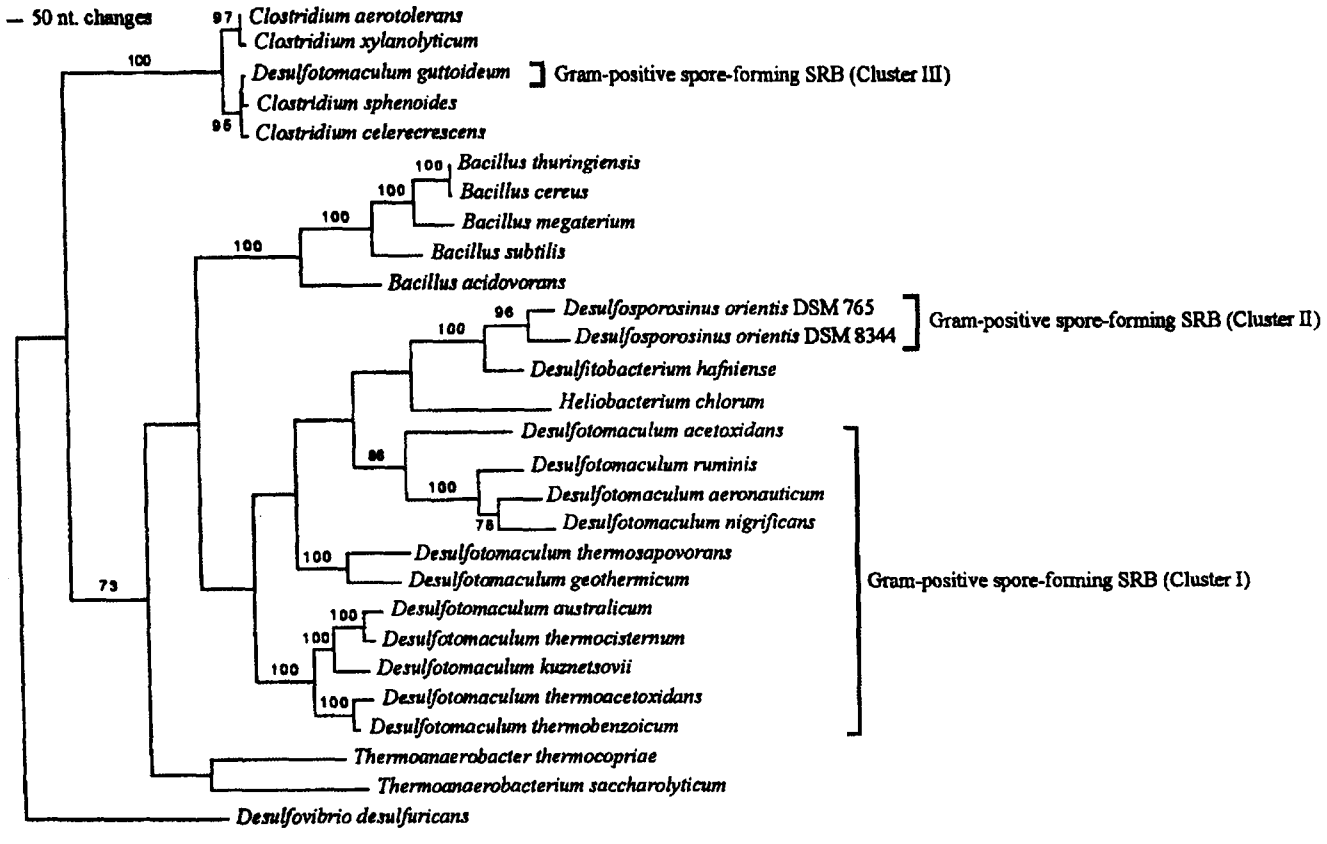


Figure 2.3c. Phylogenetic tree for the genus *Desulfotomaculum* within the cluster of low G+C content Gram-positive bacteria (Castro *et al.*, 2000).

2.3. DISSIMILATORY SULPHATE REDUCTION

Sulphur compounds are widespread and the sulphur atom has probably always been an essential component of the biosphere. Today, sulphur exists within the surface layer of the earth in a predominantly oxidised form, such as sulphates in soils, rocks, rivers and the sea, and as sulphur oxides in the atmosphere. For sulphur to be used biologically it needs to be reduced, so the biological reduction of sulphate (together with nitrogen fixation and oxygen production) has become one of the major processes on which life depends.

Sulphate reduction takes place in two ways:

a) Assimilatory reduction, whereby plants and some microbes use sulphate as their sole source of sulphur and, in doing so, incorporate it directly into their protein as sulphur containing amino acids.

b) Dissimilatory reduction, whereby the sulphate ion acts as the oxidising agent for the dissimilation of organic matter, as oxygen does in conventional respiration (Postgate, 1984).

The SRB are dissimilatory; they do assimilate a very small proportion of the sulphur, but virtually all of it is released into the external environment. Dissimilatory sulphate reduction is essentially an oxidative type of mechanism, mirroring aerobic respiration, despite the anaerobic nature of the organisms concerned. The metabolic pathway of the organism is seen in Figure 2.4, being divided into two non-oxidative stages (dissimilation of the carbon source (catabolism) and electron transport) followed by the oxidative stage of sulphate reduction.

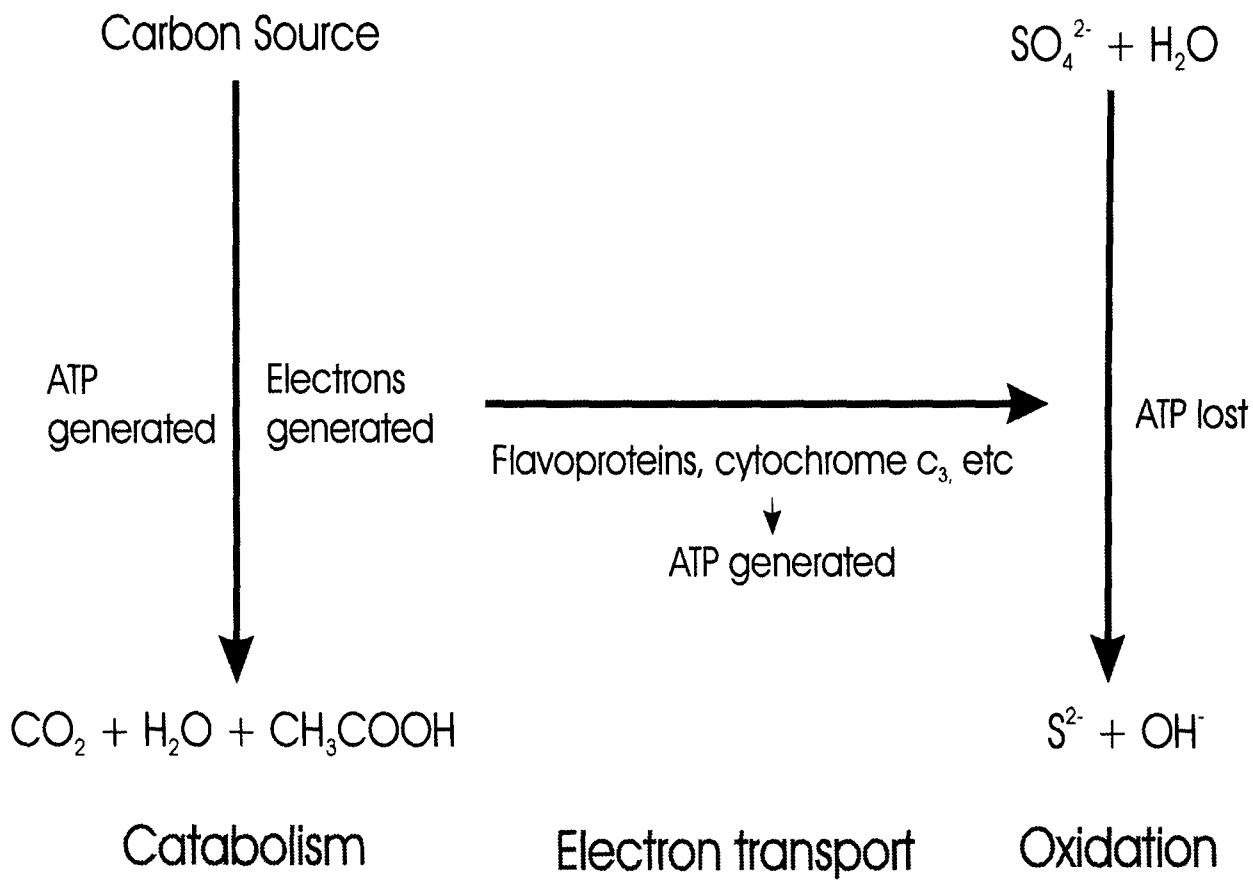


Figure 2.4. A generalised scheme for the metabolic pathway of the incompletely oxidising sulphate-reducing bacteria (Postgate, 1984).

The pathway for the oxidative sulphate reduction stage is shown in Figure 2.5. Sulphate enters the cell and is activated by the ATP-sulfurylase enzyme and thereafter reacts with adenosine triphosphate (ATP) to form adenosine phosphosulphate (APS) and pyrophosphate (PP). This reaction is driven to the right because the pyrophosphate is hydrolysed by the pyrophosphatase enzyme and then removed as inorganic phosphate (P). A further enzyme (APS reductase) then reduces the APS to adenosine monophosphate

2.3.1. The sulphur cycle

The sulphur cycle is a combination of biological and chemical interactions, with sulphur existing in multiple oxidation states spanning eight electrons (Fig. 2.6). Sulphur oxides are released into the atmosphere by the burning of fossil fuels and from volcanic and thermal emissions. The sulphur oxides are then deposited on various surfaces as sulphurous or sulphuric acids, or are washed as sulphate into soils, before being leached into rivers and the sea. Spray from these waters redistributes sulphur about the biosphere. Organic sulphur exists in the most reduced form (-2), the most important compounds being the amino acids cysteine and methionine (Postgate, 1984). Degradation of these compounds yields HS^- which can then be oxidised chemically or biologically, the end product of which is SO_4^{2-}, with intermediate products such as elemental sulphur and thiosulphate.

Sulphate-reducing bacteria are a particularly important part of this cycle, their main role being to bypass assimilatory sulphate reduction and to generate hydrogen sulphide from the large reservoirs of SO_4^{2-} available. In so doing they complement other groups of chemotrophic and phototrophic bacteria which convert sulphide, via elemental sulphur, back to sulphate (Postgate, 1984).

2.4. ENVIRONMENTAL IMPACT OF SRB

Sulphate-reducing bacteria interact with their environment and hence the effects they have on their environment can be used as tools for identifying their presence. Fractionation of sulphur isotopes, lowering of sulphate concentrations, alteration of pH, precipitation of iron sulphide and mineralization of organic matter are all heavily influenced by the activity of SRB.

Natural sulphur consists of four stable isotopes ^{32}S, ^{33}S, ^{34}S, and ^{36}S, of which ^{32}S is the major component (95%) and ^{34}S is the subsidiary (4.2%). During bacterial sulphate reduction the sulphate ions containing ^{32}S react slightly more frequently than those containing ^{34}S, thus the lighter sulphate becomes preferentially converted to sulphide; the sulphide becomes enriched in ^{32}S and the residual sulphate is enriched in ^{34}S.

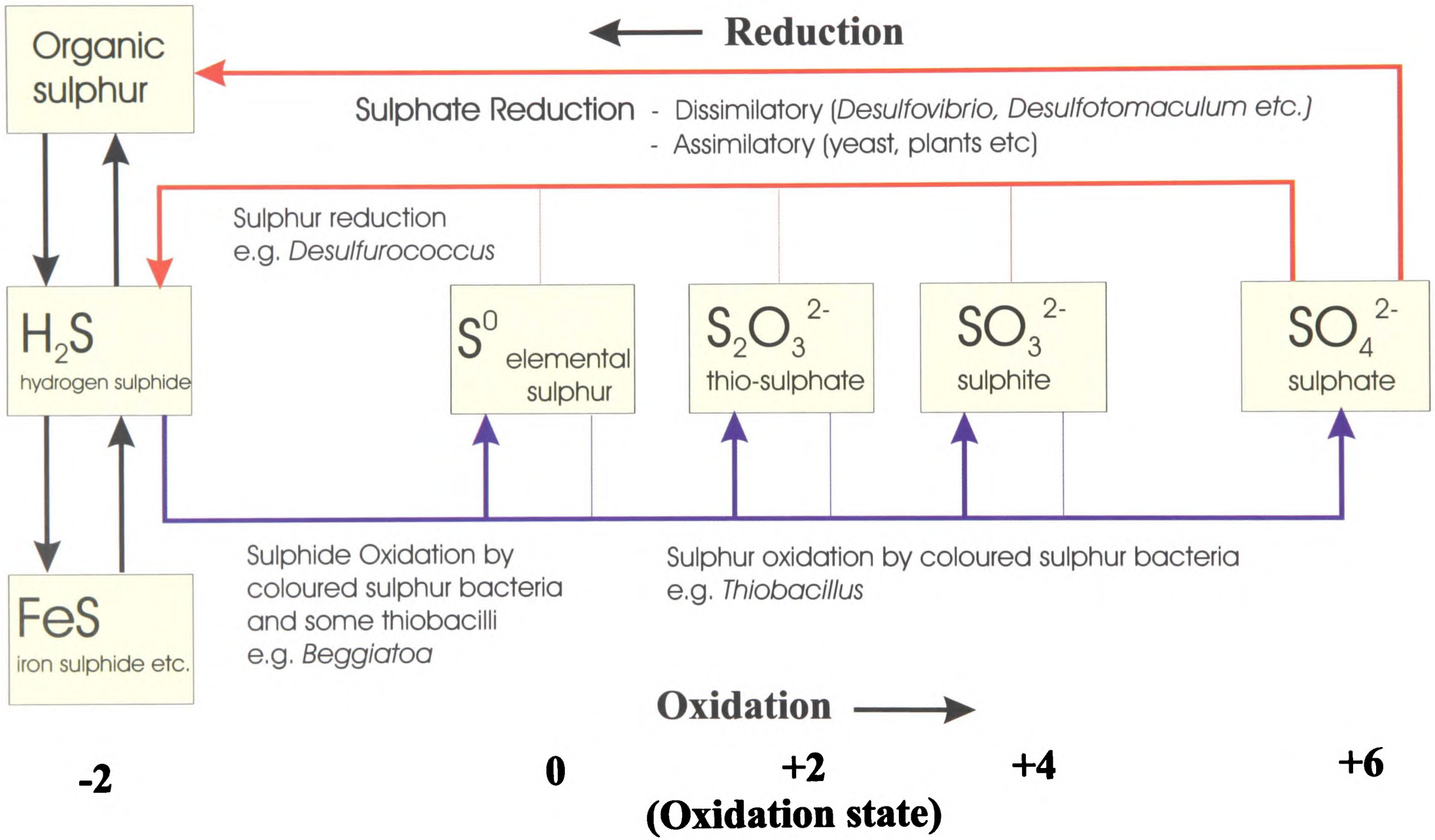


Figure 2.6. The Sulphur Cycle (after Fenchel *et al.*, 1998)

In principle the mechanism is simple; the lighter mass and greater motility of the ions containing the lighter isotope enable them to diffuse more readily to the sites of sulphate reduction and are therefore reduced more easily. The extent of isotope fractionation depends on temperature, sulphate concentration and growth rate of the SRB community, but nevertheless a negative $\delta^{34}S$ signal for pyrite (free from volcanic sulphur effects), both in modern and ancient settings, is strongly suggestive of bacterial sulphate reduction (for more detail see Chapter 5)

The metabolism of SRB also results in biochemical changes to the environment. SRB metabolise organic matter using sulphate as the terminal electron acceptor (see Section 4.4.1 for the relevant equations). The result of this process is the consumption of sulphate, the formation of hydrogen sulphide (and of mineral sulphides such as pyrite if iron is in plentiful supply), the increase in the alkalinity of the immediate environment by the addition of hydroxide ions, and the raising of carbonate alkalinity (see Chapter 4 for more detail).

Measurements of oxygen uptake and sulphate reduction rates made by Jorgensen (1982) indicate that, in coastal sediments, SRB were responsible for oxidising as much organic matter as all of the aerobes put together.

2.5. EVOLUTION OF THE SRB

By releasing H_2S as a principal metabolite which may be converted to sulphide minerals, the SRB leave vestiges of their life activities in sedimentary rocks. Here, characteristic $\delta^{34}S$ values, tending towards ^{32}S enrichment give specific evidence for the action of SRB (sulphur oxidisers show no such fractionation (Kaplan & Rittenberg, 1964)). Early workers (e.g. Goodwin *et al.*, 1976) divided the sulphur isotope record into a period before 2750Ma where the spread of $\delta^{34}S$ values is less than 10‰ and a period after this when $\delta^{34}S$ is greater than 10‰, equating this transition with the onset of microbial sulphate reduction. Subsequent authors have attempted to modify the date of the appearance of SRB, one way or the other. However, the use of the sulphur isotopes, together with the age of the sediments concerned, may produce equivocal results, as will be demonstrated in this section.

Evidence for the earliest biological sulphate reduction has been claimed from the sulphur isotope composition of Archaean pyritic sediments (~3.4Ga) and is particularly equivocal. Sedimentary pyrite from these rocks were shown to have a narrow range of sulphur isotope values (0 ± 5‰, Ohmoto *et al.*, 1993). This has been argued to result from both rapid sulphate reduction in a sulphate-rich ocean (Ohmoto & Felder, 1987; Ohmoto *et al.*, 1993) and from sulphide formation in a sulphate-poor ocean (e.g. Monster *et al.*, 1979). A sulphate-poor ocean with little or no bacterial sulphate reduction is supported by the isotope values being essentially the same as for pyrite formed in normal igneous rocks of the time (+1 ± 1‰). This contrasts with biogenic pyrite which has a large sulphur isotope range (-50 to +10‰). In addition to this, Habicht and Canfield (1996) reported that rapid sulphate-reduction under high sulphate concentrations in modern cyanobacterial mats gives rise to highly depleted sulphides (-25‰). Therefore, it had been proposed that all pyrite formed before about 2.75Ga has been formed from H_2S derived from magmas (see Schidlowski *et al.*, 1992). This would imply that before 2.75Ga, SRB had not evolved, the oceans were largely free of sulphate and the atmosphere contained virtually no free O_2.

Ohmoto *et al.* (1993), however, used new laser techniques to analyse single pyrite grains from the 3.3 - 3.4Ga Barberton Greenstone Belt, revealing a more varied isotopic signature (–3.0 to +8.6 ‰) which, they claimed, cannot be explained by Archaean basaltic magmatism nor by other non-biological means. It could, however, be explained by high rates of bacterial sulphate-reduction, comparable to the highest rates seen today in Solar Lake, in a CO_2-rich atmosphere (hence warmer, with more digestable organic matter). This requires the ocean to have substantial amounts of sulphate and, in turn, that the atmosphere contained small but appreciable amounts of free O_2. Recently, further evidence to support this point of view has been claimed. Shen *et al.* (2001) describe microscopic sulphides from the 3.47Ga North Pole formation in north-western Australia. These pyrites were found aligned along the crystal faces of supposed gypsum crystals that had subsequently been hydrothermally altered to barite. Maximum fractionation between sulphide and sulphate was 21.1‰ with an average of 11.6‰. The extent of these fractionations compare with microbial values, with ranges lying within those seen for microbes operating at high specific rates of sulphate reduction today. The sulphides are also associated with organic carbon and, since gypsum is only stable at temperatures <60°C, were unlikely to have formed hydrothermally. Runnegar *et al.* (2001a) refutes the claim that the original mineralogy of the sulphide host crystals was gypsum. By using X-ray computerised tomography, Runnegar *et al.* show the original mineralogy to have been barite. Use of sulphur isotopes shows sizeable mass independent

($\Delta^{33}S$) fractionations of the sulphate in barite, known only to occur in gas phase reactions. They state that this is consistent with shortwave UV photo-oxidation of volcanic SO_2 and claims that it is unlikely that sulphate evaporites formed in the Archaean. Runnegar *et al.* (2001b) go on to challenge the interpretation of sulphur isotope values by Shen *et al.* (2001), arguing instead that the pyrite was derived form the reduction of elemental sulphur formed, at least in part, by photochemical processes in the anoxic Archaean atmosphere.

Rasmussen & Buick (2000) describe an Early Archaean massive sulphide deposit from the Pilbarra Craton in north-western Australia. This 3235Ma deposit contains pyro-bitumen and fluid inclusions of oil in barite. It is claimed to be the oldest evidence of oil generation and is a suggested source of energy for a subsurface biota possibly metabolising hydrothermal sulphur species. Rasmussen (2000) also claims to have identified filamentous micro-organisms from the outer parts of this deposit. He suggests that the abundance of sulphur minerals in the deposit, together with the fact that the filaments are preserved as pyrite provides evidence for a chemotrophic (sulphur utilising) deep-sea hydrothermal biosphere which could have housed the earliest forms of life. Care must be taken, however, when identifying apparent micro-organisms, to ensure the specimens are bacterial in origin and not just artifacts from hydrothermal fluid flow and mineralization (cf. Brasier et al., 2002).

Definitive evidence for the widespread occurrence of SRB is not available until ~2.3Ga when it is generally accepted that the transition from an anoxic to oxic environment occurred (e.g. Kasting, 2001), increasing seawater sulphate concentration and stimulating SRB activity. This oxygenation is indicated by large negative shifts in sulphur isotope values from sedimentary sulphides (Cameron, 1982) and by the preservation of mass independent ($\Delta^{33}S$) fractionation signals in rocks older than ~2.3Ga (Kasting, 2001; Farquhar *et al.*, 2000).

Des Marais *et al.* (1992) suggest that a major burial phase of organic carbon was responsible for the release of oxidants to the earth surface at this time. Lindsay and Brasier (2002) also suggest that positive excursions in the $\delta^{13}C$ isotopic signature between 2.5 and 1.9Ga relate to carbon sequestration during ocean closure. Here, organic carbon rich sediments are subducted into and stored in the lower crust and mantle. The global ocean thereby became enriched in isotopically heavy carbon and released oxygen into the atmosphere. Kasting (2001), however, argues that the carbon isotope record of sedimentary carbonates shows that carbon burial has been fairly constant through most of geological time

and, thus, it was the oxygen sinks rather than sources which changed the oxidation state of the early earth. Catling *et al.* (2001) present the argument that hydrogen escape into space results in an irreversible net gain of oxygen in the atmosphere. After photosynthetic splitting of water into H and O_2, hydrogen is fixed in methane by methanogenesis and subsequently escapes to space from the upper atmosphere during decomposition by ultraviolet radiation. Catling *et al.* (2001) suggest that the gap between the possible emergence of photosynthetic cyanobacteria at ~2.7Ga (Brocks *et al.*, 1999) and the increased oxidation of the earth at ~2.3Ga was due the oxidation of continental crust by this newly released oxygen. This, in turn, slowly changed the oxidation state of gases released by low temperature metamorphic processes. Kasting (2001) goes on to suggest mechanisms whereby oxygen, in a low O_2, low sulphate environment, could be incorporated into the continental crust. He suggests that ferrous iron oxidation, producing banded iron formations (BIF's), and serpentinization of basalts may both have been important processes at this time.

The date of emergence of the SRB could be pushed back substantially from 2.3Ga by putative biogenic textures reported from the Ghaap Group, Northern Cape Province, South Africa by Wright and Altermann (2000). Ancient carbonate platforms of 2516 ± 4Ma (Gamohaan Formation) show intimate associations of pyrite, degraded organic material and organic laminae in carbonate cements. Isotopic evidence ($\delta^{34}S$ of –1.3 to +23.6) presented by Strauss and Beukes (1996) indicates that the pyrite formed by bacterial sulphate reduction. An absence of evidence for volcanic activity in adjacent strata would further support a biogenic origin. Kakegawa *et al.* (1998) report pyrite with $\delta^{34}S$ of –6.3 to +7.1 in the ~2.5Ga Mt McRae shales of the Hamersley Basin, W.A. This pyrite is interpreted as forming by bacterial sulphate reduction of seawater sulphate. Using these data they also propose that sulphate concentration in seawater was around one-third of its present value whilst SRB activity was significantly higher.

It is still somewhat uncertain whether SRB originated early in earth history, in response to the availability of sulphate species from volcanic vents and from anaerobic photosynthesis (produced by sulphur oxidising bacteria), or later, as a response to the changing redox status of the planet. Monster *et al.* (1979) concluded that dissimilatory sulphate reduction commenced at 2.8-3.2Ga using extrapolated $\delta^{34}S$ trends before and after this time, post-dating accumulation of oceanic sulphate and substantially predating oxygen respirers; this date lies almost half way between the proposed minimum and maximum dates. Monster *et al.* (1979) argue that the appearance of SRB was probably contingent upon

the attainment of a certain level of sulphate in the ancient oceans, provided by a combination of the various mechanisms outlined above.

Sulphate reduction in modern marine sediments is the dominant anaerobic biomineralization pathway, quantitatively equivalent to or exceeding aerobic respiration (Jorgensen, 1982). In Precambrian microbially dominated shelf ecosystems, the potential existed for bacterial sulphate reduction to operate on a large scale, leading to widespread mineralization through organic degradation. The date of emergence of the SRB is thus of great importance in constraining the age range of ancient dolomites to which a microbial dolomite model may be applied.

2.6. GROWTH / CULTIVATION

SRB grow best under slightly alkaline conditions over a relatively restricted pH range of 7.2-7.8 (Postgate 1984). The growth media must contain a carbon source and an electron donor, these usually being provided by the same substrate (e.g. lactate, acetate). Some species, however, grow mixotrophically, whereby the electron donor source (often H_2) is different from the carbon source that is incorporated into the cellular material. The growth media must also contain sulphate as the terminal electron acceptor, although some species can use thio-sulphate and sulphite instead. The exact composition of the growth media depends upon which genera or species are to be cultivated.

In the case of the Coorong sediments, it was not known in advance which SRB species were present. In this case, a medium developed by Postgate was used which was known to be suitable for the culture of *Desulfovibrio* and *Desulfotomacula*, thought to be the most common SRB in a Coorong type (hyper-saline coastal lagoon) setting. This medium was not thought to be suitable for other SRB genera, however, and so an evaluation of the total number and variety of SRB in the Coorong sediment could not, in theory, have been attempted. However, when the cultured bacteria were identified (Section 6.6 and Appendix 6) it was found that the genera present were neither *Desulfovibrio* nor *Desulfotomacula* but showed closest similarity to *delta proteobacterium strain 2550 (Desulfostipes)* (Myhr *et al.* 2002) and *Desulfosarcina* (Tanner *et al.* 2000). This suggests that this culture medium is more general

than previously thought and may be ideal for situations where the type of SRB in a sediment is unknown.

Whilst the focus of this study are the sulphate-reducing bacteria, other anaerobes survived the culturing process (Chapter 6) and are identified in Appendix 6. These are mentioned briefly as they may also have a role to play in the genesis of dolomite. Bacteria of the genus *Clostridium* were identified from both Milne Lake and McFaiden Lake, whilst a bacterium of the genus *Vibrio* was identified from Milne Lake (for a description of these genera see Section 6.6.1).

2.7. SUMMARY

- SRB are a diverse group of dominantly anaerobic micro-organisms broadly distributed over the earth but especially concentrated in anoxic marine and freshwater sediments.
- Their cells are dominantly Gram-negative with DNA that can easily be transmitted from one cell to another making them extremely adaptable.
- A taxonomic classification is difficult. More and more species and genera are being recognised by 16S rRNA technology.
- They have a dissimilatory reduction pathway relying on the sulphate ion as the terminal electron acceptor during oxidation of organic matter.
- Their environmental effects include the fractionation of sulphur isotopes (Chapter 5), alteration of pH, mineralization of organic matter and significant participation in the sulphur cycle.
- The SRB are an ancient group of microbes. The exact date of their appearance is somewhat uncertain but probably extends back to around 2.8 - 3.2Ga.
- Their age has important implications for organogenic dolomite formation throughout early geological history

CHAPTER 3



An estuarine crocodile.
One of the less friendly natives.

Chapter 3

Physiography, sedimentology and mineralogy of the Coorong ephemeral lakes

3.1. INTRODUCTION

Each of the study lakes is a dynamic system and as such exhibits changing appearances and chemistry at different times through the annual cycle. There are, however, several features which they have in common and these will briefly be described before dealing with each lake individually.

3.1.1. General Characteristics

The eight study lakes lie in a chain trending approximately NNW-SSE with Holocene calcareous dunes on the coastal side separating them from the Coorong Lagoon, which is a small inlet connected to the Southern Ocean at its NNE end (Figs 1.7 & 3.14). In pre-Holocene times there were a series of channels connecting four of the northern lakes to each other and to the Coorong Lagoon; Holocene sea level change and progradation has since left each lake isolated so that the low lying channels are now colonised by salt tolerant grasses and bushes (Von der Borch, 1965a).

Throughout the Holocene, a relative drop in sea level due to sediment accretion has resulted in the Coorong lakes evolving from a dominantly marine setting to that of distal ephemeral lakes. A sediment core from one of the lakes, Lake McFaiden, demonstrates this evolution (Fig. 3.1.). At the base of the core, a depth of c. 1m, sediments of the lagoonal facies

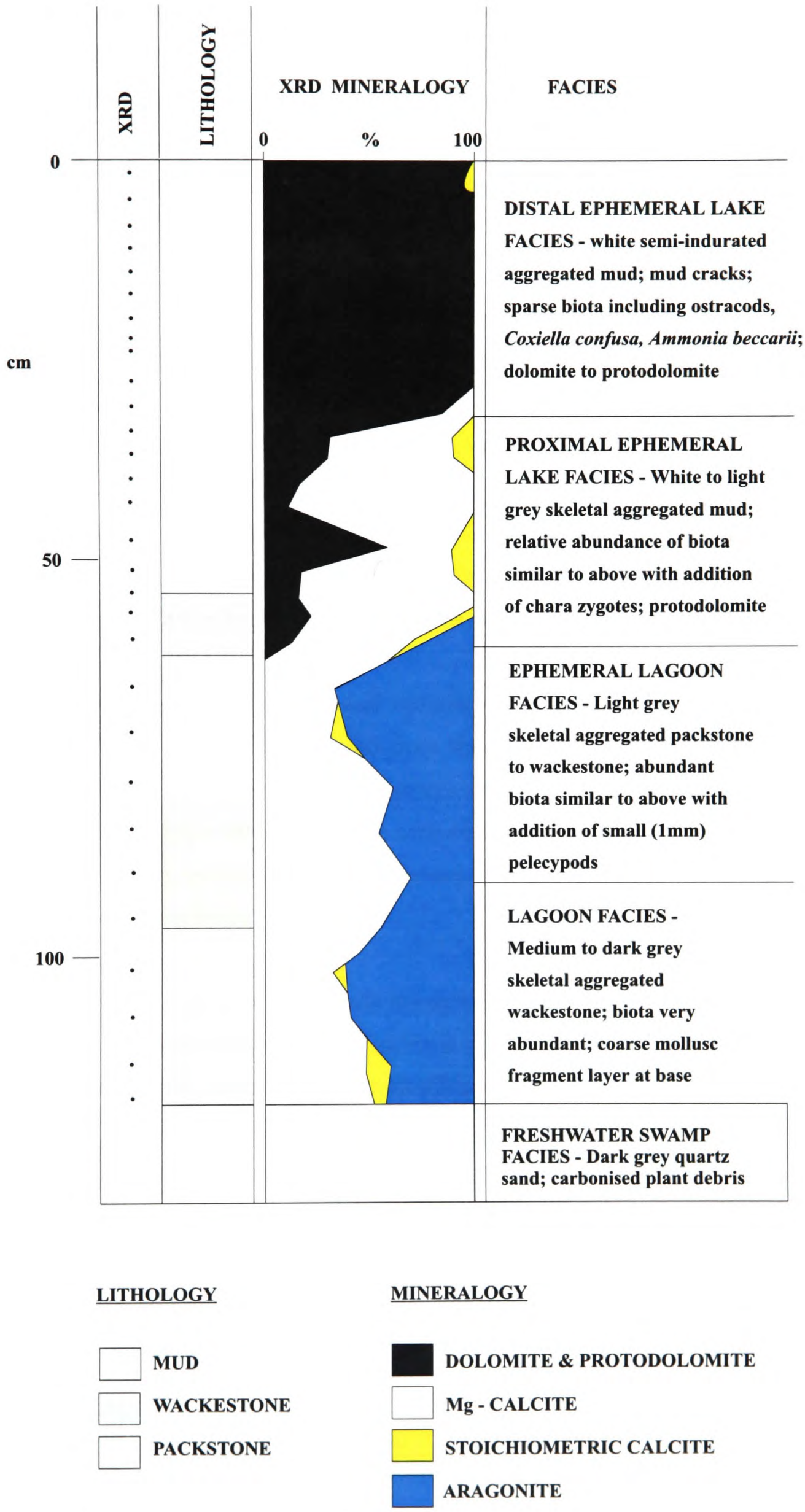


Figure 3.1. Stratigraphic log of the type core from a distal ephemeral lake. See text for full description (after Von der Borch, 1976).

occur. These are aragonite and Mg-calcite wackestone sediments with an abundant biota. A protected marine environment is indicated by a bivalve fauna (*g. Nuculana*) grading into a biota consisting of *Coxiella confusa*, a gastropod, the foram *Ammonia beccarri* (survives salinities 7‰ - 67‰; needs permanent water) and various ostracods (survive broad range of salinities up to 200%) indicating increased restriction from a marine influence (Von der Borch, 1976).

These sediments are overlain by those of the ephemeral lagoon facies (i.e. areas which were connected to the main lagoon during winter high water levels but became isolated and heavily evaporated during dry summer periods). The biota decreases in diversity and abundance and bivalves become rare or absent, mirroring increased environmental restriction. The sediment changes from a grey skeletal wackestone to a light grey/white packstone with occasional desiccation cracks. Mineralogically the sediment resembles that of the lagoonal facies, being dominated by aragonite and Mg-calcite; occasionally a little poorly ordered 'proto-dolomite' is also observed in this facies (Von der Borch, 1976).

Overlying this is the proximal ephemeral lake facies. The sediment here being generated in lakes which were isolated from the direct access of marine or lagoon waters. The sediment is a light grey to white aggregated mud with almost identical fauna to the lagoon facies. The major difference is the carbonate mineralogy: aragonite, which dominated the lower two units, is not found here, instead calcite, Mg-calcite and 'proto-dolomite' are found along with rare hydro-magnesite.

At the top of the core one finds the distal ephemeral lake facies, occurring in lakes whose floors are in excess of 1m above present mean sea level. This is the facies observed at the present day in the dolomite precipitating lakes, such as Lake McFaiden, (dolomite dated as 300 ± 250yrs old by Von der Borch *et al.*, 1964). It consists of white, semi-indurated mud with frequent desiccation cracks, teepee structures and intraclast breccias. The mineralogy is almost entirely dolomite or 'proto-dolomite', occasionally occurring with magnesite; a very sparse biota is dominated by *Coxiella confusa*.

Not all of the distal ephemeral lakes in this study contain all four sedimentary units described above. Some may have been at too high a level to be inundated by seawater to begin with, and thus contain white dolomite or dolomite/magnesite mud directly overlying Pleistocene calcrete or freshwater swamp sediments. McFaiden Lake is the most distal from

the present lagoon and is therefore the most evolved in terms of carbonate mineralogy, representing a full, idealised, Holocene stratigraphic section. Three of the study lakes (Halite, North Stromatolite and South Stromatolite) do not contain dolomite as the uppermost lake facies despite being in close proximity to dolomite precipitating lakes. Instead the carbonate mineralogy is mostly aragonite and Mg-calcite. The reasons for this difference in carbonate mineralogy forms one of the main themes for this study.

The lakes range in size from around 300m^2 (Dolomite Lake) to over 1km^2 (Milne Lake) and all are very shallow, rarely exceeding 1m water depth. Because of the shallowness of the lakes and the frequent strong onshore winds the water column in all of the lakes is well mixed and stratification does not occur; however, beneath this well mixed water column is a layer of unconsolidated sediment of yoghurt-like consistency. The density of this layer leads to stable stratification of the lowermost part of the water column during late spring to early summer. Mixing with the oxygenated waters of the upper water column is prevented by density stratification, leading to a dis-aerobic to anoxic environment around the sediment-water interface. The high concentration of suspended material in the water column also prevents much light penetrating down to this layer and together with anoxia creates an environment that, during the latter stages of the evaporative cycle, is hostile to most plant and animal life. The establishment of anoxia at, or just below, the sediment water interface is a key feature of these lakes allowing anaerobic bacteria, including SRB, to flourish at this time. This is represented in Figure 3.2 (for methodology, see Section 4.3).

Microbial mats are common components of many of the lakes, often occurring around their margins. Desiccation, during spring and summer, together with frequent winds result in much of this microbial matter being incorporated into both the lakewater and the yoghurt-like sediment. *Ruppia maritima* and Samphire (Fig. 3.13) are abundant both at the lake margins and on the lake floors themselves during much of the year, and *Ruppia*, once desiccated, becomes an especially common component of the sediment. The salinity of the lakes fluctuates from brackish during the wet winter months to hyper-saline in spring and early summer immediately before desiccation, and were all hyper-saline during the study period of October to December (see Section 4.2.). The pH is generally high (up to around 9) as are the concentrations of carbonate, sulphate and magnesium in all the lakes. The chemistry of the lakes will be dealt with in detail in Chapter 4.

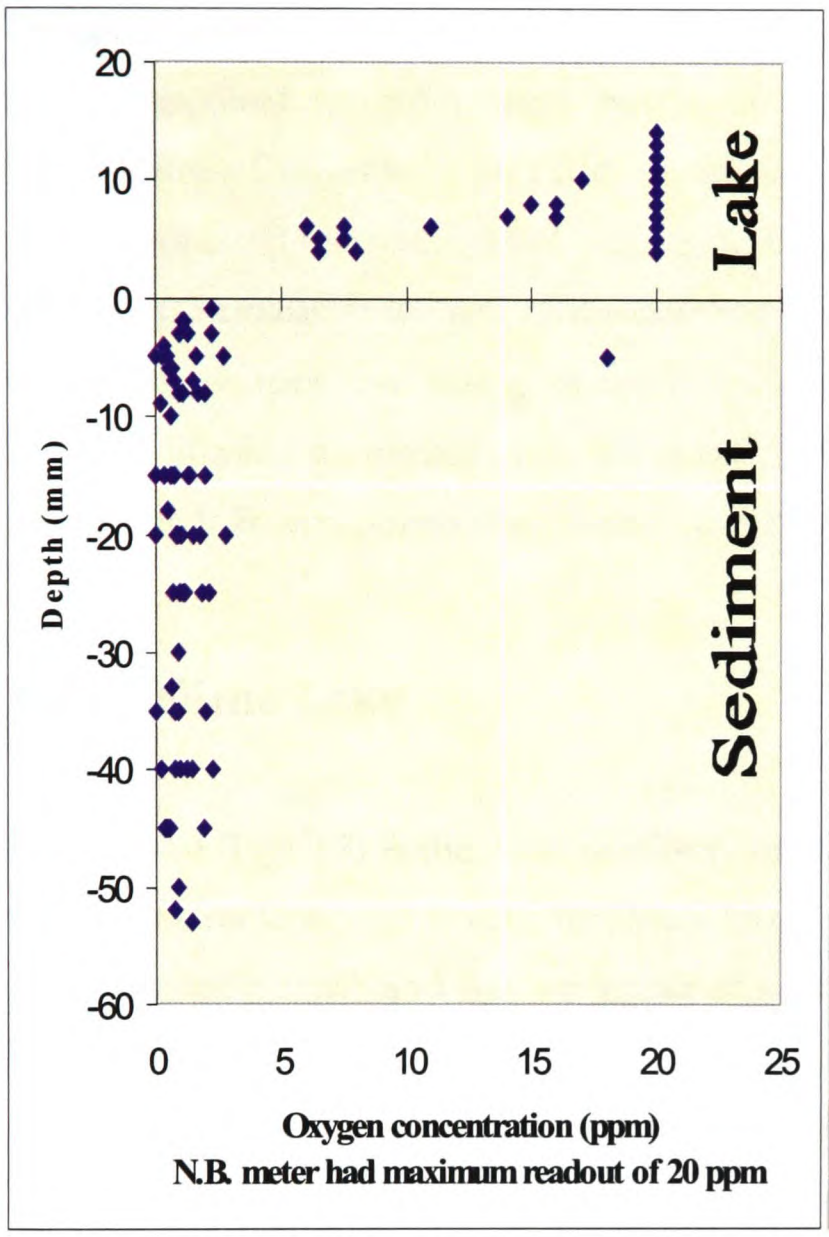




Figure 3.2.

a) Oxygen concentrations in lakewater and porewater for all the lakes studied. Data obtained in October 1998 (this study).
b) Footprint from Milne Lake showing yoghurt like sediment which is strongly disaerobic to anoxic (dark grey/black) directly below the sediment water interface. Note also the collection of organic matter (mostly *Ruppia marittima*).

3.2. PHYSIOGRAPHY AND SEDIMENTOLOGY

In this and the following chapters the four lakes which are actively precipitating dolomite will be described first, in geographical order, from North to South (Milne, Pellet, Mini Dolomite and McFaiden). A description of the three non-dolomitic lakes will then follow, again described in order from North to South (Halite, North Stromatolite and South Stromatolite). Dolomite Lake, a fifth dolomite precipitating lake, was not studied in any great detail because it was desiccated during most of the sampling period; this will be described, when appropriate, at the end of the dolomitic lake section. The sampling period was limited to the late evaporative stages of the lakes as this is the time where elevated salinity and toxicity eliminate macrofauna allowing benthic microbial communities to prosper, modifying lake and porewater chemistry to favour dolomite precipitation.

3.2.1. Milne Lake

Milne Lake (Fig. 3.3) is the most northerly of the chain of lakes and is located less than 1km from Salt Creek. Access is via a dirt track loop road. It is one of the larger lakes in the area, at approximately 1km^2, and has a number of small islands outcropping above its surface. The lake is bordered by rocky calcareous marine deposits containing numerous shell beds. The shoreline is denoted by Beaded Glasswort and *Salicornia australis* (Fig. 3.13 a, b).

During November 1998, in the latter stages of evaporation, most of the lake had water cover with only approximately the outer 30m desiccated. This region immediately adjacent to the water was characterised by a light grey yoghurt-like mud with desiccating *Ruppia maritima* grass and dead water fleas mixed within it (Fig. 3.3b). Below the upper 10-20mm, this layer was replaced by a much darker and more consolidated muddy sediment (Fig. 3.3c). Movement of the sediment caused H_2S gas to be released, recognised by its 'bad egg' like smell. This area passed shorewards into a region characterised by sediment with a plastic consistency showing polygonal desiccation cracks (Figs 3.3d & e). Around the lake margins, semi-indurated crusts of dolomite were common, often incorporating stromatolitic/microbial material. These have a mega-polygonal fracture pattern with polygons up to a couple of metres in size, formed because the crusts are aquicludes that are subject to pressure from upward migrating groundwaters. These cracks become *loci* for halite formation in the summer months. The pattern is probably inherited from the original



Figure 3.3a. Milne Lake on 10/11/99. The lake is about half full. The area immediately adjacent to the water consists of light grey yoghurt-like mud, which then passes into more consolidated light grey/brown mud undergoing early desiccation.



Figure 3.3b. Close up of the surface of Milne Lake sediment under 1-2cm of water cover. White "woolly" halite crystals can be observed attached to the *Ruppia* grass.

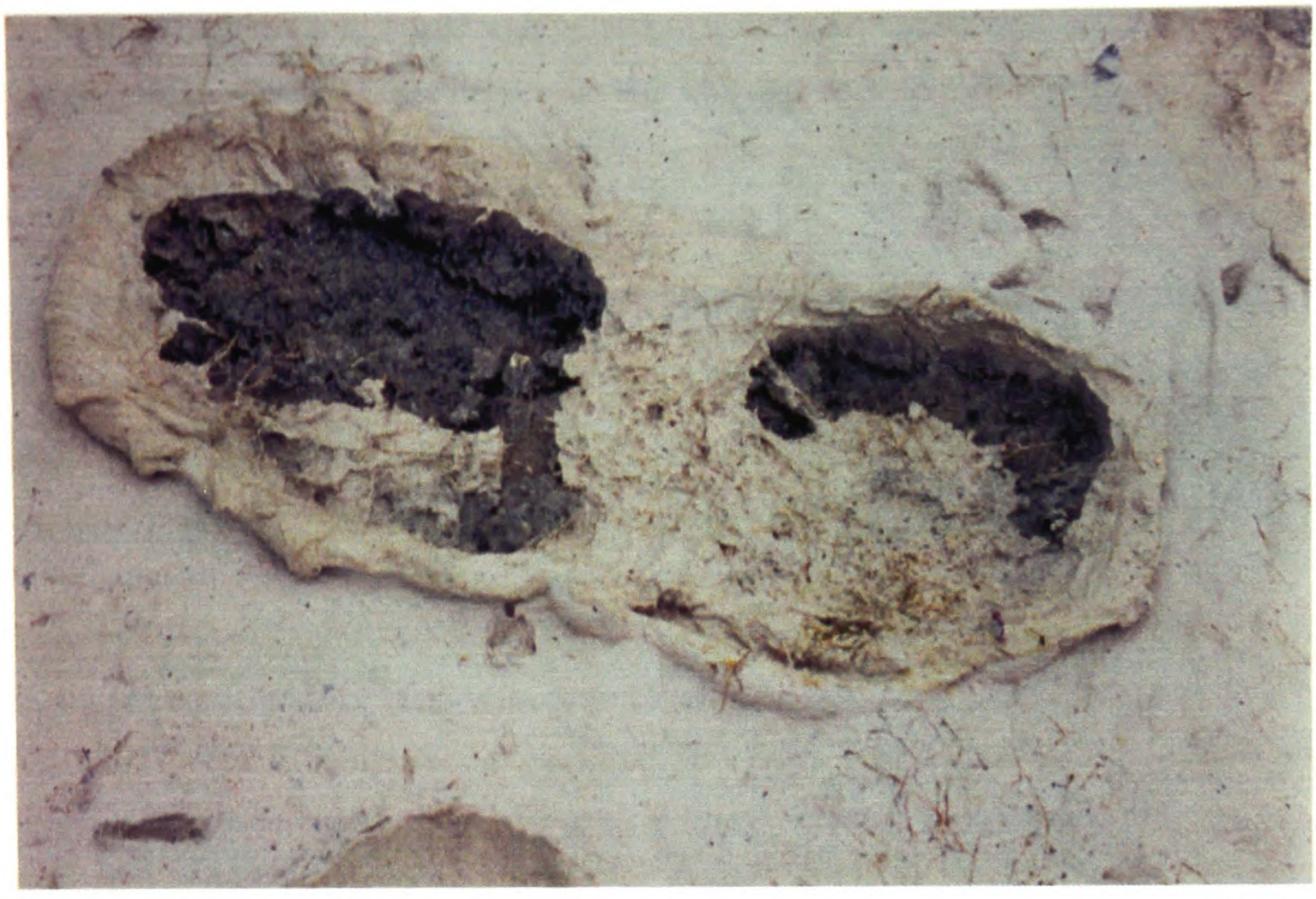


Figure 3.3c. Close up of sediment in Milne lake adjacent to area covered with water(Size 7 footprint for scale). The upper 1-2cm of the mud is of yoghurt-like consistency and contains abundant *Ruppia* grass and dead water fleas. Beneath this, the mud is darker and more coherent with a clay like texture.

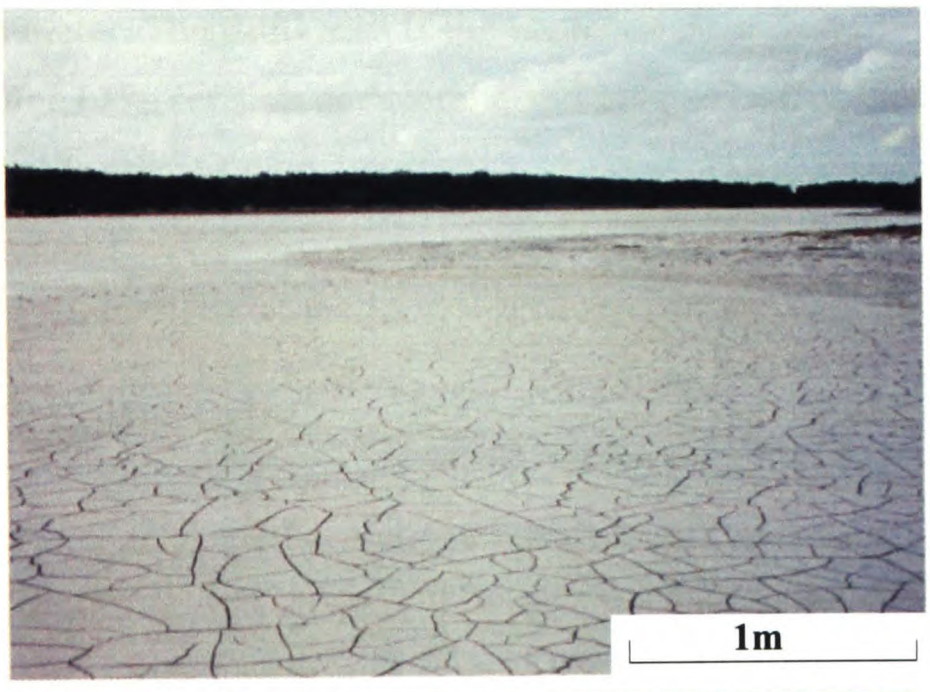


Figure 3.3d.
Milne Lake on 13/11/99.
The lake is now completely dry, with large area of yoghurt-like mud in the distance and large area of sediment with polygonal mud cracks in the foreground.

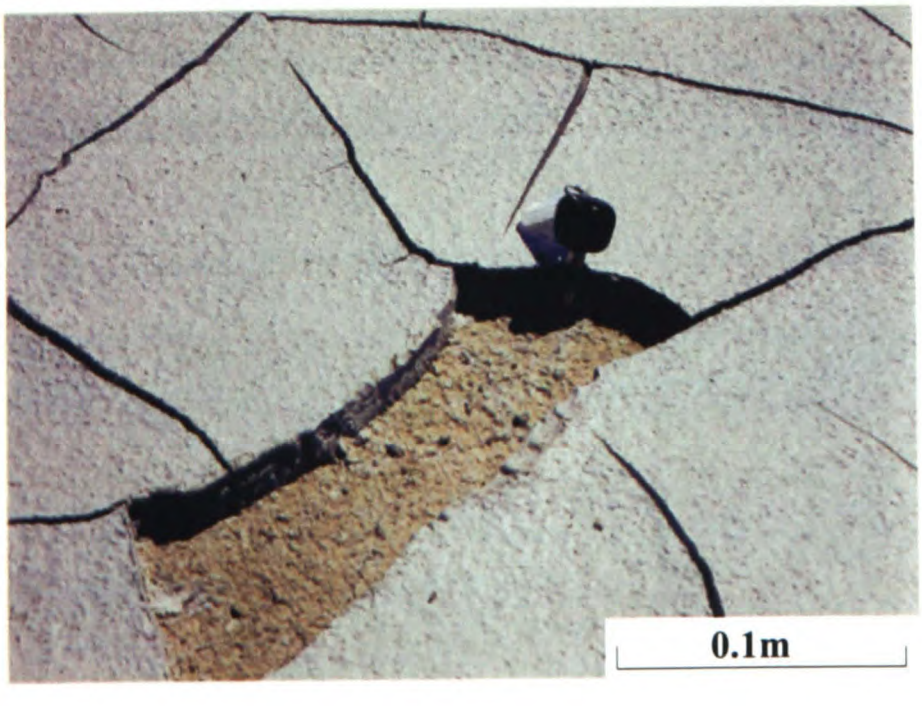


Figure 3.3e.
Close up of polygonally cracked mud. The polygons are 2-3cm thick and, at this stage, 10-20cm across. They are composed of uniform medium grey mud which is sticky and coherent (plastic) and overly a hard, pale yellow/ grey clay mud. Each polygon can be lifted out of the ground individually as seen in the photo.

desiccation pattern. The edges are often mutually upraised to form teepee structures and are then eroded to form intraclast breccia, which along with newly formed mud, infills the centre of the polygons.

In November 1999, Milne Lake was in a very different state. At the beginning of the field season it was already dryer than at any point in 1998, with a water depth rarely exceeding 50mm, even in the centre of the lake. Coring of the sediment was fairly easy; the core could be pushed the entire way in (100mm) manually. The top 10-20mm of the core was wet and yoghurt-like, while below this there was a transition to a much dryer and more clay-like texture. Desiccated *Ruppia maritima* was concentrated at the surface and coated with halite. A few long strands of grass were found at depth in the core. Within a matter of days the lake had become completely desiccated. The areas which had been yoghurt-like developed mud cracks and coring was more difficult. The entire lakebed could now be observed and could be divided into three main areas. Newly desiccated areas consisted of yoghurt-like mud. Areas which had been sub-aerially exposed for longer had metre-scale mudcracks and rare patches of stromatolitic material were observed here. The longer the exposure the more intense the cracking was, until each polygon was only a few centimetres in diameter. The third area is the shoreline described previously. The carbonate mineralogy of Milne Lake consists of dolomite and magnesite (Section 3.3.2 & Appendix 1), whilst quartz and halite are common accessories.

3.2.2. Pellet Lake

Pellet Lake is located around 150m south east of Dolomite Lake and is accessed via the low ground of a former channel that used to connect the two lakes. It is a large (approx. 1km^2) lake and is also the deepest of the lakes, with a water depth in the centre of up to 0.5-0.6m. This means that Pellet Lake is the least likely to dry out and was not seen totally dry during either of the field seasons.

There are three distinct types of sediment in Pellet Lake (compare Figs 3.4a & 3.4b). In areas where there is at least 0.1m of water cover and along the north-west margin of the lake, the typical sediment is 10-30mm of very 'gloopy' yoghurt-like dark mud (Fig. 3.4a). In the central western part of the lake, with or without water cover, the sediment is pelletal and

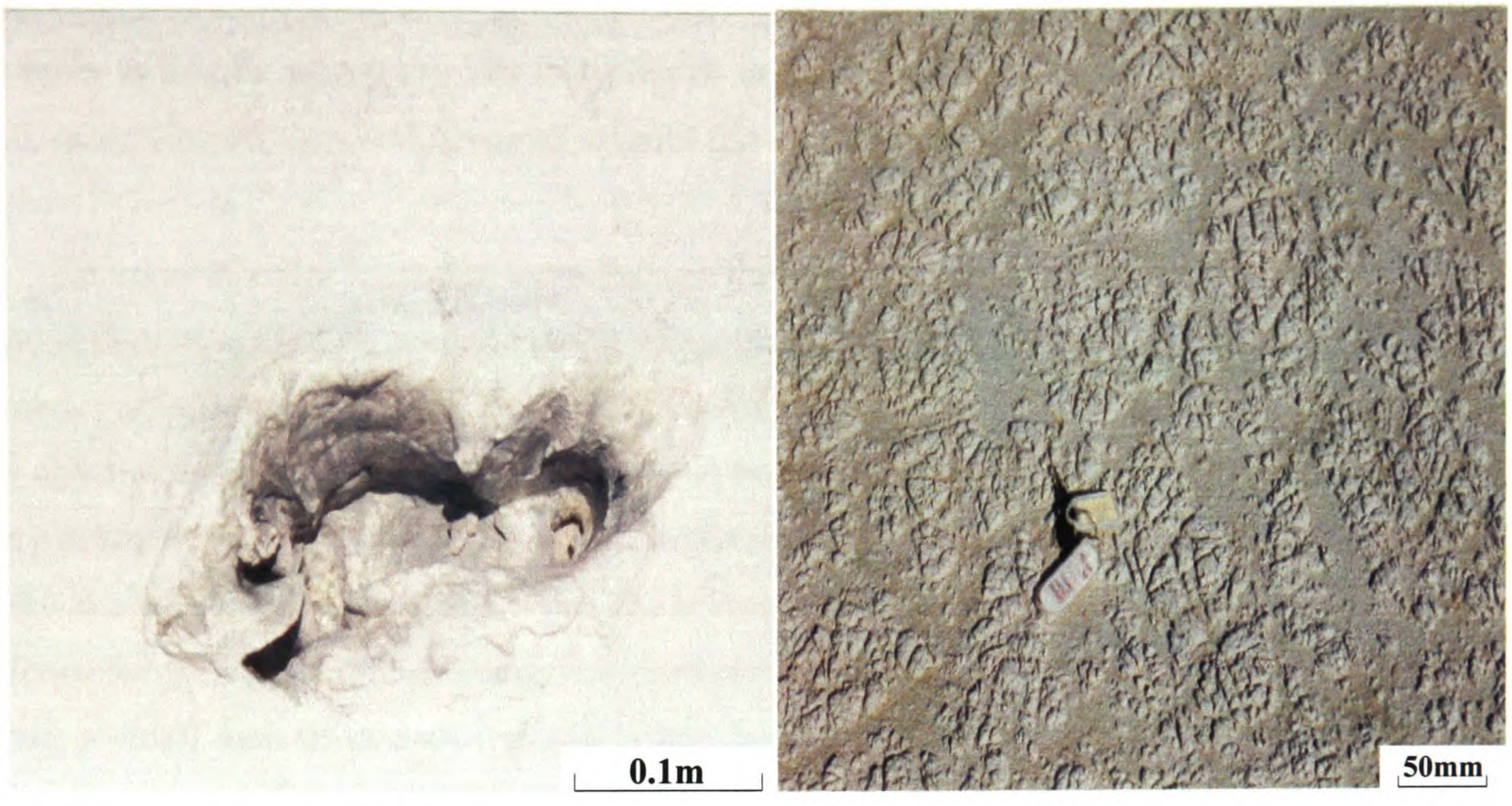


Figure 3.4 a & b. Comparison of the nature of sediment in Pellet Lake.
a) Typical light grey yoghurt-like mud passing down into a sticky darker mud.
b) Sediment unique to Pellet Lake. This is consolidated medium grey mud which is sticky on the surface but not soft enough to sink into. It occurs both on the shore and under shallow water cover.



Figure 3.4c. Southern shore of Pellet Lake looking east. Note the iron-stained lithified shoreline, composed of dolomite and stromatolite crusts and associated breccia, in close proximity to soft mud under shallow water cover. Note also the cloudiness of the water caused by fine grained dolomitic mud being disturbed by wave action.

sticky (Fig. 3.4b), but quite solid (i.e. one does not sink into it). Intermediate between these two types is a light grey putty-like mud which one sinks into only slowly. This is found in small, mostly newly exposed, areas all around the lake.

In areas covered by water, even though the water depth is only 0.5m at most, the top of the sediment cannot be seen. This is because the wind-driven waves stir the upper, fine-grained, yoghurt-like sediment, turning the lake water cloudy. *Ruppia* grass is largely absent, as is any evidence of macrofauna. The pelletal nature of much of the mud in this lake has been attributed to the digestive activity of brine shrimps (e.g. Rosen *et al.*, 1988). These may inhabit the lake in winter months, when the salinity and toxicity would permit, but no direct evidence for them was found. Polygonal mud-cracks are less common, partly because there is only a small area of desiccation and partly because the pelletal nature of the sediment makes it less susceptible to the tensional forces with lead to cracking.

The shore of Pellet Lake is also varied. Most commonly, it consists of lithified carbonate sediment with numerous shell beds and along one shoreline these are heavily iron stained (Fig. 3.4c). There are also significant areas of indurated bryozoan mounds and stromatolitic features all of which have been eroded to give intraclast breccias. The mineralogy of Pellet Lake is again dominated by dolomite with a small amount of associated halite, quartz and possible hydro-magnesite (Section 3.3.3. & Appendix 1).

3.2.3. Mini Dolomite Lake

Mini Dolomite Lake (Fig. 3.5) lies approximately 16km south of Salt Creek, just off the Princes Highway (access it via the turn off for Chinamans' Well). The lake is approximately the same size as Dolomite Lake (despite its name) and its margins are defined quite clearly by Samphire and Saltwater Paperbark trees.

Mini Dolomite Lake underwent the later stages of desiccation during both the 1998 and 1999 field seasons. The sediment is a uniform, medium grey mud with a thick yoghurt-like texture and a dense covering of *Ruppia maritima*, passing down into a sticky non-porous mud. Detectable amounts of hydrogen sulphide escaped when the uppermost sediment was



Figure 3.5a. Mini Dolomite Lake in mid November 1999 (looking south). There are just a few residual pools of water left. The sediment is a pale yellow/grey mud, topped with straw like desiccated *Ruppia* grass. In the foreground semi-lithified microbial mats can be seen.



Figure 3.5b. Mini Dolomite Lake in mid November 1998 (again looking south). Note dense cover of *Ruppia* grass which is at an earlier stage of desiccation than in 1999 (hence the fairly large colour difference). Note also the softness of sediment as evidenced by the footprints in the foreground (1).

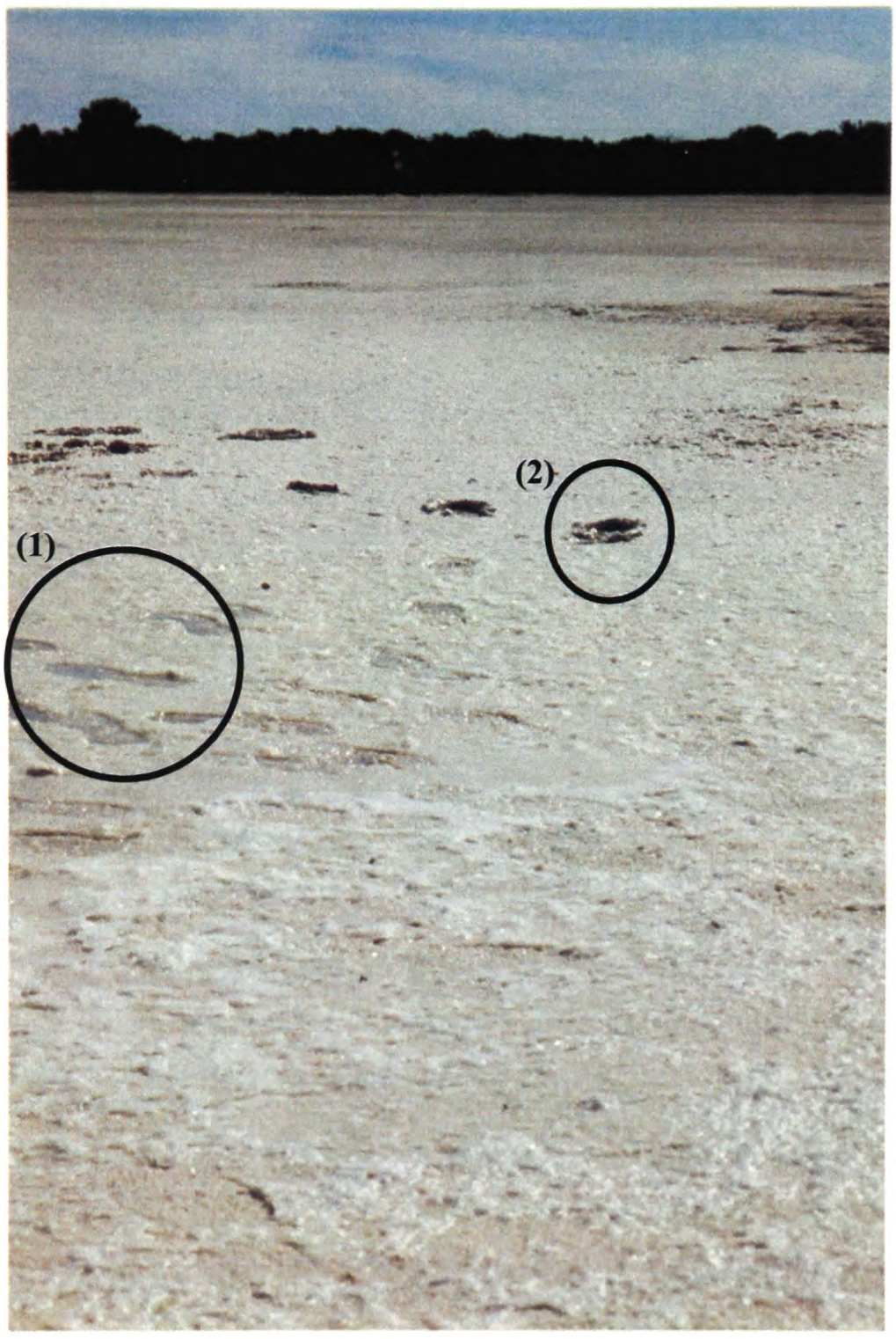


Figure 3.5c. Mini Dolomite Lake in late November 1999. The important feature to note here is the rapid mineral crystallisation as the lake finally dries up. A layer of halite forms which is almost hard enough to walk on. Beneath this, in some areas, small pockets of water are left (1). The core site is seen in the centre of the photo (2).

disturbed. The only macrofauna to be observed was the small pink gastropod, *Coxiella confusa* described from other lakes. The lake margins are composed of soft microbial mat passing quickly into dolomitic crusts, heavily eroded at their edges and often infilled with new soft sediment. In the final pools of water much halite precipitation took place and this encrusted the grass in these areas (Fig. 3.5c). As the lakebed dried the mud became lighter coloured, taking on an almost sandy appearance, while penetration below the top 20mm was difficult. Polygonal cracking was rare, possibly because of the large grass covering. The mineralogy observed in Mini Dolomite Lake is dominantly dolomite with a little halite and quartz and traces of celestine ($SrSO_4$) and kutnohorite ($CaMn_{0.6}Mg_{0.3}Fe_{0.1}(CO3)_2$) (Section 3.3.4 and Appendix 1).

3.2.4. McFaiden Lake

McFaiden Lake is situated a further 2km south of Mini Dolomite Lake and is immediately adjacent to the Princes Highway. It is a slightly unusual shape with a thin raised section topped with abundant Samphire separating it into two parts.

McFaiden Lake also went through the later stages of desiccation during both the 1998 and 1999 field seasons, so samples for data analysis could easily be obtained. The margins of the lake are mostly lined with low salt-tolerant bushes. The progressive retreat of the lake during desiccation can be traced by multiple strand lines composed of dead water fleas, gastropods and *Ruppia maritima* grass (Fig. 3.6a & b). The sediment in McFaiden Lake is a little more consolidated than in the other lakes. Small areas of thick yoghurt-like mud are observed under shallow water cover. Once exposed, however, the sediment dries quickly to a pale yellow colour and coring below the top 50mm becomes difficult. The mineralogy of the sediment in this lake is almost 100% dolomite, with small amounts of quartz and halite (Section 3.3.5 and Appendix 1).

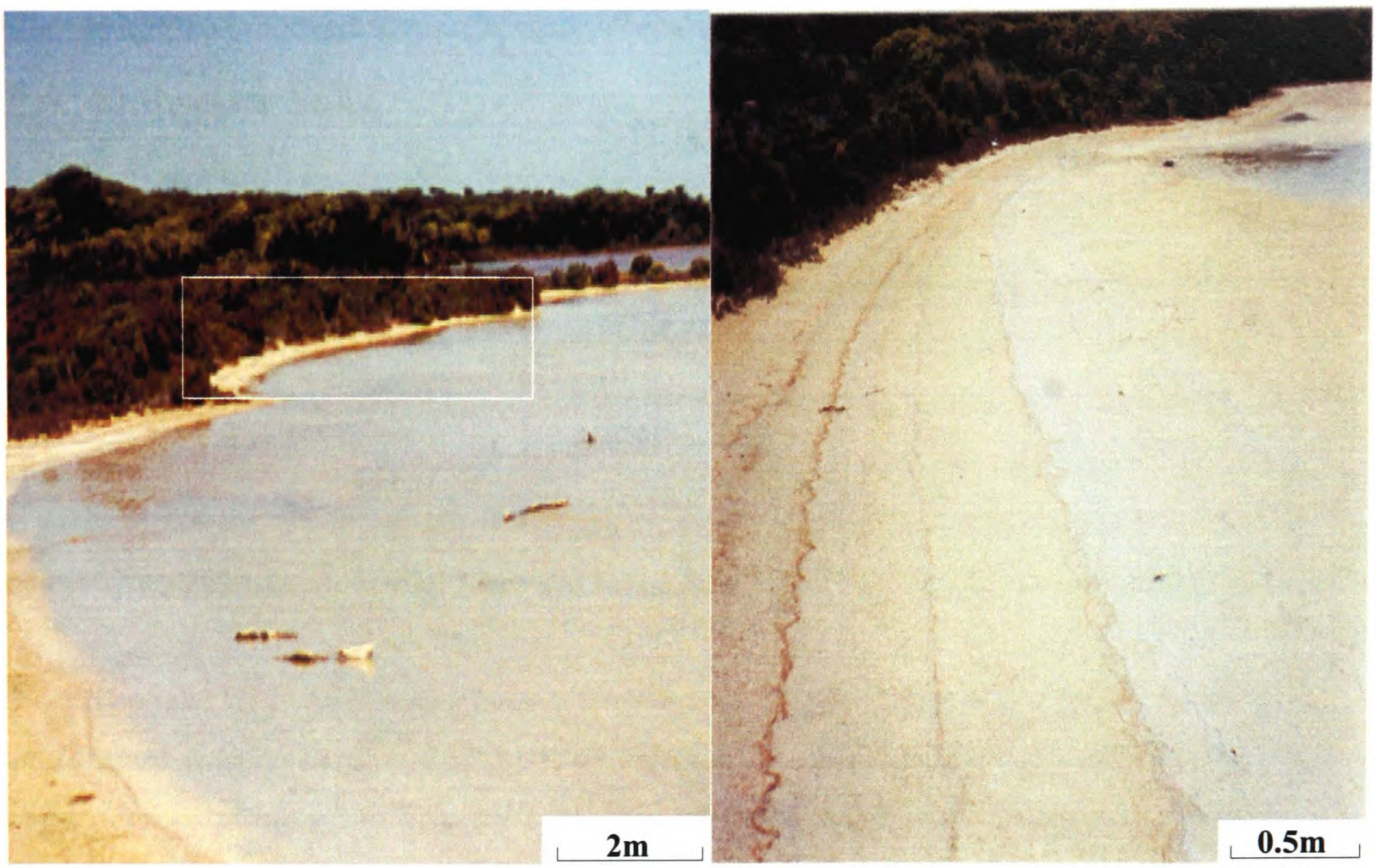


Figure 3.6. McFaiden Lake eastern shore. Fig. b) is close up of area boxed in Fig. a), demonstrating the rapid nature of desiccation. a) The lake is fairly full and one stand line can be seen denoted by dead gastropod shells and *Ruppia* grass (photo taken 30/10/98). b) Rapid retreat of the lake with multiple stand lines corresponding to daily retreats (photo taken 7/11/98).

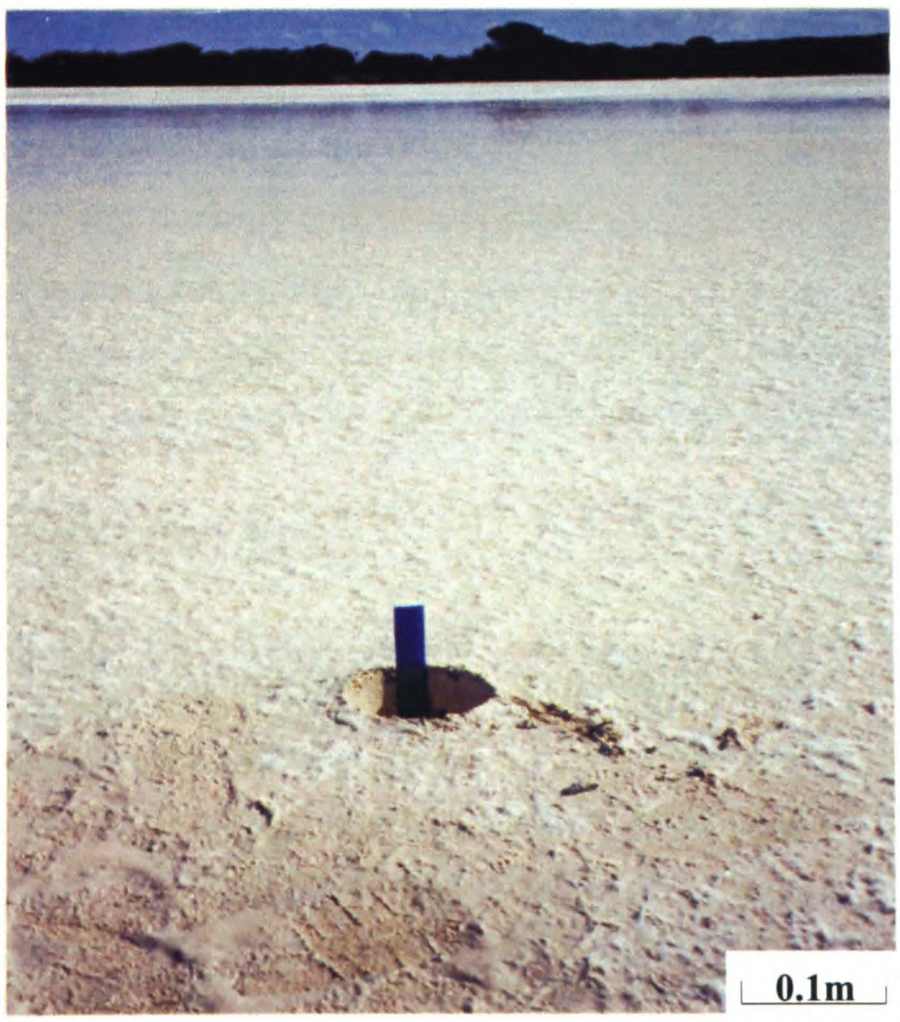


Figure 3.6c
McFaiden Lake - mid November 1999. This shows the nature of the sediment when desiccation is almost complete. The dolomitic mud is pale grey/yellow in colour with a thin covering of dead *Ruppia* grass encrusted in halite. The halite dissolves when pressure is applied, as seen in the foreground.

Note the core site in the foreground. Cores were taken in newly desiccated areas wherever possible.

3.2.5. Dolomite Lake

Dolomite Lake (Fig. 3.7) is situated around 1km south of Milne Lake and is reached via a 1.6km drive along the gravel loop road from Milne Lake. It is one of the smallest of the lakes studied and therefore experienced early drying. Approaching the lake from the road, one passes through lithified calcareous knobbly sediment which may have a stromatolitic origin. Lying unconsolidated in this low-lying area, which had been a connection to Halite Lake in the early Holocene (Rosen *et al.*, 1989), are numerous small pink gastropods (*Coxiella*) and rare bivalves (*Nuculana*). The lake margin is again denoted by a ring of halophytic samphire.

The lake had water cover only at the beginning of the 1998 field season. At this time, the sediment was very soft and sticky with a putty-like consistency, giving off a strong smell of hydrogen sulphide when disturbed. The sediment was uniform in colour and consistency, being light grey and gelatinous down to the 50mm coring level. Dense areas of *Ruppia maritima* were common and coring through it was sometimes difficult. In contrast to the area around the lake, no fossil material was observed within the lake sediment, though water fleas were common in the water. Within a week the lake was dry, an area of some $50m^2$ being desiccated in this time. The mud at this time was medium grey with a coating of brown dying grass and silvery-black dead water fleas. Some cracking was observed in the dryer areas. No sampling was possible during the 1999 field season as the lake was baked hard with multiple stages of cracking (Fig 3.7b). As a result, this lake was not studied in the same amount of detail as the other seven. The mineralogy of this lake is dominated by dolomite, this being the only carbonate phase (see Section 3.3.6. and Appendix 1). Some halite is found as surface precipitates along with a little quartz.

3.2.6 Halite Lake

Halite Lake is situated within the Salt Creek chain of lakes and lies between two dolomitic lakes, namely Milne and Dolomite Lakes. It was chosen as a comparison lake as it still has an underground connection to the Coorong Lagoon unlike any of the other study lakes (Wright, 2000). Its morphology is very different from the lakes previously described. Although small,



Figure 3.7a. Looking south-east towards desiccated Dolomite Lake. The channel from which the photograph was taken connected this lake to others in the 'Salt Creek chain' before a relative drop in sea level left each one isolated. This channel is now covered with salt tolerant plants such as Samphire and abundant gastropod shells.



Figure 3.7b. Close up of the sediment in Dolomite Lake. Small pink gastropod shells (1) and patches of desiccated *Ruppia* grass (2) can be seen. The lake has been desiccated for some time as evidenced by the multiple generations of mudcracks.



Figure 3.8a. Halite Lake in early December 1999. Note the pink tinge to the water caused by the halophylic bacteria, and the lack of grey mud. Instead the sediment is a pale brown sand with shell fragments and abundant halite.



Figure 3.8b. The core site at halite lake, showing pink tinge to the lakewater and crust of halite both on the shore and under the water.

Figure 3.8c. Top 60mm of the core, consisting of a thin crust of halite passing into 1-2mm of brown, sandy sediment. Beneath this is a uniform black sediment of fine sand texture, giving off a very strong bad egg smell.



it is fairly deep in comparison, reaching up to 1m in the centre. The water has a pink tinge, caused by the large population of halophytic bacteria (Fig. 3.8a). Despite this, the water is clear because the sediment is coarser grained so is less easily disturbed by wave action.

Differences in hydrology, vegetation and chemistry cause the sediment infill to be distinct from the other lakes in the chain. Halite crystallisation is common both on the shoreline and under water cover on the lake-bed (Fig. 3.8b). Beneath this halite layer there is a very thin (mm scale) brown sand layer which, at its base, abruptly passes into a uniform jet-black layer (Fig. 3.8c). This persists as far down as could be cored (around 1m) and smells very strongly of hydrogen sulphide. No grass or microbial material is observed but the colour and smell indicate that the sediment must have a significant organic content. The mineralogy of this lake is significantly different to those previously described, being dominated by halite, aragonite and Mg-calcite with a little quartz and gypsum (see Section 3.3.7 & Appendix 1).

3.2.7. North Stromatolite Lake

North Stromatolite Lake (Figs 3.9–3.11) is situated around 200m south east of Pellet Lake and can be accessed via a low-lying corridor of land running from the south east corner of Pellet Lake. However, this route is rather overgrown and easier access was found via a wide, low-lying area running east-west from the lake to the loop road. This used to connect the lake, and indeed the entire chain, to the Coorong lagoon during the early Holocene (Rosen *et al.*, 1989).

During the 1998 field season the lake was relatively full, no stromatolites were exposed and only a small amount data were collected. However during the November/December 1999 season, the lake became completely desiccated exposing impressive stromatolitic structures (Fig. 3.11) and also the true nature of the sediment.

Desiccated stromatolites, with mudcracks, carbonate crusts and intraclast breccia mark the lake margin, together with a large numbers of *Nuculana* bivalves and *Coxiella* gastropods. The lake is large enough to be affected by wind influenced 'tides'. During one visit the northern end was seen to be quite exposed, while a few days later, with the wind in



Figure 3.9a. North Stromatolite Lake, mid-November 1999. Once dry, the sediment becomes sandy in both texture and colour. Pale grey mud only occurs in the most recently desiccated areas and polygonal cracking is rare. This is in sharp contrast with the dolomitic lakes.

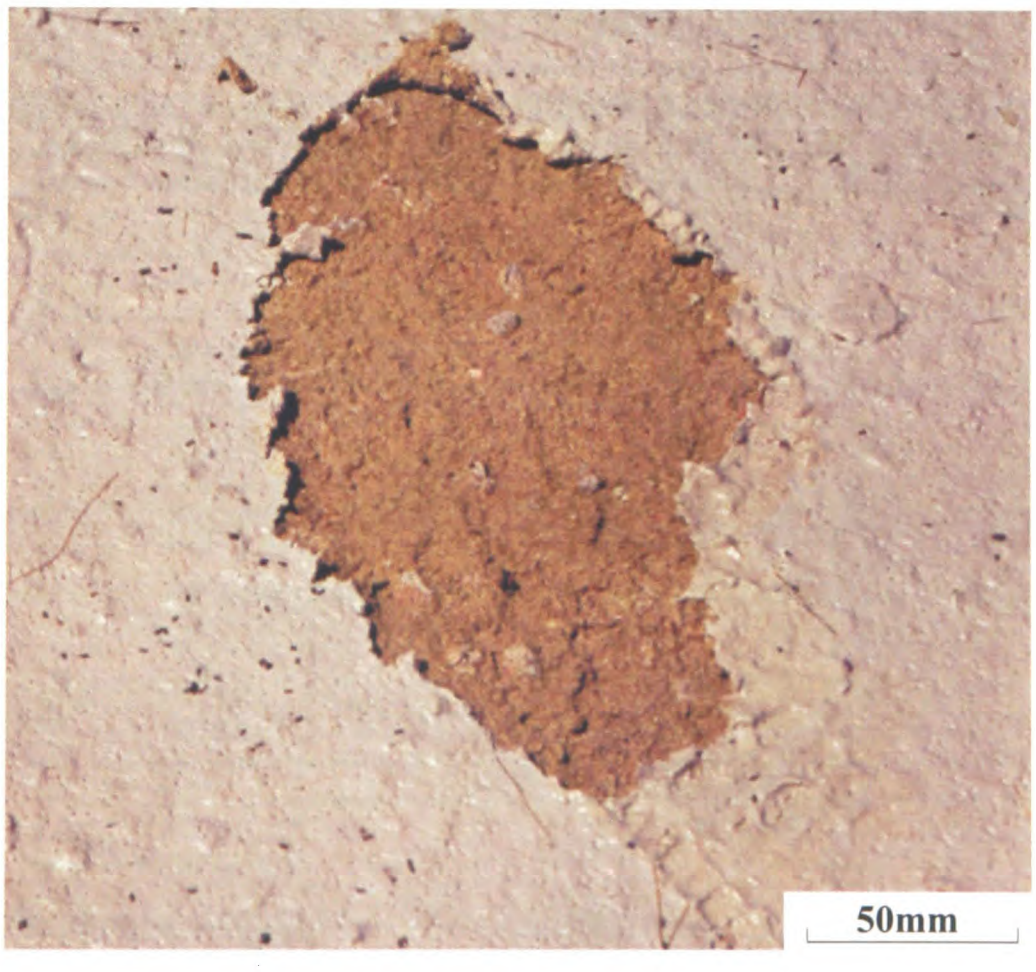


Figure 3.9b. Close up of the sediment in a newly desiccated area of North Stromatolite Lake. A very thin (<10mm) layer of damp, grey, sticky mud is soon replaced by sandy sediment with small shell fragments and rare strands of grass.

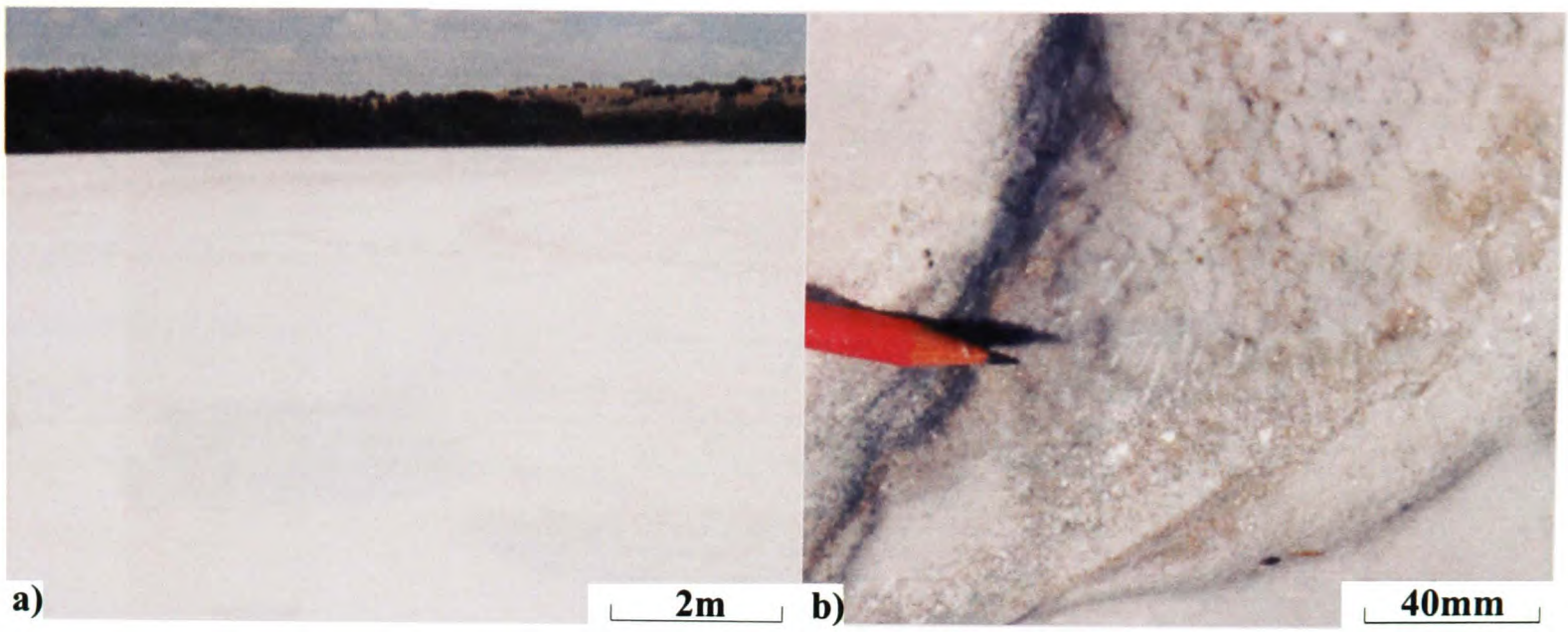


Figure 3.10a-b.
a) North Stromatolite Lake in early December. The lake is dry with a 1-2cm thick crystalline coating, resembling snow. This is composed mostly of small cubes of halite and can be walked upon without fracture. b) Close up of the crystalline surface with pencil point indicating dove tail gypsum crystals on the edge of a footprint; the rest of the footprint comprises cubes of halite.







Figure 3.10c-e.
Three examples of bioturbation of the sediment by macrofauna in North Stromatolite Lake. c) Narrow winding epichnial burrow together with abundant small shell fragments in sandy sediment. d) Branching epichnial burrow in dry mud. e) Narrow curved epichnial burrow in wet surface mud. No such traces of animal activity are found in the dolomitic lakes.









Figure 3.11 a-d.
Stromatolites / microbial mats from North Stromatolite Lake (see text for details).

the opposite direction, a large area in the south of the lake was exposed. The exposed sediment is much more compacted than in other lakes and large areas show ripples. There is a thin layer of slimy, grey mud, less than 10mm thick, which then passes into a light brown sediment of sandy texture (Fig. 3.9b). Evidence of animal activity in the surface sediment was common (Figs. 3.10c-e), though there is little or no *Ruppia* grass anywhere on the lake-bed. With further desiccation, this grey appearance disappears and the majority of the lake takes the appearance of a 'beach' with compact sand and rare shell fragments; grey rubbery stromatolites protrude upwards from this brown sediment. Polygonal cracking is rare except at the margins, which appear to be exposed all the year round. In areas covered by water, the sediment was variable; some areas were composed of yoghurt-mud (this was more waterlogged than seen in other lakes and of a dark grey to black colour) and some of pale brown carbonate sand. The mineralogy of the sediments in this lake is mainly aragonite with some hydro-magnesite and Mg-calcite present as minor carbonate phases (see Section 3.3.8 & Appendix 1).

Interestingly, at the beginning of December, a large proportion of the lake dried up very quickly, taking the form of a thin crust of tiny cubes of halite (Fig. 3.10a - it looked like it had snowed). In certain areas, such as old footprints, gypsum also crystallised (Fig 3.10b).

In the northern part of the lake, large columnar stromatolites (vertically stacked hemispheroids) were common, reaching around 0.4m in height with individual columns more than a metre in diameter (Fig. 3.11a). These were unlithified and rubbery in texture, being composed of a very fine grained carbonate mud. The internal morphology consists of numerous centimetre scale vugs connected by fairly continous, gently wavy, millemetre scale laminae. A close up of the top surface (Fig. 3.11c) reveals a small-scale knobbly, wave-like pattern, presumably resulting either from wave action of the lakewater, or wrinkling of the mat itself during desiccation. Walter *et al.* (1973) describe stratiform stromatolites with very similar internal morphology built by the cyanophyte *Microcoleus chthonoplastes* in this area, though they do not describe a columnar variety. Around the edges of the lake, low globular stromatolites are common (Fig. 3.11d); these have a dark rubbery texture despite having been dry for some considerable time. Abundant *Coxiella* shells are trapped within the nodules and their morphology is superficially very similar to the globular stromatolites described by Walter *et al.* (1973) built by *Schizothrix splendida*. The most common structure observed in this lake is a blistered microbial mat (Fig. 3.11b), varying in texture between rubbery and crusty

depending on the extent of desiccation. These are only a few centimetres thick but laterally occur in large areas, up to 100m^2.

3.2.8 South Stromatolite Lake

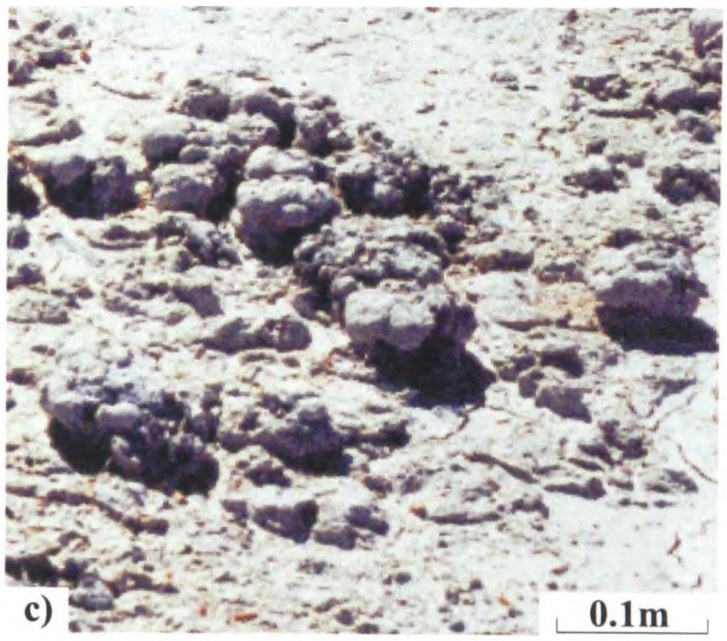
South Stromatolite Lake lies 16km south of Salt Creek immediately adjacent to Mini Dolomite Lake. Indeed the only thing which separates the two lakes is the access track to Chinamens' Well. South Stromatolite Lake is a large narrow Lake, over 1km in length north to south but only a couple of hundred metres in width. It has many similarities to North Stromatolite Lake, suffering the same 'tidal' influence, and exhibiting similar evaporative patterns.

During the 1998 field season it still contained much water and the whole northern part was inaccessible. It was noted that the water was very milky, that gastropod and bivalve shells were common over much of the lake bed and that there was much less *Ruppia* grass in the lake compared to the adjacent Mini Dolomite Lake.

In November/December 1999 the lake was much dryer and the northern part revealed impressive stromatolite structures (Fig. 3.12). Large columnar stromatolites (Fig. 3.12a) are less common than in North Stromatolite Lake, but smaller equivalents (50-100mm high) are common in the area of the lake that undergoes desiccation at the very end of the evaporative cycle (Fig. 3.11b). Globular stromatolites (Fig. 3.12c) and blistered/pustular mats (Fig. 3.12d) are again common and slightly better developed than in North Stromatolite Lake. They are mostly rubbery in texture and a transverse cross-section reveals concentric growth patterns. A fifth variety of stromatolite is seen in marginal areas of the lake, consisting of 20-30mm high colonies called 'mesas', each residing on its own mud polygon, separated by jagged cracks (Fig. 3.12e). These are identical to the stratiform stromatolites described by Walter *et al.* (1973) composed of very fine grained carbonate mud trapped by *Microcoleus chthonoplastes* with gently waving continuous laminae. They have a hard rubbery top surface and are just solid enough to walk on without sinking into them.









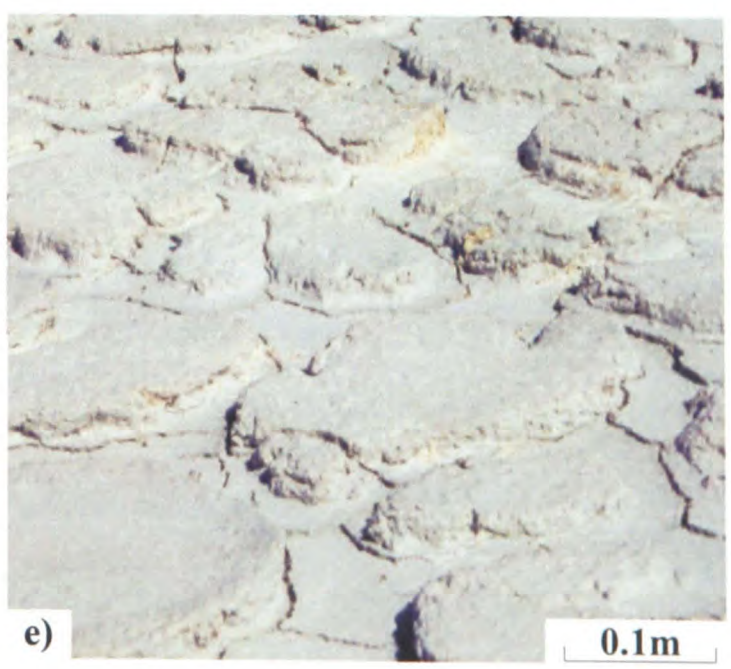


Figure 3.12 a -e. Stromatolites from South Stromatolite Lake (see text for details)



Figure 3.13. Vegetation of the Coorong region.
a) *Salicornia australis* (Samphire), common on the very edges of the lagoon and lakes.
b) Beaded Glasswort (also a Samphire), often denotes the shoreline of the ephemeral lakes.
c) Dryland Tea Tree, medium tree with cream flowers.
d) Saltwater Paperbark, bark peels off in long strips, often fringes the ephemeral lakes.
e) Silver Saltbush, 1m high shrub adjacent to the lakes.
f) Coastal Daisy, dune stabilising medium shrub.
g) Soap Mallee Tree, common on eastern side of the Coorong.
h) Pink Gum Tree, stunted tree with white flowers.
i) Bower Spinach, prostrate undershrub with small yellow flowers.
j) Coast Beard Heath, stiff upright medium shrub with flowers arranged in spikes.
k) Needle Bush, sparse stiff shrub up to 2m high.

The sediment is of similar character to North Stromatolite Lake, with large areas of carbonate sand and shell fragments around the lake margins. This is interspersed with stromatolite mounds embedded in grey, polygonally cracked mud. Towards the centre of the lake grey yoghurt-like mud takes over as the dominant constituent, this ranging from 5 to 100mm in thickness, depending on length of exposure. Beneath this, carbonate sand persists to a depth of at least 0.5m and probably below. Mineralogically, aragonite is the dominant carbonate phase with hydro-magnesite and Mg-calcite also common (see Section 3.3.9 & Appendix 1). The last residual pools of water see halite and gypsum crystallisation, although this is soon washed and/or blown away.

3.2.9. Summary of Lake Characteristics

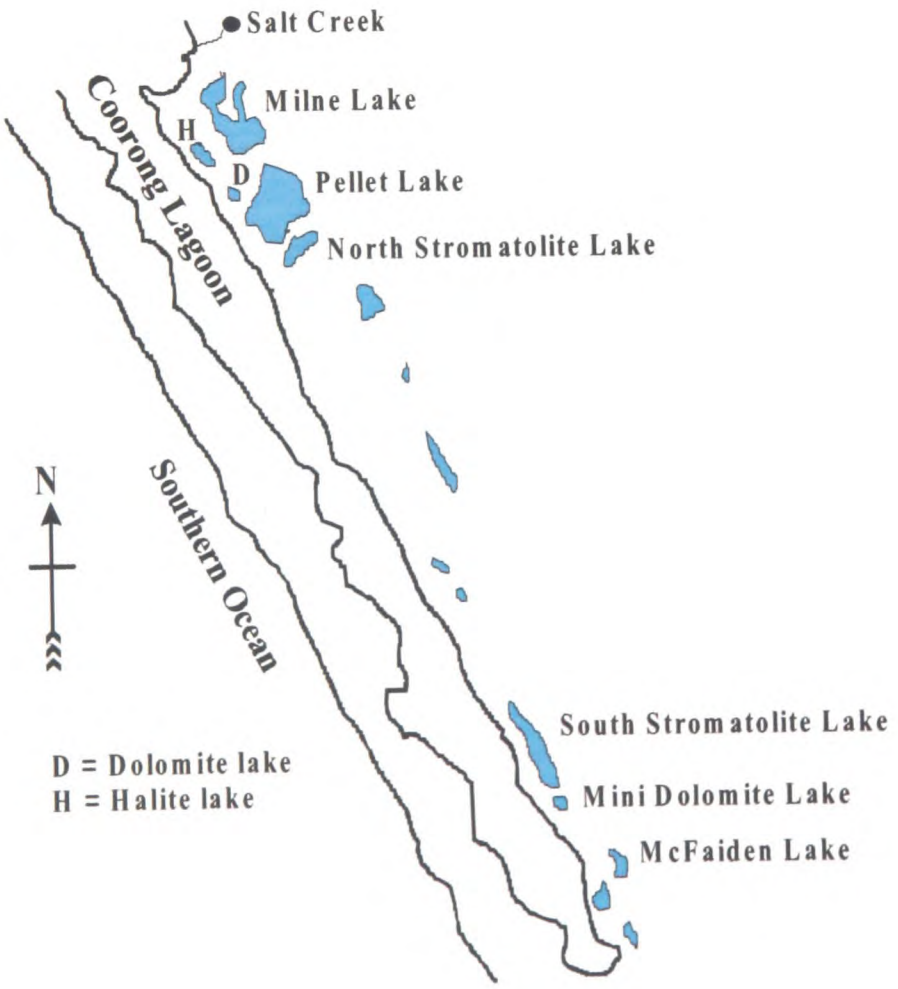


Figure 3.14. Summary of study lake locations.

	Milne	Dolomite	Pellet	Mini Dolomite	McFaiden	Halite	North Strom.	South Strom.
Dolomite	✓	✓	✓	✓	✓			
Aragonite						✓	✓	✓
Magnesite	✓							
Hydro-magnesite			✓				✓	✓
Mg-calcite						✓	✓	✓
Gypsum						✓	Rare	Rare
Pellets			✓				✓	
Strom-atolites							✓	✓
Microbial mats	Occasional	At margins	Lithified at margins	At margins	At margins		✓	✓
Dried up totally?	✓	✓		✓	✓		✓	✓
***Ruppia* grass**	✓	✓	Rare	✓	✓			Rare
Dominant texture	Mud	Mud	Mud	Mud	Mud	Sand	Sand	Sand
Animal activity			? (pellets)				✓	✓

Table 3.1. Summary of the physiography, sedimentology and mineralogy of the study lakes (all data from this study).

3.3. MINERALOGY / PETROGRAPHY

3.3.1. Methodology

Mineralogy was investigated using scanning electron microscope (SEM) analysis and confirmed by X-ray diffraction (XRD). Sediment for SEM analysis was extracted directly from cores collected during the 1999 field season. Sediment from two different depths, 10mm and 50mm, was chosen from each core as a comparison. These slices were isolated and then gently dis-aggregated using a jet of distilled water. Cover slips were prepared in triplicate for each sample; sediment was then pipetted onto each of these cover slips and then left to settle and dry on a petri dish. A photographic settling agent was added in some instances to aid this process. Once dried, the cover slips were mounted on 15mm stubs and gold coated. The stubs were viewed on a JEOL JSM-840A SEM, with Link ISIS Lab-book software and Semaphore photographic facility. It had an accelerating voltage of 20kV, a beam diameter of $< 0.5\mu m$ causing an excitation diameter of $< 3\mu m$, the images being generated by secondary electrons. Elemental analysis of the sediments, to obtain mineral stoichiometry, was performed on specially prepared polished powder sections, mounted in resin and carbon coated. These were viewed and analysed on the SEM, using a cobalt standard, calibrated for a beam current of 6×10^{-9} amps. This method has limitations because of the grain size of the sediments. Many of the studied grains were smaller than the excitation diameter created by the beam and so the resultant spectra may have had some interference from adjacent grains. For this reason multiple analyses were performed on each sample to obtain an accurate picture of mineral stoichiometry.

Sediment for use in XRD analysis was extracted directly from various cores obtained in both the 1998 and 1999 field seasons. The sediment was dried and very gently dis-aggregated to ensure crystal structure was maintained. Powder X-ray diffraction was first carried out on a Philips HT, Generator Model PW 13 20/00 at the Department of Earth Sciences, University of Oxford, using a Detector Model PW 1050. This machine was a number of years old and mineral identification had to be done manually; it was shut down during 1999. Subsequently samples were analysed on a Philips PW 1716, Generator Model PW 1729, Detector Model PW 1050/25 at the Department of Geology, University of Leicester. Here a computer program produced digital XRD traces and mineral matches, which speeded

up the process. The results of XRD analysis are given in Appendix 1, whilst representative atomic spectra and mineral stoichiometries are shown in Appendix 2.

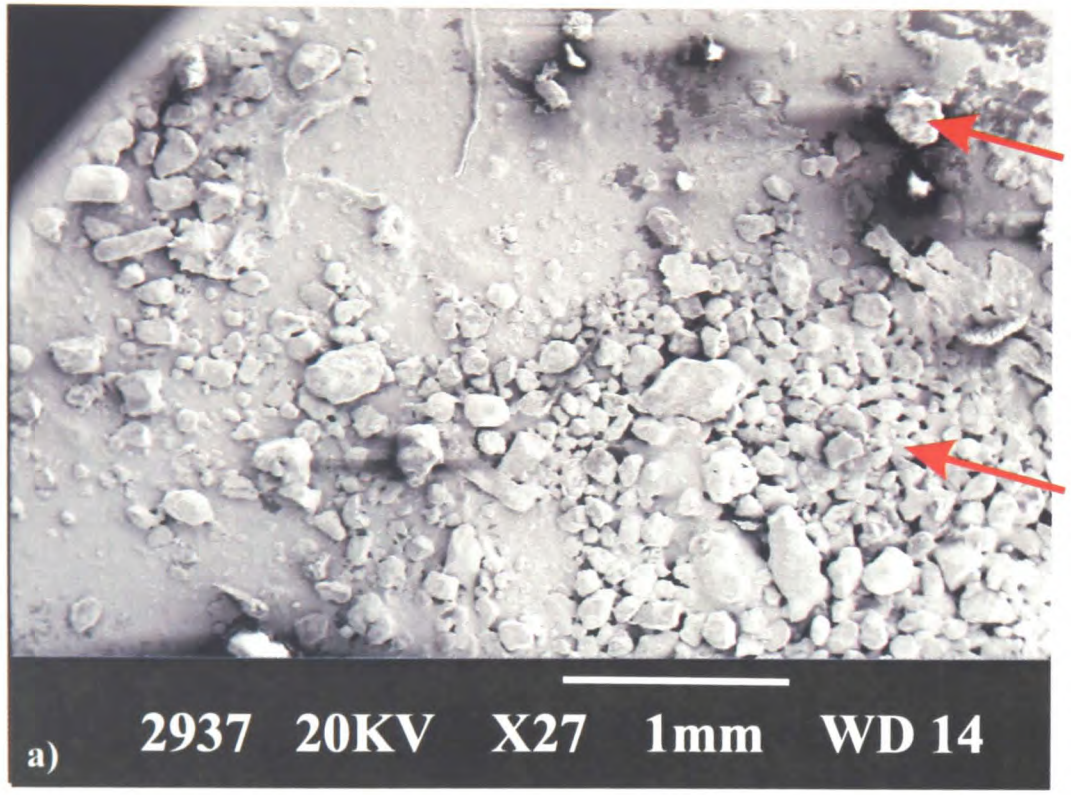
3.3.2. Milne Lake

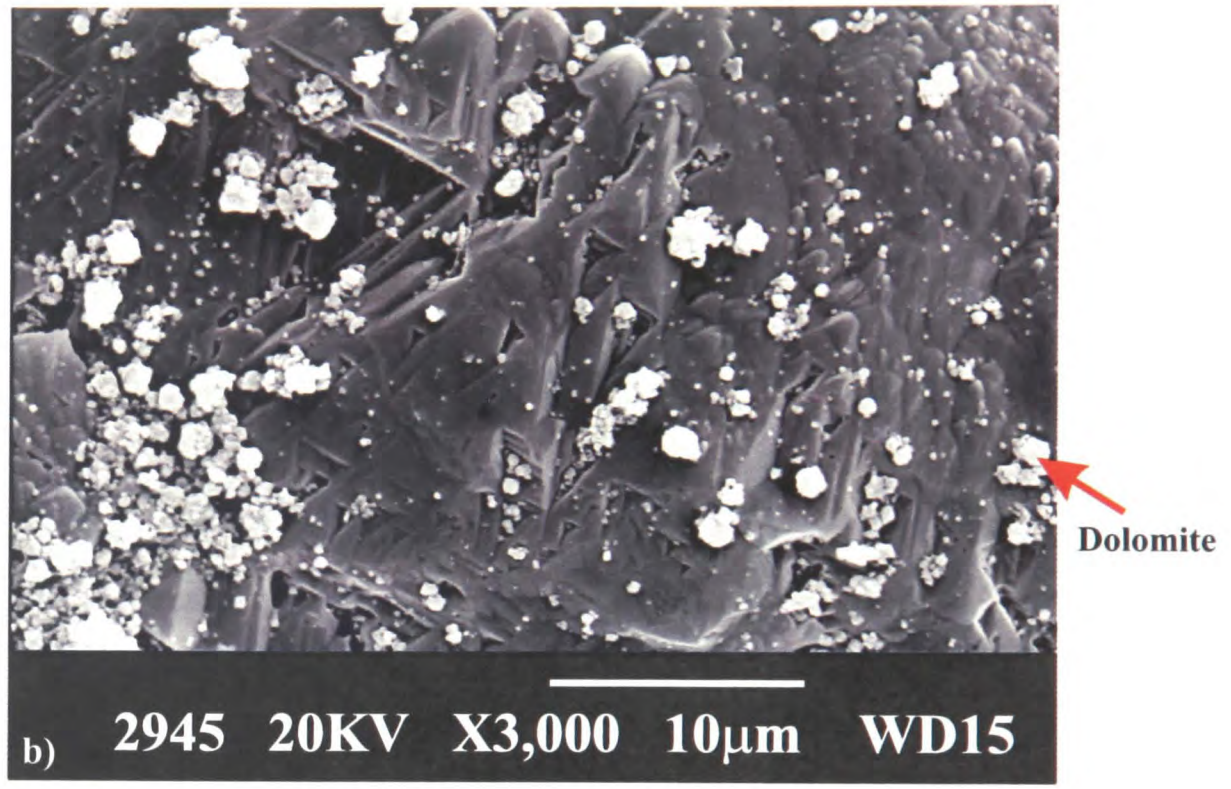
The mineralogy of the sediment in Milne Lake is dominated by dolomite, while halite is common as a thin crust during the latter stages of desiccation. Quartz is also common as is Magnesite (see Appendix 1).

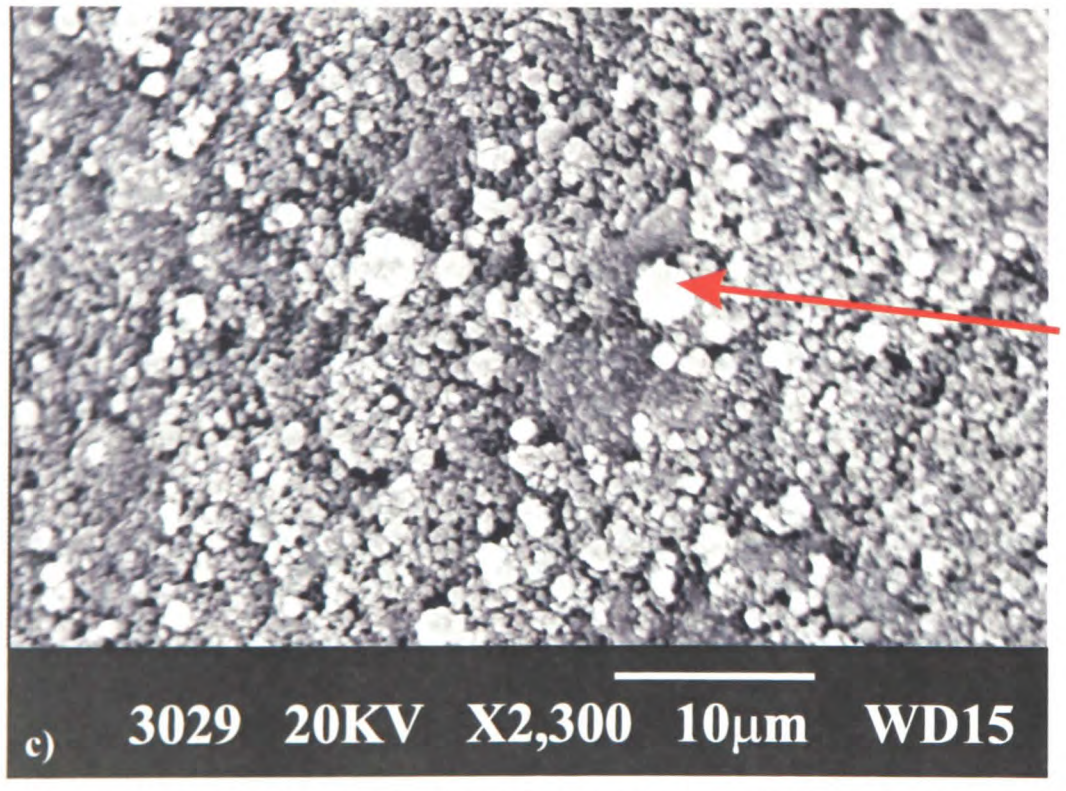
The sediment extracted from the top c.10mm of Milne Lake is shown under SEM analysis in Figure 3.15. Quartz is present comprising up to 15% of some samples, occurring as angular grains up to 0.5mm in size, along with more rounded 'grains' of dolomite of similar size (Fig. 3.15a). On closer inspection it can be seen that some of the quartz grains are partly covered in dolomite spherules (Fig. 3.15b), and the 'grains' of dolomite are in fact composed of thousands of tiny sub-micron spherules (Figs 3.15c&d).

The stoichiometry of the dolomitic sediment associated with the quartz grains is magnesium rich, with compositions up to 70% $MgCO_3$; these compositions are not found in any other lake. Similarly, the 'grains' of dolomite have Mg-rich compositions, ranging from 60% $MgCO_3$ to 90% $MgCO_3$ with the most common being around 70% $MgCO_3$ (see Appendix 2 (Table A2.1 and Figs A2.1+A2.2)). The Mg enrichment in this lake is in excess of any found in any of the other dolomitic lakes, often approaching the composition of the mineral Huntite ($Mg_{0.75}Ca_{0.25}CO_3$), although this does not appear on the XRD analysis. Aggregation of dolomite spherules is relatively rare at the surface, but some clumping does occur forming larger sub-spherical objects, 1-3μm in diameter (Fig. 3.15c).

At 50mm depth a greater proportion of the sediment is dolomite. Large quartz grains are less common, and/or more completely covered in dolomite. It is difficult to tell in some cases whether the grains are of quartz covered with dolomite, or entirely of dolomite. The sediment at this depth is more consolidated with a higher proportion of 1-3μm sub-spherical aggregates of crystals. The chemical compositions of both the individual spherules and the larger aggregates are very similar and vary little from that at the surface. Magnesium-rich







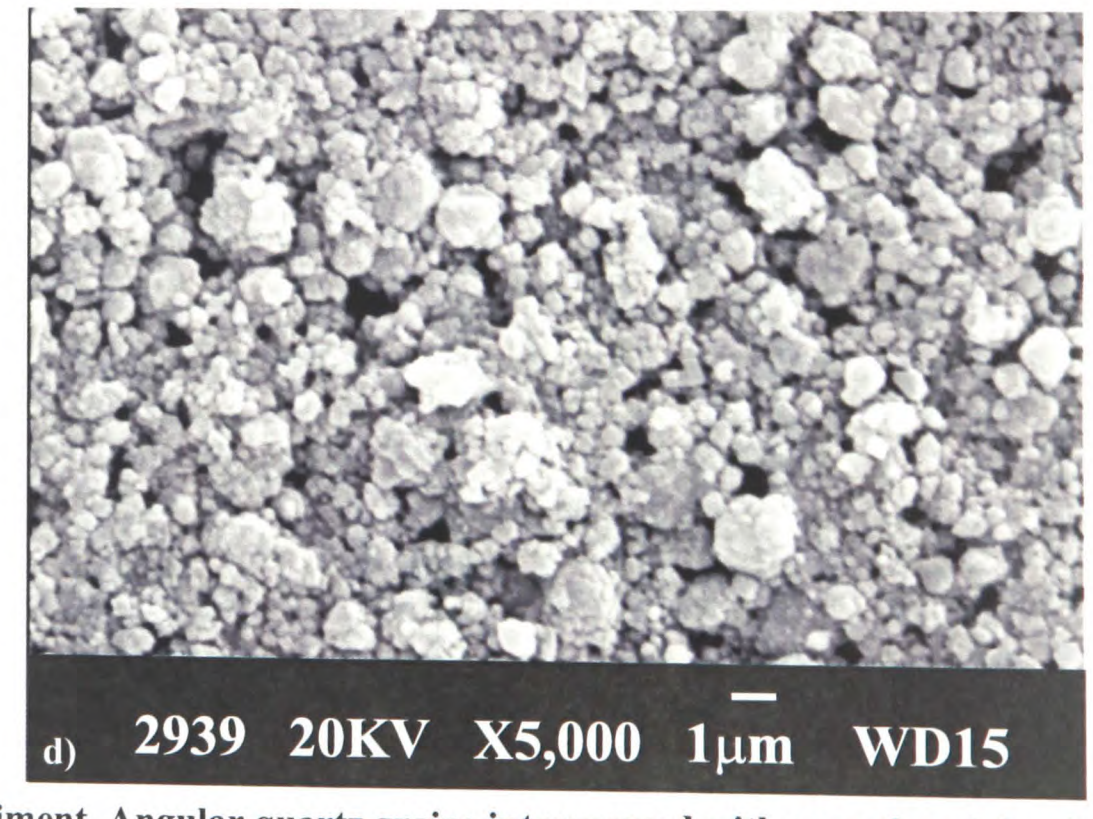


Figure 3.15. SEM images from Milne Lake. a) Quartz rich nature of the sediment. Angular quartz grains interspersed with smoother dolomite "grains" and fine powdery sediment. b) Close up of quartz grain with patchy dolomite cover. c) Aggregates of multiple spherules appearing as sub-spherical pale white objects, about 3microns in diameter (just right and just left of centre). d) An unusually calcic area at 50mm depth showing identical morphology to the more magnesium rich areas - see text for details.

grains dominate, the majority in the range of 65-70% $MgCO_3$. Only one of the areas analysed (Fig. 3.15d) had compositions a few percent more rich in calcium. Morphologically, this area is no different from the magnesium-rich areas. Principle ordering peaks for the dolomite are observed both at the surface and at 50mm depth (see Appendix 1). The degree of ordering is fairly high at the surface (approximately 75%). No discernible increase in ordering is observed with depth.

3.3.3. Pellet Lake

The mineralogy of Pellet Lake is dominated by dolomite, which appears to be the only carbonate phase found at the surface (see Appendix 1). At 50mm depth a little huntite and hydro-magnesite was found in addition to dolomite. There were also small amounts of surface halite and wind blown quartz.

Sediment taken from the uppermost layer of Pellet Lake is shown in Figure 3.16. At low magnification (Fig. 3.16a), it looks somewhat different from that in any of the other lakes, taking the form of a polygonally-cracked lumpy crust. This cracking most probably occurred as the sediment was left to dry on the slide. It mirrors the polygonal cracking seen on a larger scale in the lake when it undergoes desiccation. Under higher magnification (Fig. 3.16b), the crust is once again seen to be composed of a large number of spherules. The majority of these appear to have their grain boundaries intact but a few are coalescent. The chemical composition of these spherules is typically slightly Mg-rich, ranging from around 52% $MgCO_3$ to 68% $MgCO_3$ (see Appendix 2 (Table A2.1 and Figs A2.3+A2.4)). Occasionally there are rare grains with more Ca-rich compositions of around 60% $CaCO_3$.

Some of the crystals are more plate-like in shape, as seen in Figure 3.16b. These plates are unique to this lake and have a Mg:Ca ratio indicative of dolomite, indeed some are very close to 50:50. At very high magnification (Fig. 3.16c) many of these platelets, which themselves are not more than 1-2μm across, can be seen to have tiny spherules (< 1/10μm) adhering to them.

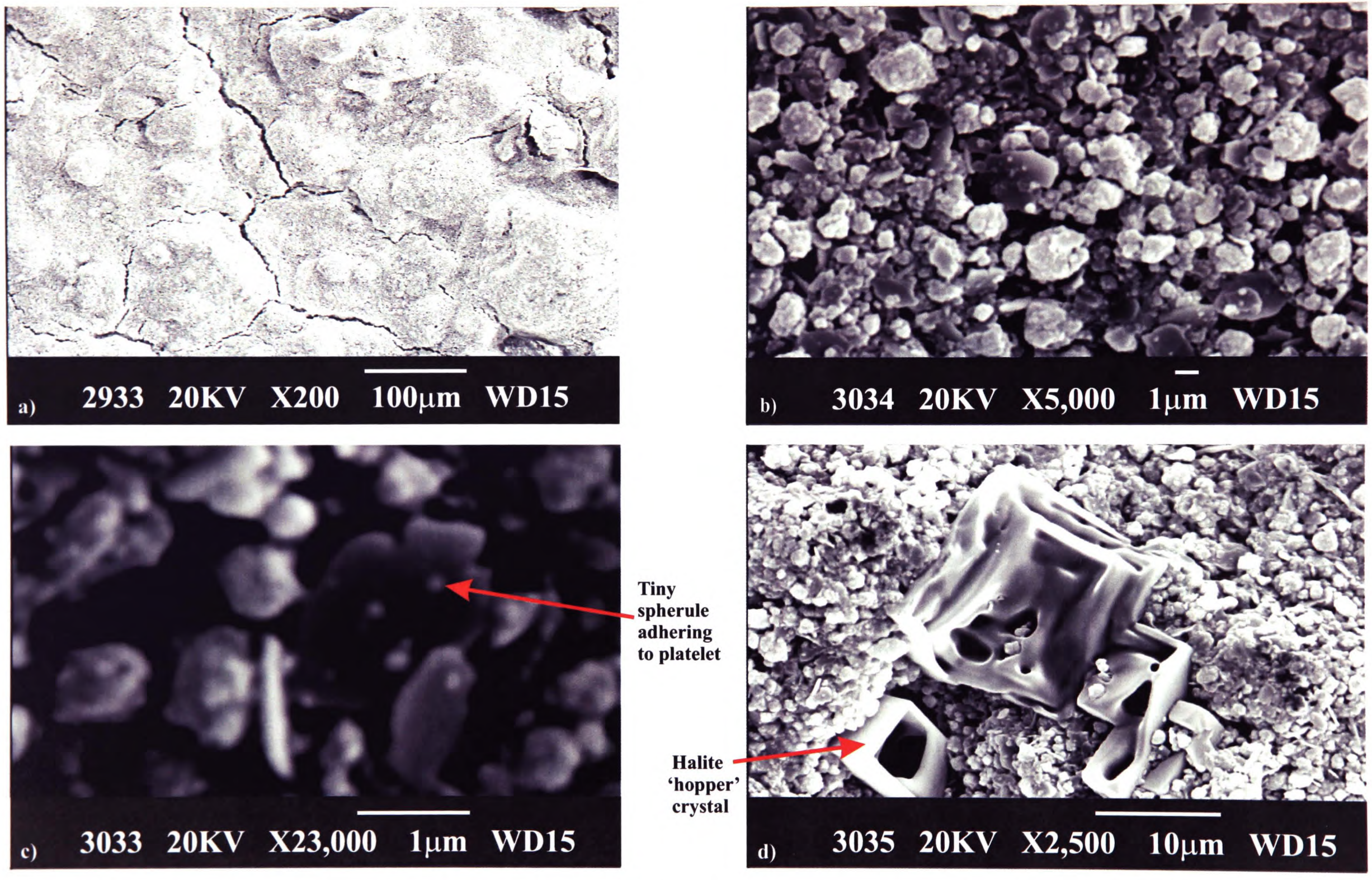


Figure 3.16. SEM images of Pellet Lake. a) Overall appearance of the sediment shows polygonally-cracked crust of small spherules. b) Many small platelets of dolomite, unique to this lake, and close to ideal dolomite composition. c) Close up of a platelet showing adherence / resorption of minute (< 0.1 micron) spherules onto its surface. d) Common halite 'hopper' crystals.

The overall appearance of sediment from 50mm depth is similar to that of the surface sediment, except that polygonal cracking is rare. Under higher magnification the sediment is unremarkable, closely resembling that at the surface. Plates with chemical compositions close to ideal dolomite are again evident, again resorbing sub-micron spherules and may be a little more common than at the surface. Occasional 'hopper halite' crystals are also observed (Fig. 3.16d), a by-product of evaporation. The dolomite from Pellet Lake does have ordering peaks but the principle ordering peak is not defined clearly enough to obtain a numerical degree of ordering (see Appendix 1).

3.3.4. Mini Dolomite Lake

The mineralogy of this lake is again dominated by dolomite, the only carbonate phase at the surface. At depth, the carbonate phase kutnohorite ($CaMn_{0.6}Mg_{0.3}Fe_{0.1}(CO3)_2$), a member of the dolomite group, may also be present in addition to dolomite. Halite and quartz are present as accessory minerals, as is celestine ($SrSO_4$) at depth (see Appendix 1).

SEM images of sediment from the top 10mm of Mini Dolomite Lake are shown in Figure 3.17. The overall nature of the sediment strongly resembles that of McFaiden Lake (Figs 3.18 & 3.19) and XRD studies (Appendix 1) have shown both to be dolomitic lakes. However, several small differences can be noted. The sediment in this lake occurs as both amorphous aggregates and distinct grains. The sediment appears to consist almost entirely of sub-micron sized dolomite crystals, and these tend to amalgamate readily into the aforementioned sprawling aggregates (Fig. 3.17b,c). A further important feature is the resorption of the sub-micron crystals into 8-10μm crystals with defined edges, seen in the centre left of Figure 3.17a. Although rare, this phenomenon occurs at a higher level (c.10mm) in the sediment column than in McFaiden Lake.

Sediment taken from c.50mm depth also shows resorption (Fig. 3.17b). Here, one can clearly see a small number of spherules in the process of being resorbed into the 10μm crystal in the centre of Figure 3.17b. The overall appearance of the sediment at this depth is of a mixture of loose dolomitic spherules, clumps of amalgamated spherules up to 100μm in size, together with a significant number of quartz grains of similar size, often partly covered with dolomite. Considerable resorption appears to be taking place at this depth because the

spherules are losing their 3D spherical nature to become more flattened and joined (Fig. 3.17c).

The chemical composition of the sediment from 10mm depth is quite wide-ranging, spanning compositions from 35% $MgCO_3$ to 55% $MgCO_3$ but the majority of grains have values around 45% $MgCO_3$ (see Appendix 2 (Table A2.1 and Figs A2.5+A2.6)). Those grains which are more Mg-rich also tend to be more consolidated, perhaps indicating some chemical substitution during crystallographic reorganisation. The chemical composition of grains at 50mm depth is commonly in the same range as at the surface. There appears to be no relationship between the size of the grains, the amount of resorption and the Mg content at this depth. The outer parts of the spherules are lighter in colour than the inner areas, as are many of the outer parts of the larger multi-spherule crystals. Fragments of grass are also observed and these are covered with dolomite spherules, suggesting an association between dolomite precipitation and organic matter. Ordering of the dolomite was investigated at 10mm and 50mm depth (see Appendix 1). Principle ordering peaks are visible at both depths and the degree of ordering increases from about 33% at 10mm to around 90% at 50mm possibly mirroring the reorganisation of the spherules into crystals with clearly defined faces.

For further comparison, sediment from c.80mm depth was viewed under SEM (Fig. 3.17d). The general appearance does not differ significantly from that at higher levels, except that rods and spicules are more common and quartz grains are absent. Some of these rods can be quite large, up to 10μm in length. The degree of connectivity between the spherules appears to be no greater than at 50mm depth, but occasional proto-rhombs are visible (Fig. 3.17d, centre); though these do not have smooth faces. The chemical composition appears similar too, with all analysed grains being slightly Ca-rich both in the individual spherules and in the more consolidated proto-rhombs. Strangely, the principle ordering peak for the dolomite appears absent from the XRD trace at this depth. This may be due to the destruction of crystal structure during sample preparation or may be a true indication of weak ordering at this depth.

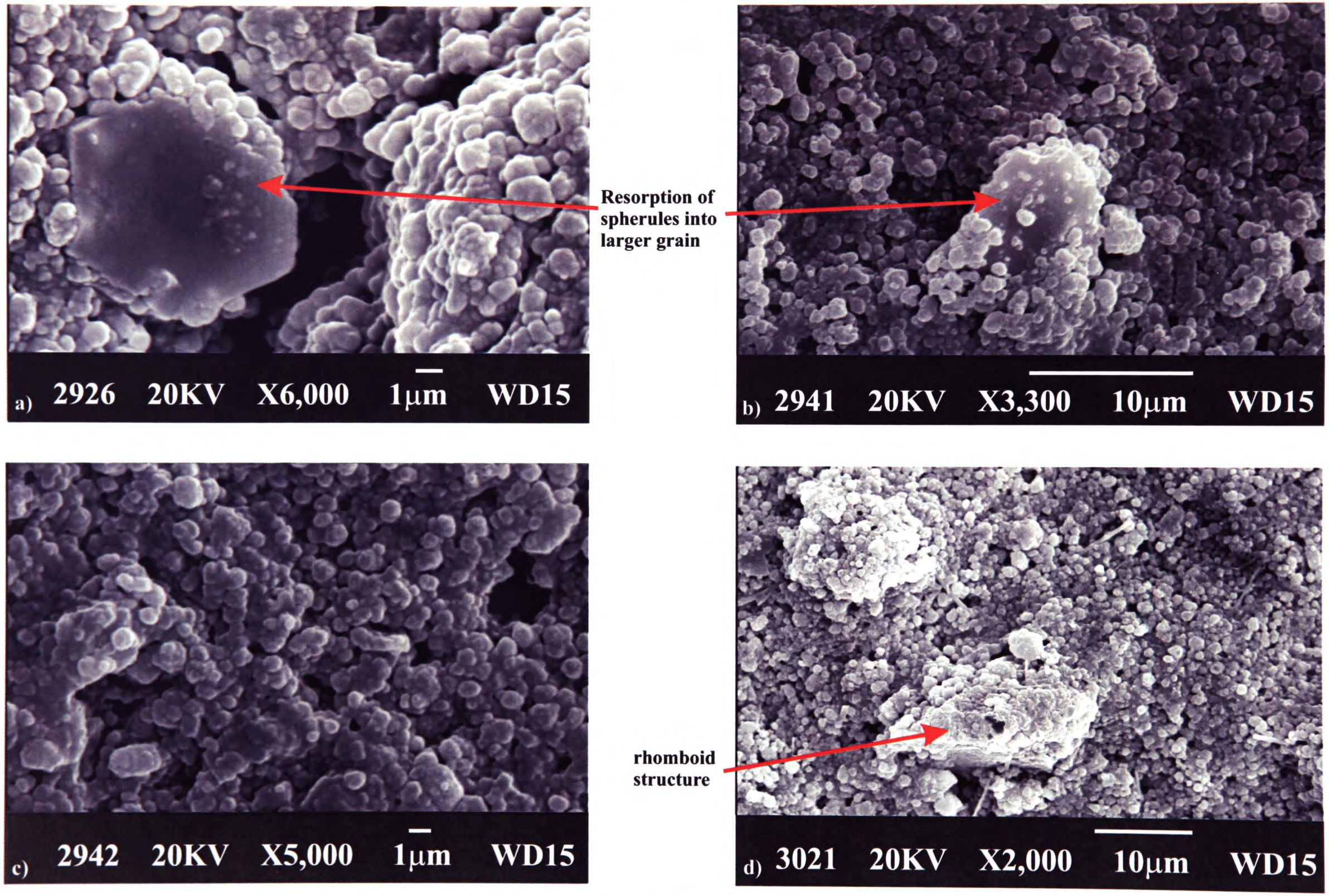


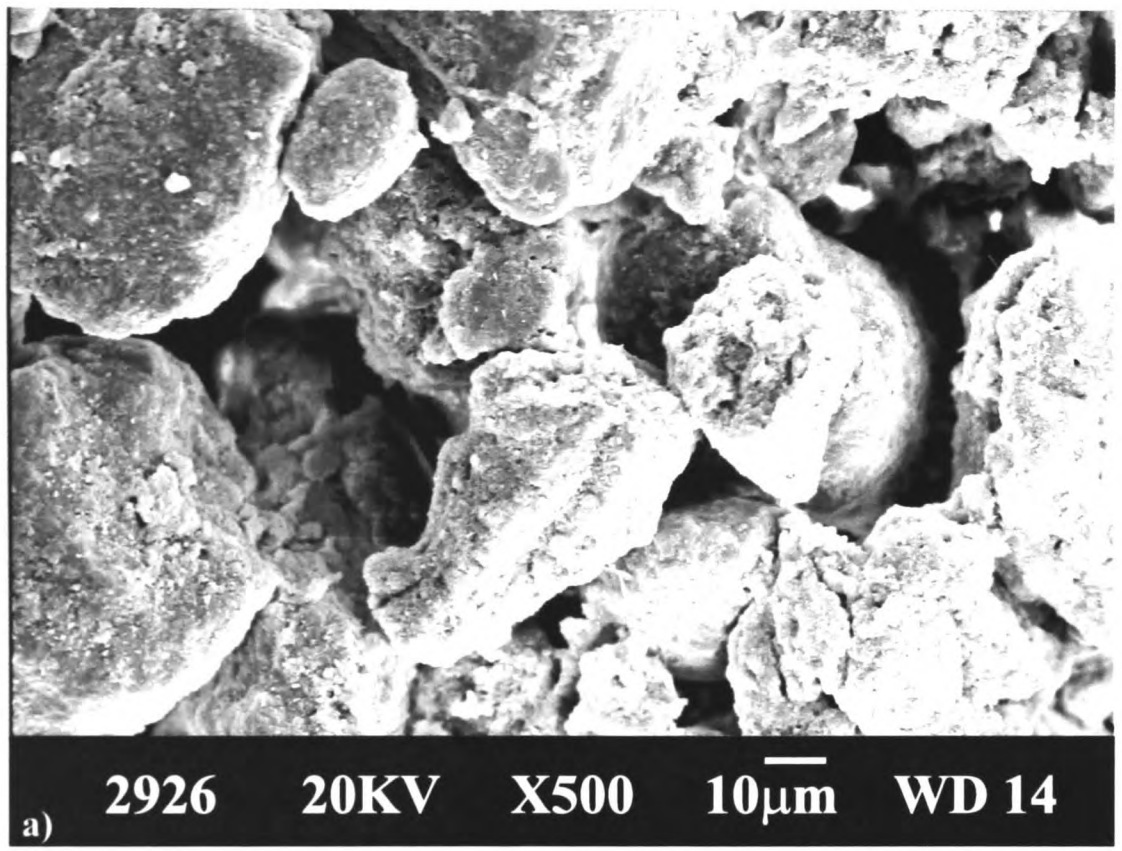
Figure 3.17. SEM images from Mini Dolomite Lake. a) Resorption of submicron grains into a large grain with defined faces (surface sediment) b) Similar resorption process at 50mm depth. c) Most spherules at 50mm depth lose individual 3D shapes and coallesce to form connected networks with smooth upper surfaces. d) Sediment at 80mm depth shows connectivity of spherules to form rhomboid structure (centre).

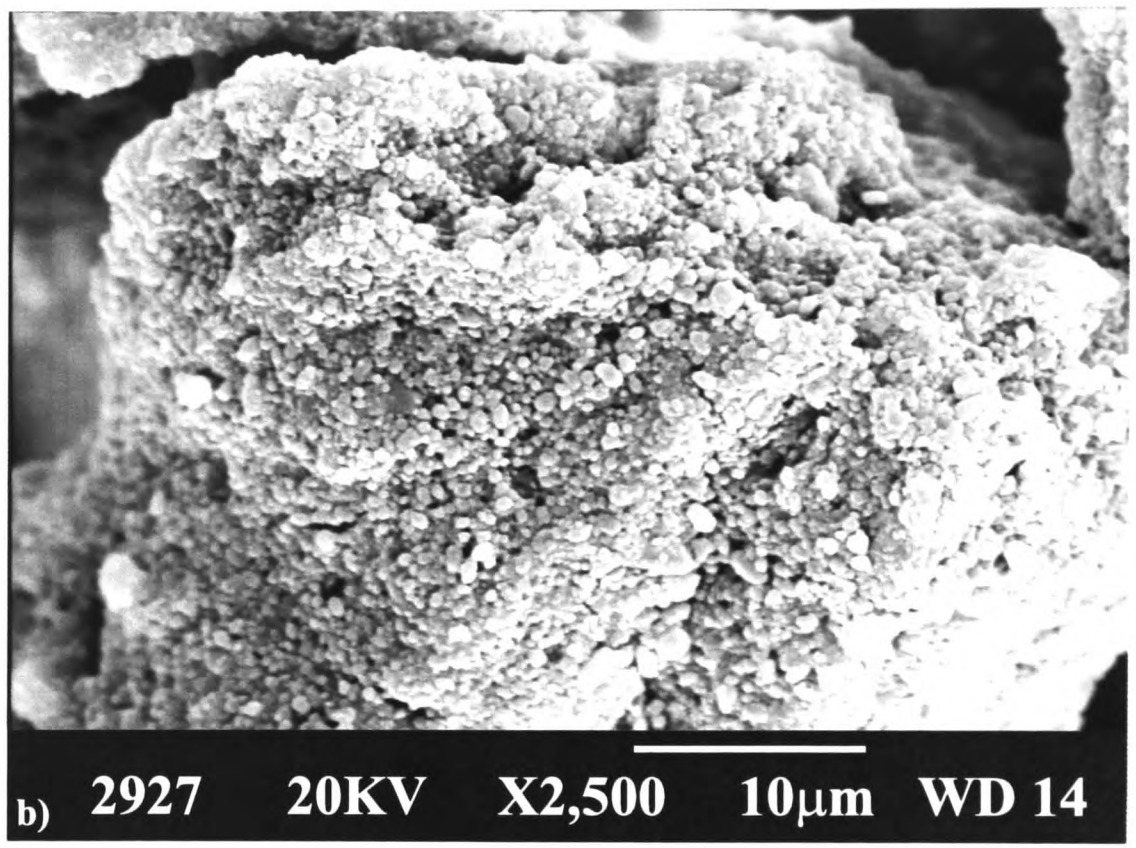
3.3.5. McFaiden Lake

The mineralogy of the sampled upper sediments of McFaiden Lake is nearly 100% dolomite, with small amounts of halite on the surface and a little accessory quartz (see Appendix 1). This lake has been reported upon the most in previous literature (e.g. Von der Borch, 1976) as it has the thickest in-fill of modern dolomite and is the most distal from the Coorong Lagoon.

Figure 3.18 shows a series of SEM images of the sediment taken from the top c.10mm of McFaiden Lake, each in turn at higher magnification. Initial examination of the sediment reveals a series of distinct 100-200μm sized grains (Fig. 3.18a). These range in shape from sub-rounded to sub angular. On closer examination, they are found to be composed of multiple sub-micron grains which are either spherical or elliptical (Fig. 3.18b). Many of these tend to be darker in the centre than around their edges (Fig. 3.18c); this may simply be an artefact of the SEM imaging, but may also suggest that the organic nanno-bacteria have acted as the nucleation sites for dolomite precipitation. The chemical composition of these sub-micron grains is fairly close to that of ideal dolomite, ranging from 45% $MgCO_3$ to 55% $MgCO_3$; the majority being slightly Ca-rich (see Appendix 2 (Table A2.1 and Figs A2.7+A2.8)). There appears to be a little heterogeneity within each large 100μm grain with some areas being a few percent more Mg-rich than others. Rarely, the sub-micron grains appear to merge with one another to form grains of around 10μm, with the beginnings of flat sides and crystal edges. Rare cubes of halite can also be observed.

Figure 3.19 shows SEM images of sediment from around 50mm depth in McFaiden Lake. Sub-micron dolomite crystals are again common, but in addition to this there are areas where the sub-micron spherules appear to be in the process of being resorbed into larger crystals (around 10μm in size) with definite, smooth crystal faces (Fig. 3.19b). There are areas where the spherules are organising themselves into a rhombic arrangement, which is the characteristic crystal shape of dolomite. The chemical composition of the sediment at this depth is much the same as in the top 10mm. Rods of dolomite up to 10μm long, with similar composition, are also observed (Fig. 3.19a) which further enhances the possibility that organic matter and bacteria are being encapsulated by dolomite. Rare, large (1mm) quartz crystals are also seen together with numerous 1-2μm cubic crystals (Fig. 3.19d) of halite





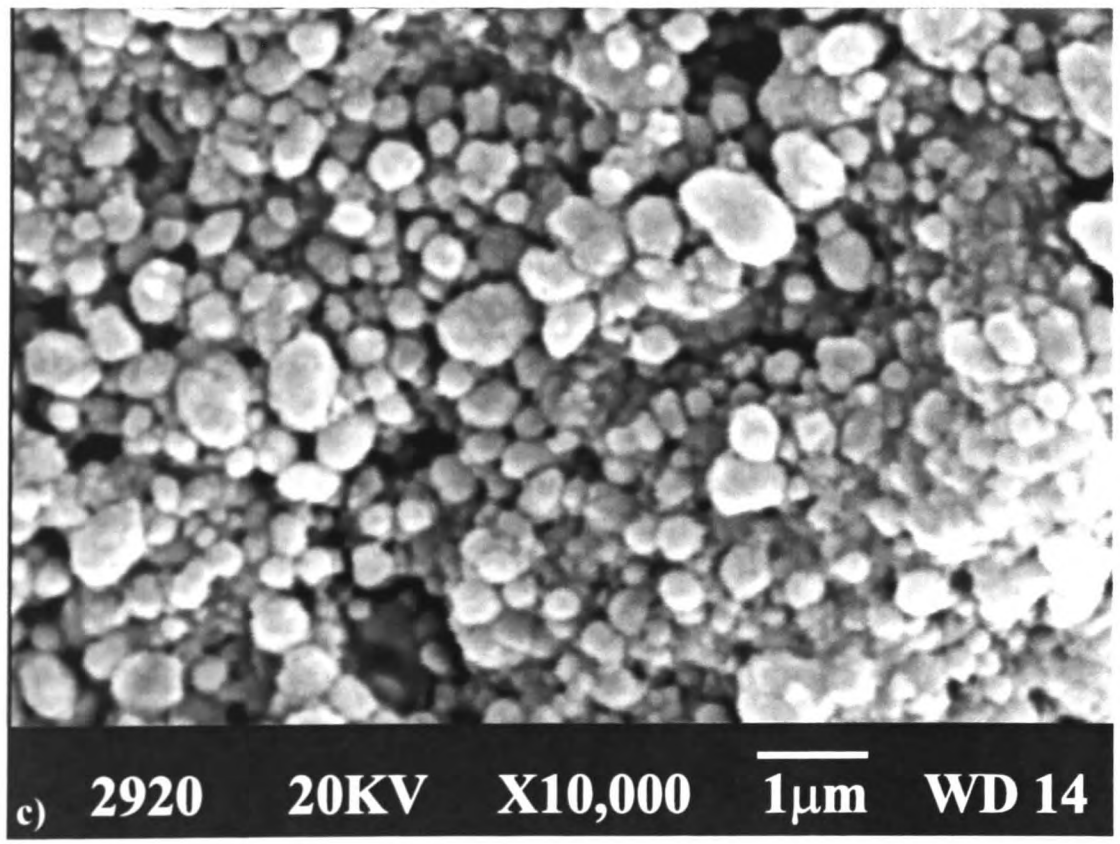
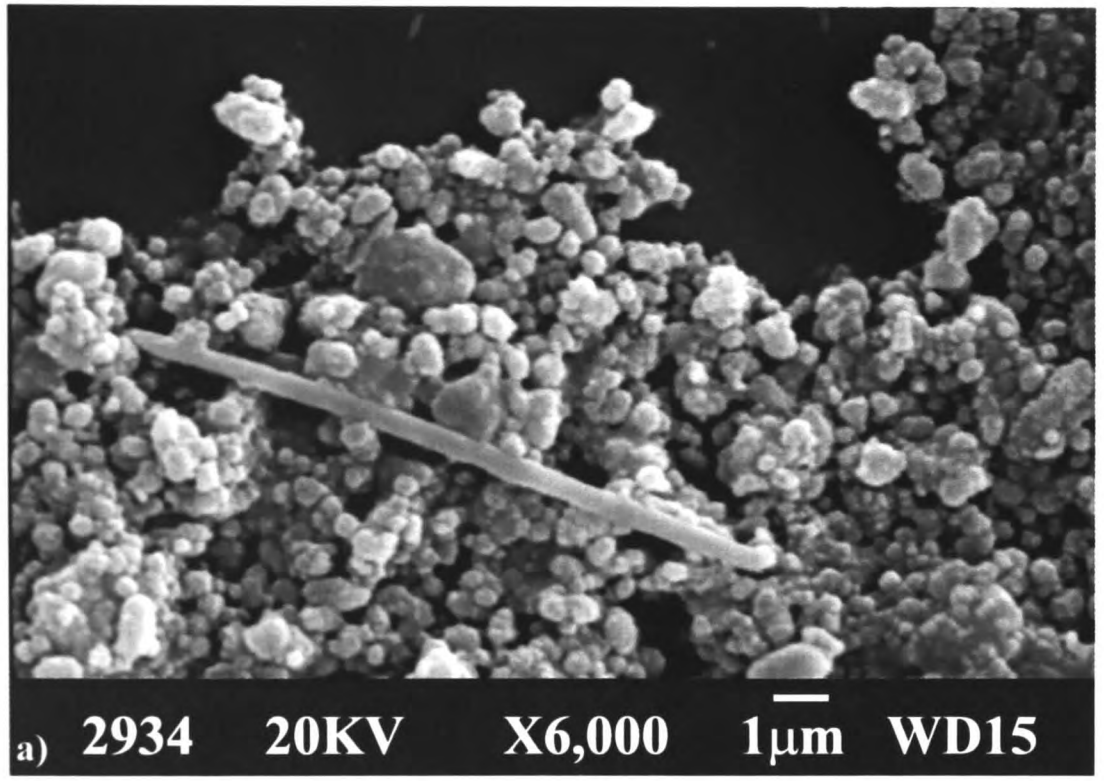
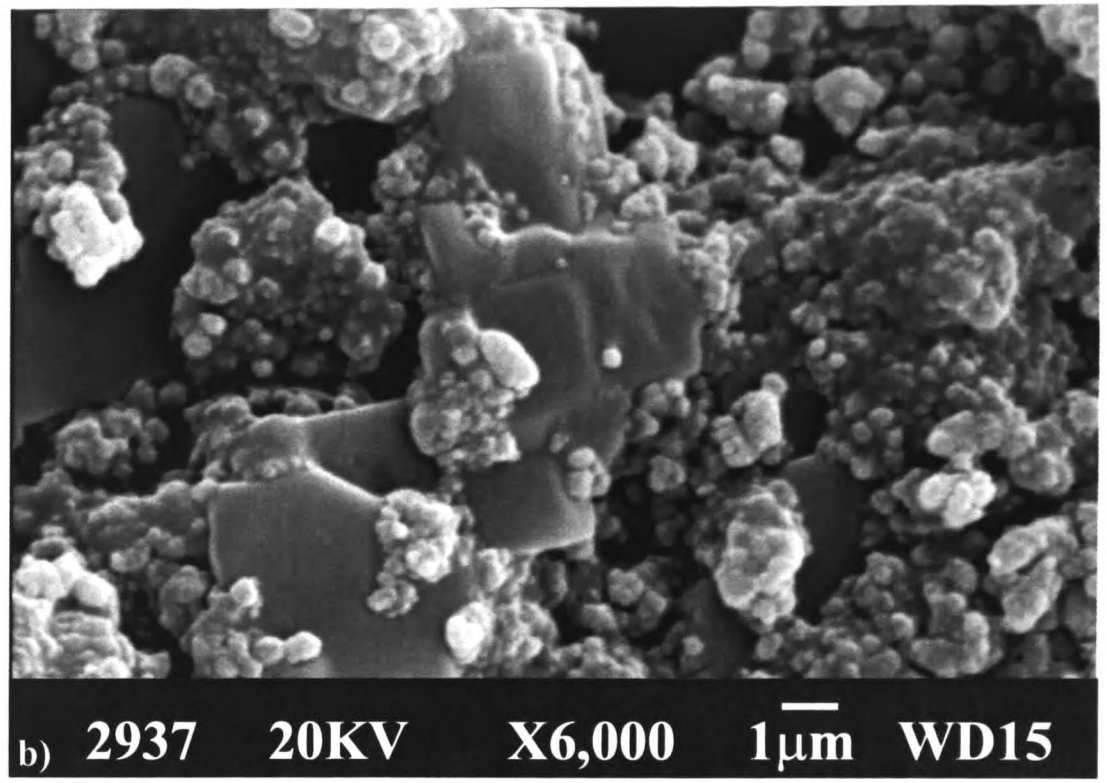
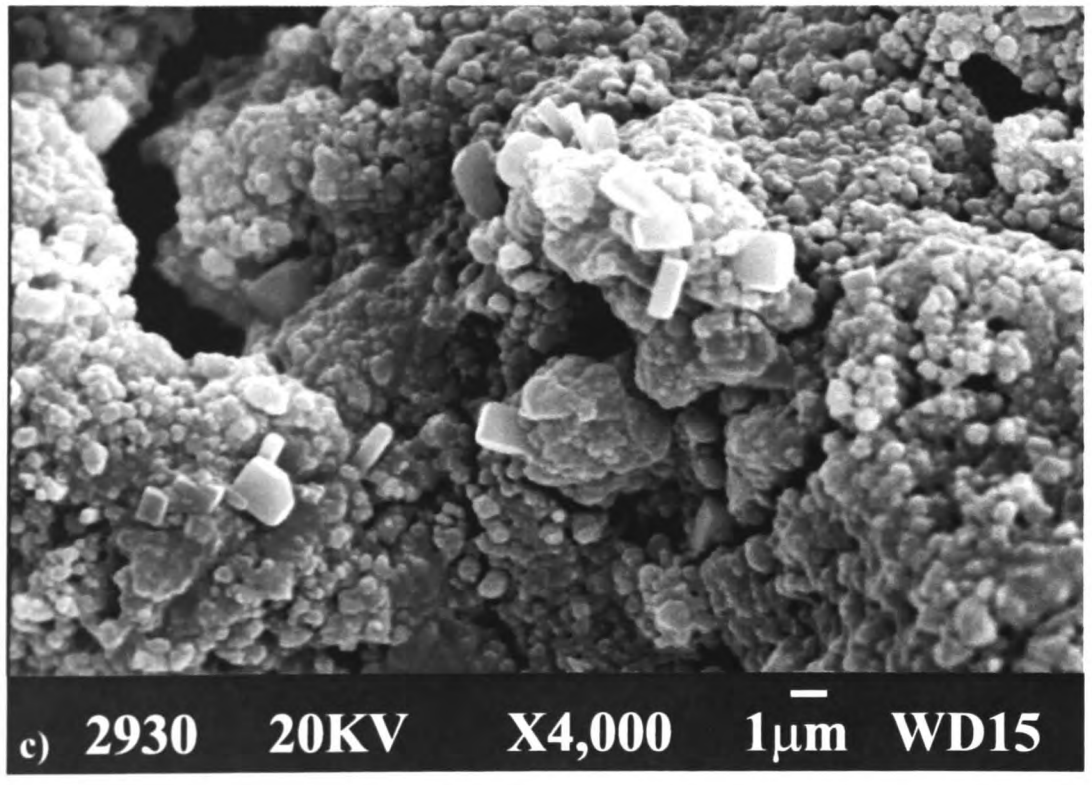


Figure 3.18. SEM images of the surface sediment in McFaiden Lake.

a) On low magnification the sediment appears to be composed of relatively small amounts of large grains, whilst on higher magnification (b) each grain is seen to be composed of multiple sub-micron spherules.
c) Individual spherules under high magnification. Note the lighter colour of the outer parts of many of the spherules, note also the coalescing of spherules in the right centre of the image.







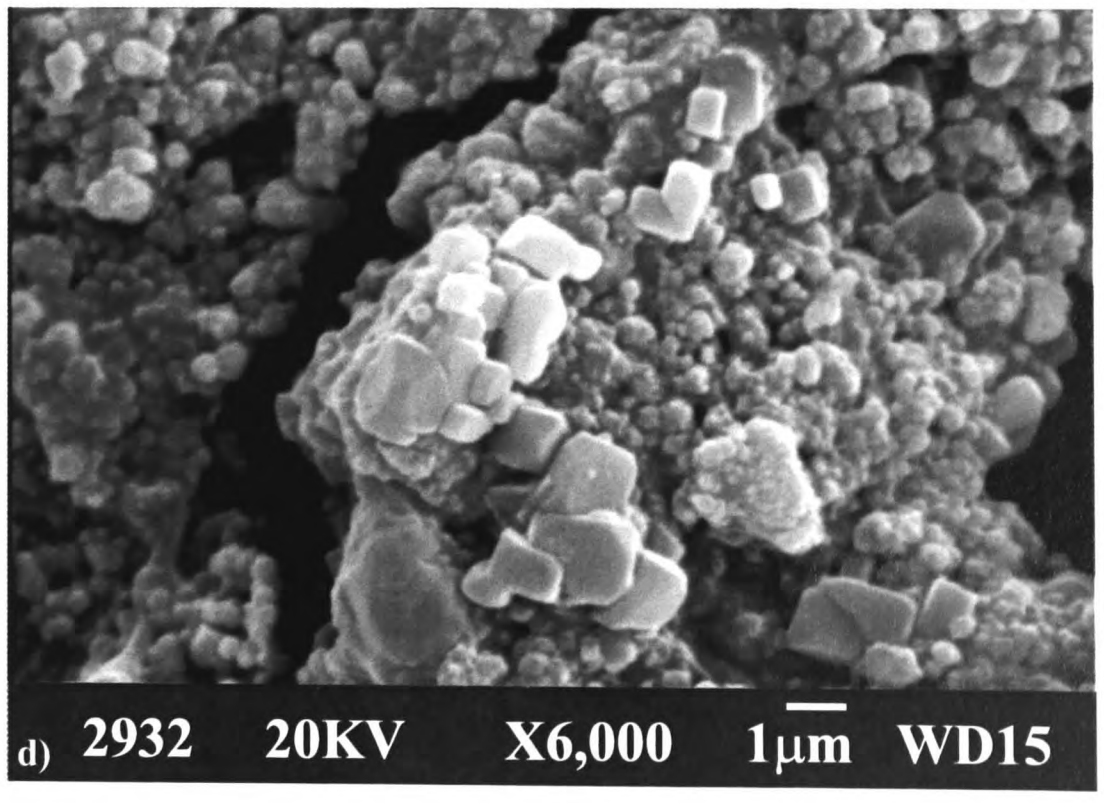


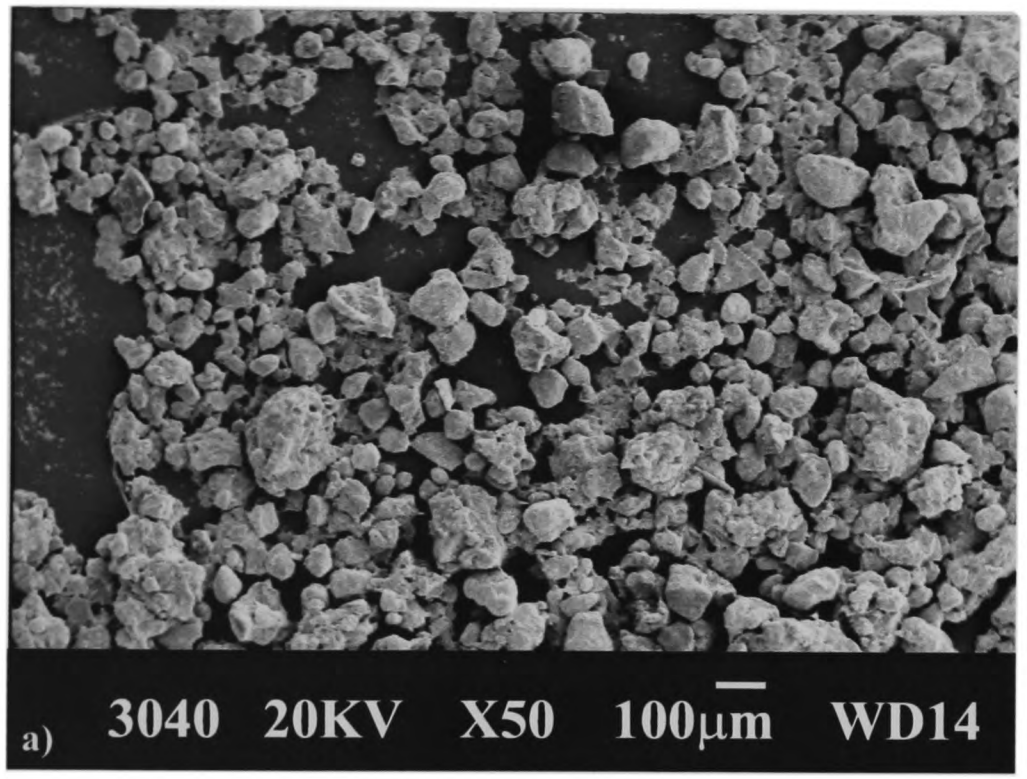
Figure 3.19. SEM images of McFaiden Lake, 50mm depth. a) Rod with dolomitic composition. b) Dolomite spherules being resorbed into larger crystal with smooth faces (centre and bottom left). c & d) Dolomite spherules coallescing and losing their individual shape. Note also bright grey-white cubic halite crystals (composition obtained from atomic absorption spectra).

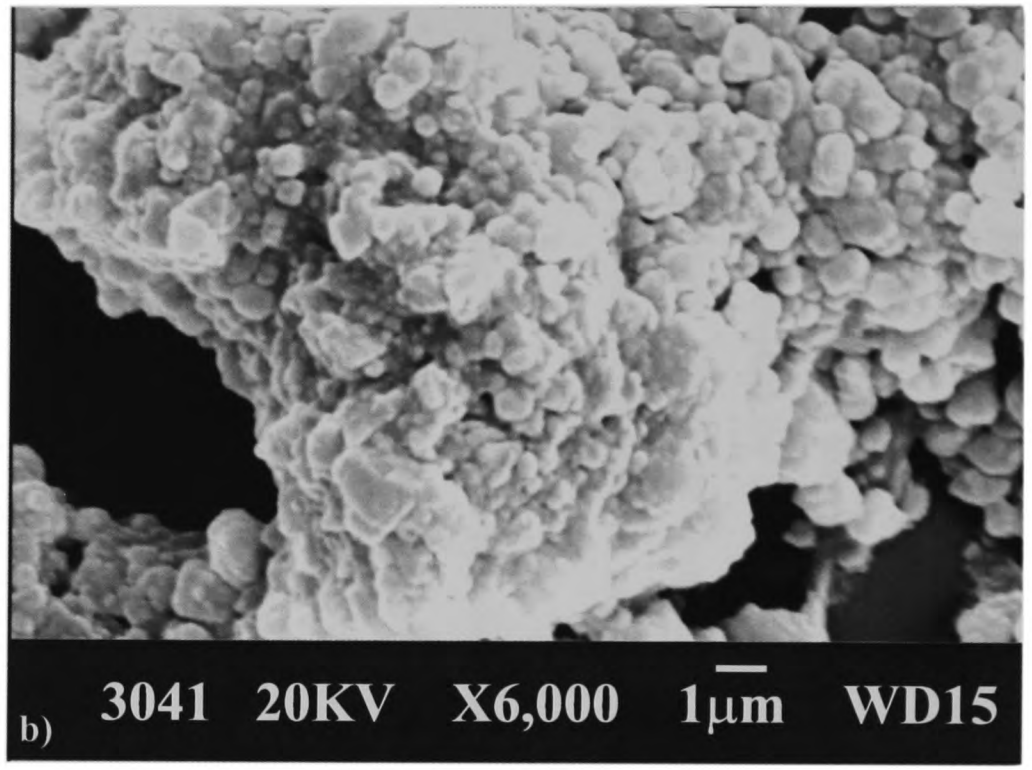
composition. Ordering peaks for the dolomite in this lake are visible on the XRD trace (see Appendix 1) but the principle ordering peak, which allows a numerical ordering percentage to be obtained, is not clearly defined. This suggests that the dolomite ordering is rather weak.

3.3.6. Dolomite Lake

The mineralogy of the uppermost sediments of Dolomite Lake is dominated by dolomite with just a little accessory quartz and halite (see Appendix 1). Figure 3.20 shows the sediment in this lake viewed under the SEM. On low magnification (Fig. 3.20a) it is seen to be composed of multiple 'grains' of dolomite ranging from around 50μm to over 200μm in size. At higher magnification these are, once again, seen to be comprised of many spherules approximately 1μm across. The stoichiometry of the dolomite is very close to that of 'ideal dolomite' spanning a fairly narrow range from 47-53% $MgCO_3$ (see Appendix 2 (Table A2.1 and Figs A2.9+A2.10)).

At 50mm depth the dolomite spherules coalesce to form aggregates, similar to those seen in Mini Dolomite and McFaiden Lakes, where only a small proportion of the original spherule boundaries are still visible (Fig. 3.20c). Compositions at this depth span the same values as at the surface. Ordering of the dolomite is surprisingly weak given the stoichiometry. Ordering peaks are visible on the XRD trace (see Appendix 1) but the principle ordering peak is weak and diffuse giving a maximum degree of ordering of only about 10%.





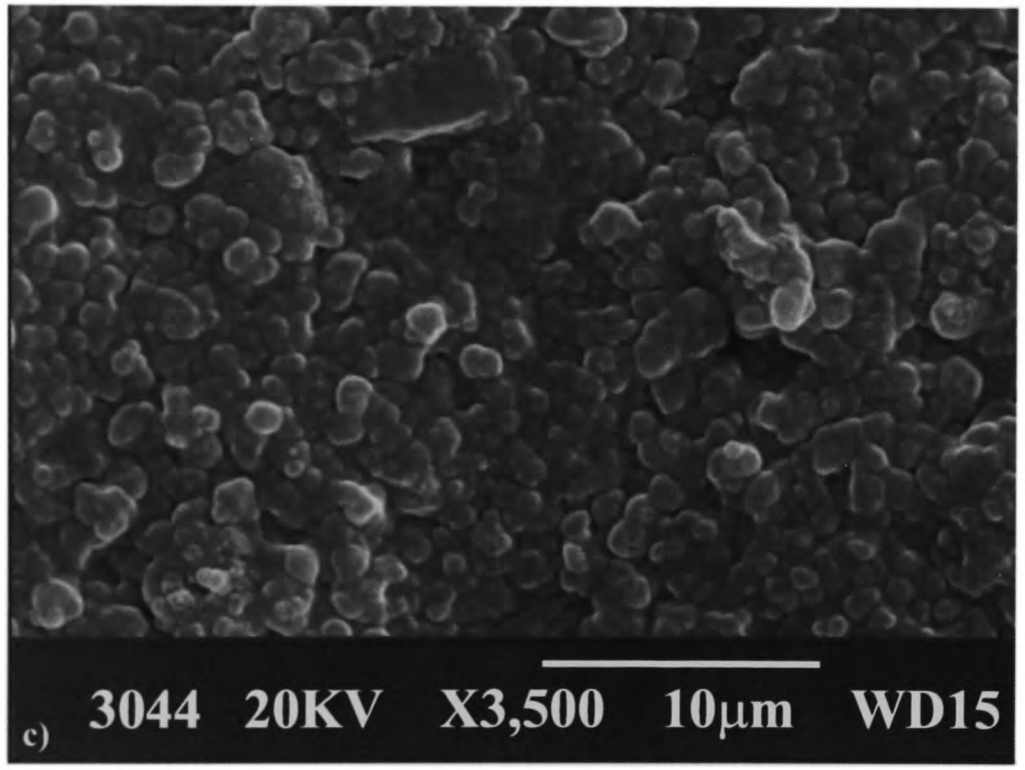


Figure 3.20. SEM images of the sediment from Dolomite Lake.
a) Overall nature of the surface sediment; a number of 100-200mm sub-rounded dolomite grains.
b) On higher magnification these are once again seen to be composed of multiple dolomite spherules.
C) Sediment at c.50mm depth. There is much consolidation of the spherules into sprawling aggregates which are flattened into a more two dimensional framework.

3.3.7. Halite Lake

The mineralogy of this lake differs markedly from that of lakes a few hundred metres away, being dominated by halite, and by carbonates of which aragonite and Mg-calcite are the main phases. Dolomite appears to be largely absent, whilst gypsum, absent in the dolomitic lakes, is seen to be present using XRD (see Appendix 1).

The sediment in this lake, when viewed under the SEM (Figure 3.21), also appears quite different from sediment in the other lakes. Masses of smooth-faced, halite crystals appear to act as a cement to the sediment. Rare blocky calcium-rich crystals appear, from their morphology and atomic spectra, to be gypsum. Gypsum also occurs as fan shaped groups of acicular crystals, each up to 10μm long. Aragonite does not occur as the needles or laths observed in North and South Stromatolite lakes but as indistinct crystals, more similar in morphology to the dolomite crystals seen elsewhere. Intermixed with the aragonite crystals, and in many areas outnumbering them, are crystals with $MgCO_3$ percentages of up to 25% (see Appendix 2 (Table A2.1 and Figs A2.11+A2.12)). These Mg-rich areas are less spherular than seen in the other lakes, usually comprising an irregular mass of indistinct grains, and appear to be Mg-calcite.

An example of the varied nature of sediment in this lake is shown in Figure 3.21a. The smooth, dark, sprawling crystals are halite, whilst the bright white block about 4μm across (middle left) is gypsum. The crystalline mass (bottom centre left) has a 90% $CaCO_3$ composition so would appear to be Mg-calcite, whereas the mass at the bottom right is close to 100% $CaCO_3$ and is therefore aragonite. Occasional strange rhombic features (Fig. 3.21b) resemble dolomite rhombs reported from ancient sediments and appear to have bacteria-shaped inclusions enclosed within them. Their compositions (c.90% $CaCO_3$), however, suggest they are Mg-calcite rhombs.

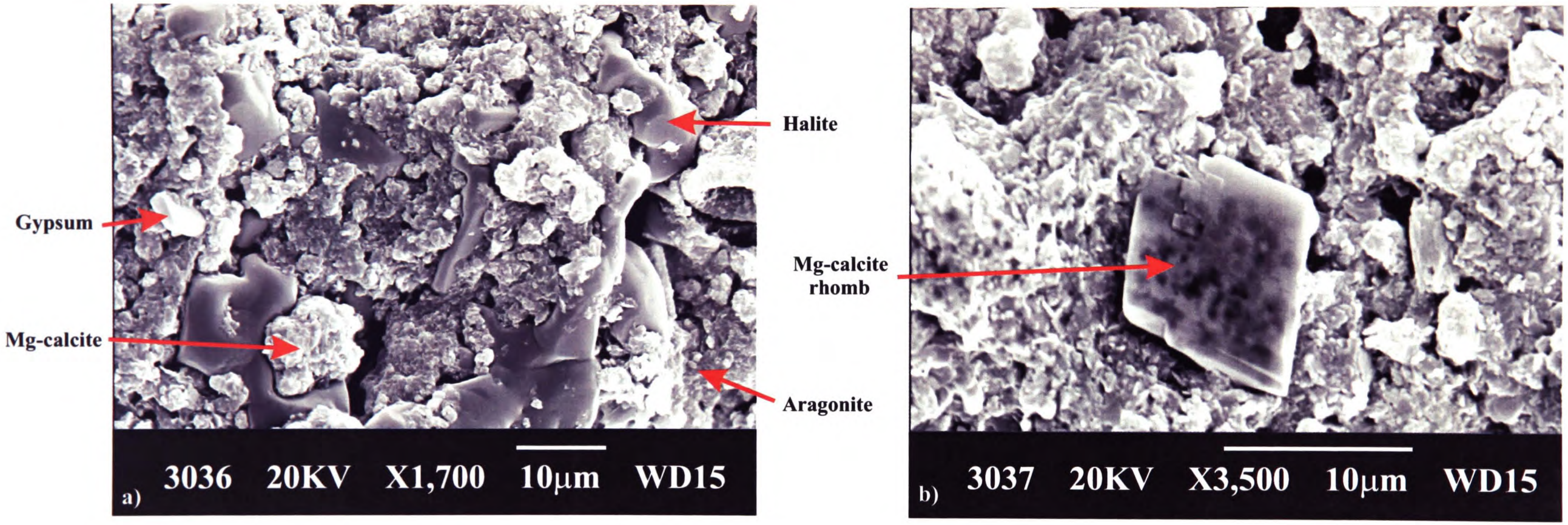


Figure 3.21. SEM images of sediment from Halite Lake. a) Smooth halite crystals intergrown with gypsum and carbonate precipitates of variable composition. b) Well formed Mg-calcite rhomb (centre) surrounded by sediment of aragonite and Mg-calcite. See text for details.

3.3.8. North Stromatolite Lake

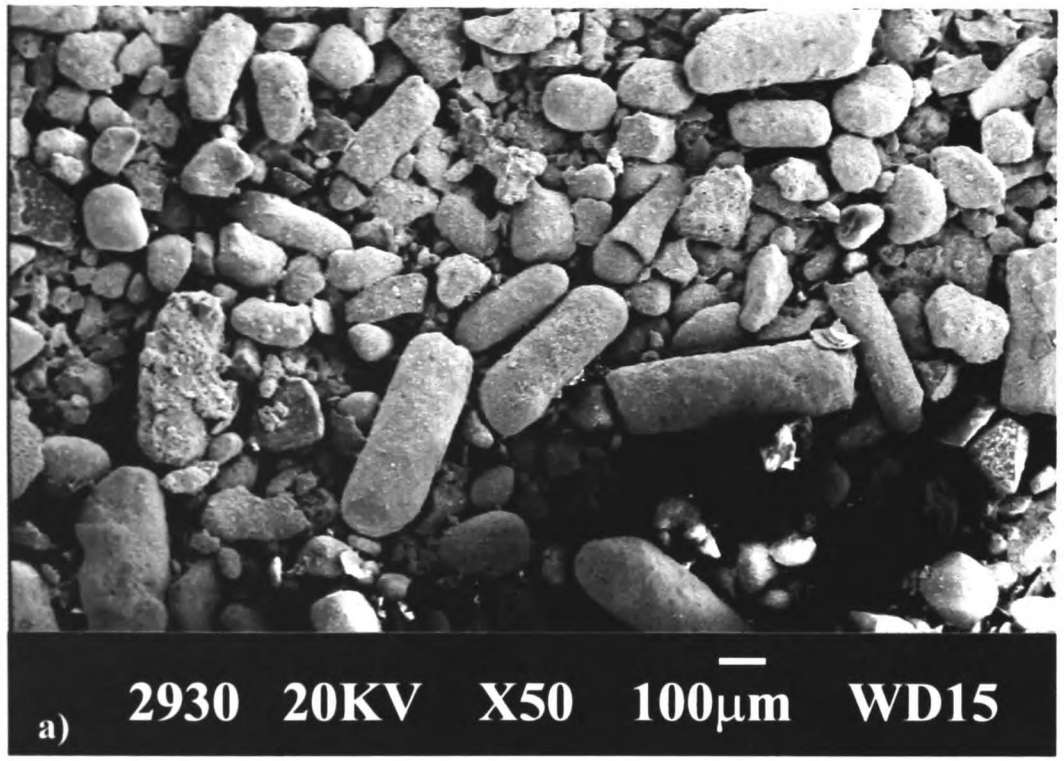
The mineralogy of this lake is dominated by aragonite, with hydro-magnesite and Mg-calcite as minor phases. Halite occurs in the upper surface layers and a little quartz is also present (see Appendix 1).

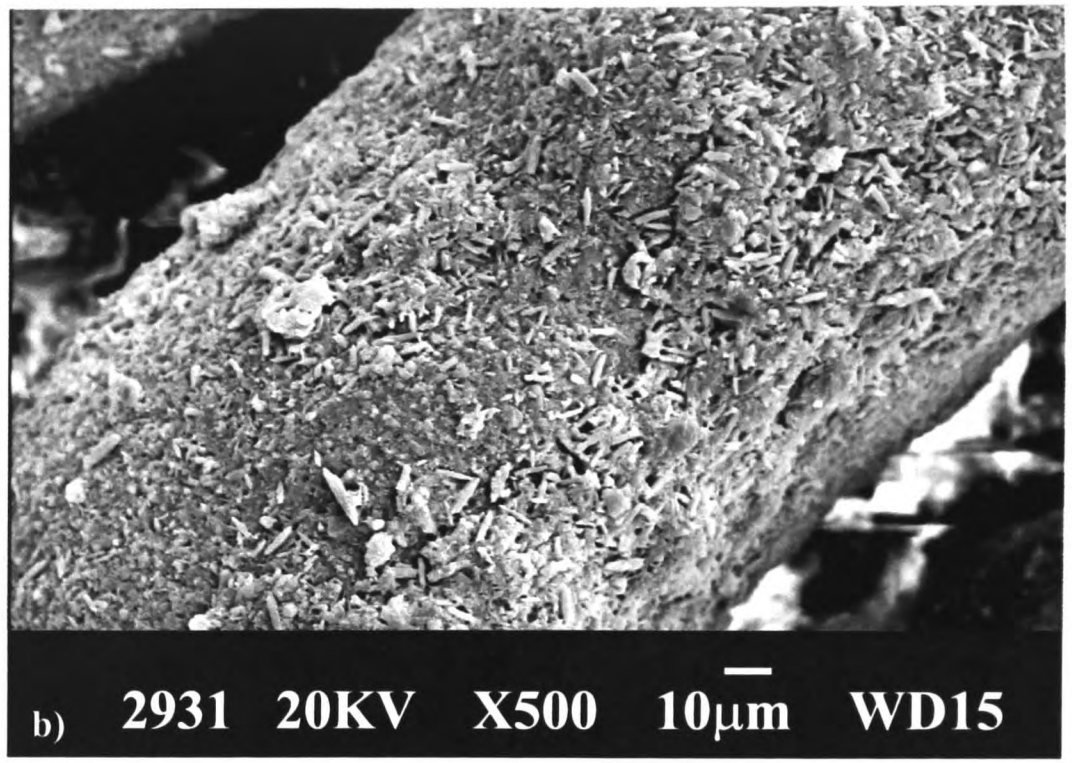
Figure 3.22 shows the nature of the sediment in North Stromatolite Lake which is very different from that seen in the lakes considered thus far. At low magnification (Fig. 3.22a) the majority of the sediment takes the form of faecal pellets which would suggest that abundant macrofauna is present at some point in the annual cycle of the lake. On closer examination, each of the faecal pellets is seen to be composed of a mass of tightly packed needles and laths (Fig. 3.22b), the vast majority of which are in the size range of 5-15μm in length. The crystals are well formed, with clear faces, and are composed mainly of aragonite, although laths of hydro-magnesite are also evident in some areas. These are present both in the upper and lower surface layers of sediment. Shell fragments are also common, and consist of almost 100% $CaCO_3$. Patches of bacterial sized subspherical grains (Fig. 3.22c) have a relatively low percentage of $MgCO_3$ (<10%), consistent with these being Mg-calcite. Occasional hydro-magnesite crystals are visible in these patches, being composed of 90-100% $MgCO_3$ (see Appendix 2 (Table A2.1 and Figs A2.13+A2.14)).

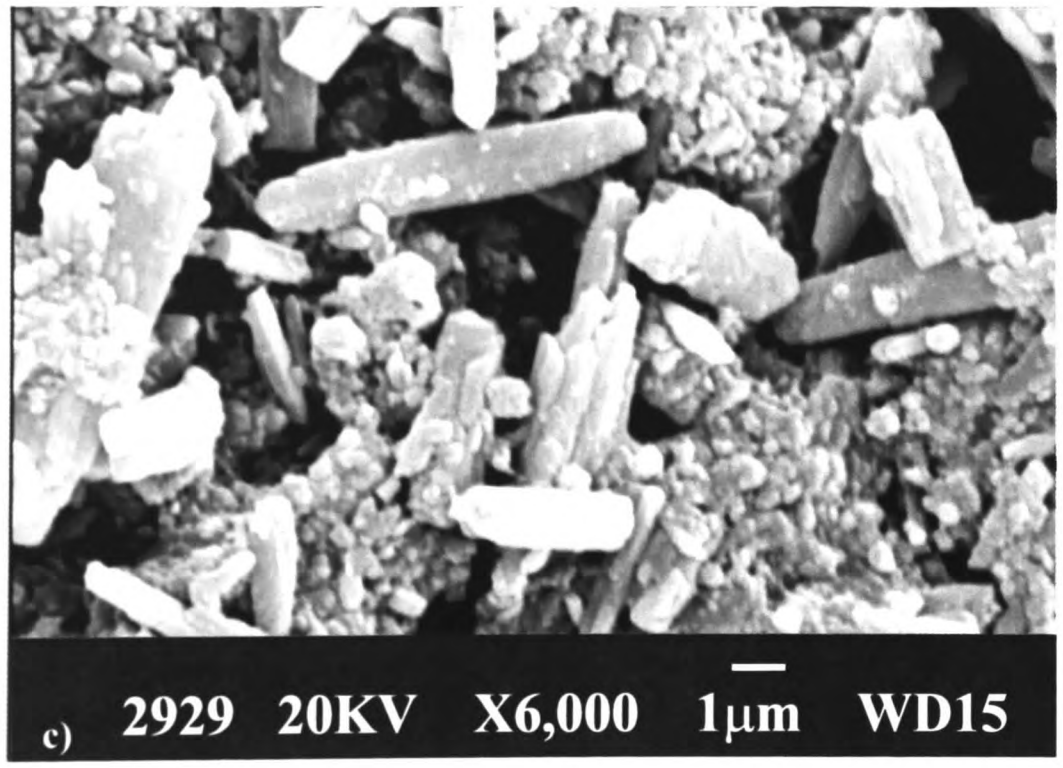
3.3.9. South Stromatolite Lake

The mineralogy of this lake is dominated by aragonite with some accessory Mg-calcite. Hydro-magnesite may also occur but this is difficult to confirm owing to the proximity of its main peak to that of quartz. Bacterial sized precipitates of both Mg-calcite and non-stoichiometric dolomite are evident under SEM analysis while halite is present as the evaporative phase. Gypsum, observed occasionally in the field, was not confirmed by XRD (see Appendix 1), so is unlikely to occur in significant amounts.

The nature of the sediment in this lake, shown in Figure 3.23, is similar to that in North Stromatolite Lake, consisting of randomly orientated needles and laths, although in







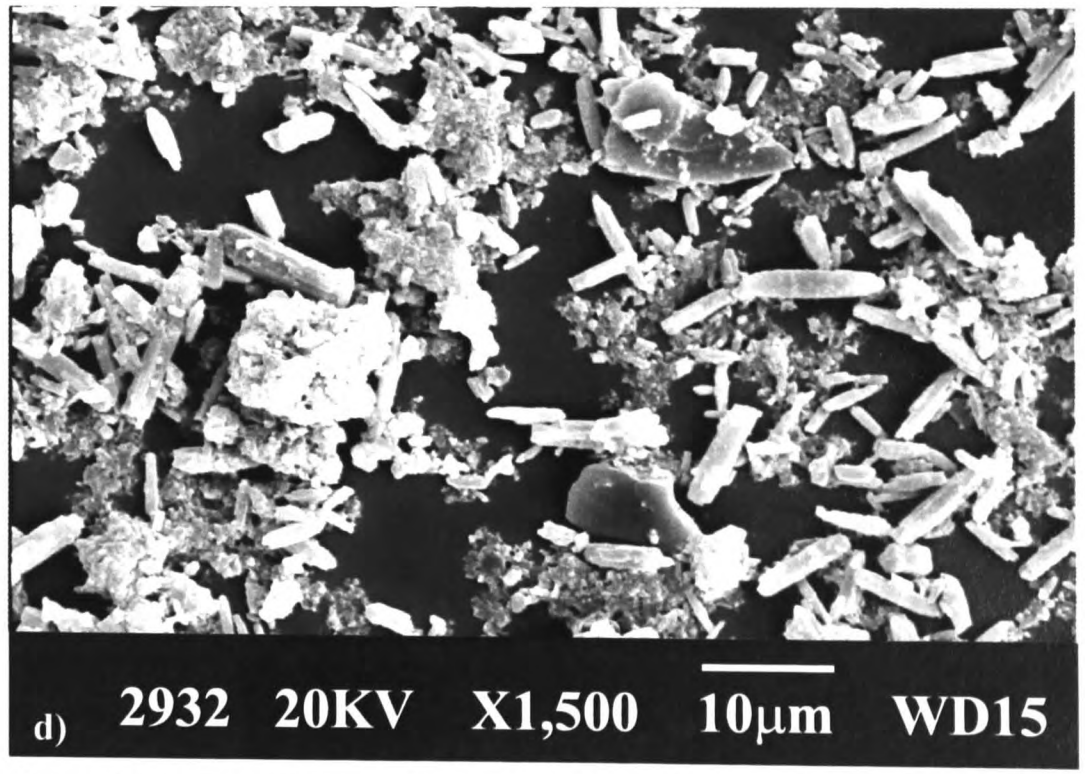
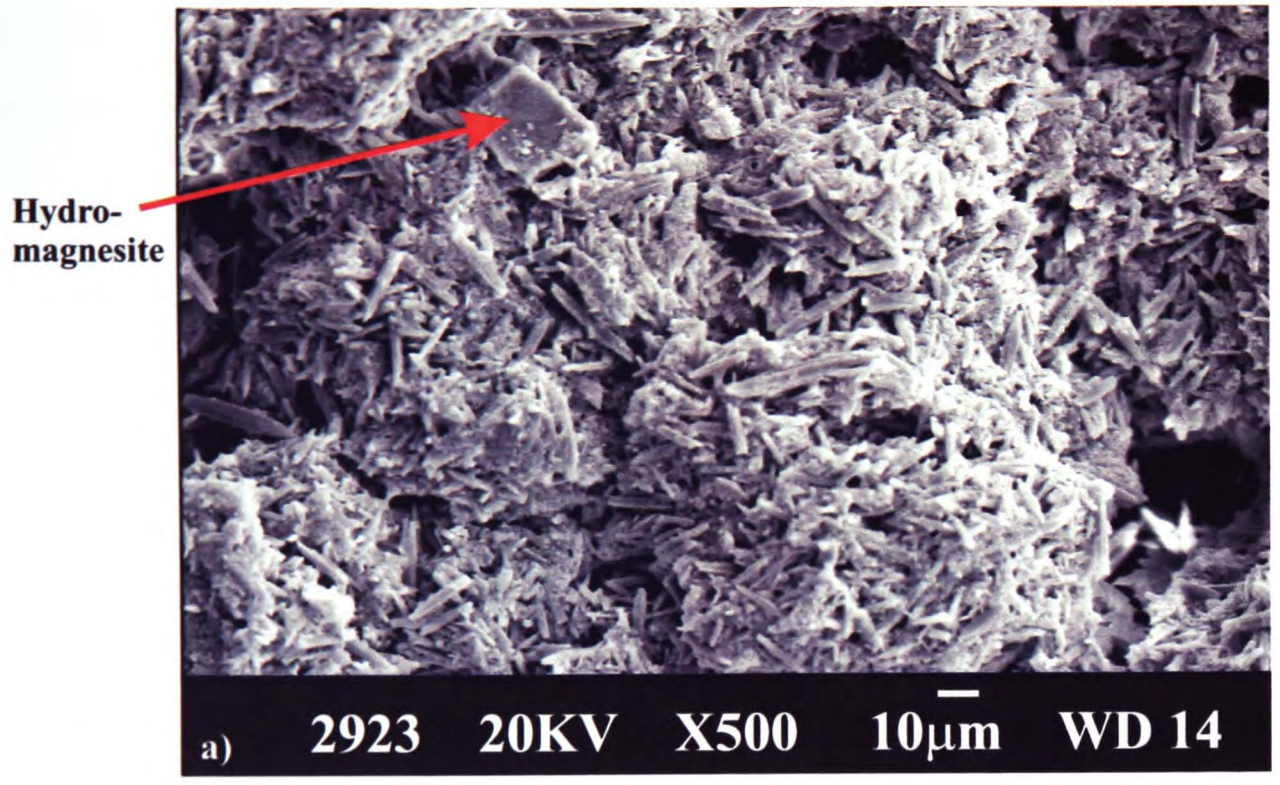
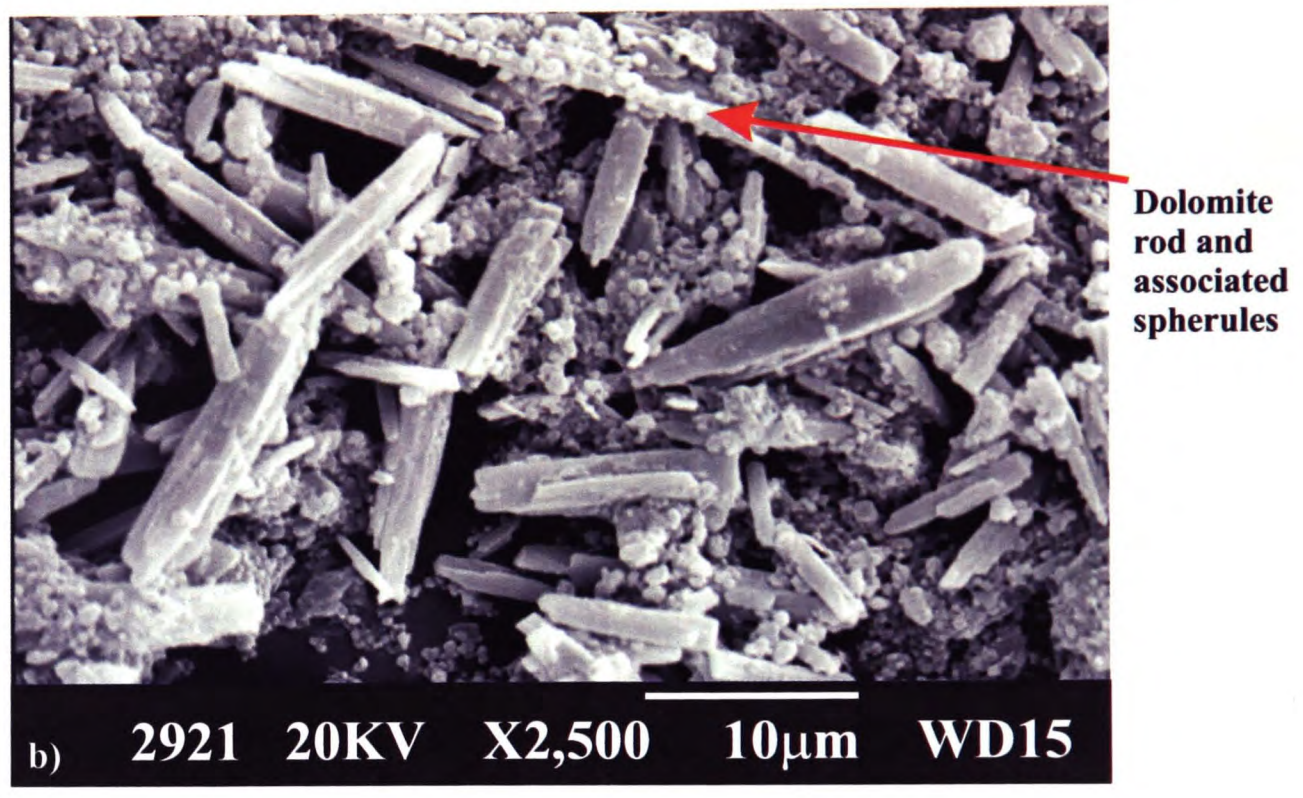


Figure 3.22. SEM images of North Stromatolite Lake. a) The majority of the sediment takes the form of rounded faecal pellets, suggesting the presence of macrofauna at some point in the annual cycle. b) Each pellet is composed of tightly packed needles and laths. c) Patches rich in spherules are common, but these have <10% Mg so are not dolomitic. These could simply be disaggregated pellets. d) Overview of the sediment, including shell fragments, aragonite needles and suspected Mg-calcite bacterial precipitates.





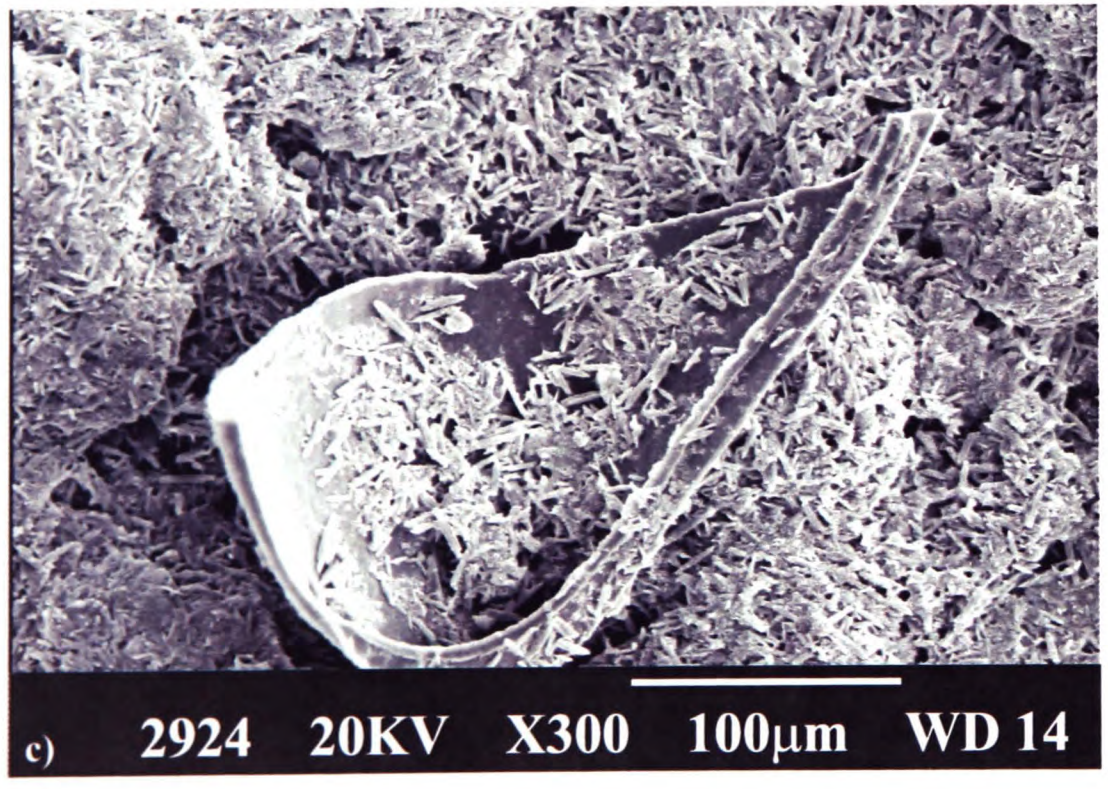


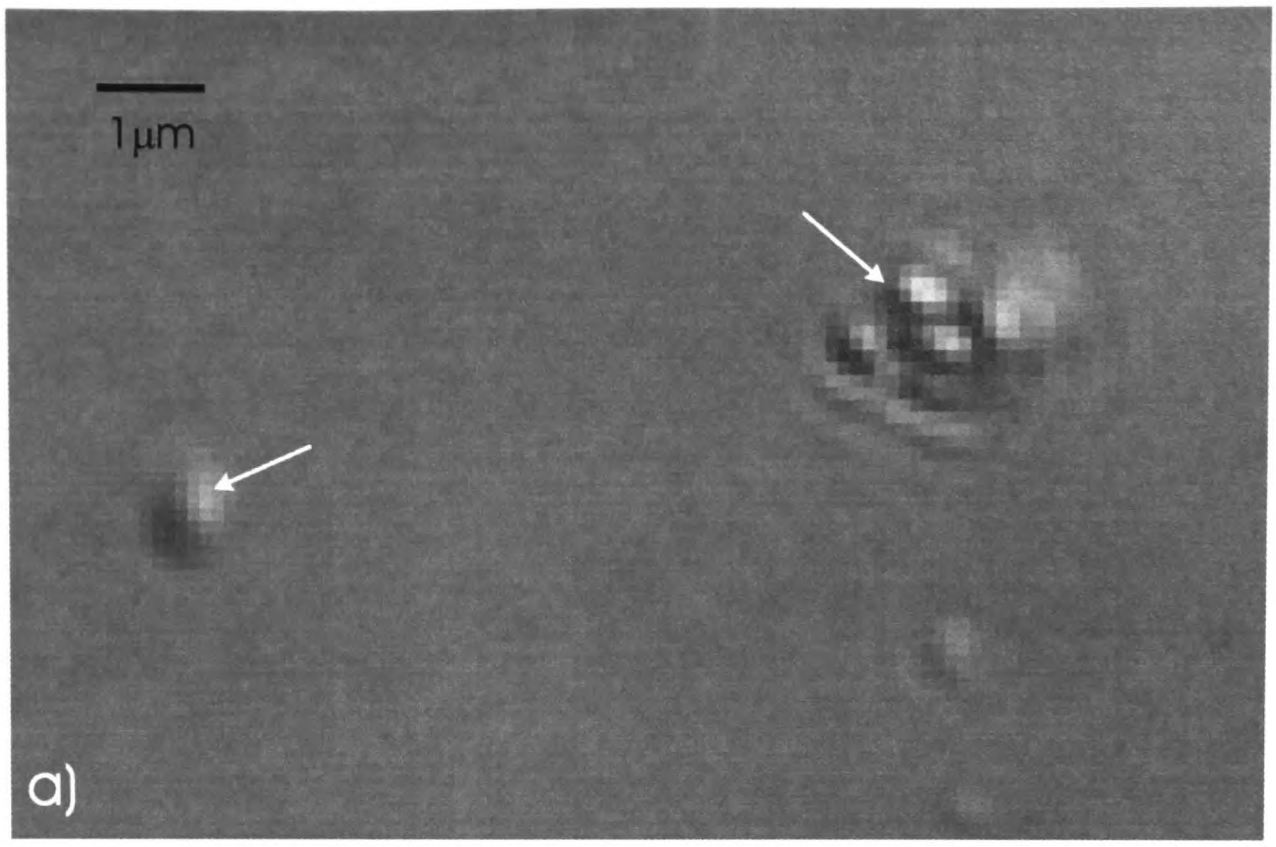
Figure 3.23. SEM images of the sediment from South Stromatolite Lake. a) General appearance of the sediment - randomly orientated needles and laths of aragonite together with rare laths of hydromagnesite. b) On closer inspection, rods (middle top of image) and spherules are visible, interspersed with the needles and laths. c) Shell fragments are fairly common in this lake and are not visibly degraded.

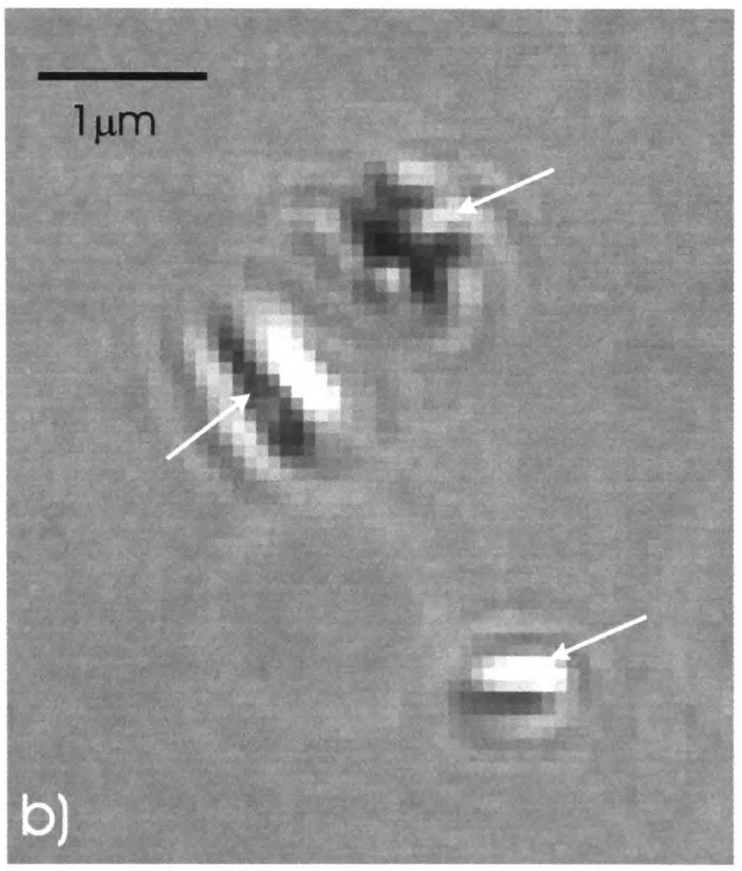
this case they are not packed into pellets (Fig. 3.23a). The crystals are mostly well formed with clear faces and are mostly of aragonite. Upper and lower surface sediment layers proved to be morphologically and mineralogically identical. Interestingly, a few sub-micron spherical grains are found to be intermixed with the larger needles (Fig. 3.23b). These grains appear to be dolomitic, and arguably of bacterial origin since they are not replacing but precipitating around the aragonite. Occasional skeletal shell fragments show no signs of degradation (Fig. 3.23c). Rods of dolomitic composition are observed (Fig. 3.23b), arguably of bacterial origin, implying the importance of organic matter in dolomite formation. Occasional cubic halite crystals are also present. The aragonitic needles typically have a composition of 97-100% $CaCO_3$. In some patches the bacterial shaped bodies have compositions similar in range to those of Mini Dolomite Lake (35-55% $MgCO_3$), whereas in others a huntite (75% $MgCO_3$) composition is achieved (see Appendix 2 (Table A2.1 and Figs A2.15+A2.16)). In the majority of areas, however, a strong calcium enrichment is observed and these crystals are most likely precipitates of Mg-calcite.

3.4. EVIDENCE FOR BACTERIAL MINERALISATION

Once lithified, bacteria cannot be revived and studied and hence evidence for their presence in ancient rocks must be somewhat circumstantial and must be based largely on their shape and size (Folk, 1993a). In modern sediments, however, such as these being studied, it is possible to find coeval living and lithified (dolomitised) bacteria.

Coeval living/dormant bacteria from the Coorong distal ephemeral lakes were imaged using Differential Interference Contrast (DIC) microscopy. This was carried out at the Department of Microbiology at Oxford University. DIC microscopy is ideal for imaging objects such as bacteria that do not show up clearly under normal bright-field illumination. It is a simple technique, requiring only a small drop of liquid from a cultured bacterial vial (see Chapter 6 for culturing technique) to be placed on a slide. The images from Vial 11 and Vial 19 are shown in Figures 3.24-3.27. Vial 11 contains bacteria from McFaiden Lake and Vial 19 bacteria from Milne Lake. Bacterial structures are clearly visible in both vials. These take a variety of forms from spherical to oval, rods, curved rods, vibrio and filaments, mostly of about 1μm in size. The size and shape of many of the bacteria is almost identical to the sediment seen in the dolomite precipitating lakes (e.g. Fig. 3.18c from McFaiden Lake).





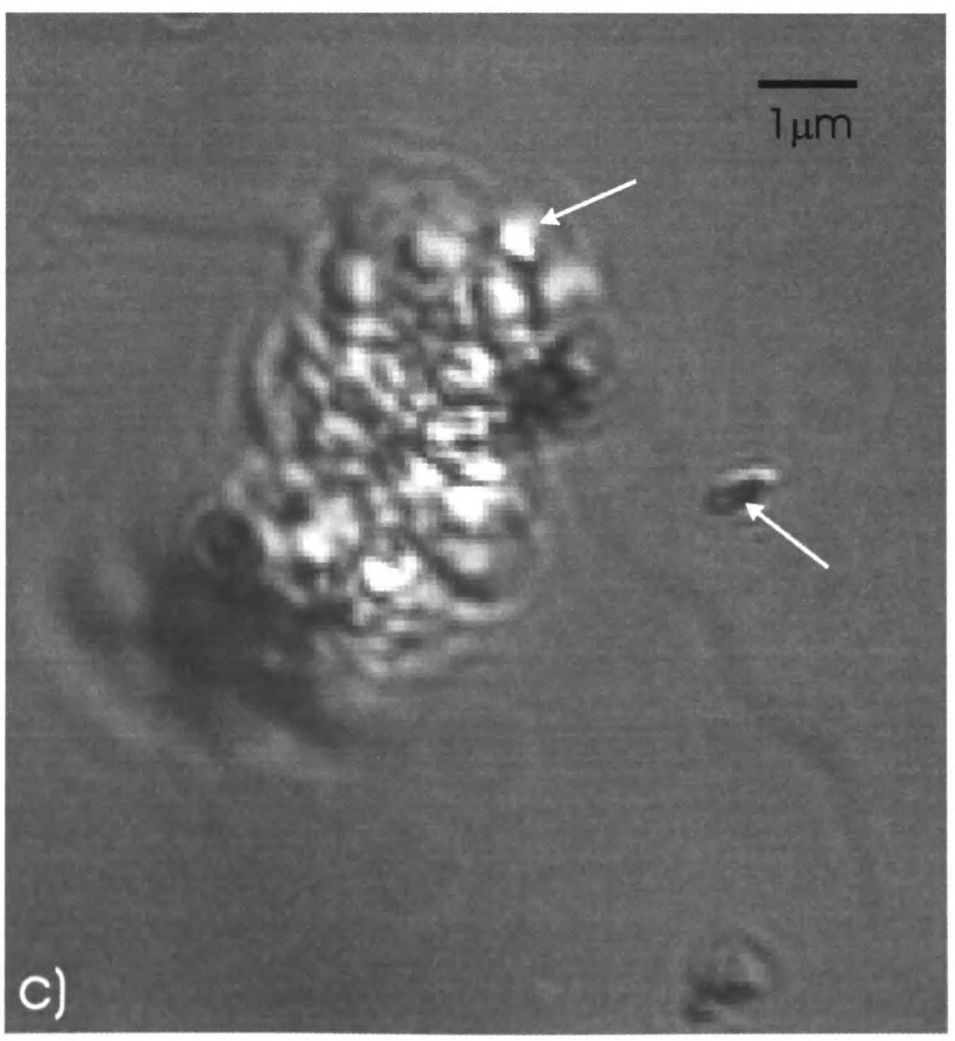
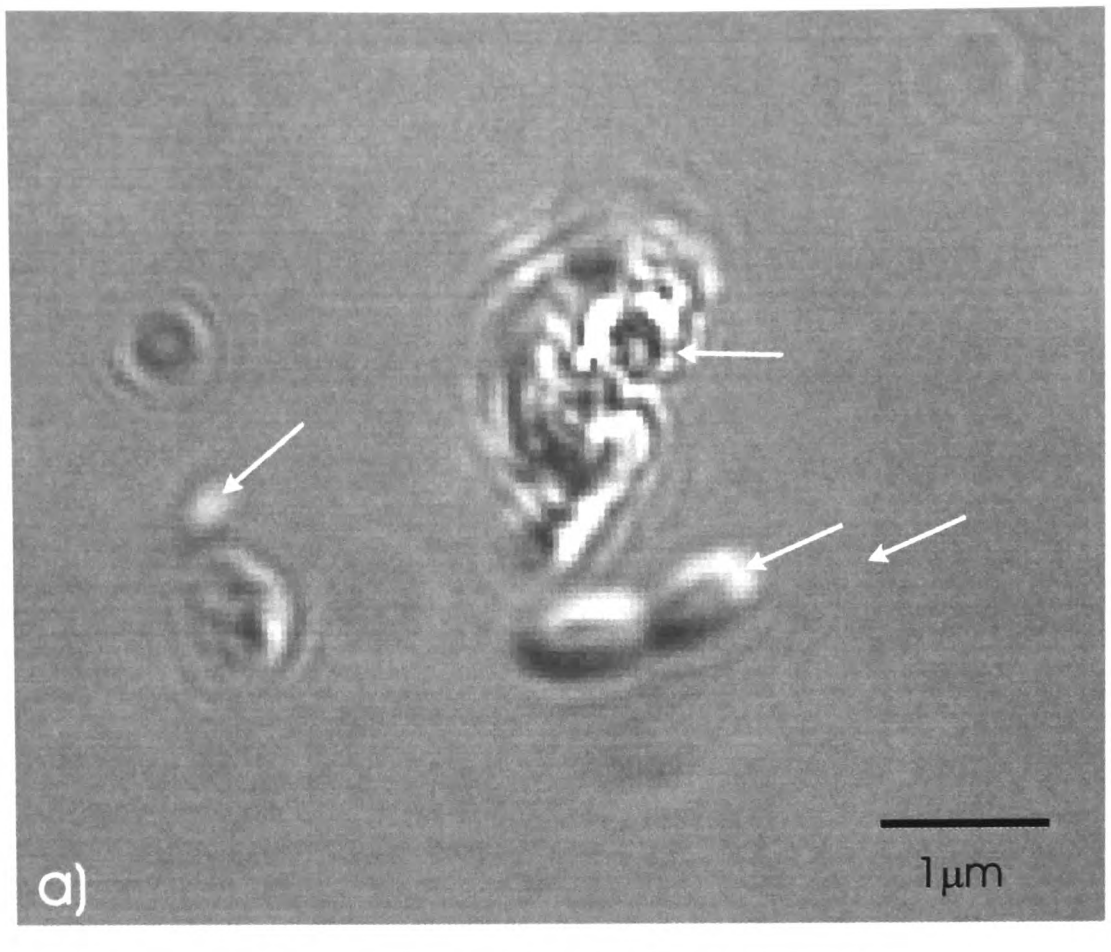


Figure 3.24. DIC images from Vial 11 (arrows indicate bacteria or possible bacteria).
a) (left to right). Single oval cell; group of at least five sub-spherical to oval cells.
b) (left to right). Rod shaped cell; cluster of small cells; small rod shaped cell.
c) (left to right). Large amount of cells possibly clustered around sediment particle or having sediment precipitate around them; single vibrio shaped cell.



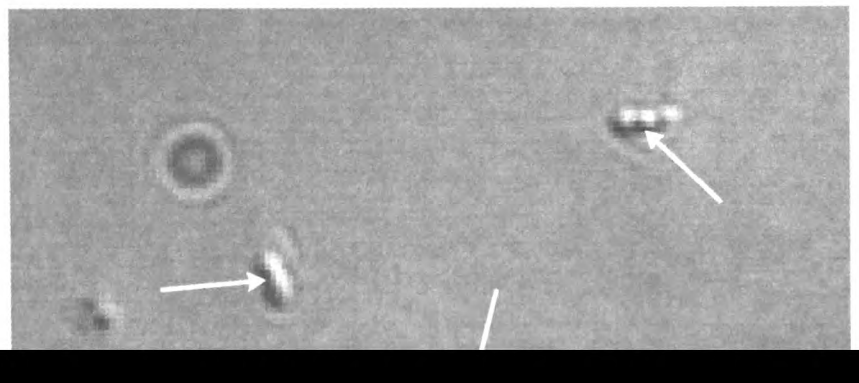


Figure 3.25. DIC images of bacteria from Vial 11 (arrows indicate bacteria or possible bacteria).
a) (left to right). Single sub-spherical cell; possible multiple cells associated with sediment; two oval cells, possibly recently divided.
b) (left to right). Single elongate cell;

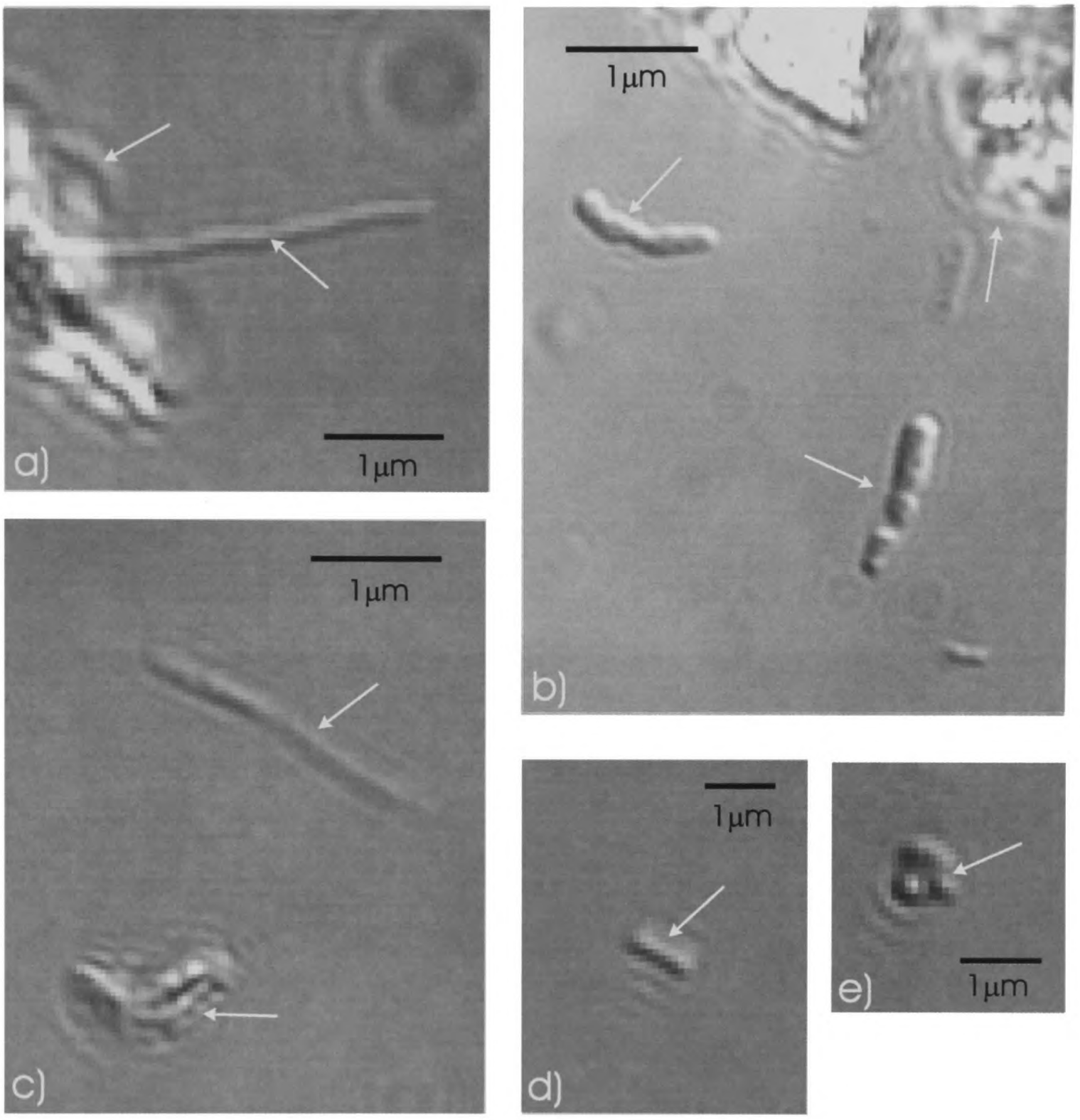
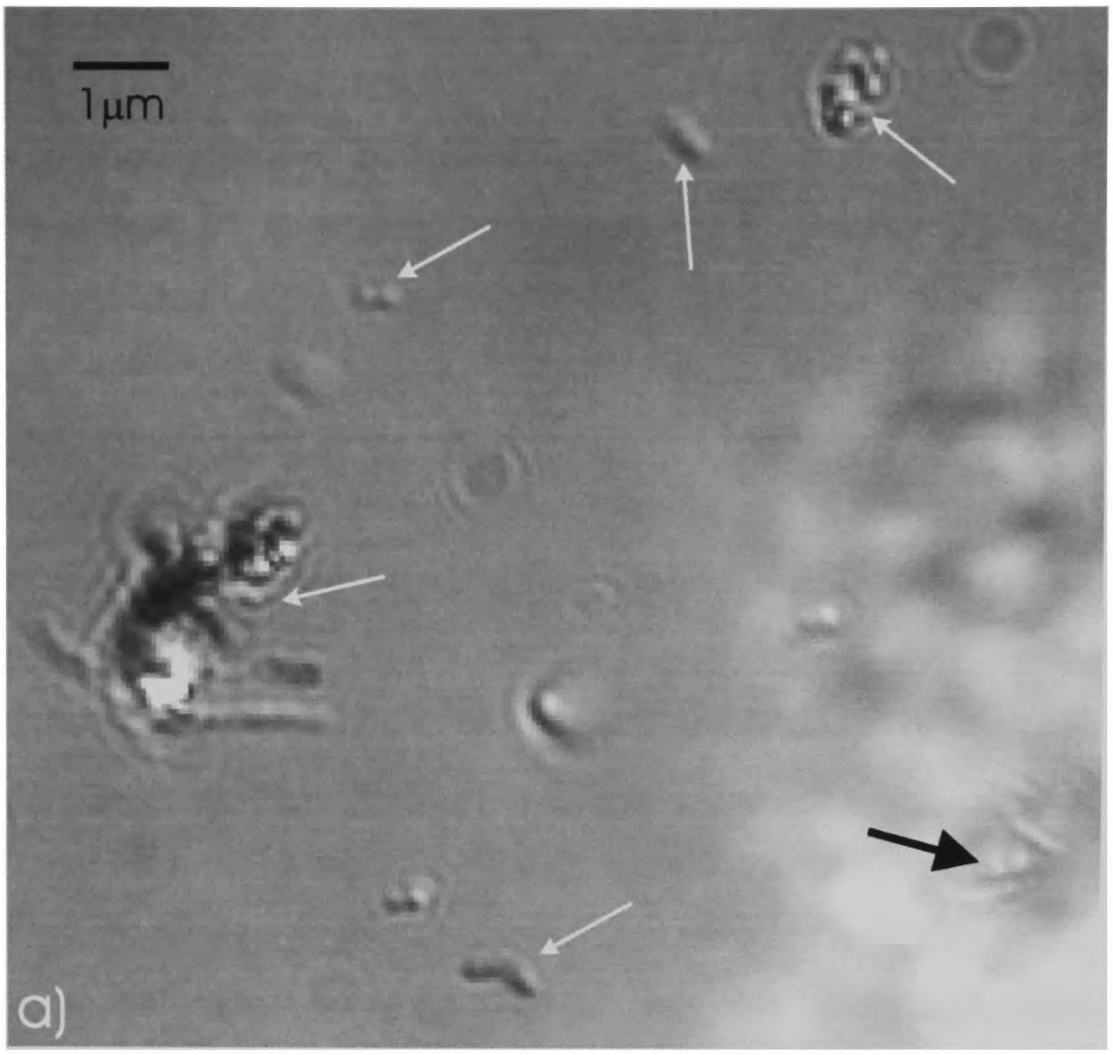


Figure 3.26. DIC images of bacteria from Vial 19 (arrows indicate bacteria or possible bacteria).
a) (left to right). Possible collection of cells associated with sediment; filamentous bacteria.
b) (left to right). Curved rod shaped cell; elongate cell, possibly dividing; sediment, possibly with multiple cells associated with it.
c) (left to right). Vibrio shaped cell; filamentous bacteria.
d) Single small rod shaped cell.
e) Collection of two spherical cells and one sub-spherical to oval cell.
f) (left to right). Curved rod/vibrio cell; rod shaped cell. Body at top of photo may or may not be bacterial



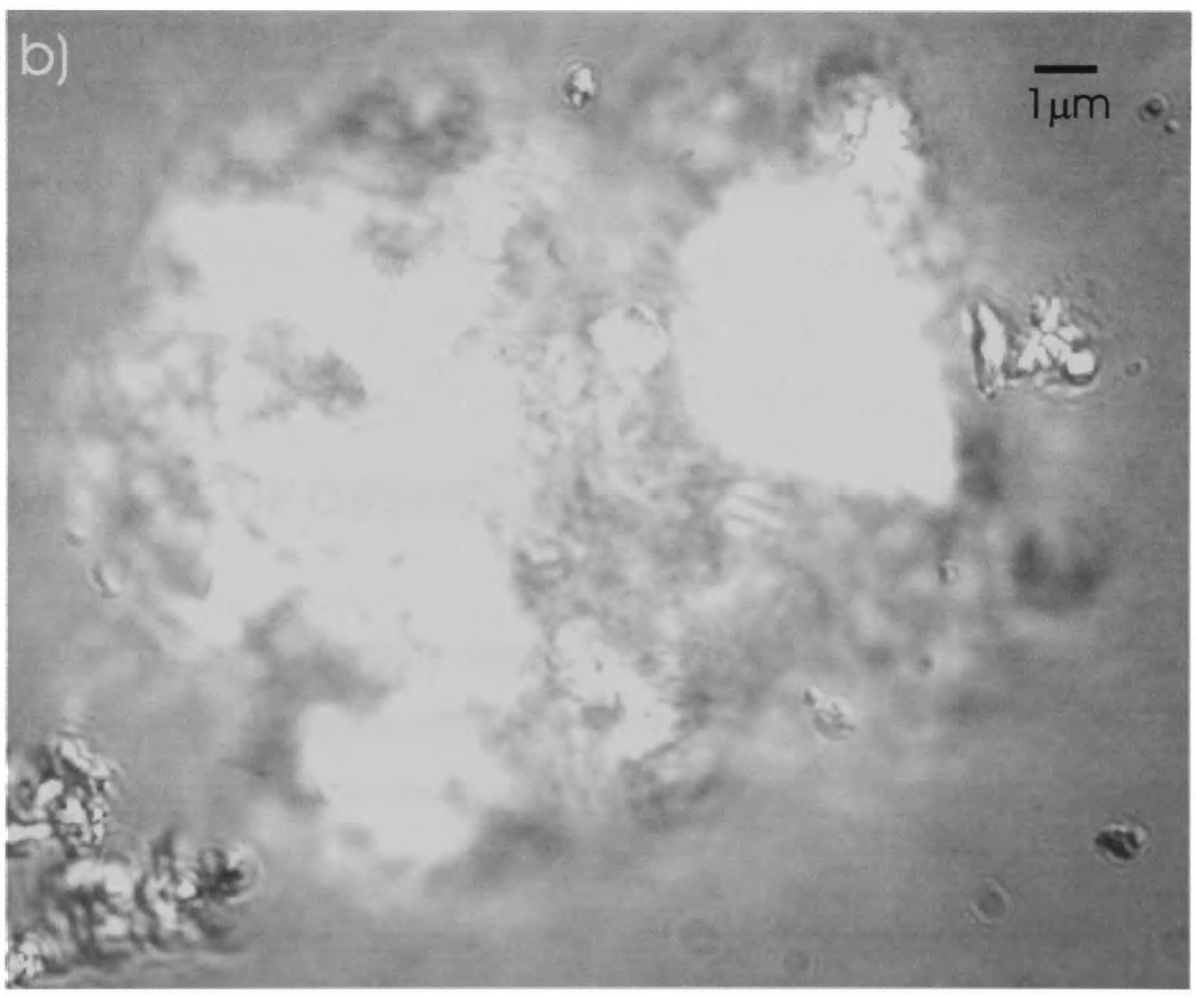


Figure 3.27. DIC images from Vial 19 (arrows indicate bacteria or possible bacteria) a) (left to right). Large collection of cells of varying morphology; small sub-spherical cells, possibly recently divided; vibrio shaped cell; oval cell; collection of multiple sub-spherical cells; rod, vibrio and sub-spherical cells partially obscured by sediment cover.
b) A view of sediment under DIC showing typical bright interference colour. A number of bacterially shaped objects can be seen around the edges of the sediment. From the evidence of previous images, one may postulate that numerous bacteria may also be found within the clumps of sediment.

This may point to the involvement of the bacteria in providing surfaces for mineral precipitation in this sediment. In addition, both the DIC and SEM images show distinct similarities to images of bacteria produced by other workers (Vasconcelos *et al.*, 1995; Vasconcelos & McKenzie, 1997; Wright, 1999; Folk, 1993a).

One question that must be asked is - if this sediment is not composed of recently dolomitized/calcified bacteria then what else can produce these distinct sub-micron, sub-spherical grains with smooth surfaces? Minerals which precipitate inorganically usually take the form of euhedra (e.g. halite cubes), needles, radial fibres and, even when spherical, tend to have a rough surfaces caused by tightly packed tiny crystallites. As previously mentioned, the sediment particles in the dolomite precipitating lakes appear to have an upper size limit of about a 1-2μm, presumably because of the vast amounts of bacterial nucleation sites – why would an inorganic mineral grain stop growing at this tiny size? When the spherular nature of Coorong type dolomite was first noted by Von der Borch and Jones (1976), the only comparable analogues were found in the laboratory. Both Muller and Fishbeck (1973) and Fritz and Smith (1970) produced proto-dolomites with a spherular structure from experimental carbonate gels. These, however, tended to have a much more variable grain size of between 1 and 40μm in keeping with the inorganic rather than bacterial nature of precipitation.

3.6. SUMMARY OF OBSERVATIONS

- During the Holocene the study area evolved from a dominantly marine setting, through a series of marginal marine restricted settings to the present day situation where each lake is isolated from one another. A sediment core from McFaiden Lake traces this evolution.
- Five of these ephemeral lakes are actively precipitating dolomite at the present day whilst, in close proximity, three similar lakes do not contain dolomite. Those which are precipitating dolomite do not contain aragonite, Mg-calcite or gypsum.
- The size, water depth and location of the lakes appears to have no relevance to the type of mineral precipitate produced, except perhaps in the case of Halite Lake which has a underground connection to the main lagoon.

- During the time of study all of the lakes evolved into inhospitable environments. They became hypersaline and anoxic below the sediment water interface. These conditions are ideal for anaerobic bacteria such as SRB to thrive especially as they then release H_2S which is toxic to many organisms.
- The dolomite containing lakes show no evidence of living macrofauna and generally have a large supply of organic matter in the form of *Ruppia maritima* and/or desiccated microbial mats; the sediment is always a grey or pale yellow mud. The non-dolomitic lakes largely lack *Ruppia maritima* and show evidence of burrowing and other animal activity; the sediment is dominantly a brown/yellow sand.
- Dolomite occurs as sub-micron spherular grains which often amalgamate to form larger spherular aggregates and proto-rhombs. In addition, tiny platelets are observed in Pellet Lake.
- The dolomite shows no evidence of replacing existing carbonate phases and is inferred to be a primary precipitate. It has a wide range of compositions ranging from slightly Ca-rich (Mini Dolomite Lake) through almost stoichiometric (McFaiden and Dolomite Lake) to Mg-rich (Pellet and Milne Lake). The degree of ordering of the dolomite is variable too; mostly it is poorly ordered but in some cases ordering is as high as 90%. Ordering and stoichiometry appear not to be linked.
- The bacterial nature of the sediment in the dolomitic lakes may be indicated by the size and shape of the grains, the existence of coeval living bacteria and the similar size and morphology of these imaged bacteria to sediment, both in this study and previous studies.

These field and petrological observations will be combined with geochemical, isotopic and microbiological observations and data in subsequent chapters to further constrain the important features of this area in relation to dolomite formation.

CHAPTER 4



The Coorong Lagoon and Young-husband Peninsula with the Southern Ocean beyond.

Chapter 4

Lakewater and porewater geochemistry

4.1. INTRODUCTION

The low activity of the carbonate ion, the presence of the sulphate ion and the high hydration enthalpy of the magnesium ion have all been cited as kinetic inhibitors to dolomite formation (see Section 1.2). This chapter investigates the geochemistry of both the lakewater and associated porewaters of the study lakes, paying particular attention to these key ions and the processes that govern their distribution. It will be proposed that these kinetic inhibitors may be removed by the action of microbes, and once this is achieved dolomite is free to precipitate.

4.2. SALINITY

Salinity, or the measure of the amount of solutes in natural waters, is theoretically defined as the total number of grams of dissolved salt ions present in 1 kg of seawater (Libes, 1992). It is an important measurement as it gives the best clue as to what stage of the evaporative cycle each lake is at and is often a contributing factor to the way different ions behave and how organisms metabolise. Salinity is difficult and time consuming to measure directly, and so the quickest and most widely used option is to infer salinity by measuring the electrical conductivity of the water (UNESCO, 1981a).

4.2.1. Field measurements

Measurements of conductivity were performed on lakewater samples collected adjacent to areas in the lake that had been cored for sediment and porewater analysis. Conductivity was measured using a probe which contains two electrodes, separated by a fixed distance. When a voltage is applied from the meter across the electrodes, the ions in solution conduct a current, which flows between the electrodes. The greater the concentration of ions in the solution, the larger the current generated and the higher the conductivity. The meter then converts the measured current to conductivity measured in microsiemens per centimeter (μs/cm). The ability of the ions to move through the solution, and conduct the current, is related to the temperature of the solution. As the temperature rises, the ions move more quickly through the solution, increasing the conductivity; the conductivity of the same solution can change by as much as 2%/°C (Association of Analytical Communities, 2002) so accurate temperature measurements must be made simultaneously to the conductivity reading. The meter has a temperature probe and converts all conductivity readings to the value that they would be at 25°C to negate these temperature effects.

4.2.2. Conversion to salinity

Conversion of conductivity measurements to salinity is defined by the 1978 Practical salinity Scale (UNESCO, 1981 a+b) using Equation 4.1. However, this is only valid for the ion ratios of standard seawater and therefore is only accurate for salinities from about 2-42.

$$S(\text{no units}) = 0.0080 - 0.1692K_{15}^{0.5} + 25.3851\,K_{15} + 14.0941\,K_{15}^{1.5} - 7.0261\,K_{15}^{2} + 2.7081\,K_{15}^{2.5} \quad (4.1)$$

where $K_{15} = C(S,15,0) / C(KCl,15,0)$

C (S,15,0) is the conductivity of the sample at 15° C and standard atmospheric pressure, and C (KCl,15,0) is the conductivity of the standard KCl solution at 15°C and standard

atmospheric pressure; and where the standard KCl solution contains a mass of 32.4356g of KCl in a mass of 1.0kg of solution. By definition, standard seawater with S=35.00 has a conductivity ratio of 1 with this standard.

The Coorong lakes are all hypersaline and so this equation gives wildly inaccurate results. An approximate relationship can be established between electrical conductivity and salinity based on known direct measurements taken from seawater samples around the globe. Average seawater salinity is 35ppt which corresponds to an electrical conductivity of 53 ms/cm. Seawater with salinity of 20ppt has electrical conductivity of 32ms/cm, that with salinity of 30ppt has conductivity of 46ms/cm, and that with salinity of 40ppt has a conductivity of 60ms/cm (Lide, 2001). From these measurements a graph of salinity versus electrical conductivity can be drawn which approximates a straight line (solid blue line on Figure 4.1), given by Equation 4.2.

$$\text{Salinity ppt} = 0.66 \times \text{Electrical Conductivity (ms/cm)} \qquad (4.2)$$

This can be extrapolated to higher salinities and, although not strictly accurate beyond around 45ppt, is a good starting approximation. At higher salinities there is a larger degree of complexing between ions. These neutral ion pairs, having no charge are not accounted for by conductivity measurements. This results in salinity in hypersaline lagoons such as those being studied being underestimated by appreciable amounts. Thus, the relationship between salinity and conductivity in the study lakes may more closely resemble the pink line of Figure 4.1. The salinities given in Figure 4.2 using Equation 4.2 are therefore only minimum values and are shown only to demonstrate that all the study lakes have salinities well in excess of seawater and thus will behave differently to seawater with respect to carbonate chemistry.

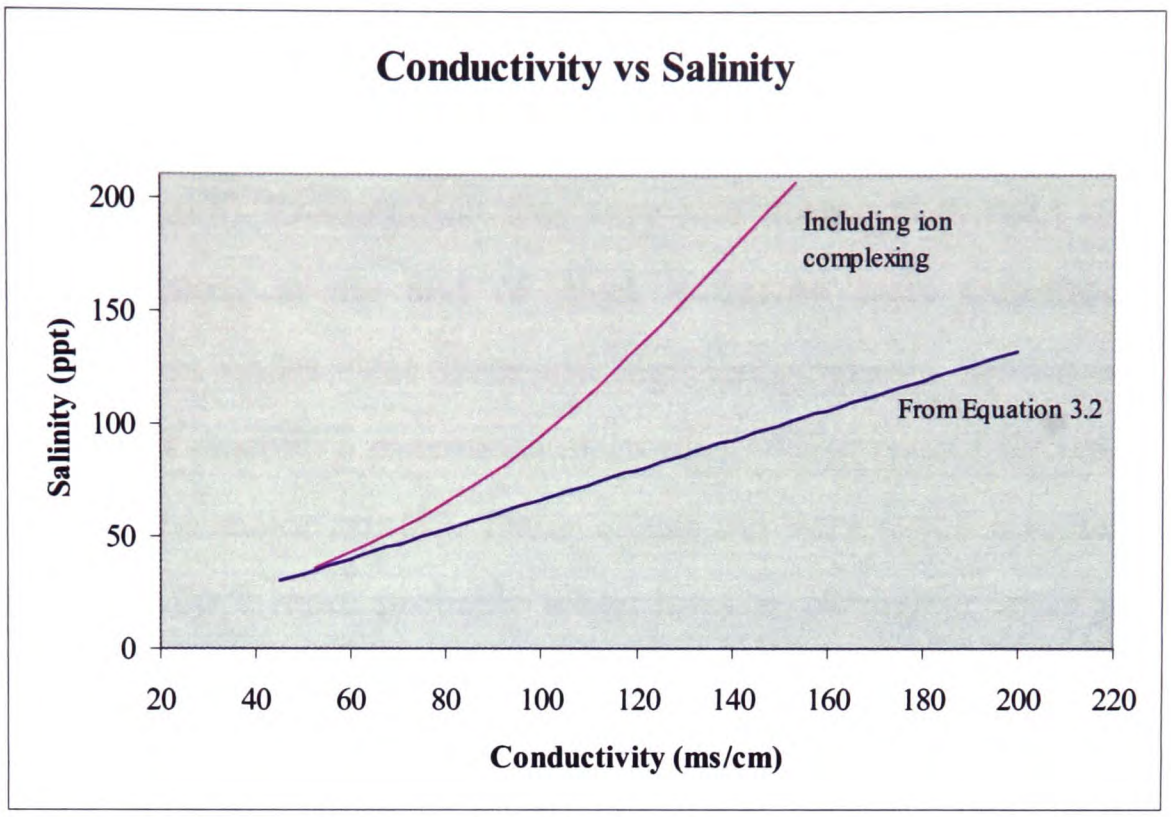


Figure 4.1. Approximate conversion between conductivity and salinity

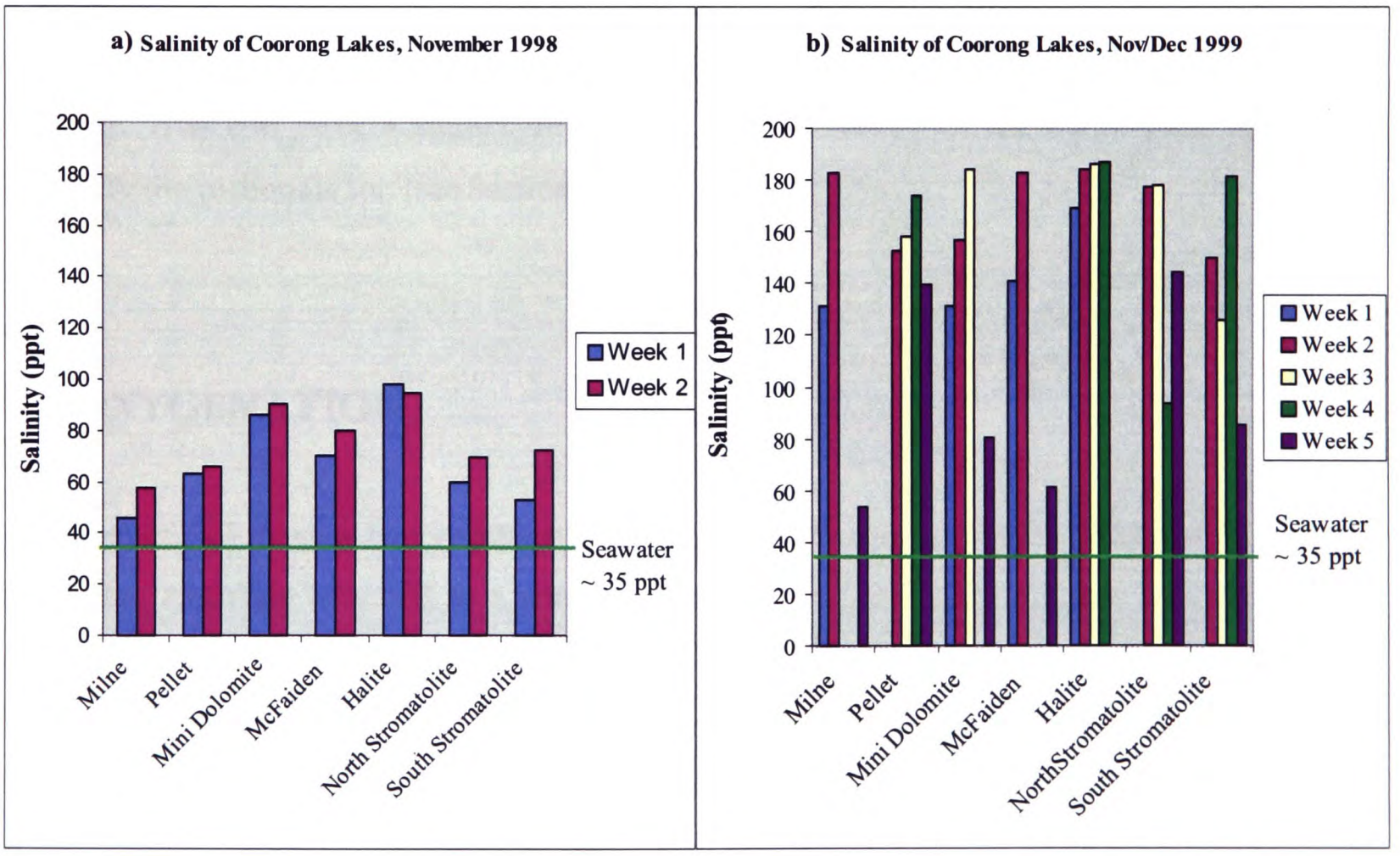


Figure 4.2. Minimum approximate salinities of the study lakes in a) 1998 field season b) 1999 field season

Note: True salinities will be much higher when ion complexing is accounted for.

4.2.3. Results

The salinity of the ephemeral Coorong lakes is related to the interplay between evaporation and precipitation (rainfall). Precipitation was very rare during both field seasons, the only appreciable amount being at the end of Week 4 during early December 1999, whilst evaporation was intense under clear skies and high temperatures. Salinities are all well in excess of seawater and reached a maximum of around 185ppt (using Equation 4.2) in all of the lakes just before the major rainfall. These values are very much a lower estimate with values approaching 400ppt more probable when ion complexing is taken into account. In addition to this, if rainfall had not occurred the lakes would have evolved into even more saline solutions. Ahmad (1996) recorded very variable salinities in these lakes with South Stromatolite having a maximum of 83ppt compared to Milne Lake at 400ppt. Von der Borch (1965a) recorded about a two fold increase in salinity (up to 100ppt) during the month of October in Milne and Mcfaiden lakes, whilst Skinner (1963) recorded values as high as 274ppt when halite began to precipitate in these lakes. It is therefore postulated that salinities during the period of mineral precipitation may be as much as ten times that of seawater. This will have a significant bearing on the activity of the major ionic species, especially the carbonate ion (see Section 4.4).

4.3. OXYGENATION

Measurement of oxygen concentration was carried out using a portable dissolved oxygen membrane electrode attached to a concentration meter. Each measurement was made by inserting the electrode in the lakewater and then at different depths in the sediment adjacent to where pH and other parameters had been measured. Careful calibration, using a standard solution, and cleaning of the membrane was required after each set of measurements.

The measurements (shown previously in Figure 3.2) demonstrate that, below the sediment water interface, all the lakes (except for one anomalous reading) are anaerobic or at least severely undersaturated with respect to oxygen. The water column on the other hand is almost always saturated with respect to oxygen; but occasionally even the water column can

become undersaturated (below 9ppm) as a result of stagnation and rapid organic degradation. Under these sort of environmental conditions sulphate-reducing and other anaerobic bacteria will flourish.

4.4. CARBONATE CHEMISTRY

One of the major inhibitors to dolomite formation is the low activity of the carbonate ion (see Section 1.2.). In most natural waters this low activity is due not only to carbonate ion concentrations being much lower than those of the cations with which they must combine to form dolomite, but also their strong tendency to complex with cations. This part of the study was undertaken to observe the effects of the chemical and bacterial processes on the concentration of the carbonate ion in the lake and porewaters.

4.4.1. Theory

The metabolism of SRB results in biochemical changes to the environment. SRB metabolise organic matter using sulphate as the terminal electron acceptor according to the following reaction:-

(4.3) $2\,CH_2O + SO_4^{2-} \text{ ----------> } H_2S + 2HCO_3^-$ (e.g. Berner, 1980)

The microbes consume cyanobacterial and other organic matter in an anoxic environment to help support their metabolism, thereby liberating ammonia, which is highly soluble. Ammonia dissolving in water significantly increases alkalinity and raises pH as a result of Equations 4.4 and 4.5.

(4.4) $NH_3 + CO_2 + H_2O \text{ ----------> } 2NH_4^+ + CO_3^{2-}$ (Berner, 1980)

or

(4.5a) $NH_3 + H_2O \text{ ----------> } NH_4^+ + OH^-$ (Slaughter & Hill, 1991)

(4.5b) $OH^- + HCO_3^- \text{ ----------> } H_2O + CO_3^{2-}$ (Slaughter & Hill, 1991)

Thus, during the process of sulphate-reduction, sulphate concentrations would be expected to decrease, whilst pH would tend to increase and carbonate ion concentration can be expected to increase.

Figure 4.3 shows the relationship of the three carbonate phases at different pH values. The general pattern is that carbonate ion concentration increases relative to other phases as pH increases. In addition to this, the carbonate phase curves have an added dimension shown in Figure 4.3b; this is salinity.

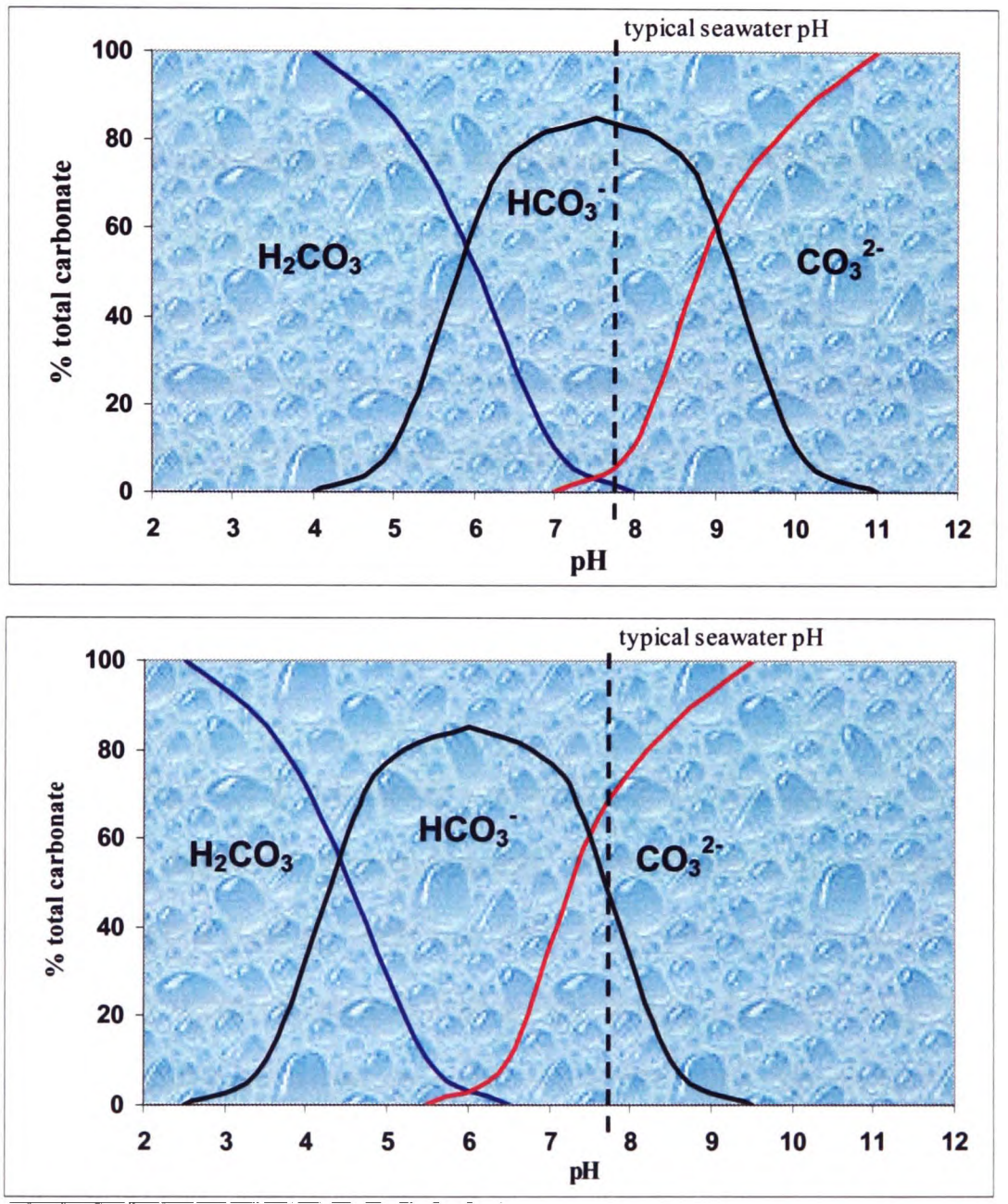


Figure 4.3. a) Relationship of carbonate phases to pH at seawater salinity. b) Relationship of carbonate phases to pH at the approximate salinity of the Coorong lakes in late November (modified from Pytkowitcz, 1983).

An increase in salinity causes the whole set of curves to shift to the left due to the effects of increased ionic strength on the HCO_3^- and CO_3^{2-} equilibrium constants and, in doing so, relatively large carbonate ion concentrations can be obtained at lower pH (Pytkowicz, 1983). The ephemeral Coorong lakes are all hypersaline (see Section 4.2) at the time of sampling and so large carbonate ion concentrations can easily be achieved at the pH of the study lakes. The combined effects of the metabolism of SRB and high salinity can thus increase carbonate ion concentration significantly, and although some of these ions may combine with various cations to form complexes, a large percentage of them become available to combine with calcium and magnesium ions to form dolomite.

4.4.2. Method for calculation of carbonate ion concentration

The calculation of carbonate ion concentration in natural waters is based upon a series of equations involving pH, pKa and the ratios of carbonate to bicarbonate ions according to the Henderson-Hasselbach equation in the carbonate system.

4.4.3 pH measurement

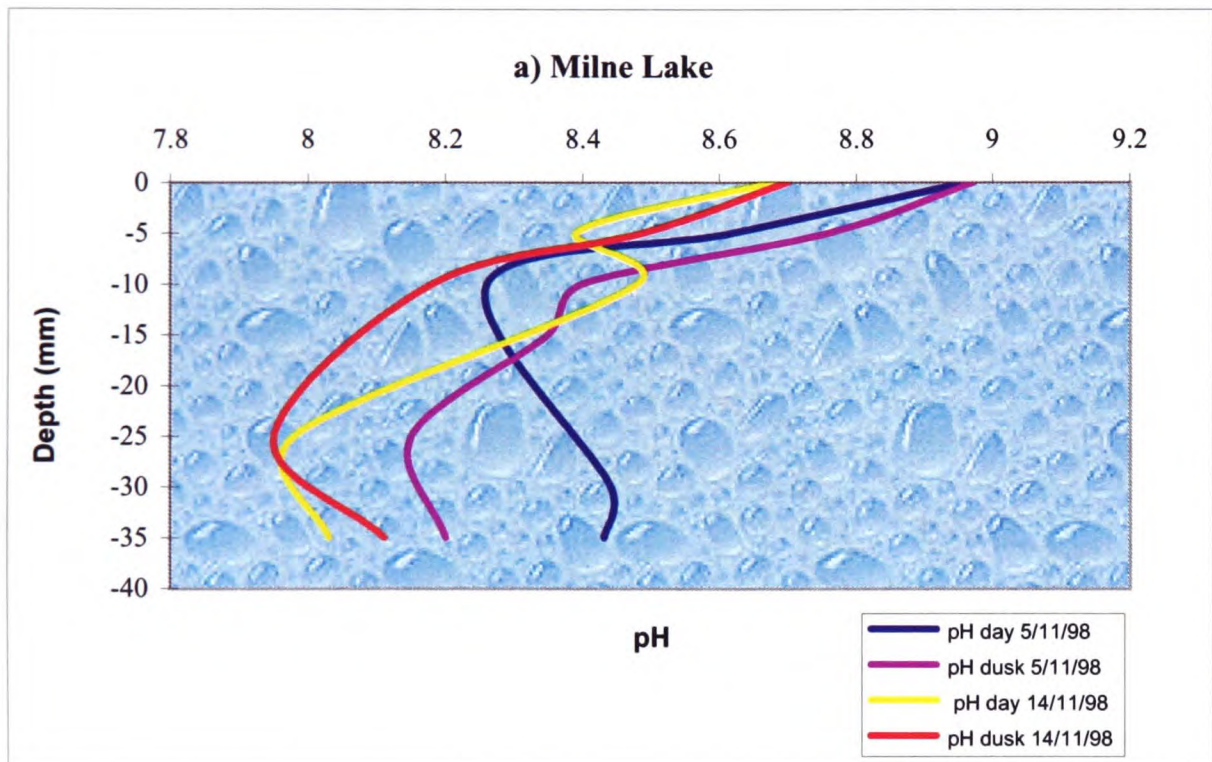
Several pH profiles (Figs 4.4 & 4.5) were constructed for the lake and porewaters of each of the lakes down to a depth of approximately 50mm below the sediment-water-interface. Profiles were constructed during both the 1998 and 1999 field seasons at various stages of lake desiccation. They were constructed in order to elucidate the impact of depth-stratified bio-geochemical processes on a micro-scale. To obtain pH values in the field, a Cyberscan pH 10 meter with automatic temperature compensation (Eutech instruments) was used. This was calibrated beforehand by using three standard pH buffers of 4.01, 7.00 and 9.20. It was re-calibrated daily to ensure reproducible results. Once in the field, measurements in the lakewater were taken by immersing the electrode in the lakewater approximately half way between the surface and the lake bed. At first readings were taken from different localities and depths in an individual lake but it was soon found that variation in pH with these

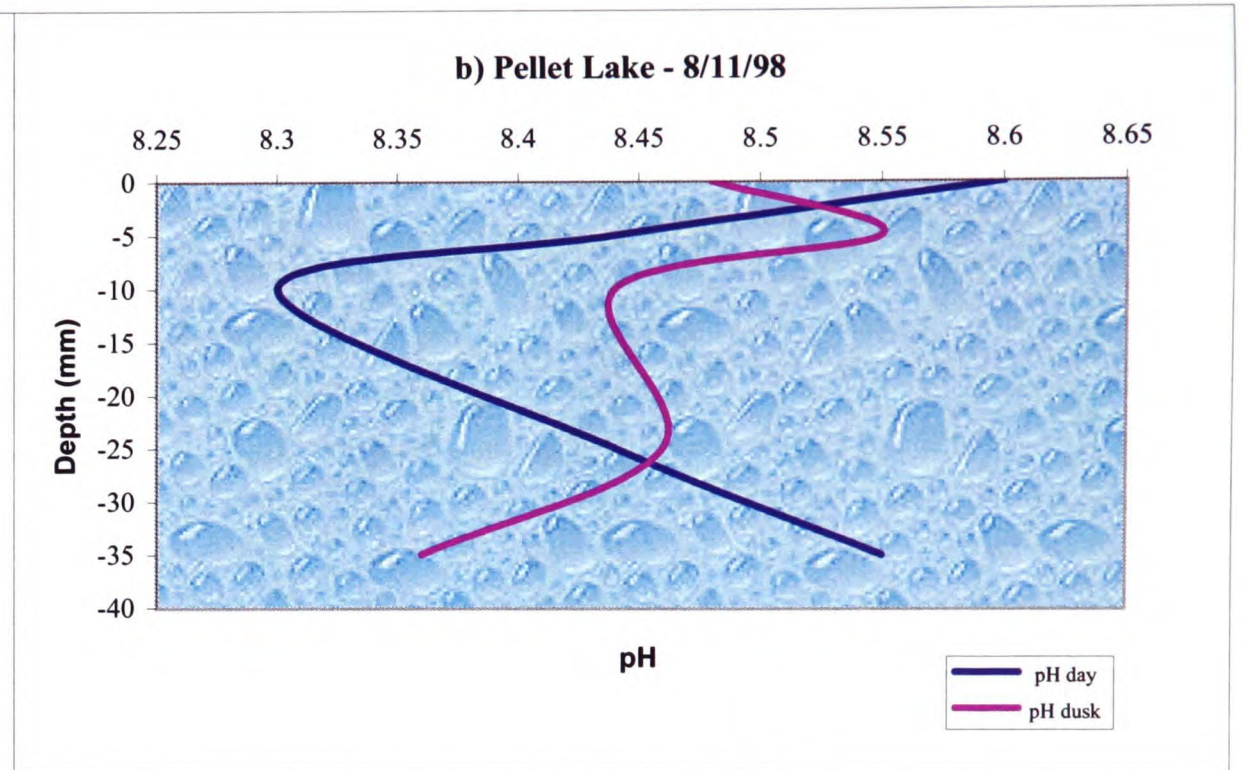
factors was minimal. Thereafter, only one reading was taken for each lake at a convenient area with water cover. Porewater pH readings were obtained by taking small cores of sediment from the margin of the lake, adjacent to where the lakewater readings were taken. The electrode was then inserted into the side of the hole created by the removal of the core at approximately 5mm intervals and as a double check it was also inserted into the core at 5mm intervals. Little variation in pH values was noted between the core and the core hole and so, thereafter, measurements were taken in the core-hole only.

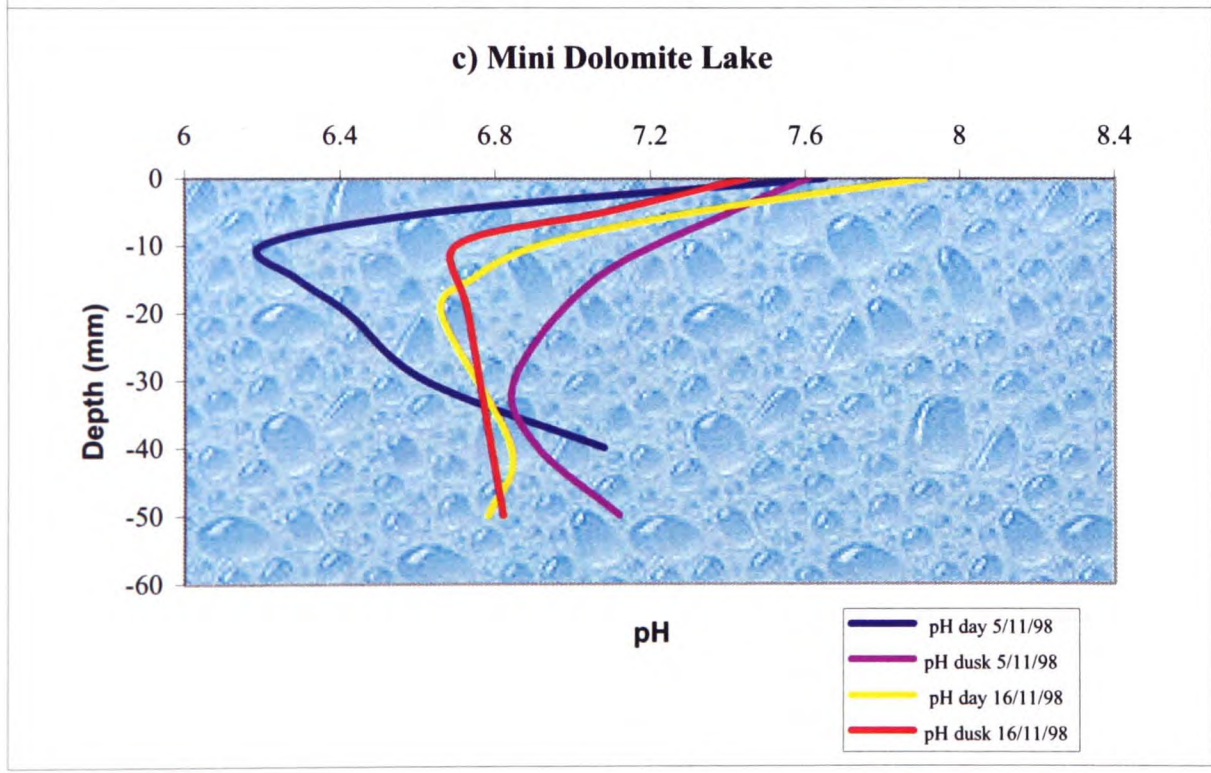
4.4.4. pH Data

Plots of pH versus depth at several times during the field seasons are shown in Figures 4.4 and 4.5. In the majority of cases, pH values in the residual lakewater are high, in excess of seawater, up to a maximum of around 9. Immediately below the sediment water interface there is a rapid decrease in pH, often as much as 0.5 to 1 pH unit within only c. 5mm depth. This decrease is attributed to H_2S gas escaping upwards from the sulphate-reduction zone below. The sulphate-reduction zone is interpreted to begin at around 5mm depth because this is where anoxia dominates, and persists down to at least 50mm depth. Beneath the top 10mm or so, a slow increase in pH is observed in many of the lakes and this is interpreted as due to the release of soluble NH_3 by SRB metabolic activity as one traverses the zone of sulphate-reduction. Deviations from this trend are attributed to bacterial communities moving up and down in the sediment column as a response to the balance between evaporation and rainfall. Wright (2000) records pH micro-profiles in a number of the lakes in this area. His Pellet Lake (south shore) profile shows a minima at 5-10mm followed by a gradual increase in pH down to 40mm. Wrights' profiles of Milne and Dolomite lakes were only sampled down to about 25mm and these show the pH decreasing to a minima below the top 5mm. No other authors have constructed depth related pH profiles for these lakes.

A further trend may be observed when pH is studied through time (Appendix 3). The pH in most lakes, both in lakewaters and in porewaters, tends to decrease as the lakes become dryer. Several authors have recorded lakewater pH values through time in these lakes. Early workers (Alderman and Skinner, 1957; Alderman, 1965) found maximum pH







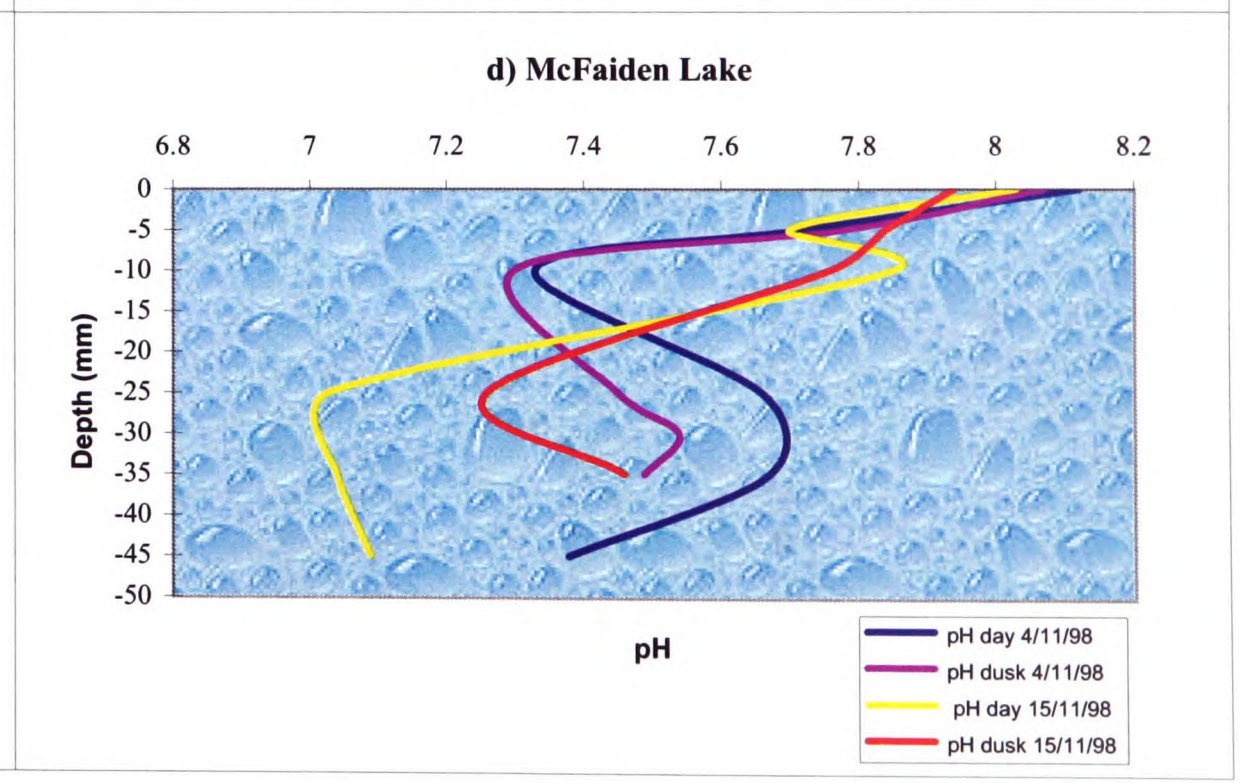
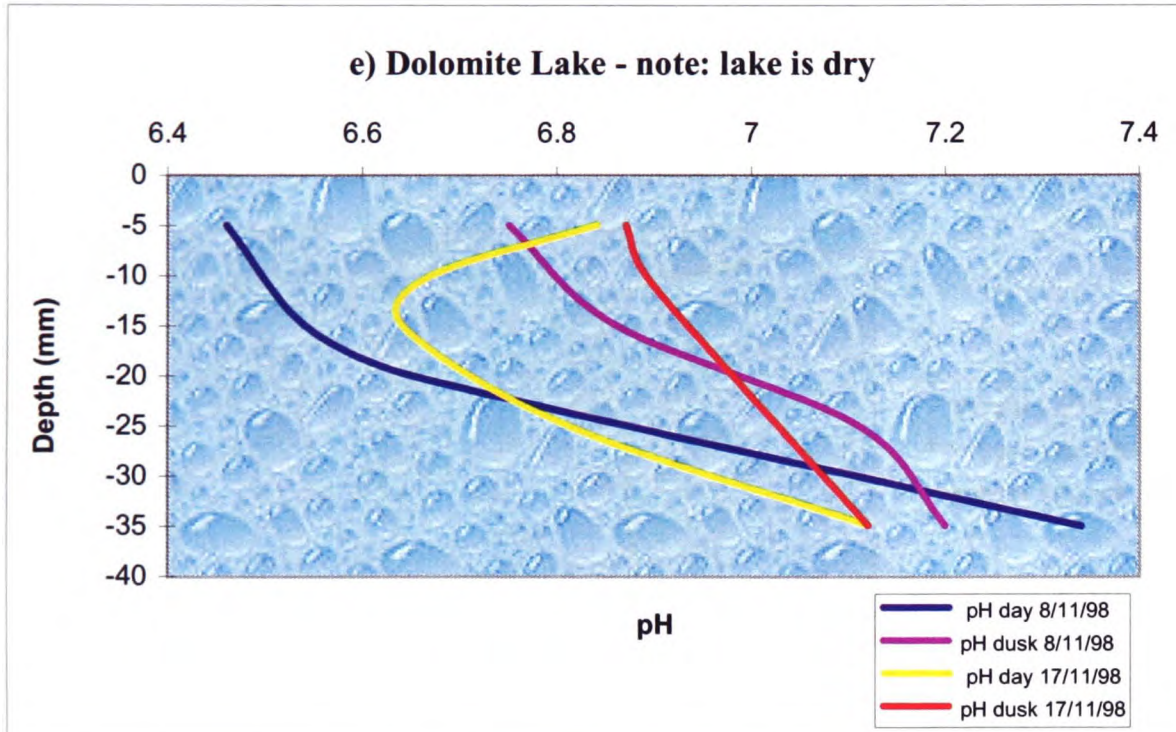
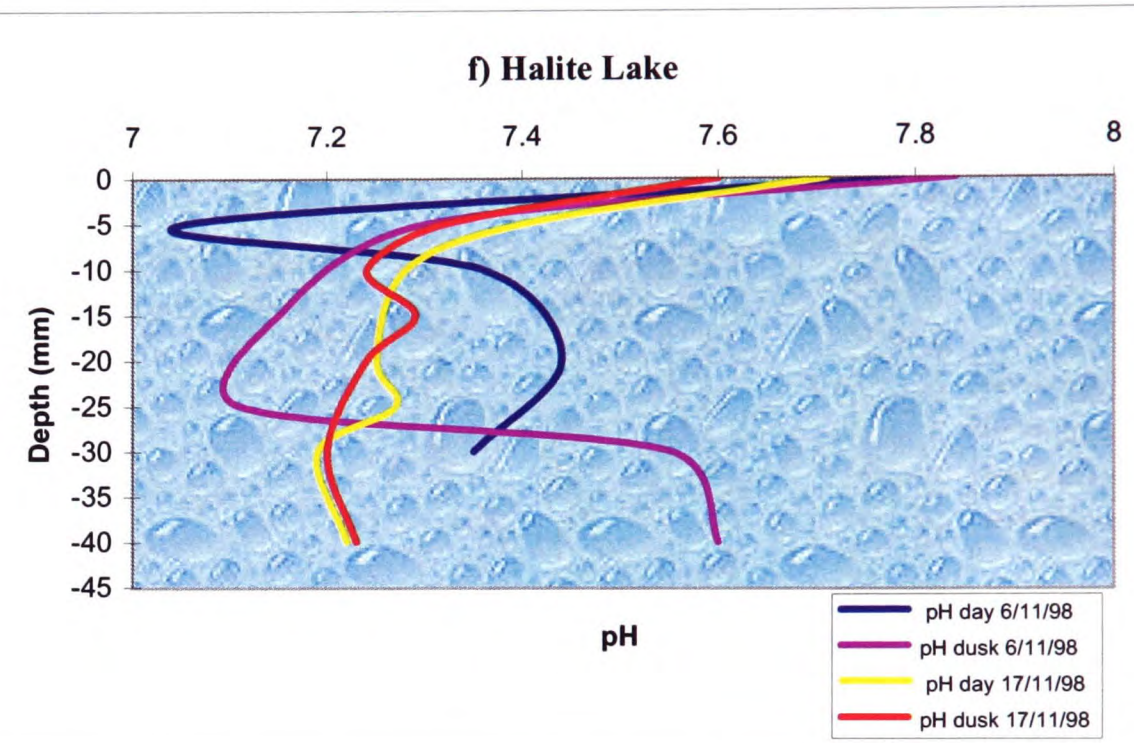
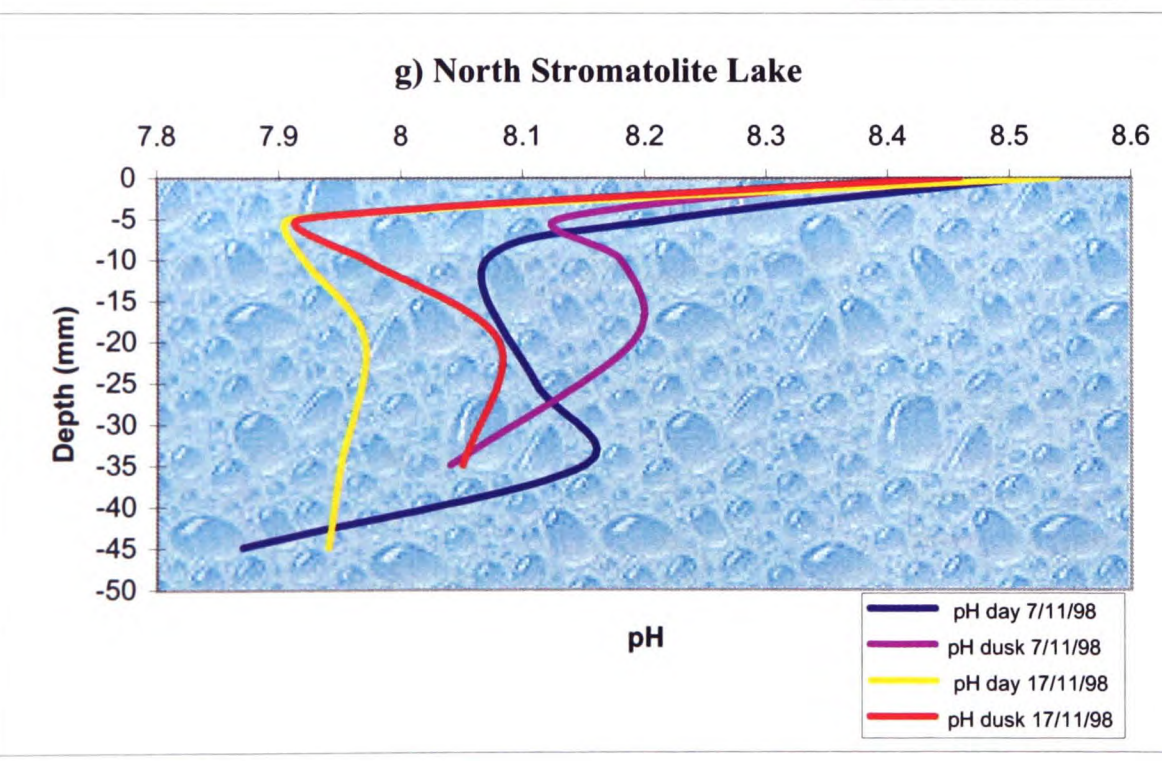


Figure 4.4a-d. 1998 pH graphs. Note: seawater pH ~ 7.8







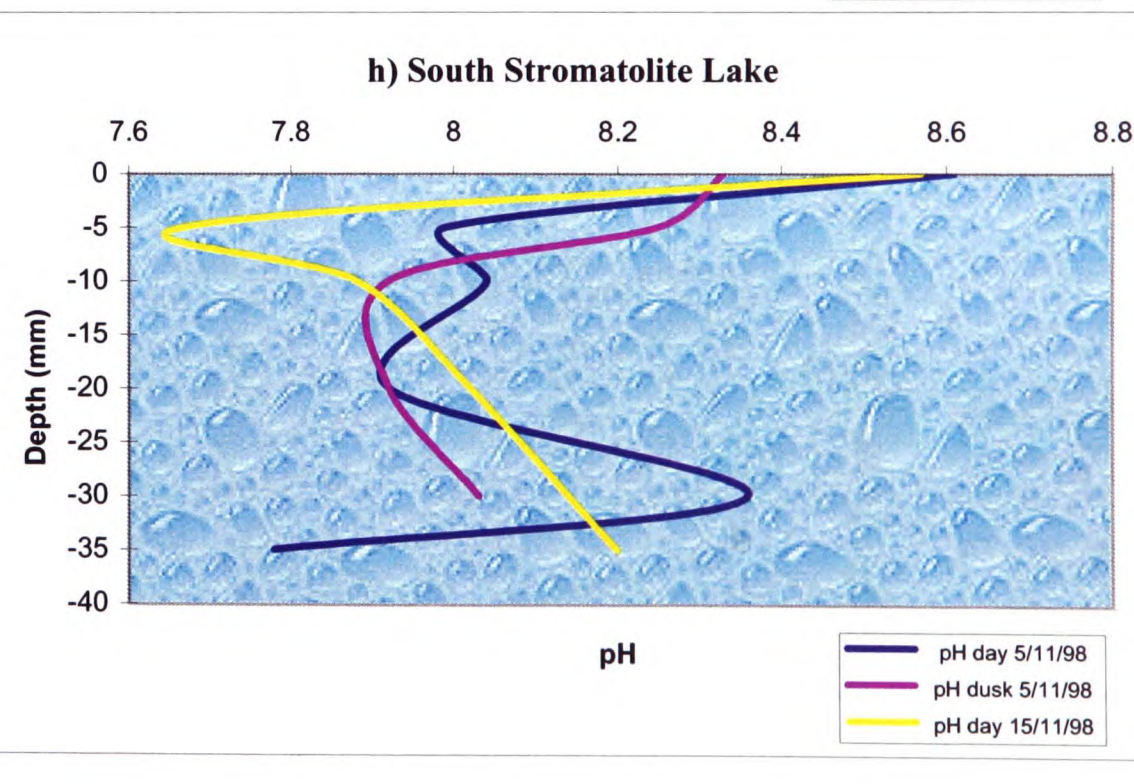
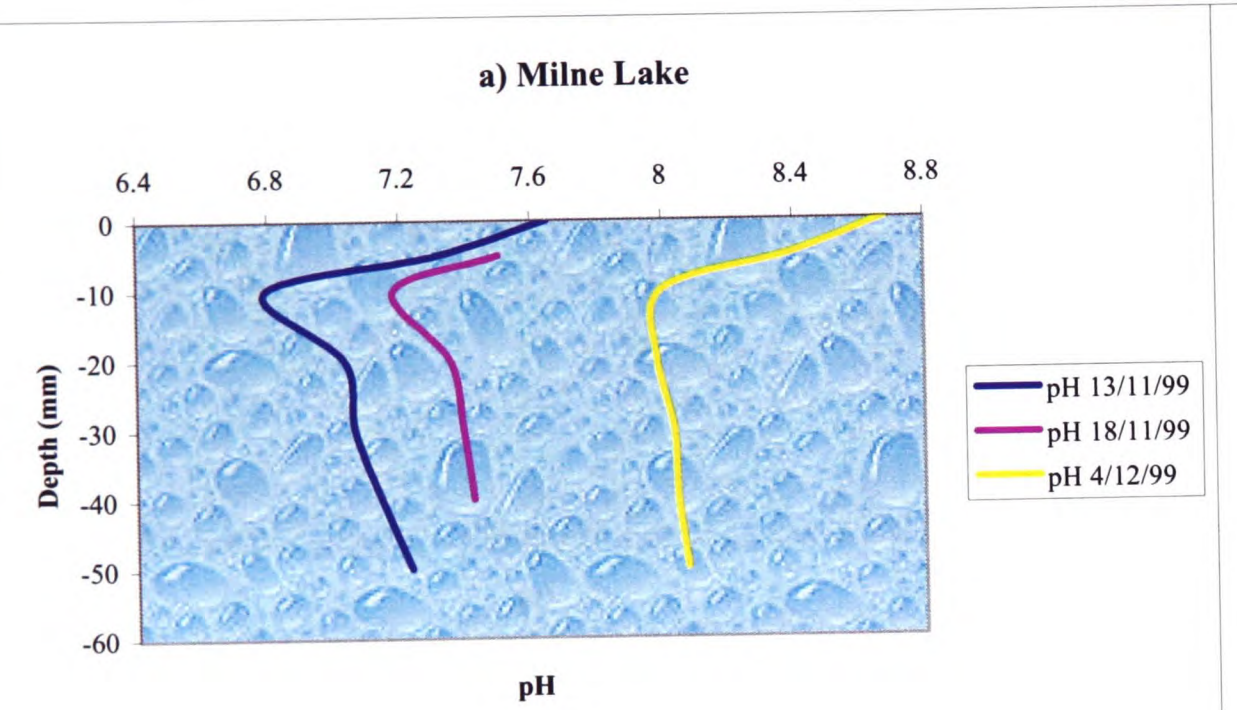
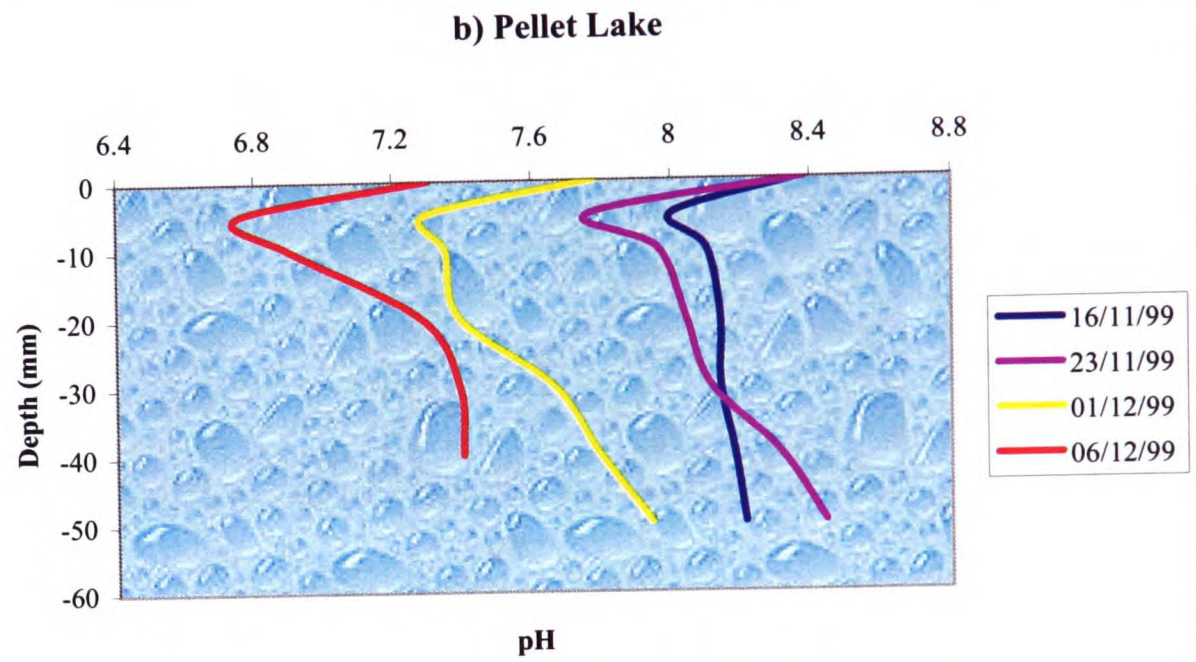
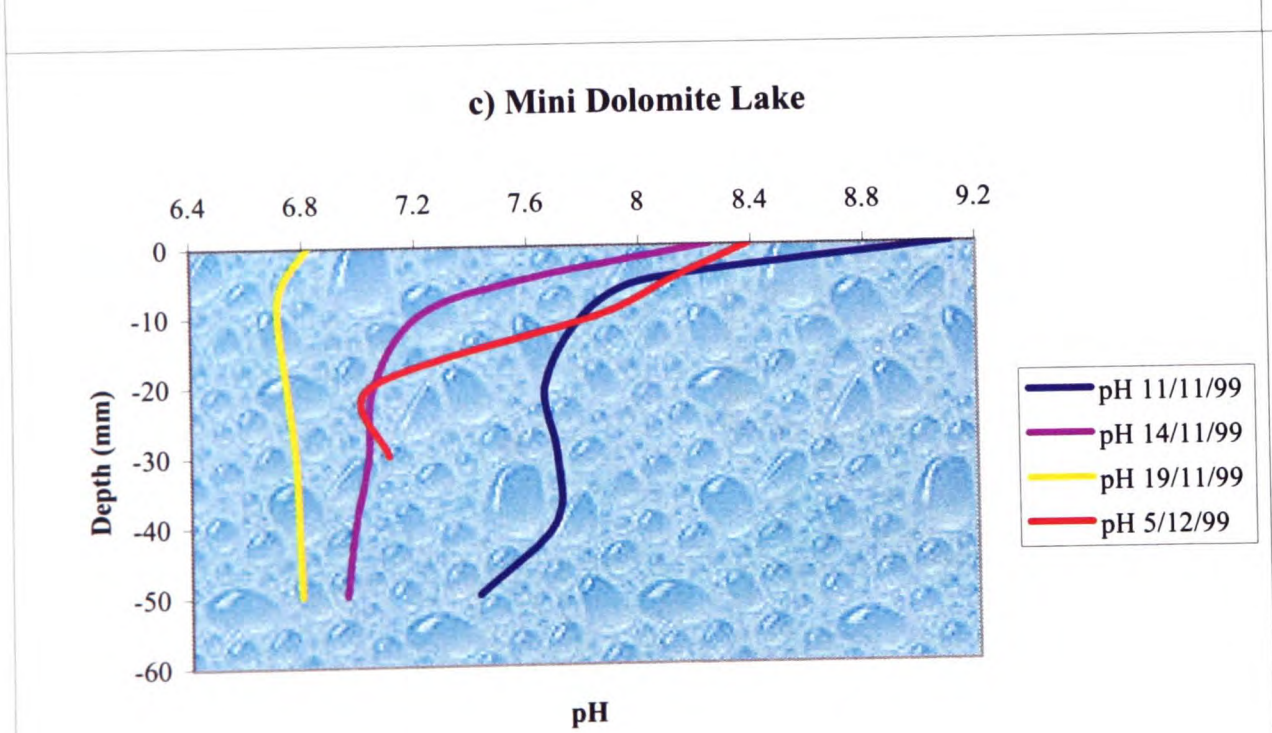


Figure 4.4e-h. 1998 pH graphs. Note: seawater pH ~ 7.8







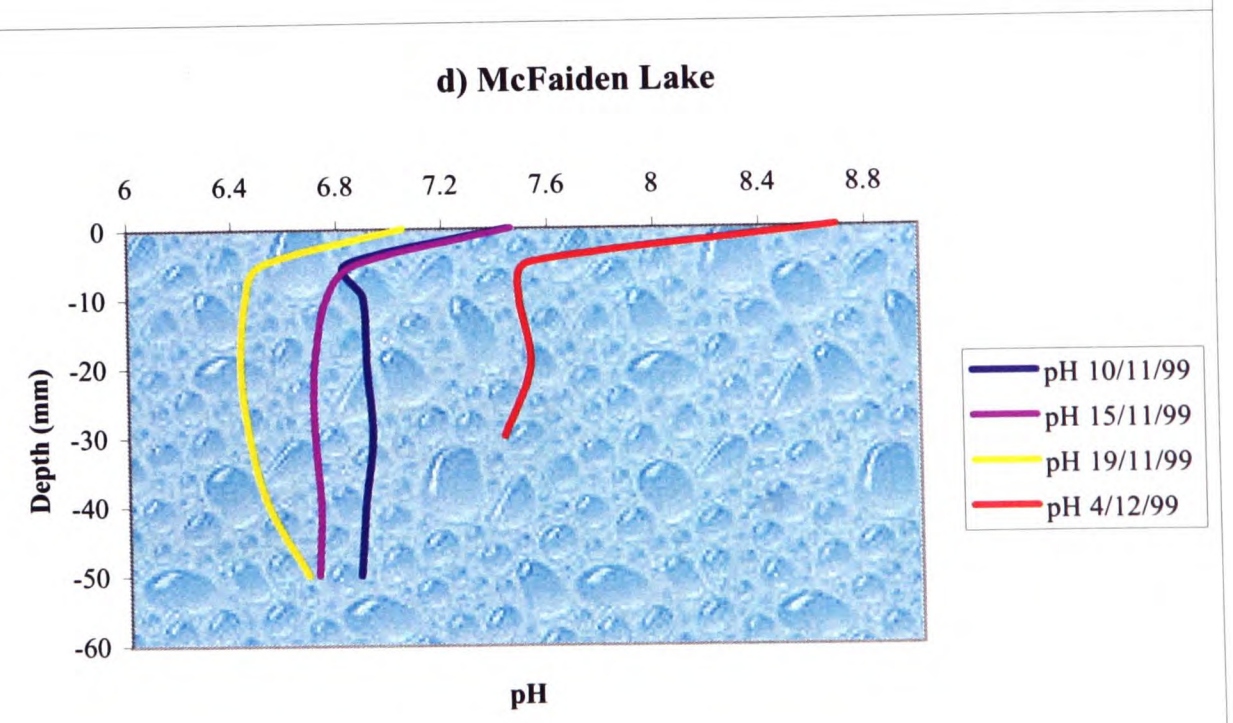


Figure 4.5a-d. 1999 pH graphs. Note: seawater pH ~ 7.8

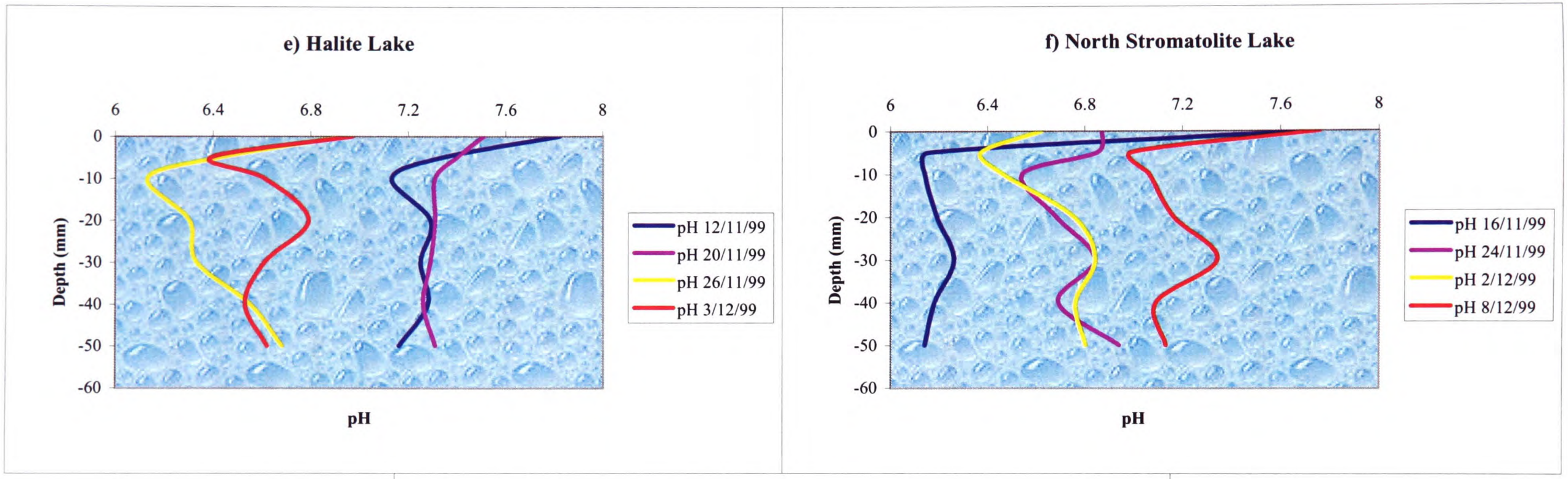


Figure 4.5e-g. 1999 pH graphs. Note: seawater pH ~ 7.8

values of 9-10 in the months of September and October. They suggested this maxima was related to intense photosynthetic activity of *Ruppia* grass. They found a drop in pH during late October and November until the lakes became completely dry. This was found to coincide with further rises in salinity inhibiting plant photosynthesis and ultimately killing off the *Ruppia* grass. Von der Borch (1965a+b) records pH maxima of over 9 in late August with significant drops by late October, whilst Wright (1999) records pH as high as 9.26 in Dolomite Lake and also records a drop in pH as desiccation proceeds. The drop in pH may also be related to carbonate precipitation at this time, to be followed after rainfall by a new cycle. The pH of the lake and pore-water is critical to the calculation of the carbonate ion concentration, as it is one of the major terms in the derivation of the Henderson-Hasselbach equation (see Section 4.4.6.).

4.4.5. The Carbonate System

The carbonate system is linked to the dissolution of atmospheric CO_2 in water to produce carbonic acid. Carbonic acid is a diprotic acid and therefore contributes two protons which require neutralisation. This is represented in Equations 4.6 – 4.8, which are controlled by pH, salinity and temperature.

$$H_2O + CO_2 \Leftrightarrow H_2CO_3\,(aq) \qquad (4.6)$$

$$H_2CO_3 \Leftrightarrow H^+ + HCO_3^- \qquad (4.7)$$

$$HCO_3^- \Leftrightarrow H^+ + CO_3^{2-} \qquad (4.8)$$

(Schulz and Zabel, 2000)

In normal seawater pH is 7.8-8.1 which is lower than the pK_a of Equation 4.8 (see next section) whereas in brines, such as found in the lake and porewaters of ephemeral Coorong lakes, pH is greater than pK_a, favouring the products of Equation 4.8 (i.e. the carbonate ion). Using simple chemical relationships contained in the Henderson-Hasselbach equation the carbonate and bicarbonate concentrations in natural waters can be calculated.

4.4.6. Derivation of the Henderson-Hasselbach Equation

Firstly, pH is defined as:

$$pH = \log_{10} \frac{1}{[H^+]} = -\log_{10} [H^+] \qquad \text{(e.g. Silberberg, 2000)} \qquad (4.9)$$

By analogy with pH, the pK of an acid is defined as the negative logarithm of the dissociation equilibrium constant of the acid, here in the HCO_3^- – CO_3^{2-} conjugate acid - base system:

$$pK_a = -\log_{10} K_a \qquad \text{(e.g. Silberberg, 2000)} \qquad (4.10)$$

Weak acids can differ widely in their strength of ionisation; for any conjugate acid – base, the proportion of acid to base is related to the ionisation state of the acid – base system (i.e. the concentration of H^+). An equation can be derived which illustrates this relationship:

$$HA + H_2O \Leftrightarrow H^+ + A^- \qquad \text{Giving} \quad K_a = \frac{[H^+]\,[A^-]}{[HA]}$$

Taking logs

$$\log_{10} K_a = \log_{10} \frac{[H^+]\,[A^-]}{[HA]}$$

This can be rearranged:

$$\log_{10} K_a = \log_{10} [H^+] + \log_{10} \frac{[A^-]}{[HA]}$$

Now if this is further rearranged as follows:

$$-\log_{10} [H^+] = -\log_{10} K_a + \log_{10} \frac{[A^-]}{[HA]} \qquad (4.11)$$

It can be seen that two of the terms in 3.11 can be replaced by terms defined in 4.9 and 4.10, resulting in:

$$pH = pK_a + \log_{10} \frac{[A^-]}{[HA]} \qquad \textbf{The Henderson-Hasselbach Equation} \qquad (4.12)$$

Now, taking into account the system of interest (carbonate system) and the two variables to be calculated the equation can be modified to:

$$pH = pK_a + \log_{10} \frac{[CO_3^{2-}]}{[HCO_3^-]}$$

Rearranging and normalising the bicarbonate term to 1:

$$pH - pK_a = \log_{10} \frac{[CO_3^{2-}]}{[HCO_3^-]} = \frac{X}{1} \qquad (4.13)$$

The Henderson-Hasselbach equation thus gives a ratio of the two components of interest if the pH and pK_a of a solution are known. However to obtain absolute concentration values it is also necessary to perform a titration to discover the amount of acid needed to neutralise the solution. The titration is also needed to obtain an absolute value for the pK_a of a solution.

4.4.7. Sample collection and titration processing

Lakewater samples were collected by immersing a 30ml collection vessel in the lake and allowing it to fill naturally. These were sealed immediately and taken back to the field base. Titrations were carried out within two hours of collection. Titrations were performed by taking a known volume of the lakewater (15ml in 1998; 2ml in 1999) and titrating it with hydrochloric acid of known molarity (0.05M). It was necessary in most cases to add a small amount of KOH of known molarity (0.076M) to ensure the pH was at a level such that all the alkali components of the lakewater solution were liberated.

Porewater samples proved more problematical to obtain and required a novel technique. The lake bed sediment was cored down to a depth of five centimetres; these cores were taken in sediment immediately adjacent to where the lakewater had been sampled. The cores were transported back to the field base and divided into 10mm thick sections. Each of these in turn were transferred to centrifuge tubes and centrifuged in a Phoenix Orbital 300 centrifuge at 3000rpm. After centrifuging for approximately five minutes a distinct water layer could be observed on the surface. This was pipetted into a new container before being titrated with hydrochloric acid as above.

4.4.8. Titration Curves (example)

An example of a titration using the inflection point titration method is shown in Figure 4.6 (McFaiden Lake 28/10/98, lakewater). To determine the inflection points (points of maximum rate of change of pH per volume of titrant added) a titration curve is plotted using change in pH versus volume of titrant added. The inflection points can clearly be seen on the example curve and the pH at which these inflection points occur corresponds to pK_a values of the solution. Since carbonic acid is diprotic the curve has two inflection points and thus two pK_a values. The one to be chosen is the one which corresponds to the conversion we are interested in, namely that from CO_3^{2-} to HCO_3^-, and so is obviously the one at higher pH. The volume of acid needed to perform the titration is also indicated on Figure 4.6 and represents the acid required to convert all carbonate species to carbonic acid; the start point of this transition is represented by the curve gradient becoming steeper and the end point is shown by the curve finally flattening out. These important values complete the data necessary for the calculation of carbonate concentration.

The calculation of carbonate concentration is thus carried out in two parts – firstly, using the Henderson-Hasselbach equation to find a ratio between carbonate and bicarbonate, and secondly, by performing a molarity calculation to obtain the absolute values.

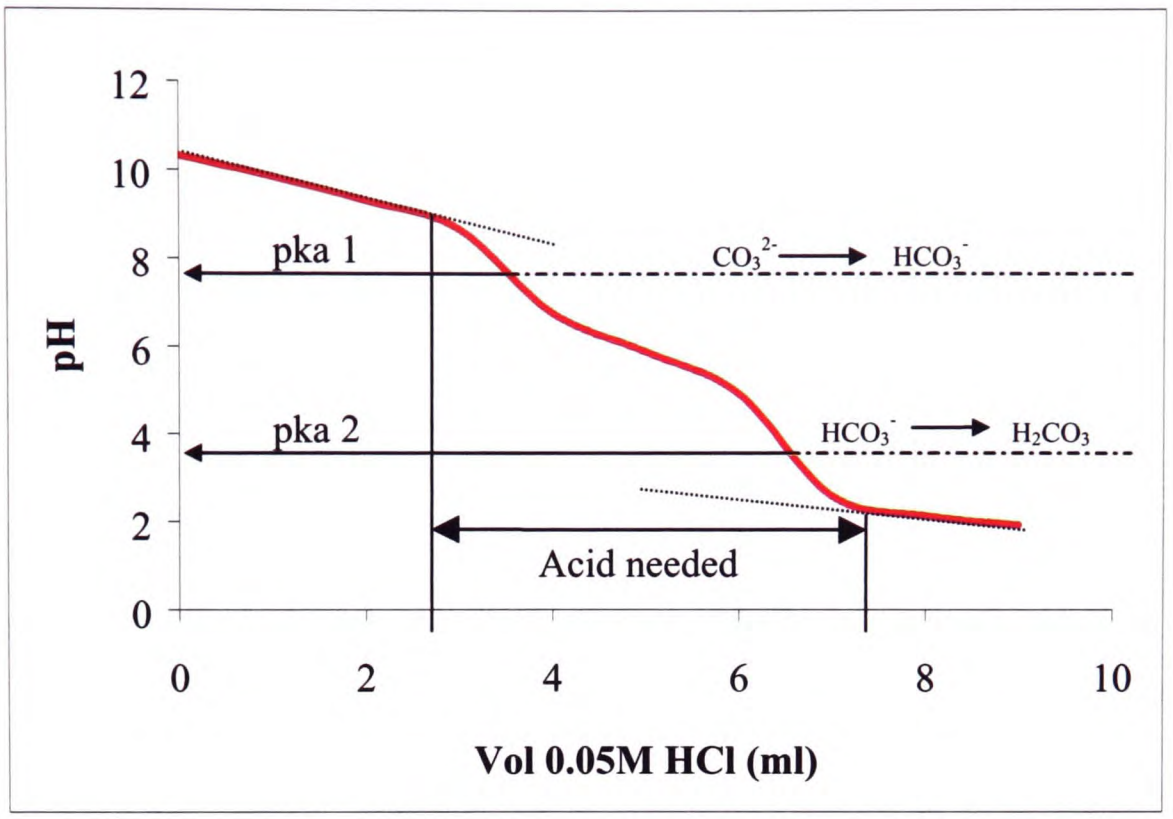


Figure 4.6 A typical titration curve (McFaiden Lake 28/10/98, lakewater). pKa = 7.8; original lakewater pH = 8.55

4.4.9. Calculation of carbonate ion concentration (example)

Measured or known values:

Vol. Sample = 15ml

pH = 8.5

pKa = 8

Vol. KOH = 2ml

Concentration KOH = 0.076M

Vol. HCl = 10.5ml

Concentration HCl = 0.05M

From the Henderson-Hasselbach Equation (Eq. 4.12):

$$pH = pk_a + \log_{10} \frac{[CO_3^{2-}]}{[HCO_3^-]}$$

Substituting known terms and rearranging:

$$8.5 - 8 = \log_{10} \frac{[CO_3^{2-}]}{[HCO_3^-]}$$

$$10^{0.5} = \frac{[CO_3^{2-}]}{[HCO_3^-]}$$

Therefore:

$$\frac{[CO_3^{2-}]}{[HCO_3^-]} = \frac{3.16}{1} \qquad (4.14)$$

From the molarity calculation:

$$\text{Moles KOH} = \text{vol.} \times \text{conc.} = 2 \times 0.076 = \frac{1.52 \times 10^4}{1000}$$

$$\text{Moles HCl} = 10.5 \times 0.05 = \frac{5.25 \times 10^4}{1000}$$

Because carbonic acid is diprotic, moles of acid = 2 x moles carbonate

Therefore:

Moles carbonate = 0.5 (5.25×10^4)

Now subtract moles KOH

Moles carbonate = $2.625 \times 10^4 - (1.52 \times 10^4) =$ **$\underline{1.105 \times 10^4 \text{ moles}}$** (4.15)

Combining 4.14 and 4.15:

Moles $CO_3^{2-} = 1.105 \times 10^4 \times (3.16/4.16) =$ **$\underline{8.4 \times 10^5 \text{ moles}}$**

Since the volume of the sample was only 15ml we must multiply by (1000/15) to get the molar value. Then, to obtain the concentration in mg/l, we must multiply first by the molecular weight and then by 1000.

Therefore:

$[CO_3^{2-}] = 8.4 \times 10^5 \times (1000/15) \times 60 \times 1000 =$ **336 mg/l**

Similarly:

$[HCO_3^-] = 1.105 \times 10^4 \times (1/4.16) \times (1000/15) \times 61 \times 1000 =$ **108 mg/l**

NB. All equations independently verified by Matthew Lloyd, Department of Chemistry, University of Oxford.

4.4.10. Results

A good data set was obtained in the 1999 field season and this can be seen in Figure 4.7 and Appendix 3, whilst the titration curves can be found in Appendix 4.

Milne, Mini Dolomite and McFaiden Lakes show similar general trends (Fig. 4.7 a-c). Carbonate ion concentrations in the lakewater are well in excess of seawater (16.2mg/l) but the majority are below about 200mg/l. A large increase in CO_3^{2-} concentrations is observed beneath the sediment-water-interface before the concentration stabilises or begins to drop off at depth (average of around 30mm). The maximum concentration varies substantially with lake and with time, from less than 200mg/l to over 1500mg/l, and the depth at which this maximum occurs is also somewhat variable. These concentrations are remarkably high, up to a maximum of around 100 times that of seawater. Very little data have been published about carbonate ion concentrations in these lakes. Skinner (1963) records carbonate ion concentrations twice as high as seawater during the month of November in Kingston Lake, a little to the south of these study lakes. Von der Borch *et al.* (1975) report groundwater in the

area enriched in carbonate ions by 10-20 times that of seawater. Wright (1999) reports lakewater concentrations in excess of seawater, using titrations performed at CSIRO, Adelaide. These were carried out some time after sample collection and are therefore likely to have underestimated carbonate ion concentrations. No previous data have been published on porewater carbonate ion concentrations in this area.

The significant increases in carbonate ion concentration can be attributed to an increase in pH, brought about by the metabolic activity of sulphate-reducers and leading to buffering by the bicarbonate ion (Eq. 4.5b). Carbonate ion concentration may also be increased by dissolution of carbonate minerals, but since November is an intensely evaporative time in the cycle, this is unlikely; there was no similar increase in calcium values in the lakewaters. The depth at which the concentration maximum occurs may reflect the distribution of the SRB community in the sediment, whilst the absolute value may reflect the balance between the intensity of sulphate-reduction and the incorporation of the carbonate ion into new mineral phases. Pellet and North Stromatolite lakes (Fig. 4.7b & f) show a marked drop in carbonate ion concentration immediately below the sediment water interface. This may be attributed either to formation of new carbonate minerals, or to the action of H_2S, making conditions less alkaline and thus favouring the conversion of the carbonate ion to the bicarbonate ion.

The results show that concentrations of the carbonate ion in all of the lakes are greatly in excess of those in seawater at all times and depths during the sampling period, consistent with the effects of microbial mediation (SRB activity) of lake and porewaters. This increase in concentration therefore favours the precipitation of carbonate phases. There are, however no straightforward and easily explained differences in CO_3^{2-} concentration between the dolomitic and non-dolomitic lakes. It is concluded that sulphate-reduction is active in all of these lakes and the level of sulphate may control precipitation of both dolomite and other carbonate phases. Unfortunately, it was not possible to calculate carbonate ion concentrations for the 1998 field season because a) porewaters could not be obtained and b) failure to note down the amount of KOH added to each lakewater sample resulted in the failure of the molarity calculation.

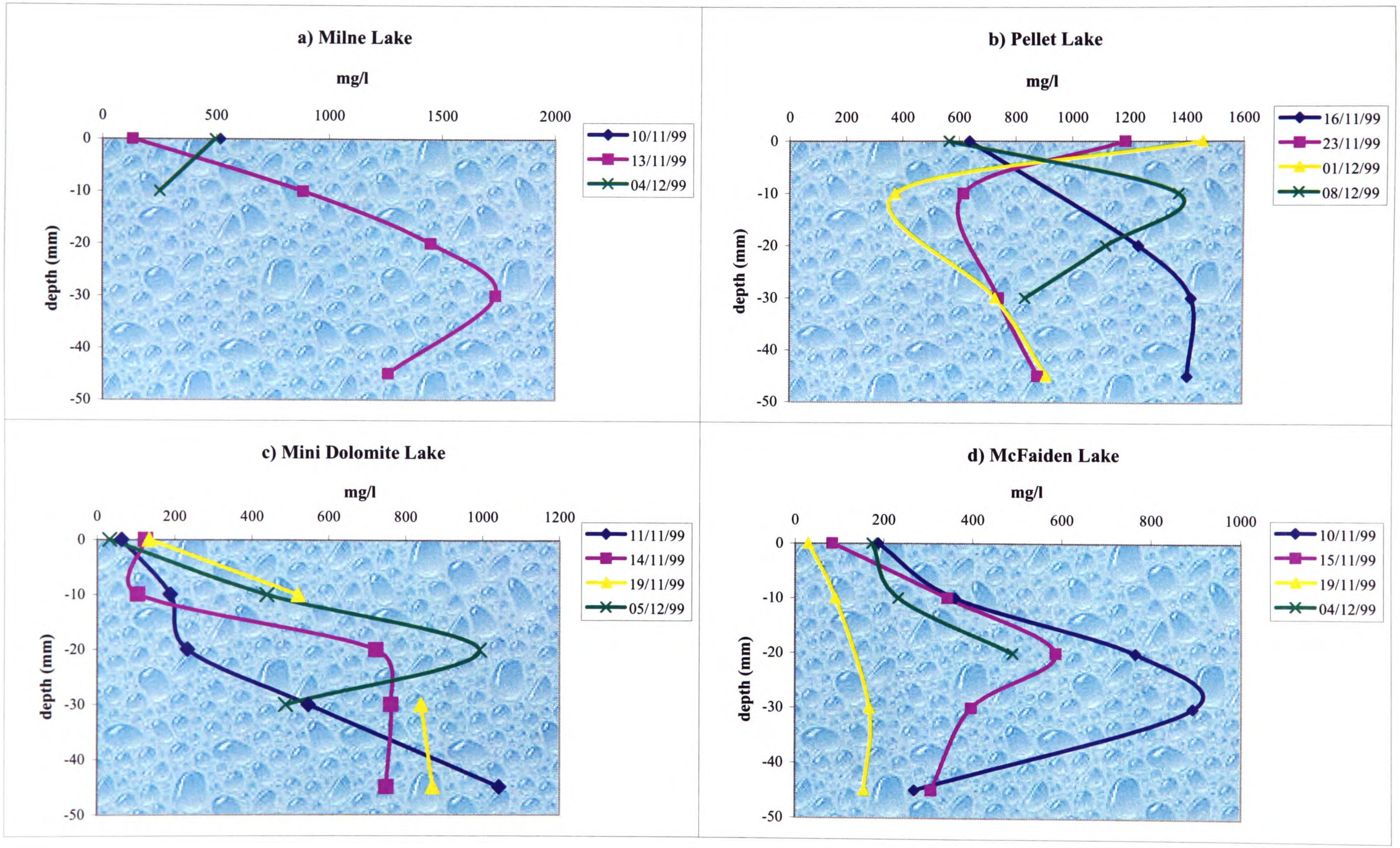
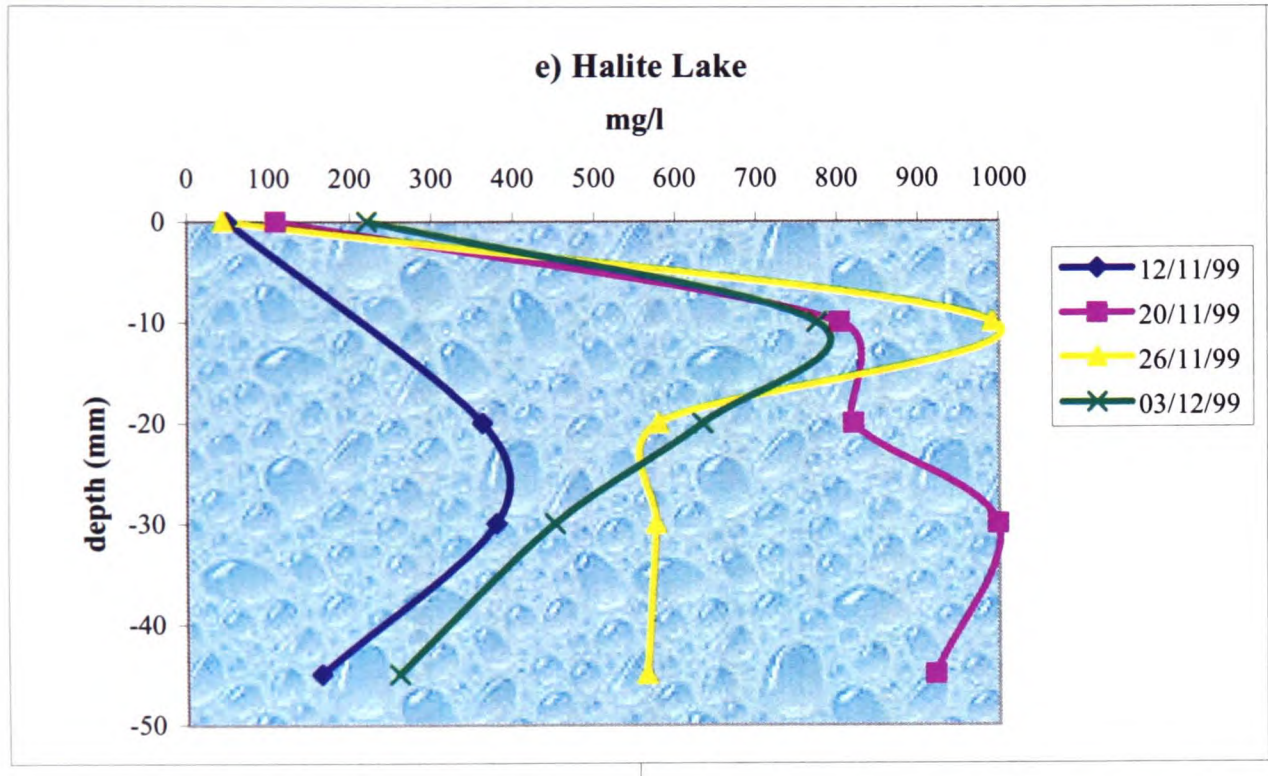
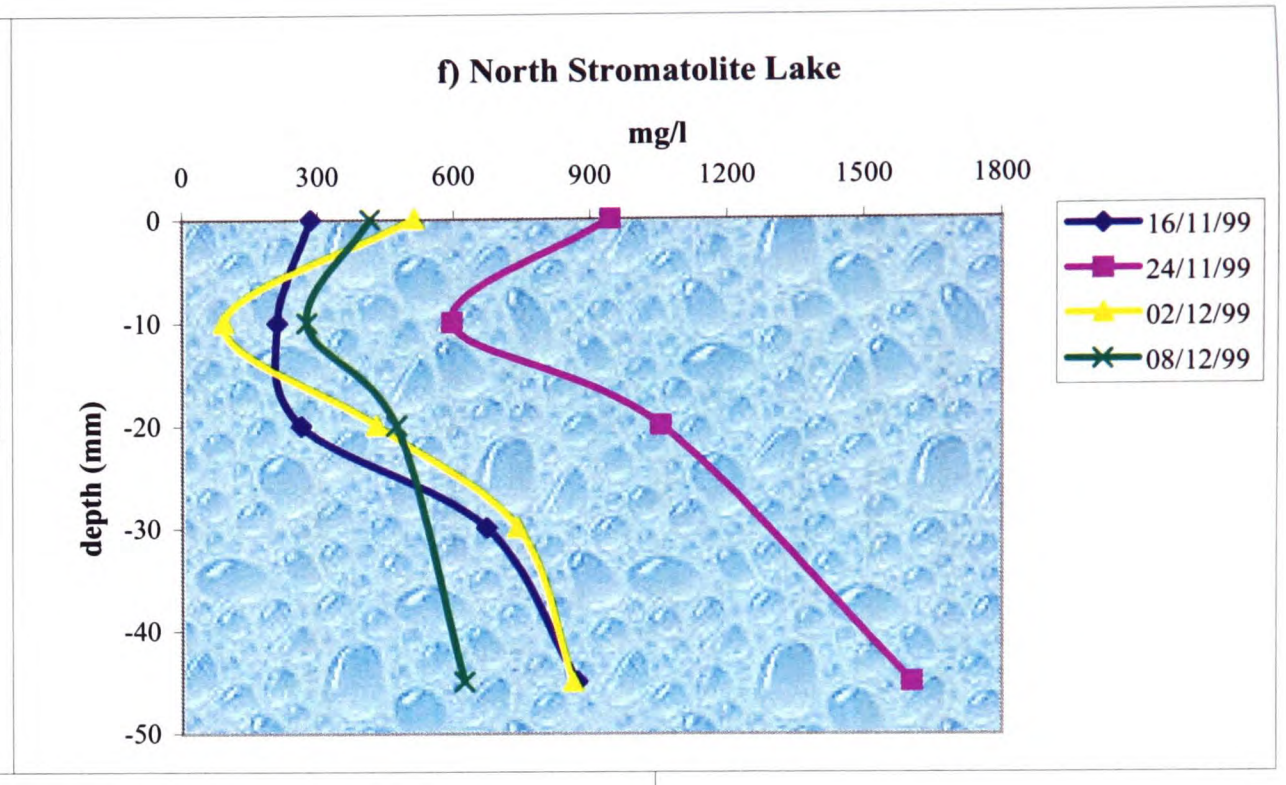


Figure 4.7a-d. Carbonate ion concentrations, 1999. Note: seawater ~ 16mg/l





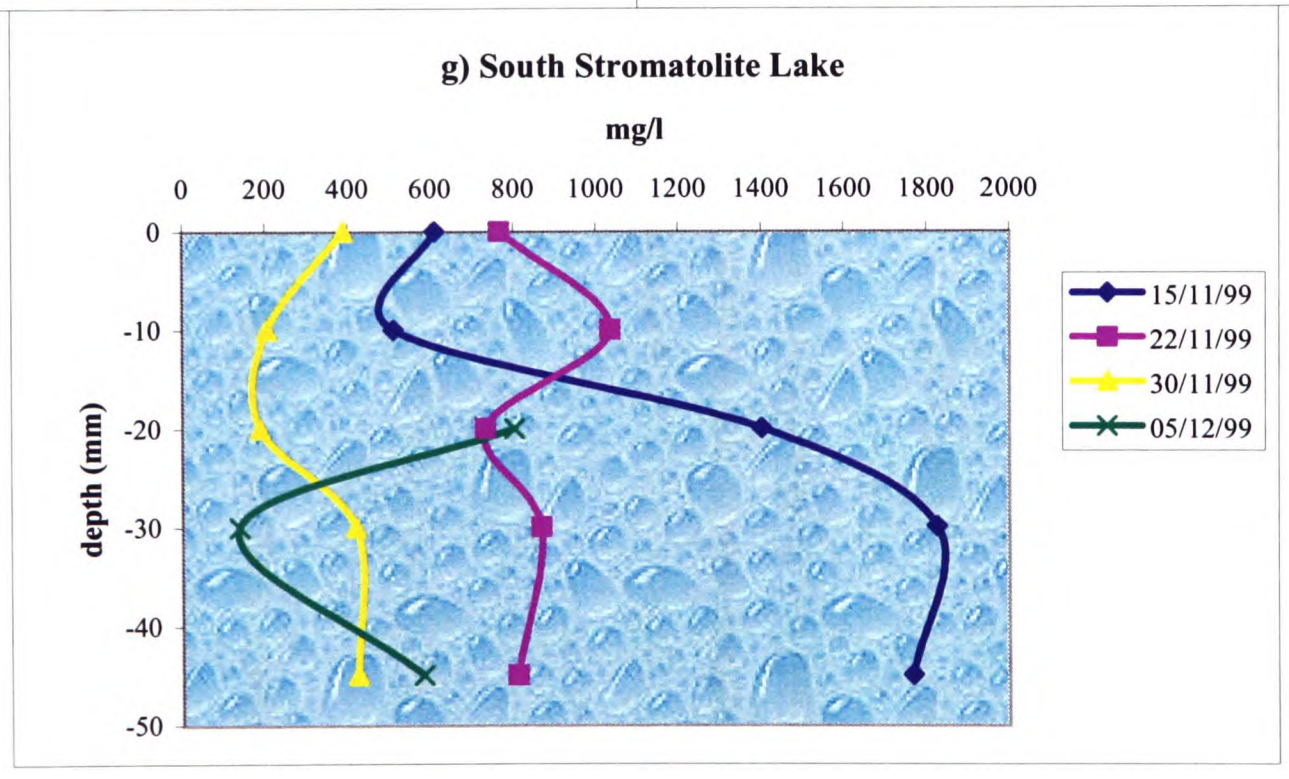


Figure 4.7e-g. Carbonate ion concentrations, 1999. Note: seawater ~ 16mg/l

4.5. SULPHATE CHEMISTRY

The measurement of sulphate ion concentrations in the lake and porewaters is critical to this study because of their inhibiting nature towards dolomite formation, and their contrasting abundance in many dolomite forming localities. The ability of sulphate ions to form neutral ion complexes with magnesium ions (Eq. 4.16), reducing magnesium ion activity and therefore inhibiting dolomite formation, is well documented (Baker & Kastner, 1981; Wright, 1999).

$$Mg^{2+} + SO_4^{2-} \text{ ----------> } MgSO_4^{\circ} \qquad (4.16)$$

Sulphate-reducing bacteria can substantially reduce concentrations of sulphate, according to Equation 4.17 (Berner, 1980):

$$2\,CH_2O + SO_4^{2-} \text{ ----------> } H_2S + 2HCO_3^{-} \qquad (4.17)$$

This section investigates how sulphate ion concentrations change during the latter stages of the evaporative cycle and whether SRB can reduce sulphate ion concentrations to levels where complexing is diminished and dolomite can precipitate.

4.5.1. Field collection and preparation

Lakewater samples for sulphate ion analyses were collected in 33ml airtight plastic containers in November 1998 (12ml containers were used in 1999). The container was submerged in the lake and allowed to fill naturally. Once filled, a small amount of gluteraldehyde was added to 'fix' the solution (i.e. to prevent further bacterial action altering the sulphate ion concentration). These were stored in a refrigerator, as a further precaution against biological activity, before being carefully shipped back to the U.K. Once back in Oxford, sulphate ion concentration was determined in the laboratory using the method outlined below (Section 4.5.3.).

Porewater samples were treated in an identical manner but the mode of collection was slightly different. Difficulties in extracting porewater from the lake sediments during the 1998 field season were so severe that no porewater sulphate data could be obtained; however, for the 1999 field season a centrifuge had been obtained which considerably aided porewater extraction.

Samples were processed as follows:

1) The lake sediments were cored adjacent to the locality of lakewater collection.
2) Cores were immediately divided into 10mm sections before being transferred to centrifuge tubes.
3) After centrifuging the porewater rose to the surface and could be pipetted into airtight plastic containers and "fixed" with gluteraldehyde.

4.5.2. Sediment dilution

Some sediment samples proved more problematical and would not yield porewater even when centrifuged. In these cases, a fixed amount of the sediment (25g) was mixed thoroughly with (50ml) of distilled water and then centrifuged and the resulting water was collected. This is not an ideal way of obtaining porewater since the exact dilution factor is not known, but limited resources in the field meant that this was the only way it could be done. Dilution factors could then be approximated using data from sediment samples which yielded porewater directly.

4.5.3. Determination of sulphate as barium sulphate

a) Overview

This method consists of the addition of warm barium chloride solution to a hot sulphate-containing solution that has previously been slightly acidified (Vogel, 1978):

$$Ba^{2+} + SO_4^{2-} \text{--------} > BaSO_4$$

The precipitation has to be carried out in a slightly acidic solution to prevent the formation of the barium salts of such ions as chromate, carbonate, nitrate and phosphate, which are insoluble in neutral solutions. Moreover, the barium sulphate crystals tend to be larger in slightly acidic solution and thus are easier to filter. Although, acidification also increases the solubility of barium chloride, it is found that this solubility is negligible in the presence of excess barium ions (Vogel, 1978). Competition from other cations such as sodium, potassium and calcium was prevented as far as possible by diluting the samples. However, the effects of these could not be removed entirely.

After the addition of barium chloride the precipitate was filtered, washed with de-ionised water, carefully ignited (see below) and weighed as barium sulphate.

b) Procedure

1. Samples were analysed in groups of six in the laboratory. Water samples from the 1998 field season had been collected in 33ml containers. It was found that this amount was in excess of what was actually needed for an accurate calculation of sulphate concentration. During the 1999 field season 12ml containers were therefore used for water collection. Each sample was emptied into a 250ml beaker, then the sample bottles and caps were washed out with de-ionised water to ensure that all the soluble sulphate was indeed in the beaker.
2. 1ml of concentrated hydrochloric acid was added to each beaker to ensure complete dissolution of carbonates.
3. The beakers were then warmed on a hot-plate with watch glasses over them to prevent evaporation - whilst this was in progress six sets of filtration equipment were erected consisting of filter funnel, conical flask and size 42 filter paper.
4. The contents of the beakers were filtered into conical flasks to remove any insoluble material, especially organic matter - the watch glasses and beakers were rinsed with de-ionised water, as were the filter papers to ensure all the material had passed through into the conical flasks. This was checked by the use of universal indicator paper to make sure the liquid coming through the filter paper is no longer acidic. The conical flasks were transferred back to the hot-plate.

5. 5 per cent barium chloride solution (i.e. 5g of $BaCl_2.H_2O$ in 100ml of de-ionised water) was prepared and warmed on the hot-plate.
6. The conical flasks were heated until they started bubbling, again with watch glasses covering the top, then the warm barium chloride was added dropwise (1 or 2ml at a time) whilst the solution was constantly stirred. If sulphate was present a white precipitate formed which settled to the bottom of the flask with time.
7. The supernatant liquid was tested for complete precipitation by adding a further few drops of barium chloride after the liquid had fully settled (after about an hour). When no further precipitation was observed the liquid was ready to be filtered - this happened after the addition of anywhere between 8ml and 50ml of barium chloride.

Filtration was carried out using the filter crucible method:

- Six Vitreosil filtering crucibles - porosity No. 4 - were cleaned in a water bath filled with de-ionised water and ignited in a furnace at 450°C. They were allowed to cool in a desiccator and then weighed on a balance accurate to five decimal places.
- Each crucible in turn was taken and inserted into the top of a side armed conical flask attached to an electric suction pump (model Capex 2D-C). Each sample was filtered under gentle to moderate suction. Care was taken to thoroughly wash out the conical flasks to get the maximum amount of precipitate through the filter system. The filter system was then washed through several times with warm de-ionised water. The base of the crucible was tested with universal indicator paper to ensure washing had been thorough and the liquid coming through was non-acid.
- The crucibles were dried in an oven at around 110°C for around 15 minutes and then transferred to the furnace to be ignited at 450°C, as the empty ones had been. These were left overnight in the furnace, then removed, left to cool in a desiccator and reweighed.

4.5.4. Data Calculation and Presentation

The difference between the weight of the crucible before and after gives the amount of barium sulphate. Because the ratio of barium to sulphate is 1:1 this can then be used to obtain the concentration of sulphate ions in the original sample. Then, for ease of comparison with other ions, this must be converted to milligrams per litre. This is a fairly simple process carried out as follows (using McFaiden Lake 10/11/99, lakewater as an example).

Weight before	15.10651g
Weight after	15.47638g

(Weight after) - (weight before) = 0.36987g

Therefore 0.36987g of $BaSO_4$ has been formed from 12ml of initial sample.

The molecular weight of $BaSO_4$ is 233.3g of which SO_4^{2-} makes up 96g

Thus the amount of SO_4^{2-} formed is 0.36987 x (96/233.3) = 0.1522g

So, there is 0.1522g in 12ml of sample

Thus, 0.1522g x 1000/12 = 12.683g in 1 litre

and 12.683 x 1000 = **12683 mg/l**

The results are presented in Table 4.1 and Figures 4.8-4.10.

	Lakewater	10mm depth	20mm depth	30mm depth	45mm depth
Milne Lake					
10/11/99	8180	8897	-	5780	3600
13/11/99	19665	-	10167	6980	3460
4/12/99	2523	11006	-	-	-
28/10/98	2751				
5/11/98	3451				
14/11/98	4751				
Pellet Lake					
16/11/99	9667	12276	8187	6306	5692
23/11/99	9726	12400	6057	5432	4879
1/12/99	12851	19282	8605	6950	-
7/12/99	11291	-	7870	5992	-
1/11/98	4904				
8/11/98	5496				
18/11/98	6389				
Mini Dolomite					
11/11/99	10698	19748	15298	24120	10110
14/11/99	17939	23027	17111	17660	13596
19/11/99	56591	21899	-	-	-
5/12/99	4868	10457	11620	14212	-
29/10/98	7107				
5/11/98	16617				
15/11/98	18554				
Mcfaiden Lake					
10/11/99	12683	16327	-	10068	9894
15/11/99	24304	29172	17075	-	-
19/11/99	40473	23160	21413	-	13140
4/12/99	3391	6800	19366	-	-
30/10/98	7568				
4/11/98	6709				
14/11/98	15528				

Table 4.1a. Sulphate ion concentrations (mg/l) in the dolomitic lakes, 1998 and 1999.

	Lakewater	10mm depth	20mm depth	30mm depth	45mm depth
Halite Lake					
12/11/99	20303	12261	14589	12012	9843
20/11/99	26955	13653	13490	13302	15006
26/11/99	33610	12104	12441	10520	8331
3/12/99	22164	17976	19585	18010	17490
29/10/98	12834				
6/11/98	12218				
16/11/98	15261				
N.Stromatolite					
16/11/99	20270	22117	19054	15367	16170
24/11/99	28311	25126	15591	17126	10568
2/12/99	75265	45550	34430	21265	15573
8/12/99	12360	12750	24156	26530	22432
1/11/98	6849				
7/11/98	8058				
17/11/98	10544				
S.Stromatolite					
15/11/99	12915	15932	13760	10245	9250
22/11/99	9670	8760	9930	7873	5719
30/11/99	32275	26194	14840	11564	-
5/12/99	5173	-	10872	12260	10292
29/10/98	3896				
6/11/98	7118				
15/11/98	7061				

Table 4.1b. Sulphate ion concentrations (mg/l) in the non-dolomitic lakes, 1998 and 1999.

4.5.5. Data analysis

The lakes were undergoing desiccation during both sampling periods. Figures 4.8 a & b both show evaporative concentration of the sulphate ion as desiccation proceeded. Sulphate ion concentrations reached higher levels in 1999 because sampling continued later in the season so that the lakes were two to three weeks further into their evaporative cycle. The major supply of the sulphate ion is seawater spray (see Section 1.7.2.) and the major sink for the sulphate ion is sulphate reduction by SRB (Chapter 2). No sulphate evaporites were observed either in the sedimentary succession or in the lakes themselves, apart from a very small amount of gypsum (Halite Lake) and celestine (Mini Dolomite Lake), even under XRD analysis (Appendix 1), so that evaporites are assumed to be unimportant in redistributing sulphate. Measurement of sulphate from local stream water and from rainwater showed negligible (< 500 mg/l) amounts present, so these can also be discounted as sources of the sulphate ion.

Patterns of sulphate concentration were disturbed by rainfall. Rainfall causes great dilution of surface waters in the lakes and can, therefore, give a false impression of sulphate ions being consumed by SRB. A torrential downpour at the start of December, 1999 resulted in dry or partially dry lakes being refilled to a level seen four to five weeks earlier in the evaporative cycle. The large dilution of sulphate concentration can be seen in all the lakes (Table 4.1) producing as much as a tenfold reduction. For this reason, data from early December are not included in Figure 4.8b. No such problems were encountered in 1998, when very occasional light rain had no significant bearing on sulphate concentrations.

From the available data, it appears that the intensity of evaporation at the very end of the evaporative cycle resulted in the last residual pools of water having very high concentrations of sulphate (between 5 and 30 times that of seawater). Undoubtedly, large quantities of sulphate were being used by the SRB in many of these lakes, but this usage is likely to have been masked by the sheer size of the sulphate reservoir. Wright (1999) is the only other author to have measured sulphate concentrations in these lakes and he reports similarly high concentrations (up to 73,400mg/l in South Stromatolite Lake) and also low

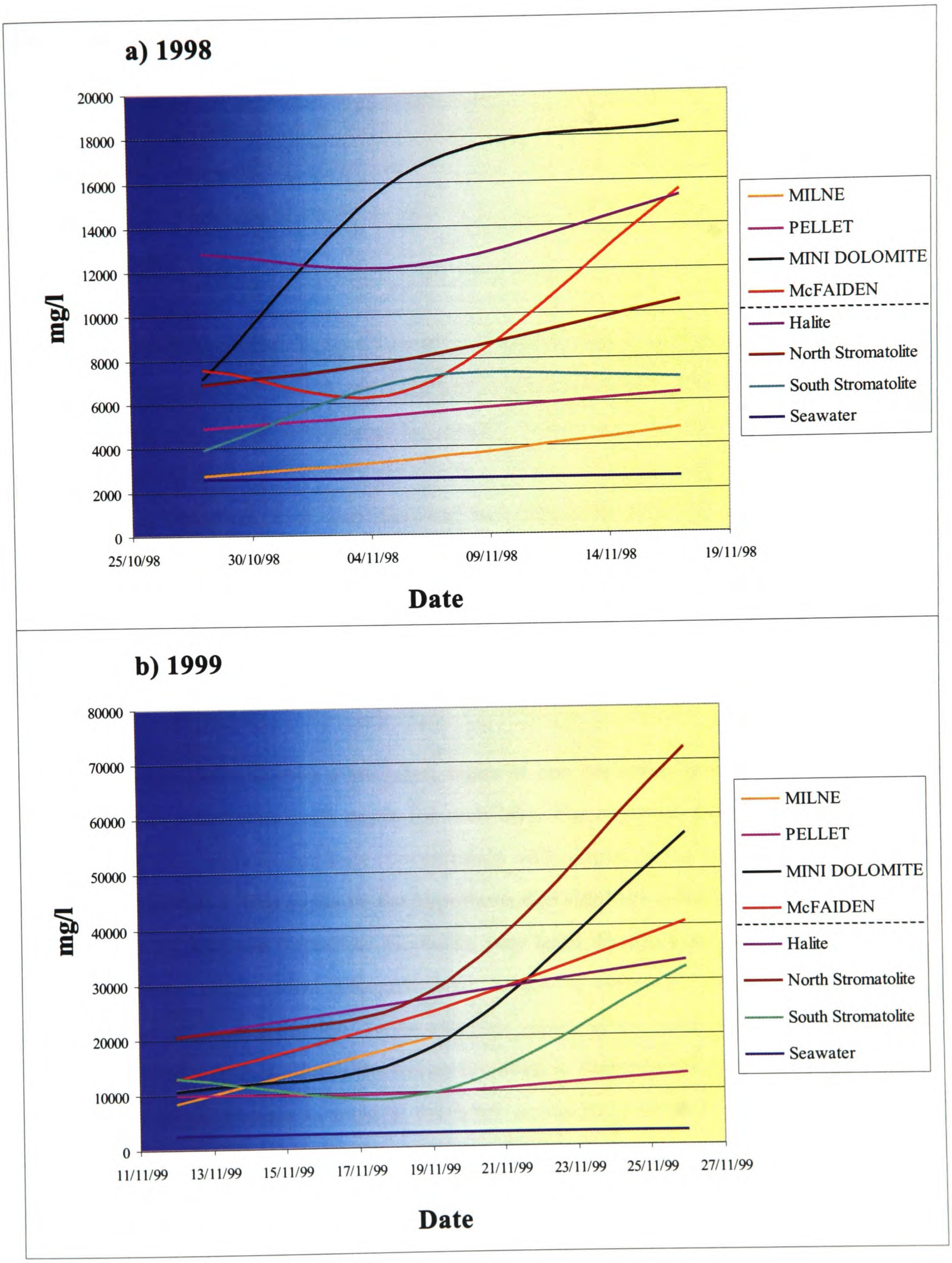


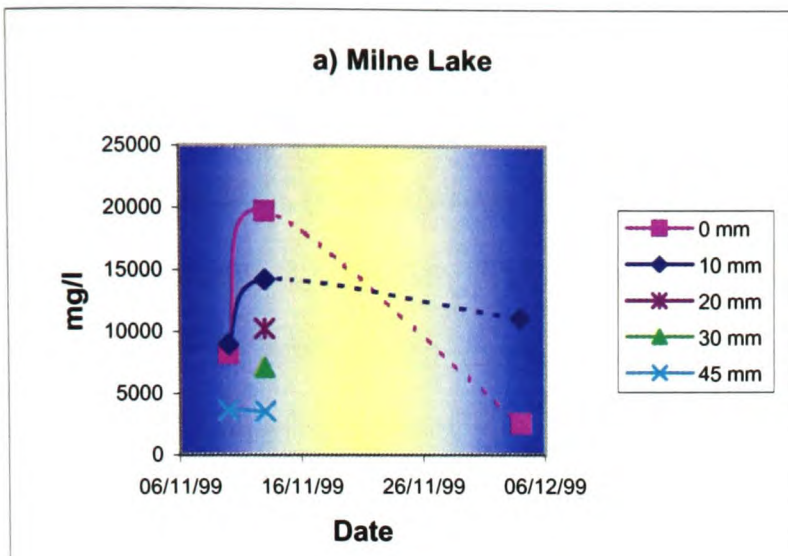
Figure 4.8. Lakewater sulphate ion concentrations
a) 1998 b) 1999

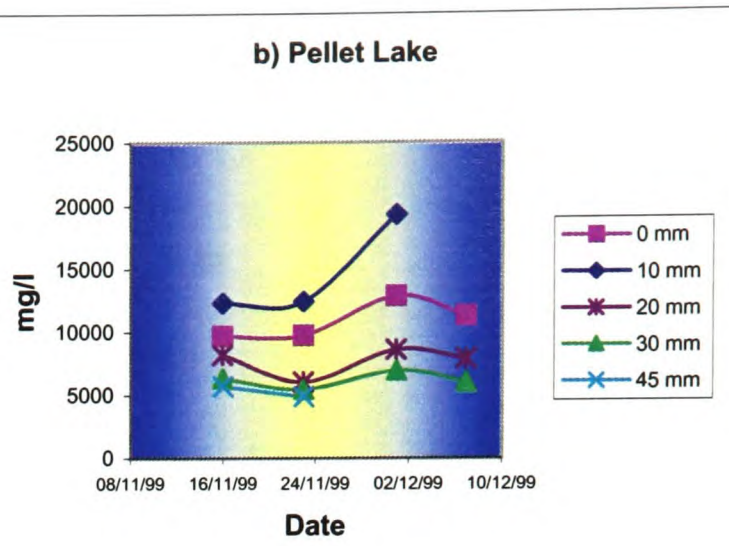
concentrations (200mg/l in residual puddles of Dolomite Lake). These low concentrations may be due to intense bacterial activity at the latest stage of desiccation.

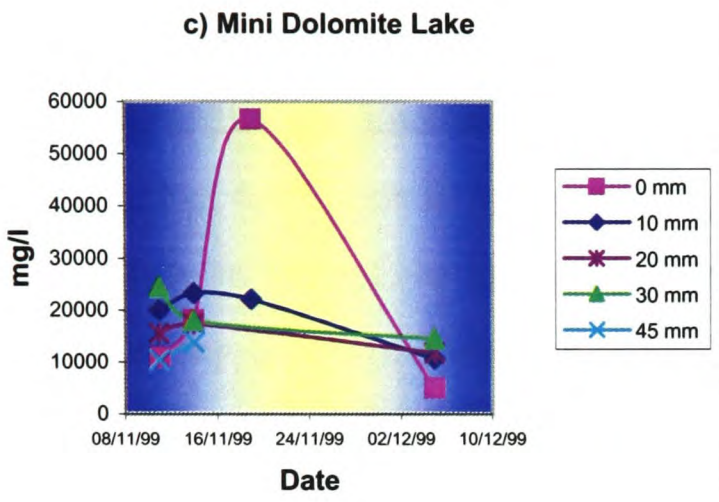
It is also necessary to investigate sulphate concentrations in the lake porewaters. Unfortunately, a successful technique for extracting these porewaters was only developed in time for the 1999 field season, and even then 100% success could not be guaranteed (e.g. data gaps in Table 4.1)

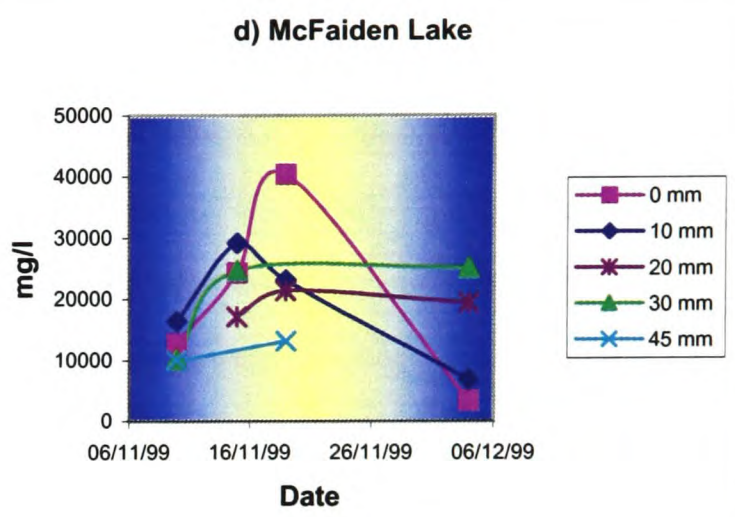
Figure 4.9 shows the change of sulphate ion concentration at different depths in each lake over a time period of around one month. Several patterns can be observed, one of which is evaporative concentration followed by rainfall. Throughout the time of sampling, the levels of sulphate in the porewaters are less than in the lakewaters and a general decrease with depth is observed. It is also observed that lakewater sulphate ion concentrations respond more rapidly and to a larger degree to changes in the environment, with greater maxima and lower minima. Porewater trends appear to be moderated somewhat and show a time lag (especially during dilution) from the lakewater values; so much so, that in early December porewater values were, unusually, higher than lakewater values.

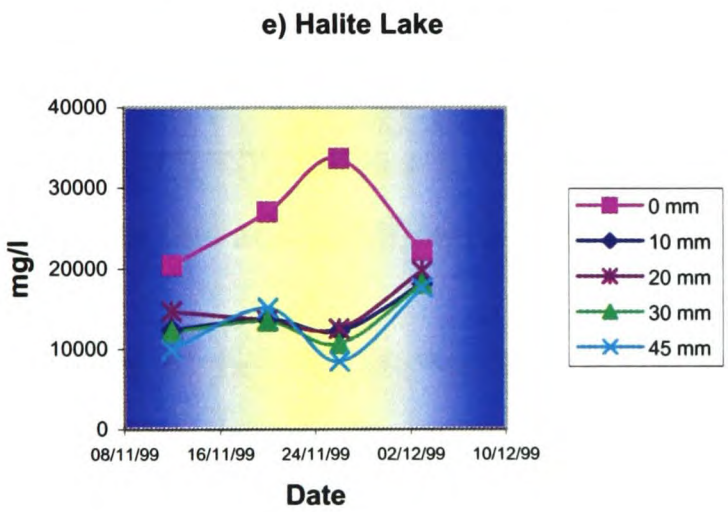
Figure 4.10a represents a snapshot, taken at one particular time, of the change in sulphate ion concentration with depth for each lake. The observed pattern is typical and shows a large decrease in sulphate concentration with depth, being greatest (82%) in the dolomitic Milne Lake. This supports the hypothesis that sulphate-reduction (hence removal) is favourable to dolomite formation. However, very large decreases are also found in non-dolomitic lakes, whilst Mini dolomite lake, which is dolomitic, shows the smallest percentage of sulphate reduction. While sulphate values never quite reach the low levels seen in seawater, extrapolation of the trends observed in Figures 4.9 and 4.10a predicts that sulphate ion concentrations in most of the lakes would drop below that of seawater at a depth of c. 60-70mm. A relatively low concentration of sulphate ions at c. 60-70mm would then favour dolomite precipitation, due to a reduced ability to complex with magnesium ions. However, one must look at sulphate ion concentrations in parallel with magnesium ion concentrations and Mg : Ca ratios in order to constrain this process more closely.

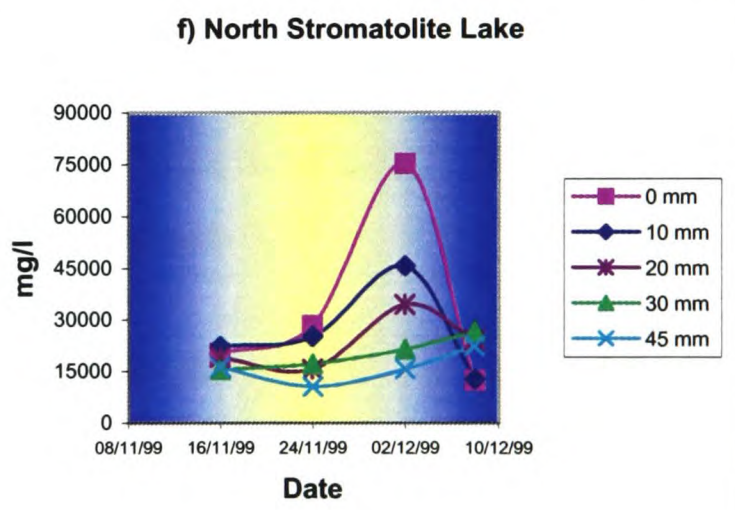












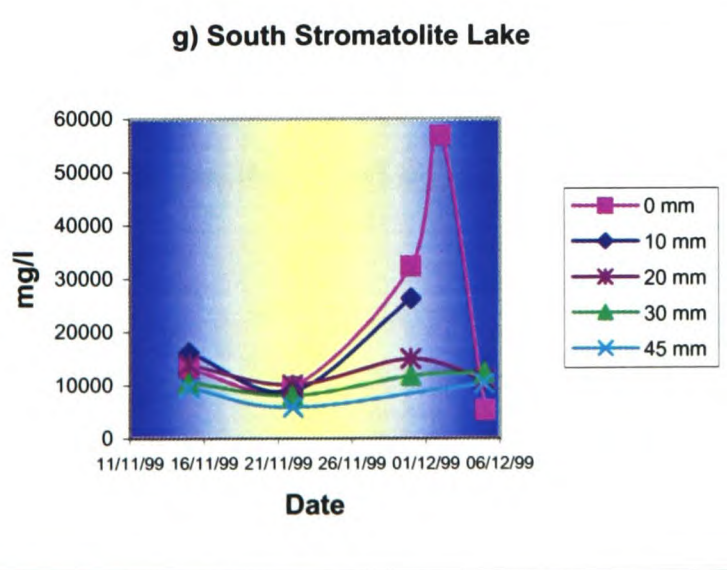


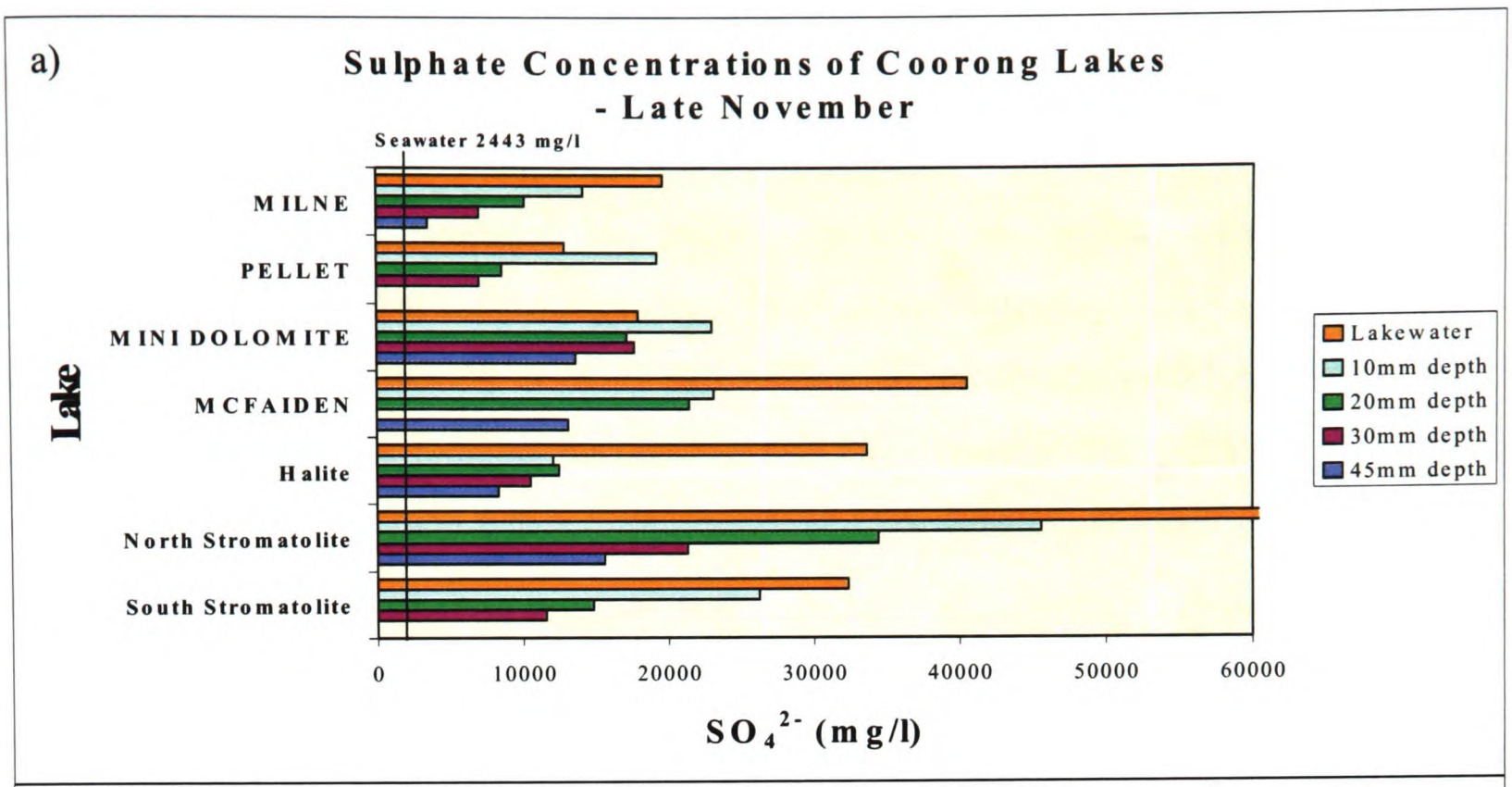
Figure 4.9a-g.
Sulphate ion concentrations in lake and porewaters, Nov/Dec 1999

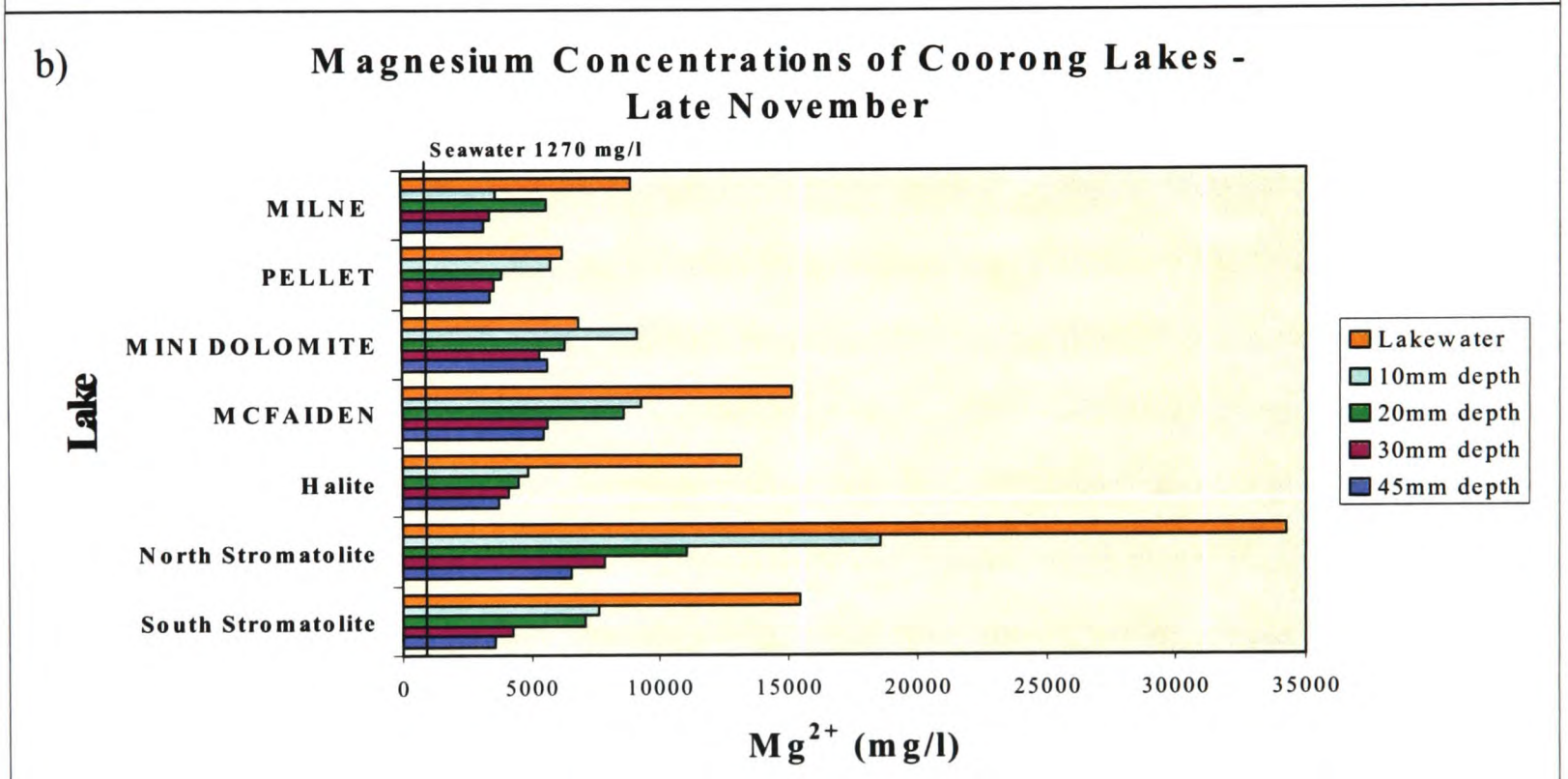
4.5.6. The magnesium / sulphate relationship

The presence of the sulphate ion inhibits dolomite formation due to its ability to complex with the magnesium ion, effectively removing magnesium from the pool of reactant ions. Wright (1999) is the only previous author to report absolute magnesium ion concentrations for these lakes. He obtained values of just over 5000mg/l in Pellet Lake and up to 28,720mg/l in South Stromatolite Lake. These compare favourably with the values seen in Figure 4.10b This is the first study to report porewater magnesium ion concentrations.

Magnesium ion concentrations in the lakes and their porewaters are seen to decrease with depth (Fig. 4.10b) but, in terms of percentage, not to such a large extent as sulphate ion concentrations. In Milne Lake for example, an 82% decrease in sulphate concentration is only accompanied by a 65% decrease in magnesium concentration and even at 45mm depth magnesium concentrations are still well in excess of those typically found in seawater. The trend observed in many of the lakes is therefore one of an increase in the Mg^{2+} to SO_4^{2-} ratio as the zone of sulphate reduction is traversed. Extrapolation of this trend would result in an excess of Mg^{2+} to SO_4^{2-} ions at depths of c. 50-60mm. When the molarity of the ions rather than their concentrations are considered (Fig. 4.10c) all lakes show a Mg^{2+} : SO_4^{2-} molar ratio in excess of one and in Milne Lake, at depth, this ratio exceeds 3.5.

The higher the Mg^{2+} to SO_4^{2-} molar ratio, the more favourable are the conditions for dolomite formation as the kinetic drive towards dolomite formation may be greater than that towards $MgSO_4^{\circ}$ complexing. $MgSO_4^{\circ}$ complexes are not stable entities as there is a continuous substitution of sulphate and magnesium ions. High Mg^{2+} to SO_4^{2-} molar ratios lead to diminished complexing and, as a consequence, Mg^{2+} ions become free to combine with readily available calcium and carbonate ions to precipitate dolomite.





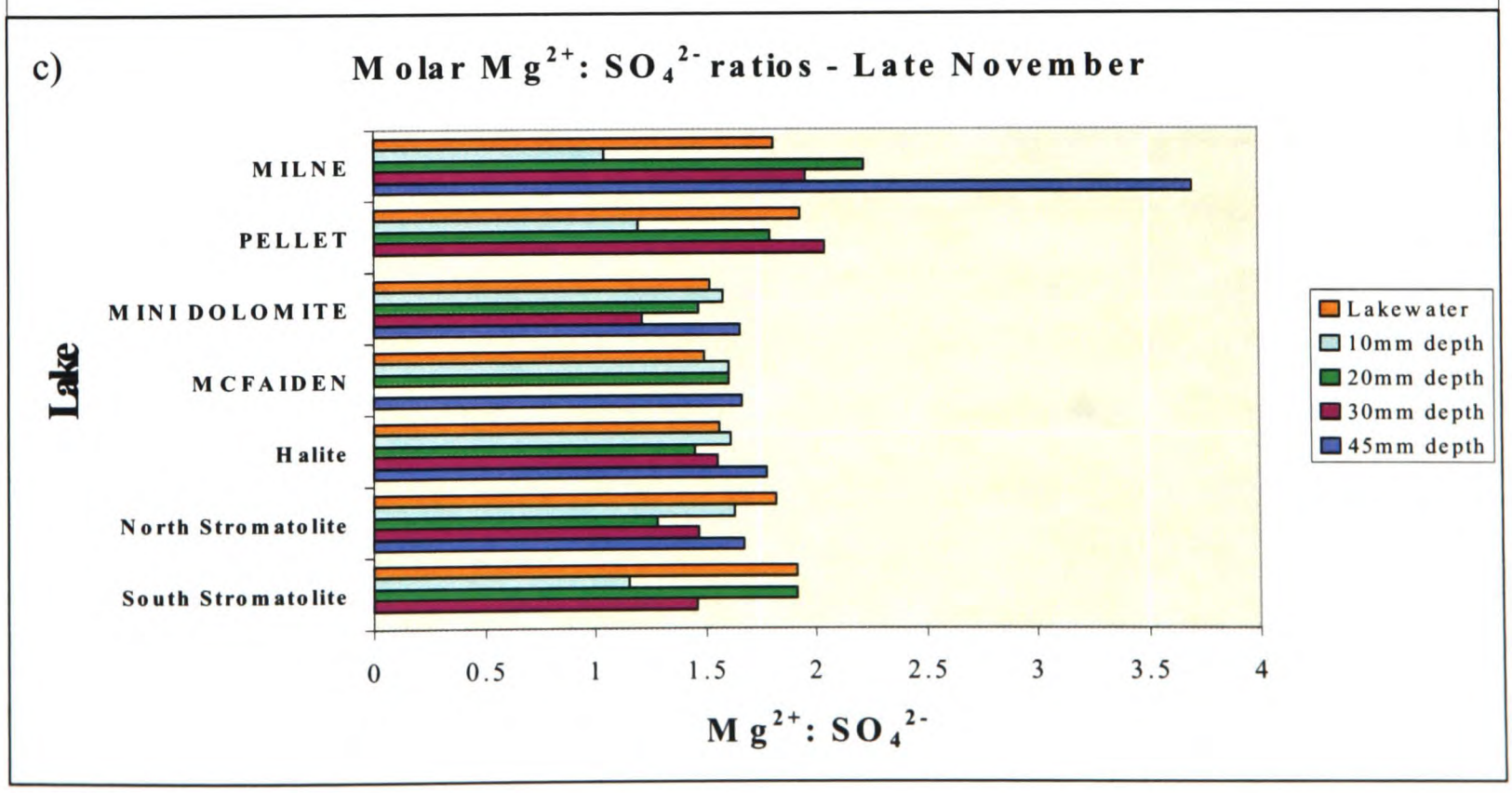


Figure 4.10. a) Change in sulphate ion concentration with depth, late November 1999
b) Change in magnesium ion concentration with depth, late November 1999
c) Molar magnesium ion to sulphate ion ratio, late November 1999

4.5.7. Magnesium to Calcium ratios

Mg^{2+} and Ca^{2+} were measured by 'Inductively Coupled Plasma, Atomic Emissio Spectroscopy' (ICP-AES) at the Geology Department, Royal Holloway University of Londor Because of the extreme salinity of the Coorong lakes, the samples were diluted in order t keep readings within the range of the machine and its software (e.g. 100,000ppm Na^{+}). On set were run at 1:10 dilution and a duplicate set at 1:100 dilution, to cover ions with ver large concentrations.

The Mg/Ca lakewater data are presented in Figure 4.11. All of the lakes exhibi much higher Mg/Ca ratios than those typical of seawater, reaching up to 110 times that o seawater in North Stromatolite Lake. The important point to note is that Mg/Ca ratios are on the whole, highest in the non-dolomitic lakes. A second trend is that of an increase i Mg/Ca ratio with time, over the relatively short sampling period. Wright (1999) report large increases in Mg/Ca with time in South Stromatolite Lake (from 2.5 to 256 in just over month) and Ahmad (1996) reports Mg/Ca ratios as high as 247. The large increase in Mg/C ratios cannot be attributed to simple evaporative concentration because calcium levels sta almost constant (this study; Wright, 1999). All of the lakes, apart from Halite Lake, hav cyanobacterial mats either within the lakes or at their margins . Cyanobacteria are known t concentrate magnesium in their sheaths by up to four times its abundance in seawate (Gebelein & Hoffman, 1973). When mats are desiccated, Mg^{2+} is released into the residua pools of water, substantially elevating magnesium concentrations late in the evaporativ cycle. In the non-dolomitic lakes any increase in Ca^{2+} due to evaporation is balanced by th incorporation of Ca^{2+} into aragonite, whilst Mg^{2+}, having a more strongly bonded hydratio shell, is the last ion to precipitate, appearing late in the evaporative cycle as hydro magnesite. During the 1999 field season, Milne and McFaiden lakes dried up for a period o 2-3 weeks (Fig. 4.11b dashed lines); when they were subsequently refilled by rainfall in earl December, the Mg/Ca ratios were found to be much lower. This may be attributed to th incorporation of Mg^{2+} from porewaters into both magnesite and Mg-rich dolomite; thi conclusion is supported by XRD studies (Appendix 1) of the sediment from Milne Lak which reveals both magnesite and Mg-rich dolomite. A second explanation involve

dissolution of Ca^{2+} minerals from the surrounding dunes, followed by runoff into the lakes. In McFaiden Lake, where only Ca rich dolomite is observed, this may be the main control.

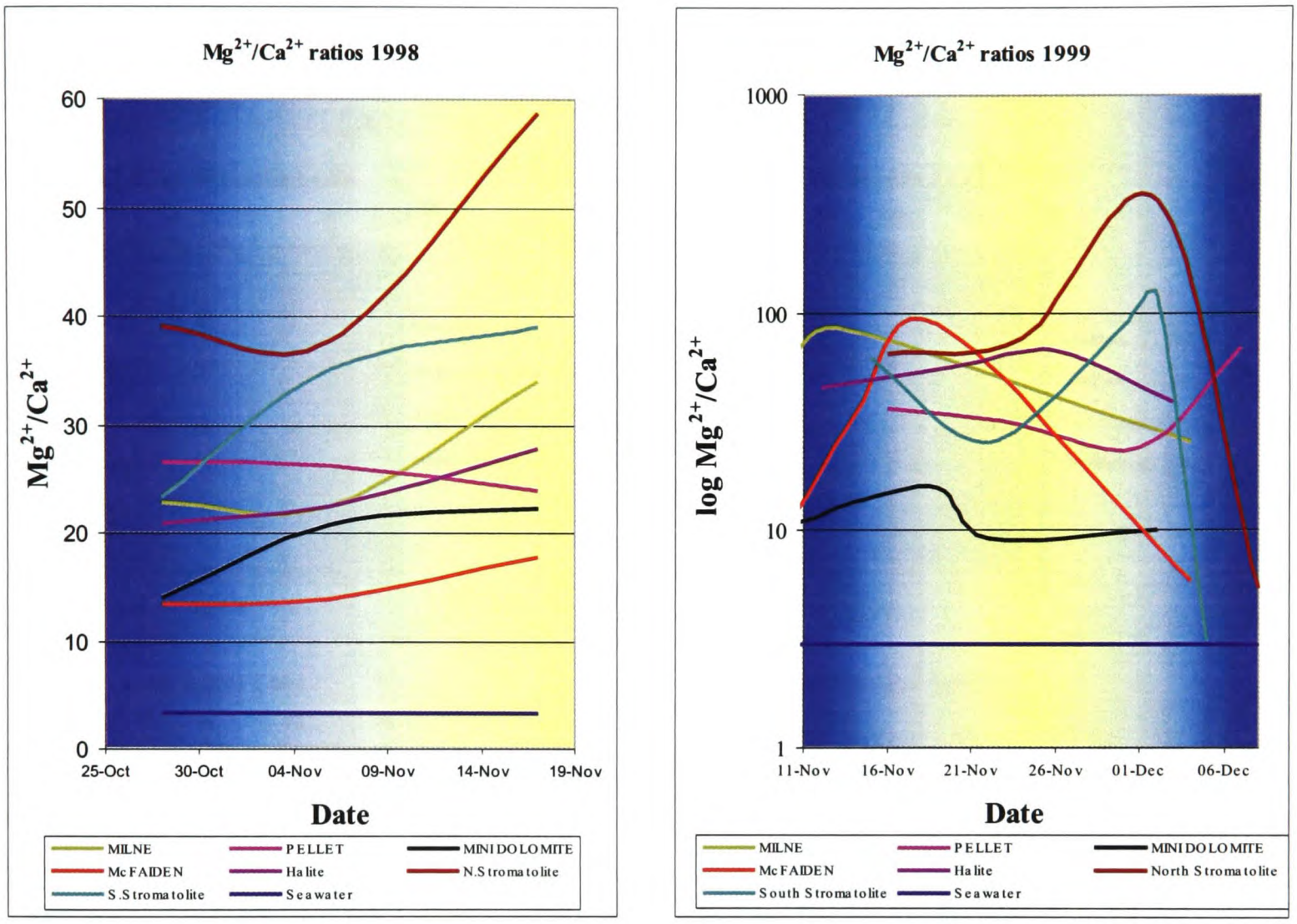
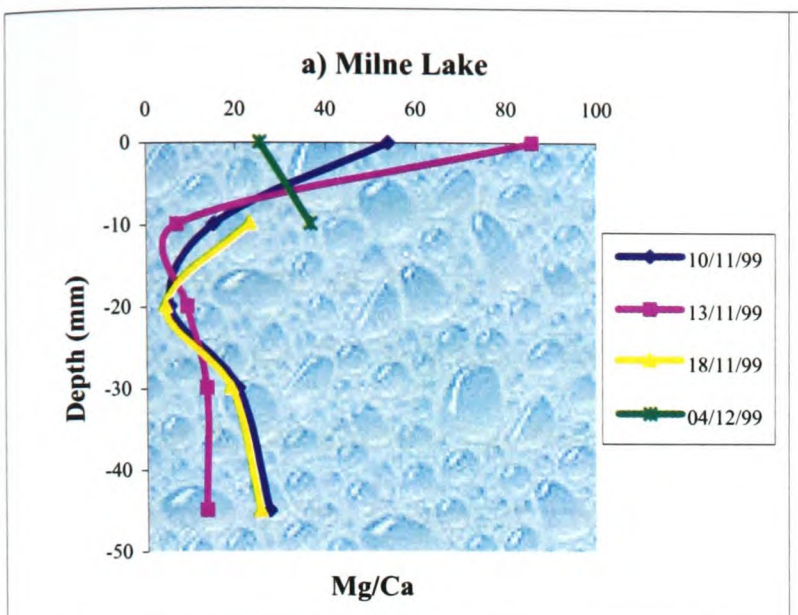
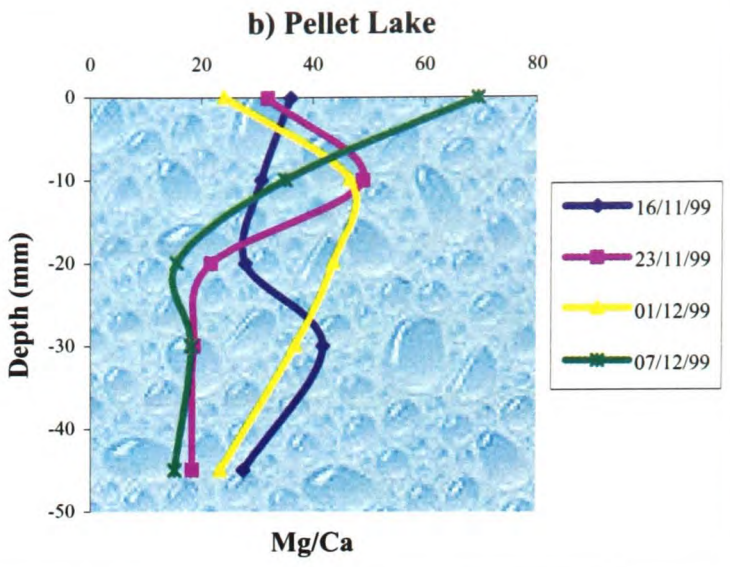
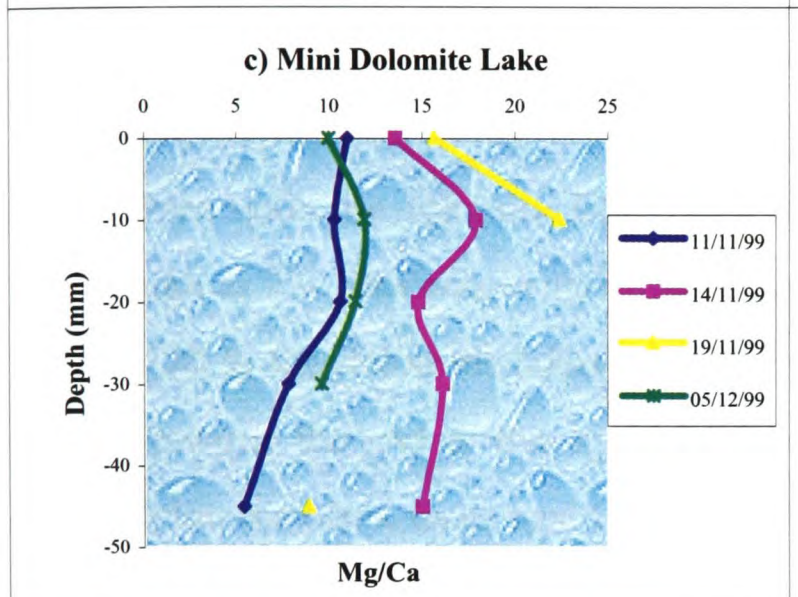


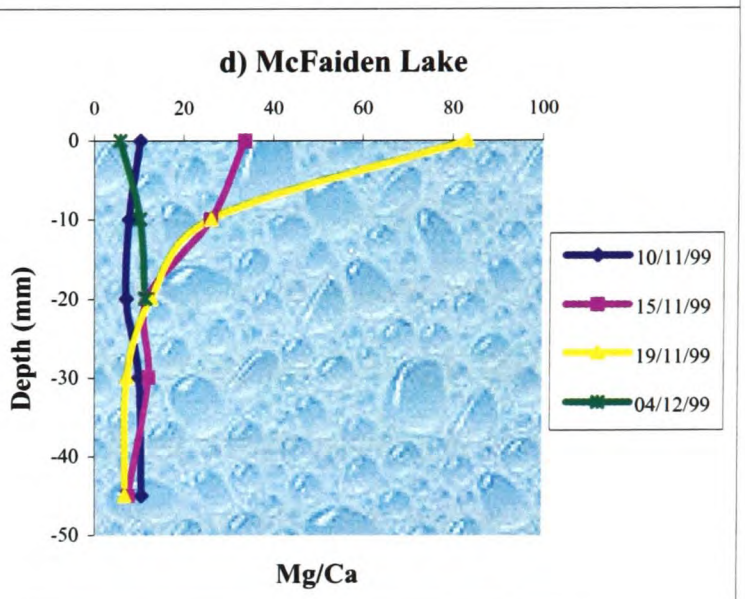
Figure 4.11. Lakewater Mg^{2+}/Ca^{2+} ratios over a period of approximately one month. Note log scale for 1999 data.

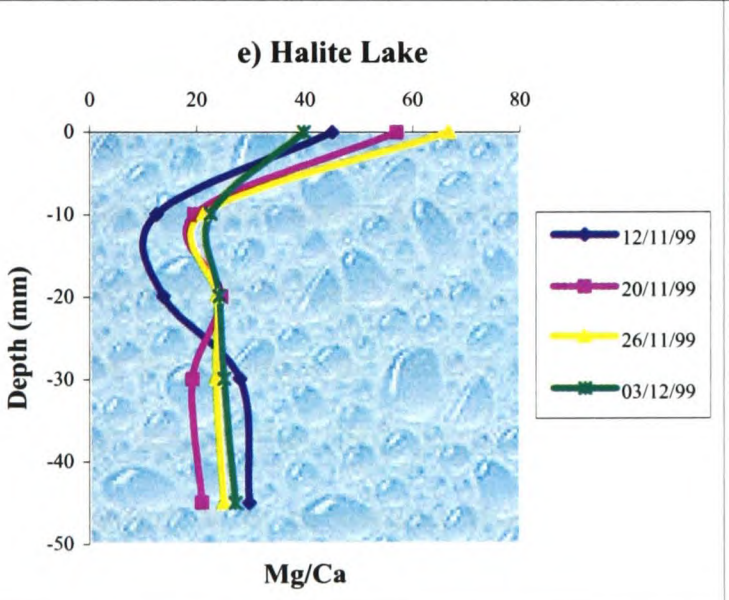
Porewater Mg/Ca ratios are shown in Figure 4.12, for the 1999 field season only. Mg/Ca ratios tend to be highest in the lakewater and generally decrease with depth, the decrease being most pronounced in the top 20mm of the sediment. Even at 45mm where the Mg/Ca ratios are lowest, they are still in excess of those found in seawater. No significant differences are observed in the trends of porewater Mg/Ca ratios in the dolomitic lakes compared to the non-dolomitic lakes.

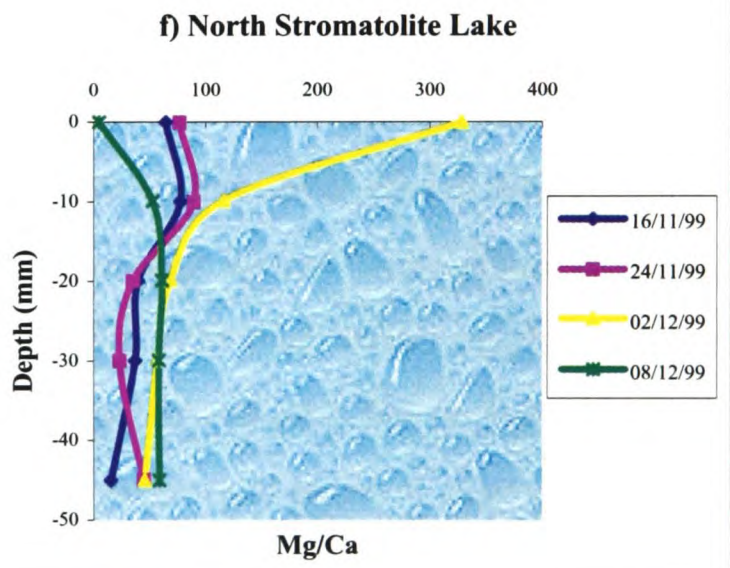












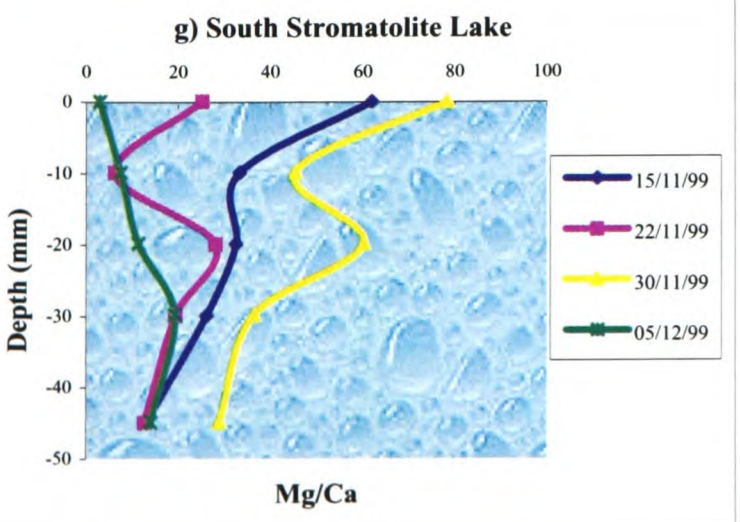


Figure 4.12a-g. Mg:Ca ratios of lake and pore-waters, Coorong distal ephemeral lakes, Nov/Dec 1999

Note use of variable x-axis scales

4.6. TOTAL ORGANIC CARBON

Measurement of total organic carbon (TOC) in each of the lake sediments was performed at the Department of Earth Sciences, University of Oxford on a Strohlein Coulomat 702 machine. The results are shown in Figure 4.13. The values obtained in 1998 (Fig 4.13a) show a marked difference between the dolomitic and non-dolomitic lakes. TOC values in the dolomitic lakes are all above 2% and often as high as 5%. TOC values in the non-dolomitic lakes are mostly between 1 and 2%. Milne Lake and Dolomite Lake show a marked increase in TOC with depth whilst the other lakes show only very small changes with depth. TOC values obtained in 1999 (Fig. 4.13b) are generally higher than those in 1998. Once again the dolomitic lakes have the higher percent TOC, mostly above 4% ranging up as high as 9%. Measurements on different dates during the sampling season show that percent TOC in the dolomitic lakes decreases as the lakes progress through their evaporative cycle. Towards the end of this cycle TOC values in these lakes approach those seen in the non-dolomitic lakes. Once again this data is almost unique with only one measurement of TOC in this area reported in previous literature. Von der Borch (1984) records a value of 2.9% at 60-80mm depth in Lake McFaiden which is consistent with the measurements made here. The high TOC values obtained in the dolomitic lakes are close to the 10% TOC reported by Vasconcelos and McKenzie (1997) for the black sludge layer of the dolomite precipitating Lagoa Vermelha. Organic matter provides the energy source for sulphate-reducing bacteria. The more organic matter that is present, together with high initial sulphate concentrations, the larger the SRB population which can be sustained and the higher its metabolic rate. Hence, it is proposed that the availability of large quantities of organic matter enhances dolomite precipitation.

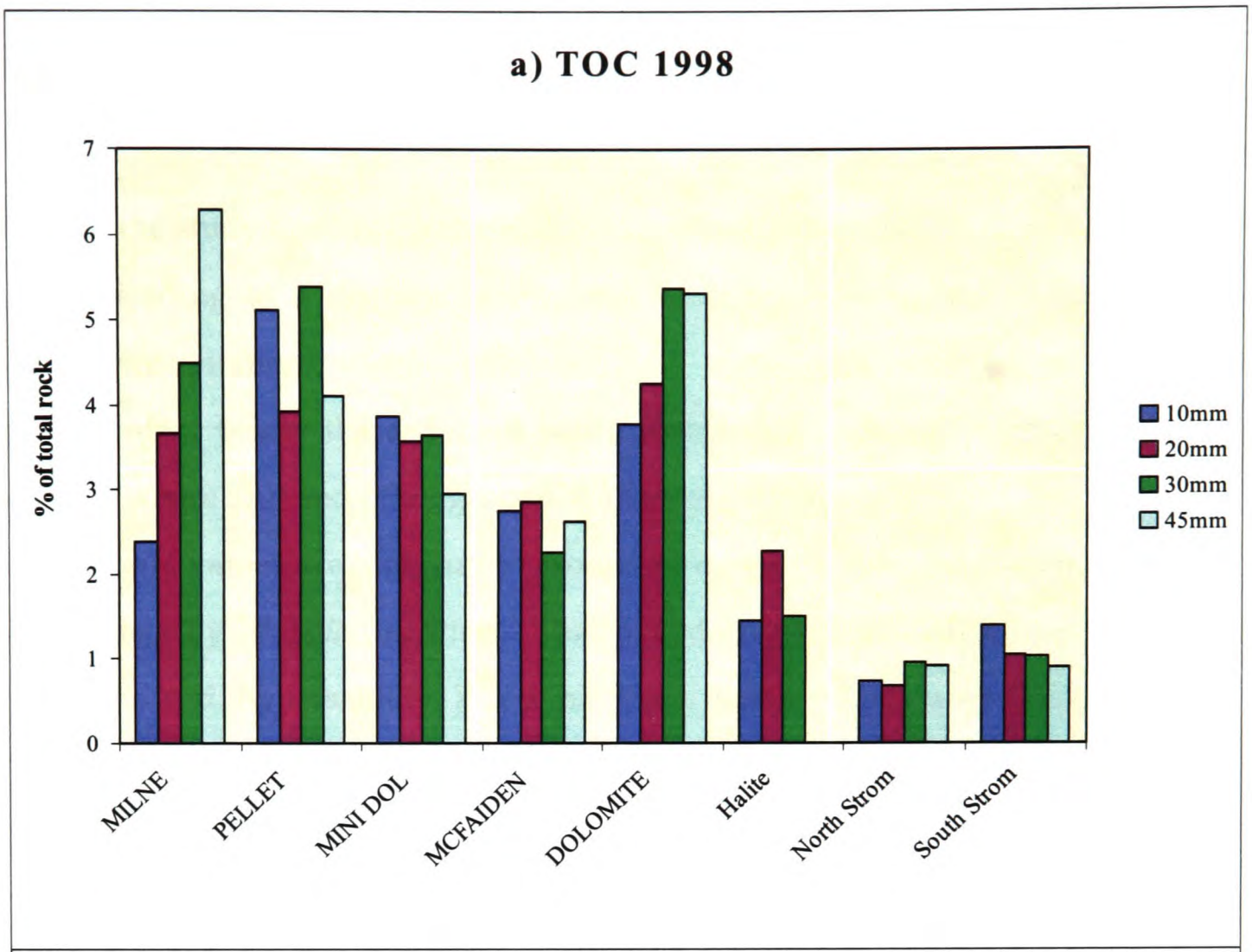


Figure 4.13. Total organic carbon values expressed as a whole rock percentage for each of the study lakes. a) 1998 b) 1999 (note analyses on more than one date for Pellet Lake and Mini Dolomite Lake)

4.7. SUMMARY

- Salinity in the study lakes is greatly in excess of seawater salinity, possibly by as much as 10 times, leading to a distribution of ionic species which is ultimately beneficial to carbonate precipitation.
- Oxygen content below the sediment water interface is minimal, leading to anaerobic conditions where SRB and other groups of anaerobes prosper.
- Lakewater pH values are high (up to around 9) raised by the photosynthetic activity of plants especially *Ruppia maritima*. The pH decreased for some time as intense evaporation and hypersalinity killed off these water plants and then increased as rainwater dilution revived them. Porewater pH is increased by the action of SRB liberating ammonia from organic matter.
- Carbonate ion concentration is greatly increased, both in the lakewaters and more importantly in the sediment porewaters, by the metabolic activity of SRB at relatively high salinity. The raised concentration and activity of this ion removes one of the major kinetic inhibitors to dolomite formation.
- Sulphate ion concentrations in the lakewaters are high, concentrated by evaporation. This gives a large sulphate reservoir for the SRB to use as terminal electron acceptors and thus large bacterial populations, metabolising relatively rapidly can be sustained.
- Porewater sulphate ion profiles show the use of this sulphate by the SRB. In so doing the kinetic inhibitor, $MgSO_4^0$ complexing, is greatly diminished, freeing dehydrated magnesium ions to participate in carbonate precipitation.
- Mg/Ca ratios are high, up to almost 100 times that of seawater.
- TOC data suggest that the supply of large amounts of organic matter may be an essential component of a dolomite precipitating environment.

CHAPTER 5



Abundant stromatolites in South Stromatolite Lake.

Chapter 5

Isotopic Analysis

Stable isotopes of three elements were used during the course of this study (sulphur, oxygen and carbon) in order to enhance understanding of the processes involved in the genesis of carbonate minerals in the Coorong Lakes. In this chapter, the theory behind each isotope system is outlined, methods of analysis are described and data are presented and discussed.

5.1. INTRODUCTION

Stable isotopes are of special interest in low temperature environments because they can be fractionated on a large scale by natural processes. Isotopic fractionation in nature takes place in two main ways (Hoefs, 1987).

1. Equilibrium isotopic exchange reactions. Fractionations of this sort are derived from small but significant differences in the thermodynamic properties between isotopes of a given element. Relative mass difference and bond strength control the fractionation and, in general, the lighter isotope forms a weaker bond than the heavier one. An example is the behaviour of oxygen during the equilibrium crystallisation of calcite with ambient water. The calcite is enriched in ^{18}O because the C- ^{18}O bond in calcite is stronger and therefore takes less energy to keep it in the solid state than the C- ^{16}O bond. The temperature at which the reaction takes place also plays a critical role in the extent of fractionation as shown in Equation 5.1.

$$1000 \ln \alpha = A (10^6 / T^2) + B \qquad (5.1)$$

where A and B are constants depending on the minerals or fluids concerned, T is in Kelvin and α is the fractionation factor. The addition of heat increases the total energy of the molecules and at high enough temperatures the vibrational energy of a molecule is increased to such an extent that differences due to variations in isotopic composition are insignificant. Therefore fractionation factors always decrease with temperature and at very high temperatures approach unity.

2. Kinetic processes. Kinetically controlled stable isotope fractionation occurs when the rate of a chemical reaction is sensitive to atomic mass at a particular position in one of the reacting species and is controlled by the ratio of the rate constants for the reaction of the light and heavy isotopes. Kinetic effects are observed when a reaction is unidirectional and depends largely on the reaction rates and reaction pathways involved. Examples include photosynthesis, where $^{12}CO_2$ gas is preferentially selected during the production of organic matter, and bacterial sulphate reduction.

Physico-chemical processes such as evaporation and condensation, diffusion and precipitation together with biogenic processes all fractionate stable isotopes but fractionation will still be governed by equilibrium or kinetic mechanisms.

5.2. SULPHUR ISOTOPES

Stable isotopes of sulphur were used in this study in order to investigate the extent of bacterial activity in the ephemeral lakes and sediments. There are four naturally occurring isotopes of sulphur:

$^{32}S = 95.02\%$

$^{33}S = 0.75\%$

$^{34}S = 4.21\%$

$^{36}S = 0.02\%$

The ratio between the two most common isotopes (^{32}S and ^{34}S) is used in geochemistry and this is expressed using the delta notation:

$$\delta^{34}S\ ‰ = \left[\frac{(^{34}S/^{32}S)_{sample} - (^{34}S/^{32}S)_{std}}{(^{34}S/^{32}S)_{std}} \right] \times 1000$$

The standard used is the Vienna Canyon Diablo Troilite (V-CDT) and results are expressed in parts per mil (‰) (Faure, 1977).

5.2.1. Distribution of sulphur isotopes

Present day sulphur-containing sediments and waters have wide-ranging isotopic signatures (Fig. 5.1). The $\delta^{34}S$ value for modern day seawater is virtually the same throughout the ocean (Claypool *et al.*, 1980) because of the relatively rapid mixing time of ocean currents ($2x10^3$yrs) compared to the residence time of sulphate in seawater ($2x10^7$yrs). A mean value of 20.99‰ determined by Rees *et al.* (1978) is used here as the accepted value. In this study sulphur isotopes were used as a tool for obtaining evidence of bacterial activity, namely anaerobic bacterial sulphate reduction, as this process is responsible for a large proportion of sulphur isotope fractionation at earth surface conditions (e.g. Canfield & Thamdrup, 1994).

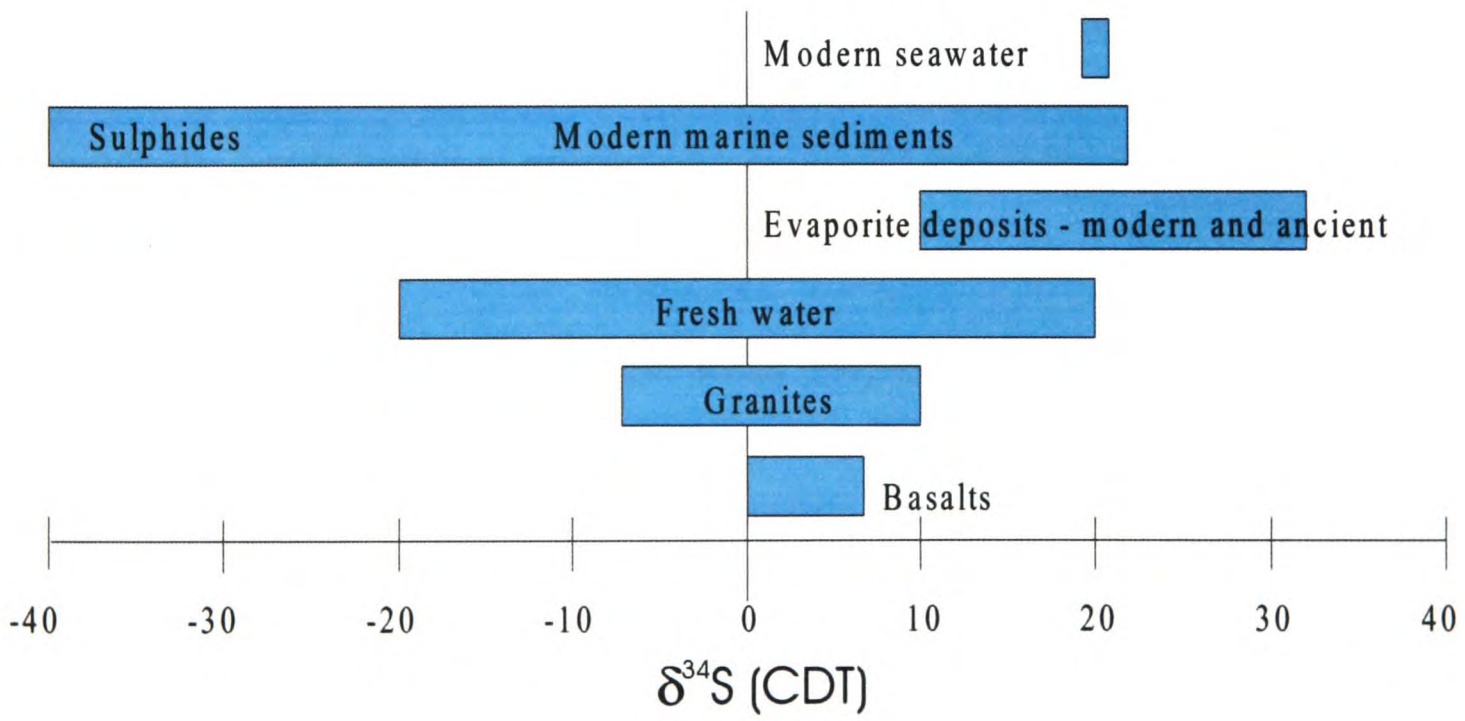


Figure 5.1. Natural isotope reservoirs of sulphur. (Adapted from Rollinson, 1993).

5.2.2. Biogenic fractionation of sulphur isotopes

Fractionation of sulphur isotopes, as with other isotopes, is controlled by a combination of equilibrium and kinetic effects. Interactions in the sulphur isotope system are complex and result in a wide range of isotopic compositions of sulphides, sulphates and intermediate sulphur species from –65 to +90‰ (Hoefs, 1987). Bacterial sulphate reduction has long since been recognised as the principle agent of sulphur isotope fractionation with sedimentary sulphides being depleted in the heavy isotope by up to about 70‰ compared with co-existing sulphate (Canfield & Thamdrup, 1994).

Many field and laboratory based studies have been performed to determine the complex array of isotope fractionation factors associated with the metabolic pathways of sulphate-reducing bacteria (SRB) and the effect that environmental conditions have on bacterial fractionation. These are necessarily reviewed here in order to understand the results of the sulphur isotope analysis in this study.

Early workers (e.g. Harrison & Thode, 1958) simply focused on the chemical kinetics of the reduction of sulphate to sulphide. When SRB reduce sulphate to sulphide, lighter isotopes of sulphur preferentially take part in the reaction, since it is kinetically easier to break bonds between lighter atoms than heavier ones. The reaction rate, determined experimentally by Harrison and Thode (1958), of the $^{32}SO_4^{2-}$ ion was 2.2% greater than the $^{34}SO_4^{2-}$ ion. Thus, if this reaction took place in one step and was unidirectional, it would result in sulphide being depleted by 22‰ relative to a sulphate source. However, the great variation in ^{32}S enrichment of sedimentary sulphides suggested that this one step reaction is an over-simplification of what is actually occurring.

Subsequent work focussed on the actual mechanism of sulphate reduction within the bacterial cells in more detail. It was proposed by Kemp and Thode (1968) that the extent of fractionation during bacterial sulphate reduction was dependent upon the mechanism and rates of the various steps of bacterial metabolism:

Step 1 - assimilation of sulphate into the cells;
Steps 2-4 – reduction within the cells;
Step 5 - passage of H_2S out of the cells.

These steps are outlined in Figure 5.2, whilst the isotope effects for each step are given in Table 5.1.

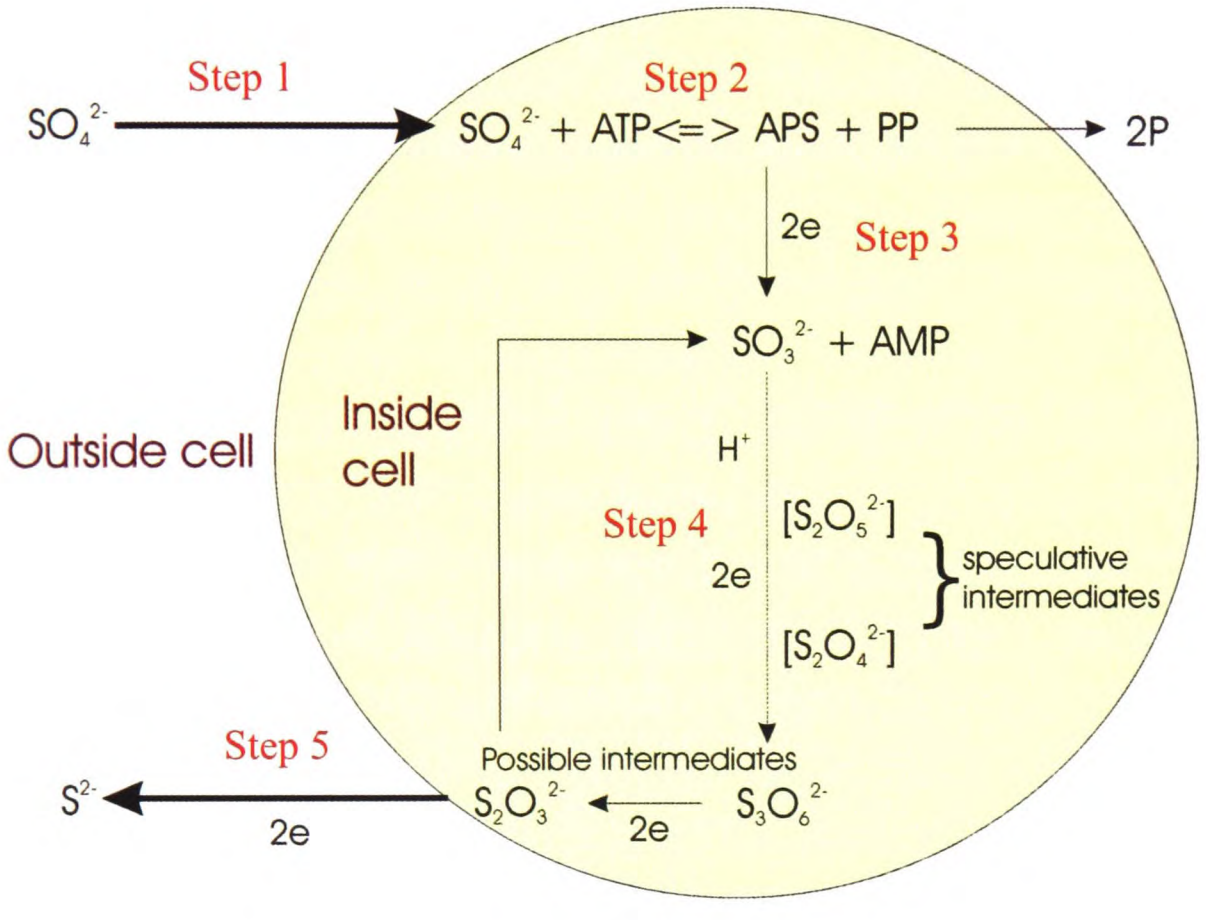


Figure 5.2. One possible metabolic pathway for the reduction of sulphate by the *Desulfovibrio* genus (redrawn from Postgate, 1984).

Step	Kinetic Fractionation	Equilibrium Fractionation	Reference
1	Maximum 2.8‰	-	Kaplan & Rittenberg (1964)
2	negligible	Steps 2 + 3 combined	Kemp & Thode (1968)
3	22‰	24‰	Harrison & Thode (1958)
4	25‰	-	Kemp & Thode (1968)
5	Rapid – cannot be rate controlling		

Table 5.1. Isotope fractionation factors associated with the different steps of bacterial sulphate reduction outlined in Figure 5.2.

The maximum isotope fractionation is obtained by addition of all of the fractionation factors until the rate-determining step is reached. Thus the maximum fractionation occurring through the mechanism outlined above would be when Steps 2 and 3 were rapid, enabling equilibrium to be established, and where Step 4 was rate controlling. This would result in an approximate 49‰ fractionation. However, when Kemp and Thode (1968) studied free energy changes for these reactions it was found that Step 4 would be more rapid than Step 3 and so sulphite would be removed rapidly and isotopic equilibrium could not be obtained in Step 3. Thus, the forward reaction of Step 3 becomes rate controlling and a kinetic fractionation of only 22‰ should be observed. They also state that at low sulphate concentrations, assimilation of sulphate into the cell may be rate controlling which can explain the smaller fractionations observed at very low sulphate concentrations. The important question that resulted from the work of Kemp and Thode and other early authors was: What processes are responsible for fractionations greater than about 25‰ which have commonly been reported in nature and in pure culture experiments? Possible solutions include:

a) **the rate of sulphate reduction, influenced by environmental factors;**
b) **species specific fractionations;**
c) **other fractionations within the sulphur cycle (biogenic and abiogenic);**
d) **open versus closed systems.**

a) Sulphate reduction rate:

Numerous experimental studies have focused on the role that *sulphate reduction rate* (SRR) has on sulphur isotope fractionation. Many authors (e.g. Kaplan & Rittenberg, 1964; Goldhaber & Kaplan, 1975; Fry *et al.*, 1988, 1995) report that the extent of isotope fractionation decreases with increasing rate of sulphate reduction. Habicht and Canfield (1997) conclude that it is the specific rate of sulphate reduction (mass/cell/time) rather than the absolute rate (mass/volume/time) that is the controlling factor, with the highest fractionations at the lowest specific rates. An explanation for this is again found in the principal steps controlling the sulphate reduction process outlined in Figure 5.2. Maximum isotope fractionation occurs when the external and internal pools of sulphate and the intermediates are in exchange equilibrium. This is best accomplished when bacterial metabolism is slow. As the metabolism increases so does the demand for sulphate and in turn the rate of sulphate transport into the cell must increase. When this rate greatly exceeds the rate at which sulphate is transported out of the cell, the internal and external pools of

sulphate are no longer in exchange equilibrium, the reduction steps within the cell are less reversible and isotopic exchange between the intermediates is hindered.

The rate of sulphate reduction is dependent upon various environmental factors such as temperature, pH, sulphate concentration and electron donor availability. Fry *et al.* (1995) found no direct correlation between $\delta^{34}S$ and temperature nor between $\delta^{34}S$ and sulphate concentration and concluded that when there was increased electron donor (organic carbon) availability, there would be increased demand for a limited sulphate supply and fractionation would be less. Canfield (2001) reinforced this argument showing that the highest fractionations (30-40‰) occurred when organic substrate was limited, limiting the activity of the bacteria. Goldhaber and Kaplan (1975) stated that the rate of sulphate reduction was dependent not only on the amount of organic matter in the sediment but also the state of complexing and hence availability of the organic matter to SRB. This is in agreement with observations that most sulphate reduction takes place within the upper few centimetres of sediment before declining rapidly at depth, mirroring the availability of suitable organic material (Trudinger, 1992).

b) Species specific fractionations:

Recently it has been argued (Detmers *et al.*, 2001) that explaining isotope fractionation factors in terms of sulphate reduction rate is an oversimplification. Detmers *et al.* (2001) selected 32 different sulphate reducers reflecting current known diversity and carried out experiments at the optimum growth conditions of each strain. They obtained fractionation factors varying from only 2‰ to 42‰. They found no correlation between these fractionation factors and salinity, temperature, pH, phylogeny or sulphate reduction rate. They found that strains that oxidised the carbon source completely to O_2 showed greater fractionation than those that only oxidised the carbon source partly to acetate. They conclude that it is the species specific physiology of each sulphate reducer that controls isotope fractionation. This was also recognised by Canfield (2001) who found that switching substrates, hence altering the physiological pathways of the bacteria, had a significant influence on the extent of fractionation.

c) Other fractionations within the sulphur cycle:

An important question that has arisen during laboratory versus field-based studies is how to reconcile the fractionation factors obtained in pure culture experiments (mostly <40‰) with those observed between sedimentary sulphides and sulphates in the rock record (as much as 70‰). Habicht and Canfield (2001) found that only between 41 and 85% of the ^{34}S depletion

found in sedimentary sulphides could be explained by sulphate reduction alone. This led both them and several other workers to conclude that additional processes must augment this fractionation in nature. These are to be found in other parts of the sulphur cycle and include oxidation of sulphide to elemental sulphur, oxidation of sulphide to thiosulphate, disproportionation of elemental sulphur, reduction and disproportionation of thiosulphate, reduction and disproportionation of sulphite. Typically 80-95% of H_2S produced from bacterial sulphate reduction is reoxidised (Jorgensen, 1982) and so these processes may be of considerable importance. The fractionation factors associated with each are outlined in Table 5.2.

Reaction	Organism	^{34}S Enrichment ‰	References
$H_2S \Rightarrow S^0$	Colourless sulphur bacteria, green and purple sulphur bacteria & anoxygenic phototrophic bacteria	~ 0	a, c, d
$H_2S \Rightarrow S_2O_3^{2-}$	Some SRB	~ 0	f
$S^0 \Rightarrow SO_4^{2-}$	SRB	+12.6 to +15.3	d, e
$\Rightarrow H_2S$	e.g. *Desulfobulbus propionicus*	-7.3 to -8.6	
$S_2O_3^{2-} \Rightarrow SO_4^{2-}$	SRB	Up to +12	b, f
$\Rightarrow H_2S$	e.g. *Desulfovibrio sulfodismutans*	Up to -12	
$S_2O_3^{2-} \Rightarrow H_2S$	SRB	-7 to -11	f,
		-10	g
$SO_3^{2-} \Rightarrow H_2S$	SRB	-6	f
$SO_3^{2-} \Rightarrow SO_4^{2-}$	SRB	+7 to +12	b, f
$\Rightarrow H_2S$	e.g. *D.sulfodismutans*	-20 to -37	

Table 5.2. Reactions in the sulphur cycle and their fractionation factors. Note: reaction with two products is a disproportionation reaction. References: a) Kaplan & Rittenberg, 1964 b) Bak & Cypionka, 1987 c) Fry *et al.*, 1988 d) Canfield & Thamdrup, 1994 e) Fuseler *et al.*, 1996 f) Habicht *et al.*, 1998 g) Smock *et al.*, 1998. Other possible reactions include the disproportionation of dithionate and of tetrathionate (Bak & Cypionka, 1987) although fractionation factors for these reactions have not yet been investigated.

It is clear that a repeated cycle of bacterial sulphate reduction followed by oxidation of H_2S and reduction and disproportionation of intermediate sulphur species can result in sulphides depleted in ^{34}S to a much greater extent than by straightforward sulphate reduction alone.

Fractionation of sulphur isotopes in the absence of bacteria is limited. Inorganic oxidation of sulphur species to sulphate or to other intermediates such as sulphite or thiosulphate has no associated isotope fractionation (Kaplan & Rittenberg, 1964; Habicht *et al.*, 1998). Pierre (1985) evaporated brines from seawater concentration to halite saturation and found an increase of only 1‰ in the $\delta^{34}S$ value of the remaining sulphate. Thode and Monster (1965) found that sulphate evaporites were concentrated in ^{34}S by 1-2‰ with gypsum, specifically, enriched in ^{34}S by 1.65 +/- 0.12‰. This process may be important in closed systems where the sulphate reservoir decreases during precipitation (Pierre, 1985) and would result in the residual sulphate becoming isotopically lighter. Sulphur isotopes can also be fractionated during temperature and pH dependent inorganic isotopic exchange reactions; however, equilibrium sulphur isotope exchange between most phases is very slow at temperatures less than 250°C (Kyser, 1987). It is concluded that bacterial activity and related kinetic effects are the predominant driving mechanisms for the fractionation of sulphur isotopes in low temperature systems (Longstaffe, 1989).

d) Open versus closed systems:

The size of the sulphate reservoir in a sulphate-reducing system can have a large influence on the $\delta^{34}S$ values of both bacteriogenic sulphides and residual sulphates. In an open system, with infinite access to dissolved sulphate, the $\delta^{34}S$ values of the H_2S and residual sulphate produced from sulphate reduction will, on average, remain essentially constant. However in a closed system, where the input of dissolved sulphate is restricted, a Rayleigh-like distillation will occur and the following equation can be applied:

$$\frac{R_f}{R_o} = f^{(\alpha-1)} \qquad (5.2)$$

Where f is the fraction of remaining reactant, R_f is the *delta* value of the reactant at some f and R_o is the *delta* value when $f=1$ (i.e. prior to the removal of any reactant).

This results in the $\delta^{34}S$ value of the sulphate increasing as its concentration drops. A parallel increase in the $\delta^{34}S$ of the produced sulphides will be seen in this scenario, assuming the

fractionation factor between sulphate and sulphide ($\Delta^{34}S$) has remained constant. Very low and relatively tightly grouped $\delta^{34}S$ values for sedimentary sulphides are characteristic of open system behaviour, whereas values that vary widely up to high $\delta^{34}S$ (e.g. –35 to +17‰, Cretaceous western interior of North America, Longstaffe 1989) are indicative of closed system behaviour due to isolation of porewater sulphate, for example during rapid sedimentation. In natural systems behaviour can be very complex and may alternate between an open and closed system, with complications resulting from additions to the residual sulphate pool and variations in the source of the sulphate.

5.2.3. Sulphur isotope methodology

Sulphur isotope values for residual lake and porewater sulphate were obtained from barite ($BaSO_4$) samples (precipitated directly from water collected in the field), in the laboratory in Oxford (see Section 4.5.3). All isotopic analyses were performed at the SUERC facility in East Kilbride, through funding obtained via the NERC Isotope Community Support Facility.

5.2.3.1. Preparation of barite sample for sulphur isotope analysis

Samples were prepared using a conventional sulphur vacuum gas extraction line, following the procedure of Coleman & Moore (1978). The barite was combusted with copper oxide and excess silica, with copper wire used to reduce any evolved sulphur trioxide to sulphur dioxide prior to collection of carbon dioxide and sulphur dioxide. The carbon dioxide was distilled using n-pentane and was discarded, whilst the sulphur dioxide was collected and its isotopic composition was analysed on a SIRA II mass spectrometer. See Appendix 5 for detailed methodology.

5.2.3.2. Data Reproducibility

The sulphur technique proved to be relatively straightforward and gave data with very good reproducibility. The error on the set of CP1 standards run with the 1998 samples was only ± 0.1‰ with a mean of –4.52‰. The quoted $\delta^{34}S$ value is –4.56‰, which is well within the error bars. There was also good internal consistency between the samples, with each lake having a

small and characteristic range of values. Yields were also high with the majority of samples having yields of between 80 and 100%. The yield percentage was shown to have no appreciable effect on the $\delta^{34}S$ value (Fig. 5.3).

The 1999 samples were run mainly with the IAEA-S-3 standard, which had an error of only ± 0.04‰ with a mean of –30.96‰ (quoted value is -31‰). Again the lakewater samples showed fairly good internal consistency although a little more variation could be expected since the lakes were very close to total desiccation. The values agree somewhat with the 1998 values, but each lake was at a slightly different evaporative stage to the previous year, so differences could again be anticipated.

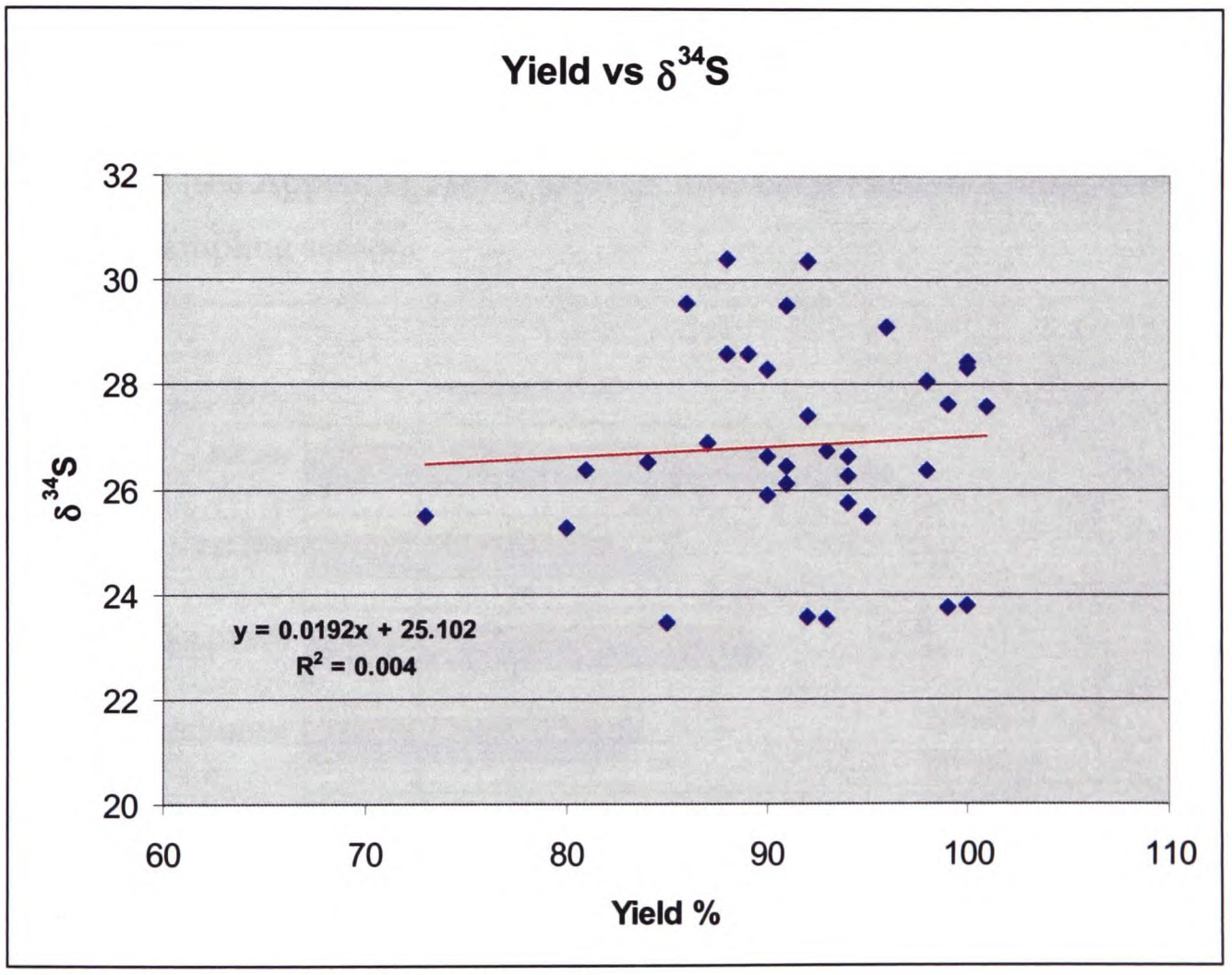


Figure 5.3. Yield versus $\delta^{34}S$ showing very low correlation. This indicates that these yields do not have a significant bearing on the isotopic composition of the gas.

5.2.4. Results

As mentioned previously, it was the residual sulphate from lake and porewaters that was analysed in this study. Unfortunately, no co-existing sulphides were isolated from these sediments because the H_2S is either re-oxidised or escapes rapidly out of the top of the sediment (illustrated by the pungent bad egg smell when the sediment is disturbed), rather than being fixed as metal sulphides.

The full set of sulphur isotope results can be found in Appendix 5. Important points that can be taken from this data set are illustrated in the following pages.

Sulphur isotopic data from the 1998 field season are shown in Figure 5.4. The main point of note is that the residual sulphate has a characteristic set of $\delta^{34}S$ values which are tightly grouped, but different for each lake; there is no significant variation between midday and dusk values (see Appendix 5) and likewise little observable difference between the start and end of the sampling season.

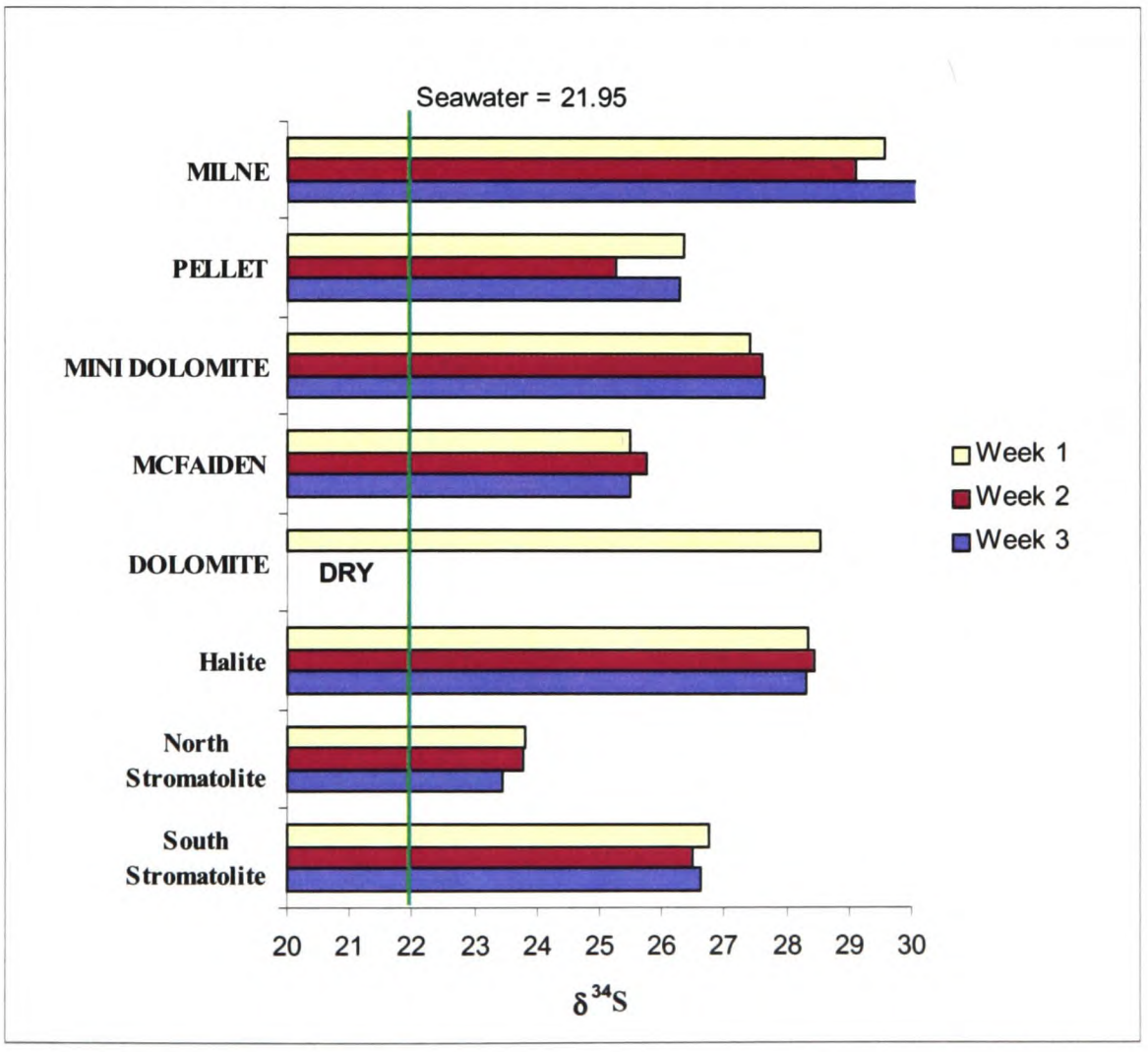


Figure 5.4. Sulphur isotope data for residual lakewater sulphates, November 1998.

All lakes show significant modification from the assumed seawater source sulphate value of +22‰ (value obtained from coastal seawater during this study; and see Section 1.7.2.) with sulphate in each lake enriched in ^{34}S. The maximum enrichment, in Milne Lake (dolomitic), being over 8‰ and the minimum enrichment in North Stromatolite Lake (non-dolomitic) being < 2‰. There are no obvious patterns in the data which discriminate the dolomitic lakes from the non-dolomitic lakes, likewise geographical location has no influence on the data.

The next logical step was to attempt to extract sulphur isotope data from the pore-waters of each of the lakes in order obtain more information on the sulphate reduction process. From the data obtained in 1998 it was assumed that the $\delta^{34}S$ of the lakewater would remain almost constant throughout the sampling season and this was reinforced by a few selected measurements in 1999. The remaining measurements in 1999 were carried out on pore-water samples, these results being shown graphically in Figure 5.5 (see Appendix 5 for complete data set).

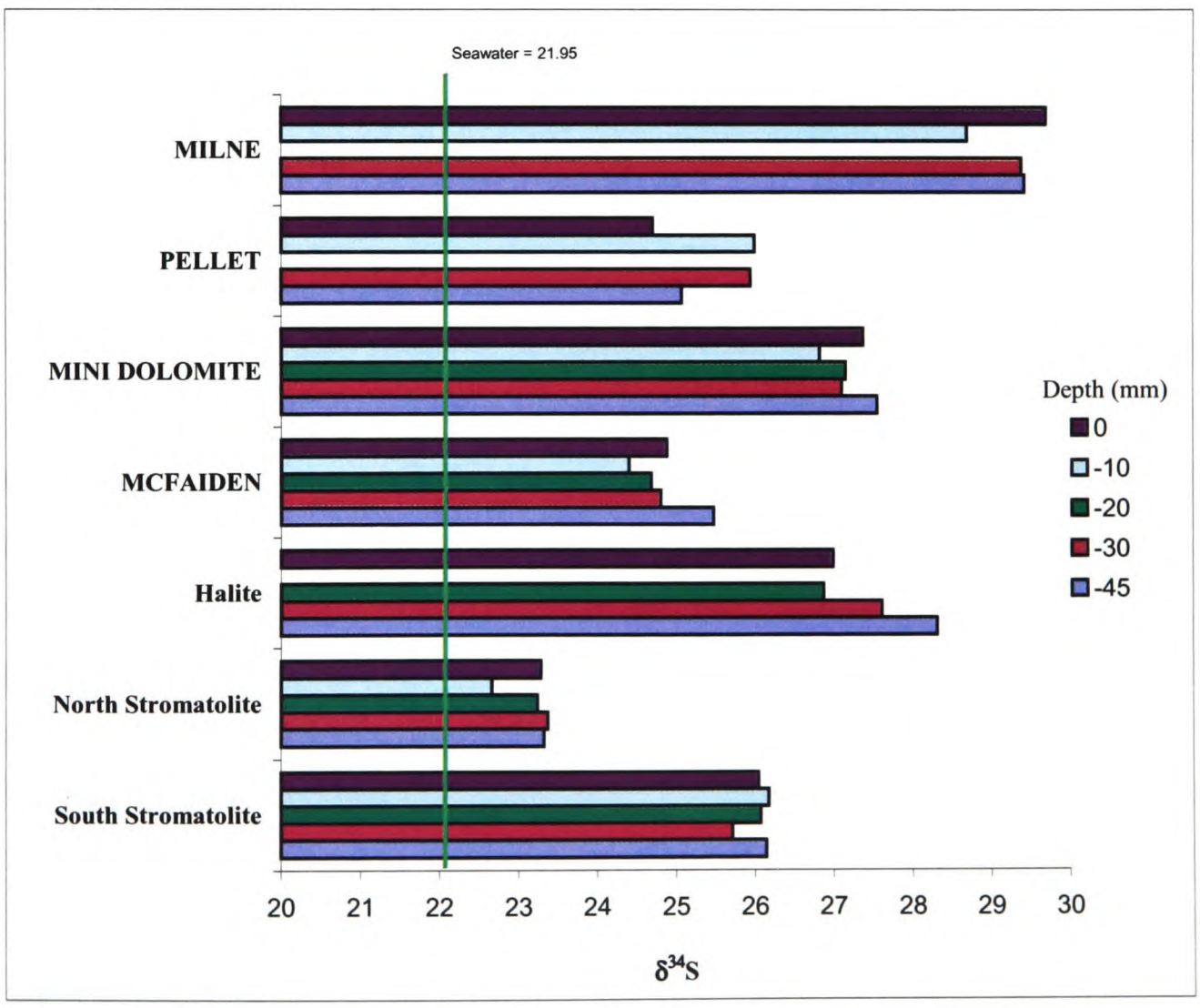


Figure 5.5. A snapshot (mid November, 1999) of sulphur isotope data for residual sulphate in both the lake and pore-water of the Coorong ephemeral lakes.

Focussing on $\delta^{34}S$ versus depth, only a little variation is noted, each lake having a fairly compact and characteristic set of values, once again significantly in excess of seawater $\delta^{34}S$. The pore-waters of Halite Lake, Mcfaiden Lake and to a certain extent Milne Lake and Mini Dolomite Lake show a pattern of increase in $\delta^{34}S$ with depth but only by relatively small amounts (1 - 1.5‰.). In all of the lakes except Milne Lake, $\delta^{34}S$ is heavier at 45mm depth than in the lakewater. Again, there are no obvious differences that distinguish the dolomitic from the non-dolomitic lakes.

5.2.5. Discussion

In a low temperature environment such as the Coorong one can be confident that any observed fractionation of sulphur isotopes away from the source value can mostly be attributed to bacterial processes. Other processes that may take place in the low temperature environment include the inorganic and biogenic oxidation of sulphide to intermediate sulphur-containing species and to sulphate and the precipitation of sedimentary sulphates. These processes, however, have little effect on sulphur isotopes; the former produces negligible fractionation (Kaplan & Rittenberg, 1964) and the latter produces $\delta^{34}S$ enrichment of only 1.65 +/- 0.12‰ (Thode & Monster, 1965). In any case, whereas halite is ubiquitous, sedimentary sulphates are striking because of their near absence in the upper sediments of the Coorong Lakes. One also needs to be confident that the results reflect bacterial processes in the lakes and are not merely due to anomalous inputs of ^{34}S enriched sulphate. It is assumed that the main source of sulphate is from seawater spray ($\delta^{34}S \sim 22‰$), since the lakes are adjacent to the coast and the prevailing wind is off the ocean (Von der Borch, 1976). In other regions, a major source of sulphate can be from groundwater discharge into the area. However the lithology in the area from which the groundwater originates here is a carbonate sequence with no evidence of evaporites from which sulphate could be dissolved (Ludbrook, 1980). Further evidence against this comes from measurements made in the field showing no significant dissolved sulphate in stream water passing into the area. Rainwater sulphate will have $\delta^{34}S$ values inherited from its source and since the weather patterns in this area mostly bring rain bearing moisture in from the sea, seawater is the assumed dominant source.

The major point for discussion must be the limited variation of isotopic signal within each lake even though it has been shown that vast amounts of SRB are present, especially in the dolomite bearing lakes (Chapter 6), and that sulphate reduction is active at this time of the year (evidenced by emission of H_2S). It is postulated that the observed, unusually small, increases in $\delta^{34}S$ values of residual sulphate could be due to one or more of the following:

1) open system behaviour with additional inputs of sulphate;
2) species specific effects;
3) re-oxidation of H_2S followed by further fractionations and transport of sulphate.

1) Are the study lakes open or closed systems? If these lakes were acting as closed systems, one would predict that as bacterial sulphate reduction proceeds in the upper few centimeters of the sediments, sulphate concentration would decrease and the residual sulphate should become increasingly enriched with respect to ^{34}S according to a Rayleigh distribution (Eq. 5.2). Sulphate concentrations generally do decrease with depth in all of these lakes; on average between 46% and 69% of sulphate is reduced in the top 50mm of the sediment (see Fig. 4.10) but $\delta^{34}S$ only increases with depth in some of the lakes and even then only by very small amounts. A plot of $\delta^{34}S$ versus sulphate concentration (Fig. 5.6a) shows very little correlation in either the dolomitic or non-dolomitic lakes when the data are grouped together.

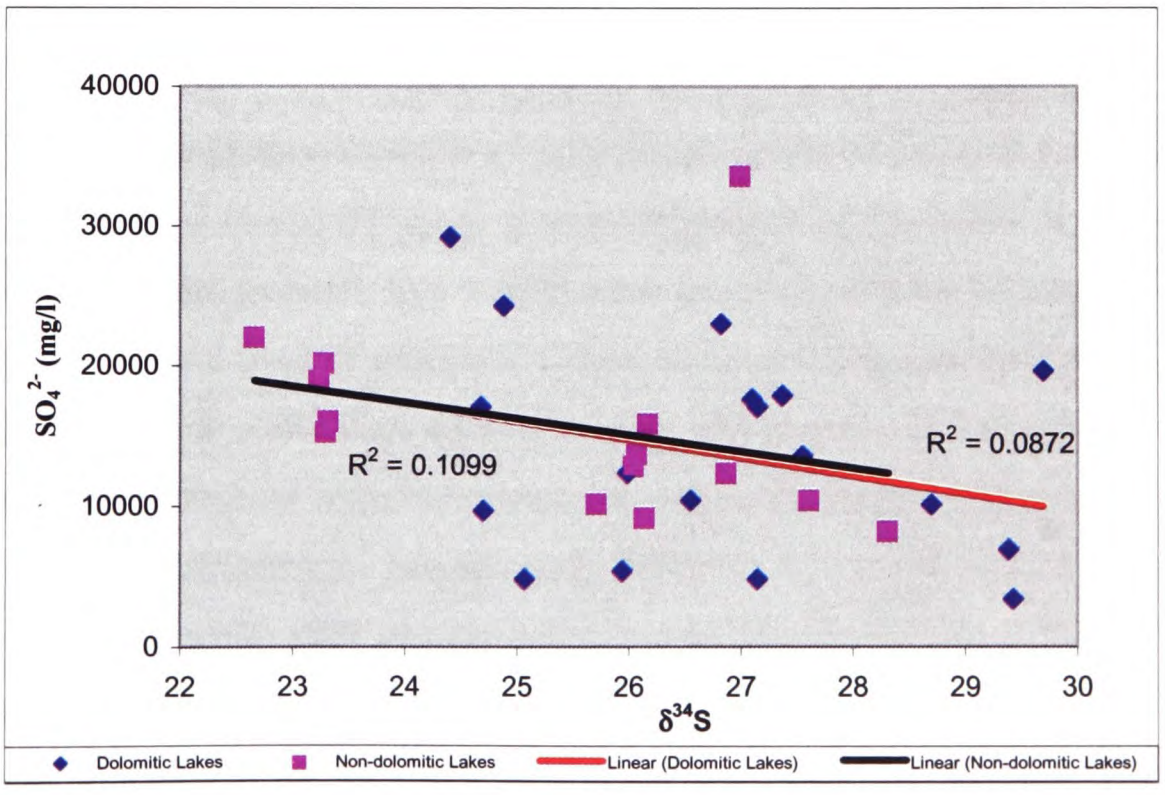


Figure 5.6a. Relationship between sulphate concentration and $\delta^{34}S$.

It could be concluded from this that the lakes are not behaving as closed systems, i.e. the porewater is not isolated and is not undergoing Rayleigh distillation. However, Figure 5.6b shows plots of $\delta^{34}S$ versus sulphate concentration for the three lakes which do show a pattern of increase in $\delta^{34}S$ with depth (Mini Dolomite, McFaiden and Halite; Milne Lake is omitted because sulphate data and $\delta^{34}S$ data were not collected on the same days). Two of these lakes (Mini Dolomite and Halite) show high correlations indicating some closed system behavior within the uppermost sediment column.

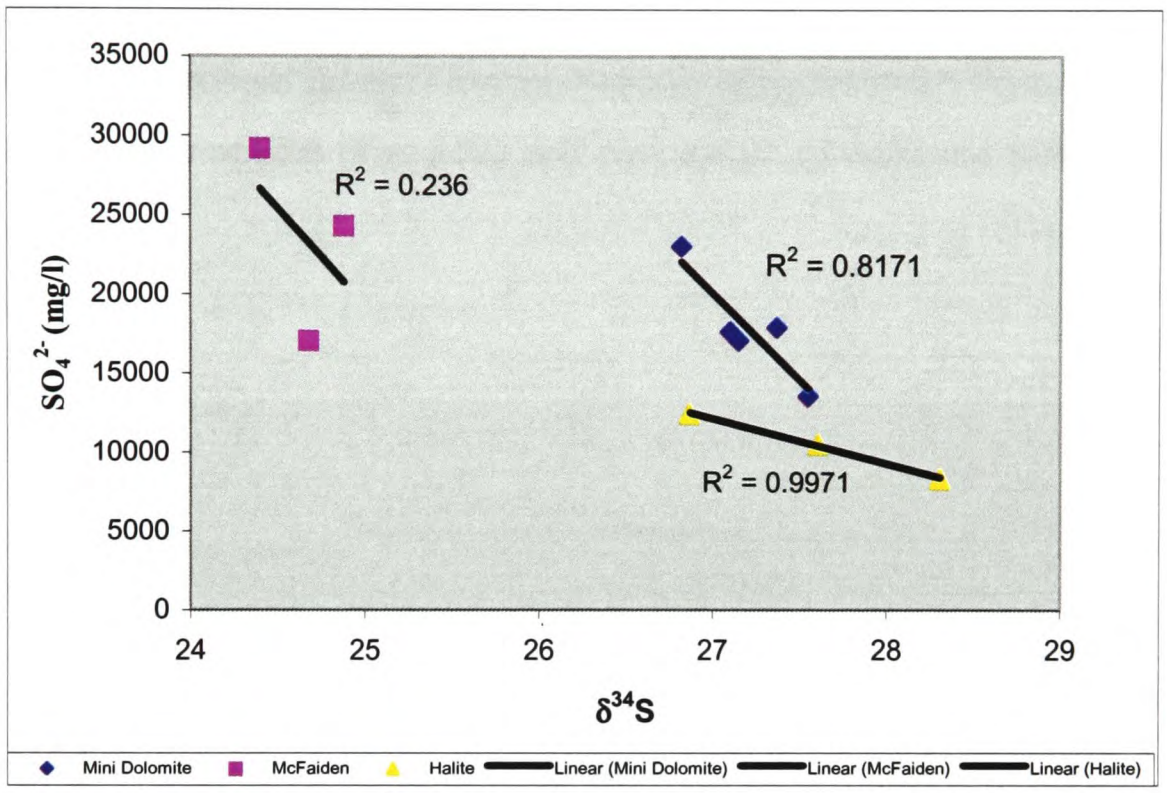


Figure 5.6b. Relationship between sulphate concentration and $\delta^{34}S$ for those lakes showing a pattern of $\delta^{34}S$ increase with depth.

The very high initial concentrations of sulphate in the lakes (Section 4.5) may go some way to explaining the predominantly open system behaviour of the lakes. If there were only small amounts of sulphate present, this would soon be exhausted by bacterial sulphate reduction, and the last residual pool of sulphate would show a strong isotopic signal. The situation in the Coorong lakes is somewhat different. Here, the source pool of sulphate is so large, even intense bacterial sulphate reduction does not reduce the concentrations to the very low levels seen in Rayleigh distillation models (e.g. Habicht & Canfield, 2001). Hence, the isotopic signal produced by the SRB is overshadowed by the initial signal from the large sulphate pool. Despite this, substantial bacterial sulphate reduction must be occurring on a lake scale to increase $\delta^{34}S$ values by as much as 8‰ (Milne Lake) compared to the seawater source sulphate.

2) Species specific effects as discussed by Detmers *et al.* (2001) may also be important in determining the $\delta^{34}S$ of each lake. Detmers *et al.* (2001) found that the fractionation factors of different species and genera growing under their optimal conditions could be vastly different, reporting a wide range between 2 and 42‰. Strains isolated from hypersaline mats, a similar environment to that of the study lakes, showed some of the smallest fractionation factors (*Desulfovirio halophilus* = 2‰, *Desulfovibrio oxyclinae* = 4.5‰) whilst a strain which has been identified in McFaiden Lake, *Desulfosarcina variabilis*, shows the lowest fractionation factor of the complete oxidizing species tested (15‰).

Two plots where positive correlations might previously have been expected are $\delta^{34}S$ versus the number of SRB (Fig. 5.7a) and percentage of sulphate reduced versus number of SRB (Fig. 5.7b).

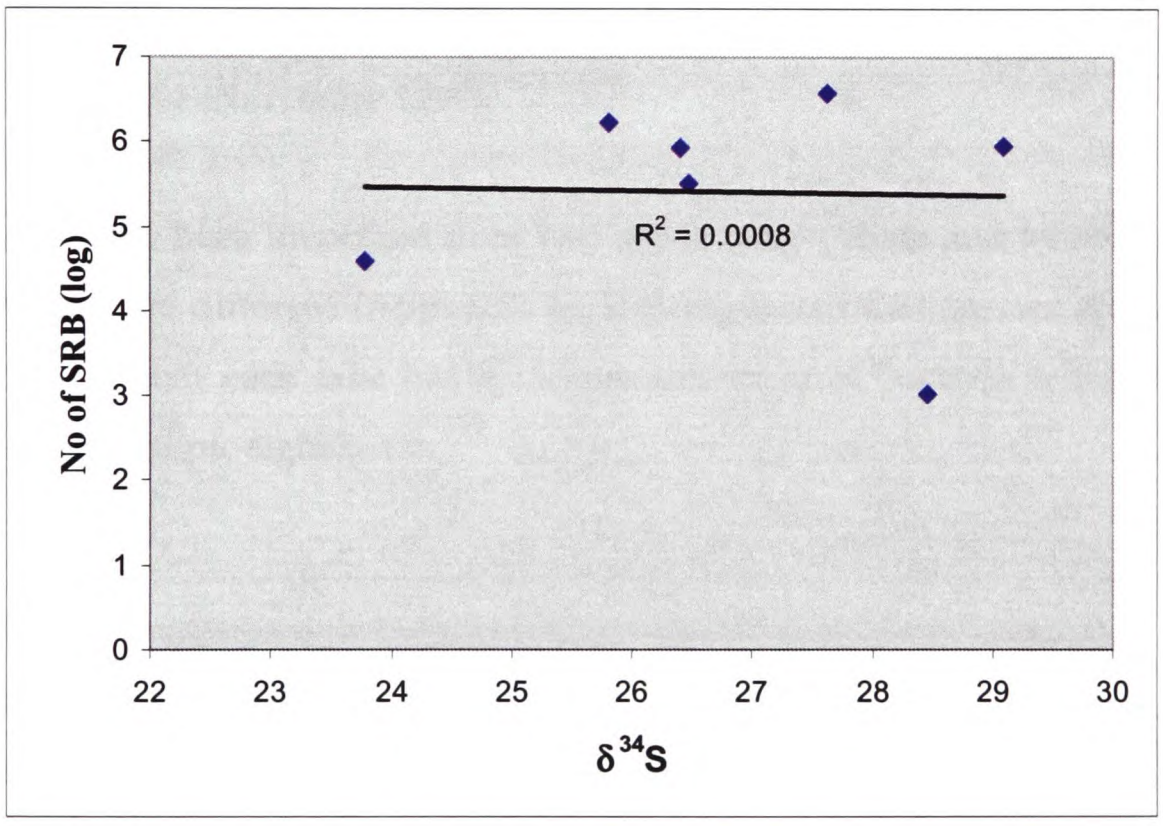


Figure 5.7a. A plot of $\delta^{34}S$ (lakewater sulphate) versus the number of SRB (per ml of sediment) in each lake (November 1998).

It may be expected that a larger number of SRB would be able to reduce more sulphate and hence result in a heavier $\delta^{34}S$ signal. However, neither of these plots show a correlation. This may be because a larger population of bacteria, competing for limited nutrients, will not function so efficiently as a smaller population whose nutrients are not limited and, therefore, the amount of sulphate reduced is independent of population size.

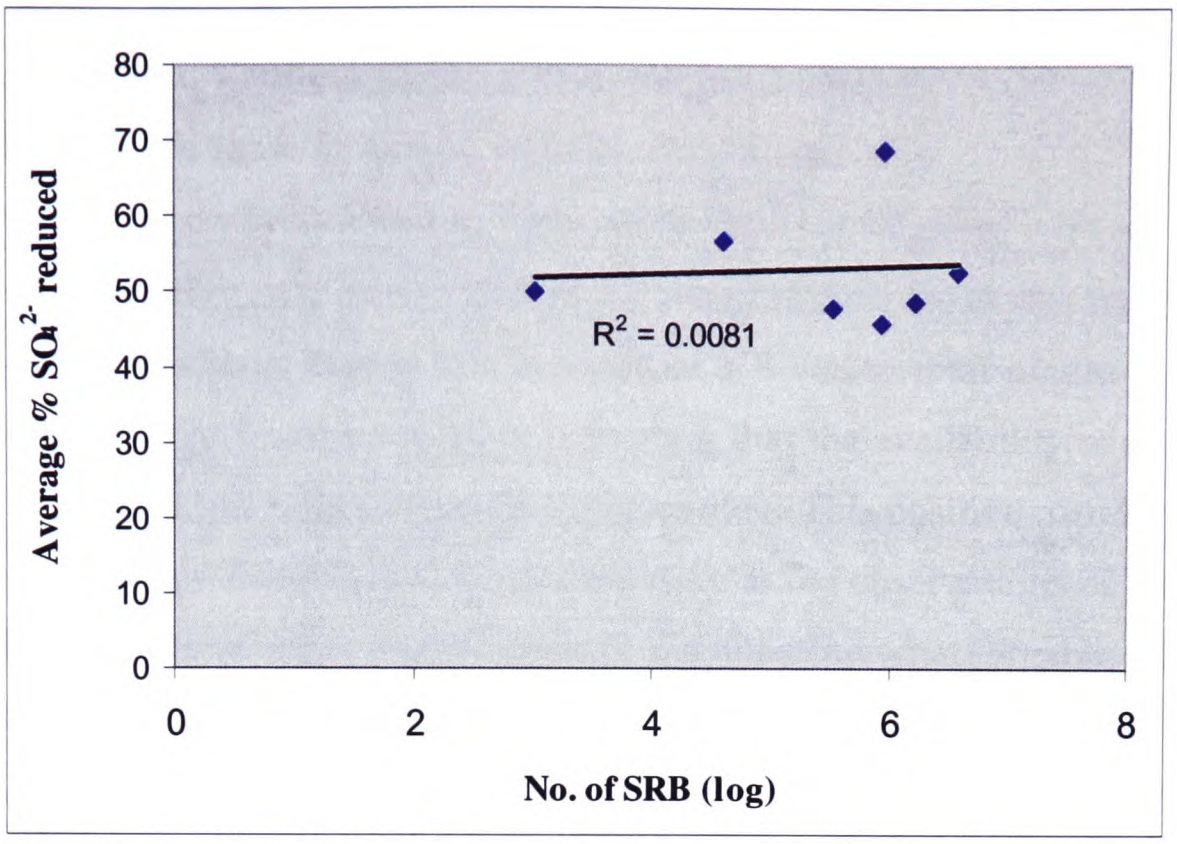


Figure 5.7b. A plot of the number of SRB (per ml of sediment) versus the average amount of sulphate reduced in the top 50mm of sediment in each lake (November 1999).

SRB species have been identified from two of the lakes (Milne and McFaiden) and have been shown to be quite different (Appendix 6). It is suggested that species specific effects may be important and that each lake has a unique collection of bacteria which in turn give it its characteristic isotopic signal.

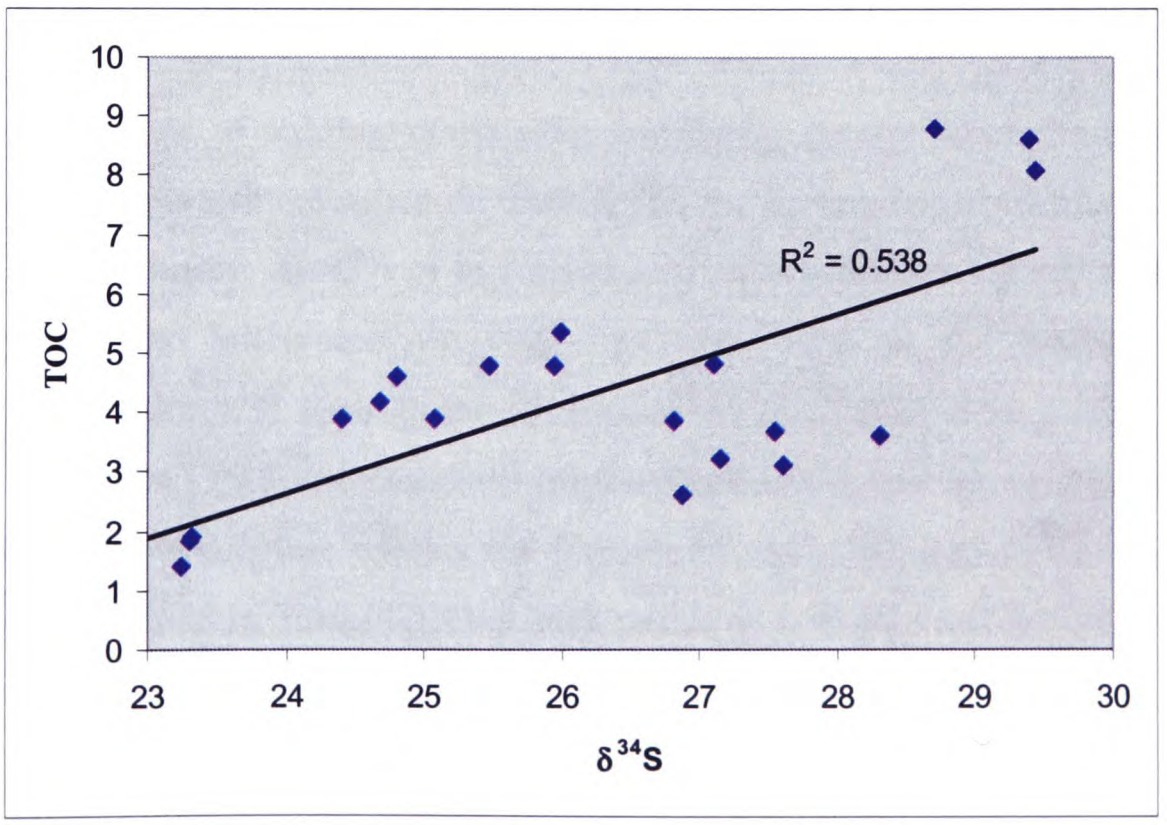


Figure 5.7c. Plot of $\delta^{34}S$ versus total organic carbon (TOC) showing a moderate correlation.

In addition, Canfield (2001) found that very variable fractionation factors could be obtained using the same strains of bacteria but changing their physiological pathways by using different growth substrates. Thus, even if different lakes contain similar bacterial populations, the lakes may inherit different isotopic signals due to the type of organic matter available to the bacteria. Figure 5.7c is a plot of $\delta^{34}S$ versus total organic carbon (TOC) and shows a 95-99% significant correlation indicating that the availability of organic matter may result in slightly larger sulphur isotope fractionations. This positive correlation between TOC and sulphur isotope fractionation is contradictory to the observations of Fry *et al.* (1995) and Canfield (2001) who record a higher isotopic fractionation when organic substrate is limited, because bacterial activity is lower and there is less competition for a limited sulphate supply. In the Coorong lakes, sulphate concentrations (see Section 4.5.4) may be high enough to support this increased bacterial activity associated with large concentrations of organic matter. It must be stated, however, that this correlation is governed only by the values at low (<2%) and high (<7%) TOC. Removing these five data points would result in no significant correlation, so it may be other factors such as the type of organic matter rather than the amount that are most important.

Much of this discussion can only be speculation at this time since some key data are unavailable. A full characterization of the bacterial populations in all of the study lakes, together with information on their sulphur isotope fractionation factors using a variety of substrates is necessary before this speculation can be substantiated.

3) Transformations of sulphur-containing species by means other than sulphate reduction may have an important influence on the sulphur isotope signal in each lake. Jorgensen (1982) states that, commonly, 80-95% of H_2S produced from sulphate reduction is reoxidized. H_2S escaping into the lakewater can easily be reoxidised as the lakewater is fairly well oxygenated (Section 4.3). Even in the absence of oxygen, nitrate and/or nitrite can be used by bacteria to oxidize H_2S to intermediate sulphur-containing species such as elemental sulphur. Once intermediate sulphur species are formed (S^0, S_2O_3, SO_3 etc) these can undergo further reactions as outlined in Table 5.2. One such pathway is shown in Figure 5.8 and would result in the residual sulphate becoming progressively isotopically lighter.

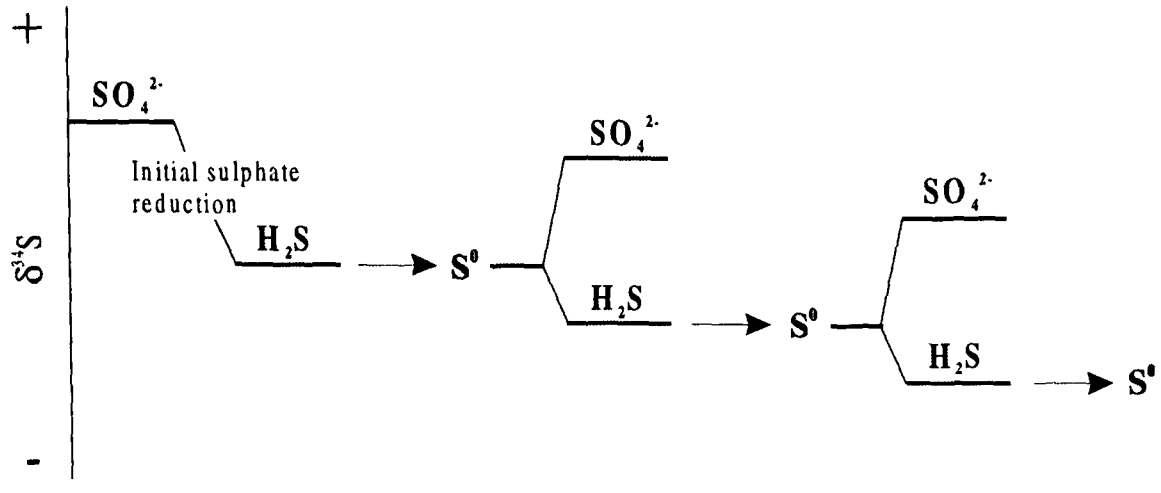


Figure 5.8. A generalized scheme showing how repeated sulphide oxidation followed by disproportionation can result in the residual sulphate reservoir becoming depleted in ^{34}S (redrawn from Canfield & Thamdrup, 1994).

This, together with similar disproportionation reactions for sulphite and thiosulphate may balance much of the heavy isotope enrichment caused by sulphate reduction resulting in each lake obtaining a relatively steady isotopic state. Although this theory is inevitably somewhat speculative, it is supported by oxygen isotopes in the lakewater sulphate, suggesting oxidation of sulphur in the lakewater (see Section 5.3.2) and by the immensely high concentrations of sulphate in the lakewaters, suggesting sulphate recycling.

5.3. OXYGEN ISOTOPES

Oxygen isotopes were used in this study in a threefold manner in order to:

a) elucidate the relationship between the carbonate minerals and the water from which they precipitated;
b) trace the evolution of the evaporating brines;
c) demonstrate microbial activity.

Oxygen has three stable isotopes:

$^{16}O = 99.763\%$

$^{17}O = 0.0375\%$

$^{18}O = 0.1995\%$

The ratio between ^{18}O and ^{16}O is used in oxygen isotope studies and is calculated from the following equation:

$$\delta^{18}O\ ‰ = \left[\frac{(^{18}O/^{16}O)_{sample} - (^{18}O/^{16}O)_{standard}}{(^{18}O/^{16}O)_{standard}} \right] \times 1000$$

The standards used here are V-PDB (from belemnites in the Cretaceous Peedee Formation of South Carolina) or a water sample distributed from the Atomic Energy Agency in Vienna, known as V-SMOW and the results are again expressed as parts per mil (‰).

Results using the V-SMOW standard are related to those using V-PDB as follows:

$$\delta^{18}O_{V\text{-}SMOW} = 1.03086\ \delta^{18}O_{V\text{-}PDB} + 30.86 \quad \text{(Hoefs, 1987)} \qquad (5.3)$$

and

$$\delta^{18}O_{V\text{-}PDB} = 0.97002\ \delta^{18}O_{V\text{-}SMOW} - 29.98 \quad \text{(Coplen } et\ al.\text{, 1983)} \qquad (5.4)$$

5.3.1. Distribution of oxygen isotopes

Two complementary $\delta^{18}O$ reservoirs are found in nature. Igneous, metamorphic and sedimentary rocks are mostly enriched in ^{18}O relative to the mantle value (~5.7‰), whilst seawater and meteoric waters are depleted (Fig. 5.9).

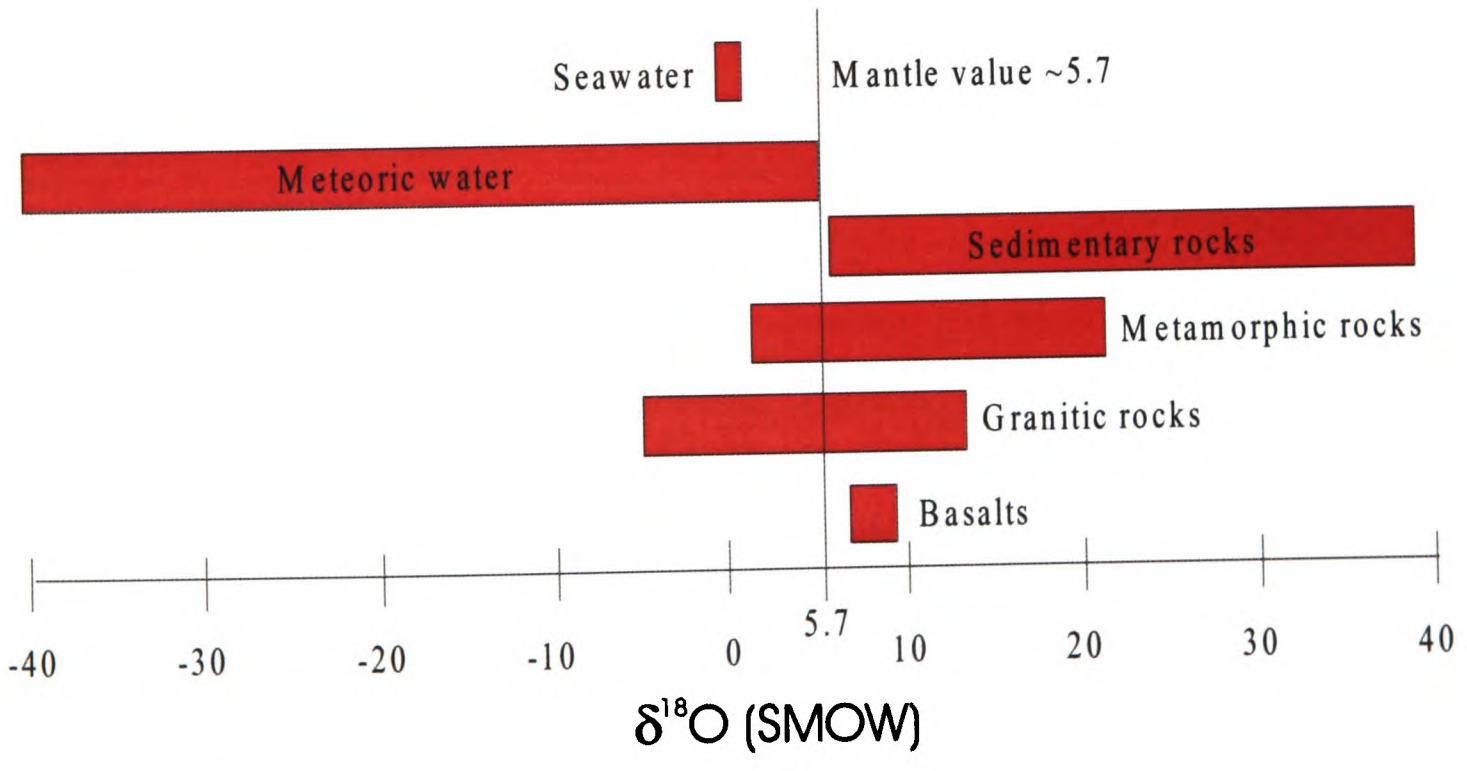


Figure 5.9. Natural isotope reservoirs of oxygen (adapted from Hoefs, 1987).

In this study the reservoirs of interest are:

a) Natural waters
b) Phases common in the Coorong Lake environment (i.e. carbonates and sulphates).

a) Natural waters

The oxygen isotope composition of natural waters is strongly influenced by evaporation and condensation (Faure, 1977). During evaporation isotopic fractionation is controlled by the difference in vapour pressure between molecules containing the heavier or lighter isotope. It follows that the lighter molecular species are concentrated in the vapour phase because less energy is needed to keep them in this phase. The *extent* to which evaporation or condensation has occurred is also important. Vapour produced from net evaporation of the oceans ($\delta^{18}0 \sim 0‰$) at low latitudes is enriched in ^{16}O. Atmospheric circulation carries this vapour polewards, the drop in temperature causing some to condense. Since ^{18}O is more likely to condense than ^{16}O the remaining water vapour becomes progressively depleted in ^{18}O, and so any further condensate will itself be depleted in ^{18}O. This process is another example of Rayleigh Distillation (Eq. 5.2) and results in meteoric water at low latitude being isotopically heavier than that at high latitude (see the meteoric water line of Figure 5.15).

Conversely, residual water from which ^{16}O rich water vapour has evaporated will be enriched with isotopically heavy ^{18}O, and so in an environment like the Coorong distal ephemeral lakes where evaporation greatly exceeds precipitation for large parts of the annual cycle, extensive ^{18}O enrichment is expected. This will be discussed in more detail in Section 5.3.4 where brine evolution is considered.

b) Carbonates and sulphates

The $\delta^{18}O$ of sedimentary carbonates depends largely upon equilibrium exchange reactions between CO_2, H_2O and various carbonate species, proceeding through dissolution, precipitation reactions and through diffusional mechanisms.

$$\text{e.g. } CaC^{16}O^{16}O^{16}O + H_2{}^{18}O \Leftrightarrow CaC^{18}O^{16}O^{16}O + H_2{}^{16}O$$

This causes calcite to be considerably enriched in ^{18}O at equilibrium, by 28.6 ‰ at 25°C (O'Neil & Epstein, 1964). Other carbonate minerals are likewise enriched. Heavy isotopes

tend to be concentrated in more closely packed structures, with ions that have a high ionic potential (charge/size ratio) concentrating heavy isotopes to a greater degree. The C^{4+} ion in carbonate does this to great effect, with the mass effect of the divalent cation playing a more minor part. Experimental studies indicate dolomite should be enriched in ^{18}O by 5-7‰ compared to co-existing calcite at 25°C (O'Neil & Epstein, 1966; Sheppard & Schwarcz, 1970). In most natural samples this difference is significantly less; this has been explained by dolomite being precipitated as 'protodolomite' in which the fractionation factor with water is less, or because of miscalculations of the dolomite-calcite fractionation factor. Unfortunately, because dolomite had not, until very recently, been precipitated in the laboratory under natural conditions, experimental isotopic equilibrium fractionation factors for the mineral are poorly defined, but do remain useful (see Section 5.3.5). Biogenic (vital) effects such as differences in species, growth rate, metabolic and reaction pathways result in *isotopic disequilibrium* and so deviations from expected isotopic distribution patterns often indicate the action of biological processes. A good example of this is the $\delta^{18}O$ values of sulphate ions as discussed in the following sub-sections.

5.3.2. Oxygen isotopes from SO_4^{2-}

5.3.2.1. Methodology

Oxygen isotope values for residual lake and porewater sulphate were obtained from barite ($BaSO_4$) samples precipitated directly from water collected in the field, in the laboratory in Oxford (see Section 4.5.3). As with the sulphur isotope analyses, oxygen isotopic analyses were performed at the SUERC facility in East Kilbride, through funding obtained via the NERC Isotope Community Support Facility. Samples for oxygen isotope analysis were prepared following the procedure of Hall *et al.* (1991). The barite was combusted with graphitic carbon at around 1350°C (by induction heating of a clean platinum crucible) for a period of between one and three hours. During gas extraction, any CO produced is converted to CO_2 via a high voltage discharge unit held at liquid nitrogen temperature. This is then added to produced CO_2 and quantitatively measured and collected for later isotopic analysis on a SIRA 10 mass spectrometer (see Appendix 5 for the detailed methodology).

5.3.2.2. Data reproducibility

The sulphate oxygen technique is acknowledged to be one of the most difficult to execute to produce good quality data. As a result, oxygen isotope data proved problematical to deal with. The reproducibility of the standards was again good but as soon as samples were run, problems were encountered. Initially, yields were very low which resulted in anomalous $\delta^{18}O$ values when the mass spectrometer analysed the gas. Some time was spent experimenting with the intensity and length of combustion before relatively high yields were obtained. It was found that the period of combustion had to be increased threefold in comparison with the standard, whereas the intensity could only be increased very gradually whilst at the same time carefully checking that no plasma was being created in the heating tube. Emission of such plasma can lead to anomalous results. Since the yield appeared to have some bearing on the $\delta^{18}O$ values (in the experience of the SUERC laboratory, low yields tend to give anomalously high $\delta^{18}O$ (Adrian Boyce, Pers. Comm.)), samples with yields below 60% or above 100% were discarded. As a result quality data have only been obtained from a small proportion of the samples analysed.

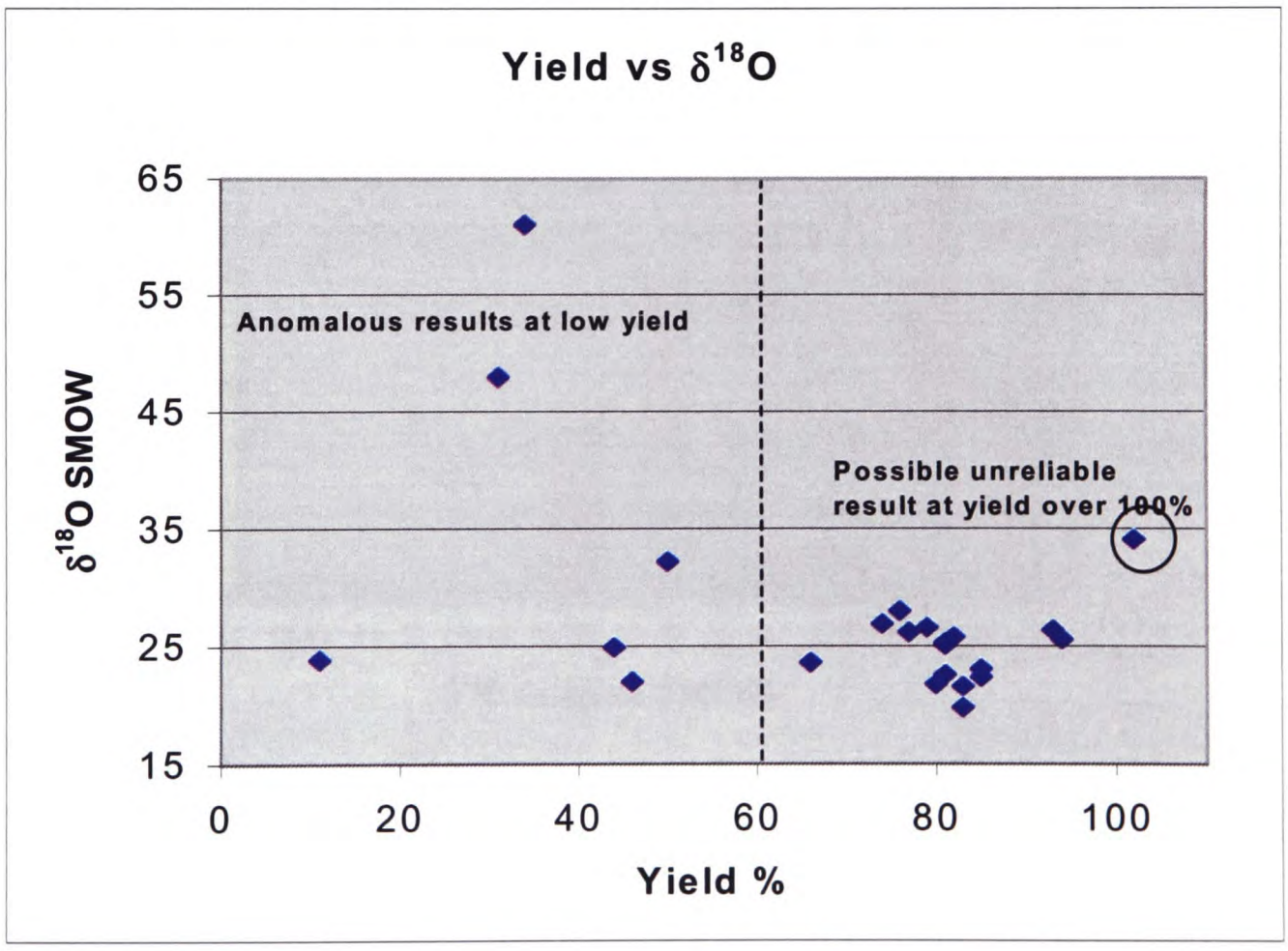


Figure 5.10. Yield versus $\delta^{18}O$ showing that anomalous results may be caused by very low or very high yields. Data from yields below 60% and above 100% were subsequently discarded.

5.3.2.3. Results

Figure 5.11 shows the range of $\delta^{18}O$ values found in the residual sulphate of the Coorong Lakes. The $\delta^{18}O$ of seawater sulphate obtained in this study is also represented for comparison. $\delta^{18}O$ of the lakewater sulphate in the dolomitic lakes ranges from 19.9 to 28.1‰ with a mean of 24.3‰, whilst the range for the non-dolomitic lakes is from 21.9 to 26.7‰ with a mean of 23.9‰. These values are well in excess of the sulphate from coastal seawater measured in this study (10.4‰ and 11.3‰). No other sulphate oxygen data exists for these lakes and indeed very little sulphate oxygen data has been reported for any saline lake settings. Longinelli and Craig (1967) report enrichments of 7-23‰ in a variety of saline lakes, the highest being from Searles Lake (+23.16‰) where the sulphate concentration was 48,700ppm which is on the same scale as that observed in these lakes.

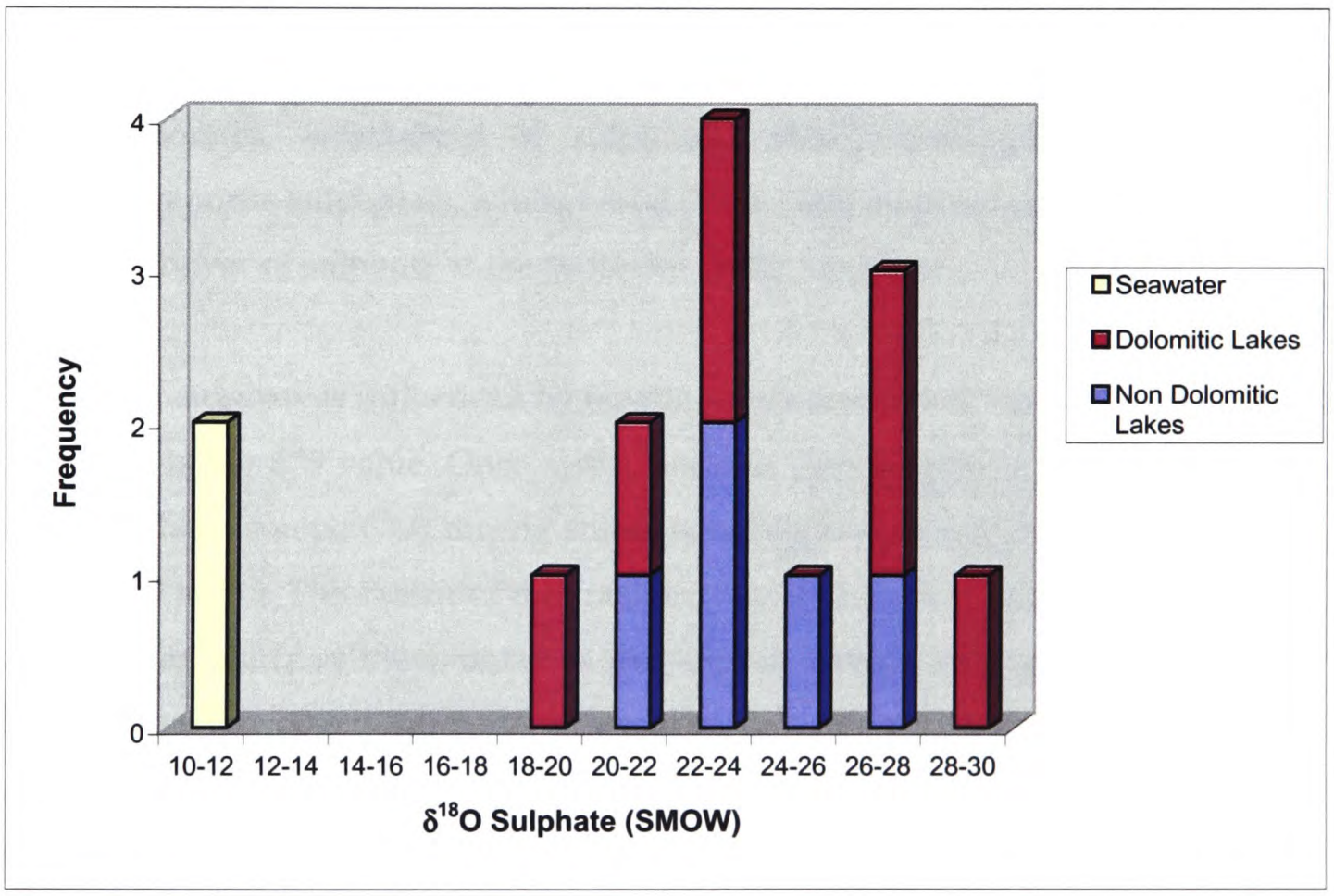


Figure 5.11. Sulphate oxygen isotope results from seawater and the Coorong study lakes

5.3.2.4. Discussion

The behaviour of oxygen isotopes in the sulphate-water system has, somewhat surprisingly, received little attention in the geological community, with very few studies reported in the literature. For this reason, the interpretation of this limited data set is somewhat difficult. The equilibrium fractionation factor for isotopic exchange between oceanic water ($\delta^{18}O \sim 0‰$) and sulphate ions as determined by Mitzutani (1972) is 28.3‰ at 25°C increasing to 33.1‰ at 5°C. Yet sulphate ions in seawater have a relatively constant $\delta^{18}O$ of only 9.7‰ (Lloyd 1968). Hence, it is clear that the oxygen in the sulphate ion does not obtain isotopic equilibrium with the oxygen in seawater, and instead reflects the source of the sulphate. It was found that the sulphate ion, once formed, is extremely stable with respect to oxygen isotope exchange and so the isotope content of a given sulphate ion remains uniquely characterized by its mechanism of formation (Lloyd 1967). Lloyd (1968) calculated that periods of time of the order of at least 10^3 years were required to attain isotopic equilibrium. While the $\delta^{18}O$ value of 9.7‰ is universally regarded as correct for seawater sulphate, how it is achieved is still somewhat controversial. Holser *et al.* (1979) maintain that it is due to a balance of inputs (erosion of evaporates, weathering of sulphides) and outputs (sulphate reduction, precipitation of evaporite sulphates), whilst Lloyd (1967,1968) emphasised the importance of rapid bacterial turnover of sulphate at the sediment water interface.

The $\delta^{18}O$ of sulphate is influenced by kinetic effects associated with bacterial sulphate reduction, just as is the $\delta^{34}S$ value. Once again, bacteria discriminate in favour of sulphate containing the lighter isotope (^{16}O) during sulphate reduction leaving the residual sulphate reservoir enriched in ^{18}O. The extent of the fractionation is debatable and unfortunately has not been studied in nearly as much detail as the sulphur isotope system has. Lloyd (1968) reported a kinetic effect of around 4.6‰ using pure cultures of *D.desulfuricans* and mixed cultures from black muds. Other authors (Holser *et al.*, 1979; Pierre 1985) prefer to use a ratio of sulphur to oxygen enrichment ($\varepsilon^{34}S/\varepsilon^{18}O$). This ratio commonly ranges between 2.5 and 4 (Pierre 1985) and hence, if one knows the sulphur isotope enrichment, the equivalent oxygen enrichment can be calculated. This implies that the process of sulphate reduction will lead to covariance of sulphur and oxygen isotopes in the residual sulphate. A plot of $\delta^{18}O$ versus $\delta^{34}S$ for the sulphate analysed in this study is given in Figure 5.12a.

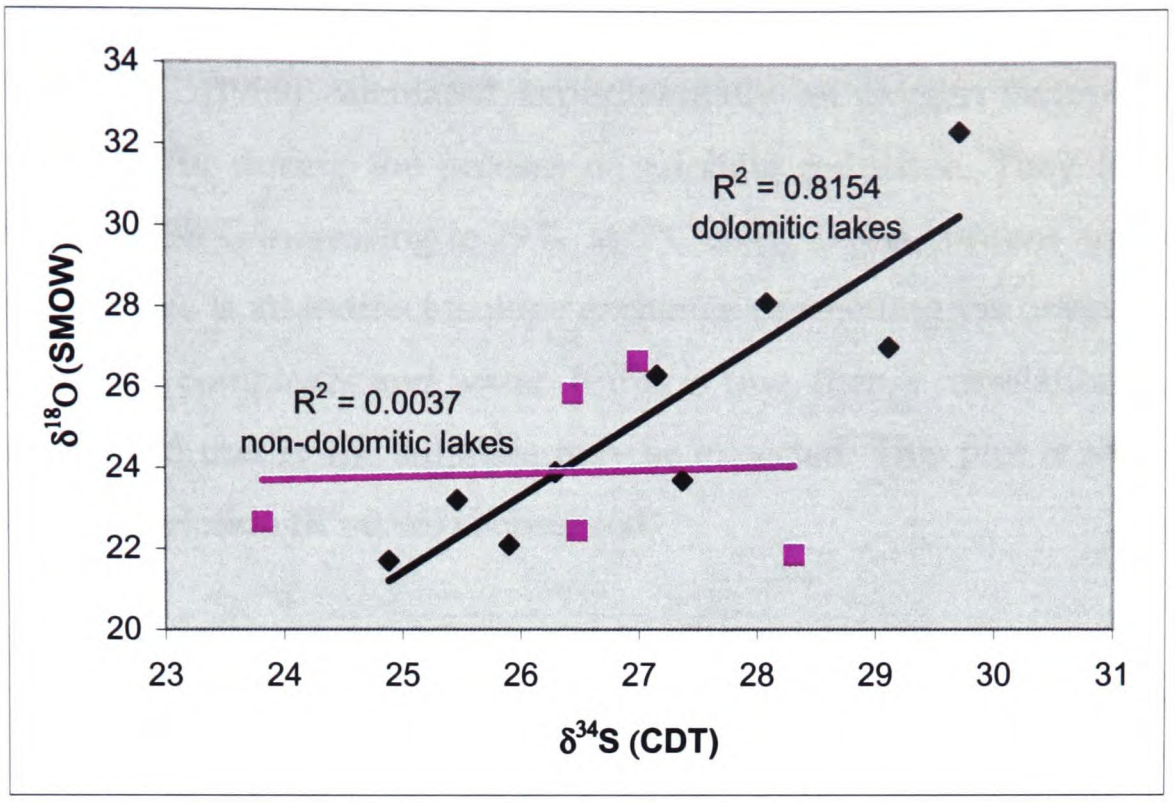


Figure 5.12a. Relationship between $\delta^{34}S$ and $\delta^{18}O$ in the residual lakewater sulphate in both dolomitic and non-dolomitic lakes.

A significant correlation is noted for the dolomitic lakes, with an increase in $\delta^{34}S$ being accompanied by an increase in $\delta^{18}O$. These are the first isotopic parameters for which a significant difference is observed between dolomitic and non-dolomitic lakes, perhaps suggesting that bacterial sulphate reduction is better developed in the dolomitic lakes. A similar positive correlation between $\delta^{34}S$ and $\delta^{18}O$ of residual sulphate was recorded by Böttcher *et al.* (1999) in a sulphate reducing environment from bottom sediments of the Western Mediterranean. If one assumes the source of sulphate is seawater ($\delta^{18}O$=+9.7‰ and $\delta^{34}S$=+21‰) then the $\varepsilon^{34}S/\varepsilon^{18}O$ enrichment ratio is only ~ 0.4 for the dolomitic lakes. This is much less than the common range of 2.5 to 4 and lower even than the value of 1.5 found by Pierre (1985) for the marine salt pans of Salin-de-Giraud (south of France). However, this $\varepsilon^{34}S/\varepsilon^{18}O$ ratio has been obtained from relatively small amounts of data in a closed system. Since it has already been shown that the $\delta^{34}S$ of sulphate depends on many factors such as reaction rate, temperature, amount of available organic matter, substrate and, possibly most importantly, species specificity then it can be assumed that the $\delta^{18}O$ of sulphate may also depend on these same variables. Thus the $\varepsilon^{34}S/\varepsilon^{18}O$ ratio can be expected to vary widely. In addition, such high $\delta^{18}O$ values suggest that a sulphate source other than seawater may also be important. As noted during the discussion of sulphur isotopes, much of the sulphate reduced may be recycled via bacterial oxidation and disproportionation reactions before being reduced once more and thus an original seawater sulphate ion will inherit the $\delta^{18}O$ value associated with the fluids in the area it is re-oxidised (i.e. the lakewater).

Fritz *et al.* (1989) calculated experimentally an oxygen isotope exchange between sulphate and water during the process of sulphate reduction. They found a fractionation factor of 25‰ at 30°C increasing to 29‰ at 5°C using *D.desulfuricans* and a lactate substrate. They state that this is an indirect isotope exchange proceeding via oxygen exchange between sulphate-enzyme complexes and water. If this is true, then a correlation between the $\delta^{18}O$ of the lakewater and that of the sulphate may be expected. This plot is shown in Figure 5.12b and a strong correlation (R^2=0.96) is observed.

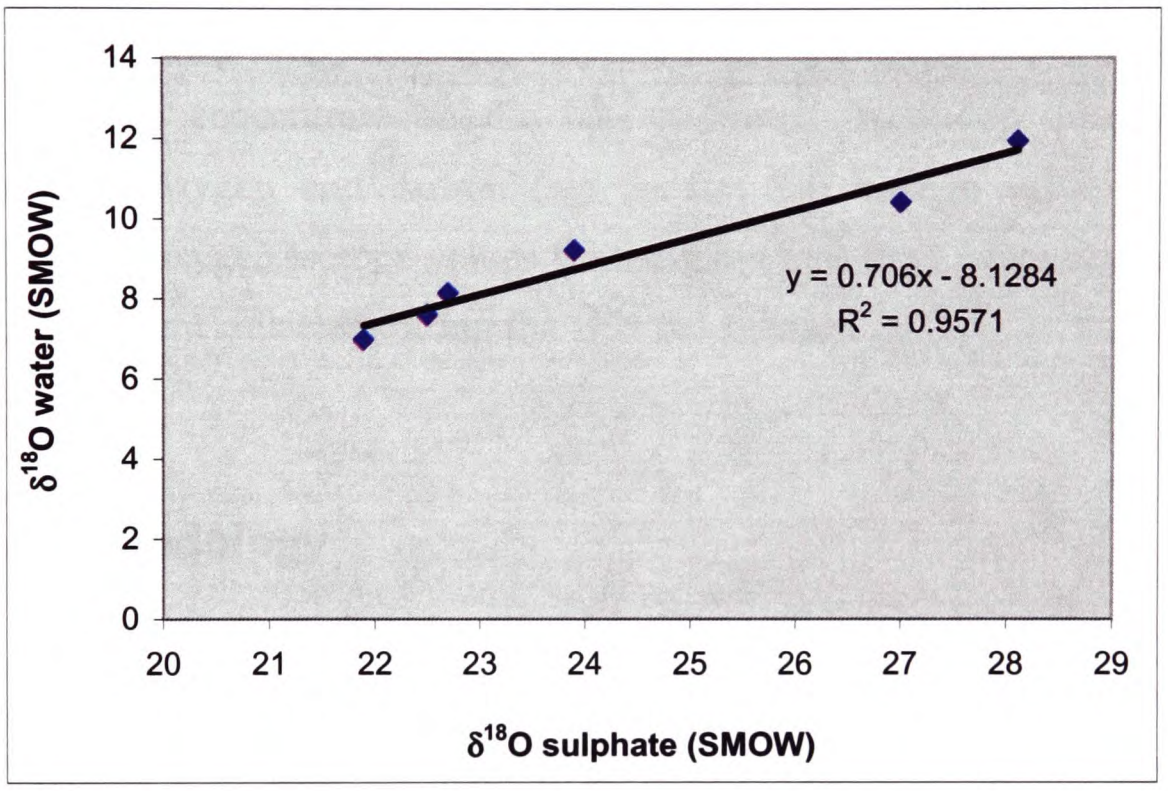


Figure 5.12b. Relationship between $\delta^{18}O$ in the lakewater and that in the residual lakewater sulphate (November 1998)

This not only supports the existence of an oxygen isotope exchange during sulphate reduction but also the recycling of sulphate mentioned in the previous paragraph. The difference between the $\delta^{18}O$ of the sulphate and that of the water ($\Delta^{18}O_{sulphate\text{-}water}$) is not as great as that calculated by Fritz *et al.* (1989) having a mean of only 15.3‰. This is not unexpected, however, because Fritz *et al.* (1989) used a closed system and calculated their fractionation factors from experiments where <2% of the original sulphate remained. In the case of the Coorong lakes, a much higher percentage of sulphate remains and the signal may be complicated by inputs from sea spray ($\delta^{18}O$ ~10‰) and by the fact that different species and concentrations of vital components exist in these lakes when compared with the Fritz *et al.* (1989) experiments.

Despite the problems caused by the lack of thorough investigation into sulphate oxygen isotopic signals in the past and the small data set obtained here, tentative conclusions can be drawn that support the activity of SRB as a major factor contributing to the distribution of observed $\delta^{18}O$-sulphate in this setting. Indeed, it is the first isotopic parameter to show a significant distinction between the dolomitic and non-dolomitic lakes.

5.3.3. $\delta^{18}O$ of the carbonates

The next logical step after obtaining sulphur and oxygen isotopic data from the residual sulphate was to concentrate on the lake sediment itself and investigate its isotopic characteristics. Oxygen and carbon (see Section 5.4) isotope values for the carbonate sediments, plus oxygen isotope values for the lakewater fluid, were obtained directly from water and sediment collected during the 1999 field season.

5.3.3.1. Methodology

Isotopic analysis was again performed at SUERC, using a relatively new piece of apparatus from *Analytical Precision*, which made preparation and processing both rapid and accurate. Traditionally the measurement of ^{13}C and ^{18}O from carbonate samples has been made using a Dual Inlet Isotope Radio Mass Spectrometer, either interfaced with an automated sample preparation system or using samples extracted off-line. This yields reliable data but results in a relatively low daily throughput and high costs. The new apparatus from *Analytical Precision* consists of a fully automated sample preparation module and a sample processing module, interfaced to a dedicated Isotope Ratio Mass Spectrometer. The simplified instrumentation allows high throughput at relatively low cost. In addition, because each sample is prepared and reacted with acid individually, 'memory' effects, often observed when common acid baths were in use, are removed, and a variety of carbonate minerals can be analysed during a given run. See Appendix 5 for more detailed methodology.

5.3.3.2. Data Reproducibility

The reproducibility of data from the AP2003 unit at East Kilbride is excellent since each sample tube was run several times, producing replicate peaks. An internal standard (Mab2b) was used whose accepted value is $\delta^{18}O = -2.404$ ‰ PDB and reproducibility was ± 0.2 ‰.

5.3.3.3. Results

The oxygen isotope data obtained from sediment within the study lakes are shown in Figure 5.13. $\delta^{18}O$ values have a narrow range between 33.7 and 36.4‰, lying in the field of normal sedimentary rocks but towards the higher end (Fig. 5.8). There is no obvious trend as far as dolomitic versus non dolomitic lakes are concerned, neither is there any consistent trend with depth. From this data alone little can be deduced about the processes operating, but these data may be useful when combined with those obtained from the fluid lakewater (Section 5.3.6) and $\delta^{13}C$ data from the carbonates (Section 5.4).

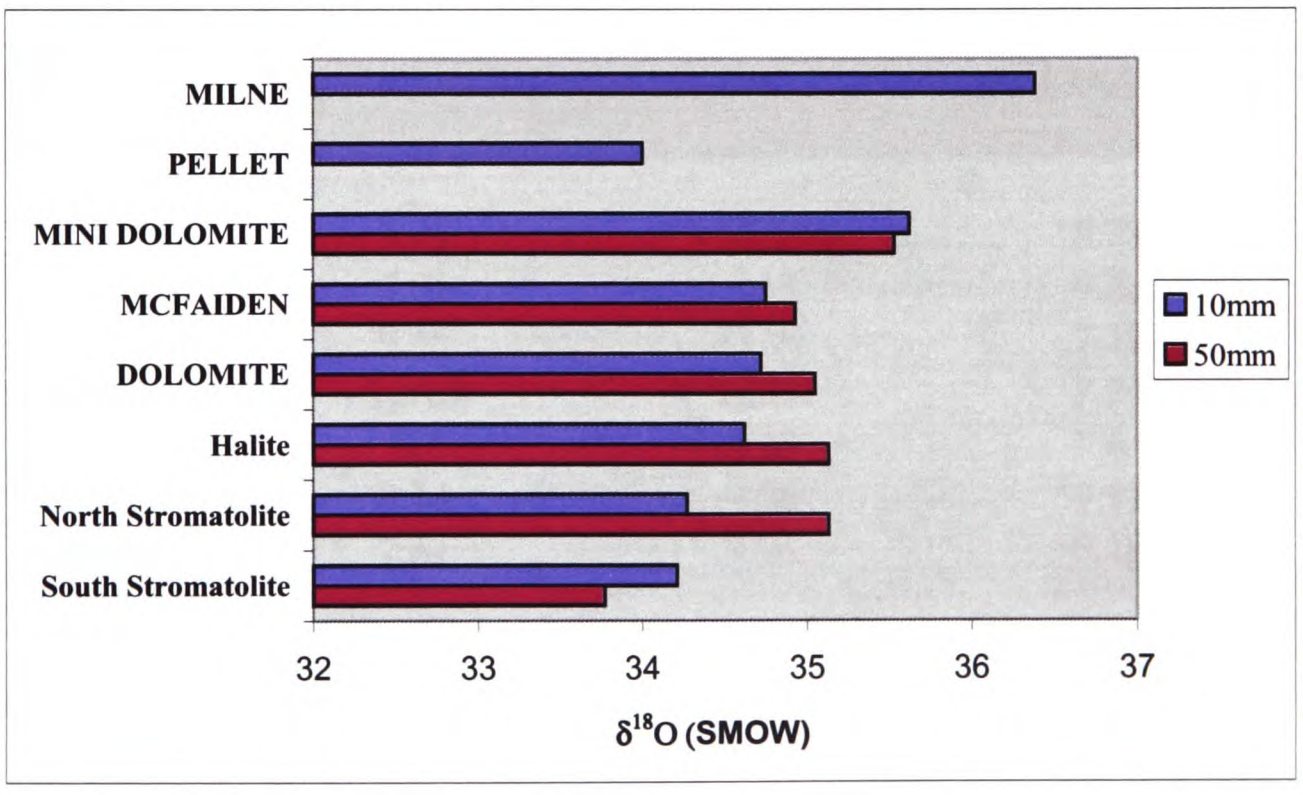


Figure 5.13. $\delta^{18}O$ data for carbonates in the Coorong ephemeral lakes.

N.B. Lakes in capitals are dolomitic whilst those in lowercase are aragonitic.

5.3.4. Lakewater $\delta^{18}O$

Water samples were run on the same apparatus as the carbonate samples and the methodology is described in Appendix 5. Oxygen isotope data from water taken from the study lakes at several times during the sampling season are presented in Table 5.3 and Figure 5.14. $\delta^{18}O$ values span a large range of 5.7 to 12.3‰, these values being very heavy when compared to seawater which by definition, on the V-SMOW scale, is approximately zero. The lakes are situated in a seawater-groundwater mixing zone and in addition are often refilled directly with meteoric water. During a substantial part of the year, all of these lakes undergo intense evaporation, which concentrates ^{18}O in the residual lakewater. This enrichment effect was maximised because samples were collected near the end of the annual evaporative cycle of the lakes. The driest lakes, at the time of sampling (McFaiden and Mini Dolomite), show the greatest ^{18}O enrichment up to the week ending 8th November. Beyond this date, three of the lakes show increased ^{18}O enrichment with increased evaporation, as expected. Four of the lakes, however, (significantly the driest four) show the reverse pattern, indicating that a significant opposing process may be taking place. Since there was no substantial rainfall in this period, and since different lakes are responding in different manners, an input of meteoric water can be discounted.

Lake	$\delta^{18}O$ (‰ V-SMOW)		
	W/end 1/11/98	W/end 8/11/98	W/end 22/11/98
MILNE	9.91	10.43	8.78
PELLET	7.01	7.13	9.23
MINI DOLOMITE	9.45	11.95	7.12
MCFAIDEN	12.13	12.29	7.74
Halite	5.7	6.43	7
North Stromatolite	8.16	9.26	9.91
South Stromatolite	7.61	9.96	8.18

Table 5.3. Oxygen isotope values of lakewater in Coorong distal ephemeral lakes, November 1998

Craig and Gordon (1965) modeled the process of $\delta^{18}O$ enrichment of evaporating low salinity waters showing that $\delta^{18}O$ increases until the final stages of drying when a steady state is reached due to the back transport of water molecules from the atmosphere. The

steady state $\delta^{18}O$ value in that situation depends upon relative humidity and the $\delta^{18}O$ value of the atmospheric moisture in the area.

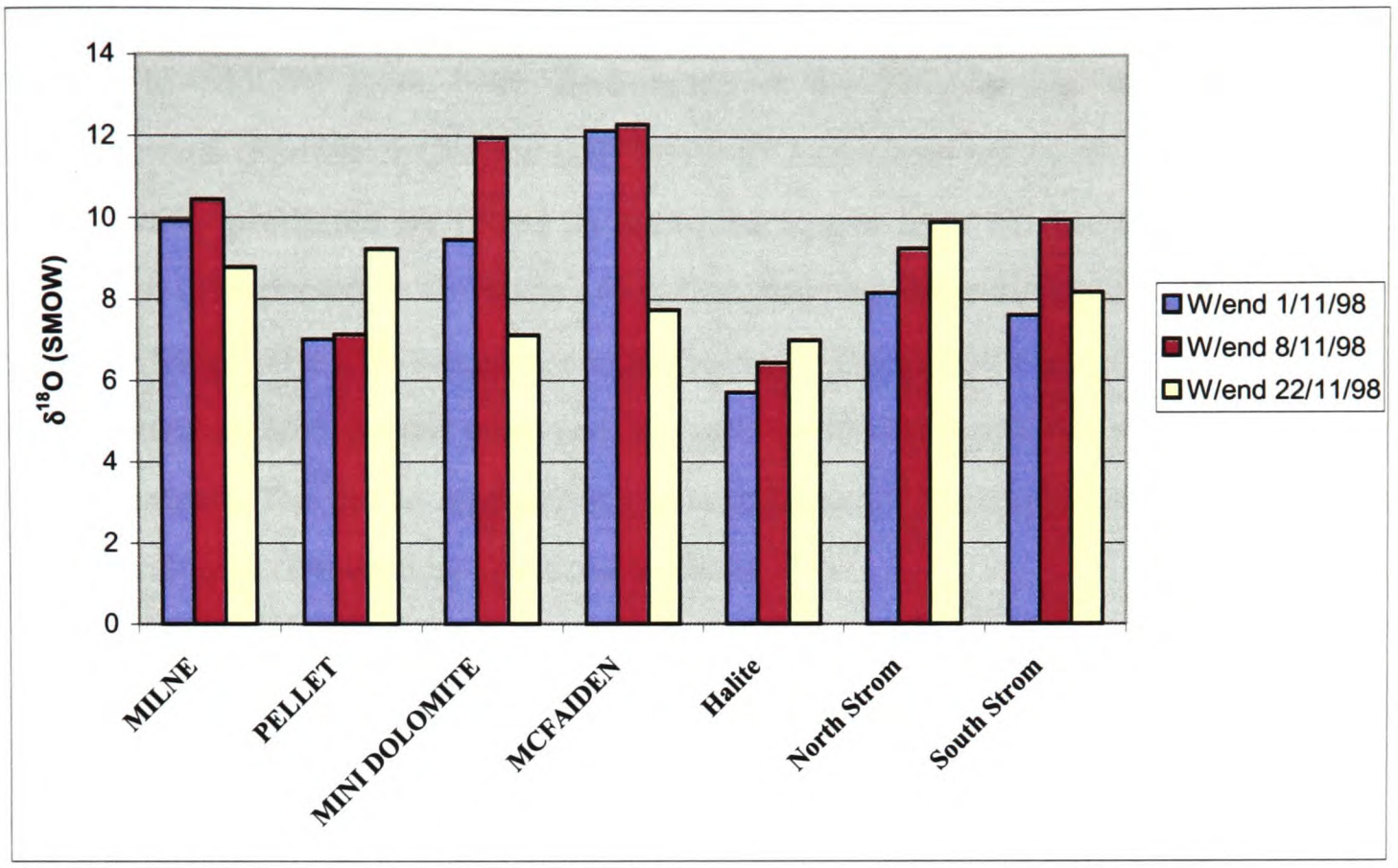


Figure 5.14. Graphical representation of data from Table 4.1.

A rather different situation is seen in water bodies of high salinity such as those in the Coorong. Laboratory experiments by Lloyd (1966) backed up by observations in natural settings, show that the heavy isotope content of the residual brine increases at first but then reverses, without a steady isotope composition being reached. For example brines in the Persian Gulf were shown to increase to $\delta^{18}O = +5‰$ at a salinity of 150‰ but then decrease slowly at higher salinities (Lloyd, 1966). Lloyd (1966) concluded that a maximum $\delta^{18}O$ enrichment of about 6‰ could be reached by the evaporation of coastal seawater brines and that further enrichment would be retarded by back exchange of atmospheric moisture with the evaporating fluid. Knauth & Beeunas (1986) summarize the $\delta^{18}O$ evolution of a residual seawater brine, extending its evolution to extreme 'halite facies' evaporation and beyond producing, (when plotted against hydrogen isotopes (δD)), a hooked trajectory (Figure 5.15).

As salinity increases there is an increase in the relative numbers of water molecules tied up in hydration spheres around cations. Isotopic exchange between these molecules, unbound water, water leaving the liquid-air interface and atmospheric water is believed to cause the hook (Holser, 1979; Knauth and Beeunas, 1986) with its exact shape depending upon climatic variables. Evaporating meteoric water will follow a path similar to that for sea water except that the starting point will be somewhere on the meteoric water line. Because

the concentrations of dissolved constituents are much less in meteoric water, evaporation may have to proceed to greater concentrations and greater ^{18}O enrichments before the hooked trajectory appears (Knauth & Beeunas, 1986). Thus, ^{18}O enrichments in excess of 30‰ relative to SMOW have been demonstrated for evaporating meteoric waters in arid environments (Fontes & Gonfiantini, 1967). $\delta^{18}O$ enrichments in all of these lakes are greater than the 6‰ predicted by Lloyd as being the upper limit for the evaporation of seawater. This is not unexpected as the lakes are fed not only by seawater but also by groundwater and meteoric water. The $\delta^{18}O$ values for Mini Dolomite Lake have been plotted on Figure 5.15 and I have fitted an interpreted evaporation curve to the lakewater even though no data for δD were obtained. The curve represents a best estimate of the evolution of the lakewater based on curve shapes obtained by previous authors.

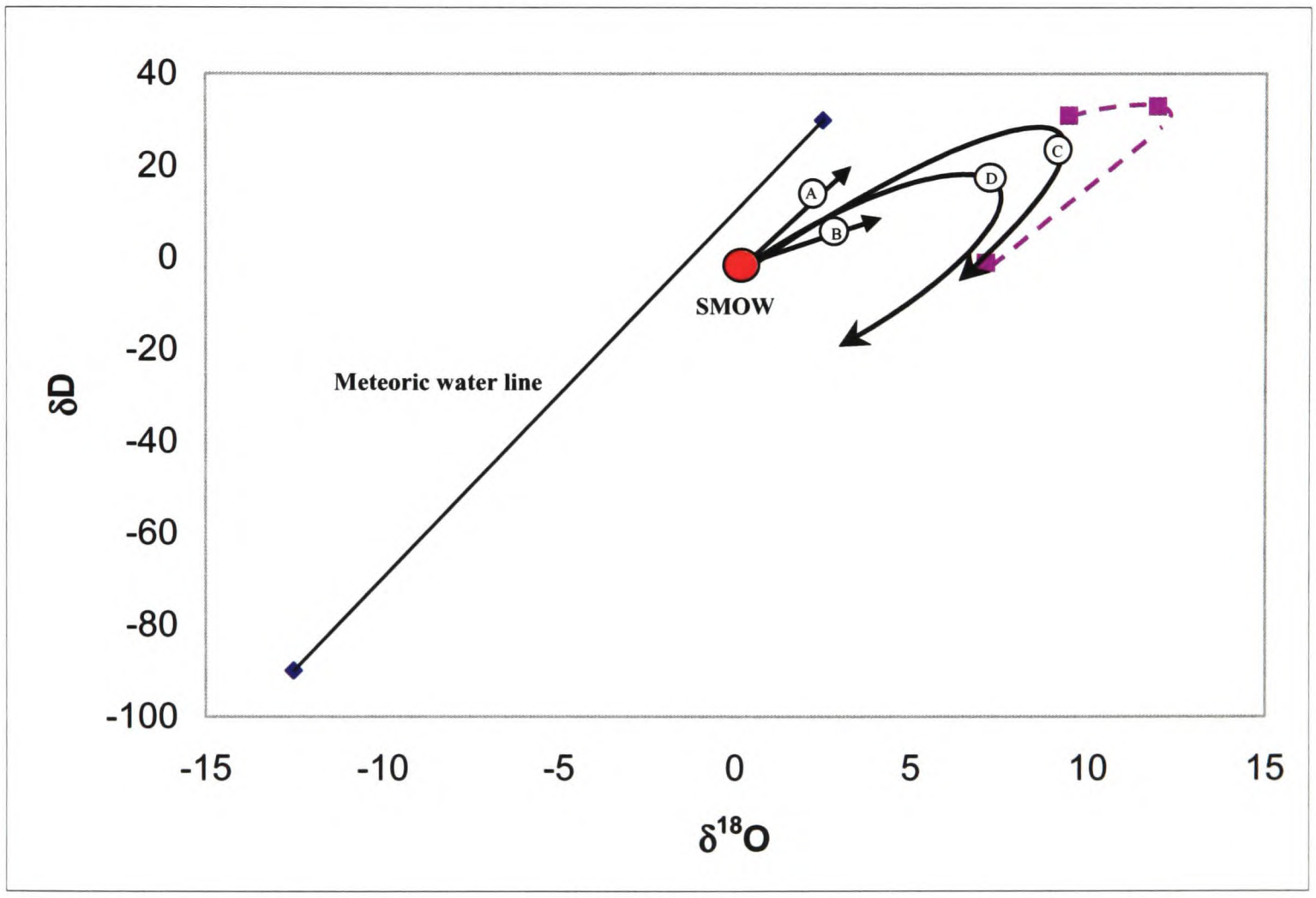


Figure 5.15. Paths taken by evaporating seawater. Curve A under humid conditions; curve B under arid conditions (Knauth & Beeunas, 1986). Curve C is Holser's estimate (Holser, 1979) for evaporating sweater to 10X concentration. Curve D is from Pierre *et al.* (1984). The dashed curve represents a best estimate (interpretation) of the evaporation path taken by water in Mini Dolomite Lake in the absence of δD data.

Observations over a longer timescale together with δD data are necessary to constrain the evolution of the water more tightly. Even then, similar isotopic data can be obtained from both evaporating marine and meteoric waters and so chemical data combined with isotopic data is necessary to fully understand the source and evolution of brines. From the data available at present one is able to conclude that each lake has its own individual evaporation cycle, resulting in different maximum enrichments in ^{18}O at slightly different times of the year. A further factor that could result in the $\delta^{18}O$ of the lakewater decreasing is mineral precipitation. This is dealt with in the following section, where the dynamically changing $\delta^{18}O$ of the lakewater may be used to constrain where and when the carbonate minerals precipitate.

5.3.5. Mineral-water interactions

A mineral-water interaction is a further possible solution to the drop in $\delta^{18}O$ values in the four lakes that are closest to the end of their evaporative cycles. As the lakes desiccate, minerals will precipitate; each mineral has an isotopic fractionation factor governing the way isotopes in the formation water will behave during precipitation. Water-mineral interactions result in the shift of $\delta^{18}O$ values of the mineral and the water away from their initial values. If the oxygen reservoir in the water is much greater than that in the mineral/rock, the mineral/rock values will be shifted but the water values will remain essentially constant, e.g. seawater values remain constant when calcite precipitates because the seawater oxygen reservoir is so large. The converse situation may occur when the water reservoir is relatively small – is this the case in the Coorong lakes?

Carbonate mineral phases in these four lakes, as observed by X-ray diffraction (Appendix 1) are dominantly dolomite (or poorly ordered dolomite) and aragonite; the mineral-water oxygen isotope fractionation equations for these are as follows.

$$1000\ln\alpha \text{ (dolomite-water)} = 3.20 \times 10^{6}T^{-2} - 1.50 \quad \text{(Friedman \& O'Neil, 1977 after Northrop \& Clayton, 1966)} \quad (5.5)$$

$$1000\ln\alpha \text{ ('proto-dolomite'-water)} = 2.78 \times 10^{6}T^{-2} + 0.11 \quad \text{(Fritz \& Smith, 1970)} \quad (5.6)$$

$$1000\ln\alpha \text{ (aragonite-water)} = 18.45 \times 10^{3}T^{-1} - 32.54 \qquad \text{(Bohm } et\ al.\text{, 2000)} \qquad (5.7)$$

This gives enrichment in the mineral phase of ^{18}O with respect to the formation water, when in equilibrium at 25°C with that water, as follows.

Dolomite = 35‰
'Proto-dolomite' = 31.4‰
Aragonite = 29.4‰

It can be seen that such large isotope fractionations in favour of the heavy isotope entering the mineral might easily account for associated decreases in $\delta^{18}O$ observed in the residual pools of water in the lakes.

Temperature of precipitation – equilibrium or dis-equilibrium?

As temperature increases, the fractionation factor between mineral and formation water decreases. Increased energy in the system results in bonds being broken and formed more easily and thus the isotopic mass difference is less critical. This temperature effect can be used to deduce the temperature at which a given mineral precipitated, so long as the mineral precipitated in equilibrium with that water. In the case of the Coorong lakes, data have already been presented on the $\delta^{18}O$ of both the sediment and of the water at a particular time in the evaporative cycle of the lakes. The average ambient temperature of the lakes is also known (20-30°C), so using the Equations 5.5-5.7 it is possible to deduce whether the sediment precipitated in equilibrium with those particular waters. Figures 5.16a-c plot fluid $\delta^{18}O$ versus temperature and are contoured in units of $\delta^{18}O$-sediment for dolomite, 'proto-dolomite' and aragonite respectively.

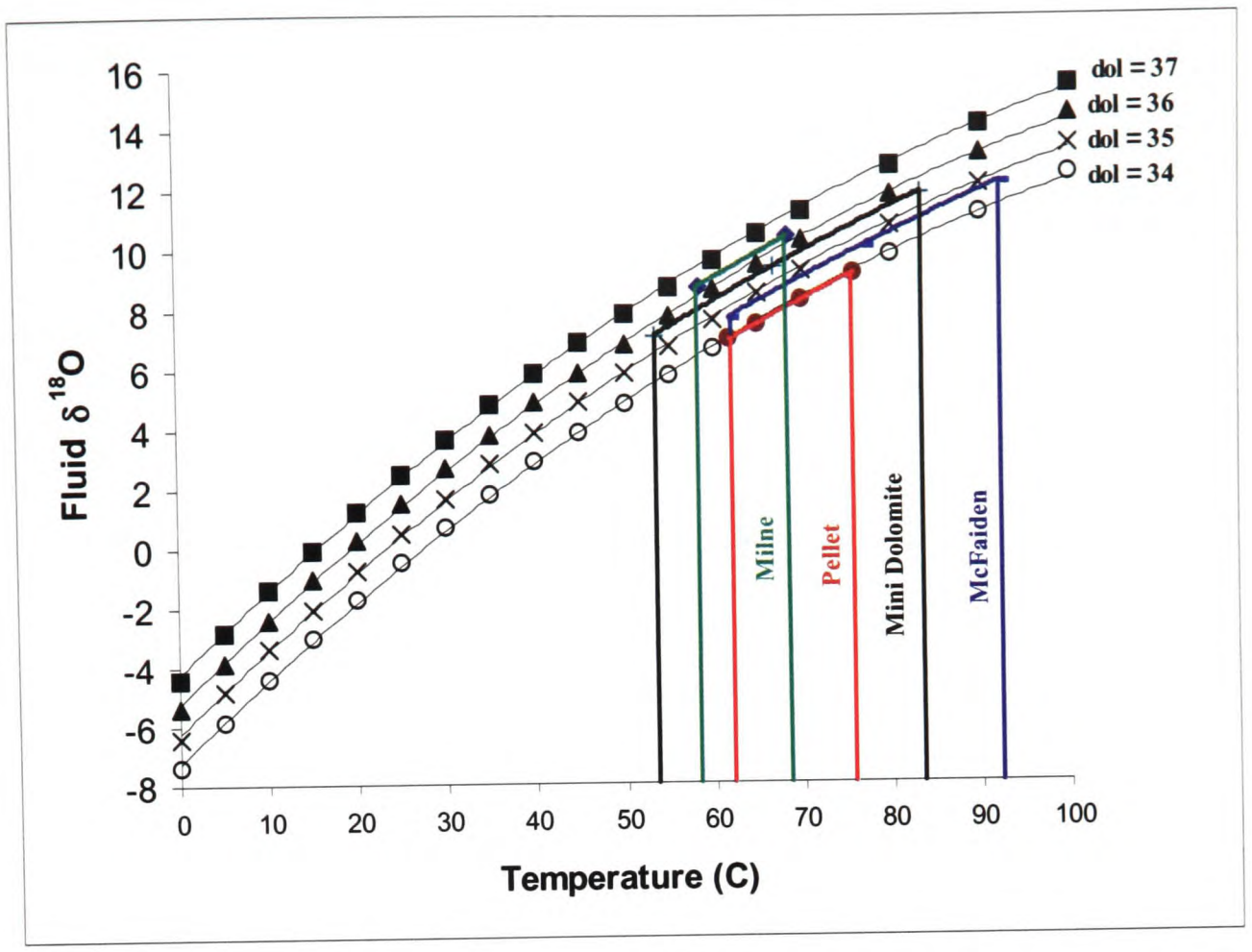


Figure 5.16a. Plot of temperature versus $\delta^{18}O$ (SMOW) fluid contoured for dolomite.

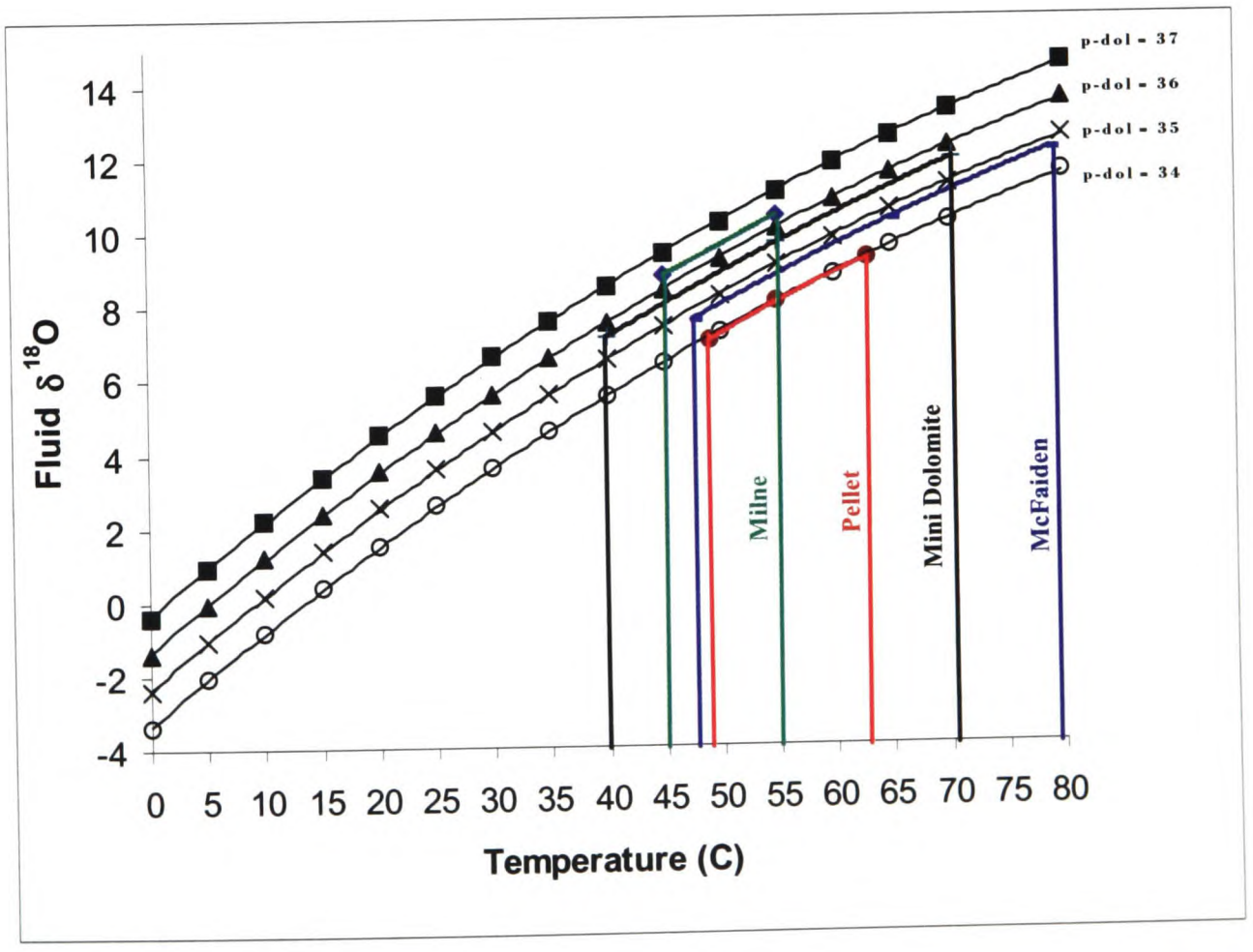


Figure 5.16b. Plot of temperature versus $\delta^{18}O$ (SMOW) fluid contoured for proto-dolomite.

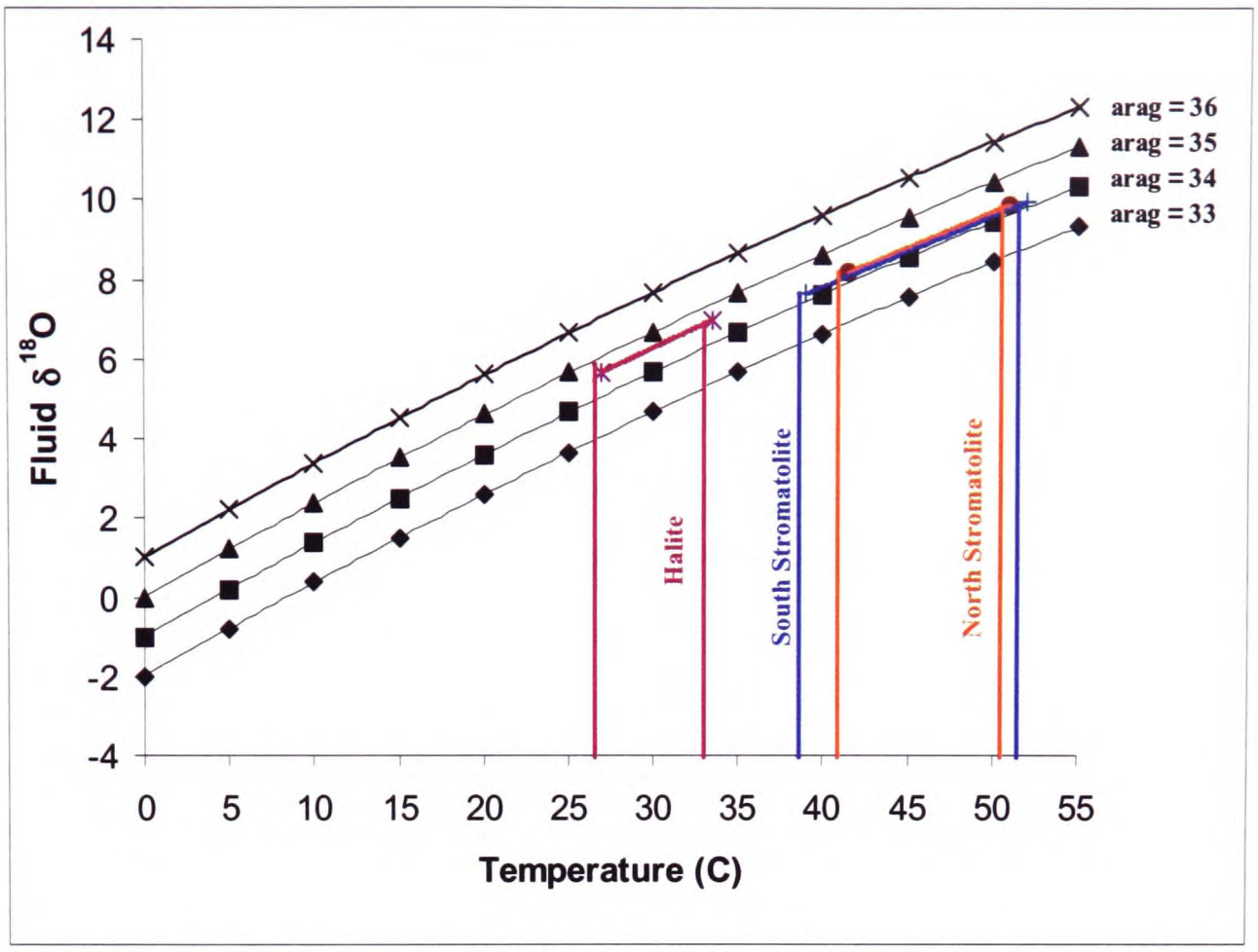


Figure 5.16c. Plot of temperature versus fluid $\delta^{18}O$ (SMOW) contoured for aragonite.

An explanation of the plots is necessary and for this purpose Halite Lake is taken as an example. The surface aragonite sediment in Halite Lake has a known $\delta^{18}O$ value of 34.62‰ (this study), drawn as a contour on the diagram. The measured fluid $\delta^{18}O$ values were between 5.7 and 7‰ (this study) which, given the 34.62‰ contour line, must correspond to a temperature of formation of between about 27°C and 33°C. All the other lakes are plotted in exactly the same way and the range of temperatures at which the minerals precipitated, if in equilibrium with the formation waters, are enclosed by the solid vertical lines. This data is useful and may be used to answer two questions posed earlier.

1) Is mineral precipitation responsible for the lowering of $\delta^{18}O$ of the fluid?
2) Were the precipitates formed in equilibrium with the November lakewaters?

1) Mineral precipitation does not appear to be the mechanism by which the $\delta^{18}O$ of the fluid is lowered. If this was so, the minerals would have a much heavier $\delta^{18}O$, reflecting precipitation from a brine with $\delta^{18}O$ = 10 to 12‰. Instead it appears that the drop in $\delta^{18}O$-lakewater in the four driest lakes is indeed due to the 'hook effect' from intense evaporation described in the previous section.

2) Given the fluid and sediment data for each lake, it can be seen that lakewater temperatures in excess of those actually encountered would be needed to satisfy the oxygen isotope fractionation equation for the minerals observed. For dolomite to have precipitated in equilibrium with these waters, temperatures ranging from 53-92°C would be necessary. More realistically the dolomite precipitates as poorly ordered dolomite but even then temperatures of 39-79°C would be required. Aragonite in Halite Lake would require temperatures of 27-33°C whilst in North and South Stromatolite Lakes temperatures of 39-52°C would indicate equilibrium precipitation. Only in Halite Lake were temperatures actually observed which correlate with these theoretical equilibrium precipitation values.

For poorly ordered dolomite to have precipitated at a realistic temperature (15-35°C), waters with $\delta^{18}O$ between about 0.5 and 6‰ would be required. Hence, either the dolomite precipitates at some shallow depth in the sediment in equilibrium with porewaters which have not experienced such intense evaporation and therefore have significantly lower $\delta^{18}O$ values, or they precipitate from lakewaters at some other time in the evaporitic cycle of the lakes. The time of precipitation cannot be earlier in the evaporitic cycle because SRB do not flourish at this time but may be a little later in the cycle where the interpreted 'hook effect' lowers $\delta^{18}O$ significantly. Unfortunately $\delta^{18}O$ values were not obtained for the porewater, mainly due to difficulties in extraction. However, if these values do prove to be slightly lower than in the lakewater, this (coupled with an increase in temperature) would suggest that dolomite precipitates at a few centimetres depth in the lakes. More data are required before a firm conclusion can be drawn. These data potentially provide a test by which the position and timing of precipitation can be deduced (as long as the mineral has precipitated in equilibrium with the water).

5.4. CARBON ISOTOPES

Stable carbon isotopes were used in this study to further investigate microbial activity and to attempt to constrain the source of the carbon in the carbonate sediments of the Coorong region.

Carbon has two stable isotopes:

$^{12}C = 98.89\%$

$^{13}C = 1.11\%$

The ratio of ^{13}C to ^{12}C is used in carbon isotopic studies and is calculated as follows:

$$\delta^{13}C\ ‰ = \left[\frac{(^{13}C/^{12}C)_{sample} - (^{13}C/^{12}C)_{standard}}{(^{13}C/^{12}C)_{standard}} \right] \times 1000$$

The standard used (V-PDB) is CO_2 gas obtained by reacting Peedee belemnites with 100% phosphoric acid. This standard is used because its ^{13}C and ^{18}O values are close to that of average marine limestone (Rollinson, 1993).

5.4.1. Distribution of Carbon Isotopes

Carbon can exist in oxidized, native and reduced forms in modern sedimentary environments and its isotopic composition can vary depending on temperature, pH, oxygen fugacity, concentration of carbon bearing species in the system and, most importantly, the mechanism by which the carbon isotopes have been fractionated. Two main present day carbon reservoirs exist:

i) Organic carbon;
ii) Inorganic carbon species and sedimentary carbonates.

These are isotopically quite distinct from one another since kinetic effects determine the $\delta^{13}C$ values of the organic carbon reservoir whilst equilibrium fractionations control the $\delta^{13}C$ composition of the inorganic carbonate reservoir.

i) Organic carbon

During photosynthesis, isotopic fractionation is controlled by a kinetic effect. Fixing of inorganic carbon from the atmosphere during photosynthesis may be represented by the following reaction:

$$6CO_2 + 6H_2O \longrightarrow C_6H_{12}O_6 + 6O_2$$

Reaction kinetics dictates that reaction of $^{12}CO_2$ proceeds faster then reaction of $^{13}CO_2$, hence the enrichment of biologically produced organic matter in ^{12}C and the depletion of residual CO_2 in ^{12}C relative to atmospheric carbon dioxide ($\delta^{13}C$ ~ –7.0‰, Faure, 1977). The exact nature of fractionation depends on reaction rate, temperature and nature of the vegetation involved and, while largely beyond the scope of this study, reviews can be found in Deines (1980) and O'Leary (1981). For the purpose of this study, it will suffice to point out that Recent plant matter has $\delta^{13}C$ values ranging from –5 to -35‰, with organic matter in Recent sediments closely mirroring these values at –10 to -30‰ (Eckelman *et al.*, 1962). In addition to this, very low $\delta^{13}C$ values (–50 to –110‰) are characteristic of the modification of organic matter by methanogenic bacteria. Microbial degradation of organic matter by SRB releases the light carbon stored in organic matter. Hence, carbonates that formed in a sulphate-reducing environment often have strongly negative $\delta^{13}C$ values. For example, carbon isotope minima in the interstitial water and sediments of deep-sea cores are often attributed to the activity of SRB, with typical values of ~ -20‰ (e.g. Böttcher *et al.*, 1999). It is worth noting, however, that the $\delta^{13}C$ signal attributable to SRB depends largely on the $\delta^{13}C$ value of the organic matter being metabolised. It is also worth noting that the isotopically heaviest biomass encountered on earth has been furnished by benthic cyanobacterial communities from two hypersaline lagoons (Solar Lake and Gavish Sabkha), whose $\delta^{13}C$ signals are as high as –3.5‰ (Shidlowski *et al.*, 1985). A similar community can be envisaged living in the Coorong hypersaline lakes and so only a relatively small negative $\delta^{13}C$ signal may be expected in the sediments of these lakes. Further assessment of the isotopic composition of the local cyanobacterial community is recommended to test for this possibility.

ii) Inorganic carbonate

The isotopic composition of carbonates precipitated from aqueous solutions is controlled largely by equilibrium isotope exchange between CO_2 gas, carbonate and bicarbonate ions in solution and the solid carbonate. This, in turn, is controlled by the temperature of equilibration, the pH (controlling the abundance of bicarbonate and carbonate ions in the system) and, of course, the initial $\delta^{13}C$ value of the CO_2 gas. Fractionation factors between each of the carbon containing species are outlined below at the average ambient temperature of the Coorong lakes (25°C).

$CO_{2\,(g)} \Leftrightarrow CO_{2\,(aq)}$	1.00106	(Vogel *et al.*, 1970)
$HCO^-_{3\,(aq)} \Leftrightarrow CO_{2\,(aq}$	1.00901	(Mook *et al.*, 1974)
$CO^{2-}_{3\,(aq)} \Leftrightarrow CO_{2\,(aq}$	1.00759	(Ohmoto & Rye, 1979)
Calcite $\Leftrightarrow CO_2$	1.00983	(Deines *et al.*, 1974)
	1.01022	(Ohmoto & Rye, 1979)
Calcite $\Leftrightarrow HCO^-_{3\,(aq)}$	1.00197	(Deines *et al.*, 1974)
$CO^{2-}_{3\,(aq)} \Leftrightarrow HCO^-_{3\,(aq)}$	1.00039	(Mook *et al.*, 1974)
Dolomite – Calcite	1.0022 – 1.0026	(Sheppard & Schwarcz, 1970 extrapolated from high temperatures)

It can be seen that through isotopic equilibration, aqueous carbonate species tend to be enriched in ^{13}C by around 7-10‰ with respect to atmospheric CO_2 (Emrich *et al.*, 1970; Deines *et al.*, 1974)(Fig. 5.17). Fractionation between aqueous species and solid calcite is small (<2‰), whilst ordered dolomite precipitating under equilibrium conditions should be around 2.4‰ heavier in $\delta^{13}C$ than in coexisting calcite. Reaction rates can affect the carbon isotopic composition of carbonates whereby rapidly precipitating crystals sequester the component of interest (CO_3^{2-}) from solution so quickly that equilibrium processes, limited by the slowest reaction step, cannot prevail. Rapidly precipitated carbonates may therefore inherit a kinetic effect and carry a lighter $\delta^{13}C$ signal relative to a pure equilibrium precipitate (Turner, 1982; Michaelis *et al.*, 1985).

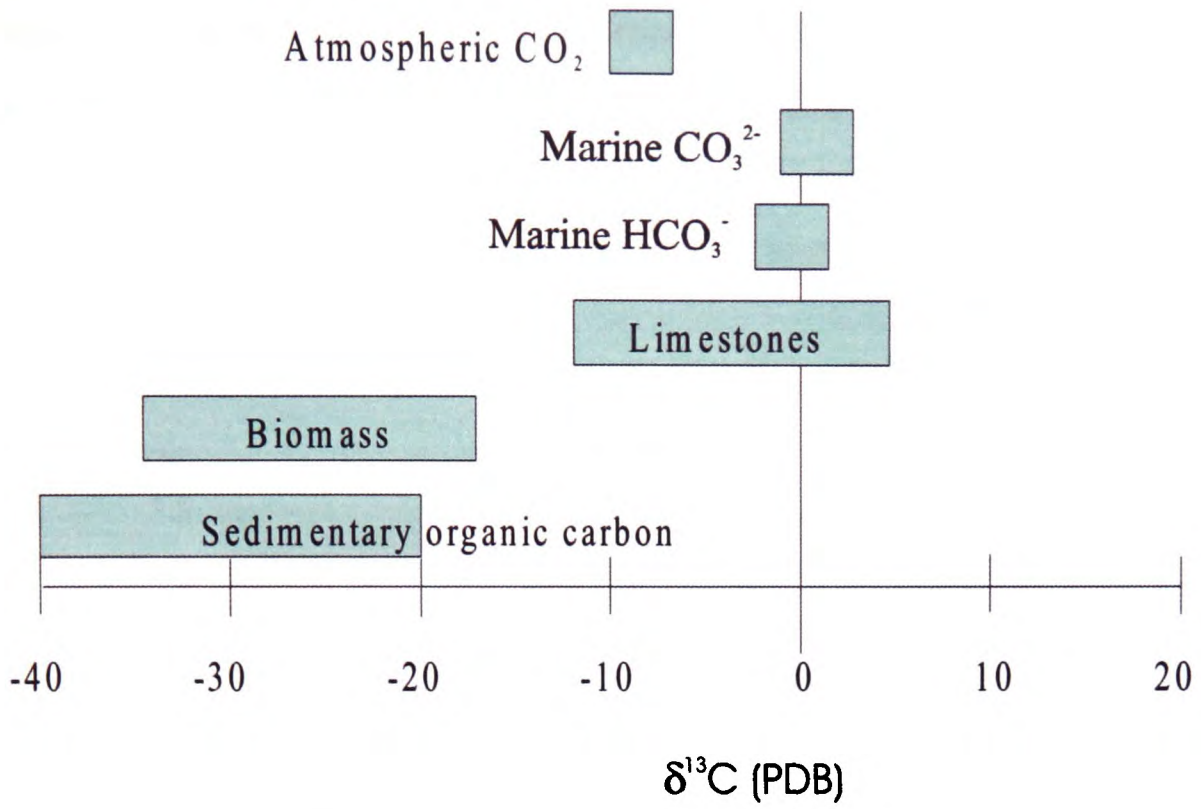


Figure 5.17. Natural isotope reservoirs of carbon (adapted from Rollinson, 1993).

5.4.2. Results

Carbon isotope analyses of the carbonate sediments were performed on the same apparatus as for oxygen and a detailed methodology can be found in Appendix 5. The internal Mab2b standard was again used whose accepted value is +2.480‰ PDB and reproducibility was ±0.08‰. The full set of results also appear in Appendix 5, along with a table of isotopic data obtained by two previous authors for the Coorong lakes.

The carbon isotope data are represented graphically in Figure 5.18 (plotted against $\delta^{18}O$ values). $\delta^{13}C$ values range from –1.19 up to +3.22‰ for the dolomitic lakes, whereas the non-dolomitic lakes have a more closely spaced $\delta^{13}C$ range from +1.12 to +3.07‰. These values fall into the field of normal marine or freshwater carbonate sediments (Fig. 5.16).

In order to extract as much information as possible from the carbon isotope data, graphical plots of $\delta^{13}C$ versus several other parameters were constructed. Plots of $\delta^{13}C$ versus dolomite ordering, versus total organic carbon (TOC) and versus $\delta^{18}O$ (where a relationship between the variables might be expected) were constructed (Figs 5.19a-c) and these will be discussed in the next section. Plots of $\delta^{13}C$ versus other parameters such as pH, sulphate ion concentration and carbonate ion concentration were attempted but were not informative

since these parameters vary widely, both from week to week and with depth, mirroring the dynamic nature of each of the lakes. The $\delta^{13}C$ of the sediment is a single measurement reflecting the lake conditions at the particular time of precipitation and so correlations with such dynamically changing parameters need not be expected.

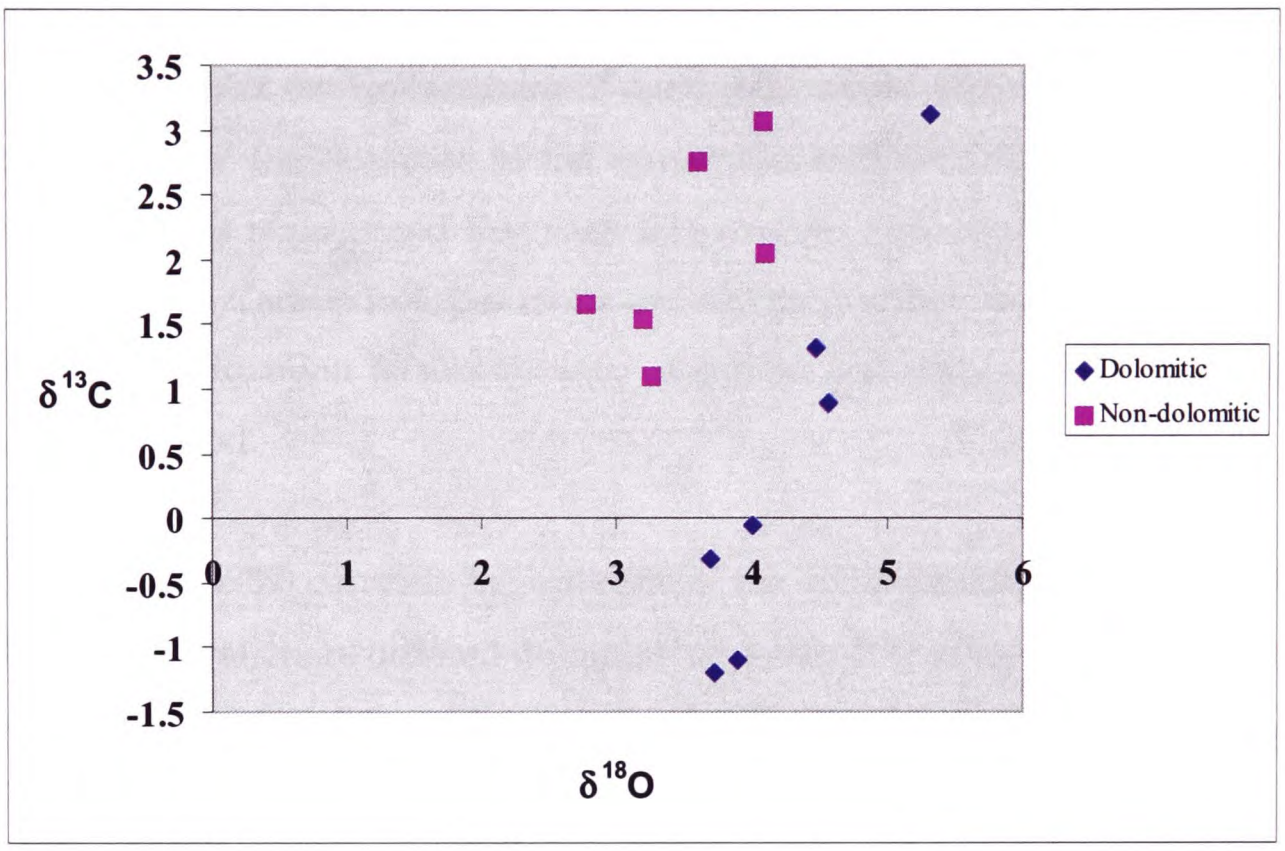


Figure 5.18. Carbon isotope values of carbonates from the Coorong ephemeral lakes. Note use of PDB scale in this figure.

5.4.3. Discussion

Previous studies of the Coorong lakes (Botz & Von der Borch, 1984; Rosen *et al.*, 1989) found similar patterns in the carbon isotope data to those presented here. They found that McFaiden and Dolomite Lake possessed largely negative $\delta^{13}C$ values, whilst the remaining dolomitic lakes were positive, with values ranging up to 4.1‰. These data were interpreted as representing two different types of dolomite. Botz & Von der Borch (1984) interpreted the isotopically light dolomite as forming from evaporitically modified continental groundwater, whereas the isotopically heavy dolomite was interpreted as forming in equilibrium with atmospheric CO_2 by the dolomitization of aragonite. Botz & Von der Borch (1984) based this latter assumption upon the close correlation of $\delta^{13}C$ values for aragonite and dolomite, suggesting one was a precursor to the other. Similar data from Solar Lake (Aharon *et al.*,

1977) appeared to reinforce this view. However, on further examination the two apparently similar data sets can be seen to tell different stories. In Solar Lake, aragonite is found co-existing with calcite and shows dissolution textures and so a replacement origin may be supported. In this study, however, it has been shown that the isotopically heavy dolomite is identical in morphology to the light dolomite and aragonite does not co-exist in any of the dolomite precipitating lakes. The lack of co-existing aragonite and dolomite in any one lake rules out the possibility of equilibrium co-precipitation and the lack of dissolution textures in the aragonite also rules out replacement of one by the other. There is abundant evidence in this study that all of the dolomite in the uppermost sediments is likely to be of primary origin. In addition, it is proposed that each lake evolves individually, with its own unique mineral assemblage. Carbon isotopes alone are unable to either support or refute this, since carbon isotope fractionation factors between dolomite and other carbon containing species are poorly understood.

Rosen *et al.* (1989) correlate the ordering of the dolomite with its isotopic composition stating that, in general, more ordered dolomite has lower $\delta^{13}C$ values, presumably suggesting that an increase in ordering accompanies recrystallisation in the presence of ^{12}C rich porewater. This conclusion is not supported by this study, which finds no significant correlation (Fig 5.19a).

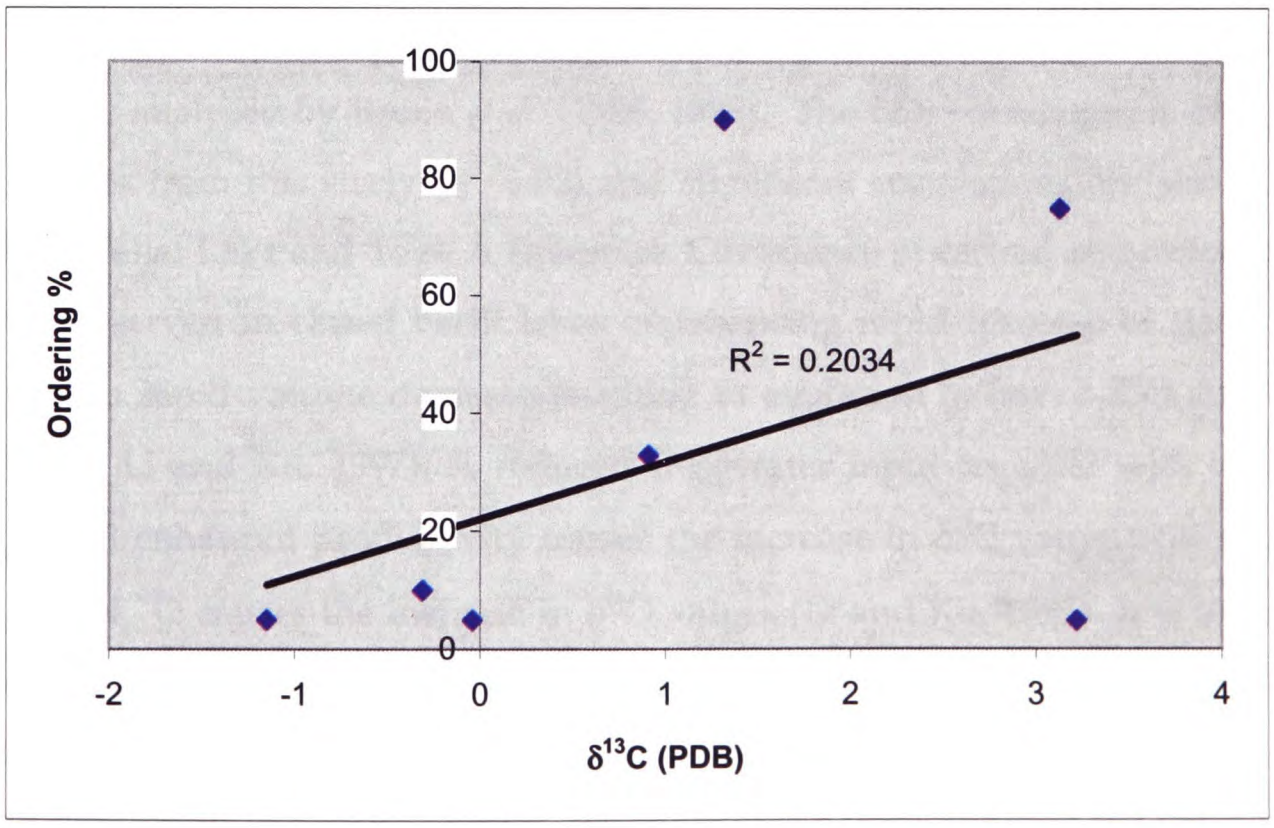


Figure 5.19a. Relationship between $\delta^{13}C$ and the extent of ordering of the dolomite.

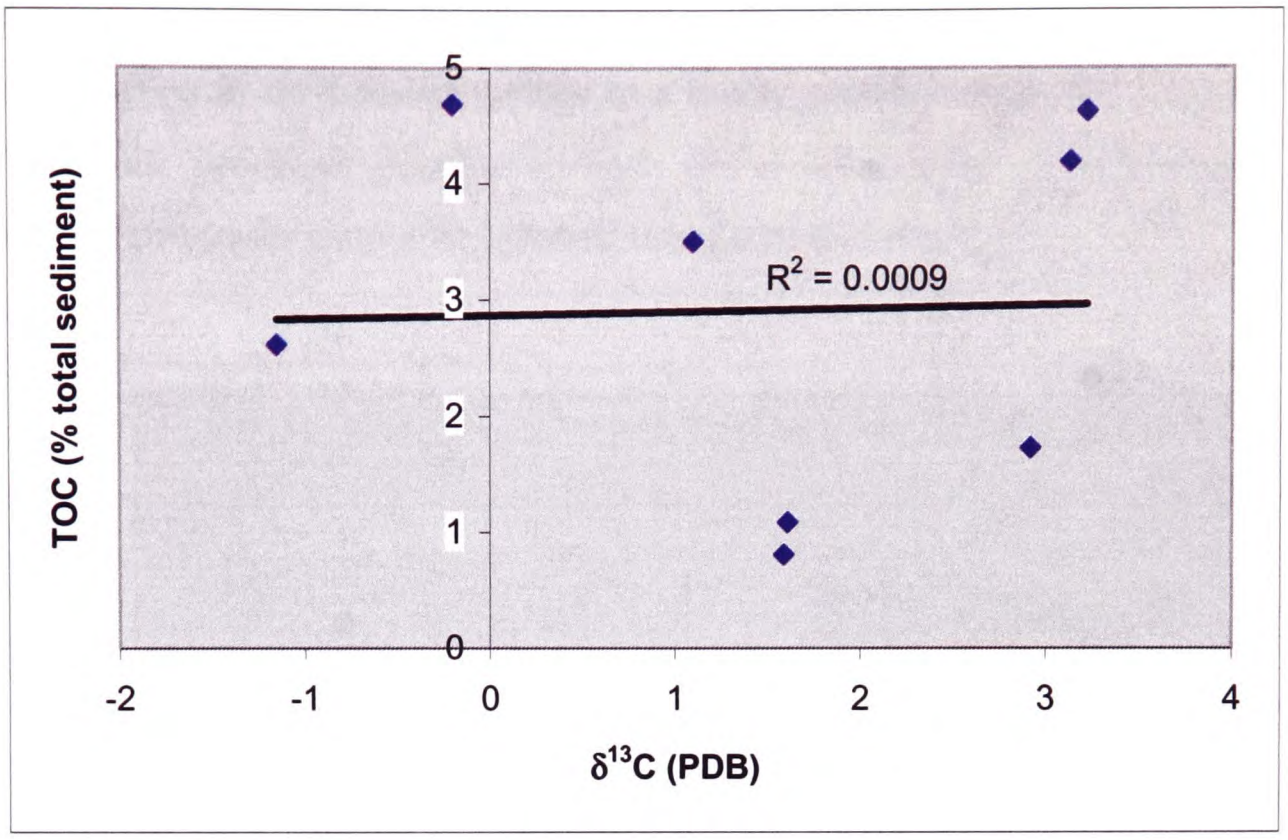


Figure 5.19b. Relationship between $\delta^{13}C$ and amount of total organic carbon (TOC) in each of the study lakes.

Figure 5.19b shows the relationship between $\delta^{13}C$ and TOC. A negative correlation may have been expected between these variables, as a plentiful supply of organic carbon for bacteria to oxidize would result in a larger contribution from the organic carbon reservoir to the carbonate $\delta^{13}C$ signal. Once again, this preconception is not supported by the data. Figure 5.20 shows the correlation between $\delta^{13}C$ and $\delta^{18}O$ analysed from the carbonates in this study and also those analysed by Rosen *et al.* (1988, 1989). The best correlation is observed in the dolomitic lakes from this study (R^2=0.92) and significant correlations are also observed for Rosen *et al's* Pellet Lake and Type A Dolomite. Covariance of carbon and oxygen isotopes is commonly observed in closed basin lakes experiencing rapid increase or decrease in lake volume with a rapid volume decrease resulting in evolution to heavy $\delta^{18}O$ and $\delta^{13}C$ values (Talbot, 1990; Li and Ku, 1997). A reduced freshwater input together with increased CO_2 degassing and enhanced productivity causes the increase in $\delta^{13}C$ values whilst preferential evaporation of ^{16}O causes the increase in $\delta^{18}O$ values (Li and Ku, 1997). It is interesting that the dolomitic lakes in this study span a different range of values to those found by Rosen *et al.* (1988, 1989). Once again this emphasizes the dynamic nature of these lakes, suggesting that small differences in sample locality, depth and time (lake volume) can have a significant effect on the data. The dolomitic and non-dolomitic lakes from this study occupy distinctly different areas of the $\delta^{13}C$ - $\delta^{18}O$ cross plot, suggesting that the two sets of lakes have

inherently different chemistries. The variation in isotopic signal cannot be explained by equilibrium precipitation from similar formation waters because, in that case, the dolomite should be enriched in the heavier isotope to a much greater extent ($\delta^{13}C \sim 2‰$, $\delta^{18}O \sim 6‰$). Instead, dynamic processes peculiar to each set of lakes must be responsible. The exact nature of these processes cannot be inferred using a plot of this type.

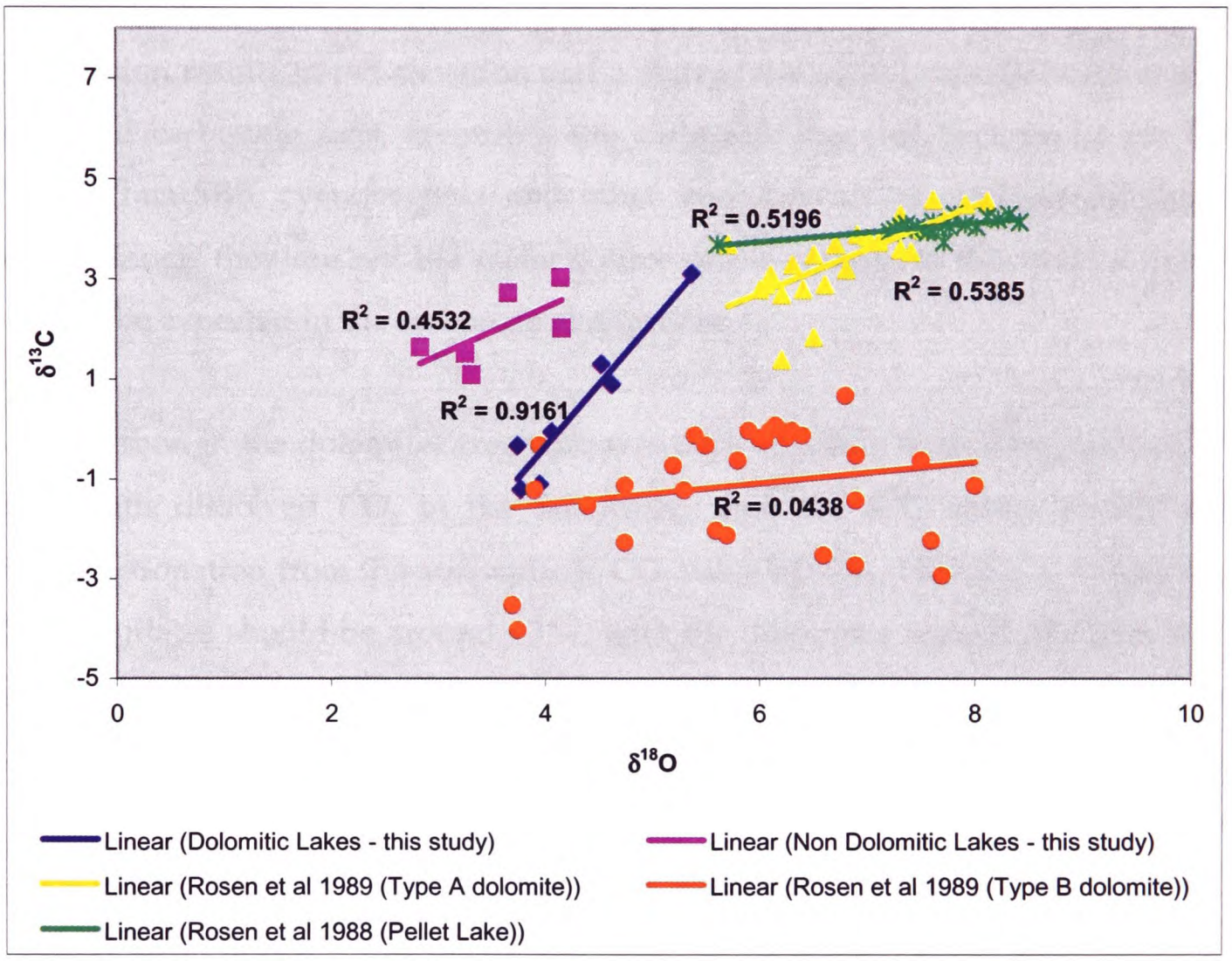


Figure 5.20. Plot of $\delta^{13}C$ versus $\delta^{18}O$ for the carbonates in this study and also for those in two studies by Rosen *et al*. Note use of PDB scale in this diagram.

In general, carbonates with strongly negative $\delta^{13}C$ values are interpreted as resulting from the incorporation of carbon arising from the oxidation of ^{12}C-enriched organic matter. It might therefore be expected that carbonates from the Coorong lakes would yield a light signature since it is postulated that carbonate precipitation in these lakes is associated with microbial degradation. Only two of the lakes exhibit a light signature (McFaiden Lake and Dolomite Lake (Fig. 5.18)) and even here the values are much heavier than expected for organically derived carbon. Since these carbonates do not have the expected negative signature, previous authors have rejected the possibility that an organogenic dolomite model might still be applicable (e.g. Botz & Von der Borch, 1984; Rosen *et al.*, 1988). However, the situation in these lakes is not so straightforward. Carbon isotopes alone are not a sufficient

tool for determining the role of organic matter in dolomitization (Hill, 1990), nor indeed for tracking other microbially-driven carbonate precipitation. While strongly negative $\delta^{13}C$ values may suggest the incorporation of carbon from oxidized organic matter, slightly negative to slightly positive values, such as those found here, do not rule out a role for bacterial processes. Geochemical modeling indicates that the carbonate ions being incorporated into these carbonates can originate from inorganic bicarbonate already present in the lakewater whilst their availability is still controlled by bacterial processes. Bacterial sulphate-reduction results in pH elevation and a shift of the equilibrium between inorganic bicarbonate and carbonate ions, favouring the carbonate ion (see Section 4.4 for theory behind this). Thus SRB, cyanobacteria and other microbes act as catalysts for dolomite precipitation though they are not the major source of the carbon. In this way, a light $\delta^{13}C$ value need not be expected in the carbonate precipitates.

If the carbon in the dolomite/aragonite was derived solely from inorganic species in equilibrium with dissolved CO_2 in the lakewater, then the $\delta^{13}C$ values should reflect equilibrium fractionation from the atmospheric CO_2 value of -7‰. Hence $\delta^{13}C$ values for the aragonite precipitates should be around +3‰, with the dolomites around 2‰ heavier. It is clear that the majority of lakes are not precipitating carbonate in equilibrium with atmospheric CO_2 and that some input from isotopically light carbon, especially in McFaiden and Dolomite lakes, is involved. It is concluded that the carbon isotope signature is unique to each lake, resulting from precipitation of carbonate minerals at different times in the annual evaporative cycle of each lake, allowing varying amounts of mixing of heavy carbon from the inorganic reservoir and light carbon from the organic reservoir.

5.5. SUMMARY OF ISOTOPIC DATA

- A single isotopic system is not sufficient to constrain the genesis of the carbonate minerals in the Coorong ephemeral lakes. Even a combined approach using three stable isotope systems can lead to equivocal interpretation of the data.
- Sulphur isotopes in residual lakewater sulphate exhibit a heavy signal, modified from that of the seawater source by between 2 and 8‰.
- Each lake appears to act as a separate system with respect to sulphate $\delta^{34}S$, each having a unique and tightly spaced range of values.

- There is minimal variation of $\delta^{34}S$ over the 4-6 week sampling period and this steady state is emphasized by the reproducibility of the data from one year to the next.
- The expected pattern of an increase in $\delta^{34}S$ with depth, as sulphate is consumed, is not marked, nor is there any correlation between $\delta^{34}S$ and the number of SRB.
- This rather complex pattern may be explained by a combination between open system behaviour, high initial sulphate concentrations, species specific physiological pathways and bacterial transformations of other sulphur containing species.
- A correlation between $\delta^{34}S$ and $\delta^{18}O$ in the sulphate is clearly observed in the dolomitic lakes. No such correlation is observed in the non-dolomitic lakes. This suggests that the process of bacterial sulphate reduction is better developed in the dolomitic lakes.
- The $\delta^{18}O$ of the lakewater sulphate is excessively heavy and does not reflect the seawater source. This data suggest that at least some of the sulphate is formed in the lakewater itself by re-oxidation of H_2S and other sulphur species, thus reinforcing the suggestion made by the $\delta^{34}S$ data that additional bacterial transformations of sulphur species are taking place in the sediment and lakewater.
- A 'hook effect' during the evolution of the brines has been interpreted for the lakewater $\delta^{18}O$ data due to increased water molecule complexing around cations at high salinity.
- Combined analysis of the $\delta^{18}O$ signal of the lakewater and of the carbonates themselves show that the carbonates in all but one of the lakes are not precipitating in equilibrium with the November lakewaters. In combination with other data, precipitation may be shown to occur at some shallow depth below the sediment water interface or at a different time in the evaporative cycle.
- The carbon isotope signal is not derived directly from organic matter oxidised by the SRB; the carbonates fall within the normal marine range. The dolomitic lakes have a wider $\delta^{13}C$ range but the data do not lend further support to the suggestion made by previous authors that two different types of dolomite are present in the uppermost sediments. Dolomitization of precursor aragonite is not supported by these or by sedimentological data obtained in this study. The $\delta^{13}C$ signal can be explained if the carbon was derived mostly from bicarbonate in the inorganic pool as a result of microbial mediation of ambient waters. Some contribution from the organic carbon pool is, however, suspected in all the lakes, and especially in McFaiden Lake and Dolomite Lake which show negative $\delta^{13}C$ signals. More rapid precipitation in these lakes, preventing the establishment of equilibrium, could provide an additional explanation for the lighter isotopic signal.

CHAPTER 6



Sand dunes separating the Coorong distal lakes from the main Coorong lagoon and the Southern Ocean.

Chapter 6

Bacterial enumeration, identification and precipitation experiments

6.1. INTRODUCTION

Combined geochemical and isotopic data from both laboratory and field work (Chapters 4 and 5), give convincing though indirect evidence for the presence of sulphate-reducing bacteria. The next logical step was to carry out experiments to physically prove that the sulphate reducers were present in the lake sediments. Once their presence was confirmed, it was necessary to discover their abundance and approximate proportion relative to the *total* bacterial population. Further experiments were then undertaken using natural populations of bacteria and replicated lakewaters in order to attempt to precipitate dolomite in the laboratory. Identification of bacteria from these natural populations was attempted using 16S rRNA sequencing.

6.2. SRB ENUMERATION

This was achieved by using two techniques outlined in the following sub-sections:

- The most probable number (MPN) statistical technique. (Hurley & Roscoe, 1983)

- The acridine orange direct counts (AODC) technique. (Kirchman *et al.*, 1982; Fry, 1988, 1990).

6.2.1. Collection and storage of SRB-containing sediment

Lake sediments to be used in culture experiments were collected from each study lake in 5ml open ended syringes. Each syringe was gently inserted (vertically) into the top of the sediment. At the same time, the plunger was gently pulled out. This method was employed to minimise any compaction of the sediment during collection. The sediment was then injected with a small amount of gluteraldehyde to stabilise the bacteria. The syringes were sealed with butyl rubber stoppers to exclude oxygen and then carefully labelled with lake name, depth and date. Within about an hour of collection they had been refrigerated at c. 3°C as further precaution against bacterial activity. The samples were brought back to the UK surrounded by gel ice packs to keep them refrigerated.

6.2.2. Culturing Method for SRB from Coorong Lakes

The sealed syringes were transferred to the laboratory of Dr. John Parkes and Dr. Barry Cragg at the Department of Geomicrobiology, University of Bristol, where a culturing technique for SRB is well established. The technique involves the following steps :

Step 1 – Create culture medium

The ingredients of the culture media were weighed out according to the following recipe for Postgate Media B (Postgate 1984), here modified to adapt to lake conditions:

KH_2PO_4	1.00 g
NH_4Cl	2.00 g
Sodium acetate (anhhyd.)	0.90 g
Sodium lactate (liquid)	1.76 g
Yeast extract	2.00 g
Ascorbic acid	0.20 g
$CaSO_4$	2.00 g

$FeSO_4.7H_2O$	1.00 g
$MgSO_4.7H_2O$	4.00 g
$MgCl_2.6H_2O$	11.00 g
NaCl	59.00 g
Resazurin (0.1 %)	2.00 ml
Water (anoxic)	~2000 ml

Note.

Acetate and lactate act as the substrate.

SO_4^{2-} ions act as the electron acceptors.

$MgCl_2$ and NaCl are added in the ratio 6:32 to adjust sample salinity.

NaOH is added to adjust the pH to that of the lakes (~ 8).

Resazurin is a dye added to indicate if any oxygen enters the vials.

The media is made up to 2 litres using anoxic water (obtained by constant bubbling with nitrogen).

Once these ingredients were added, the medium was autoclaved, to ensure that anaerobicity and sterility was maintained, and then placed in an anaerobic cabinet, where two further ingredients were added:-

$NaHCO_3$	5.04 g
Thioglycollic acid	0.20 g

Step 2 – Injection of culture media (all done in the anaerobic cabinet)

Thirteen empty 50ml vials were taken and injected, using thirteen sterile 50ml syringes, with 10ml of the culture medium. Thirteen vials were required because it was surmised that large amounts of SRB would be present in the sediment samples. A 1:5 dilution series (that is, 1ml of sediment to 5ml of medium), performed thirteen times, was estimated to be sufficient to account for the largest numbers of SRB ever previously found in 1ml of sediment (~10^6/ml, Bak & Pfennig 1991).

Following correct experimental practice (B. Cragg, pers. comm.), each of the thirteen dilution series was performed in triplicate, requiring thirty-nine 10ml vials. Into each of these, 5ml of culture medium was then injected. Hence, for each original sediment sample to be investigated, a total of thirteen large dilution vials and thirty nine smaller vials were required. All the vials were sealed with butyl rubber septa to prevent any gaseous diffusion into them, before being taken out of the anaerobic cabinet, crimped with aluminium tops and autoclaved at 121°C overnight.

Step 3 – Transference of sediment into Vial 1

All the vials were labelled with sample identification and dilution number. The first lake-sediment sample was removed from the refrigerator, where it had been kept at 3°C, and transferred to the anaerobic cabinet together with a sterile open-ended syringe, a sterile petri dish and large (50ml) dilution Vial 1.

The rubber bung was removed from the sample core, the syringe was inserted and 4 or 5ml of sample was withdrawn. The first millilitre of sample was extruded and wiped off with the side of the sterile petri dish; this was then injected into a vial containing formaldehyde, thus preserving it in readiness to perform the acridine orange direct counts technique at a later date (Section 6.3). The next 2.5ml of sample was the part required for the MPN analysis, since this was the depth at which geochemical data suggested most of the SRB's were concentrated. The first dilution vial was opened carefully by removing the crimp top and septum. The septum must be held between thumb and forefinger without touching the inside of it because it must remain sterile. The 2.5ml of sediment sample was extruded into the vial and the septum carefully replaced. Any other sediment left over was kept for XRD analysis at a later date. This procedure was repeated with the other sediment samples.

Step 4 – The multiple injection stage (carried out in a laminar flow cabinet.)

The first sample was taken and a dilution series was completed. This involved transferring 2.5ml from Vial 1 (i.e. the one made up in Step 3 that has all the sediment in it) to Vial 2. Hence one obtained 2.5ml from Vial 1 in a total of 12.5ml in Vial 2 - a 1:5 dilution. Vial 2 was

shaken to mix it and then 2.5ml was taken from it and injected into Vial 3. This step was repeated all the way down to Vial 13, each becoming more and more dilute with respect to the original sample. Correct experimental procedure (B. Cragg, pers. comm.) required that each injection be done with a new sterile syringe and needle tip. Each syringe was gassed with nitrogen several times before use and all the vial tops were dabbed with alcohol to maintain sterility.

This completed the dilution series. Next it was necessary to transfer material from each of the large (50ml) dilution vials to the small (10ml) vials in triplicate, which could then be incubated. The transfer was done in reverse (i.e. most dilute first); in this way one syringe could be used all the way through, but again a new needle tip was needed for each triplicate set.

Three millilitres was taken from large (50ml) dilution Vial 13 and 1ml was injected into each of the three 10ml '13^{th} dilution' vials. Again 1ml in 5 ml of media is a 1:5 dilution. This procedure was repeated all the way back to dilution Vial 1. During injection, a relief syringe was placed in each vial so that a little gas could escape; injection would otherwise have been impossible due to pressure effects. Finally, all the vials were injected for around 1 second with nitrogen to keep them under positive pressure. All the injections were done around the edges of the septa where they are thickest, to prevent putting a permanent hole in the septum and thereby making the vial oxic. The Resazurin indicator within the medium acted as an oxygen indicator, turning pink if oxygen is present. If this occurs, the vial must be discarded.

Step 5 - Incubation

All of the 10ml vials were then transferred to a thermostatically controlled cabinet which was set to the average temperature of the lakes in the Coorong, around 23°C, and incubated for up to two months, or until there was no obvious further growth. Vials with bacteria in them, ('positive vials'), turned black and showed an obvious growth ring owing to the precipitation of FeS_2.

6.2.3. Numbers of positive vials

The dilution series was performed to a factor of 1:5 thirteen times in all, resulting in total dilutions as shown in Table 6.1 below.

Dilution Level	Dilution Factor
1	0.2
2	0.04
3	0.008
4	0.0016
5	0.00032
6	0.000064
7	0.0000128
8	0.00000256
9	0.000000512
10	0.0000001024
11	0.0000000205
12	0.0000000041
13	0.0000000008

Table 6.1. Total dilution factors for each dilution level

The original inoculated volume of sediment was 1ml and incubation was at 25°C for a period of approximately one month. The results (i.e. how many of each set of triplicate dilution vials produced obvious growth) are shown in Table 6.2, for seven of the Coorong lakes; four dolomitic lakes (McFaiden, Mini Dolomite, Milne and Pellet) and the three non-dolomitic lakes (North Stromatolite, South Stromatolite and Halite).

		Dilution Series												
Source	**Date examined**	**1**	**2**	**3**	**4**	**5**	**6**	**7**	**8**	**9**	**10**	**11**	**12**	**13**
McF	18/02/99	3	3	3	3	3	2	0	0	0	0	0	0	0
	24/02/99	3	3	3	3	3	2	0	1	0	0	0	0	0
	03/03/99	3	3	3	3	3	3	2	2	2	0	0	0	0
	12/03/99	3	3	3	3	3	3	3	3	1	0	0	0	0
	26/03/99	3	3	3	3	3	3	3	3	2	0	0	0	0
Mini Dol	18/02/99	3	3	3	3	3	2	3	2	1	0	0	0	0
	24/02/99	3	3	3	3	3	3	3	3	1	1	0	0	0
	03/03/99	3	3	3	3	3	3	3	3	2	1	0	0	0
	12/03/99	3	3	3	3	3	3	3	3	2	1	0	0	0
	26/03/99	3	3	3	3	3	3	3	3	2	2	0	0	0
Milne	18/02/99	3	3	3	3	0	3	0	0	0	0	0	0	0
	24/02/99	3	3	3	3	3	3	0	1	0	0	0	0	0
	03/03/99	3	3	3	3	3	3	1	1	2	0	0	0	0
	12/03/99	3	3	3	3	3	3	3	1	2	0	0	0	0
	26/03/99	3	3	3	3	3	3	3	2	2	1	0	0	0
Pellet	20/09/00	3	3	2	1	1	1	0	0	0	0	0	0	0
	02/10/00	3	3	2	3	2	1	0	0	0	0	0	0	0
	16/10/00	3	3	3	3	3	1	2	0	1	0	0	0	0
	27/10/00	3	3	3	3	3	2	2	1	1	0	0	0	0
	06/11/00	3	3	3	3	3	2	2	2	2	0	0	0	0
	20/11/00	3	3	3	3	3	3	3	2	2	0	0	0	0
N. Strom	20/09/00	3	3	1	1	0	0	0	0	0	0	0	0	0
	02/10/00	3	3	3	2	0	0	0	0	0	0	0	0	0
	16/10/00	3	3	3	3	1	1	1	0	0	0	0	0	0
	27/10/00	3	3	3	3	3	2	1	0	0	0	0	0	0
	06/11/00	3	3	3	3	3	2	1	0	0	0	0	0	0
	20/11/00	3	3	3	3	3	3	1	0	0	0	0	0	0
S. Strom	20/09/00	3	3	2	0	0	0	0	0	0	0	0	0	0
	02/10/00	3	3	2	1	1	0	0	0	0	0	0	0	0
	16/10/00	3	3	2	2	1	0	1	0	0	0	0	0	0
	27/10/00	3	3	3	3	3	2	1	0	0	0	0	0	0
	06/11/00	3	3	3	3	3	2	1	1	0	0	0	0	0
	20/11/00	3	3	3	3	3	3	3	2	0	0	0	0	0
Halite	20/09/00	3	1	0	0	0	0	0	0	0	0	0	0	0
	02/10/00	3	2	0	0	0	0	0	0	0	0	0	0	0
	16/10/00	3	3	1	0	0	0	0	0	0	0	0	0	0
	27/10/00	3	3	2	1	1	0	0	0	0	0	0	0	0
	06/11/00	3	3	2	1	1	1	0	0	0	0	0	0	0
	20/11/00	3	3	3	2	1	1	0	0	0	0	0	0	0

Table 6.2 Numbers of vials from the ephemeral lakes which contained a black pyritic precipitate, indicating bacterial growth. Each dilution level was done in triplicate and each value indicates how many of these showed growth on the stated date.

6.2.4. Most Probable Numbers

The numbers of positive vials from each dilution level were entered into a computer program written in the BASIC programming language (Hurley & Roscoe, 1983, Appendix A). This generates a most probable number of bacteria per millilitre of each sample by solving the following equation:

$$\sum_{i=1}^{k} \frac{v_i d_i p_i}{1 - e^{-v_i d_i x}} = \sum_{i=1}^{k} v_i d_i n_i$$

where k = number of levels of dilution

n_i = number of subsamples at level i

p_i = number of positive subsamples at level i

d_i = dilution factor at level i

= volume of main sample in subsample

---

volume of subsample e.g. 0.1 for a 1 in 10 dilution

v_i = volume of each subsample at level i

x = estimated density of organisms per unit volume of the original sample from which the diluted samples were taken

e = exponential function

The BASIC computer program not only generates a most probable number but also a 95% confidence interval and a deviance value. The deviance of the MPN indicates whether there has been handling errors in the laboratory when the dilution series was set up and for the count to be valid the value must be less than the 5% chi-squared level at $k - 1$ degrees of freedom. 95% confidence intervals are necessary because this technique is of low precision compared to direct counts.

The results (MPN and 95% confidence interval) for each lake are given in the following pages and are represented graphically in Figure 6.1.

Milne Lake:

MPN = 921,600 ml^{-1}

95 % Confidence Interval (C.I.) = 304,088 to 2,792,543 ml^{-1}

These are often expressed as logs since the numbers are so large

log MPN = 5.96

log 95 % C.I. = 5.48 to 6.44

Deviance = 3.705 < (95 % X^2 = 16.92), therefore not significant = valid count

Pellet Lake:

MPN = 863,200 ml^{-1}

95 % C.I. = 288,403 to 2,630,268 ml^{-1}

log MPN = 5.94

log 95 % C.I. = 5.46 to 6.42

Deviance at 95 % C.I. is not significant, indicating a valid count

Mini Dolomite Lake:

MPN = 3,737,600 ml^{-1}

95 % C.I. = 1,173,545 to 11,931,636 ml^{-1}

log MPN = 6.57

log 95 % C.I. = 6.06 to 7.07

Deviance at 95 % C.I. is not significant, indicating a valid count

McFaiden Lake:

MPN = 1,715,200 ml^{-1}

95 % C.I. = 537,426 to 5,474,073 ml^{-1}

log MPN = 6.23

log 95 % C.I. = 5.73 to 6.74

Deviance at 95 % C.I. is not significant, indicating a valid count

Halite Lake:

MPN = 1063 ml^{-1}

95 % C.I. = 348 to 3244 ml^{-1}

log MPN = 3.02

log 95 % C.I. = 2.54 to 3.51

Deviance at 95 % C.I. is not significant, indicating a valid count

North Stromatolite Lake:

MPN = 40,000 ml^{-1}

95 % C.I. = 13,320 to 120,116 ml^{-1}

log MPN = 4.60

log 95% C.I. = 4.12 to 5.08

Deviance at 95 % C.I. is not significant, indicating a valid count

South Stromatolite Lake:

MPN = 332,800 ml^{-1}

95 % C.I. = 106,706 to 1,037,949 ml^{-1}

log MPN = 5.52

log 95 % C.I. = 5.03 to 6.02

Deviance at 95 % C.I. is not significant, indicating a valid count

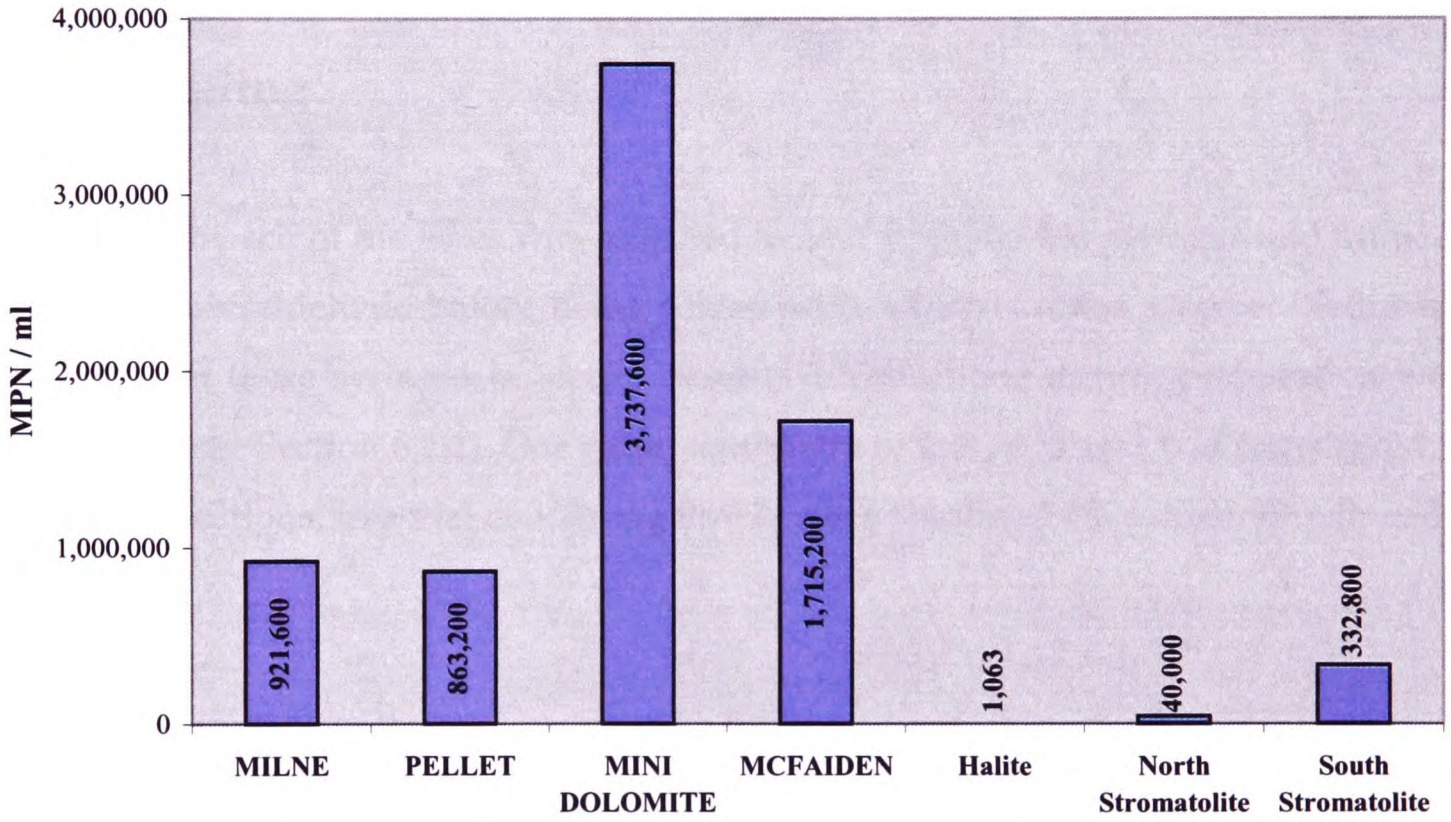


Figure 6.1. A graphical comparison of the most probable number (MPN) of SRB per millilitre of sediment in the dolomitic (caps) versus the non-dolomitic study lakes.

6.3. ACRIDINE ORANGE DIRECT COUNTS (AODC)

AODC counts were performed to estimate the total number of bacteria in 1ml of each sediment sample. The results of AODC were then compared to those of the MPN technique (Section 5.8) to establish what proportion of the total bacterial population were SRB. It could then be determined whether this proportion is significant enough for SRB to substantially modify their surrounding environment.

The technique used to calculate total bacteria in a soil/mud sample is the Acridine Orange Direct Count Method (AODC; see Kirchman *et al.*, 1982; Fry 1988, 1990).

6.3.1. Sampling

Sediment from each of the lakes was collected in $5cm^3$ open-ended syringes and immediately fixed with gluteraldehyde before being sealed with a butyl rubber stopper. Sediment was extracted from these syringes in sterile, anaerobic conditions during preparation work for MPN counts (see Section 6.2.2). One cubic centimetre of this sediment was transferred, under the above conditions, to a vial containing 9ml of filter sterilized 4% formaldehyde and made into a slurry.

6.3.2. Analytical procedure

Analysis of each sample was carried out using the reagents and procedure outlined below; the procedure was once again performed at the Geomicrobiology unit of Bristol University, where there was easy access to both equipment and expertise.

Reagents:

1. Formaldehyde saline solution (2% - 20ml of 40% commercial formaldehyde solution and 35g NaCl dissolved in 1 litre of de-ionised water). This was filtered through a 0.2µm filter (Vacucap 0.2ml bottletop vacuum filter unit, Gelman Sciences), into a desiccated Duran

bottle which had been heated to 450°C for approximately 2 hours. (In sediments with high carbonate content, such as those from the Coorong, formaldehyde was used that was made with 2.5% acetic acid, which dissolves much of the debris during staining).

2. Acridine Orange Solution: $1gl^{-1}$ dissolved in 2% acetic acid, filter-sterilised (0.2 µm ministart filters; Sartorious) into Sterilin containers. This acted as the stain.

3. Oxalate solution: This was a filter sterilised (0.2µm filter) solution of 28g of ammonium oxalate and 15g oxalic acid per 1000ml.

4. Hydroxylamine solution: 0.25N hydroxylamine in 0.25N HCl (filter-sterilized, 0.2µm).

Microscope slide preparation:

1. 10ml of formaldehyde was filter-sterilised (0.1µm; Amotop-25) into a sterile Sterilin bottle.

2. 5-100µl of sediment slurry from the sample vial was then added (the aim being to end up with approximately 50-75% coverage of the field of view with sediment particles). At this stage oxalate solution may be added at the rate of 9µl oxalate per 1µl of sample if iron oxyhydroxide floc is prevalent. Alternatively, hydroxylamine solution may be added at the rate of 16µl per 1 µl of sample if manganic oxyhydroxide floc is a problem. These problems were not encountered.

3. 50µl of acridine orange solution was added. This gave a final concentration of 5mg/l. The solution was vortex mixed by rapid spinning and left to stain for 3 minutes.

4. The stained sample was vacuum filtered through a 25mm black nucleopore filter (0.2µm pore size, polycarbonate membrane), then rinsed with a further 10ml of filter-sterilised formaldehyde. A gentle vacuum was applied until the filter appeared dry.

5. The filter was mounted, within a medium of liquid paraffin, on a glass slide and a cover-slip was placed over it using another drop of liquid paraffin. The filter was then fixed firmly in place by gently pressing down on the slide. Three replicate filters were prepared for each sample to minimise the variance of the counts.

6. The slide was viewed under epifluorescent illumination and 1000 times magnification (Zeiss Axioskop microscope fitted with a 50-W mercury vapour lamp, a wide band interference filter set for blue excitation, a 100x Plan Neoflar objective lens, and 10x eyepiece). The bacteria showed up as predominantly green-fluorescing, bacterially shaped objects (rods, spheres, filaments) with fairly sharp outlines, whilst the debris stained orange or red. Non-bacterially-shaped objects (i.e. large, fluorescent, amorphous blobs and objects with jagged edges) were ignored.

Counting:

All of the cells in a fixed number of graticule squares were counted (3 x 3 to 10 x 10, depending on cell abundance). It was recommended (B. Cragg, Pers. Comm.) to aim for at least 20 cells per field of view. In my samples there were often many more than 20 cells per field of view.

I moved from one field of view to another without looking at the filter to ensure fields were randomly selected. Each field of view was counted rapidly to avoid problems caused by the rapid fading of the fluorochrome (the part of the cell that is picked up in UV light).

It was recommended (B. Cragg, Pers. Comm.) that a minimum of 400 cells or 200 fields of view should be counted, and that at least 20 fields of view should be counted, no matter how abundant the cells are, to avoid statistical bias. This was done working in linear transects back and forth across the membrane.

The cells were classified according to 'on-particle', 'off-particle', dividing and divided cells (and 'filamentous' cells where relevant).

'On-particle': cells which were apparently attached to the upper surface of a particle. The number of bacteria 'on-particles' were doubled in the calculations to account for those hidden from view.

'Off-particle': Cells attached to the side of a particle, where the black membrane was visible around three sides of the cell, together with cells attached to either transparent objects or with no attachment.

Dividing cells: bacterial cells that exhibited a clear invagination were counted as one cell in both the total count and dividing cell count.

Divided cells: recently divided bacteria appeared as closely adjacent identical cells (with a visible gap between them) and were counted as two cells in both the total count and dividing cell count.

6.3.3. Spreadsheet Calculations

All the critical data obtained from the AODC technique was entered into a spreadsheet (Table 6.3). The various parts of the spreadsheet are briefly explained below. It has columns A-W (see below) and several rows corresponding to different lake samples and controls.

There are two controls, CONTROL and BLANK.

CONTROL = 1ml of formaldehyde from an unused sample vial put through the entire staining and counting process.

BLANK = 50µl of acridine orange in 10ml of filter sterilized formaldehyde.

What follows is an explanation of the abbreviations used for each of the columns in Table 6.3 based upon the numbers in Row 5 (the first Mini Dolomite Lake count).

A = Sample identifier

B = Dilution factor of sample vial

C = Grid counted – in this case 10 x10

SAMPLE	DIL.	GRID	µm2 CTD	VOL µl	ON PART	OFF PART	VIEW COUNT	DIVG	DIVD	MEMB. TOT. CT.	TOT CT - (BL+C)	LOG CT	MEAN	ST DEV	95% C.L.	DIVIDING CELLS	LOG DIV CELLS	MEAN	TOTAL CELLS	DIVIDING CELLS	% DIV CELLS	MEAN % DIV CELLS
A	B	C	D	E	F	G	H	I	J	K	L	M	N	O	P	Q	R	S	T	U	V	W
	0.100	10	9801	10.0	230	425	25	20	38	1421980	1421980000	9.1529				170970099	8.2329		1421980000	170970099	12.02	
Mini Dolomite	0.100	10	9801	10.0	184	442	25	24	51	1363561	1363561077	9.1347				218569341	8.3396		1363561077	218569341	16.03	
	0.100	10	9801	10.0	286	501	25	12	46	1702957	1702956683	9.2312	9.1729	0.0513	0.1274	186196026	8.2700	8.2808	1702956683	186196026	10.93	13.00
	0.025	10	9801	15.0	193	278	66	13	22	394926	1053135057	9.0225				105043634	8.0214		1053135057	105043634	9.97	
Milne	0.025	10	9801	15.0	155	322	67	17	31	385237	1027299722	9.0117				138368113	8.1410		1027299722	138368113	13.47	
	0.025	10	9801	15.0	211	304	66	10	18	420521	1121388180	9.0498	9.0280	0.0196	0.0487	84770148	7.9282	8.0302	1121388180	84770148	7.56	10.33
	0.025	10	9801	15.0	178	369	30	15	32	969940	2586506055	9.4127				309087651	8.4901		2586506055	309087651	11.95	
McFaiden	0.025	10	9801	15.0	195	410	30	27	33	1078635	2876359811	9.4588				363346400	8.5603		2876359811	363346400	12.63	
	0.025	10	9801	15.0	256	447	30	21	44	1292353	3446274268	9.5373	9.4696	0.0630	0.1566	433799441	8.6373	8.5626	3446274268	433799441	12.59	12.39
CONTROL	0.100	10	9801	1000.0	0	0	2000	0	0	0		0										
CONTROL	0.100	10	9801	1000.0	0	0	2000	0	0	0		0										
CONTROL	0.100	10	9801	1000.0	0	0	2000	0	0	0		0										
			SUM	3000.0	0	0	6000	0	0	0	0	0	0									
BLANK		10	9801		0	1	400	0	0	88												
BLANK		10	9801		0	1	400	0	0	88												
BLANK		10	9801		0	1	400	0	0	88		0										
		10	9801	SUM	0	3	1200	0	0	88	29	0	0									

Table 6.3. Spreadsheet for Acridine Orange Direct Counts. See text for details

D = Area counted = C5 x C5 x 98.01 (98.01 = area of one grid square in μm^2)

E = Volume of sample used

F = On-particle count

G = Off-particle count

H = Number of fields of view counted

I = Number of dividing cells

J = Number of divided cells

K = Calculated total cells on membrane:

((((F5x2) + G5 + I5 + (2xJ5) + ((F5/(F5 + F5 + G5)) x (I5 + (2xJ5))))/H5)
x 346360000/D5)

Note: 346360000 = total filtered area (μm^2) of a 25mm diameter nucleopore filter, based on the area of the base of the filter funnel.

L = Corrected count (takes into account control, blank, sample volume and sample dilution factor):

((K5 – ((E5 x L20) + L25)) x (1000/E5)) / B5

M = Log count (i.e. log L5)

N = Mean

O = Standard deviation

P = Confidence interval

Q = Dividing cells – corrected numbers:

(((((I5 + (2xJ5) + ((F5/(F5 + F5 + G5)) x (I5 + (2xJ5))))/H5) x (346360000/D5)) -
((E5 x N20) + N20)) x (1000/E5)) / B5

R = Log dividing cells (log Q5)

S = Mean

T = Total cells

U = Dividing cells

V = Percentage of dividing cells = (U5 x 100) / T5

W = Mean percentage of dividing cells, indicating whether the bacterial population was healthy.

6.3.4. Results

The important numbers to be taken from Table 6.3 are those in columns L, M and N, and then also from columns V and W.

Column L gives the total cell count for the lake sediment sample, which is then expressed in columns M and N as logs, making the numbers easier to manipulate (Table 6.4).

Lake	Total counts (mean)	Log total counts
Mini Dolomite	1496010274	9.1729
Milne	1066689631	9.0278
McFaiden	2969298690	9.4696

Table 6.4. Total bacterial counts from three dolomitic lakes. (NB. Total counts could not be obtained from the remainder of the study lakes owing to budget considerations.)

Columns V and W are used to show whether the population was healthy at the time of counting. The indicator for this is the percentage of the total cells that are currently dividing. If this percentage is very low then it can be assumed that the sample had not been stored correctly and, if this is the case, the total count procedure will underestimate population numbers. In these samples however the percentages are quite high at over 10% so the population can be assumed to be healthy, and the counts to be accurate.

6.3.5. Bacterial Clustering

An important point that arose from the bacterial counting procedure was the way the bacteria were distributed under the microscope. A typical field of view is shown in Figure 6.2. The bacteria are seen as sub-micron sized, green, fluorescing objects with smooth outlines. It can be seen that there are large areas with no bacteria visible and then other areas where there are clusters. It is proposed that these clusters are associated with clumps of organic matter that provide favourable micro-environments for the growth of the bacteria by supplying high concentrations of readily oxidizable material.

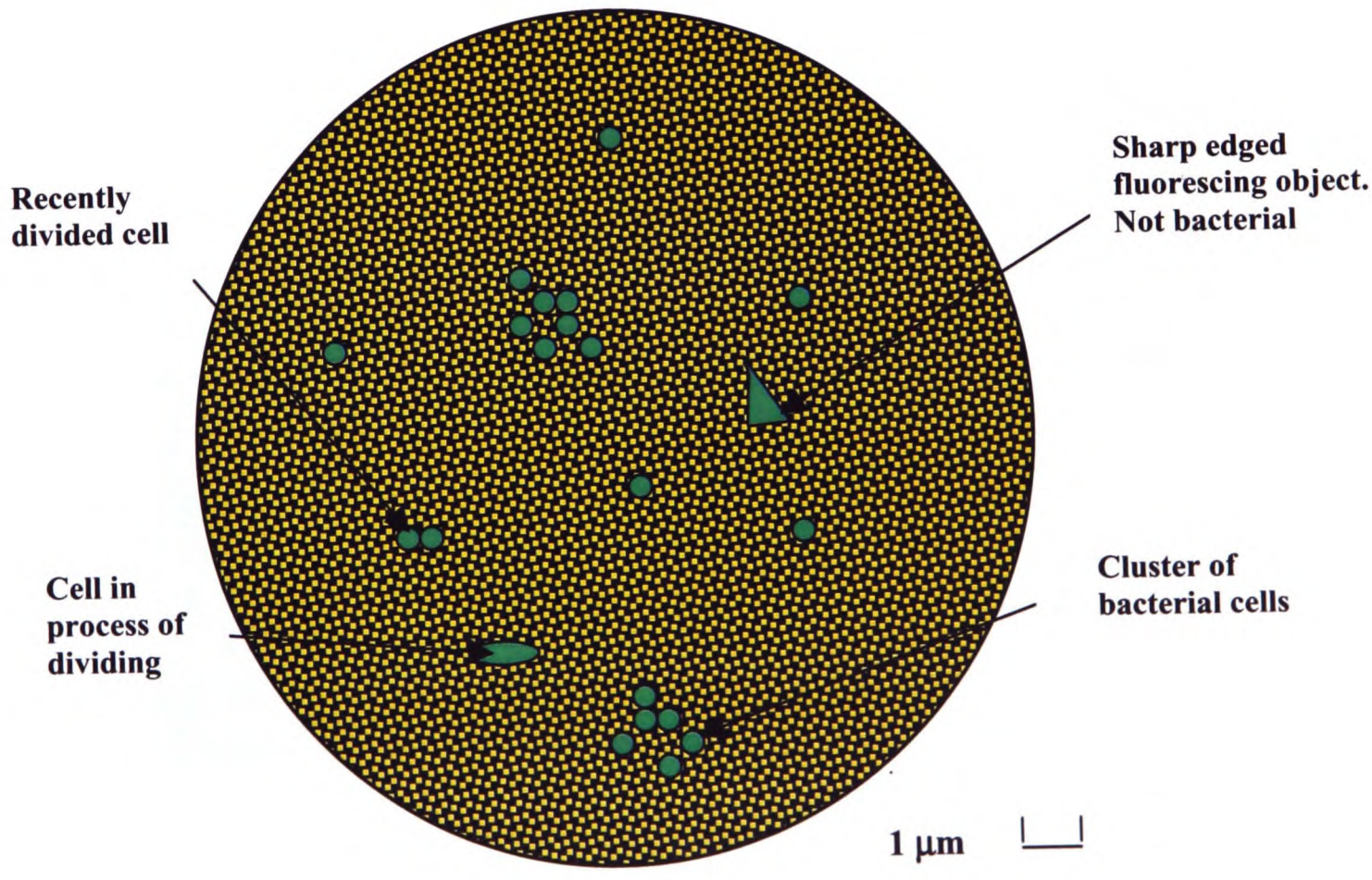


Figure 6.2. Typical field of view of bacterial cells during AODC work.

6.4. COMPARISON OF AODC AND MPN VALUES

Lake	AODC	log AODC	MPN	log MPN	% SRB
Mini Dolomite	1496010274	9.1729	3737600	6.573	**0.25**
Milne	1066689631	9.0278	921600	5.965	**0.086**
McFaiden	2969298690	9.4696	1715200	6.23	**0.06**

Table 6.5. A comparison of AODC and MPN values. Note: MPN technique underestimates the numbers of SRB by up to a factor of 1000 (see text for details).

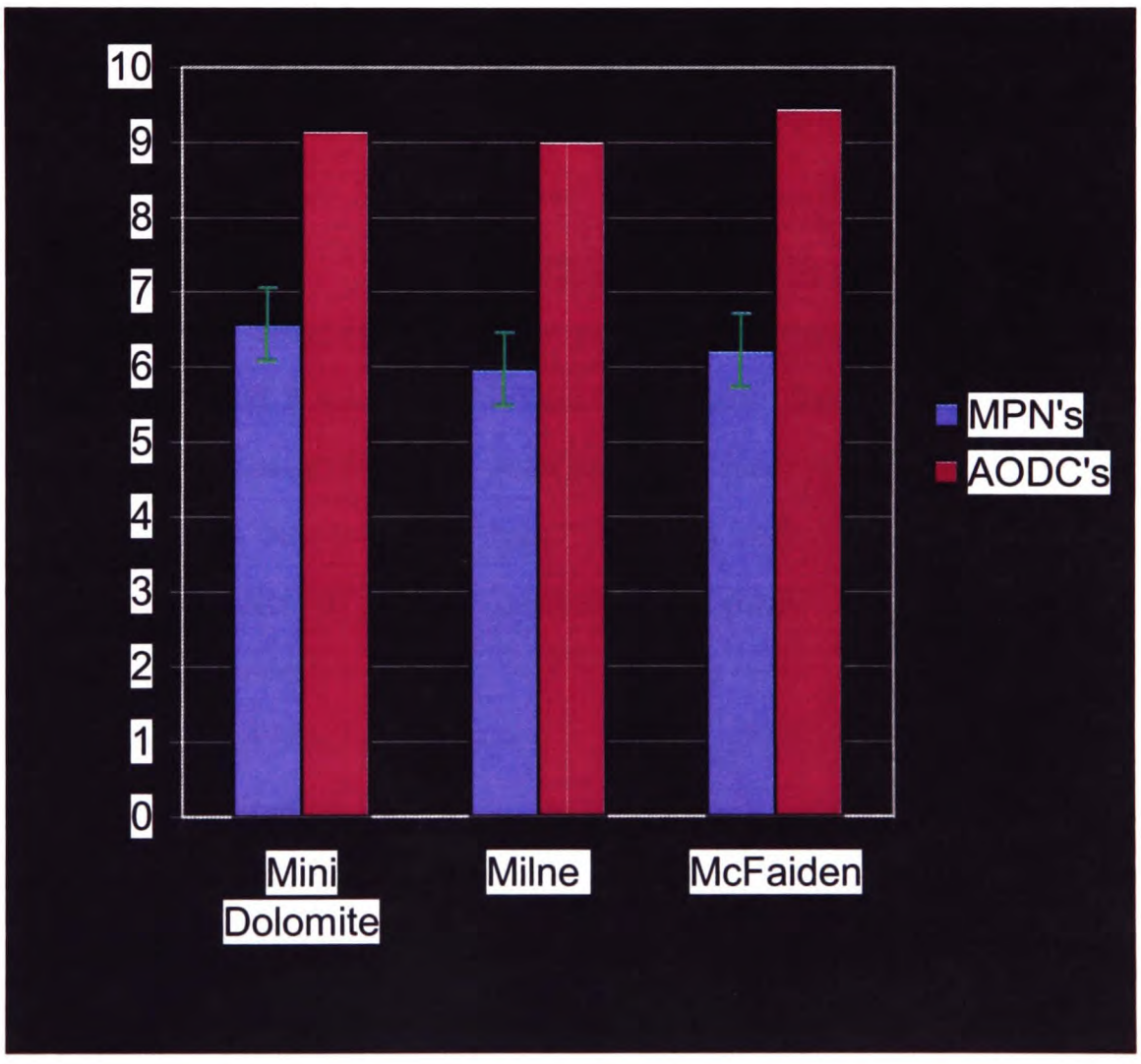


Figure 6.3. A graphical comparison of the two bacterial counts (Note the logarithmic scale and the 95% confidence intervals on the MPN data). The MPN count gives the number of viable SRB in 1ml of sediment, whilst the AODC count gives the *total* number of bacteria in 1ml of sediment. A comparison of the two counts thus approximates the proportion of total bacteria that are SRB's.

6.5. DISCUSSION

The MPN technique counts the number of viable, cultivable, metabolically active sulphate reducers isolated from a lake-bed sample, using a specific culture media and a dilution series. The AODC technique counts the *total* number of bacteria in the same sediment sample. Using these techniques one can obtain a rough estimate of the proportion of the total bacterial population that are sulphate reducers.

The amount of sulphate reducers, given as a percentage of the total bacterial population, is shown in Table 6.5. These values initially appear to be very low and suggest that SRB are not an important part of the bacterial population. This, however, is very misleading. It is well known that only approximately 0.1% of a general bacterial population is recoverable by culture-dependent processes such as MPN counts (Jannasch & Jones, 1959; Staley & Konopka, 1985). This has usually been attributed to the inadequacy of the culture media, but there is a more fundamental reason underlying this. Viable but non-culturable cells account for much of the total bacterial population and activity *in situ*. These cells, although viable in a given media, may not grow beyond a few cell divisions and thus will not be picked up in the MPN counts (Teske *et al.*, 1996). An example of this comes from Binnerup *et al.* (1993) where the bacterium *Pseudomonas flourescens* was investigated. They found that after 40 days 0.21% of the bacterial population was still cultivable. Originally 20% of the population had been identified as viable but non-culturable (i.e. could form micro-colonies but not beyond a few cell divisions). Hence, the viable cultivable population was only 1% of the viable non-culturable population. Direct cell counts such as AODC count all viable bacteria and so one would expect a direct cell count to be around two orders of magnitude greater than a culture-dependent count. Further evidence showing SRB populations to be underestimated by MPN counts was found by Teske *et al.* (1996). Here denaturing gradient gel electrophoresis (DGGE) was performed on PCR amplified nucleic acids. This technique shows the presence of bacterial populations but not their metabolic activity. It was found that the major bands of the DGGE pattern did not match the genera obtained from MPN isolates, suggesting that MPN dilutions may not recognise the most abundant viable genera in an SRB population.

From the evidence presented above and knowing that direct cell counts such as AODC count all viable bacteria, one might expect a direct cell count to be around two orders of magnitude greater than a culture-dependent count. However, Teske *et al.* (1998) used

measurements of specific sulphate reduction rate to show that MPN counts underestimate the amount of metabolically active SRB by as much as ten fold (one order of magnitude). Adding this observation to those made previously a direct count which is as much as three orders of magnitude higher than a MPN count is therefore not unexpected.

Further to this, when dealing with SRB, the growth substrate needs to be considered. As discussed previously (Section 5.7), the culture medium in this study was chosen because many types of *Desulfovibrio* and *Desulfotomacula* thrive in it and these were thought to be the most common sulphate reducers in an ephemeral lake setting. The growth substrate in this medium was a mixture of lactate and acetate. Although many SRB genera do grow on these substrates, they do not account for all genera. Teske *et al.* (1996) used three separate substrates: lactate, acetate and acetate + H_2 in obtaining values of ~10^6 cells/ml in the sediments of Mariager Fjord, Denmark whilst Teske *et al.* (1998) used lactate, acetate and formate in obtaining values between 0.9 and 11.6 x 10^6 cells/ml at various depths in microbial mats in Solar Lake. A wide variety of substrates must be used to fully characterise the SRB population and, due to financial constraints, this was not achievable during this study.

Bacterial strains most closely related to *S2550 (Desulfostipes saporovans)* and *Desulfosarcina* were subsequently identified, using 16S rRNA sequencing, growing in this medium (Section 6.6). This medium may not have been the *most* beneficial to their growth and, consequently, their numbers may have been somewhat under-estimated. It was also noted (Teske *et al.* 1996; Castro *et al.*, 2000) that the genus *Desulfosarcina*, a non-motile acetate-oxidising genus, often experiences cell clumping leading to underestimates of its numbers.

It is useful to have a reference frame for the counts obtained in this study. Other workers have performed population counts of SRB in a wide range of different settings and have often found lower numbers of sulphate reducers (Table 6.6). The data given in Table 6.6 shows that the numbers of SRB recorded in this study are comparable to the highest ever recorded in anoxic sediments. When the percentages of SRB in Table 6.5 are re-examined with the knowledge of the numerous limitations of the MPN technique, discussed above, the values start to look remarkably high, especially in Mini Dolomite Lake (0.25%). This is reinforced when compared to values obtained from other locations; for example Teske *et al.* (1998) obtained *total* bacterial counts in Solar Lake of ~ 1 x 10^{11}/ml giving the percentage of SRB in Solar Lake as only around 0.001%; a couple of orders of magnitude less than found in these study lakes.

Location	Population of SRB (measured by MPN dilution series)	Reference
Mini Dolomite Lake	3.73×10^6 /ml	This study
Microbial mat, Solar Lake	~ 10^6 /ml (in all mat layers)	Teske *et al.*, 1998
	2×10^6 /ml	Jorgensen & Cohen, 1977
Lake Constance (freshwater)	6.3×10^6 /ml. (Highest number ever reported at the time)	Bak & Pfennig, 1991
Lagos Lagoon (polluted)	$4.23 \times 10^2 - 7.6 \times 10^4$ /ml (sediment) $28 - 5.71 \times 10^3$ /ml (water)	Esiobu *et al.*, 1991
Cold marine sediments, Norway	$4.3 \times 10^4 - 2.3 \times 10^5$ /ml	Knoblauch, 1997
Eastern Baltic Sea	$4 \times 10^2 - 7 \times 10^4$ /ml	Bussmann & Reichardt, 1991
Oil field formation waters, China	1000 /ml	Nazina *et al.*, 2000
Stratified marine water column	25 /ml above chemocline 250 /ml below	Teske *et al.*, 1996
Bottom sediments, Gulf of Gdansk	$0.76 \times 10^3 - 1.27 \times 10^4$ / g wet sediment	Mudryk *et al.*, 2000
Shallow water hydrothermal vent	Max 1.4×10^5 / g wet sediment	Sievert *et al.*, 1999

Table 6.6. A comparison of reported SRB populations with data obtained in this study. All counts were obtained using the MPN dilution technique, except for Bak & Pfennig (1991) where both MPN and agar was used. Data from Mudryk *et al.* (2000) and Sievert *et al.* (1999) has units of 'per gram of wet sediment.' The density of this sediment is not stated but an approximate conversion factor of 1.75 (average bulk sand) may be applied to obtain units of 'per ml'

Field evidence also suggests that SRB are present in very high numbers. Firstly, the lake sediment is anoxic immediately below the sediment water interface so this limits the bacterial population to anaerobes. Secondly, when the lake sediment was disturbed a pungent 'bad egg' smell, corresponding to the release of H_2S was noted. H_2S is the main metabolic product of bacterial sulphate reduction and so bacterial sulphate reduction would appear to be one of the dominant processes taking place in these lakes. It is therefore proposed that SRB are present in the lakes in such large quantities that their activity can be expected to have a profound effect on the chemistry of the surrounding micro-environment.

A comparison of the MPN counts of SRB from dolomite and non-dolomite precipitating lakes reveals that, although numbers are high in all the lakes, the dolomite precipitating lakes have significantly larger SRB populations. This may be a key factor in whether dolomite precipitates in preference to other carbonate phases. A larger SRB population may result in greater mediation of porewater chemistry, in particular an increase in the activity of the carbonate ion and an increase in free magnesium ions. Bacterial precipitation experiments were designed in the laboratory to further constrain the conditions required to precipitate dolomite and attempt to confirm that SRB are indeed the active agent of dolomite precipitation (see Section 6.7).

6.6. BACTERIAL IDENTIFICATION

The next logical step in this project was to identify the bacteria in the study lakes. Vials containing mixed cultures of bacteria from the study lakes were sent to Amodia, a bacterial identification company in Germany. They used the 16S rRNA method of Schwieger and Tebbe (1998) for the detection of bacterial DNA and subsequent identification. The GenBank database (http://www.ncbi.nlm.nih.gov) was used to classify the detected products. Again, due to financial constraints, only bacteria form Milne Lake, Mini Dolomite Lake and McFaiden Lake were able to undergo the identification process.

6.6.1. Results

The complete DNA sequencing results are given in Appendix 6, whilst a summary is shown in Table 6.7, below.

Lake	Product Identity	Closest Relative	Other Closely Related Bacteria
Milne (product 1)	98%	*Vibrio harveyi*	Vibrio sp. BV25Ex
Milne (product 2)	91%	*Clostridium propionicum*	Uncultured Clostridiaceae
McFaiden (product 1)	97%	*Desulfostipes saporovans*	*Desulfosarcina* Sulphate-reducing bacterium AK-01
McFaiden (product 2)	96%	Unidentified eubacterium	*Clostridium propionicum*

Table 6.7. 16S rRNA sequencing results for Milne and McFaiden Lakes. NB. Universal screening for bacterial DNA produced no products in Mini Dolomite Lake.

The results obtained from Amodia were somewhat unexpected. The vial containing bacteria cultured from Mini Dolomite Lake did not produce any DNA products, whilst Milne Lake showed one significant and three weak products and McFaiden Lake showed three weak products (one product corresponds to one organism). Two of the weak products from Milne Lake and one from McFaiden Lake could not be identified because of the very small amount of DNA involved. These results were very surprising considering the large amounts of bacteria shown to be present by MPN and AODC techniques. It is thought that these poor results were due to the quality of preservation of the DNA. The vials had been stored for a considerable amount of time (~2 years) before identification was attempted and it had already proved impossible to extract 'clean' DNA when attempted at the Department of Biochemistry in Oxford.

Nevertheless, four products were obtained whose closest relatives are described below:

1) *Vibrio harveyi* (98% similarity)

These anaerobic, Gram-negative curved rods are around 0.5μm in width and up to 2.6μm in length, motile with an optimum temperature of 20-30°C. They are found in a wide range of

aquatic environments, tolerating a wide range of salinities. Indeed, sodium ions are a requirement of most species (Holt *et al.*, 1994). A species with 98% gene similarity to *V. harveyi* was found in Milne Lake. This can utilise some of the same substrates as the SRB (e.g. lactate, acetate) and can also reduce nitrate.

2) *Clostridium propionicum* (91% similarity)

Members of the genus *Clostridium* are metabolically diverse, gram positive, spore forming rods that are strictly anaerobic, belonging to the family *Bacillaceae*. They are motile, found ubiquitously in nature, especially in soils, at temperatures of between 10 and 65°C. When the environment is favourable they exist as long drumsticks with a bulge at their terminus end sometimes linked to form chains, but when the environment turns hostile they produce spores which can tolerate the extreme conditions (including oxygen) that the active bacteria cannot. Some species are responsible for diseases in humans such as botulism (*C. botulinum*) and tetanus (*C. tetani*). They employ butyric fermentation pathways to produce energy and thus often give off foul odours. Usually they metabolise carbohydrates and peptones producing organic acids and alcohols (Holt *et al.*, 1994). They are closely related to the genus *Desulfotomaculum* though they themselves do not carry out sulphate reduction. A species with 91% gene similarity to *C. propionicum* was identified in these lakes. In terms of genetics, this is not a high degree of similarity and this species is likely to be an, as yet, uncharacterised bacteria.

3) *Desulfostipes saporovans* (97% similarity)

This new species was submitted to GenBank by Myhr *et al.* in 1999. It also goes by the title of *delta proteobacterium S2550.* At present, no further literature is available documenting the features of this taxon. The most closely related bacterium as identified by GenBank is the genus *Desulfosarcina*, represented only by *D. variabilis*. This is a member of Subgroup 3 of the sulphate-reducing bacteria described briefly in Section 2.2. Cells may be oval, rod shaped or coccoid, up to 2.5mm in length and are non spore forming. They stain gram negative and may be motile by the use of single polar flagella. They are strictly anaerobic using H_2, lactate, formate and higher monocarboxylic acids as electron donors; they may also grow

autotrophically. Their optimum temperature range of 33°C and optimum pH of 7.6 are very close to conditions experienced in the Coorong ephemeral lakes.

4) *Eubacterium* (96% similarity)

Members of the genus *Eubacterium* are very closely related to *Clostridium*, the only difference being that *Eubacterium* is non spore forming (Holt *et al.*, 1994). Indeed poorly sporing strains of *Clostridium* may be confused with *Eubacterium*. Again strict anaerobes, they have a fermentative metabolism producing mixtures of acids such as butyric, acetic and formic acid, together with H_2 gas. Their preferred habitat is black anoxic mud. Both *Clostridium* and *Eubacterium* are closely related to the Gram-positive spore forming SRB *Desulfotomaculum*.

It is worth noting that the species identified here may not be representative of the species present in the lakes. They may be a result of preferential selection and evolution of certain strains by the culture media.

6.7. BACTERIAL PRECIPITATION EXPERIMENTS

The data obtained from both the field and laboratory presented in previous chapters is consistent with microbial mediation of the precipitation of dolomite. The conclusion to this project uses bacteria, obtained and cultured in the laboratory from the study lakes, to further understand the conditions that lead to dolomite precipitation. Conditions found in the natural lake setting were replicated and in some cases subtly altered in the laboratory to see if a reproducible environment could be created which facilitated dolomite precipitation.

6.7.1. Initial Components of the vials

A series of experimental vials were established using a simple culture media (Postagate B (Section 6.2.2)), mineral seeds of quartz, aragonite or glass beads and natural bacterial populations cultured from the lake sediments. Control vials were created with no bacteria in them. As with the initial culturing described in Section 6.2, these experiments had to be handled with great care in order to maintain an anaerobic environment for the SRB. The culture medium and selected mineral seed were added to 12ml vials in an anaerobic cabinet

(anaerobic work was performed in the Department of Chemistry, whilst all other work was carried out in the Department of Earth Sciences, both in Oxford). Vials were labelled, sealed and clamped. Bacterial populations were then extracted from liquid culture vials and carefully injected into these experimental vials. The vials were stored for approximately two months at the ambient temperature of the lakes to allow the bacteria to adjust to their new environment and to see if the populations could be sustained. A sustainable population was indicated by a significant drop in sulphate concentration in the vials after two months of storage (Section 6.7.2a).

Subsequent to this, selected vials were injected with additional components to enhance the possibility of dolomite precipitation using knowledge obtained from previous field and laboratory observations. These additional components included one or more of: concentrated seawater (brine); brine with extra magnesium sulphate and organic matter (see Table 6.8). Concentrated seawater was added to mimic the water available in the natural lake environment, i.e. high salinity. Extra magnesium sulphate was added as this has the dual effect of increasing the Mg^{2+}/Ca^{2+} ratio (mirroring the release of magnesium from desiccated cyanobacterial sheaths) and increasing the amount of electron acceptors, in the form of SO_4^{2-}, for the oxidation of organic matter by the SRB. Organic matter (ground up *Ruppia* grass) was added to a small number of vials to keep pace with the expected increased activity of bacterial sulphate reduction, i.e. to provide additional oxidisable matter. It was hoped that these would provide both plentiful material that the bacteria could metabolise and the required ions for incorporation into the dolomite lattice.

The vials were then left at the approximate ambient temperature of the lakes and observed at regular intervals for any sign of precipitation. Approximately two weeks after the extra components were added a change was noted in some of the vials. A distinct layer of precipitate was observed. Vial 6, which appeared to have the greatest amount of precipitate, was left for a further two weeks and then opened. Vials 1, 8, 10 and 21 were taken as a representative cross section of all of the vials and these were opened a month later. Vials 7 and 15 were used for more careful monitoring of pH and sulphate concentration before being opened.

6.7.2. Chemical analyses of the vials

a) Sulphate concentrations

Measurements of the changes in sulphate concentration in the vials were used as a measure of bacterial activity. Initially the change in sulphate concentration was used to indicate successful transfer and acclimatization of bacteria into the experimental vials. Subsequently it was found that, even in the vials containing no bacteria, there was some drop in sulphate concentration due to inorganic precipitation of sulphate minerals. However, the drops in sulphate concentration in the vials containing bacteria were substantially greater than in the control vials (Fig. 6.4).

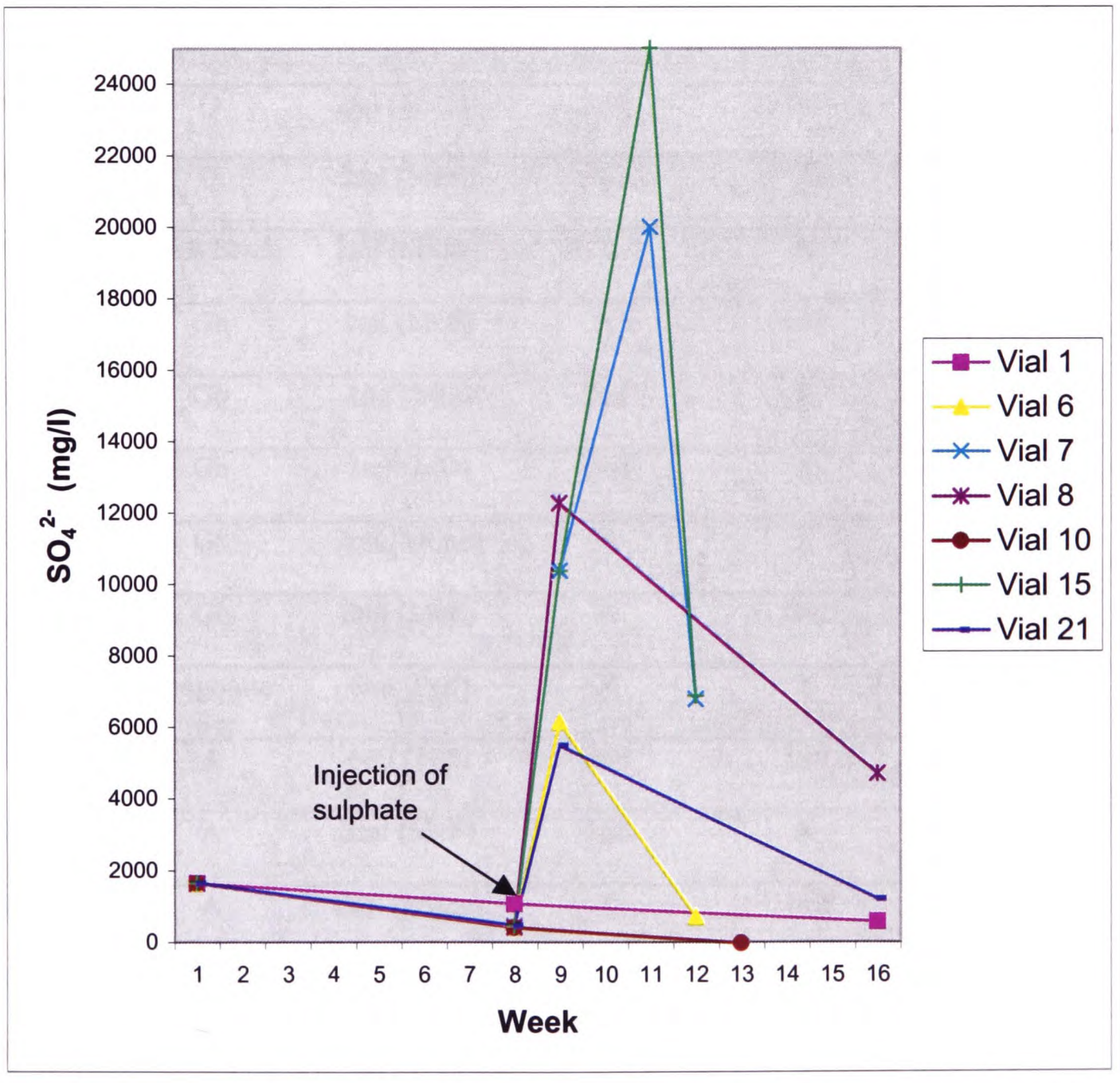


Figure 6.4. Change in sulphate ion concentration in the experimental vials over a period of 3-4 months. Vial 1 acted as a control vial with no bacteria present. Vial 10 was also a control vial monitoring background use of sulphate by relatively dormant bacteria. The remaining vials were all injected with various additional components (see Table 6.8) including $MgSO_4$ at the end of week 8 which is inferred to have stimulated bacterial metabolism.

Vial	Mineral seed	Bacteria (lake)	Conc. sea water	$MgSO_4$ in brine	Organic matter
1	Quartz	X	X	X	X
2	Glass beads	X	X	X	X
3	Aragonite	X	X	X	X
4	Quartz	1ml (Milne)	X	X	X
5	Q	1ml (McF)	2ml	1ml	1ml
6	Q	1ml (MD)	X	1ml	1ml
7	Q	2ml (MD)	X	6ml	X
8	Q	2ml (Milne)	2ml	1ml	X
9	Q	2ml (McF)	X	X	1ml
10	Glass beads	1ml (Milne)	X	X	X
11	Gb	1ml (McF)	X	1ml	1ml
12	Gb	1ml (MD)	2ml	X	1ml
13	Gb	2ml (MD)	2ml	X	X
14	Gb	2ml (Milne)	X	X	1ml
15	Gb	2ml (McF)	X	6ml	X
16	Aragonite	6ml (Pell)	X	X	X
17	A	6ml (Pell)	2ml	1ml	1ml
18	A	3ml (McF)	2ml	X	1ml
19	A	2ml (Milne)	X	1ml	1ml
20	A	2ml (McF)	X	X	1ml
21	A	2ml (MD)	X	1ml	1ml

Table 6.8. Starting components in each of the experimental vials.
Note: A = aragonite **McF = Mcfaiden Lake**
Q = quartz **MD = Mini Dolomite Lake**
Gb = glass beads **Pell = Pellet Lake** **X = no addition**
Lake names in brackets refer to the lake the bacteria were initially extracted from.

b) pH

Vials 7 and 15 were used to monitor the change in pH after the addition of extra magnesium sulphate to the vials. This was intended to reveal the nature of reactions occurring in these vials and establish whether pH would increase as the sulphate was used by SRB to metabolise the organic substrate. The pH of the two vials was measured by extracting a small amount of liquid using a sterile syringe, being careful not to allow any oxygen to enter the vial. 2ml of $MgSO_{4(aq)}$ (pH 7.35) was then injected into each and the pH was measured at regular intervals for 1 week. At the beginning of week 2 a further 2ml of $MgSO_{4(aq)}$ (pH 7.35) was added and the measurements repeated for a further 2 weeks.

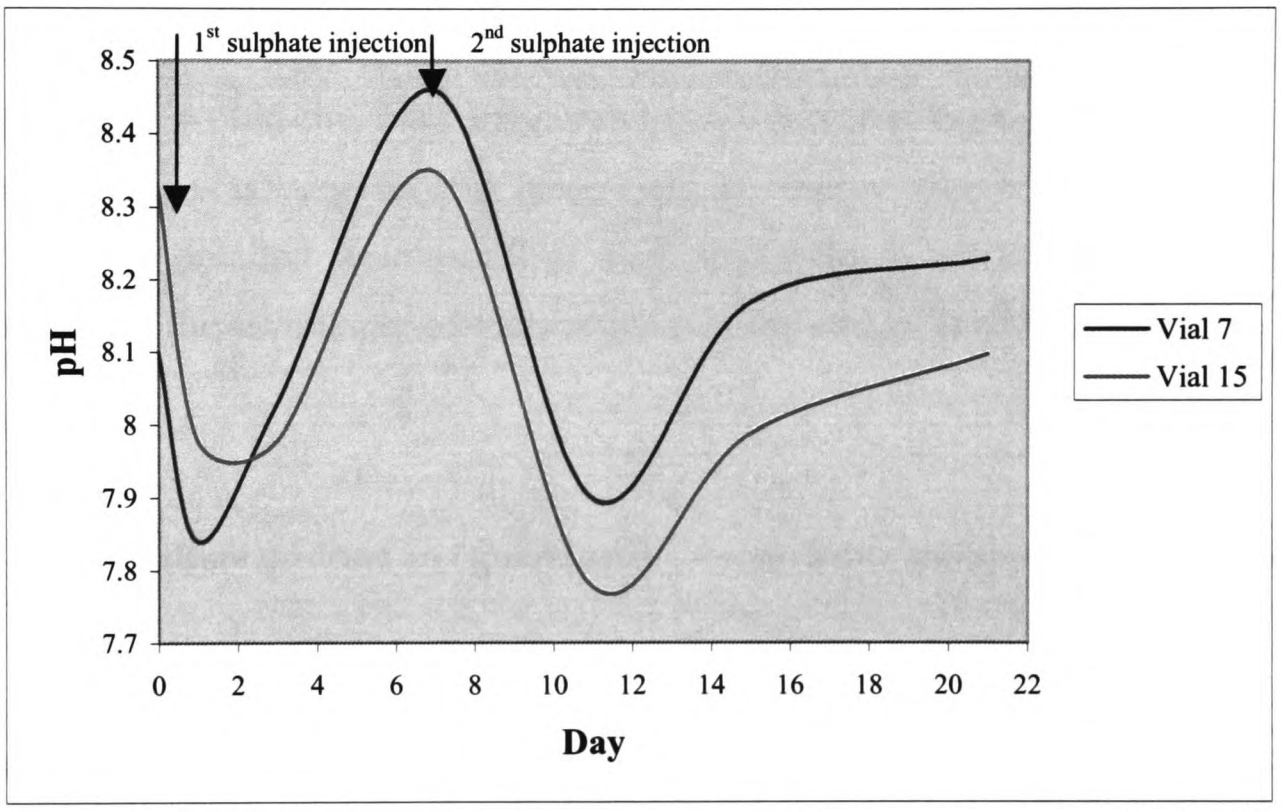


Figure 6.5. Evolution of the pH in Vial 7 and Vial 15 after successive injections of $MgSO_{4(aq)}$

Figure 6.5 traces the evolution of pH in the two vials and shows a similar pattern in each case. Immediately after injection of the $MgSO_4$ the pH drops from over 8 because the sulphate solution had a pH of 7.35. One metabolic product of the BSR is H_2S which is acidic and this may also assist the drop in the pH. Since there were sufficient Fe ions in the culture media to fix most of this H_2S as FeS, its effect upon pH should, however, be very small. The pH measurement on day 2 begins to show a rise which continues until the end of week 1. A second injection of $MgSO_4$ then brings about another sharp fall in pH but once again pH quickly begins to recover. After day 14, pH increases less rapidly and then slowly reaches equilibrium. No further pH measurements were made after day 21 because the liquid in the vials was exhausted.

The significant rise in pH is attributed to bacterial action and the release of ammonium compounds from the organic substrates that are being oxidised. The gradual levelling out of pH after week 2 is attributed to a drop in metabolic activity of SRB owing to exhaustion of the organic substrate and/or to the vials reaching an equilibrium state with respect to pH, close to that seen in the Coorong lakes.

6.7.3. Vial Precipitates

The final contents of the vials were analysed by X-ray Diffraction (XRD) and Scanning Electron Microscopy (SEM). Only a representative cross section of the vials were analysed since anaerobic conditions could not be re-established once they were opened and the bacterial populations would die. Had the correct conditions not been established in one of these opened vials it was necessary to have vials in reserve where conditions could be further modified. A detailed description of each vial follows whilst a summary of the products analysed in the seven opened vials is given at the end in Table 6.9 (p250).

6.7.3.1. Vial 1 (Culture medium and quartz seed ⟶ halite and smectite precipitate)

This was a control vial, the only contents being a clean quartz mineral seed and sterile culture medium. Sulphate concentration dropped from an initial value of 1650mg/l to 1100mg/l after week 8 and then to 800mg/l after week 16. This background drop in sulphate concentration must be taken into account when observing subsequent vials. The sediment from Vial 1, as viewed under the SEM, is shown in Figure 6.6. The initial appearance under low magnification is of numerous sub-rounded quartz grains (Appendix 7, spectrum 1), cemented in places, but elsewhere very little precipitate (Fig. 6.6a). The cementing precipitates are halite crystals (Appendix 7, spectrum 2) with an almost perfect cubic morphology, contoured with greater precipitation adjacent to the quartz grains (Fig. 6.6a). There is little precipitation on the quartz grains themselves, except in preferable sites such as indentations and cracks. Here, halite is again common, with minor Fe, Mg, K and Ca clays of the smectite group (Appendix 7, spectrum 5) although precise identification is difficult due to their small size and masking by background quartz counts. Occasionally these clay-mineral precipitates appear to be embedding themselves into the quartz grains (Fig. 6.6c).

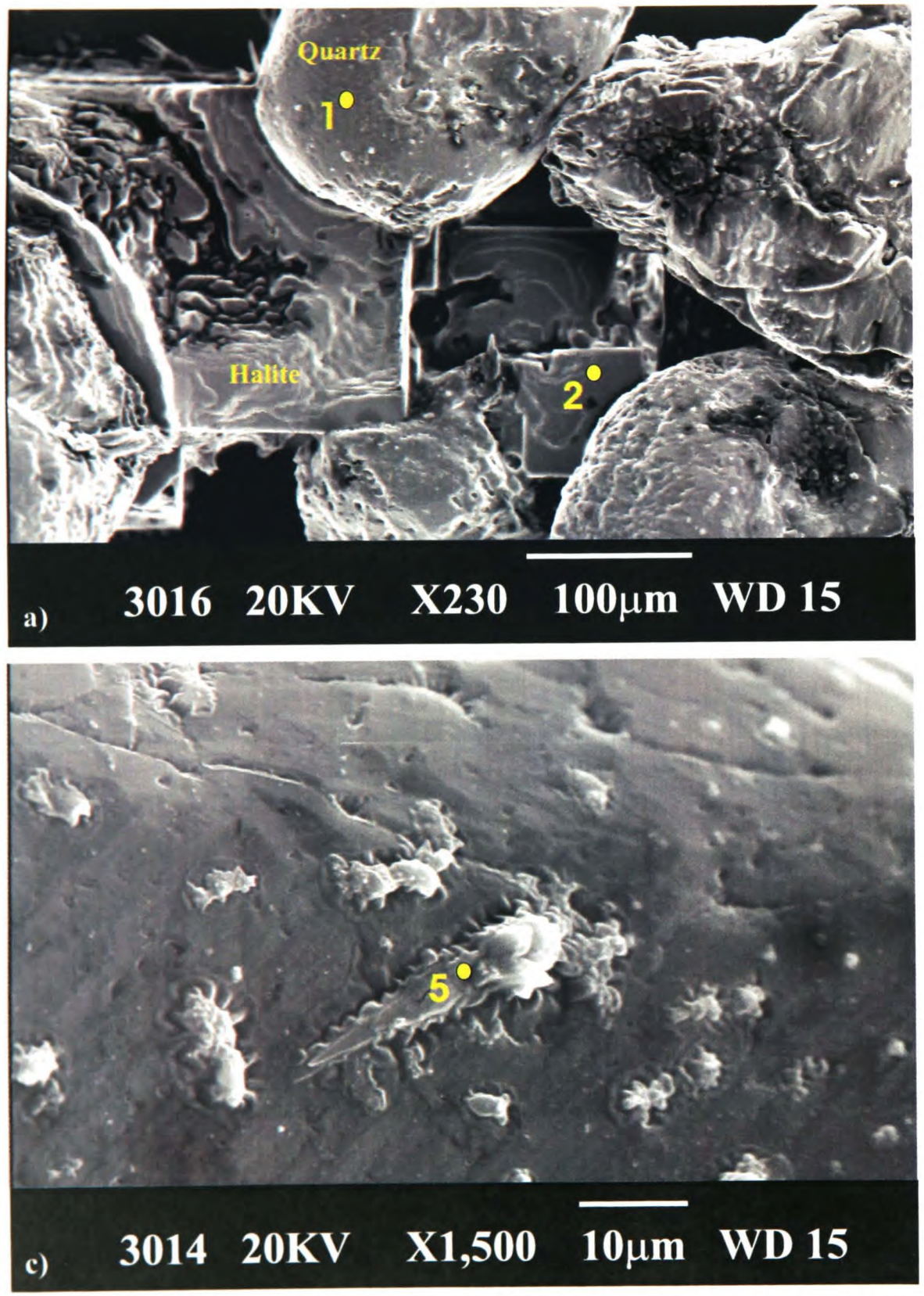


Figure 6.6. SEM images from Vial 1. a) Cubic halite crystals cementing quartz. b) Variety of chemical precipitates of chlorides and sulphates - see text and spectra (Appendix 7) for details. c) Clay mineral precipitates embedded in a quartz grain. d) Fan shaped morphology of multi-cation chloride. Numbers refer to atomic spectra in Appendix 7.

Loose sediment lying away from the quartz grains is rare and of varied mineralogy; small halite crystals are again present and, in addition to these, there appear to be other chlorides with cations not only of sodium (Appendix 7, spectrum 3) together with a Na-Ca sulphate (Appendix 7, spectrum 4). Examples of these are seen in Figures 6.6 b+d. One particular type of chloride assumes a fan/rose shape arrangement of crystals as shown in Figure 6.6d. This proved to be a multi-cation chloride with varying amounts of Ca, Na, Mg and K (Appendix 7, spectrum 6).

All of the ions needed for inorganic chemical precipitation of the above phases were present in the culture medium described in Section 6.2.2 and were evidently present in concentrations high enough for precipitation both in the vial and on the cover slip during drying. When examining the remainder of the vials, these phases were discounted as being of bacterial origin, where they occurred with the same morphology and mineral relations.

6.7.3.2. Vial 6 (Quartz seed, culture medium, SRB, $MgSO_4$ and organic carbon ⟶ halite, dolomite, montmorillonite, hydro-glauberite and mixed chloride precipitate)

Significant quantities of precipitate were observed in this vial shortly after injection of magnesium sulphate (in concentrated seawater) and organic matter at the end of week 8. An initial drop in sulphate concentration to <500mg/l during acclimatization of the bacteria was followed by a more rapid consumption of sulphate once the additional components were in place. Almost 90% of the added sulphate was consumed within 3-4 weeks.

The overall appearance of the sediment from this vial (Fig.6.8) shows numerous large quartz grains (Appendix 7, spectrum 7) up to 200μm across with various precipitates on their surfaces, and a scattering of sediment between. Figure 6.8b is a close up of one of these quartz grains. Two distinct precipitates can be seen. The smooth cubic crystals are halite (Appendix 7, spectrum 8) whilst the clumps of micron sized sub-spherular material are a Ca-Mg carbonate (Appendix 7, spectrum 9). Figure 6.8c is an enlargement of the centre of Figure 6.8b showing the spherules in more detail. A little amalgamation of the spherules can be seen in this area with some of the multi-spherule crystals beginning to exhibit a smooth appearance. The chemical composition cannot be established accurately as these gold-coated stubs only allow qualitative rather than quantitative analysis, but the spectra (Appendix 7,

spectra 9 and 10) appear to show some magnesium enrichment. XRD analysis (Fig. 6.7) indicates the presence of poorly ordered dolomite.

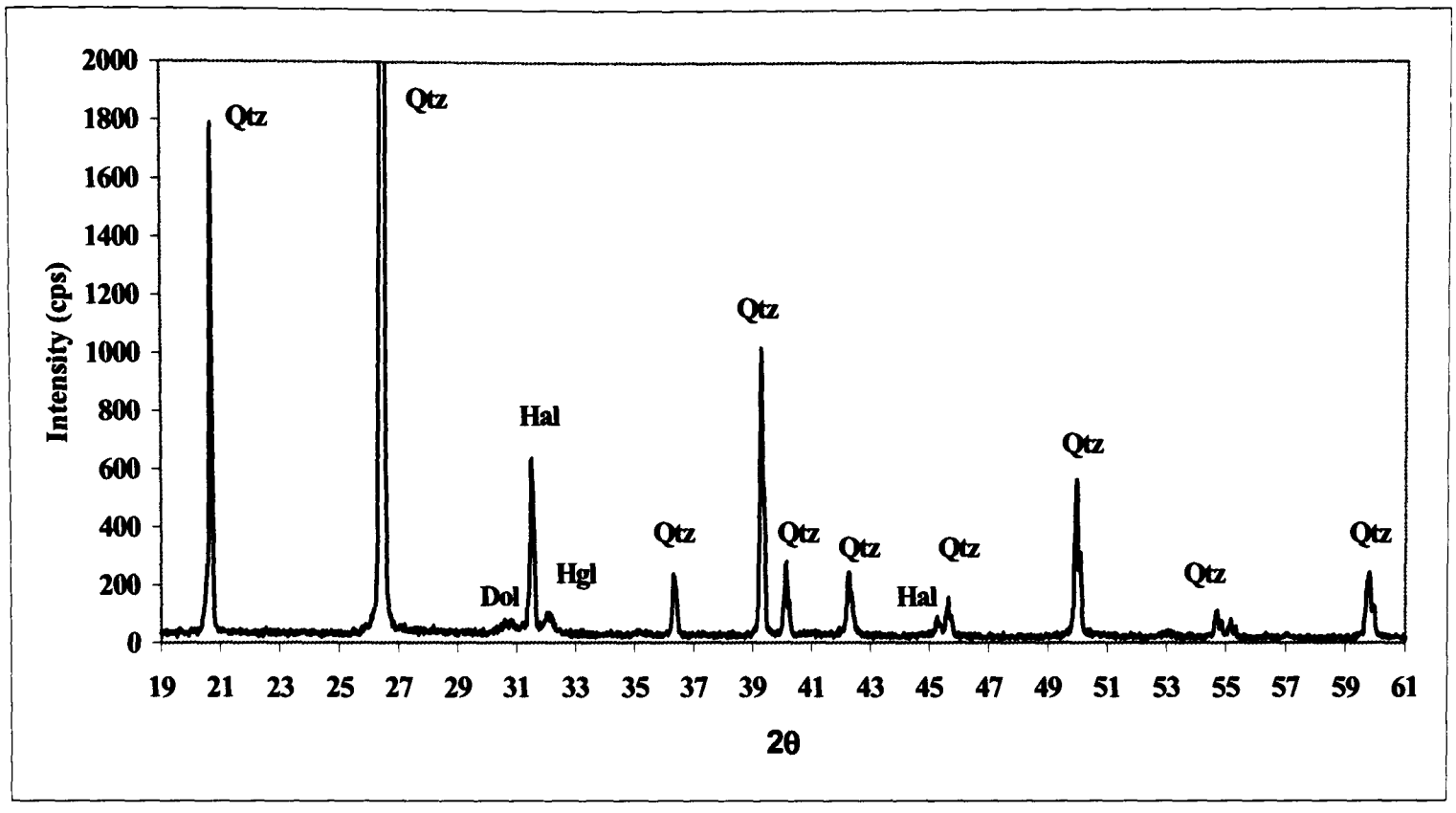
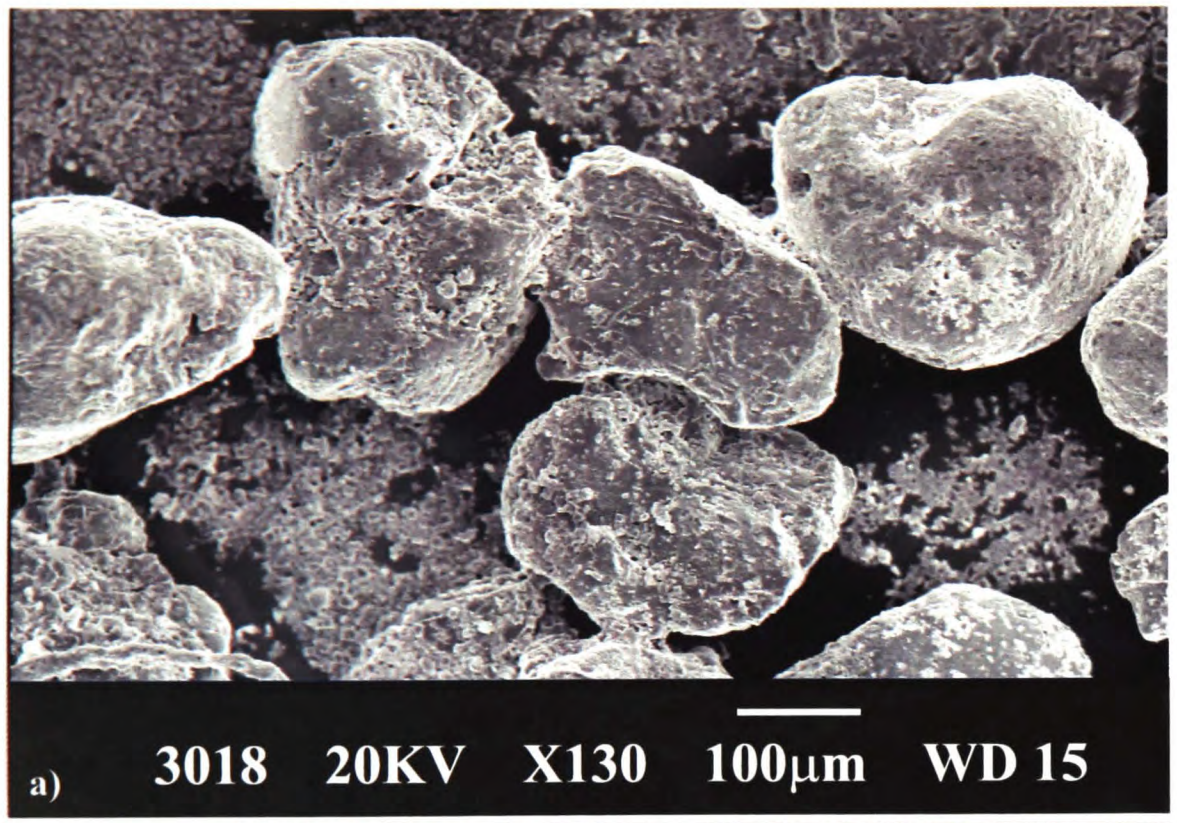
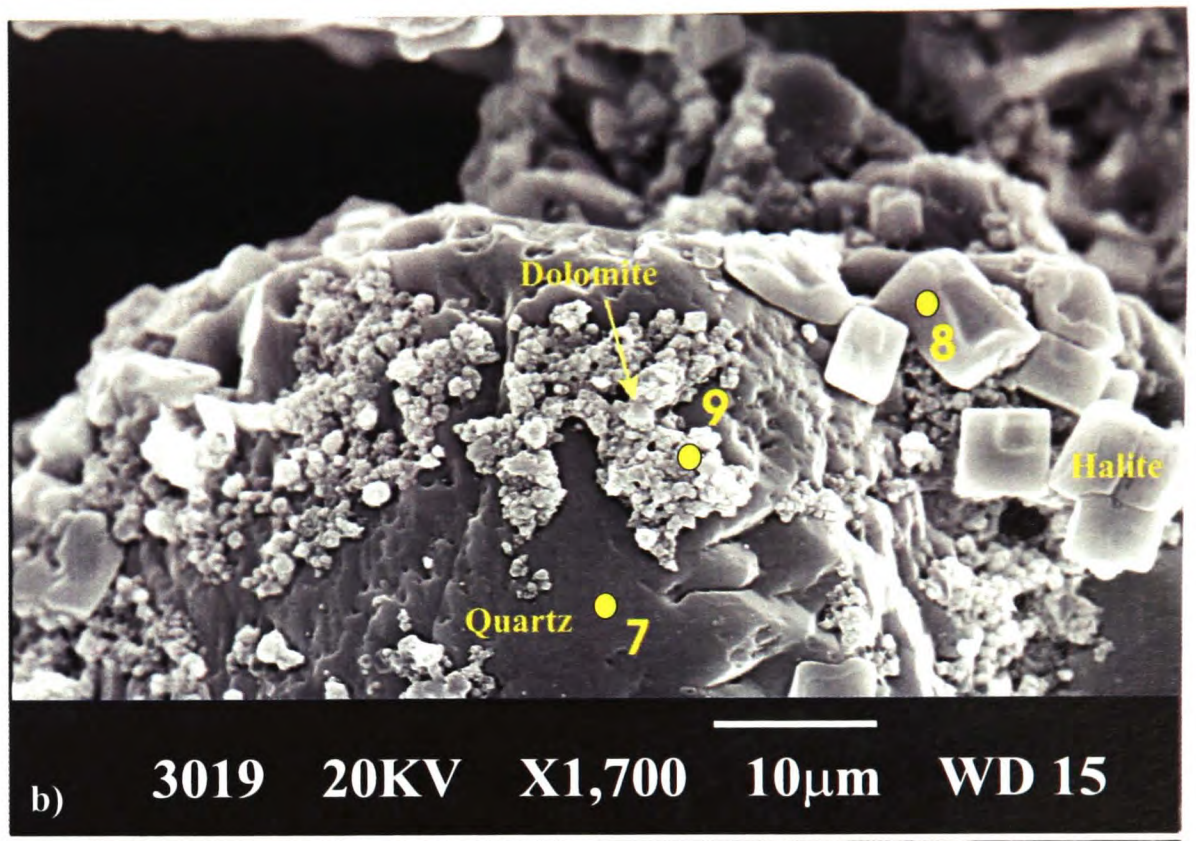


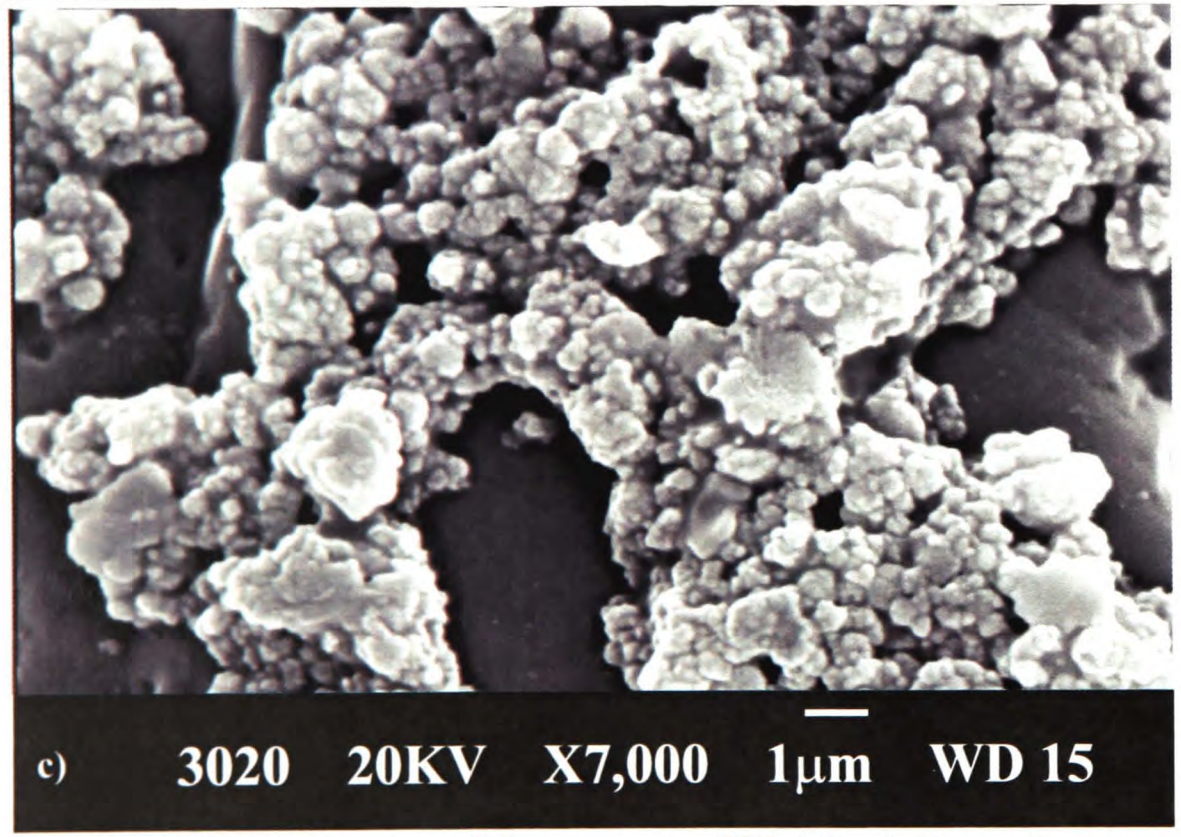
Figure 6.7. X-Ray diffractogram of sediment extracted from Vial 6. Note dolomite peak.

The quartz grains are unaltered and the halite appears to be a later precipitate than the dolomite. Figure 6.8d shows how the dolomitic material clusters around favourable growth sites on the quartz grains with very little precipitation over the rest of the quartz grain, except for late halite precipitates (centre right and top). Here, as in many other places, spectral analysis of the carbonate is hampered by background counts from the quartz substrate (e.g. Appendix 7, spectrum 10).

Chlorides occur as large (>100μm) flat crystals with cubic symmetry, over much of the area between quartz grains or as rapidly formed hopper crystals with cubic outlines and almost hollow centres. These are not solely NaCl as they have Mg and Ca rich areas (Appendix 7, spectrum 11). Much of the groundmass appears to be carbonate rich in nature with a granular appearance. X-ray analysis reveals much of this material to be dolomitic spherules cemented by late stage chlorides (see Figs 6.8 f+g). Some quartz grains have very tiny elliptical bodies on them, too small for X-ray analysis and may be the remains of bacteria (left side of Fig. 6.8e). Other rare mineral precipitates are shown in Figures 6.8 f+g. In Figure 6.8f, very rare brick-shaped calcian sulphates (Appendix 7, spectrum 13), approximately 10μm in length, sometimes also containing Na (XRD analysis (Fig. 6.7), imply hydro-







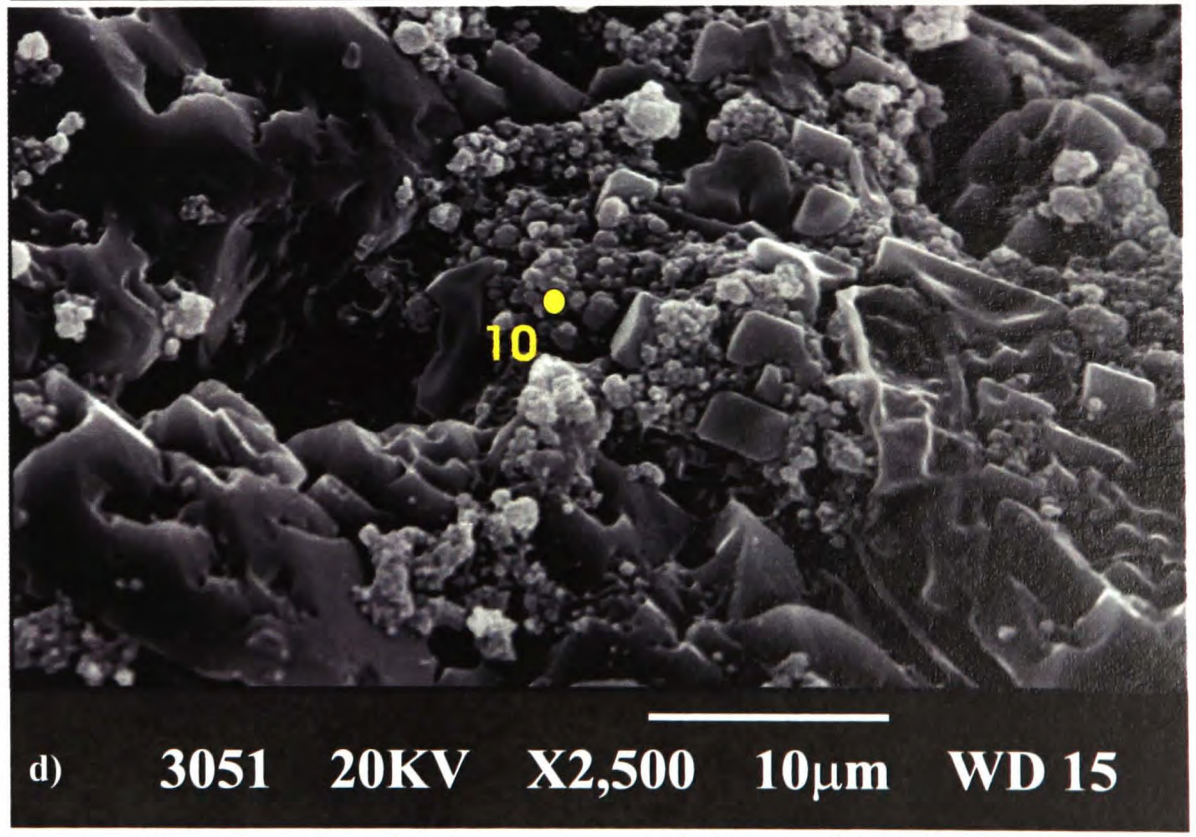
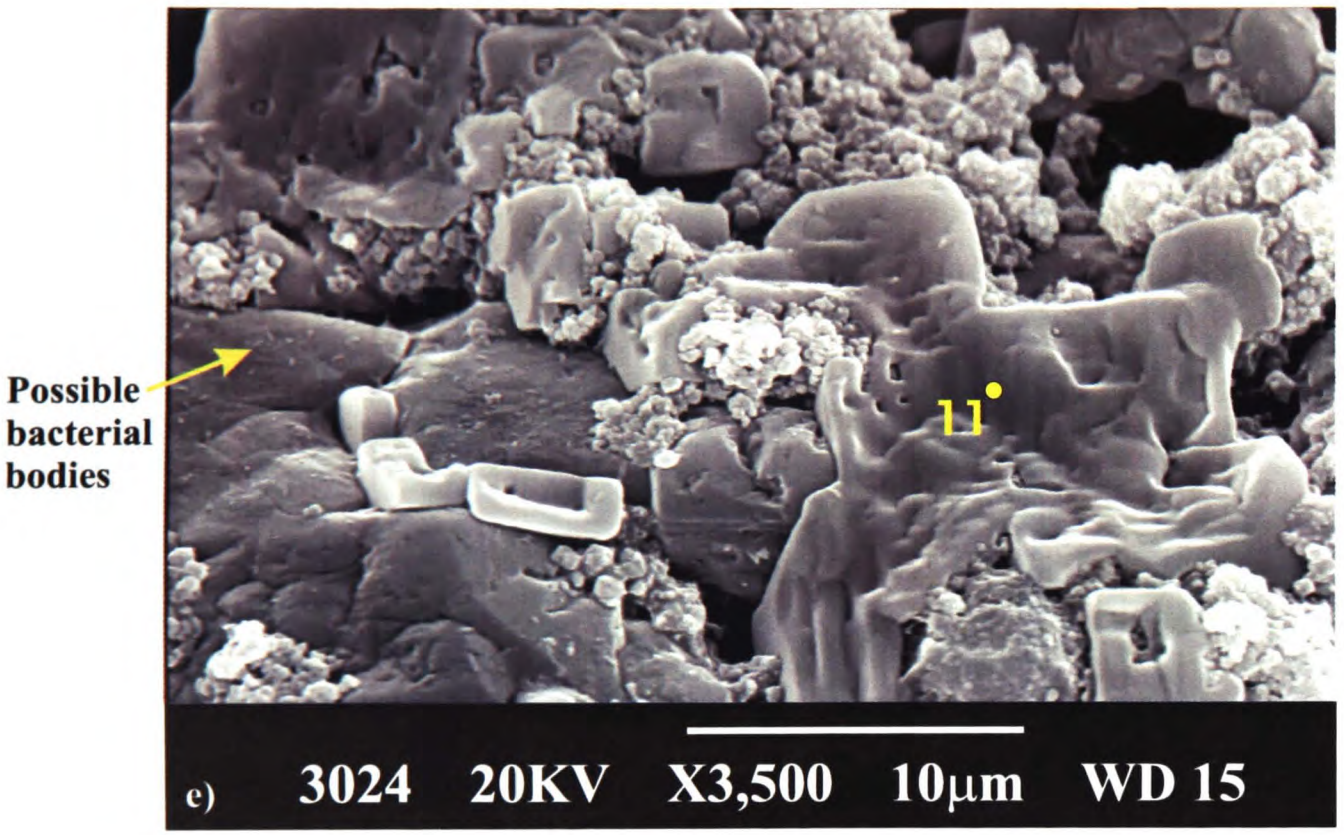
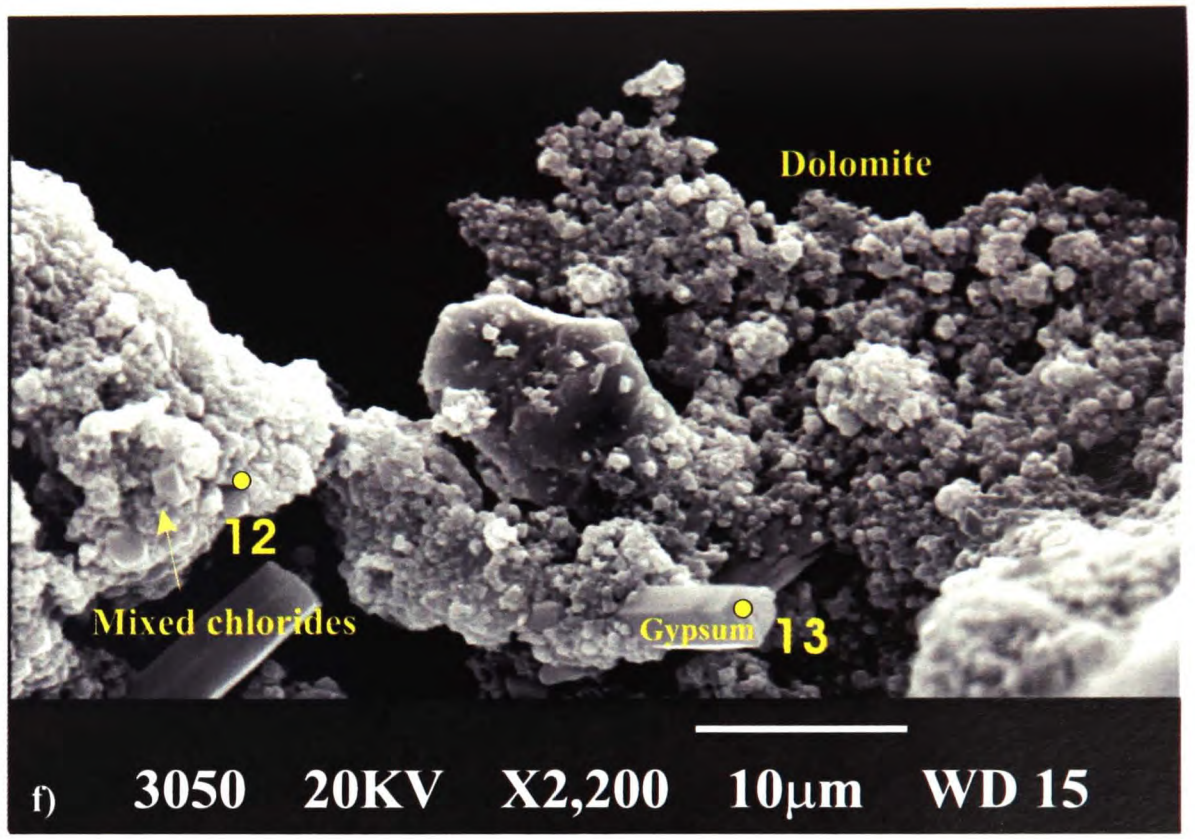


Figure 6.8. SEM images of the contents of Vial 6. a) General appearance of the quartz mineral seed and subsequent precipitates. b) Halite and dolomite precipitate on quartz grain. c) Close up of centre of (b). d) Clustering of the dolomite precipitate at favourable nucleation sites. Numbers refer to the atomic spectra in Appendix 7.





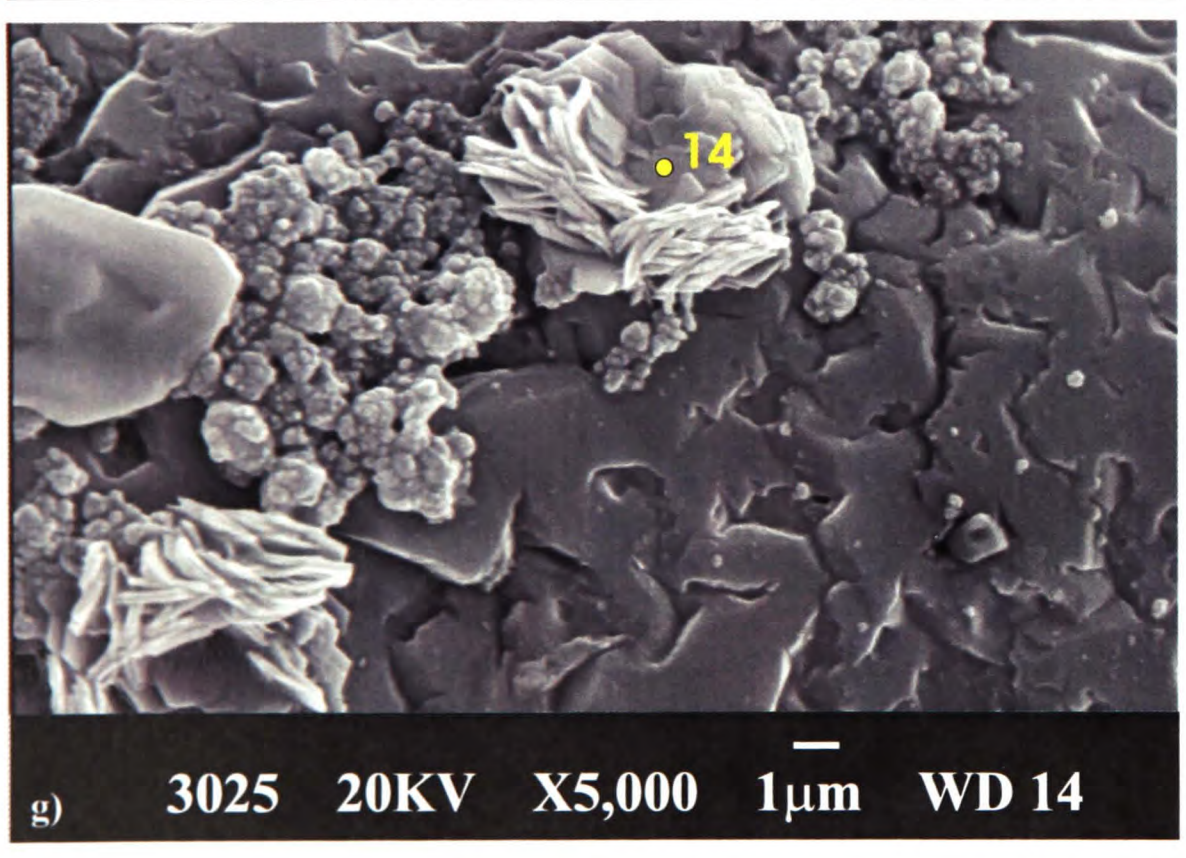


Figure 6.8 (continued). SEM images of the sediment from Vial 6.

e) Possible bacterial bodies on the quartz grain, centre left of picture.

f) Rare gypsum crystal in association with dolomite and various chloride precipitates.

g) $(KMg)Cl_2$ plates with rose head morphology.

Numbers refer to the atomic spectra in Appendix 7.

glauberite) appear in close proximity to dolomite. This could suggest that hydro-glauberite precipitation further reduces sulphate concentrations, creating conditions even more favourable for dolomite precipitation. Mixed chlorides are also common (Appendix 7, spectrum 12). A particularly noticeable chloride is the rose-shaped potassium magnesium chloride (Appendix 7, spectrum 14) which appears in close association with dolomite on the surface of quartz grains (Fig. 6.8g).

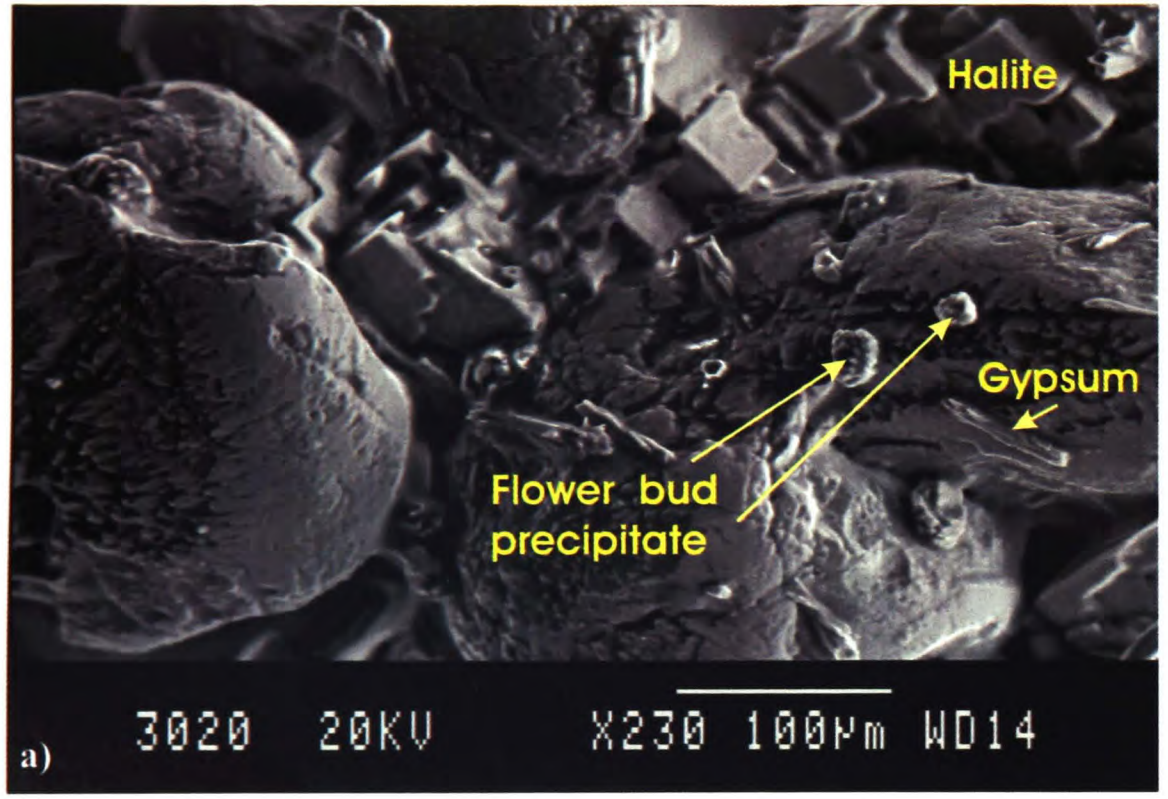
Abundant halite can be attributed to the large amount of NaCl in both the culture media and the injected concentrated seawater. The lack of gypsum in comparison to halite is attributed to efficient removal of most sulphate ions by the sulphate-reducing bacteria, as shown by measurements of sulphate concentrations in the liquid prior to opening the vial. Mixed chlorides are likewise due to high ionic concentrations in the solution.

The formation of dolomite is attributed to the action of the bacteria in the presence of organic matter, since in vials without organic matter little or no dolomite has been found (e.g. Vials 7, 8, 10 and 15), and in vials lacking both bacteria and organic matter (Vial 1) only chemical precipitates of chlorides, sulphates and clays were found.

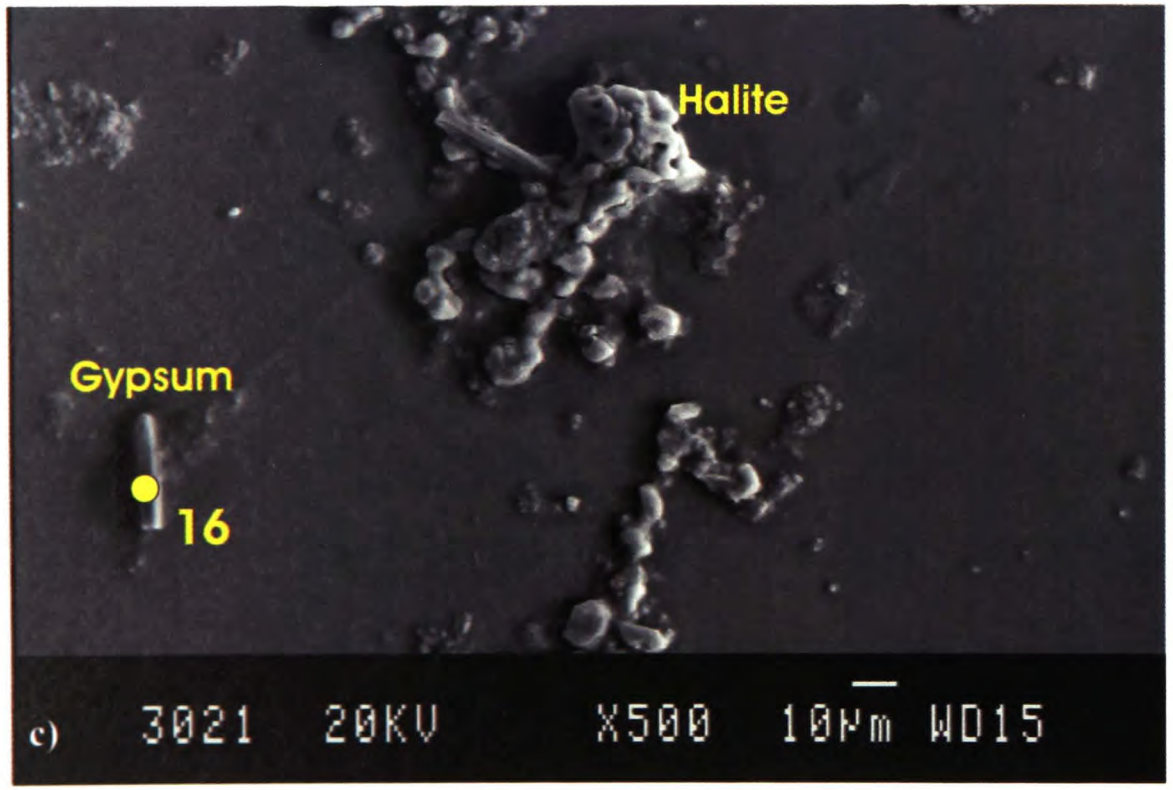
6.7.3.3. Vial 7 (Quartz seed, culture medium, SRB and $MgSO_4$ ⟶ halite, hydro-magnesite and smectite precipitate)

The initial components of this vial were a quartz mineral seed, culture medium and bacteria from Mini Dolomite Lake. The vial recorded a drop in sulphate concentration over the first 8 weeks (Fig. 6.4). Two subsequent injections of $MgSO_4$ were made, one at the end of week 8 and another during week 10. Sulphate ion concentration dropped from a maximum of 20,000mg/l to 6,800mg/l in just over a week, a drop of 65%.

The sediment extracted from Vial 7 is shown in Figure 6.9. Quartz grains are cemented by abundant halite (Fig. 6.9a) and have two types of precipitate on their surfaces. The first of these has flower-bud morphology at low magnification (Fig. 6.9a) and smooth, blocky crystal faces (Fig. 6.9b), possibly being composed of two or more intergrown minerals and apparently nucleated upon indentations in the quartz grain. Neither XRD nor atomic spectra (Appendix 7, spectrum 15) were particularly helpful in resolving the mineralogy.







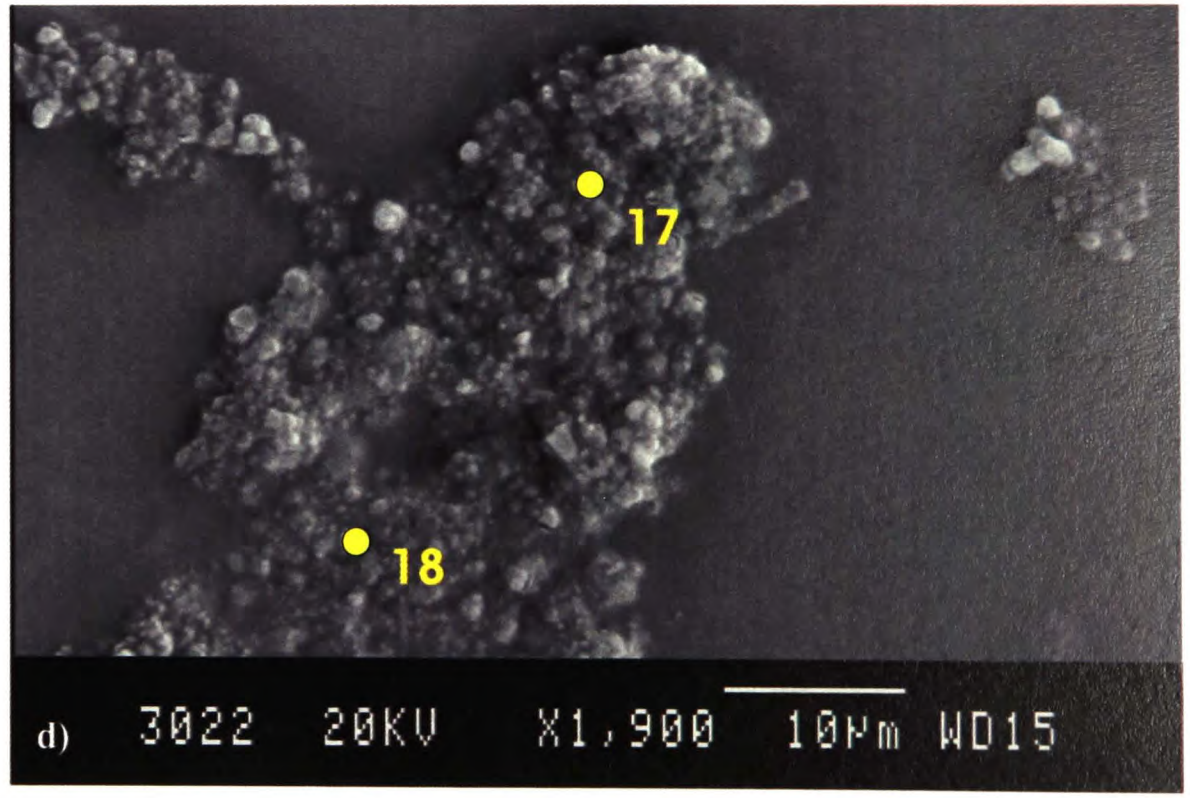


Figure 6.9. SEM images of the sediment extracted from Vial 7. a) Quartz grains cemented by halite with precipitates of gypsum and a mixed sulphate-chloride. b) Close up of mixed sulphate-chloride on quartz grain. c) The precipitate away from quartz grains is dominated by halite and gypsum. d) Bacteria-shaped objects of variable mineralogy (see text for details). Numbers refer to atomic spectra in Appendix 7.

Inter-grown chloride and sulphate seems most likely, based upon observations in other vials. The second type of precipitate on the quartz grains is stick- or rope-like. These are gypsum crystals (Appendix 7, spectrum 16) but they are much more fibrous than seen in any other vials. Precipitation over the rest of the quartz grain surface is absent, in contrast to Vials 6, 15 and 21 where sub-micron objects are common on the substrate. Free lying sediment is dominated by halite with accessory gypsum (Fig 6.9c) or, less commonly, by micron sized granular structures which resemble bacterial precipitate observed in Vial 6 and 21. Atomic spectra (Appendix 7, spectra 17-18) are ambiguous and the precipitate could combine a mixture of clays, chlorides and carbonates. The XRD analysis (Fig. A7.2a) of this vial shows the presence of smectitic clays and hydro-magnesite. Hence, the precipitate is inferred to be a mixture of these two minerals plus a small amount of a chloride.

6.7.3.4. Vial 8 (Quartz seed, culture medium, SRB, $MgSO_4$ and brine ⟶ gypsum and sauconite precipitate)

This vial, having initial components of quartz mineral seed, culture medium and bacteria from Milne Lake, recorded a drop in sulphate concentration from 1650mg/l to <500mg/l after 8 weeks. During week 9 concentrated seawater and extra magnesium sulphate were introduced to stimulate bacterial growth and mimic lake conditions. A substantial decrease in sulphate concentration was observed between week 9 and week 16, with over 60% of the sulphate being consumed.

The sediment extracted from Vial 8 after week 16 is shown under SEM in Figure 6.10. Many of the quartz grains are cemented by sub-cubic halite precipitates. This halite is attributed to the increase in ionic concentrations achieved by adding concentrated seawater. A little of the cementing agent is magnesium calcium chloride (Fig. 6.10a) (Appendix 7, spectrum 19). Brick-shaped bright white gypsum (Appendix 7, spectrum 20) crystals are commonly hexagonal in cross section (Figs 6.10a+b), reflecting the monoclinic structure, although there is some heterogeneity and the appearance of potassium ions in places. These crystal faces are well formed but have a patchy spotted appearance. On close examination many of the $MgCl_2$ and NaCl crystals also have a spotted appearance.

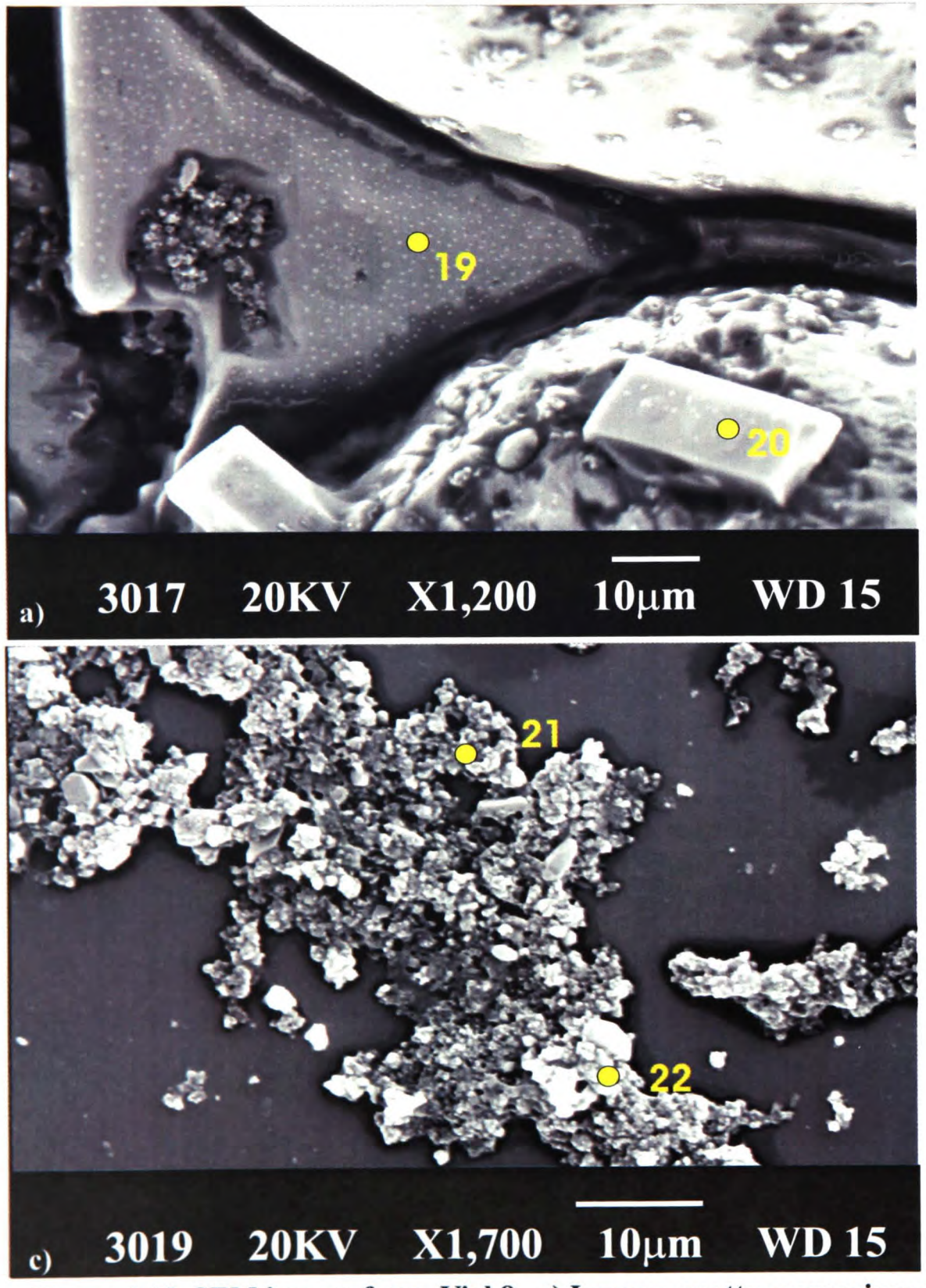


Figure 6.10. SEM images from Vial 8. a) Impure, spotty magnesium chloride cementing quartz and brick like gypsum crystals. b) Gypsum in cross section. c) Clumps of chloride and clay precipitates. d) Well formed plates of $KMgCl_2$ associated with largely unidentifiable precipitates. Numbers refer to the atomic spectra in Appendix 7.

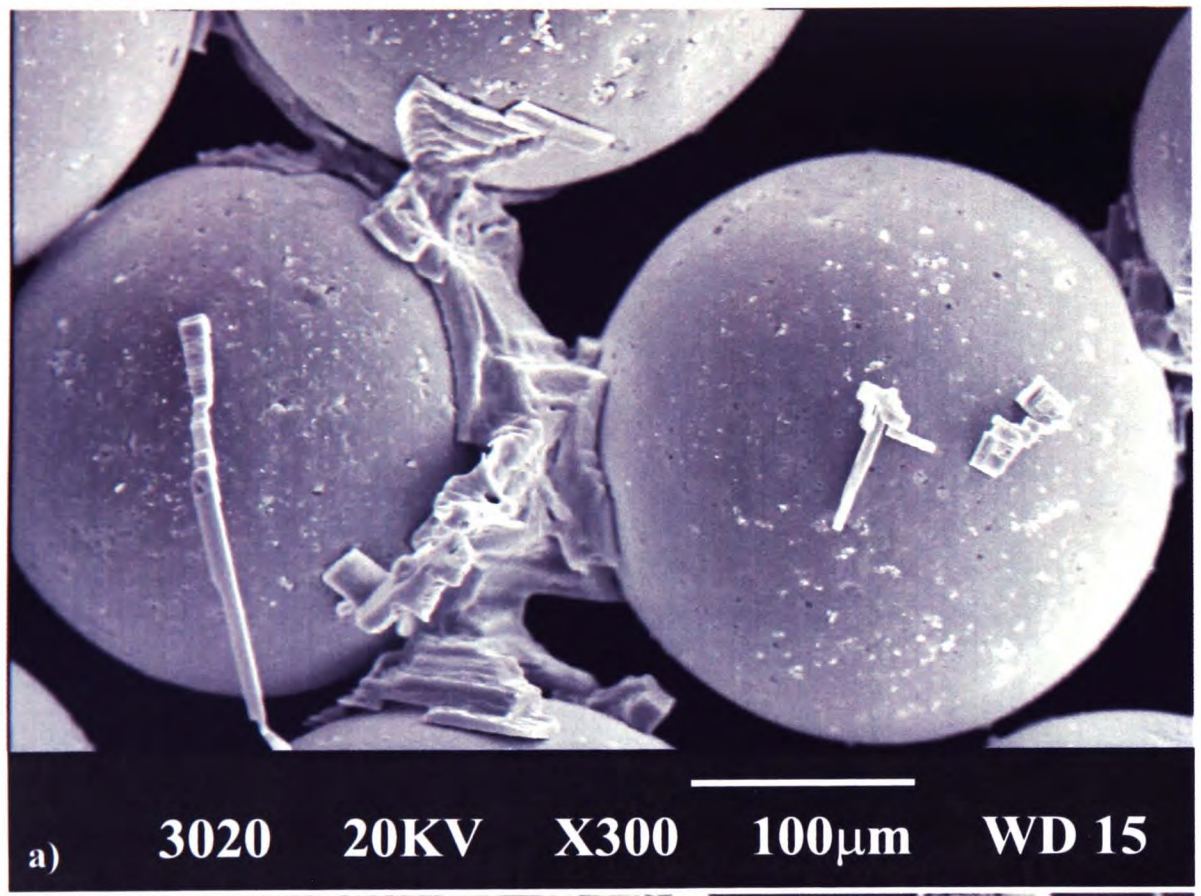
Precipitate is also found on the cover slip (Fig. 6.10c). This is heterogeneous, granular in appearance and associated with hexagons of gypsum. Although it looks similar to clumps of dolomite spherules observed in the lake sediments, the mineralogy is different. XRD analysis (Fig. A7.2b) shows not dolomite but chlorides and clays (Appendix 7, spectra 21-22). The exact mineralogy is indeterminable from the atomic spectra, but XRD (Fig. A7.2b) suggests sauconite ($Na_{0.3}Zn_3Si_3AlO_{10}(OH)_2.4(H_2O)$). Well-formed plates of potassium magnesium chloride (Appendix 7, spectrum 23) are also common (Fig. 6.10d). Precipitation on quartz grains is rare except for small clay minerals (Fig. 6.10b).

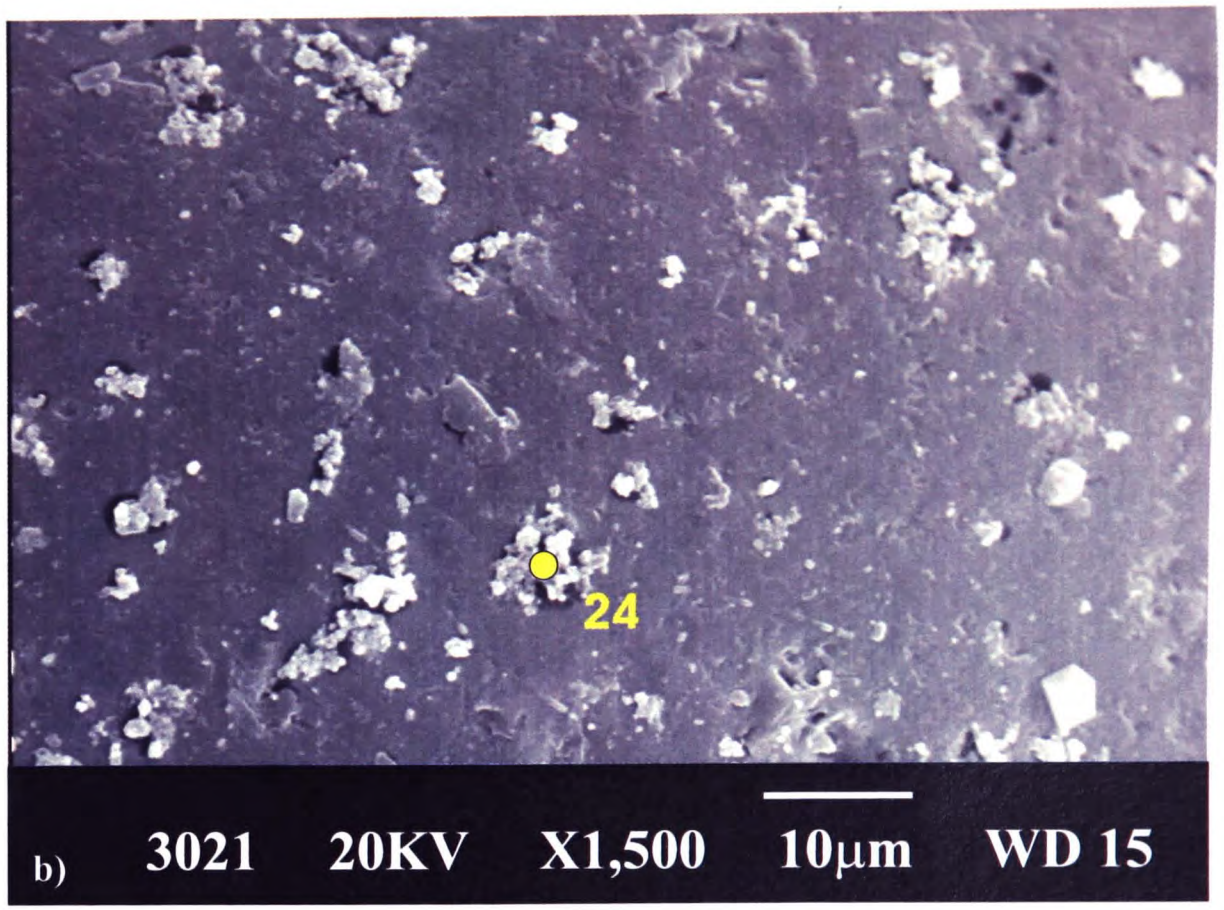
The precipitation of gypsum can be attributed to the addition of magnesium sulphate to stimulate bacterial growth. Although bacteria used much of this sulphate, as much as 40% remained for precipitation as gypsum. The abundance of magnesium chlorides can also be explained by the addition of magnesium sulphate to the vial. Since the size and shape of the spots are of bacterial size the spotted appearance of many of the crystals may be attributed to bacterial growth. It is proposed that, despite the addition of bacteria, a deficiency in supply of metabolisable organic matter prevented the bacteria reducing sulphate concentrations and elevating carbonate alkalinity to the extent where dolomite could precipitate.

6.7.3.5. Vial 10 (Glass bead seed, culture medium, SRB ⟶ halite, clays, chlorides)

The initial contents of this vial were a glass bead mineral seed, culture medium and bacteria from Milne Lake. Unlike many of the vials, there were no additives injected after week 8 to stimulate bacterial growth or provide extra ions. Sulphate concentration decreased steadily from 1650mg/l until undetectable after week 12.

The sediment extracted from Vial 10 is shown in Figure 6.11. At low magnification, the spherical glass beads (c. 300μm in diameter) are occasionally cemented by halite (Fig.6.11a). They have a slightly speckled appearance and, on closer examination, have numerous small crystals growing upon them (Fig. 6.11b). Some clustering is evident, similar to that commonly seen when SRB are observed under the microscope. The exact mineralogy of the clustered precipitates is difficult to ascertain due to their size but the atomic spectrum (Appendix 7, spectrum 24) suggests clay minerals. Bulk powder XRD analysis (Fig. A7.3a)





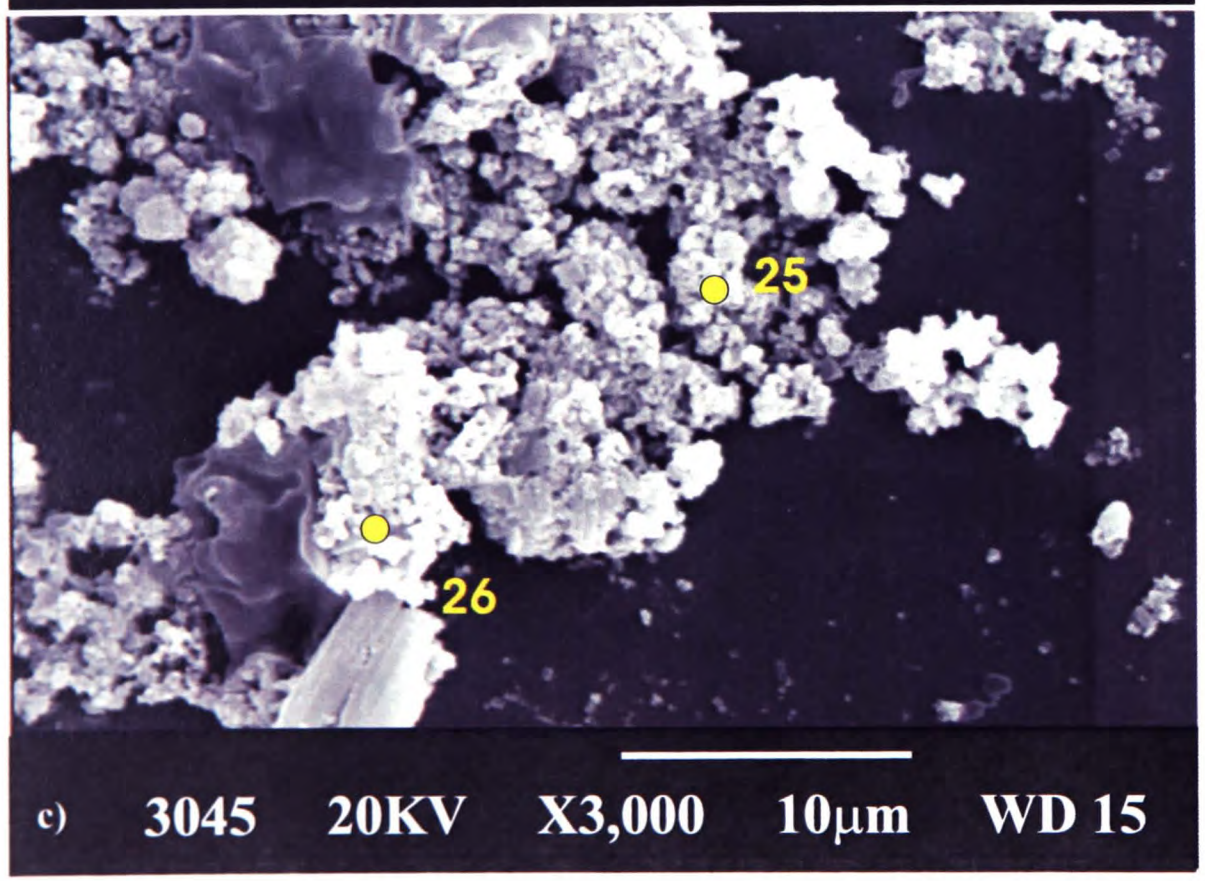


Figure 6.11. SEM images from Vial 10.

a) Glass bead mineral seed cemented by halite.

b) Speckly nature of the glass beads with small clusters of precipitate, possibly bacterially induced.

c) Clusters of precipitate not associated with the glass beads. Suspected mineralogy includes chlorides and clays.

Numbers refer to the atomic spectra in Appendix 7.

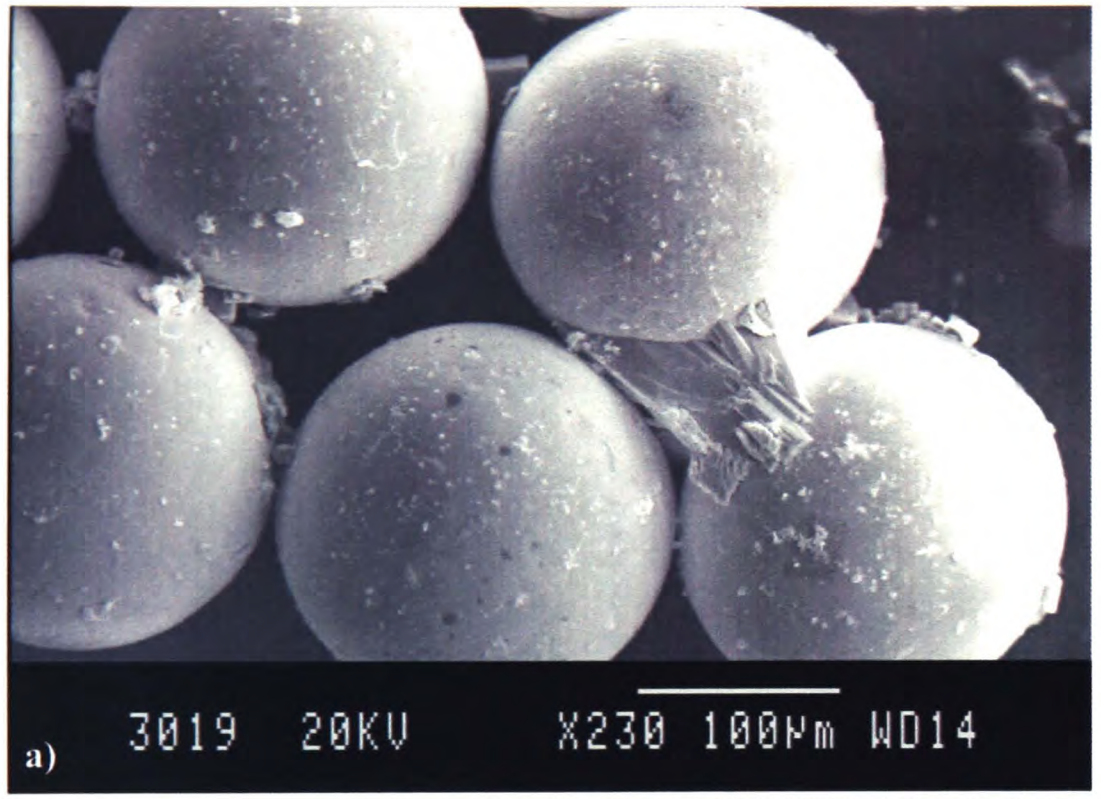
failed to identify the mineralogy owing to interference from the amorphous glass beads. There are also some clusters of precipitate away from the glass beads (Fig. 6.11c). Here, smooth halite crystals are common and granular areas of precipitate have a heterogenous mineralogy, with both chlorides and clays inferred (Appendix 7, spectra 25-26). The precise mineralogy was unobtainable since atomic spectra from gold-coated stubs only gives the elements present, not their relative abundances. Since the majority of precipitate is similar to that in control Vial 1, it can be interpreted as having formed inorganically. Some of the morphology suggests contribution from bacteria, possibly as nucleation sites when alive or after sulphate was consumed and the bacteria ceased metabolising.

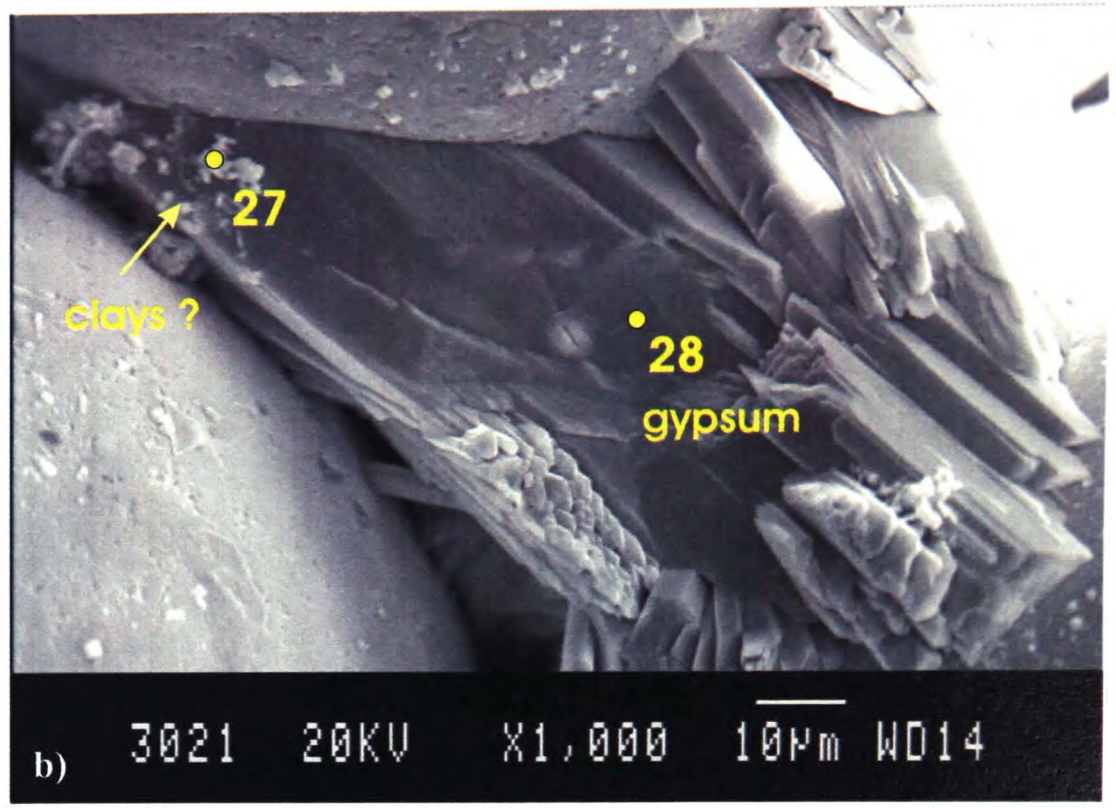
6.7.3.6. Vial 15 (Glass bead seed, culture medium, SRB, $MgSO_4$ ⟶ halite, gypsum, clay and chloride precipitates)

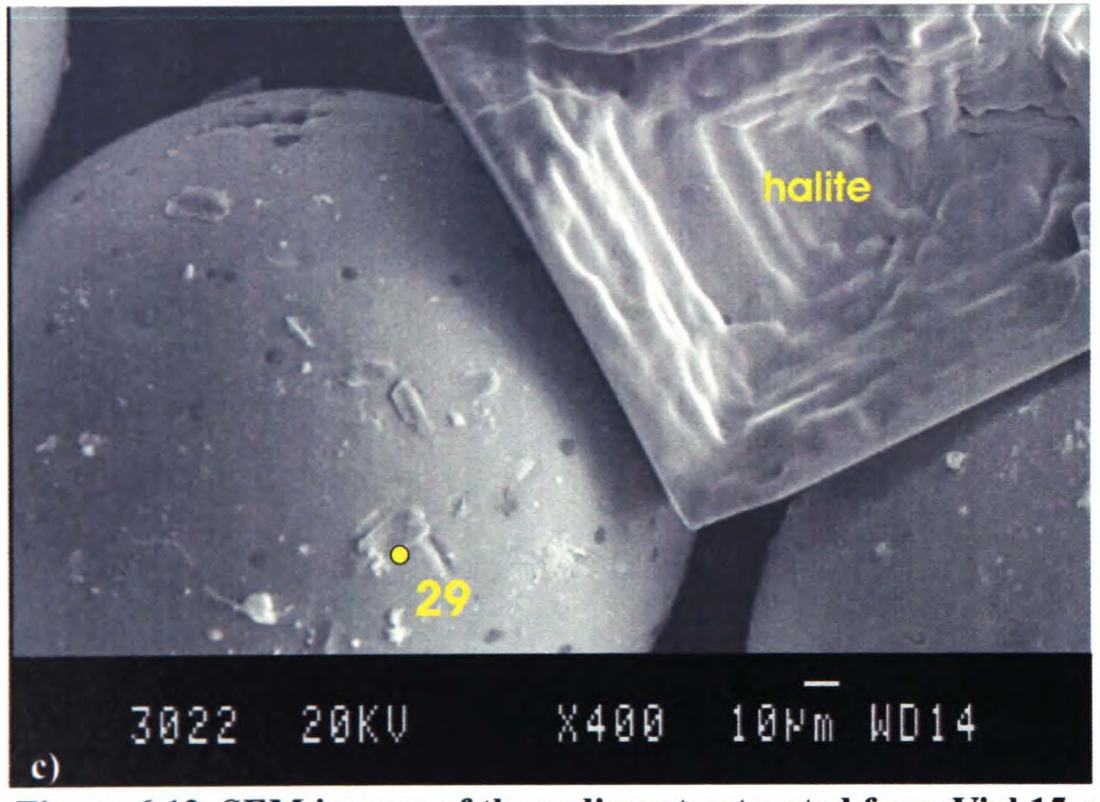
Initially this vial contained a glass bead mineral seed, culture medium and bacteria from McFaiden Lake. As with the other vials containing bacteria the concentration of sulphate dropped from 1650mg/l to <500mg/l after week 8 consistent with bacterial metabolism. This vial was then used to monitor the change in pH after addition of $MgSO_4$, firstly at the beginning of week 9 and then again during week 10. Sulphate concentration dropped from a maximum of 25000mg/l to 6,900mg/l (a 72% drop) in a period of just two weeks.

Figure 6.12 shows SEM images of the sediment extracted from Vial 15 at the end of week 12. A small number of the glass beads are cemented by gypsum (Fig. 6.12a+b, Appendix 7, spectrum 28) whilst one large halite crystal (~200μm across) joins three of the glass beads (Fig. 6.12c). Small (1-5μm) clay precipitates are common on and adjacent to the glass beads (Appendix 7, spectrum 27). A further precipitate on the surface of the glass beads comprises 10-20μm sub-rectangular grains. Their atomic spectrum mainly contains magnesium, silicon and chloride (Appendix 7, spectrum 29) and these are interpreted as $MgCl_2$ crystals with some interference from the background SiO_2 counts of the glass beads.

The most interesting component of this vial is observed at high magnification (Fig. 6.12d). Here are seen hundreds of rounded sub-micron objects, usually occurring singly but occasionally grouped together. These are too small for accurate determination of any mineralogy though their atomic spectra are all nearly identical (Appendix 7, spectrum 30). It is difficult to deduce whether these spectra are merely an artefact of the glass beads on which







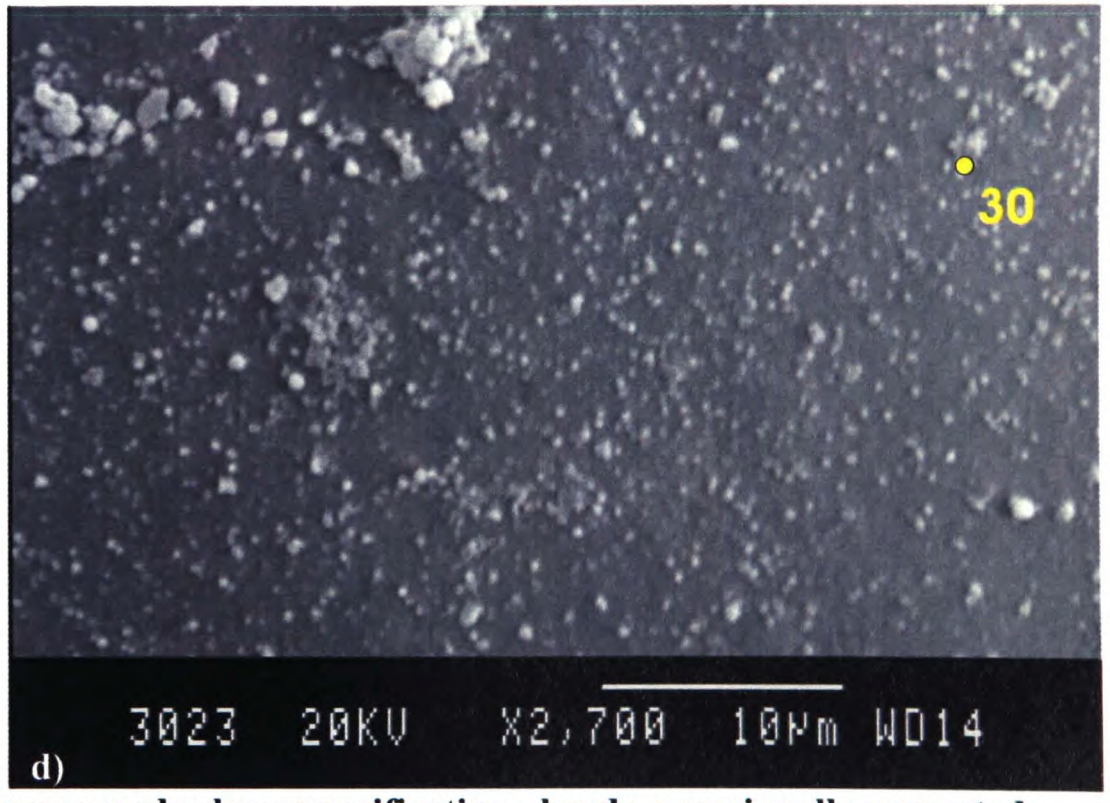


Figure 6.12. SEM images of the sediment extracted from Vial 15. a) Appearance under low magnification - beads, occasionally cemented, with obvious surface precipitate. b) Close up of the two beads on the right of a), cementing agent is gypsum with clays common on and around the beads. c) Large halite crystal growing in the space between three glass beads. Surface of bead has several Mg-rich precipitates. (dark grey spots are an artefact of the SEM. d) Large amount of sub-micron objects on the surface of a glass bead (see text for details). Number refer to spectra in Appendix 7.

they sit. The objects resemble bacteria in size and shape as well as particles of Mg-Ca carbonate observed in other vials (cf. Fig. 6.8). Powder XRD analysis of this vial (Fig. 7.3b) only picks up the amorphous nature of the glass beads with a couple of halite peaks. Other minerals may be present but the peaks are masked.

6.7.3.7. Vial 21 (Aragonite seed, culture medium, SRB, $MgSO_4$, organic matter ⟶ dolomite, halite and other chloride precipitates)

This vial had aragonite grains as a mineral seed, plus culture medium and bacteria from Mini Dolomite Lake. By week 8 sulphate concentration had, once again, fallen below 500mg/l indicating bacterial metabolism. Subsequently, extra magnesium sulphate and a quantity of organic matter (washed and crushed *Ruppia* grass) were injected into the vial before it was left for a further two months. 80% of the sulphate was consumed by this time and the sediment extracted is shown in Figure 6.13.

An immediate observation at low magnification is the quantity of precipitate (Fig. 6.13a). The cover slip is largely covered with precipitate and the majority of the initial aragonite grains have partial or full cover. The initial aragonite seed grains were of many different sizes and shapes ranging from only a few microns to over 100μm, as identified by both X-ray analysis (Fig. 6.14) and atomic spectra (Appendix 7, spectrum 31). A second carbonate mineral is also observed (centre right of Figure 6.13b), distinguished from the larger aragonite grains by its spherular/granular morphology of many sub-micron spherical grains. This is identified as dolomite both by XRD (Fig. 6.14) and atomic spectra (Appendix 7, spectra 32, 34 and 36). Analysis of the atomic peak heights shows that the dolomite is of variable composition (compare spectra 32, 34 and 36) but no further conclusions may be drawn since only qualitative analysis was attempted. The aragonite grains are largely unaltered and the dolomite is inferred to be precipitating around and between the aragonite grains rather than replacing them. The abundance of mineral surfaces, however, may aid the nucleation of dolomite crystals. Chlorides are again abundant. Halite dominates but sodium calcium chloride (Appendix 7, spectrum 33) is also common (top left of Figure 6.13b).

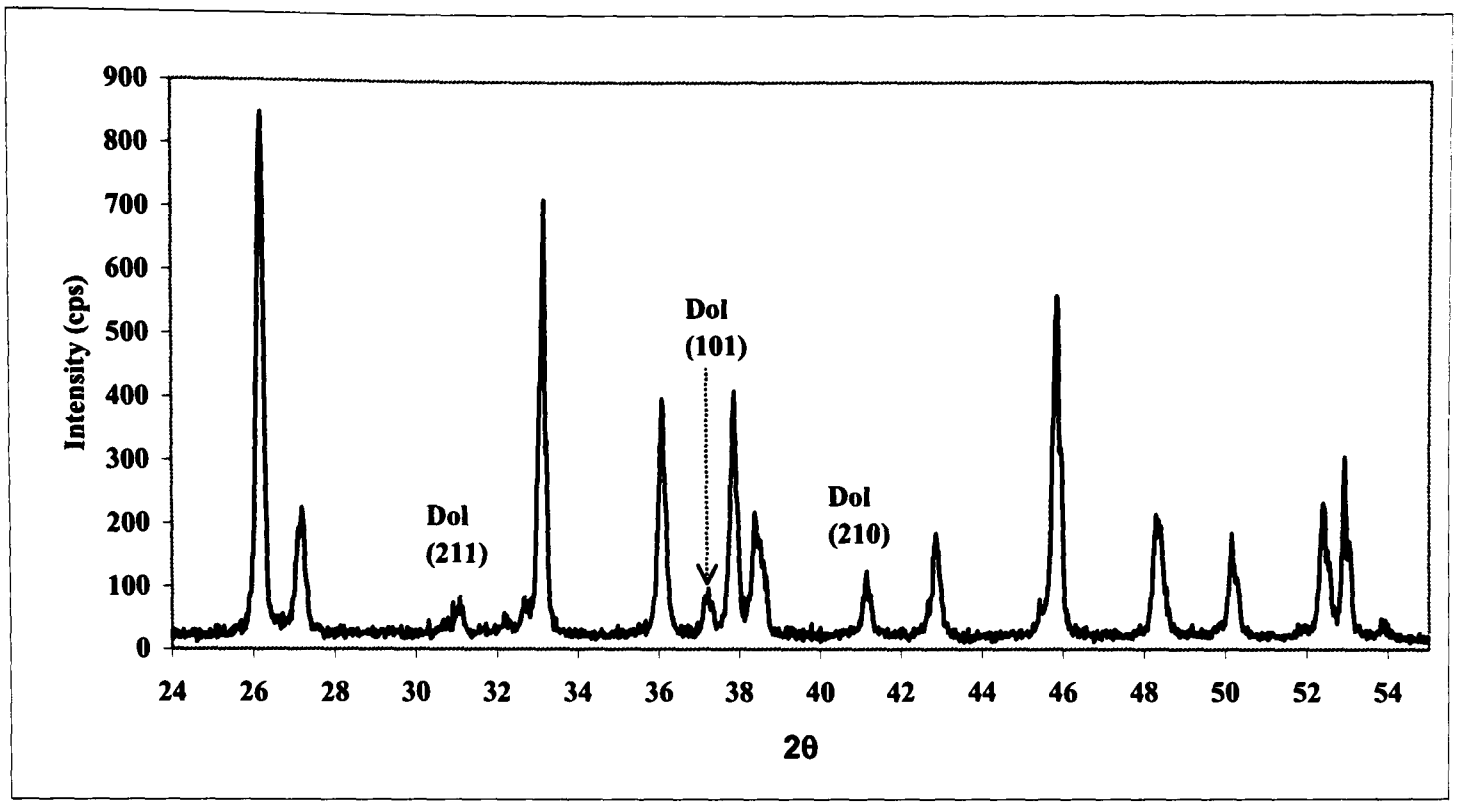
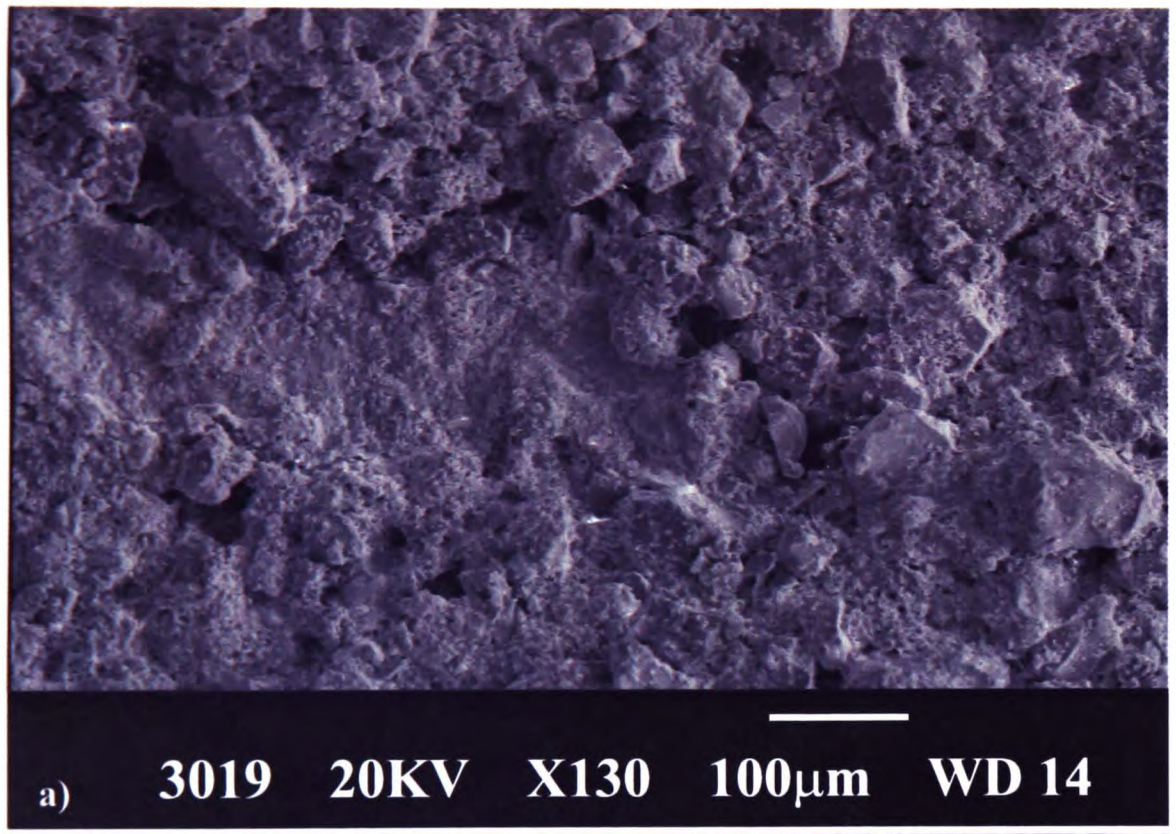
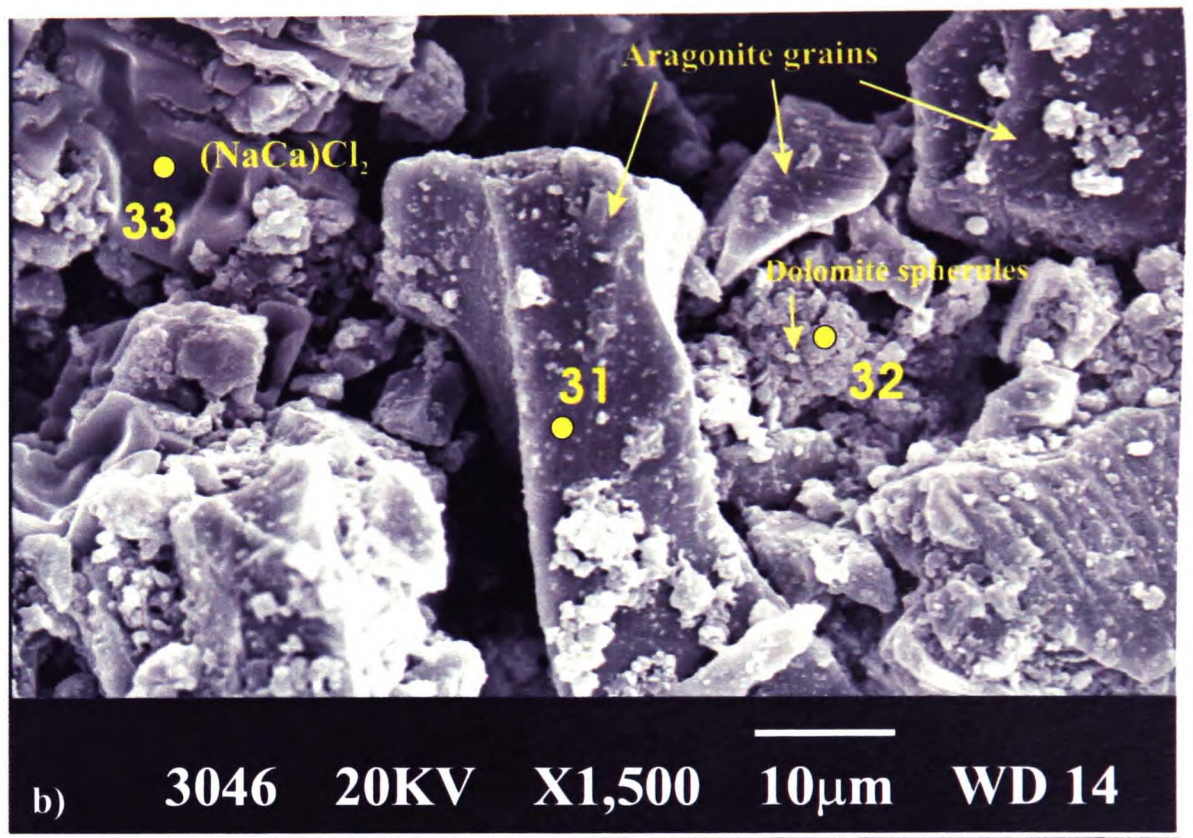
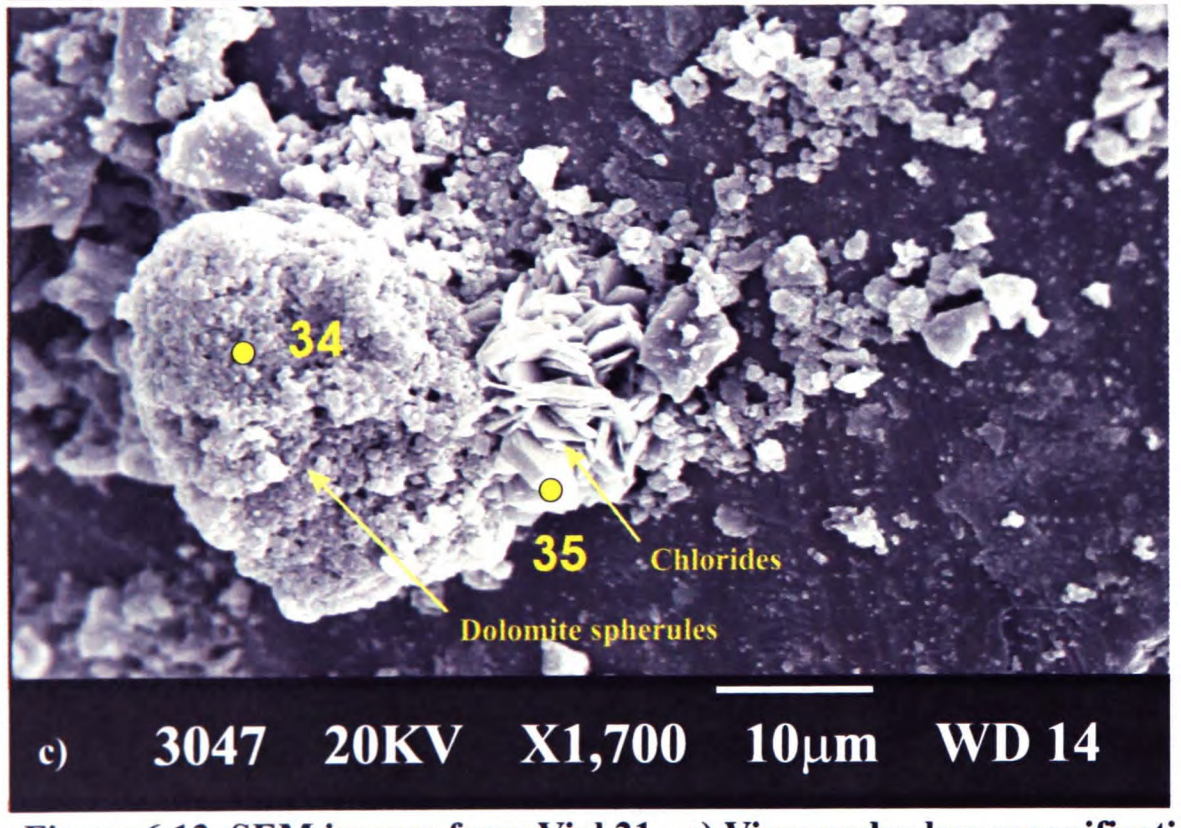


Figure 6.14. X-Ray diffractogram of the sediment extracted from Vial 21. Note dolomite peaks at 2θ = 30.98, 37.5 and 41.2. Remaining peaks are from aragonite mineral seed.

A third type of chloride has a lath/plate-like morphology similar to crystals seen in many other vials and proves to be a potassium- and calcium-rich chloride (Appendix 7, spectrum 35). Figure 6.13c shows this mineral in close association with a clump of dolomitic material and some small aragonite grains. Note that these are all positioned upon a large aragonite grain that still has a smooth, non-degraded surface. The occurrence of dolomite as clusters of spherules mirrors the clustering of bacteria observed under the microscope (cf. Fig. 6.2) while the good preservation of aragonite grains also suggests primary precipitation rather than replacement for the dolomite. Magnesium chlorides and/or sulphates are absent in this vial, suggesting that all the available magnesium was being channelled into the dolomite lattice. Figure 6.13d shows a mass of dolomite associated with evaporitic chlorides. Here the outlines of the spherulitic mass assume approximately straight edges, giving the appearance of a half rhomb. This implies reorganisation into rhomb-like morphology.







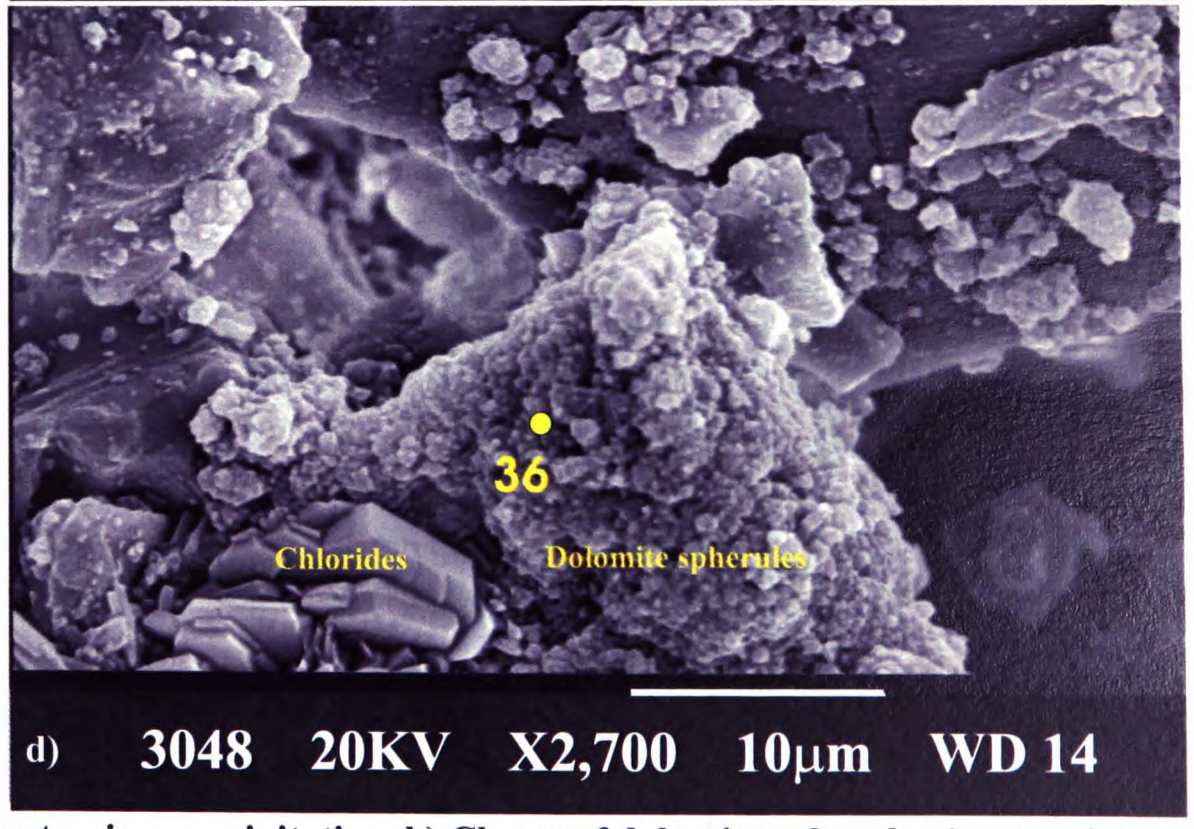


Figure 6.13. SEM images from Vial 21. a) View under low magnification showing extensive precipitation. b) Clump of dolomite spherules (centre right) adjacent to large aragonite grains. c) Aggregation of dolomite spherules associated with $(KCa)Cl_2$ growing on apparently non-degraded aragonite grain. d) Clump of dolomite spherules undergoing reorganisation into rhomb like morphology. Numbers refer to the atomic spectra in Appendix 7.

6.8. SUMMARY

Vial	Products (Determined by X-ray Diffraction)
1 (control)	(Quartz) Halite Smectite
6 (SRB, $MgSO_4$, C)	(Quartz) Halite Montmorillonite Hydroglauberite **Dolomite**
7 (SRB, $MgSO_4$)	(Quartz) Halite Hydromagnesite Smectite
8 (SRB, brine, $MgSO_4$)	(Quartz) Gypsum Sauconite
10 (SRB control)	(Amorphous glass beads) – no XRD peaks
15 (SRB, $MgSO_4$)	(Amorphous glass beads) Halite
21 (SRB, $MgSO_4$, C)	(Aragonite) Halite **Dolomite**

Table 6.9. Contents of the experimental vials as determined by X-ray diffraction. Minerals in brackets were already in the vials as the mineral seed.

NB: **Sauconite = $Na_{0.3}Zn_3Si_3AlO_{10}(OH)_2.4(H_2O)$**

Hydroglauberite = $Na_4Ca(SO_4)_3.2(H_2O)$

Hydromagnesite = $Mg_5(CO_3)_4(OH)_2.4(H_2O)$

- Culturing was carried out using a Postgate B medium (Postgate 1984). Estimations of the total number of bacteria and of the number of SRB were performed using 'acridine orange direct' counts and 'most probable number' counts respectively. A comparison of the two counts gave the approximate proportion of total bacteria that are SRB.
- Mean counts of SRB ranged from just over 1000 per cubic centimetre of sediment in Halite Lake to over 3.5 million/cm^3 in Mini Dolomite Lake. The counts from the dolomitic lakes are amongst the highest ever recorded using this method.
- AODC performed on three of the dolomitic lakes resulted in values of up to $3x10^9$ bacteria/cm^3. During AODC it was observed that the bacteria appear to cluster in favourable sites.
- A discussion of the inadequacies of the MPN counting technique include the underestimation of metabolically active SRB (Teske *et al.*, 1998) and the failure to account for viable but unculturable SRB (e.g. Binnerup *et al.*, 1993). It is concluded that a direct count might normally be expected to be some three orders of magnitude greater than an MPN count. Restricted variety of substrate and cell clumping may also reduce MPN counts.

- In this study, total counts are shown to be much less than three orders of magnitude greater than SRB counts, suggesting that SRB constitute an unnaturally large proportion of the bacterial population. Since field evidence supports this, it is proposed that SRB are present in large enough numbers to significantly modify the chemical conditions in several Coorong distal ephemeral lakes, consistent with the provision of favourable sites for dolomite precipitation.
- Bacterial detection and identification was performed using the 16SrRNA method of Schwieger and Tebbe (1998) with subsequent classification using GenBank. Problems were encountered owing to the length of storage of the bacteria resulting in poorly preserved bacterial DNA. Only four DNA products were identified with between 91% and 98% similarity to organisms stored in the GenBank database.
- A series of experimental vials were set up to test whether dolomite could be precipitated, in the laboratory, under conditions similar to those of the Coorong lakes. Each vial was subtly different to the next attempting to create the ideal conditions for dolomite precipitation. Sulphate concentration and pH were monitored as two key components, with concentrated seawater, different mineral seeds and organic matter as further variables.
- Dolomite was successfully precipitated in two (Vial 6 and Vial 21) out of seven vials, identified both by XRD and SEM. Vial 6 used quartz as a mineral seed whilst Vial 21 utilized aragonite. This suggests that the type of mineral seed is not a key variable in dolomite precipitation. Both vials, however, contained culture medium, SRB, additional magnesium sulphate (in brine) and organic matter in the form of *Ruppia* grass. This combination of components appears to be ideal for dolomite precipitation. If one or more of these components are omitted, precipitates of different mineralogy are found. Hence, SRB are directly linked to dolomite precipitation in the presence of suitable amounts of $MgSO_4$ and organic matter. In addition, the morphology of the dolomite precipitate closely resembles that found in the Coorong lakes and in other modern microbial settings (e.g. Lagoa Vermelha).

CHAPTER 7



Sunset over Coorong Lagoon

Chapter 7

Conclusions

This study comprises a detailed documentation of the mineralogy, geochemistry, isotopic characteristics and microbial populations of several ephemeral lakes in the Coorong region of South Australia. In addition, it presents experimental proof that dolomite formed under environmental, microbiological and geochemical conditions that prevailed in the late evaporitic stages of the dolomitic Coorong lakes, and further demonstrates that bacterial sulphate reduction is responsible for removing kinetic inhibitors to dolomite formation that operate in saline solutions.

Dolomite occurs in the upper sediments of five of the study lakes (Milne, Dolomite, Pellet, Mini Dolomite and McFaiden) associated with large quantities of organic matter, in particular from *Ruppia maritima* grass and desiccated microbial mat. All of the lakes show TOC values in excess of most near-shore and deep sea sediments (usually < 1% TOC) and are comparable to exceptionally high TOC values in areas of upwelling (Schulz and Zabel, 2000), while TOC values in the dolomitic lakes (up to 9%) are substantially in excess of those in the non-dolomitic lakes (<3%). Thus, organic matter, by implication, provides the energy source for sulphate-reducing bacteria (SRB). Where more organic matter is present, together with high initial sulphate concentrations, a larger bacterial population with a higher metabolic rate can be sustained. It is therefore proposed that the availability of large quantities of organic matter enhances the precipitation of dolomite.

SRB enumeration, using MPN counts, reveal extremely large populations of SRB in the dolomite containing lakes. These populations are amongst the highest concentrations ever recorded using this technique (~10^6/ml). Much fewer SRB are present in the non-dolomitic lakes (10^3-10^4/ml). Field evidence and counting techniques show that, in the

dolomitic lakes, SRB comprise a significant (up to 0.25%) proportion of the total bacterial population and, in turn, they substantially modify the surrounding micro-environment, creating conditions favourable for dolomite formation. Microbial mats are also common components of the lakes and it is suggested that the cyanobacteria, as well as being a source of organic matter, may play a vital role in dolomite genesis by providing a concentrated supply of magnesium ions to the lake- and pore-waters as they are degraded.

SEM studies of lake sediments show that the dolomite grains are sub-micron in size with spherical or elliptical morphology. DIC imaging of coeval living bacteria show strong similarities in size and shape, both with this dolomitic sediment and with organogenic sediments studied by other authors (e.g. Folk, 1993a; Vasconcelos *et al.*, 1995; Vasconcelos & McKenzie, 1997; Wright, 1999; Wartmann *et al.* 2000). The morphology of the dolomite, together with the absence of coexisting aragonite leads to the conclusion that this sediment is likely to be a primary precipitate of bacterial origin. The morphology also suggests that the bacteria themselves may act as favourable nucleation sites for dolomite precipitation. DNA products, identified from two dolomitic lakes, are closely related to *Desulfostipes* sp., *Desulfosarcina* sp. and *Desulfotomaculum* sp. SRB populations vary between lakes and are different from those identified by Vasconcelos & McKenzie (1997) as being associated with dolomite formation in Lagoa Vermelha, Brazil. Using these two examples, it appears that generic differences between SRB populations have little effect on dolomite precipitation. It would be interesting, however, to investigate which genera are *most efficient* at mediating chemistries and enhancing dolomite precipitation.

In this study detailed investigations into geochemical parameters reveal rapid changes with depth and time, consistent with microbial activity. Exponential rises in the concentrations of carbonate ions with depth and time result in carbonate ion concentrations and activities that are two orders of magnitude higher than those found in standard seawater (where bicarbonate is the dominant ion). Increasing carbonate ion concentrations seen with depth in the dolomitic lakes are found to be associated with decreasing sulphate ion concentrations and with populations of SRB that are larger than found in the non-dolomitic lakes. Magnesium ion concentrations in all the lakes increase dramatically at a late stage in the evaporative cycle, as do Mg/Ca ratios, owing to release of magnesium ions from desiccated cyanobacterial sheaths. Since the highest Mg/Ca ratios are found in the non-

dolomitic lakes, it follows that the Mg/Ca ratio of the waters cannot alone be a controlling factor in dolomite formation. Magnesium ion concentrations decline steadily with depth from extremely high concentrations of c. 28000 mg/l, in lakewater samples down to c. 3000 mg/l in pore-water samples at 4.5cm depth. If this rate of decline in sulphate and magnesium ion concentrations (e.g. in Milne Lake) is extrapolated beyond the sampled depth, it appears that the two trends converge and cross-over below c. 5cm, so that sulphate ion concentrations will then be lower than those of magnesium ions. The critical depth at which free Mg^{2+} is available may migrate towards the surface as bacterial sulphate reduction progresses and more sulphate ions are consumed. The total lack of precipitated sulphate minerals in the lake sediments (except for Halite Lake, which exceptionally is connected to the Coorong Lagoon by a subterranean channel) demonstrates that sulphate ions are eventually consumed entirely, thereby removing a key kinetic inhibitor to dolomite formation.

While carbonate ion concentrations are also high in the non-dolomitic lakes, the total number of SRB are 2-3 orders of magnitude lower, and sulphate ion concentrations remain higher for longer. In the non-dolomitic lakes, therefore, the aragonite and hydromagnesite mineralogy of precipitated carbonate may reflect the presence of high carbonate ion concentrations in the presence of sulphate ions. The increase in carbonate ion activity up to levels many times that seen in seawater may be explained as an interplay between the inter-linked processes of plant photosynthesis, degradation of organic matter, elevation of pH and elevation of salinity. Few modern natural settings would appear to have this combination of processes operating simultaneously, together with intense bacterial sulphate reduction, and this may, perhaps explain the relatively few occurrences of modern dolomite.

Although the observed geochemical trends are far from perfect, it must be remembered that these lakes are dynamic systems with continuously changing chemistries caused by both physical and biological processes. Each lake is a slightly different size, depth, height above the water table and distance from the source of ions; each lake was therefore at a different stage in its evaporative cycle during the sampling period. Sampling over a fairly short space of time can only give a brief snapshot into the evolving nature of each lake, so that simple patterns in the data are not to be expected. Even so, recorded differences in TOC

values, Mg^{2+} to SO_4^{2-} ratios, CO_3^{2-} activities and SRB numbers all point to the critical role of bacterial sulphate reduction in dolomite formation.

Isotopic studies reinforce geochemical and microbial findings. Carbon isotopes, in particular, shed light on the role that SRB may play in increasing the activity of the carbonate ion. The dolomitic lakes ($\delta^{13}C$ = -1.19 to +3.22‰) do not posses the strongly negative $\delta^{13}C$ signal to be expected if the carbon in the dolomite lattice originated solely from an organic reservoir. Instead, it is inferred that the carbonate ions are being incorporated into the lattice from inorganic bicarbonate already present in the lakewater. In this context, the action of the microbes results in pH elevation and a shift in the bicarbonate-carbonate equilibrium towards stability of the carbonate ion. In this way, SRB may therefore act as the catalyst for dolomite precipitation but not as a major source of carbon. A minor contribution to the carbon reservoir from these organic species can be invoked for carbonates of Mcfaiden and Dolomite lakes, however, since these reveal slightly negative $\delta^{13}C$ values. This has significant implications for interpreting carbon isotope signals of dolomite in the geological record.

Oxygen isotopes help to enhance our understanding of the timing and depth of dolomite precipitation. If the $\delta^{18}O$ signal of the carbonates is combined with $\delta^{18}O$ of the lakewater, it allows an estimation of the temperature of precipitation of the carbonate minerals, assuming that precipitation took place in equilibrium with the measured (November) lakewaters. Using isotopic fractionation factors for both dolomite and protodolomite, temperatures of between 39°C and 92°C are required to satisfy the oxygen isotope fractionation equation for these minerals. Temperatures of this high level were not, however, recorded in the field. The temperatures required for aragonite precipitation appear more realistic, especially in Halite Lake (27-33°C). It is concluded from this that dolomite may either precipitate at a few centimetres depth where temperatures are higher and $\delta^{18}O$-pore-water may be lower, or at some other time in the evaporative cycle, where the $\delta^{18}O$ of the lakewater is lower so that lower temperatures are required to fulfill the equation. A distinct 'hook effect', interpreted from lakewater $\delta^{18}O$ patterns, means the minerals could precipitate either earlier or later in the evaporative cycle. Of these, later precipitation is preferred since bacterial action is more intense, sulphate ionic concentration lower and free Mg^{2+} higher at this time. The morphology of the dolomite changes little with depth; occasionally an increased amalgamation of the spherules is observed leading to the

formation of larger multi-spherular grains with straight crystal faces. There is little evidence, however, to contradict the inference of dolomite precipitation at some shallow depth.

Two further isotopic correlations were discovered with important implications for lake geochemistry. A strong correlation was noted between the $\delta^{18}O$ of lakewaters and of residual sulphate ions in the lakewater. An indirect isotopic exchange, proceeding by oxygen exchange between sulphate enzyme complexes and water (Fritz *et al.*, 1989) is inferred to result in a $\delta^{18}O$ of lakewater sulphate that reflects that of the evaporitically modified lakewater (rather than of the original seawater source). This provides a strong argument for the case that many of the lakewater sulphate ions are formed *in situ* within the lake system from re-oxidation of H_2S and other sulphur species. This, in turn, has important implications for the $\delta^{34}S$ signal in these lakes. Re-oxidation of H_2S by various types of bacteria including some SRB, is likely to result in the formation of intermediate sulphur species, such as elemental sulphur, sulphite and thiosulphate. These, in turn, can experience further oxidation, reduction and disproportionation. Repeated cycles of oxidation, reduction and disproportionation could therefore result in residual lake- and pore-water sulphate becoming progressively ^{32}S-enriched. This would balance much of the heavy $\delta^{34}S$ signal inherited from straightforward sulphate reduction and could explain both the relatively small total ^{34}S enrichments found in these lakes and the minimal variation of $\delta^{34}S$ between the dolomitic and non-dolomitic lakes. A further explanation for the latter was found when bacterial species-specific effects were investigated. Sulphur isotope fractionation factors for different species of SRB can differ greatly (Detmers *et al.*, 2001) ranging between 2‰ and 42‰, under each species ideal growth conditions. Several genera of bacteria have been identified in this study from Milne and McFaiden lakes. If each lake has a distinctive bacterial population, it is possible that this may determine the lakes' isotopic signal. Further work is needed into the fractionations of sulphur isotopes by different bacterial taxa, isolated from these lakes, in relation to metabolic rates, substrates, population sizes and sulphate ion concentrations before these isotopic signals can be fully understood.

A second covariant positive correlation is observed between sulphate $\delta^{18}O$ and $\delta^{34}S$ in the lakewater of the dolomitic lakes. No such correlation was observed in the non-dolomitic lakes. This same correlation has been observed previously in sulphate-reducing

environments (Bottcher *et al.* 1999) suggesting that bacterial sulphate reduction may control the isotopic signal of sulphates in the dolomitic lakes. It follows that bacterial sulphate reduction is likely to be more active in the dolomitic lakes than in the non-dolomitc lakes, consistent with the other geochemical and microbial data presented here.

Sulphate-reducing bacteria interact with their environment through organogenic degradation and this can be used as a tool to identify their presence. Consequences of SRB metabolism include: fractionation of sulphur and oxygen isotopes, lowering of sulphate concentrations, increase of alkalinity and carbonate ion concentrations, hydrogen sulphide generation and carbonate mineral precipitation. These trends are here demonstrated from the Coorong dolomitic lakes during the late stages of evaporation, when benthic microbial communities dominate the lake ecosystem.

Dolomite is shown to precipitate in laboratory experiments that simulate the microbiogeochemical conditions prevailing during the late stages of evaporation in the distal, ephemeral, hypersaline dolomitic lakes of the Coorong. Successful replication and maintenance of key components of the dolomitic Coorong lakes allowed precipitation of nano-grains of dolomite on both quartz and aragonite mineral seeds, after just one month of incubation. Dolomite was only precipitated in vials containing culture medium, SRB, additional $MgSO_4$ and a quantity of ground up organic matter; 80-90% of the sulphate was consumed at the same time. Where one or more of these components are absent, precipitates of different mineralogy are found, further emphasing the link between SRB, organic matter, high initial sulphate concentrations and release of free Mg^{2+} with dolomite formation.

The results from this study are a little difficult to put into a general context since the Coorong is a rather specialized environment. Data from this study, however, may be compared to data obtained from the Lagoa Vermelha area where primary dolomite is also precipitating at the present day (Vasconcelos *et al.*, 1995; Vasconcelos and McKenzie, 1997; Warthmann *et al.*, 2000). The Coorong Lakes and Lagoa Vermelha are similar in many ways. Both are relatively small and shallow; Lagoa Vermelha is 2.4km^2 in area with a maximum depth of 1.7m whilst many of the Coorong lakes are around 1km^2 with a maximum depth of <1m. Algal mats border both Lagoa Vermelha and the dolomite precipitating Coorong lakes and clastic material is largely absent. Their hydrological settings are similar; both are fed by a mixture of meteoric water and seawater seeping into the groundwater and both areas are

separated from a major ocean by a narrow barrier dune. In both areas salinities vary substantially from brackish to hypersaline. The major difference in the hydrological regime of Lagoa Vermelha compared to the Coorong lakes is that it does not dry out completely at any time of the year. The dolomite in Lagoa Vermelha is made up of aggregates of sub-micron spherical and elliptical bodies, assumed to be forming in an anoxic organic rich sludge layer under hypersaline conditions; it is poorly ordered and calcium rich. The dolomite in the Coorong lakes is almost identical in morphology but has a wider range of compositions ranging from slightly calcium rich (55% $CaCO_3$) to magnesium rich (70% $MgCO_3$). The lake chemistries of the two environments also show some significant similarities including pH's often in excess of 8 and key ionic concentrations in excess of seawater. Sulphate ion concentrations span a much greater range in the dolomite precipitating Coorong lakes than in Lagoa Vermelha with substantially greater maxima and lower minima, whilst magnesium ion concentrations and Mg/Ca ratios are significantly greater in all of the Coorong lakes. Oxygen isotope data show a $\delta^{18}O$ maximum of 3.82‰ (SMOW) in Lagoa Vermelha compared to over 12‰ (SMOW) in one of the Coorong lakes (McFaiden Lake). These data suggest that while the two environments are broadly similar, and both favourable to dolomite formation, the Coorong experiences greater climatic and geochemical extremes. Porewater chemistries cannot be compared and contrasted as no data has been published on Lagoa Vermelha porewaters.

The successful engineering of microbiogeochemical conditions, enhancing dolomite precipitation, has implications for further work. Scaling up of this process from vials to tanks would result in a larger quantity of dolomite precipitate, allowing $\delta^{13}C$ and $\delta^{18}O$ isotopic analysis to compare the bacterial signals in these artificial precipitates with those obtained from both modern and ancient natural examples. Full microbial population analysis of each of the lakes and isolation of selected SRB genera may result in the discovery of taxa that are particularly efficient in enhancing dolomite precipitation. These could then be sought in other modern dolomite precipitating environments. The introduction of iron salts into the tanks (to precipitate iron sulphides), would allow sulphur isotopic fractionation factors for Coorong SRB to be investigated more thoroughly and the isotopic patterns observed in the lakes to be better understood. Importantly, microbiogeochemical processes operating in the Coorong distal lakes and in the laboratory today shows that bacterial sulphate reduction can provide a 'process analogue' for the formation of dolomite through biosphere-hydrosphere-lithosphere interaction, not only in modern environments but wherever such conditions prevailed in the past.

In studies to date, the role of bacteria in dolomite formation has only been investigated in a small number of specialised environments and in laboratory experiments. Any attempt to assess the importance of bacteria in dolomite formation in non-specific environments, needs to examine the variations in abundance of dolomite through geological time and to equate this both with changes in ocean and atmosphere chemistry and with microbial activity. It has for long been accepted that almost all large bodies of sedimentary dolomite form by replacement of previously deposited calcium carbonates by dissolution-reprecipitation reactions involving fluids of seawater or modified seawater composition (e.g. Lippmann 1973). Most models of dolomite formation in the literature are physico-chemical ways to move seawater or modified seawater through calcium carbonate sediment but they fail to account for the kinetic controls operating during the reprecipitation reaction.

Observations from Precambrian dolomites may imply a link between microbes and dolomite formation at this time. Most modern dolomite is found in intertidal to supratidal environments (including alkaline lakes), whereas most Precambrian dolomite was deposited in shallow subtidal marine settings. However, a common factor linking both modern and ancient dolomites is their frequently observed association with benthic microbial communities, typically as stromatolites and cyanobacterial mats, and this association may not be coincidental. SRB today are universally distributed in marine sediments and microbial mats (Teske et al., 1998), and have a long history, arguably extending back to the Archaean (Trudinger 1992; Ohmoto *et al.*, 1993; Strauss and Beukes 1996; Kakegawa et al. 1998). In living microbialites, SRB occur from just beneath the sediment-water interface to variable depths in sediments, wherever anoxic conditions prevail; they account for a significant fraction (30±40%) of organic carbon consumption despite the presence of oxygen at the surface (Reid et al., 2000). Sulphate reduction in marine sediments is the dominant anaerobic biomineralization pathway, quantitatively equivalent to or exceeding aerobic respiration (Jorgensen, 1982). In modern stromatolites, pervasive carbonate precipitation has also been documented in association with SRB and decaying organic matter (Sprachta et al. 2001). In Precambrian microbially dominated shelf ecosystems, the potential may have existed for bacterial sulphate reduction to operate on the large scale, leading to widespread mineralization through organic degradation

The ubiquitous presence of bacteria in modern aquatic systems and their ability tc overcome the kinetic inhibitors to dolomite formation by removing SO_4^{2-} ions (thereby

reducing the solubility of Mg^{2+} and Ca^{2+} ions, and raising carbonate alkalinity) makes them extremely important agents in driving both modern and many ancient geochemical cycles. Such microbial ecosystems arguably dominated the depositional environments during the Late Archaean and Proterozoic, often building up thick, platformal sequences. By analogy with modern stromatolites, it follows that taphonomic processes associated with sulphate reduction and organic diagenesis could have been prevalent in anoxic conditions beneath microbial mats, thereby creating the geochemical conditions necessary for dolomite formation which may have led to the accumulation of thick, platformal, microbialitic dolostone seen in the rock record. Microbial mediation of ambient waters is therefore likely to be an important process in the transfer of carbon, calcium and magnesium ions from the hydrosphere and biosphere to the lithosphere.

It is of interest to note the variation in dolomite abundance during the Phanerozoic, which shows peaks in the Ordovician/Early Silurian and again in the Early Cretaceous. These peaks cannot easily be explained using physico-chemical parameters in seawater such as Mg/Ca ratio, sulphate ion concentration, saturation state or pCO_2 because they suggest that dolomite should have been less abundant than usual at these times. These large-scale changes in ocean chemistry during the Phanerozoic may be more easily explained as a response to more rapid dolomite formation. A microbial explanation deserves analysis here. A negative correlation between the abundance of dolomite and modelled atmospheric O_2 levels (Burns *et al.*, 2000) implies that periods of low seawater oxygen might have been more conducive to massive dolomite formation, because this creates an environment in which SRB can prosper. Increased rates of seafloor hydrothermal activity, leading to large sulphide fluxes into the deep sea and then to consumption of oxygen through both organic and inorganic reactions may therefore control massive dolomite formation on a global scale.

Whilst it is clear that a microbial model cannot be invoked for all dolomites (e.g hydrothermal and early Archaean dolomite), data presented here and in the last ten years has demonstrated that the involvement of microbes in dolomite formation is much more widespread than previously thought. Investigations in the coming years will, in the opinion of this author, demonstrate the importance of microbes in both modern and ancient dolomite formation to an even greater extent.

Bibliography

ADAMS J. E. and RHODES M. L. (1960) Dolomitization by seepage refluxion. *American Association of Petroleum Geologists Bulletin* **44**, 1912-1921.

AHARON P., KOLODNY Y. and SASS E. (1977) Recent hot brine dolomitization in the "Solar Lake," Gulf of Elat, isotopic, chemical, and mineralogical study. *Journal of Geology* **85**, 27-48.

AHMAD R. (1996) Late Holocene major Australian arid period revealed by direct sedimentological evidence from lakes in the Coorong region of South Australia. *Geology* **24**, 619-622.

ALDERMAN A. R. (1965) Dolomitic sediments and their environment in the South-East of South Australia. *Geochimica et Cosmochimica Acta* **29**, 1355-1365.

ALDERMAN A. R. and SKINNER H. C. W. (1957) Dolomite sedimentation in the South-East of South Australia. *American Journal of Science* **255**, 561-567.

ASSOCIATION OF ANALYTICAL COMMUNITIES (AOAC) (2002). AOAC official method 973.40. Specific conductance of water. *http://www.southerndatastream.com/maerc/sop/conuctivity.htm*

AUSTRALIAN BUREAU OF METEOROLOGY (2001) Rainfall and temperature graphs for South Australia. *http://www.bom.gov.au*

BADIOZAMANI K. (1973) The Dorag dolomitization model – application to the middle Ordovician of Wisconsin. *Journal of Sedimentary Petrology* **43**, 965-984.

BAK F. and CYPIONKA H. (1987) A novel type of energy metabolism involving fermentation of inorganic sulphur compounds. *Nature* **326**, 891-892.

BAK F. and PFENNIG N. (1991) Sulphate-reducing bacteria in littoral sediment of Lake Constance. *FEMS-Microbiology-Ecology* **85**, 43-52.

BAKER P. and KASTNER M. (1981) Constraint on the formation of sedimentary dolomite. *Science* **213**, 214-216.

BALE S. J., GOODMAN K., ROCHELLE P. A., MARCHESI J. R., FRY J. C., WEIGHTMAN A. J. and PARKES R. J. (1997) *Desulfovibrio profundus* sp. nov., a novel barophilic sulfate-reducing bacterium from deep sediment layers in the Japan Sea. *International Journal of Systematic Bacteriology* **47**, 515-521.

BERNER R. A. (1980) Early Diagenesis. Princeton University Press, 241pp.

BINNERUP S. J., JENSEN D. F., THORDAL-CHRISTENSEN H. and SORENSEN J. (1993) Detection of viable but non-culturable *Pseudomonas flourescens* DF57 in soil using a microcolony epiflouresence technique. *FEMS-Microbiology-Ecology* **12**, 97-105.

BOHM F., JOACHIMSKI M. M., DULLO W. C., EISENHAUER A., LEHNERT H., REITNER J. and WORHEIDE G. (2000) Oxygen isotope fractionation in marine aragonite of coralline sponges. *Geochimica et Cosmochimica Acta* **64**, 1695-1703.

BORCHERT H. and MUIR R. O. (1964) Salt Deposits: the origin, metamorphism and deformation of evaporites. Van Nostrand Reinhold, London, 338pp.

BÖTTCHER M. E., BERNASCONI S. M. and BRUMSACK H-J (1999) Carbon, sulfur and oxygen isotope geochemistry of interstitial waters from the Western Mediterranean. *Proceedings of the Ocean Drilling Program, Scientific Results* **161**, 413-421.

BOTZ R. W., and VON DER BORCH C. C. (1984) Stable isotope study of carbonate sediments from the Coorong region, South Australia. *Sedimentology* **31**, 837-849.

BRASIER M. D. (1977) An Early Cambrian chert biota and its implications. *Nature* **268**, 719-720.

BRASIER M. D., GREEN O. R., JEPHCOAT A. P., KLEPPE A. K., VAN KRANENDONK M. J., LINDSAY J. F., STEELE A. and GRESSINEAU N. V. (2002) Questioning the evidence for Earth's oldest fossils. *Nature* **416**, 76-81.

BROCKS J. J., LOGAN G. A., BUICK R. and SUMMONS R. E. (1999) Archean molecular fossils and the early rise of eukaryotes. *Science* **285**, 1033-1036.

BURNS S. J., MCKENZIE J. A. and VASCONCELOS C. (2000) Dolomite formation and biogeochemical cycles in the Phanerozoic. *Sedimentology* **47** (Supp. 1), 49-61.

BUSSMANN I. And REICHARDT W. (1991) Sulphate-reducing bacteria in temporarily oxic sediments with bivalves. *Marine Ecology Progress Series* **78**, 97-102.

BUTLER G. P. (1969) Modern evaporite deposition and geochemistry of coexisting brines, the sabkha, Trucial Coast, Arabian Gulf. *Journal of Sedimentary Petrology* **39**, 70-89.

CAMERON E. M. (1982) Sulphate and sulphate reduction in early Precambrian oceans. *Nature* **296**, 145-148.

CANFIELD D. E. (2001) Isotope fractionations by natural populations of sulfate-reducing bacteria. *Geochimica et Cosmochimica Acta* **65**, 1117-1124.

CANFIELD D. E. and DES MARAIS D. J. (1991) Aerobic sulphate reduction in microbial mats. *Science* **251**, 1471-1473.

CANFIELD D. E. and THAMDRUP B. (1994) The production of 34S-depleted sulfide during bacterial disproportionation of elemental sulfur. *Science* **266**, 1973-1975.

CARBALLO J. D., LAND L. S. and MISER D. E. (1987) Holocene dolomitization of supratidal sediments by active tidal pumping, Sugarloaf Key, Florida. *Journal of Sedimentary Petrology* **57**, 153-165.

CARPENTER A. B. (1980) The chemistry of dolomite formation I: the stability of dolomite. In: Zenger D.H., Dunham J.B. and Ethington R.L. (Eds). Concepts and models of dolomitization. *S.E.P.M Special Publication* **28**, 111-121.

CASTRO H. F., WILLIAMS N. H. and OGRAM A. (2000) Phylogeny of sulfate-reducing bacteria. *FEMS Microbiology Ecology* **31**, 1-9.

CATLING D. C., ZAHNLE K. J. and McKAY C. P. (2001) Biogenic methane, hydrogen escape and the irreversible oxidation of early earth. *Science* **293**, 839-843.

CHAMBERS L. A. and TRUDINGER P. A. (1975) Are thiosulfate and trithionate intermediates in dissimilatory sulfate reduction? *Journal of Bacteriology* **123**, 36-40.

CLAYPOOL G. E., HOLSER W. T., KAPLAN I. R., SAKAI H. and ZAK I. (1980). The age curves of sulfur and oxygen isotopes in marine sulfate and their mutual interpretation. *Chemical Geology* **28**, 199-260.

COLEMAN M. L. and MOORE M. P. (1978) Direct reduction of sulfates to sulfur dioxide for isotopic analysis. *Analytical Chemistry* **50**, 1594-1595.

COPLEN T. B., KENDALL C. and HOPPLE J. (1983) Comparison of stable isotope reference standards. *Nature* **302**, 236-238.

CRAIG H. and GORDON L. I. (1965) Isotope oceanography - deuterium and oxygen-18 variations in the ocean and marine atmosphere. *Symposium on Marine Geochemistry, 1964*, 277-374.

CURTIS R., EVANS G., KINSMAN D. J. J. and SHEARMAN D. J. (1963) Association of dolomite and anhydrite in the Recent sediments of the Persian Gulf. *Nature* **197**, 679-680.

DEINES P. (1980) The isotopic composition of reduced organic carbon. Pages 329-406 of: Fritz P. and Fontes J.C. (Eds.) Handbook of Environmental Isotope Geochemistry, Volume 1. Elsevier, New York Amsterdam, 545pp.

DEINES P., LANGMUIR D. and HARMON R. S. (1974) Stable carbon isotope ratios and the existence of a gas phase in the evolution of carbonate ground waters. *Geochimica et Cosmochimica Acta* **38**, 1147-1164.

DES MARAIS D. J., STRAUSS H., SUMMONS R. E. and HAYES J. M. (1992) Carbon isotope evidence for the stepwise oxidation of the Proterozoic environment. *Nature* **359**, 605-609.

DETMERS J., BRUCHERT V., HABICHT K. S. and KUEVER J. (2001) Diversity of sulfur isotope fractionations by sulfate-reducing prokaryotes. *Applied and Environmental Microbiology* **67**, 888-894.

DEVEREUX R., HE S. H., DOYLE C. L., ORKLAND S., STAHL D. A., LEGALL J. and WHITMAN W. B. (1990) Diversity and origin of Desulfovibrio spp. Phylogenetic definition of a family. *Journal of Bacteriology* **172**, 3609-3619.

DEVEREUX R., DELANEY M., WIDDEL F. and STAHL D. A. (1989) Natural relationships among sulphate-reducing eubacteria. *Journal of Bacteriology* **171**, 6689-6695.

DILLING W. and CYPIONKA H. (1990) Aerobic respiration in sulfate-reducing bacteria. *FEMS Microbiology Letters* **71**, 123-128.

ECKELMAN W. R., BROECKER W. S., WHITLOCK D. W. and ALLSUP J. R. (1962) Implications of carbon isotopic composition of total organic carbon of some recent sediments and ancient oils. *A.A.P.G. Bulletin* **46**, 699-704.

EMRICH K., EHHALT D. H. and VOGEL J. C. (1970) Carbon isotope fractionation during the precipitation of calcium carbonate. *Earth and Planetary Science Letters* **8**, 363-371.

ESIOBU N., AMUND O. O., FAKILE O. O. and POPOOLA O. H. (1991) Occurrence and distribution of sulphate-reducing bacteria in a polluted lagoon. *Biomedical Letters* **46**, 129-132.

FARQUHAR J., BAO H. and THIEMENS M. (2000) Atmospheric influence of earth's earliest sulfur cycle. *Science* **289**, 756-758.

FAURE G. (1977) Principles of Isotope Geology (1st Edition). Wiley, New York, 464pp.

FENCHEL T., KING G. M. and BLACKBURN T. H. (1998) Bacterial Biogeochemistry: the Ecophysiology of Mineral Cycling (2nd Edition). Academic Press.

FERNANDEZ-DIAZ L., PUTNIS A., PRIETO M. and PUTNIS C. V. (1996) The role of magnesium in the crystallization of calcite and aragonite in a porous medium. *Journal of Sedimentary Research* **44**, 482-491.

FINDLEY J. E. and AKAGI J. M. (1968) Lysis of Desulfovibrio vulgaris by ethylenediaminetetraacetic acid lysozyme. *Journal of Bacteriology* **96**, 1427-1428.

FLOEGEL H. (1972) The position of the lower Tertiary artesian aquifer within the hydrogeology and hydrogeochemistry of the Gambier Embayment area. Ph.D. thesis, Fakultät für Allgemeine Wissenschaften der Technischen Universität, München.

FOLK R. L. (1993a) S.E.M. imaging of bacteria and nannobacteria in carbonate sediments and rocks. *Journal of Sedimentary Petrology* **63**, 990-999.

FOLK R. L. (1993b) Dolomite and dwarf bacteria (nannobacteria). *Geological Society of America, Annual Meeting (Abtracts)*, 397pp.

FOLK R. L. and LAND L. S. (1975) Mg/Ca ratio and salinity: Two controls over crystallization of dolomite. *AAPG Bulletin* **59**, 60-68.

FONTES J. C. and GONFIANTINI R. (1967) Comportement isotopique au cours de l'evaporation de deux basins Sahariens. *Earth and Planetary Science Letters* **3**, 258-266.

FRIEDMAN I. and O'NEIL J. R. (1977) Compilation of stable isotope fractionation factors of geochemical interest. *U.S. Geological Survey Professional Paper* **440-KK**, 49p.

FRITZ P. and SMITH D. G. W. (1970) The isotopic composition of secondary dolomite. *Geochimica et Cosmochimica Acta* **34**, 1161-1173.

FRITZ P., BASHARMAL G. M., DRIMMIE R. J., IBSEN J. and QURESHI R. M. (1989) Oxygen isotope exchange between sulphate and water during bacterial reduction of sulphate. *Chemical Geology (Isotope Geoscience Section)* **79**, 99-105.

FRUND C. and COHEN Y. (1992) Diurnal cycles of sulphate reduction under oxic conditions in cyanobacterial mats. *Applied and Environmental Microbiology* **58**, 70-77.

FRY J. C. (1988) Determination of Biomass. Pages 27-72 of: Austin B. (Ed.) Methods in Aquatic Bacteriology. Wiley, Chichester, 425pp.

FRY J. C. (1990) Methods in Microbiology (Vol. 22). Academic Press, San Diego.

FRY B., GEST H., and HAYES J. M. (1988) $^{34}S/^{32}S$ Fractionation in sulfur cycles catalysed by anaerobic bacteria. *Applied and Environmental Microbiology* **54,** 250-256.

FRY B., GIBLIN A., DORNBLASER M. and PETERSON B. (1995) Stable sulfur isotopic compositions of chromium reducible sulfur in lake sediments. Pages 397-411 of: Vairavamurthy M.A. and Schoonen M.A.A. (Eds.) Geochemical Transformations of Sedimentary Sulfur. American Chemical Society, Washington, 467pp.

FUSELER K., KREKELER D., SYDOW U. and CYPIONKA H. (1996) A common pathway of sulfide oxidation by sulfate-reducing bacteria. *FEMS Microbiology Letters* **144**, 129-134.

GARRELS R. M. and THOMPSON M. E. (1962) A chemical model for seawater at 25°C and one atmosphere total pressure. *American Journal of Science* **260,** 57-66.

GARRELS R. M., THOMPSON M. E. and SIEVER R. (1960) Stability of some carbonates at 25 degrees C and one atmosphere total pressure. *American Journal of Science* **258,** 402-418.

GEBELEIN C. D. and HOFFMAN P. (1973) Algal origin of dolomite laminations in stromatolitic limestone. *Journal of Sedimentary Petrology* **43**, 603-613.

GOLDHABER M. B. and KAPLAN I. R. (1975) Controls and consequences of sulphate reduction rates in recent marine sediments. *Soil Sciences* **119**, 42-55.

GOODWIN A. M., MONSTER J. and THODE H. G. (1976) Carbon and sulfur isotope abundances in Archean iron-formations and Early Precambrian life. *Economic Geology* **71**, 870-891.

HABICHT K. S. and CANFIELD D. E. (1996) Sulphur isotope fractionation in modern microbial mats and the evolution of the sulphur cycle. *Nature* **382**, 342-343.

HABICHT K. S. and CANFIELD D. E. (1997) Sulfur isotope fractionationduring bacterial sulfate reduction in organic-rich sediments. *Geochimica et Cosmochimica Acta* **61**, 5351-5361.

HABICHT K. S. and CANFIELD D. E. (2001) Isotope fractionation by sulfate-reducing natural populations and the isotopic composition of sulfide in marine sediments. *Geology* **29**, 555-558.

HABICHT K. S., CANFIELD D. E. and RETHMEIER J. (1998) Sulfur isotope fractionation during bacterial reduction and disproportionation of thiosulfate and sulfite. *Geochimica et Cosmochimica Acta* **62**, 2585-2595.

HALL A. J., BOYCE A. J., FALLICK A. E. and HAMILTON P. J. (1991) Isotopic evidence of the depositional environment of Late Proterozoic stratiform barite mineralisation, Aberfeldy, Scotland. *Chemical Geology (Isotope Geoscience)* **87**, 99-114.

HALLA F. and RITTER F. (1935) Eine Methode zur Bestimmung der Anderung freien Energie bei Reaktionen das Typus A(s) + B(s) = AB(s) und ihre Anwendung auf das Dolomit Problem. *Zeitschrift fur Phyzikalische Chemie* **175**, 63-82.

HANSHAW B. B., BACK W. and DEIKE R. G. (1971) A geochemical hypothesis for dolomitization by groundwater. *Economic Geology* **66**, 710-724.

HARDIE L. A. (1987) Dolomitization: a critical view of some current views. *Journal of Sedimentary Petrology* **57**, 166-183.

HARRISON I. R. and THODE H. G. (1958) Mechanism of the bacterial reduction of sulphate from isotope fractionation studies. *Transactions of the Faraday Society* **54**, 84-92.

HILL R. J. (1990) Field evidence for the role of organic matter in dolomitization. *Master's abstract, Colorado School of Mines.*

HOEFS J. (1987) Stable isotope geochemistry (3rd Edition). Springer-Verlag, Berlin, 241pp.

HOLSER W. T. (1979) Trace elements and isotopes in evaporites. Pages 295-346 of: Burns R.G. (Ed.) Marine Minerals. *Mineralogical Society of America, Reviews in Mineralogy.*

HOLSER W. T., KAPLAN I. R., SAKAI H. and ZAK I. (1979) Isotope geochemistry of oxygen in the sedimentary sulfate cycle. *Chemical Geology* **25**, 1-17.

HOLT J. G., KRIEG N. R., SNEATH P. H. A., STALEY J. T. and WILLIAMS S. T. (1994) Bergey's manual of determinative bacteriology (9th Edition). Williams and Wilkins, Baltimore, 787pp.

HORN R. A. (1969) Marine Chemistry: The Structure of Water and the Chemistry of the Hydrosphere. Interscience, New York, 568pp.

HSU K. J. (1967) Chemistry of dolomite formation. Pages 169-191 of: Chillingar G.V., Bissel H.J. and Fairbridge R.W. (Eds.) Carbonate Rocks: origin, occurrence and classification. Elsevier, Amsterdam, 471pp.

HSU K. J. and SIEGENTHALER C. (1969) Preliminary experiments and hydrodynamic movement induced by evaporation and their bearing on the dolomite problem. *Sedimentology* **12**, 11-25.

HURLEY M. A. and ROSCOE M. E. (1983) Automated statistical analysis of microbial enumeration by dilution series. *Journal of Applied Bacteriology* **55**, 159-164.

HUTTON J. T. (1974) Chemical characterization and weathering changes in Holocene volcanic ash in soils near Mount Gambier, South Australia. *Royal Soc. South Australia Trans.* **98**, 179-183.

JANNASCH H. and JONES G. E. (1959) Bacterial populations in seawater as determined by different methods of enumeration. *Limnology and Oceanography* **4**, 128-139.

JORGENSEN B. B. (1982) Mineralization of organic matter in the sea bed – the role of sulphate reduction. *Nature* **296**, 643-645.

JORGENSEN B. B. and COHEN Y. (1977) Solar Lake (Sinai). The sulfur cycle of the benthic cyanobacterial mats. *Limnology and Oceanography* **22**, 657-666.

JORGENSEN B. B., ISAKSEN M. F. and JANNASCH H. W. (1992) Bacterial sulfate reduction above 100°C in deep-sea hydrothermal vent sediments. *Science* **258**, 1756-1757.

KAKEGAWA T., KAWAI H. and OHMOTO H. (1998) Origins of pyrites in the ~2.5Ga Mt. McRae Shale, the Hamersley District, Western Australia. *Geochimica et Cosmochimica Acta* **62**, 3205-3220.

KAPLAN I. R. and RITTENBERG S. C. (1964) Microbiological fractionation of sulphur isotopes. *Journal of General Microbiology* **34**, 195-212.

KASTING J. F. (2001) The rise of atmospheric oxygen. *Science* **293**, 819-820.

KELTS K. and McKENZIE J. A. (1982) Diagenetic dolomite formation in Quaternary anoxic diatomaceous muds of Deep Sea Drilling Project Leg 64, Gulf of California. Pages 553-569 of: Initial Reports of the Deep Sea Drilling Project, Volume 64, Part 2; Mazatlan, Mexico to Long Beach, California.

KEMP A. L. W. and THODE H. G. (1968) The mechanism of the bacterial reduction of sulphate and of sulphite from isotope fractionation studies. *Geochimica et Cosmochimica Acta* **32**, 71-91.

KIRCHMAN D., SIGDA J., KAPUSCINSKI R. and MITCHELL R. (1988) Statistical analysis of the direct count method for enumerating bacteria. *Applied and Environmental Microbiology* **44**, 376-382.

KNAUTH P. L. and BEEUNAS M. A. (1986) Isotope geochemistry of fluid inclusions in Permian halite with implications for the isotope history of ocean water and the origin of saline formation waters. *Geochimica et Cosmochimica Acta* **50**, 419-433.

KNOBLAUCH C. (1997) Sulphate-reducing bacteria in cold marine sediments. *(Abstracts) Fifth European Marine Microbiology Symposium.*

KOBAYASHI K., TACHIBANA S. and ISHIMOTO M. (1969) Intermediate formation of trithionate in sulfite reduction by sulfate-reducing bacterium. *Journal of Biochemistry* **65**, 155-157.

KRAUSKOPF K. (1995) Introduction to Geochemistry (3rd Edition). McGraw-Hill Book Company, New York, 647pp.

KYSER T. K. (1987) Equilibrium fractionation factors for stable isotopes. Pages 1-84 of: Kyser T.K. (Ed.) Stable isotope geochemistry of low temperature processes. *Mineralogical Association of Canada Short Course Handbook* **13**.

LAND L. S. (1991) Dolomitization models – seawater mixing zones. *Dolomieu Conference on Carbonate Platforms and Dolomitization (abstracts)*, p144.

LINDSAY J. F. and BRASIER M. D. (2002) Did global tectonics drive early biosphere evolution? Carbon isotope record from 2.6 to 1.9Ga carbonates of Western Australian basins. *Precambrian Research* **114**, 1-34.

LIBES S. M. (1992) An Introduction to Marine Biogeochemistry. Wiley, New York, 734pp.

LIDE D. R. (2001) CRC Handbook of Chemistry and Physics, 81st Edition. CRC Press, 2415pp.

LIPPMANN F. (1973) Sedimentary Carbonate Minerals. Springer-Verlag, Berlin, 228pp.

LLOYD R. M. (1966) Oxygen isotope enrichment of sea water by evaporation. *Geochimica et Cosmochimica Acta* **30**, 801-814.

LLOYD R. M. (1967) Oxygen–18 composition of oceanic sulfate. *Science* **156**, 1228-1231.

LLOYD R. M. (1968) Oxygen isotope behaviour in the sulfate-water system. *Journal of Geophysical Research* **73**, 6099-6110.

LONGINELLI A. and CRAIG H. (1967) Oxygen-18 variations in sulfate ions in sea water and saline lakes. *Science* **156**, 56-59.

LONGSTAFFE F. J. (1989) Stable isotopes as tracers in clastic diagenesis. Pages 201-277 of: Hutcheon I.E. (Ed.) Short Course in Burial Diagenesis. *Mineralogical Association of Canada Short Course Series, Volume 15.*

LUDBROOK N. H. (1980) A guide to the geology and mineral resources of South Australia. Department of Mines and Energy, South Australia, 230pp.

LUDBROOK N. H. (1961) Stratigraphy of the Murray Basin in South Australia. *Bulletin of the Geological Survey of South Australia* **36.**

MACHEL H. G. and MOUNTJOY E. W. (1986) Chemistry and environments of dolomitization – a reappraisal. *Earth-Science Reviews* **23**, 175-222.

McKENZIE J. A. (1981) Holocene dolomitization of calcium carbonate sediments from the coastal sabkhas of Abu Dhabi, U.A.E.: a stable isotope study. *Journal of Geology* **89**, 185-198.

MICHAELIS J., USDOWSKI E. and MENSCHEL G. (1985) Partitioning of ^{13}C and ^{12}C on the degassing of CO_2 and the precipitation of calcite – Rayleigh-type fractionation and a kinetic model. *American Journal of Science* **285**, 318-327.

MITZUTANI Y. (1972) Isotopic composition and underground temperature of the Otake geothermal water, Kyusha, Japan. *Geochemical Journal* **6**, 67-73.

MOOK W. G., BOMMERSON J. C. and STAVERMAN W. H. (1974) Carbon isotope fractionation between dissolved bicarbonate and gaseous carbon dioxide. *Earth and Planetary Science Letters* **22**, 169-176.

MONSTER J., APPEL P. W. U., THODE H. G., SCHIDLOWSKI M., CARMICHAEL C. M. and BRIDGWATER D. (1979) Sulfur isotope studies in early Archaean sediments from Isua, West Greenland; implications for the antiquity of bacterial sulfate reduction. *Geochimica et Cosmochimica Acta* **43**, 405-413.

MORROW D. W. and RICKETTS B. D. (1988) Experimental investigation of sulfate inhibition of dolomite and its mineral analogues. In: Sedimentology and Geochemistry of Dolostones (Shukla V. and Baker P.A. eds). *S.E.P.M. Special Publication* **43**, 27-38.

MUDRYK Z. J., PODGORSKA B., AMERYK A. and BOLALEK J. (2000) The occurrence and activity of sulphate –reducing bacteria in the bottom sediments of the Gulf of Gdansk. *Oceanologia* **42**, 105-117.

MULLER G. and FISCHBECK R. (1973) Possible natural mechanism for protodolomite formation. *Nature* **242**, 139-141.

MYHR S., LILLEBO B-L. P., SUNDE E., BEEDER J. and TORSVIK T. (2002) Inhibition of microbial H_2S production in an oil reservoir column by nitrate injection. *Appl. Microbiol. Biotechnol.* **58**, 400-408.

NAZINA T. N., XUE Y. F., WANG X. Y. and GRIGORIYAN A. A. (2000) Diversity and activity of microorganisms in the Daqing oil field of China and their potential for biotechnological applications. *Resource and Environmental Biotechnology* **3**, 161-172.

NORTHROP D. A. and CLAYTON R. N. (1966) Oxygen-isotope fractionations in systems containing dolomite. *Journal of Geology* **74**, 174-196.

O'DRISCOLL E. P. D. (1960) The hydrology of the Murray Basin province in South Australia. *Bulletin of the Geological Survey of South Australia* **35**, p148.

O'LEARY M. H. (1981) Carbon isotope fractionation in plants. *Phytochemistry* **20**, 553-567.

O'NEIL J. R. and EPSTEIN S. (1964) Oxygen isotope fractionation between dolomite and calcite. *Transactions of the American Geophysical Union* **45**, 113p.

O'NEIL J. R. and EPSTEIN S. (1966) Oxygen isotope fractionation in the system dolomite-calcite-carbon dioxide. *Science* **152**, 198-201.

OHMOTO H., KAKEGAWA T. and LOWE D. R. (1993) 3.4-Billion-year-old biogenic pyrites from Barberton, South Africa: Sulfur isotope evidence. *Science* **262**, 555-557.

OHMOTO H. and FELDER R. P. (1987) Bacterial activity in the warmer, sulphate bearing, Archaean oceans. *Nature* **328**, 244-246.

OHMOTO H. and RYE R. O. (1979) Isotopes of sulfur and carbon. Pages 509-567 of: Barnes H.L. (Ed.) Geochemistry of Hydrothermal Ore Deposits. John Wiley & Sons, New York, 798pp.

PAUSTIAN T. (2002) The Cell Wall. University of Wisconsin-Madison.
http://www.bact.wisc.edu/microtextbook/BacterialStructure/CellWall.html

PIERRE C. (1985) Isotopic evidence for the dynamic redox cycle of dissolved sulphur compounds between free and interstitial solutions in marine salt pans. *Chemical geology* **53**, 191-196.

PIERRE C., ORTLIEB L. and PERSON A. (1984) Supratidal evaporitic dolomite at Ojo de Liebre lagoon: mineralogical and isotopic arguments for primary crystallization. *Journal of Sedimentary Petrology* **54**, 1049-1061.

PISCIOTTO K. A. and MAHONEY J. J. (1981) Isotopic survey of diagenetic carbonates, Deep Sea Drilling Project Leg 63. Pages 595-609 of: Initial Reports of the Deep Sea Drilling Project, Volume 63; Long Beach, California to Mazatlan, Mexico.

POSTGATE J. R. (1984) The Sulphate-Reducing Bacteria (2nd Edition). Cambridge University Press, 208pp.

PYTKOWICZ R. M. (1983) Equilibria, Nonequilibria and Natural Waters: Wiley, New York, 704pp.

RASMUSSEN B. (2000) Filamentous microfossils in a 3,235-million-year-old volcanogenic massive sulfide deposit. *Nature* **405**, 676-679.

RASMUSSEN B. and BUICK R. (2000) Oily old ores: Evidence for hydrothermal petroleum generation in an Archaean volcanogenic massive sulfide deposit. *Geology* **28**, 731-734.

REES C. E., JENKINS W.J. and MONSTER J. (1978) The sulphur isotopic composition of ocean water sulphate. *Geochimica et Cosmochimica. Acta* **42**, 377-381.

REID R. P., VISSCHER P. T., DECHO A. W., STOLZ J. F., BEBOUT B. M., DUPRAZ C., MACINTYRE I. G., PAERL H. W., PINCKNEY J. L., PRUFERT-BEBOUTK L., STEPPE T. F. and DESMARAIS D. J. (2000) The role of microbes in accretion, lamination and early lithification of modern marine stromatolites. *Nature* **406**, 989-992.

ROBIE R. A. and WALDBAUM D. R. (1968) Thermodynamic properties of minerals and related substances at 298.15K (25°C) and one atmosphere (1.013 bars) pressure and at higher temperatures. *U.S. Geological Survey Bulletin* 1259.

ROLLINSON H. (1993) Using Geochemical Data: Evaluation, Presentation, Interpretation. Longman Group, 352pp.

ROSEN M. R., MISER D. E. and WARREN J. K. (1988) Sedimentology, mineralogy and isotopic analysis of Pellet Lake , Coorong region, South Australia. *Sedimentology* **35**, 105-122.

ROSEN M. R., MISER D. E., STARCHER M. A. and WARREN J. K. (1989) Formation of dolomite in the Coorong region, South Australia. *Geochimica et Cosmochimica Acta* **53**, 661-669.

RUNNEGAR B., DOLLASE W. A., KETCHAM R. A., COLBERT M. and CARLSON W. D. (2001a) Early Archean sulfates from Western Australia first formed as hydrothermal barites not gypsum evaporites. *GSA Annual Meeting (abstracts).*

RUNNEGAR B., COATH D., MOJZSIS S. J., FARQUHAR J., LYONS J. R., MCKEEGEN K. D. and HARRISON T. M. (2001b) Sulfur isotope evidence for atmospheric but not bacterial processes in formation of Early Archean sedimentary sulfides and sulfates. *GSA Annual Meeting (abstracts).*

SCHIDLOWSKI M., MATZIGKEIT U., MOOK W. G. and KRUMBEIN W. E. (1985). Carbon isotope geochemistry and 14C ages of microbial mats from the Gavish Sabkha and the Solar Lake. Pages 381-401 of: Friedman G. M. and Krumbein W. G. (Eds). Hypersaline Ecosystems: The Gavish Sabkha. *Ecological Studies* **53**.

SCHIDLOWSKI M., GOLUBIC S., KIMBERLEY M. M., McKIRDY D. M. and TRUDINGER P. A. (Eds). (1992) Early Organic Evolution: Implications for Mineral and Energy Resources. Springer-Verlag, Berlin, 555pp.

SCHULZ H. D. and ZABEL M. (2000) Marine Geochemistry. Springer-Verlag, Berlin, 455pp.

SCHWIEGER F. and TEBBE C. C. (1998) A new approach to utilise PCR-single-strand-conformation polymorphism for 16S rRNA gene based microbial community analysis. *Applied and Environmental Microbiology* **64**, 4870-4876.

SHEN Y., BUICK R. and CANFIELD D. E. (2001) Isotopic evidence for microbial sulphate reduction in the early Archaean Era. *Nature* **410**, 77-81.

SHEPPARD S. M. F. and SCHWARCZ H. P. (1970) Fractionation of carbon and oxygen isotopes and magnesium between coexisting metamorphic calcite and dolomite. *Contributions to Mineralogy and Petrology* **26**, 161-198.

SIBLEY D. F. (1980) Climatic control of dolomitization, Seroe Domi Formation (Pliocene), Bonaire, N.A. *S.E.P.M. Special Publication* **28**, 247-258.

SIEVERT S. M., BRINKHOFF T., MUYZER G., ZIEBIS W. and KUEVER J. (1999) Spatial heterogeneity of bacterial populations along an environmental gradient at a shallow submarine hydrothermal vent near Milos Island, Greece. *Applied and Environmental Microbiology* **65**, 3834-3842.

SILBERBERG M. S. (2000) Chemistry (The Molecular Nature of Matter and Change), 2nd Edition. McGraw-Hill, 1086pp.

SIMMS M. (1984) Dolomitization by groundwater-flow systems in carbonate platforms. *In: Transactions of the 34th annual meeting, Gulf Coast Association of Geological Societies*, 411-420.

SINGLETON P. (1997) Bacteria in Biology, Biotechnology and Medicine (4th Edition). Wiley, New York, 403pp.

SKINNER H. C. W. (1963) Precipitation of calcian dolomites and magnesian calcites in the southeast of South Australia. *American Journal of Science* **261**, 449-472.

SLAUGHTER M. and HILL R. J. (1991) The influence of organic matter in organogenic dolomitization. *Journal of Sedimentary Petrology* **61**, 296-303.

SMOCK A. M., BOTTCHER M. E. and CYPIONKA H. (1998) Fractionation of sulfur isotopes during thiosulfate reduction by *Desulfovibrio desulfuricans*. *Archives of Microbiology* **169**, 460-463.

SPRACHTA S. G., CAMOIN G., GOLUBIC S. and LE CAMPION T. H. (2001) Microbialites in a modern lagoonal environment: nature and distribution, Tikehau atoll (French Polynesia) *Palaeogeography, Palaeoclimatology, Palaeoecology* **175**, 103-124.

SPRIGG R. C. (1952) The geology of the southeast province of South Australia, with special reference to Quaternary coastline migrations and modern beach development. *Bulletin of the Geological Survey of South Australia* **29**.

STALEY J. T. and KONOPKA A. (1985) Measurement of *in situ* activities of no-photosynthetic microorganisms in aquatic and terrestrial habitats. *Annual Reviews in Microbiology* **39**, 321-346.

STANIER R. Y., INGRAHAM J. L., WHEELIS M. L. and PAINTER P. R. (1986) General microbiology (5th Edition). Macmillan Education Ltd., London, 689pp.

STEINEN R. P., MATTHEWS R. K. and SEALY H. A. (1978) Temporal variation in geometry and chemistry of the freshwater phreatic lens: the coastal aquifer of Christ Church, Barbados, West Indies. *Journal of Sedimentary Petrology* **48**, 733-742.

STRAUSS H. and BEUKES N. J. (1996) Carbon and sulfur isotopic compositions of organic carbon and pyrite in sediments from the Transvaal Supergroup, South Africa. *Precambrian Research* **79**, 57-71.

TANNER M. A., EVERETT C. L., COLEMAN W. J., YANG M. M. and YOUVAN D. C. (2000) Complex microbial consortia inhabiting hydrogen sulfide-rich black mud from marine coastal environments. *Biotechnology et alia* **8**, 1-16.

TESKE A., WAWER C., MUYZER G. and RAMSING N. B. (1996) Distribution of sulphate-reducing bacteria in a stratified Fjord (Mariager Fjord, Denmark) as evaluated by most-probable-number counts and denaturing gradient gel electrophoresis of PCR-amplified ribosomal DNA fragments. *Applied and Environmental Microbiology* **62**, 1405-1415.

TESKE A., RAMSING N. B., HABICHT K. S., FUKUI M., KUVER J., JORGENSEN B. B. and COHEN Y. (1998) Sulfate-reducing bacteria and their activities in cyanobacterial mats of Solar Lake (Sinai, Egypt). *Applied and Environmental Microbiology* **64**, 2943-2951.

THODE H. G. and MONSTER J. (1965) Sulfur-isotope geochemistry of petroleum, evaporites and ancient seas. *American association of Petroleum Geologists memoirs* **4**, 367-377.

TRUDINGER P. A. (1992) Bacterial sulphate reduction: current status and possible origin. Pages 367-377 of: SCHIDLOWSKI M., GOLUBIC S., KIMBERLEY M. M., McKIRDY D. M. and TRUDINGER P. A. (Eds.) Early Organic Evolution: Implications for Mineral and Energy Resources. Springer-Verlag, Berlin, 555pp.

TUCKER M. E. (2001) Sedimentary Petrology: an introduction to the origin of sedimentary rocks, 3rd Edition. Blackwell Science, 262pp.

TURNER J. V. (1982) Kinetic fractionation of carbon-13 during calcium carbonate precipitation. *Geochimica et Cosmochimica Acta* **46**, 1183-1191.

UNESCO (1981a) The practical salinity scale 1978 and the international equation of state of seawater 1980. *UNESCO Technical Papers in Marine Science* **36**, 25pp.

UNESCO (1981b) Background papers and supporting data on the practical salinity scale, 1978. *UNESCO Technical Papers in Marine Science* **37**, 144pp.

USDOWSKI H. E. (1967) The formation of dolomite in sediments. Pages 21-32 of: Recent Developments in Carbonate Sedimentology in Central Europe (Eds G. Muller, and G.M., Friedman), Springer-Verlag, Berlin.

VASCONCELOS C., McKENZIE J. A., BERNASCONI S., GRUJIC D. and TIEN A. J. (1995) Microbial mediation as a possible mechanism for natural dolomite formation at low temperatures. *Nature* **377**, 220-222.

VASCONCELOS C. and McKENZIE J . A. (1997) Microbial mediation of modern dolomite precipitation and diagenesis under anoxic conditions (Lagoa Vermelha, Rio de Janeiro, Brazil). *Journal of Sedimentary Research* **67**, 378-390.

VOGEL A. I. (1978) Textbook of quantitative inorganic analysis (4th Edition). Longman Group, 1216pp.

VOGEL J. C., GROOTES P. M. and MOOK W. G. (1970) Isotope fractionation between gaseous and dissolved carbon dioxide. *Zeitschrift fur Physik* **230**, 255-258.

VON DER BORCH C. C. (1965a) The distribution and preliminary geochemistry of modern carbonate sediments of the Coorong area, South Australia. *Geochimica et Cosmochimica Acta* **29**, 781-799.

VON DER BORCH C. C. (1965b) Source of ions for Coorong dolomite formation. *American Journal of Science* **263**, 684-688.

VON DER BORCH C. C. (1976) Stratigraphy and formation of Holocene dolomitic carbonate deposits of the Coorong area, South Australia. *Journal of Sedimentary Petrology* **46**, 952-966.

VON DER BORCH C. C. and JONES J. B. (1976) Spherular modern dolomite from the Coorong area, South Australia. *Sedimentology* **23**, 587-591.

VON DER BORCH C. C., LOCK D. E. and SCHWEBEL D. (1975) Ground-water formation of dolomite in the Coorong region of South Australia. *Geology* **3**, 283-285.

VON DER BORCH C. C. and LOCK D. (1979) Geological significance of Coorong dolomites. *Sedimentology* **26**, 813-824.

VON DER BORCH C. C., RUBIN M and SKINNER B. J. (1964) Modern dolomite from South Australia. *American Journal of Science* **262**, 1116-1118.

WAGNER P. D. (1983) Geochemical characterization of meteoric diagenesis in limestone – development and applications (unpublished PhD dissertation), Brown University.

WALTER M. R., GOLUBIC S., PREISS W. V. (1973) Recent stromatolites from hydromagnesite and aragonite depositing lakes near the Coorong Lagoon, South Australia. *Journal of Sedimentary Petrology* **43**, 1021-1030.

WARREN J. K. (1990) Sedimentology and mineralogy of dolomitic Coorong lakes, South Australia. *Journal of Sedimentary Petrology* **60**, 843-858.

WARTHMANN R., VAN LITH Y., VASCONCELOS C., McKENZIE J. A. and KARPOFF A. M. (2000) Bacterially induced dolomite precipitation in anoxic culture experiments. *Geology* **28**, 1091-1094.

WRIGHT D. T. (1993) Studies of the Cambrian Eilean Dubh Formation of north-western Scotland. Unpublished D. Phil. Thesis, University of Oxford, 336pp.

WRIGHT D. T. (1997) An organogenic origin for widespread dolomite in the Cambrian Eilean Dubh formation, North-western Scotland. *Journal of Sedimentary Research* **67**, 54-64.

WRIGHT D. T. (1999) The role of sulphate-reducing bacteria and cyanobacteria in dolomite formation in distal ephemeral lakes of the Coorong region, South Australia. *Sedimentary Geology* **126**, 147-157.

WRIGHT D. T. (2000) Benthic microbial communities and dolomite formation in marine and lacustrine environments – a new dolomite model. Pages 7-20 of: Glenn C. R., Prevot L. L. and Lucas J (Eds). Marine authigenesis; from global to microbial. *S.E.P.M. Special Publication* **66**.

WRIGHT D. T. and ALTERMANN W. (2000) Microfacies development in Late Archaean stromatolites and oolites of the Ghaap Group of South Africa. In: INSALACO E., SKELTON P. W. and PALMER T. J. (Eds). Carbonate paltform systems: components and interactions. *Geological Society of London, Special Publications* **179**, 51-70.

APPENDICES



An echidna

APPENDIX 1

X-RAY DIFFRACTOMETRY OF THE LAKE SEDIMENTS

The Coorong distal lake sediments were examined using X-Ray diffractometry to accurately establish their mineralogy and, in the case of dolomitic samples, to estimate their degree of ordering. Fifty millimetre cores from each lake were divided into 10mm sections and then gently disaggregated using a mortar and pestle. Disaggregation was done slowly and as gently as possible to minimise crystal structure deformation. The powders from the top 10mm of each core were mounted and run on a Philipps HT Generator Model PW 13 20/00 at the Department of Earth Sciences, University of Oxford, using a diffractometer Model PW 1050. Subsequently this machine was shut down and the remainder of samples were run on a Philips PW1716 diffractometer with a PW1729 generator and PW1050/25 detector at the Department of Geology, University of Leicester. The XRD analyses are shown in Figures A1.1 - A1.8. The results are summarised below.

Lake	Carbonate Mineralogy (in order of abundance)	Accessory Minerals (in order of abundance)
Milne	Dolomite, Magnesite	Quartz (v.abundant), Halite
Pellet	Dolomite, Huntite, Hydro-magnesite	Halite, Quartz
Mini Dolomite	Dolomite, (Kutnohorite?)	Halite, Quartz, (Celestine?)
Mcfaiden	Dolomite	Halite, Quartz
Dolomite	Dolomite	Halite, Quartz
Halite	Aragonite, Mg-calcite, (Dolomite?)	Quartz, Halite, Gypsum
North Stromatolite	Aragonite, Hydro-mag., Mg-calcite	Quartz, Halite
South Stromatolite	Aragonite, Mg-calcite, Hydro-mag.	Halite, Quartz

Table A1.1. Mineralogy of the Coorong study lakes as determined by X-ray diffraction

It can be seen that five lakes; Milne, Pellet, Mini Dolomite, McFaiden and Dolomite Lakes contain abundant dolomite with accessory quartz and halite. Milne Lake is slightly different

to the other four, being very quartz rich and also containing abundant magnesite. The remaining three lakes (Halite, North Stromatolite, South Stromatolite) are dominated by aragonite, with calcite, hydromagnesite, halite and quartz also present.

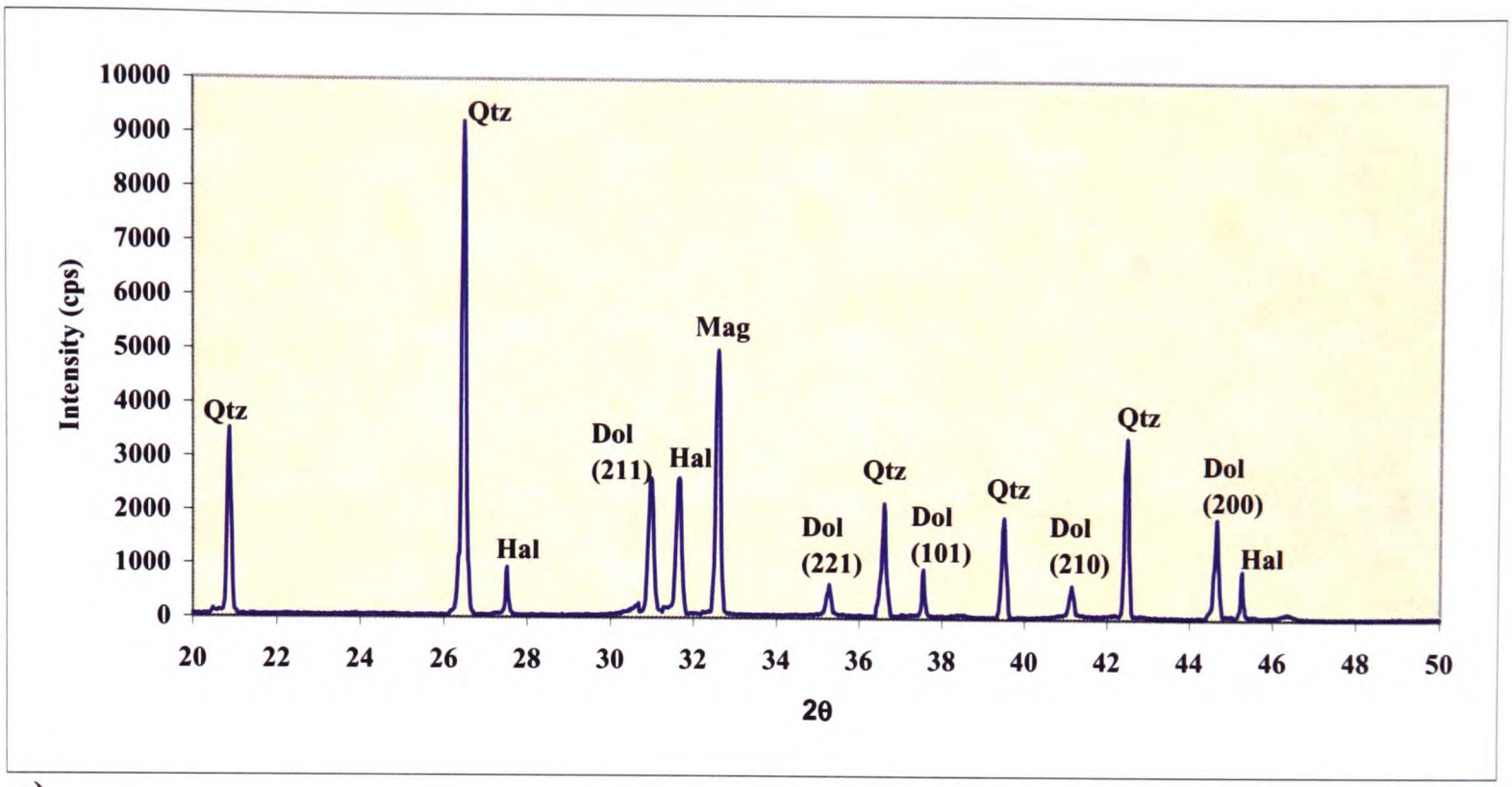
Degree of ordering in the dolomite

The basal cation planes in dolomite are alternately occupied by Ca and Mg resulting in a lowering of symmetry compared to that in calcite. The Additional X-ray reflections observed for dolomite, which result from this alternation of cation planes, are called ordering reflections. At the range of 2θ values which these samples were run at, there are three principle order reflections at 2θ = 22.1°, 35.3° and 43.8°, corresponding to the crystallographic planes (100), (221) and (111), together with a lower order reflection at 2θ = 33.6° corresponding to the basal (222) plane. The major dolomite reflection in all of the samples was at 2θ = 31° corresponding to the (211) plane. All of the dolomites show at least one order reflection and are therefore true dolomites.

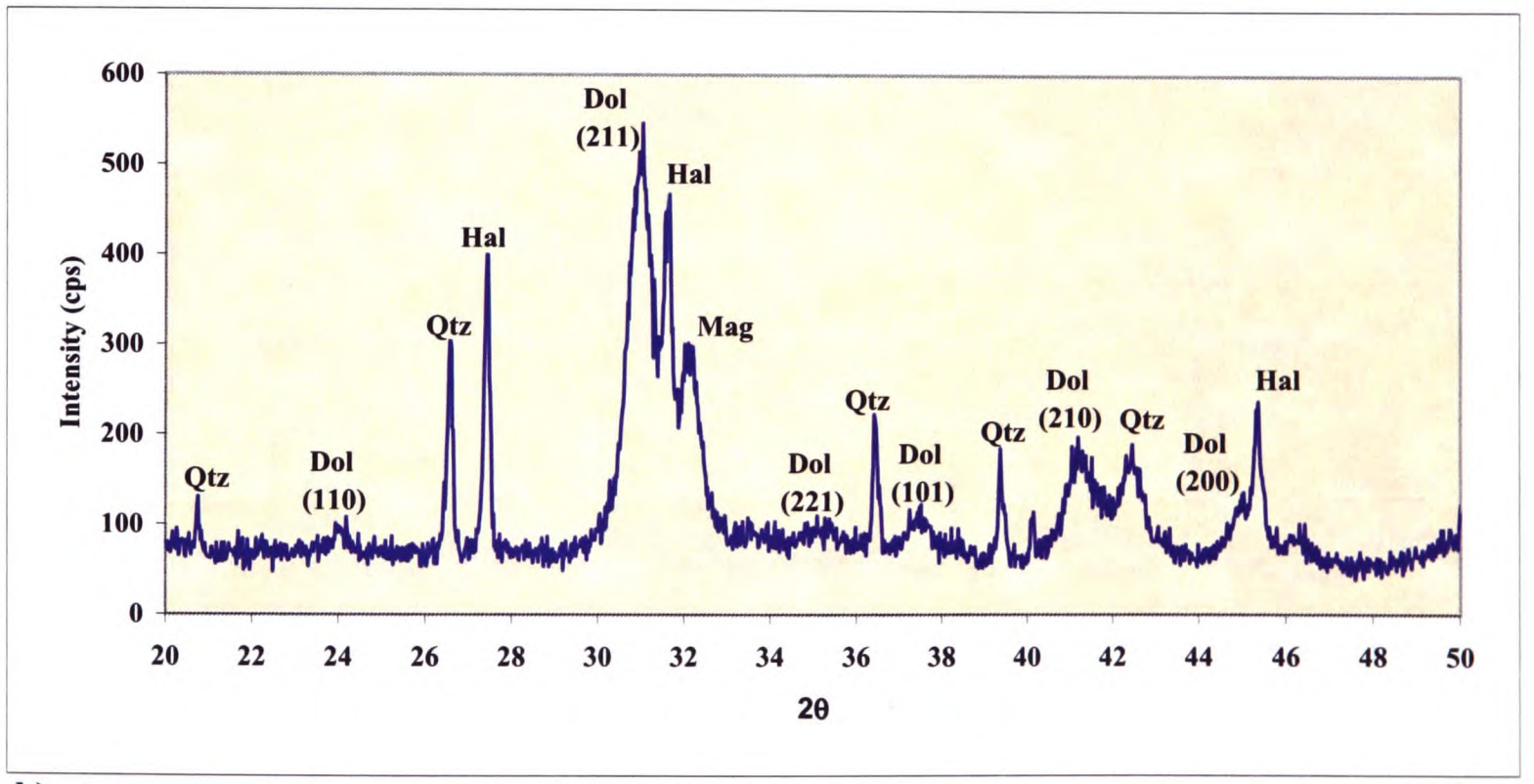
Only two of the lakes (Milne and Mini Dolomite) show definite principle ordering peaks at (221), whilst Dolomite Lake shows evidence of a slight bulge around 2θ = 35.3° but no real peak. To assess the degree of ordering in the dolomites, the intensity of the ordering peak (221) is divided by the intensity of a dolomite reference peak (101), which has no influence from the ordered cation planes. The intensity of the (221) ordering peak decreases when positions in the lattice, which in ideal dolomite are occupied by magnesium, are instead occupied by heavier cations leading to increased scattering of the X-rays. The greater the ratio of (221)/(101), the greater the degree of ordering. The results are shown in Table A1.2.

Lake	Ordering	
	Surface	**50mm**
Milne	~ 0.75	~ 0.75
Mini Dolomite	~ 0.333	~0.90
Dolomite	~ 0.100	(221) peak diffuse
Pellet	(221) peak not clearly defined	
McFaiden	(221) peak not clearly defined	

Table A1.2. Degree of ordering of the dolomite in Coorong lakes

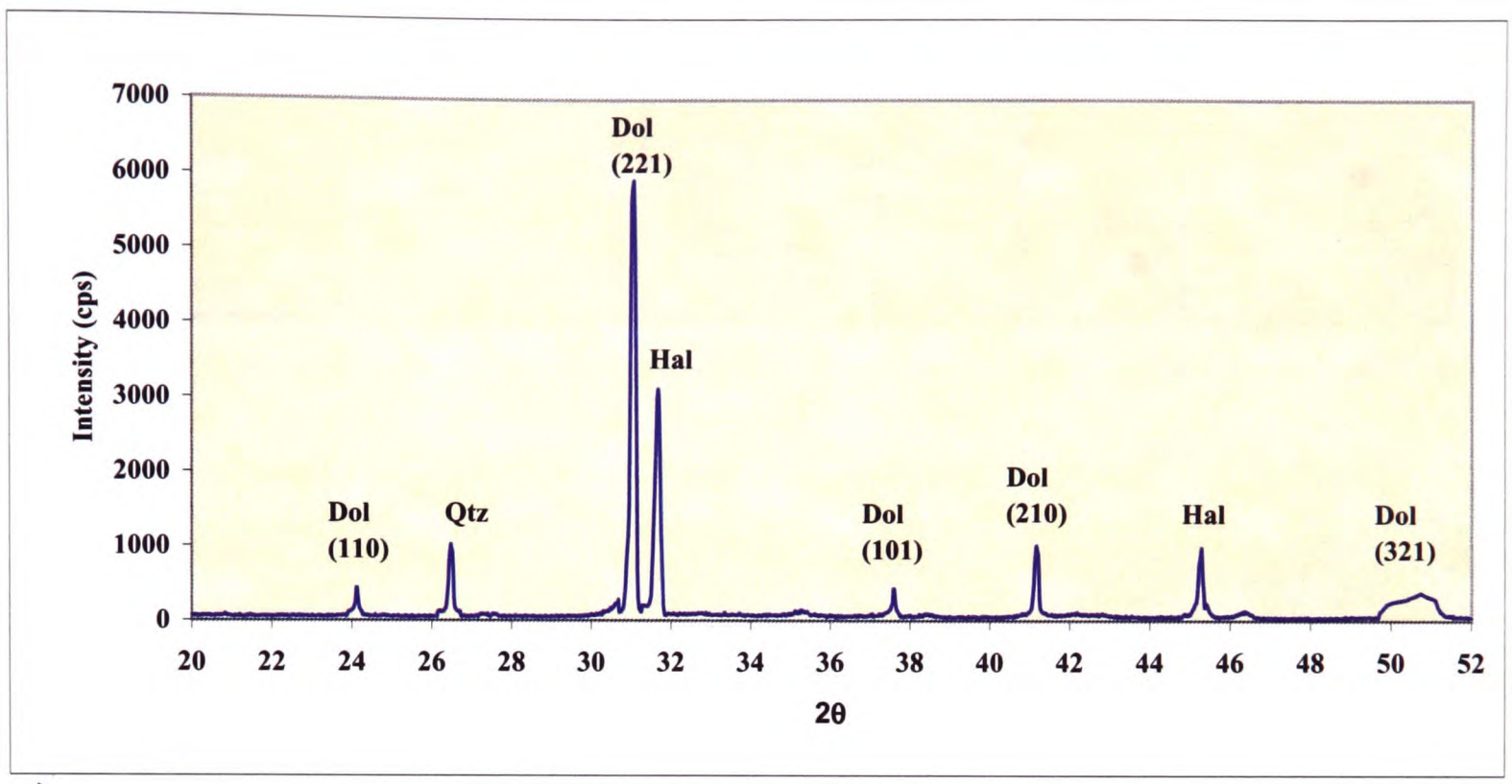


a)

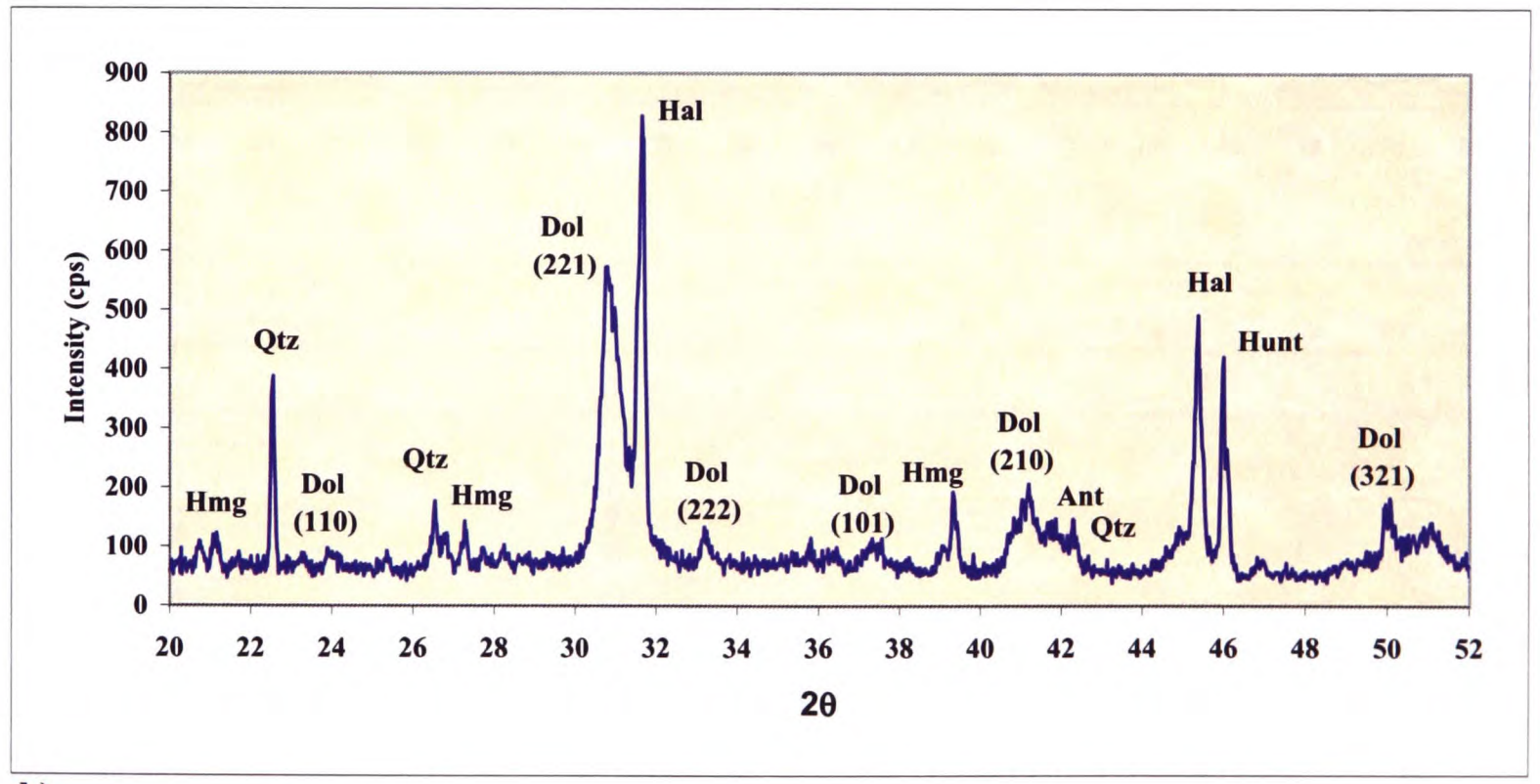


b)

Figure A1.1. X-ray diffractograms from Milne Lake
a) Surface sediment b) Sediment from 50mm depth

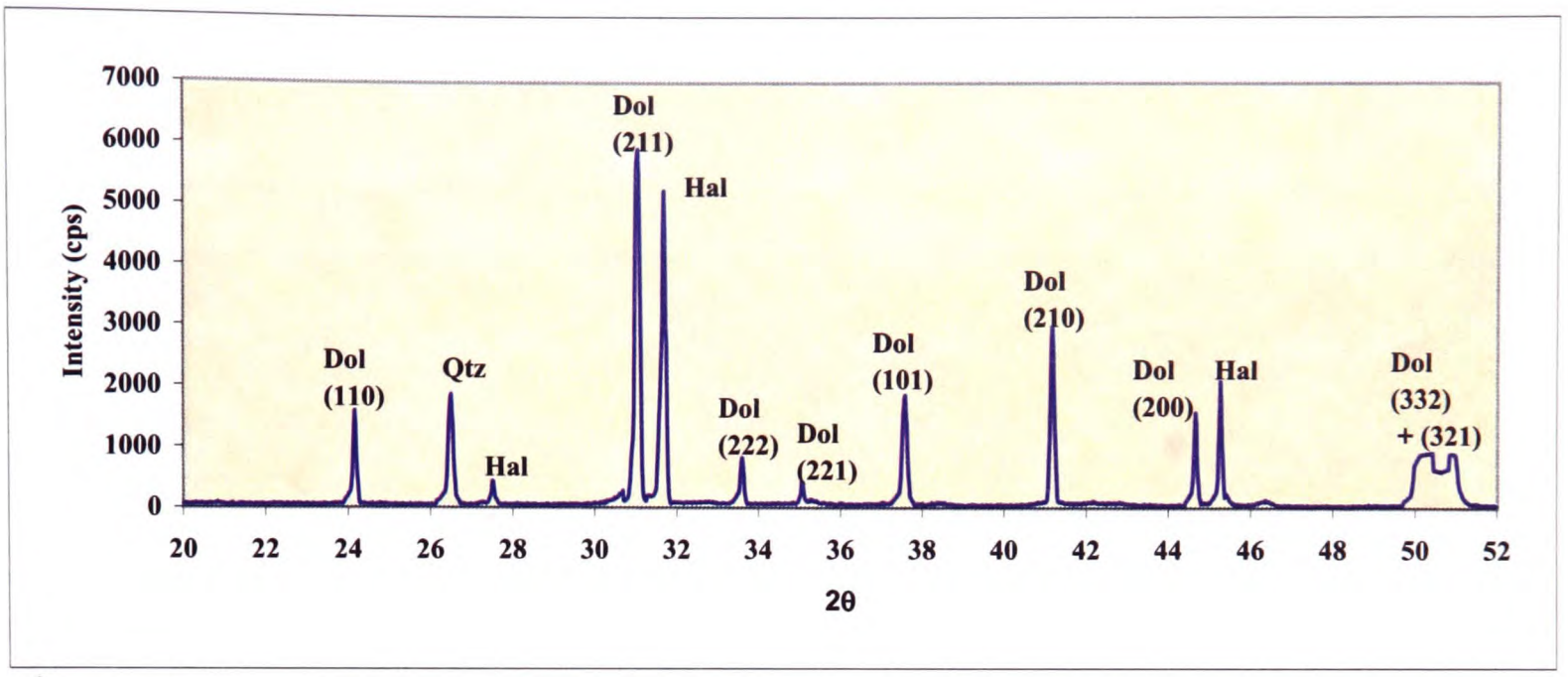


a)

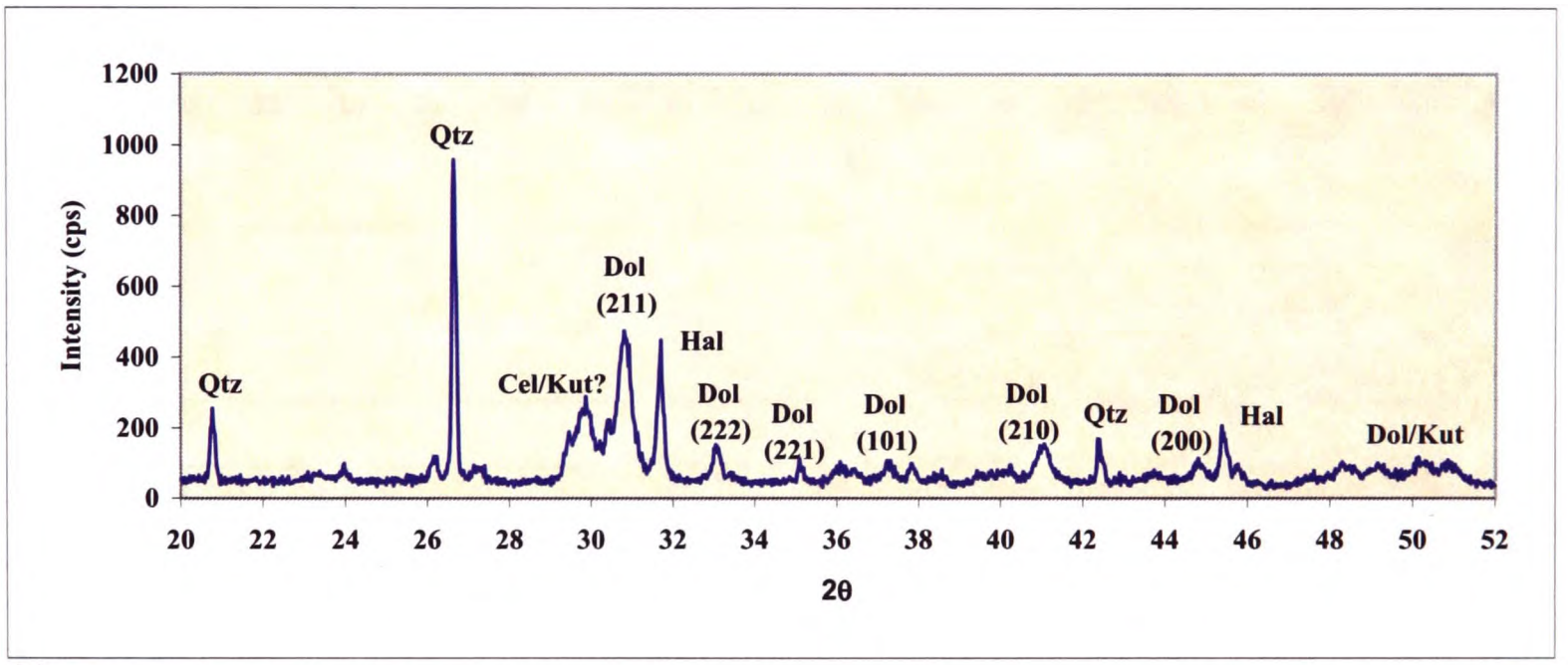


b)

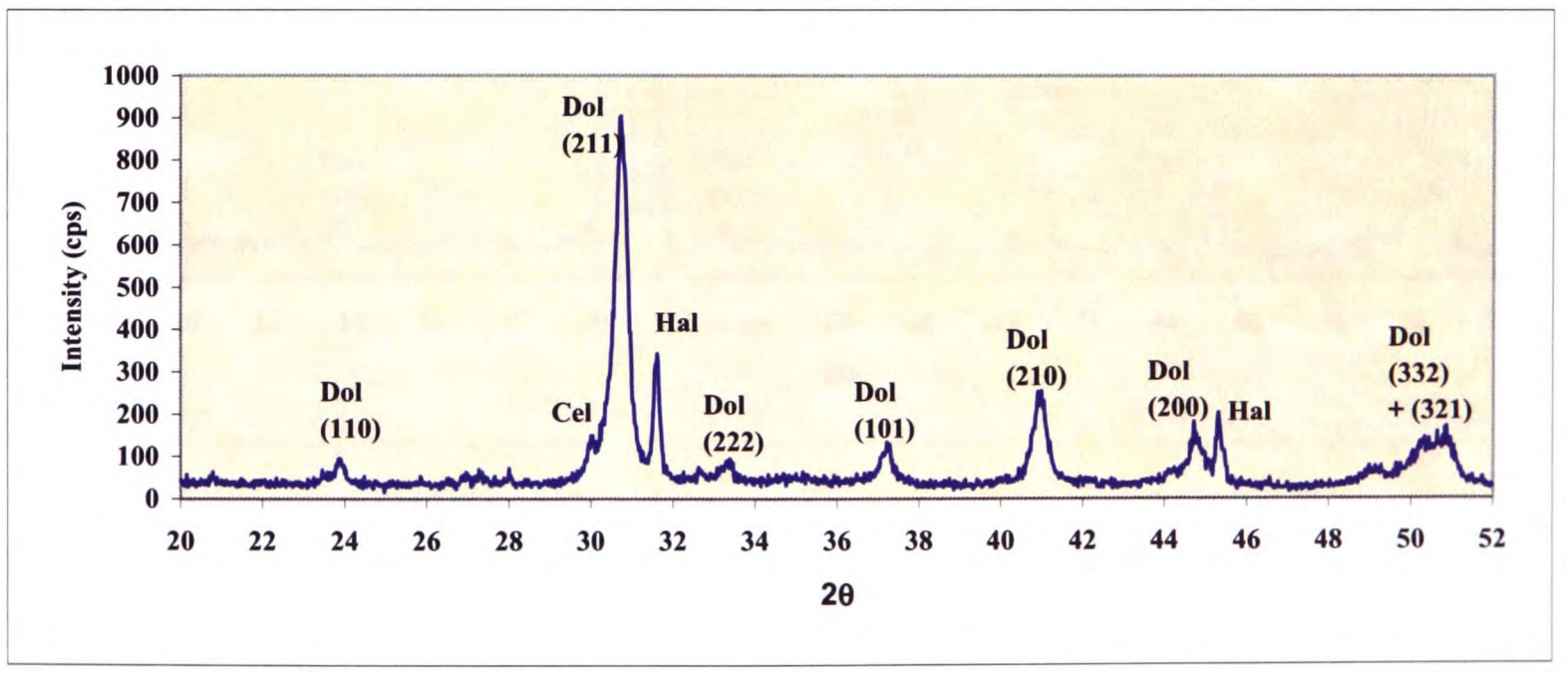
Figure A1.2. X-ray diffractograms from Pellet Lake
a) Surface sediment b) Sediment from 50mm depth



a)

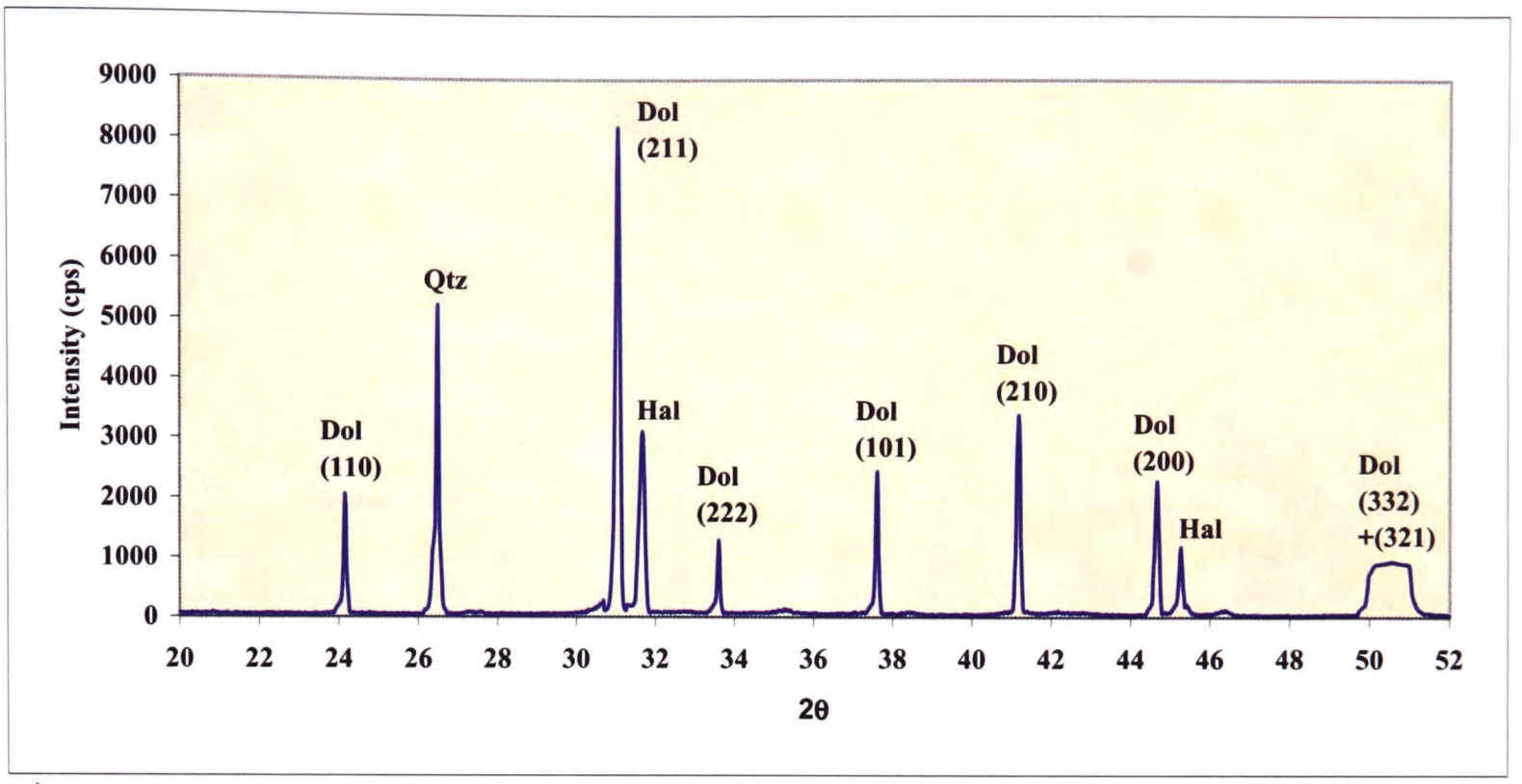


b)

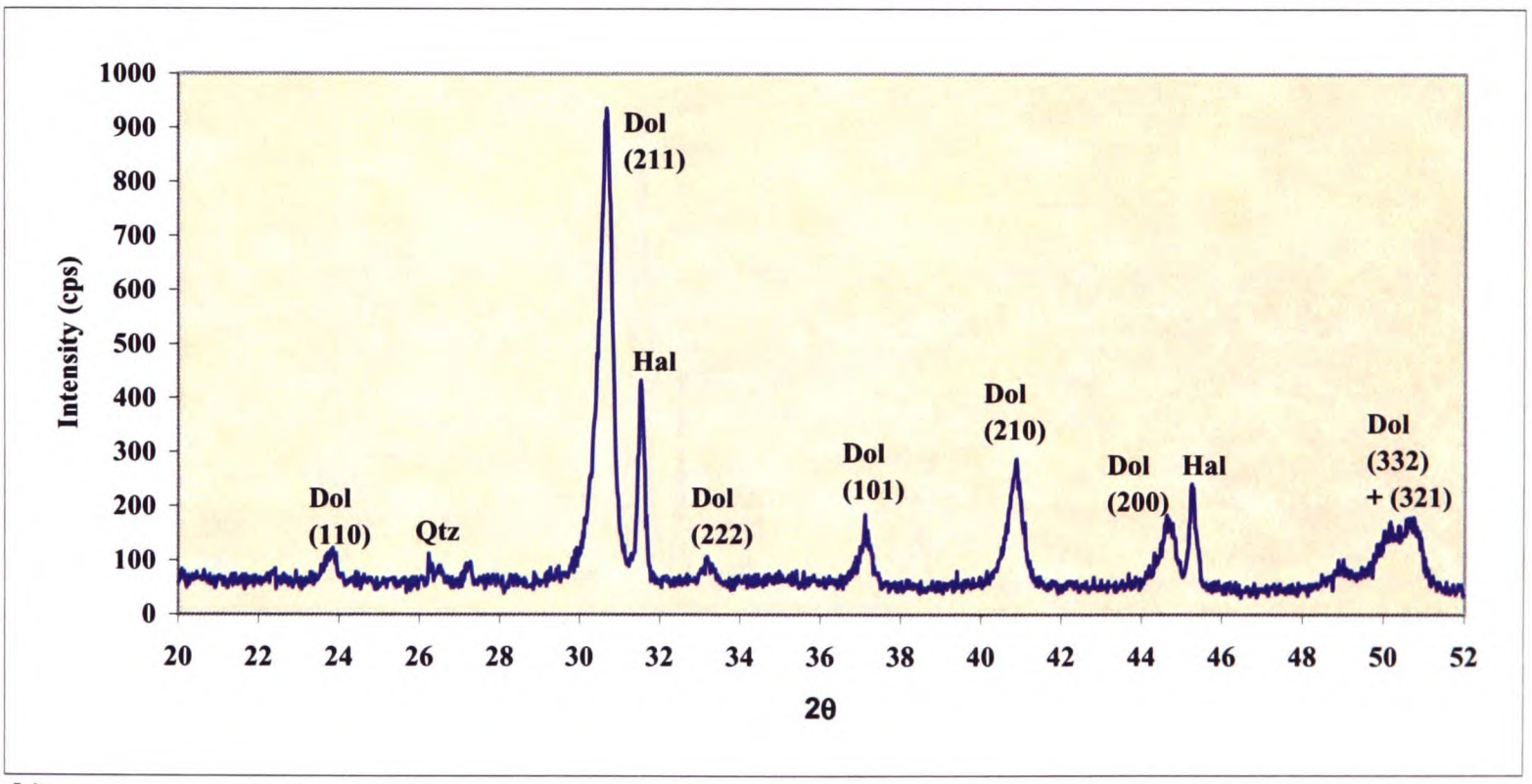


c)

Figure A1.3. X-ray diffractograms from Mini Dolomite Lake
a) Surface sediment b) 50mm depth c) 90mm depth

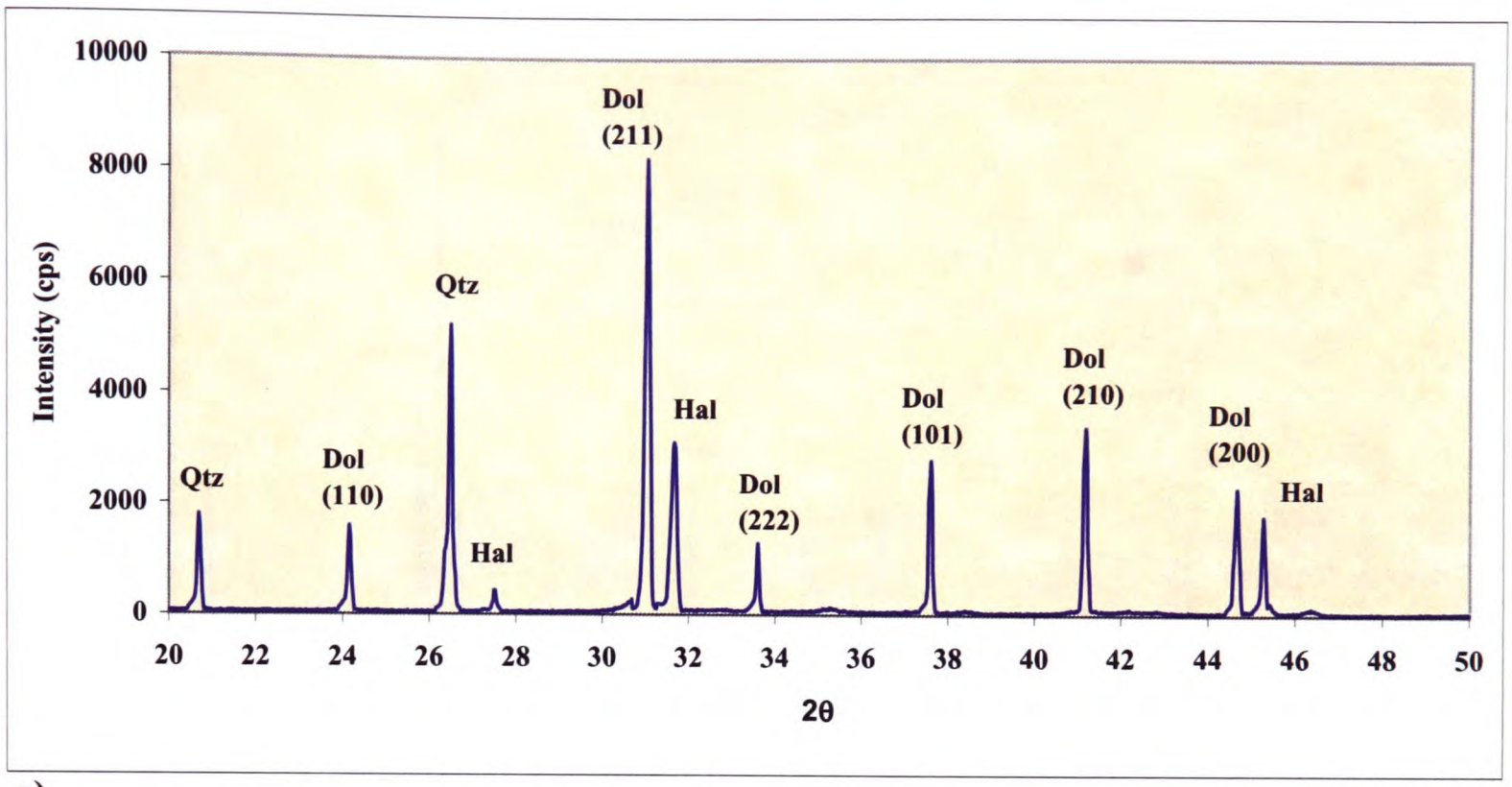


a)

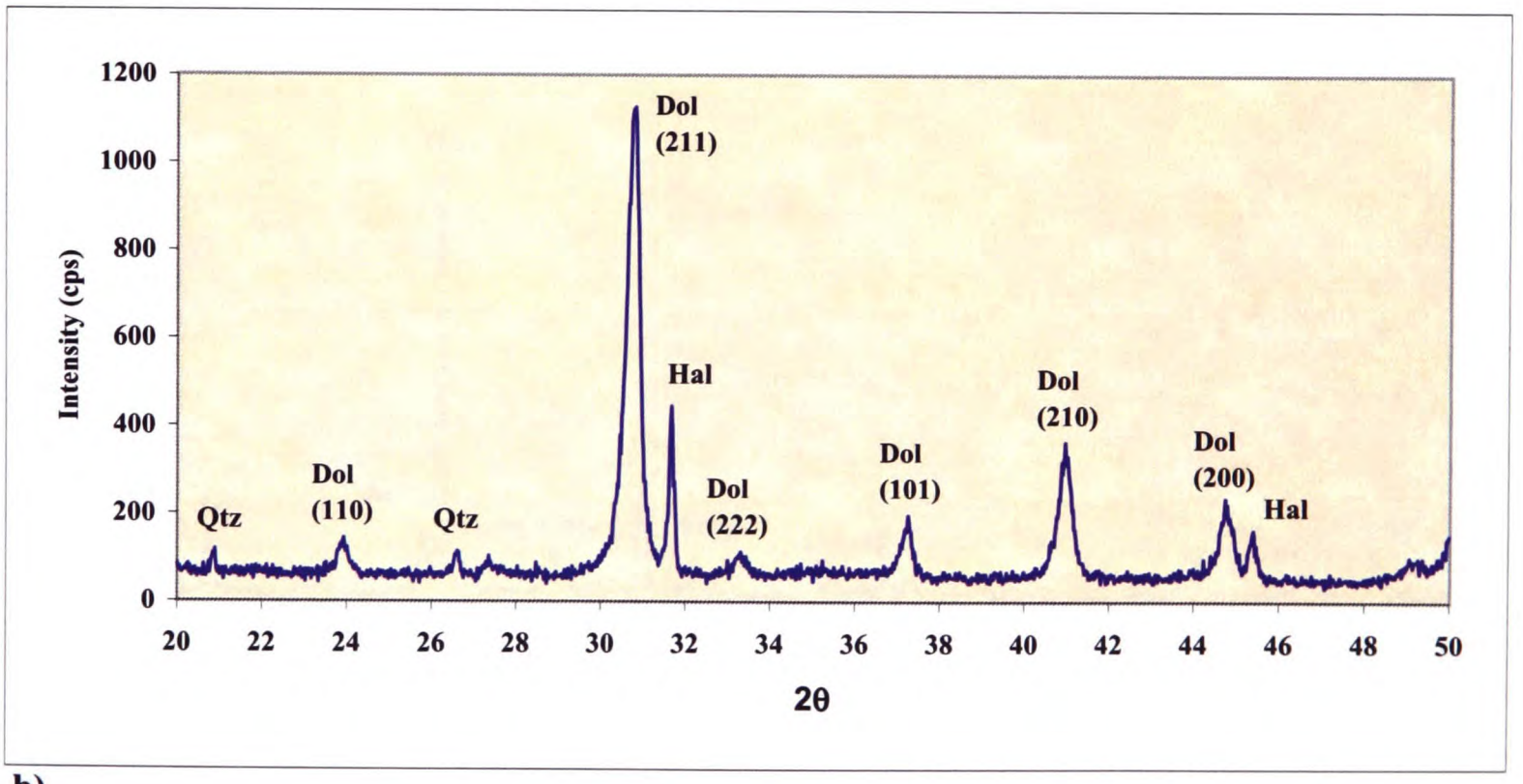


b)

Figure A1.4. X-ray diffractograms from McFaiden Lake
a) Surface sediment b) Sediment from 50mm depth

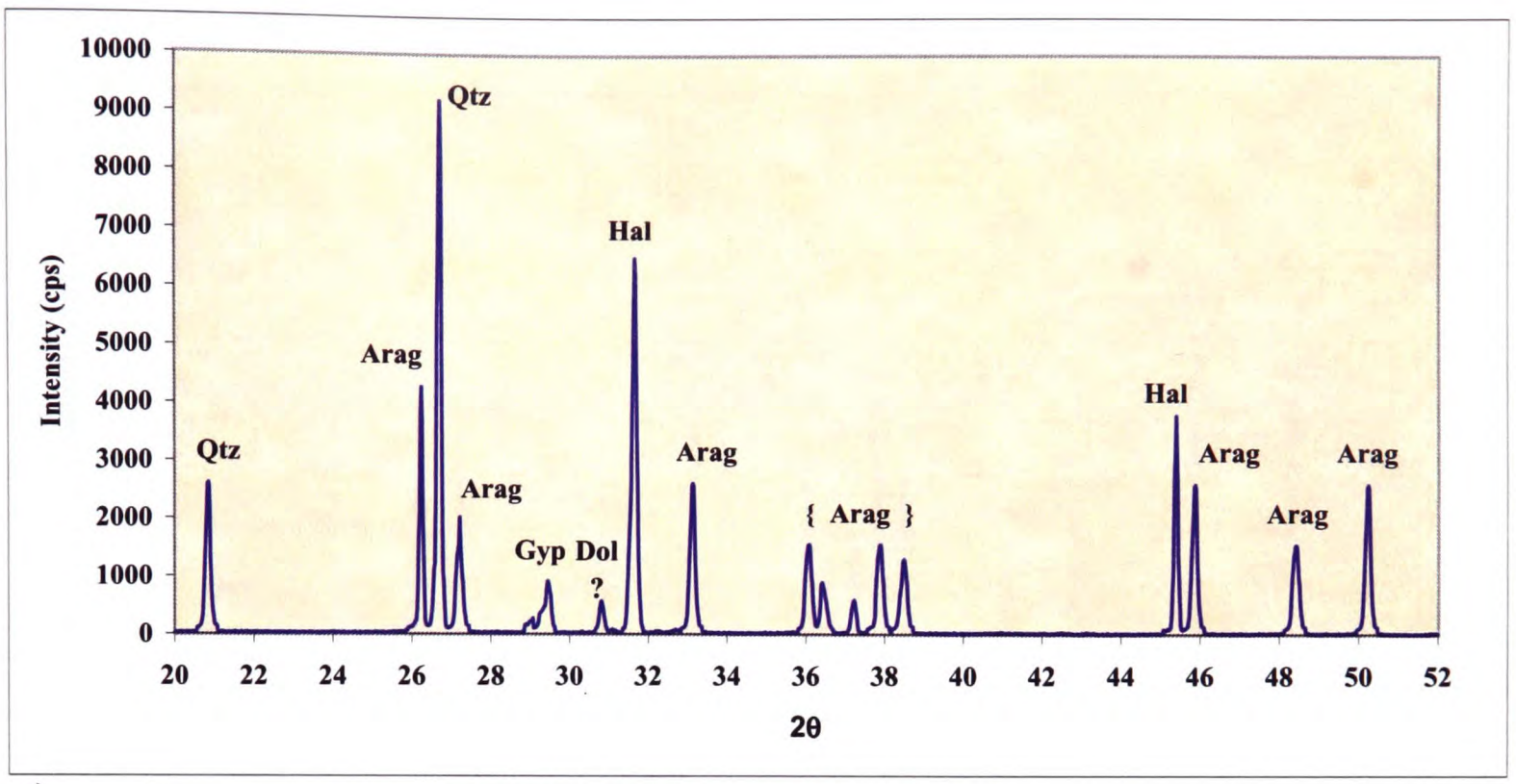


a)

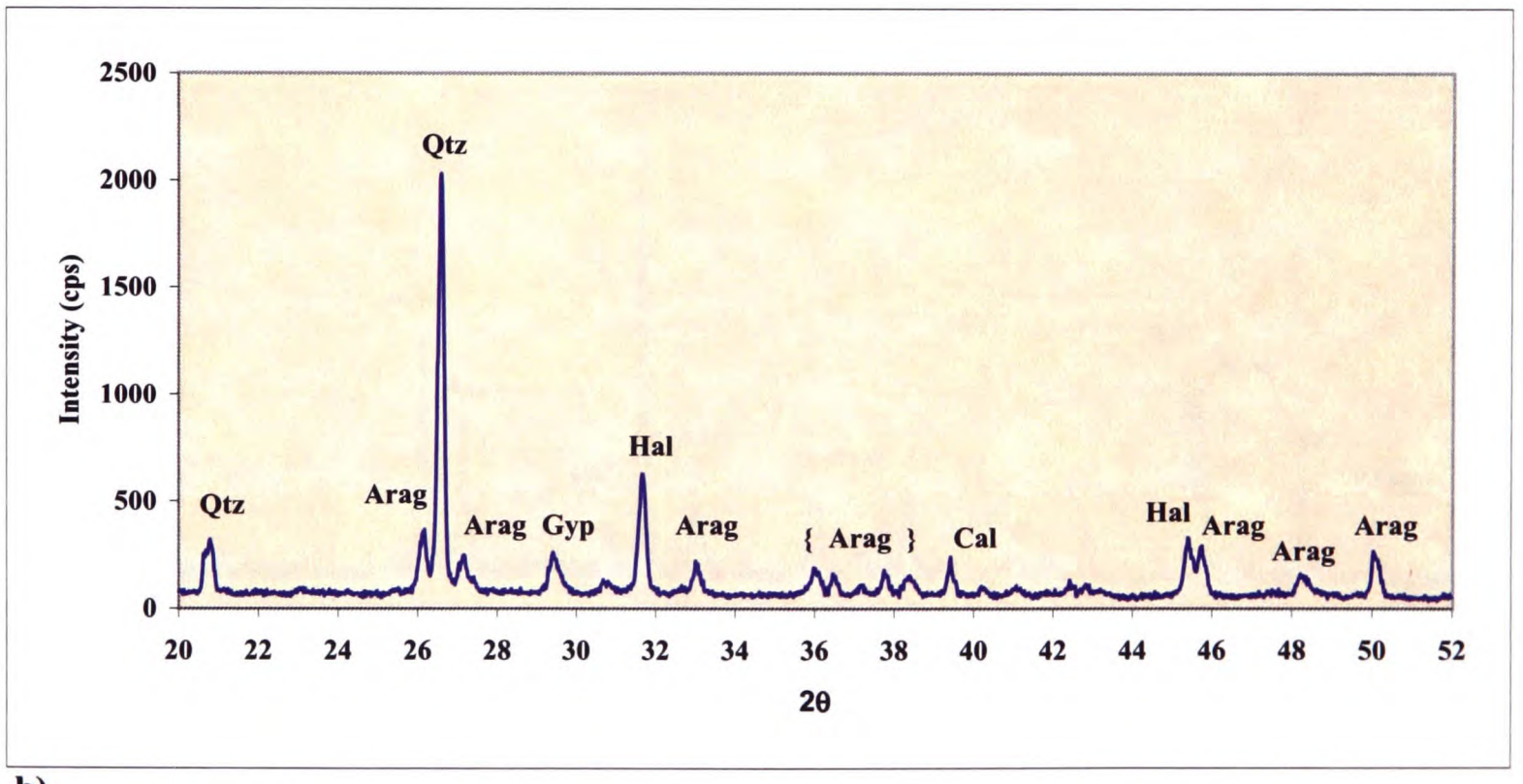


b)

Figure A1.5. X-ray diffractograms from Dolomite Lake
a) Surface sediment b) Sediment from 50mm depth

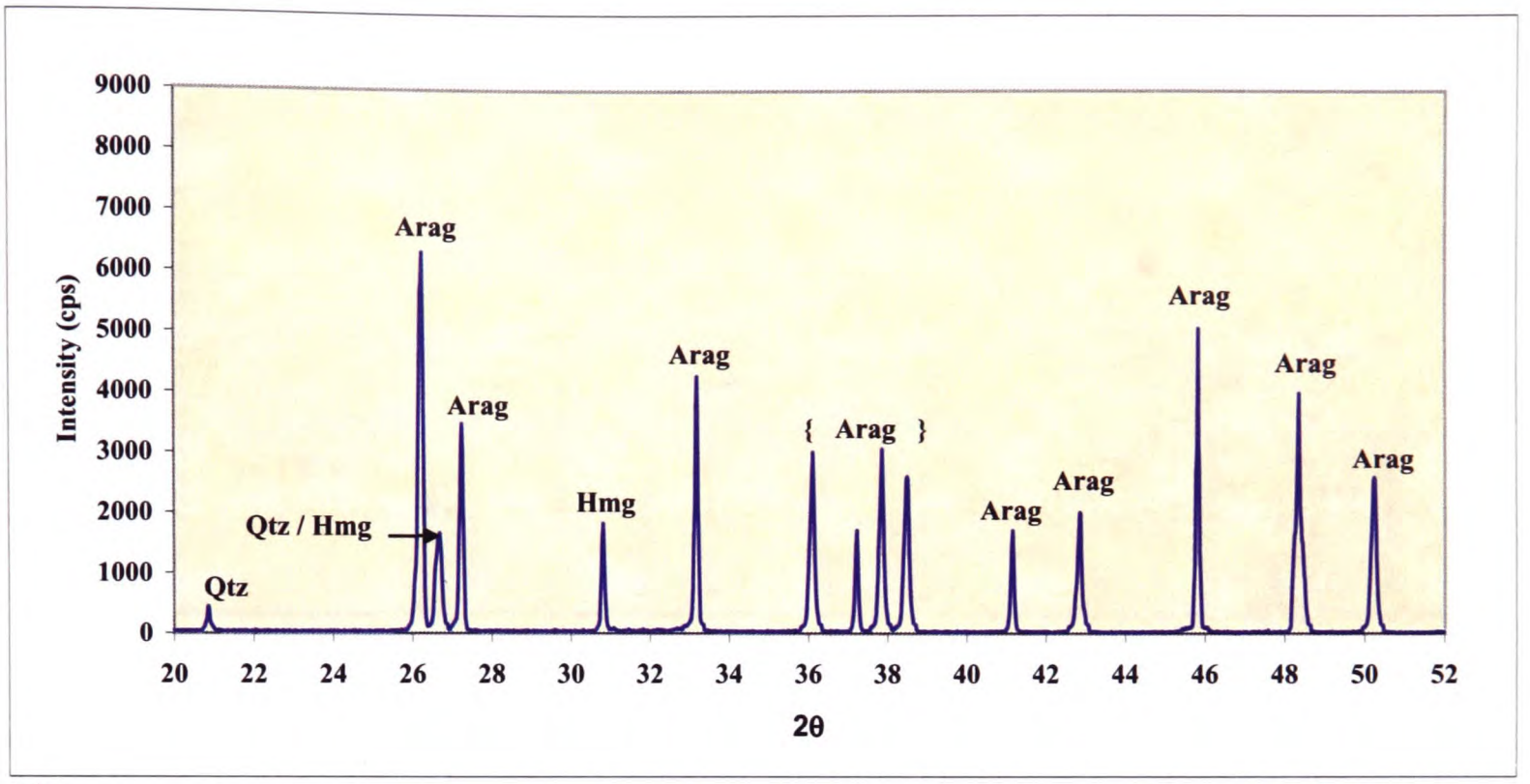


a)

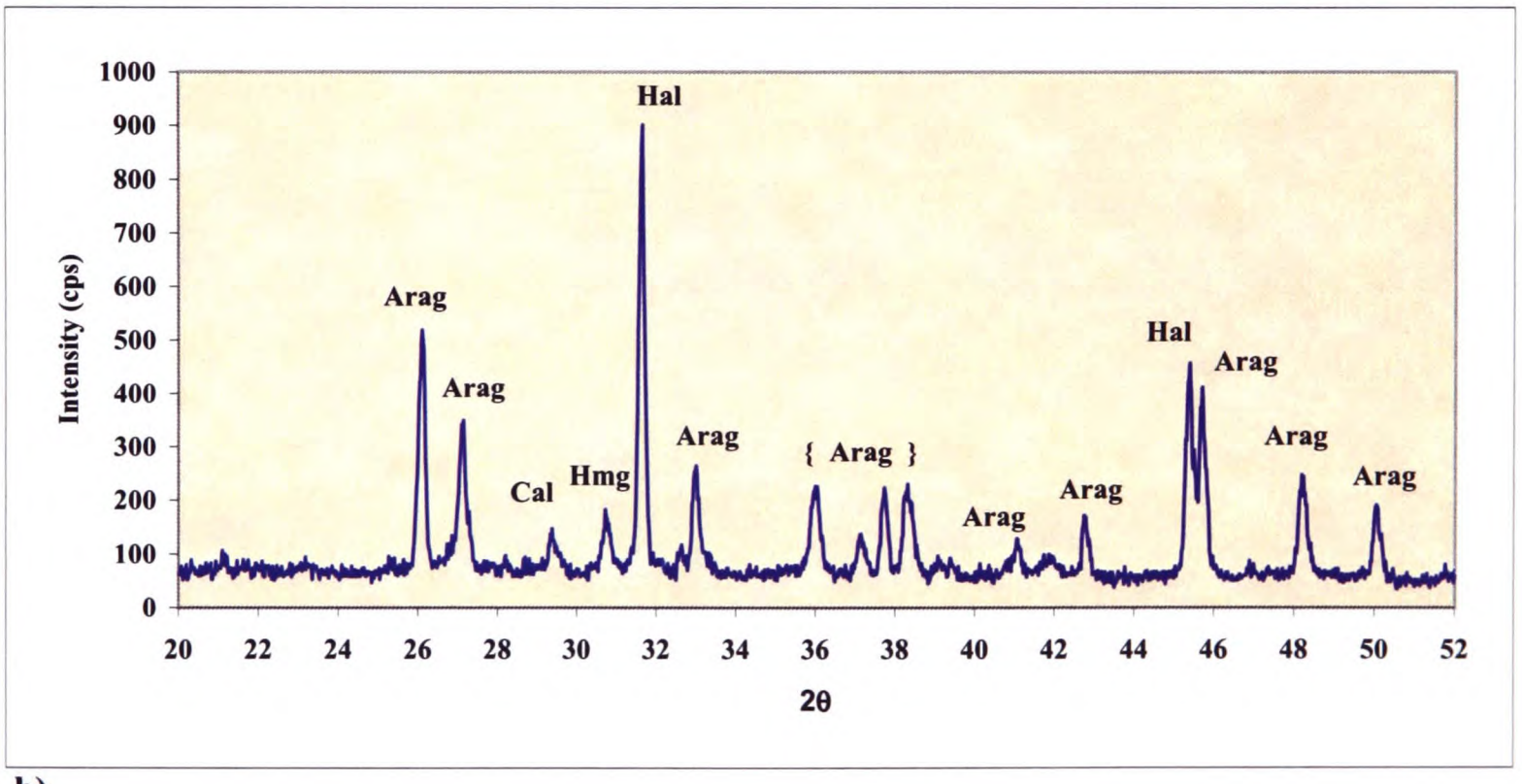


b)

Figure A1.6. X-ray diffractograms from Halite Lake
a) Surface sediment b) Sediment from 50mm depth

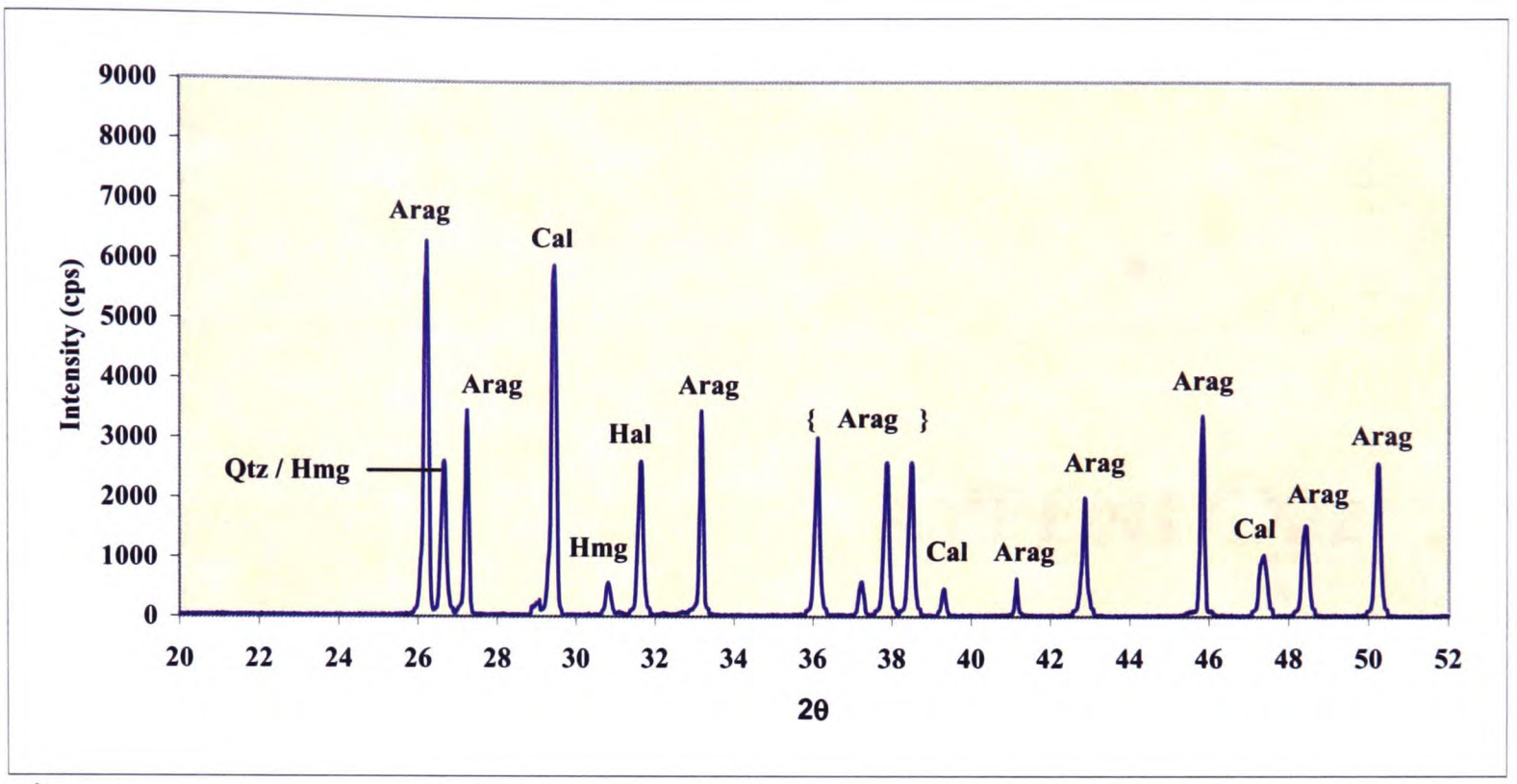


a)

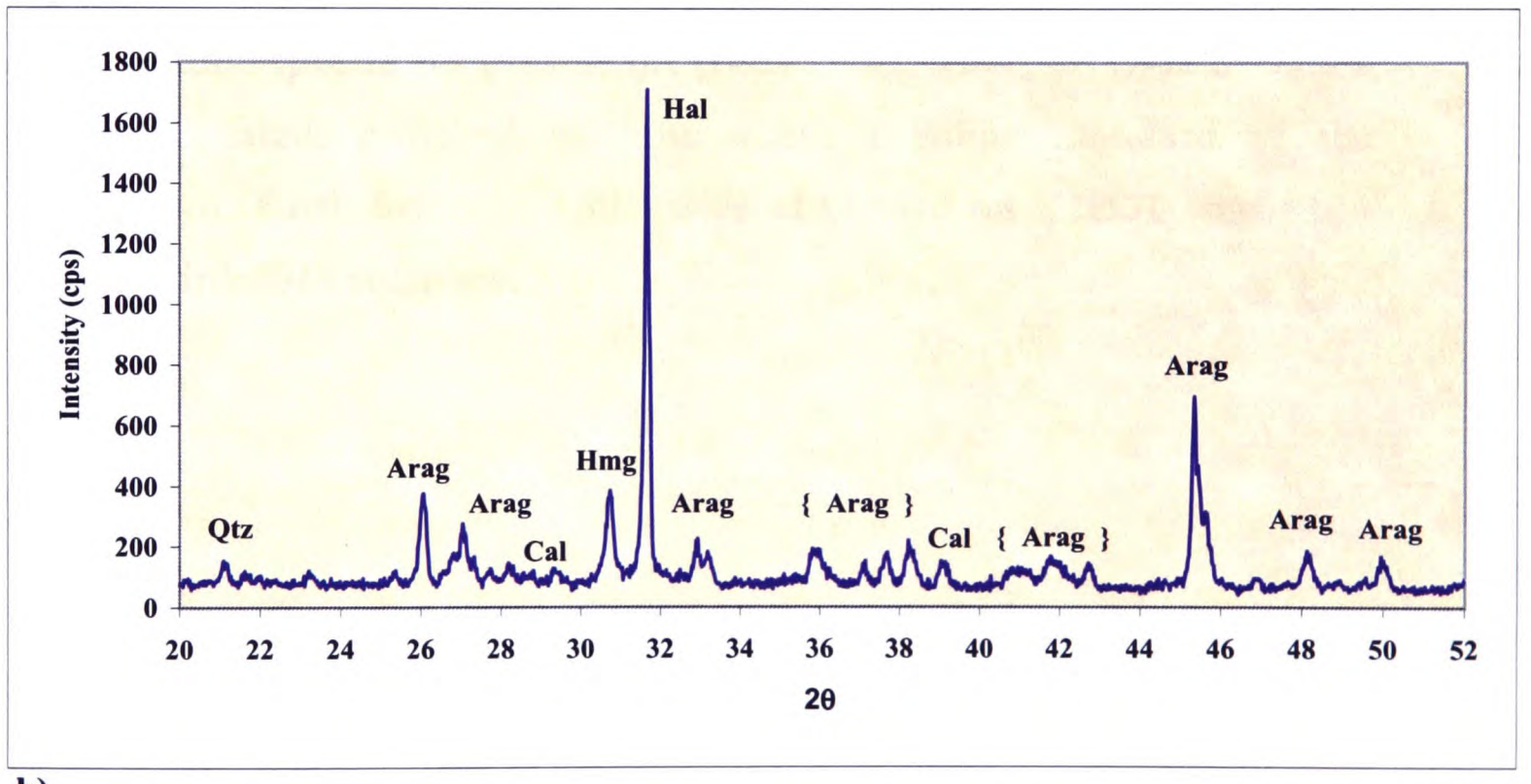


b)

Figure A1.7. X-ray diffractograms from North Stromatolite Lake
a) Surface sediment b) Sediment from 50mm depth



a)



b)

Figure A1.8. X-ray diffractograms from South Stromatolite Lake
a) Surface sediment b) Sediment from 50mm depth

APPENDIX 2

Mineral Analyses

This Appendix contains mineral analyses, back-scattered electron images and microprobe spectra for each of the study lakes. Analyses were obtained on carbon coated, polished sections using a cobalt standard at the Department of Earth Sciences, University of Oxford on a JEOL JSM-840A SEM with Link ISIS software.

Sample : Milne Lake

Spectra	1	2	3	4	5	6	7	8
Wt %								
Mg	0.01	37.25	48.77	32.74	34.19	44.34	36.35	42.22
Ca	-	18.74	9.21	25.72	25.51	12	23.92	8.87
Fe	-	0.57	0.09	0.04	-	0.24	0.14	0.33
Mn	-	-	-	0.08	0.17	0.11	0.14	-
Na	-	0.28	0.5	0.28	0.51	0.28	0.29	0.55
K	-	0.09	0.07	0.11	-	0.19	0.08	0.18
Mg:Ca	**-**	**77:23**	**90:10**	**68:32**	**69:31**	**86:14**	**71:29**	**89:11**
Mineral	Quartz	Dol/ Huntite	Huntite/ Magnesite	Dol	Dol	Huntite/ Magnesite	Dol	Huntite/ Magnesite

Sample : Pellet Lake

Spectra	1	2	3	4	5	6
Wt %						
Mg	11.57	10.81	10.84	11.05	11.33	8.14
Ca	10.76	10.78	9.35	11.14	10.27	10.7
Fe	0.11	0.17	0.13	0.11	0.07	0.08
Mn	-	-	-	0.02	-	-
Na	0.32	0.26	0.24	0.28	0.29	0.32
K	-	0.05	0.09	0.03	-	-
Mg:Ca	**64:36**	**62:38**	**66:34**	**62:38**	**65:35**	**56:44**
Mineral	Dol	Dol	Dol	Dol	Dol	Dol

Table A2.1. Mineral analyses and Mg:Ca ratios

Sample : Mini Dolomite Lake

Spectra	1	2	3	4	5	6	7	8	9	10
Wt %										
Mg	0.04	5.35	5.52	6.85	1.18	9.06	11.14	6.18	9.51	1.83
Ca	0.04	10.97	10.71	14.55	3.03	12.53	18.51	10.4	17.05	3.89
Fe	-	0.22	0.29	0.34	0.06	0.34	0.27	0.12	0.31	0.1
Mn	0.06	-	0.01	0.07	0.03	-	0.02	0.05	-	-
Na	-	0.19	0.08	0.28	0.03	0.16	0.24	0.1	0.38	-
K	-	0.07	0.08	0.07	0.04	0.05	0.01	-	0.03	0.04
Mg:Ca	**-**	**45:55**	**46:54**	**44:56**	**39:61**	**54:46**	**50:50**	**50:50**	**48:52**	**44:56**
Mineral	Quartz	Dol	Dol	Dol	Dol	Dol	Dol	Dol	Dol	Dol

Sample : Mcfaiden Lake

Spectra	1	2	3	4	5	6	7	8	9	10	11
Wt %											
Mg	10.02	10.76	1.31	9.09	5.59	14.66	9.24	11.11	10.46	9.76	11.26
Ca	18.39	18.91	2.69	16.57	9.66	20.53	16.36	19.66	18.79	18.82	19.01
Fe	0.08	-	0.49	0.09	0.16	-	0.07	0.03	0.05	0.02	0.07
Mn	0.03	-	0.03	0.03	0.05	0.07	-	-	0.03	0.05	0.03
Na	0.17	0.34	1.59	0.26	0.17	0.49	0.31	0.45	0.19	0.31	0.23
K	0.05	-	2.02	0.05	0.03	-	0.12	0.05	0.09	0.07	0.04
Mg:Ca	**47:53**	**48:52**	**45:55**	**48:52**	**49:51**	**54:46**	**48:52**	**48:52**	**48:52**	**46:54**	**49:51**
Mineral	Dol	Dol	? Bad Spectra	Dol	Dol	Dol	Dol	Dol	Dol	Dol	Dol

Table A2.1. Mineral analyses and Mg:Ca ratios

Sample : Dolomite Lake

Spectra	1	2	3	4	5	6	7	8
Wt %								
Mg	8.92	7.74	8.5	3.99	7.32	7.81	7.2	8.09
Ca	14.22	12.17	14.83	7.31	9.83	12.49	12.56	11.75
Fe	0.16	0.07	0.12	0.13	0.04	0.05	0.04	0.07
Mn	-	0.05	-	-	0.01	0.05	0.03	0.08
Na	0.3	0.16	0.4	0.13	0.36	0.2	0.22	0.04
K	0.05	0.09	-	0.06	0.03	0.02	0.07	0.12
Mg:Ca	**51:49**	**51:49**	**49:51**	**47:53**	**55:45**	**51:49**	**49:51**	**53:47**
Mineral	Dol	Dol	Dol	Dol	Dol	Dol	Dol	Dol

Sample : Halite Lake

Spectra	1	2	3	4	5	6	7	8	9
Wt %									
Mg	0.31	0.01	0.22	0.51	1.46	0.32	1.09	0.62	3.99
Ca	31.7	0.1	28.7	10.31	13.5	17.66	23.53	17.98	19.99
Fe	0.03	0.02	0.13	0.13	0.26	0.05	0.09	0.13	0.84
Mn	-	-	-	-	-	0.05	0.03	0.02	0.11
Na	0.36	-	0.23	0.04	0.22	0.26	0.25	0.32	0.09
K	-	-	0.07	0.02	-	0.02	0.02	0.04	-
Mg:Ca	**2:98**	**-**	**1:99**	**8:92**	**15:85**	**3:97**	**7:93**	**5:95**	**25:75**
Mineral	Arag	Quartz	Arag	MgCal	MgCal	Arag	MgCal	Arag	MgCal

Table A2.1. Mineral analyses and Mg:Ca ratios

Sample : North Stromatolite Lake

Spectra	1	2	3	4	5	6	7
Wt %							
Mg	3.74	0.03	2.26	0.82	0.05	2.42	13.93
Ca	27.81	36.02	23.94	1.09	6.19	29.44	1.37
Fe	0.21	-	0.05	-	0.37	-	0.51
Mn	0.09	-	-	0.26	0.1	0.02	0.05
Na	0.17	0.25	0.47	46.54	-	0.29	-
K	0.05	0.07	0.04	-	0.16	0.06	0.1
Mg:Ca	**18:82**	**0:100**	**13:87**	**-**	**1:99**	**12:88**	**94:6**
Mineral	MgCal	Arag	MgCal	Halite	Arag	MgCal	Hydromag

Sample : South Stromatolite Lake

Spectra	1	2	3	4	5	6
Wt %						
Mg	0.03	0.05	1.94	12.76	2.88	8.74
Ca	17.78	30.93	27.19	0.95	6.68	4.9
Fe	0.02	-	0.06	0.47	0.24	0.12
Mn	0.06	-	-	0.05	-	0.04
Na	-	0.24	0.17	0.03	0.01	0.08
K	0.03	-	0.01	0.09	0.03	0.07
Mg:Ca	**0:100**	**0:100**	**9:91**	**96:4**	**42:58**	**75:25**
Mineral	Arag	Arag	Arag/ MgCal	Hydromag	Dol	Huntite?

Table A2.1. Mineral analyses and Mg:Ca ratios

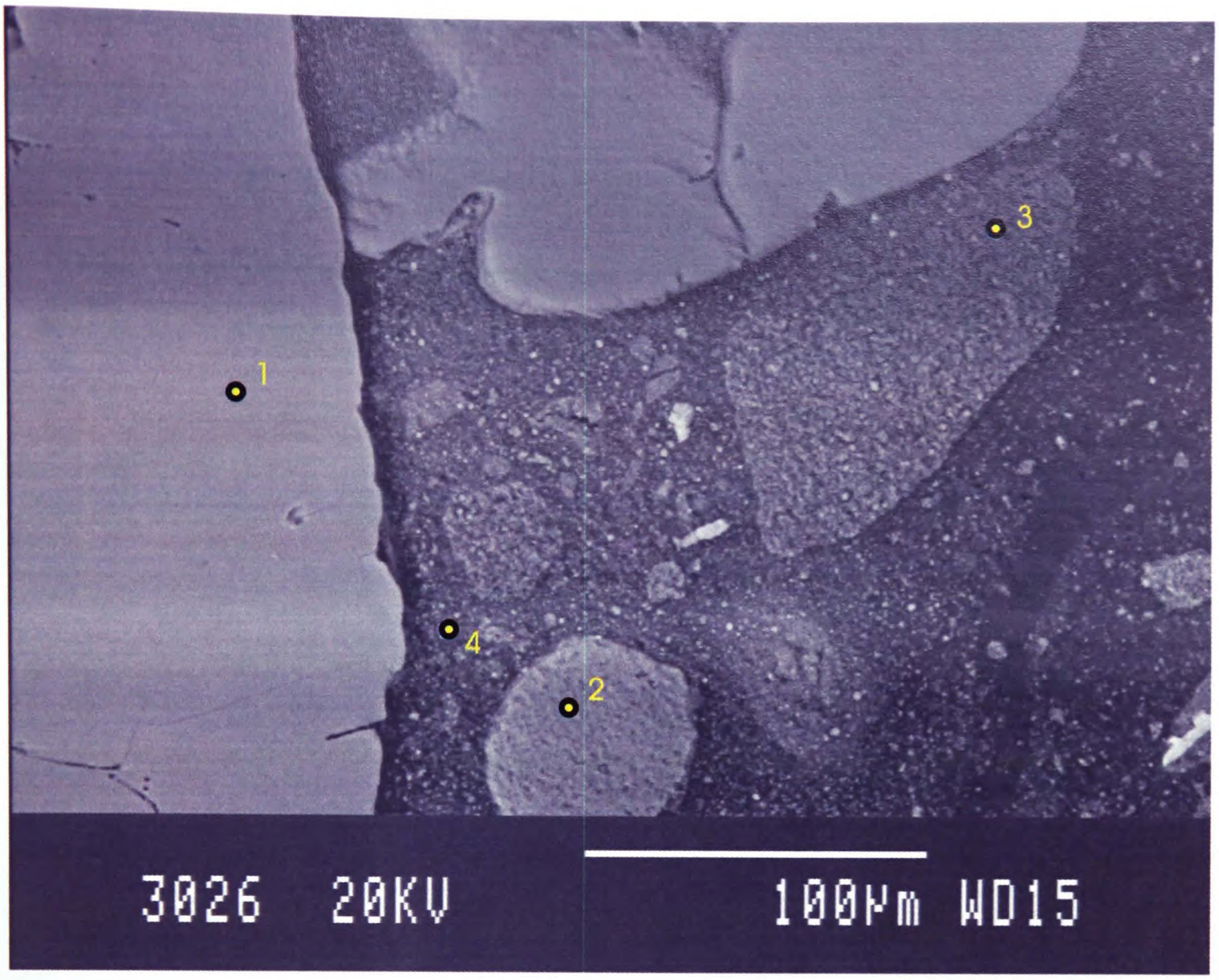


Figure A2.1. Back-scattered electron images of the sediment from Milne Lake showing points of compositional analysis. Numbers refer to the spectra number in Fig. A2.2 and Table A2.1.

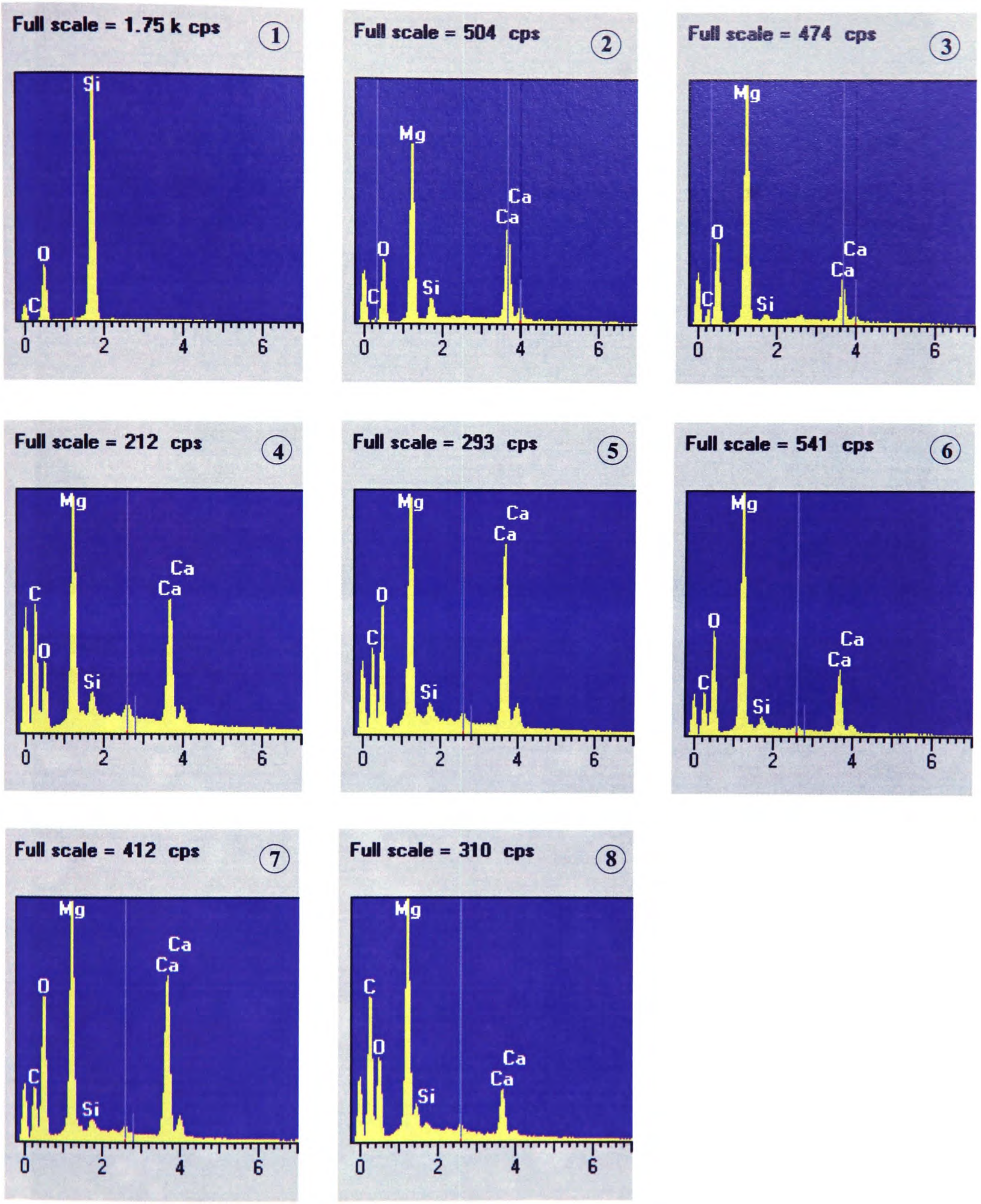
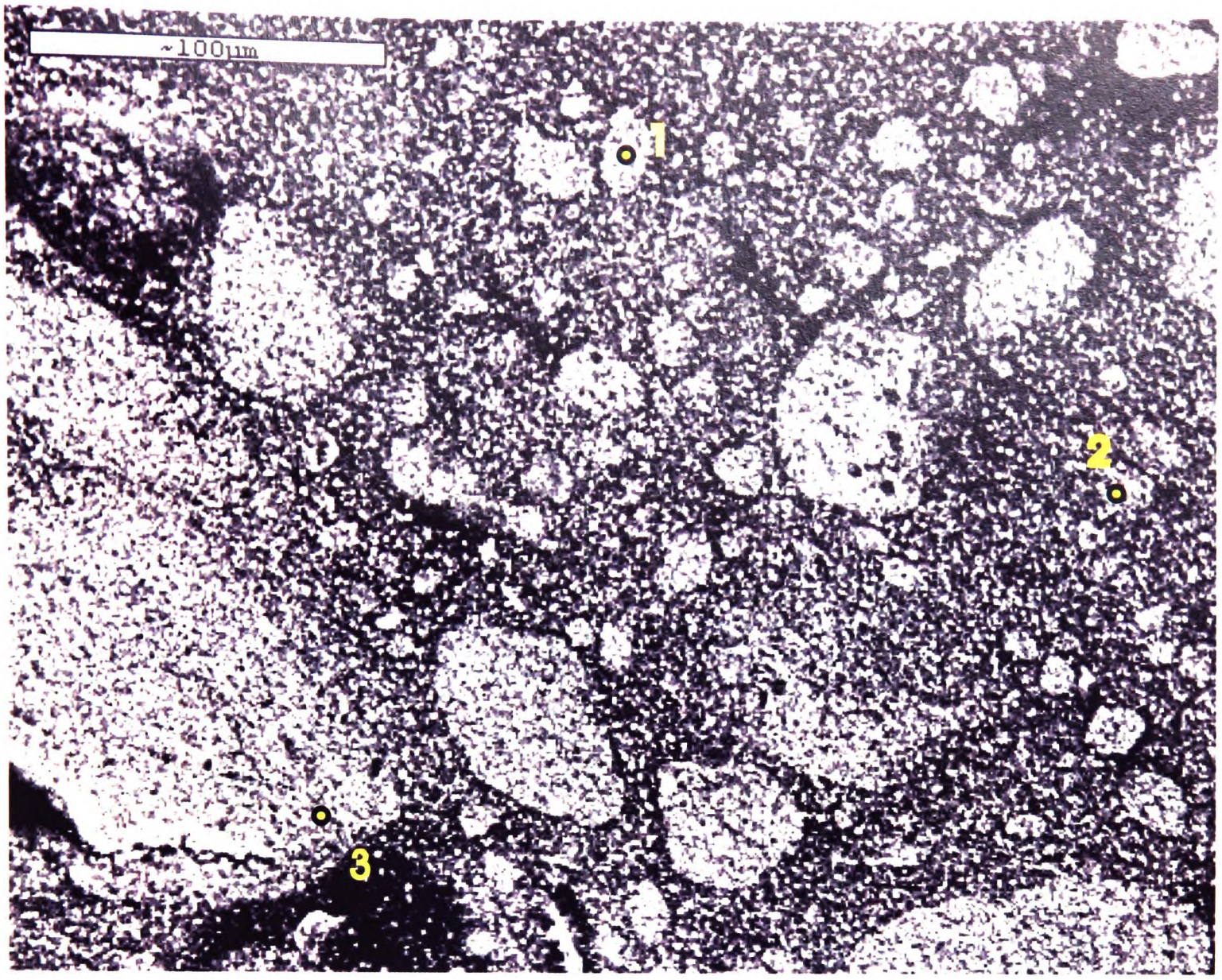


Figure A2.2. Milne Lake. Atomic spectra for the sediment shown in Fig. A2.1.



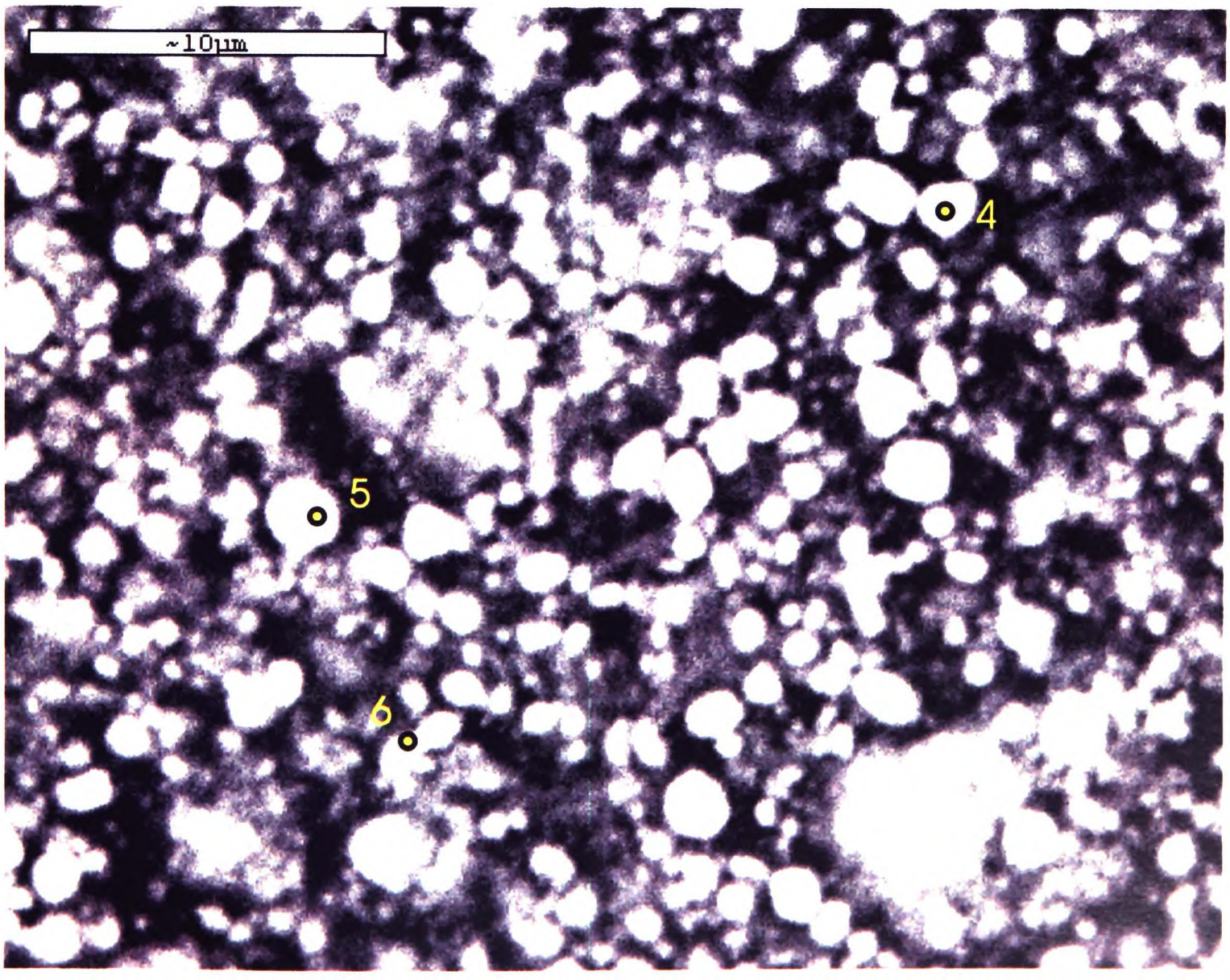


Figure A2.3. Back-scattered electron images of the sediment from Pellet Lake showing points of compositional analysis. Numbers refer to the spectra number in Fig. A2.4 and Table A2.1.

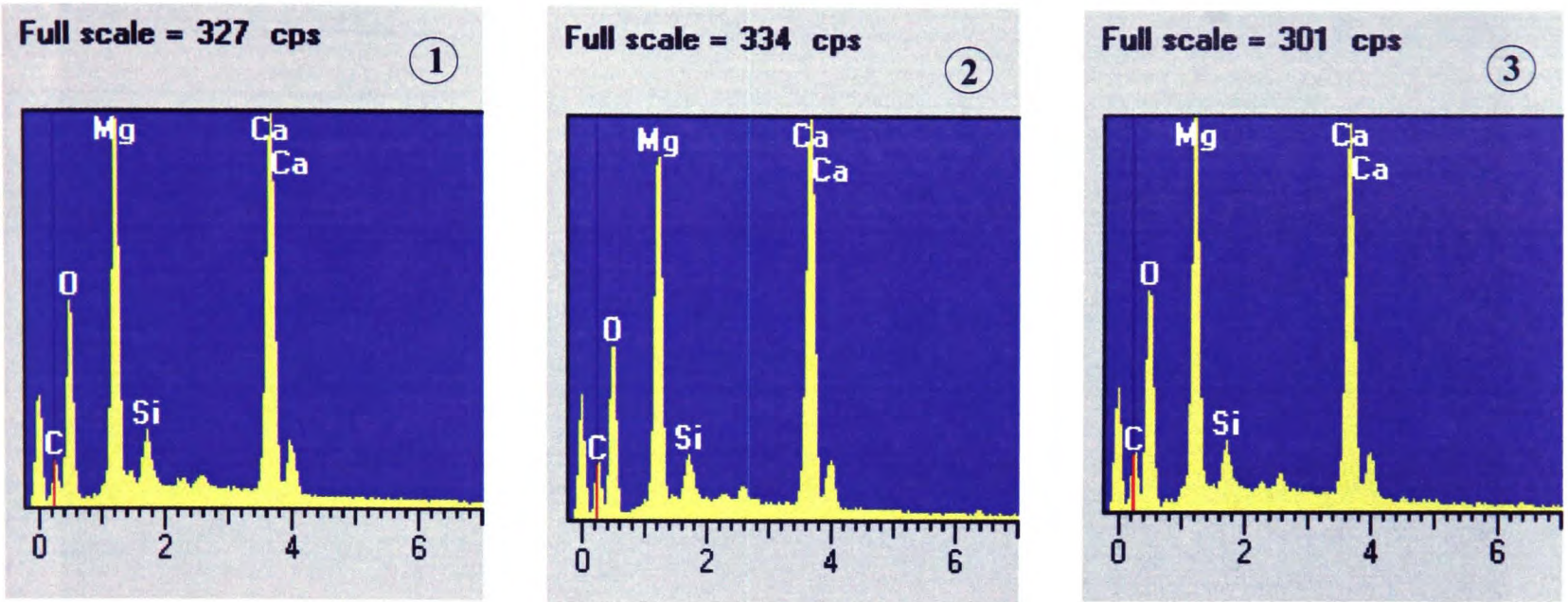
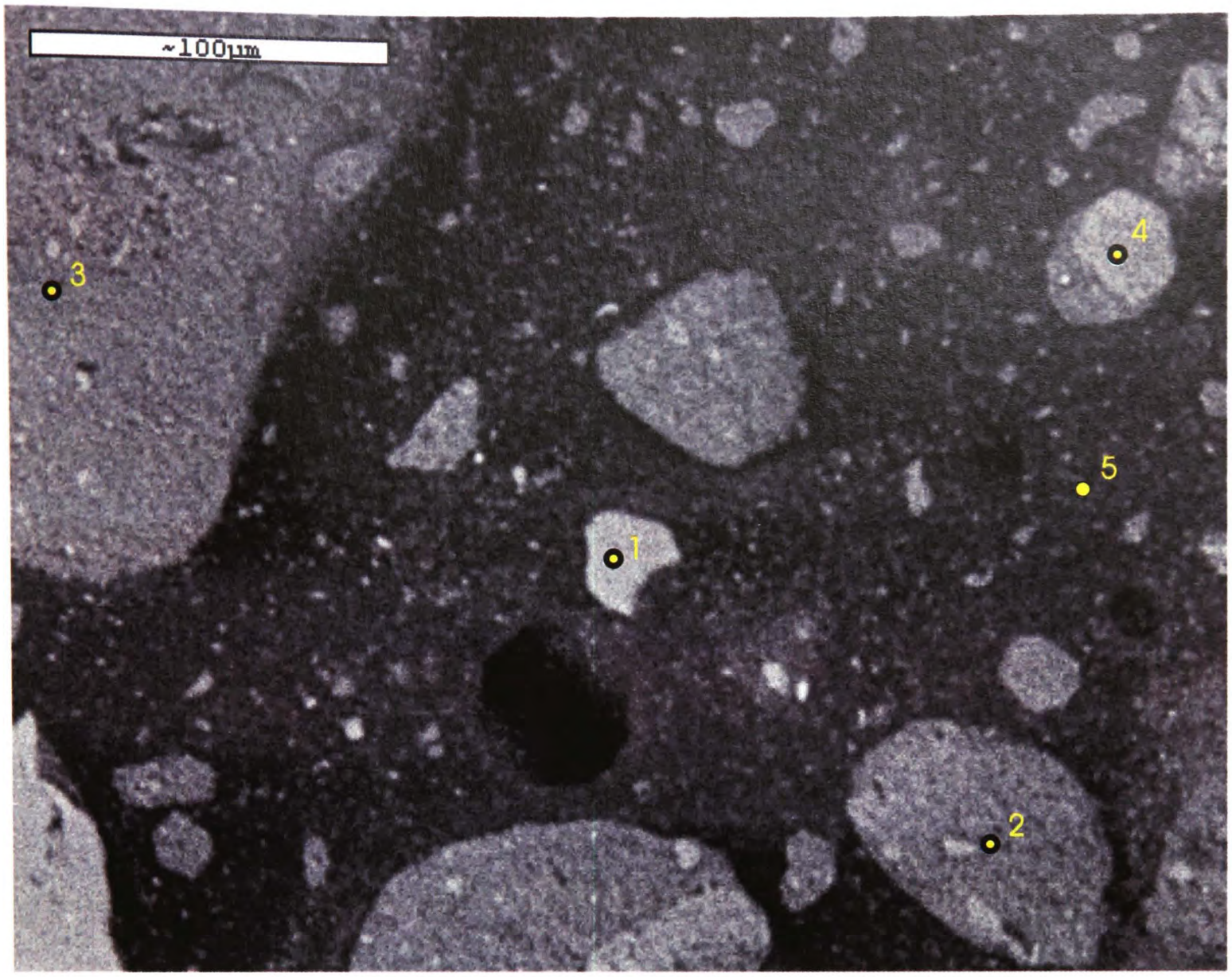


Figure A2.4. Pellet Lake. Atomic spectra for the sediment shown in Fig. A2.3



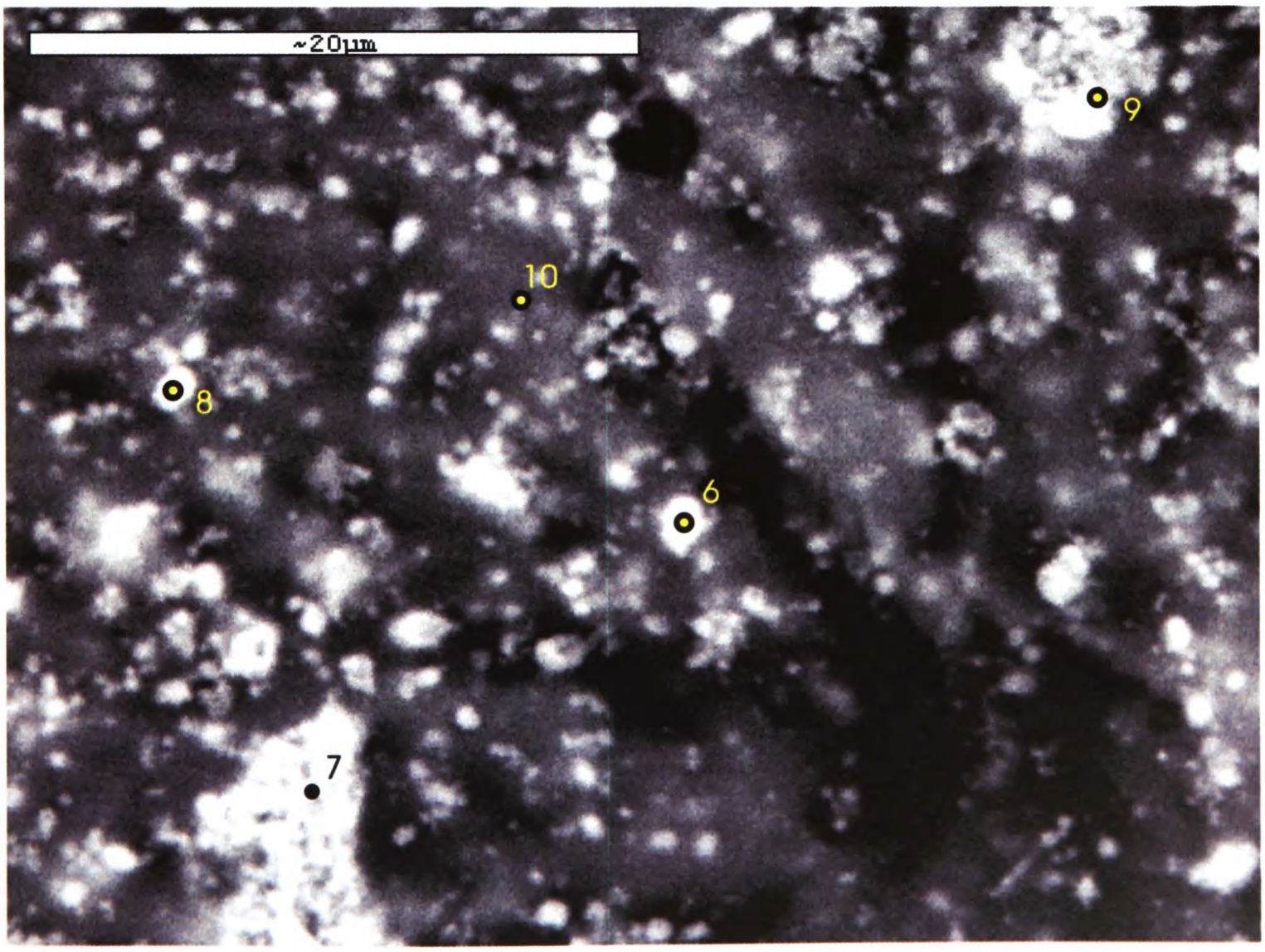


Figure A2.5. Back-scattered electron images of the sediment from Mini Dolomite Lake showing points of compositional analysis. Numbers refer to the spectra number in Fig. A2.6 and Table A2.1.

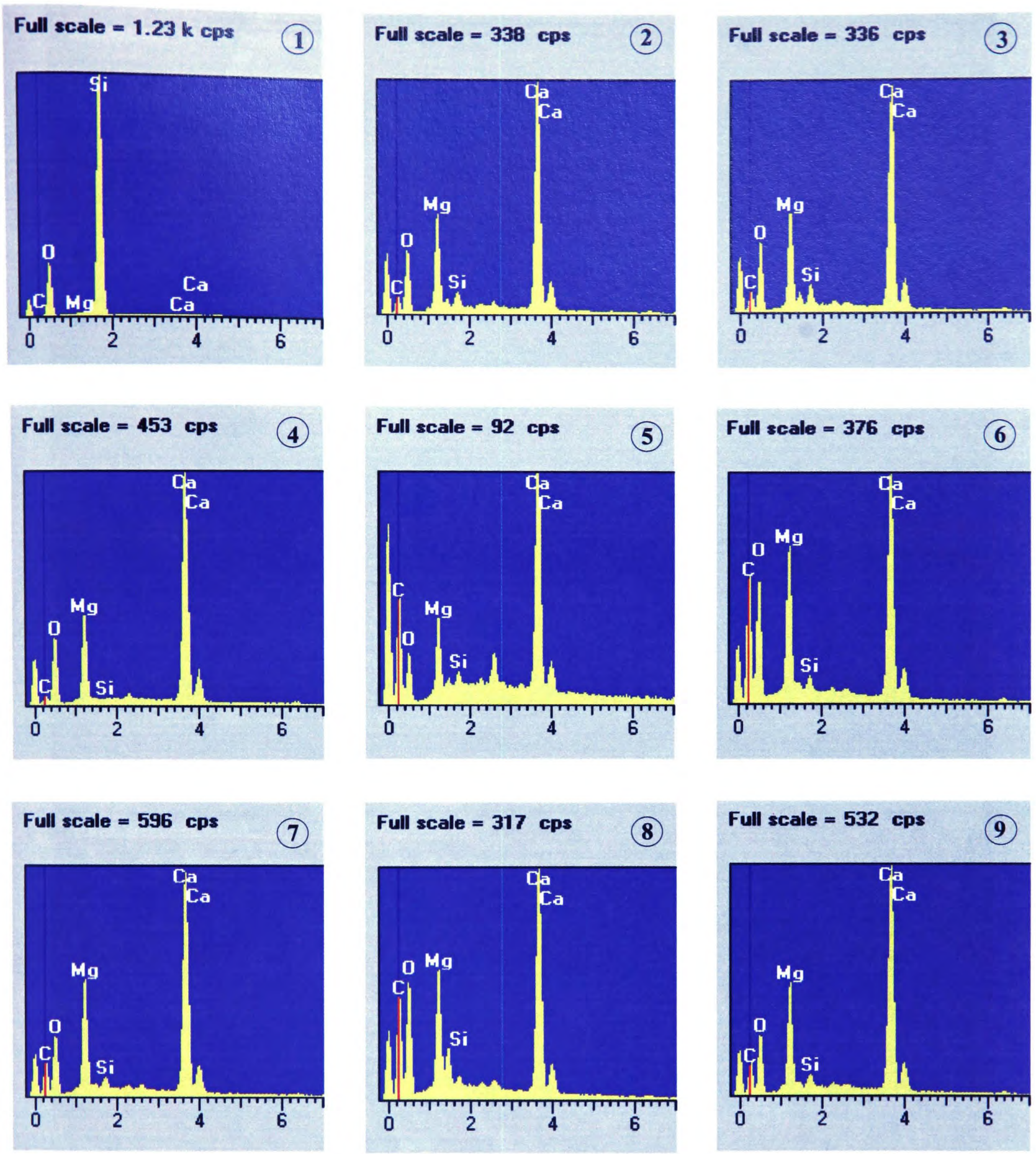
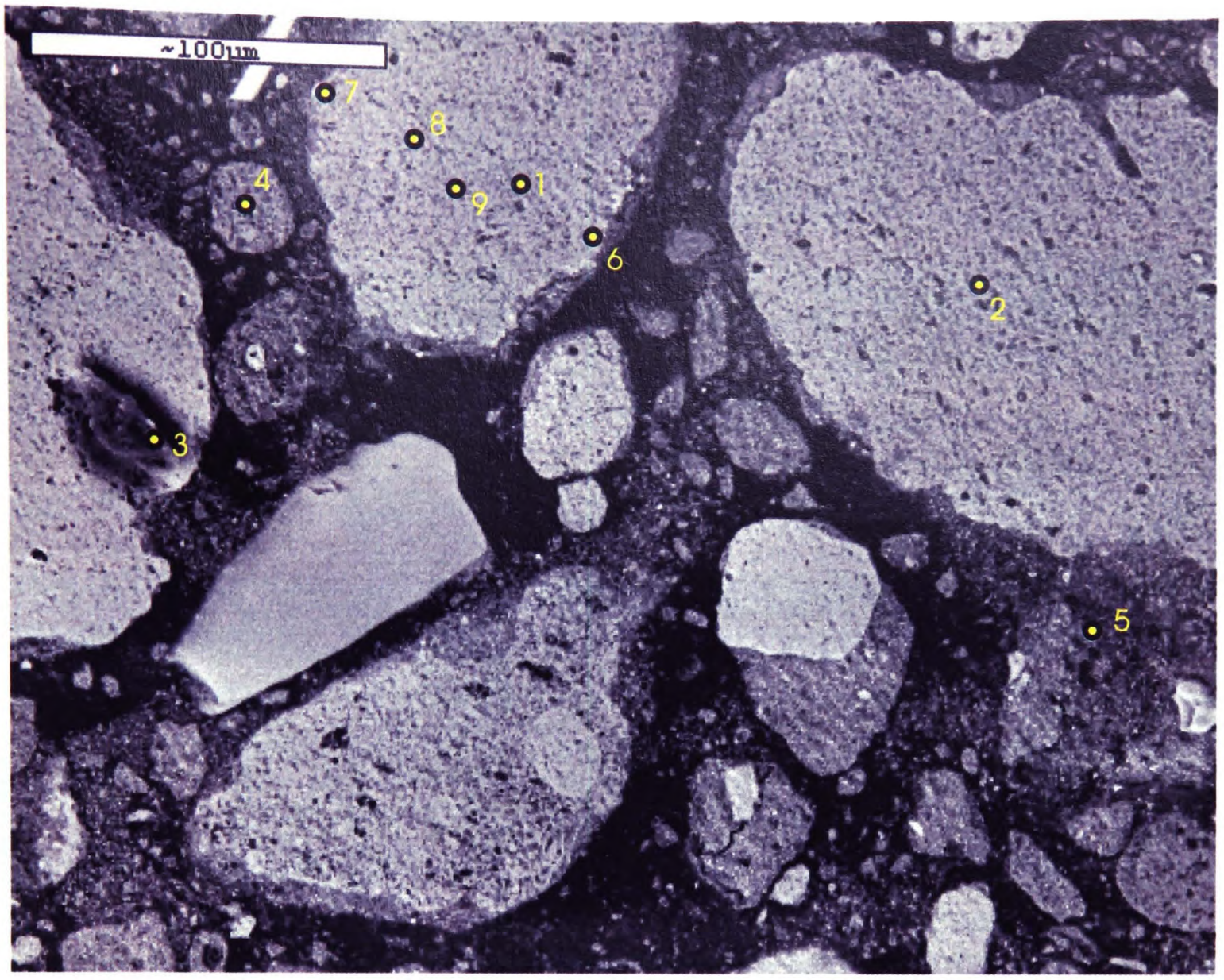


Figure A2.6. Mini Dolomite Lake.
Atomic spectra for the sediment shown in Fig. A2.5.



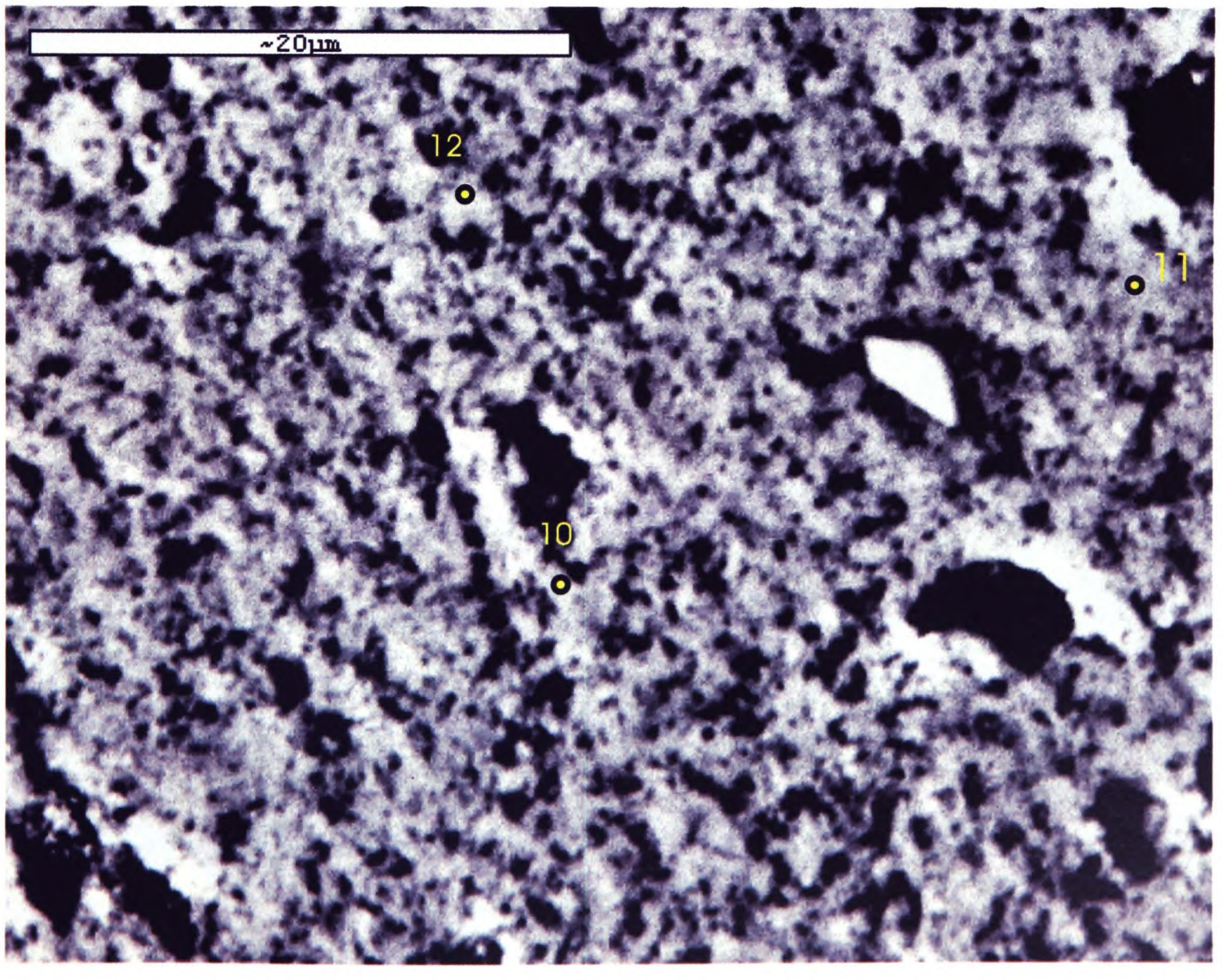
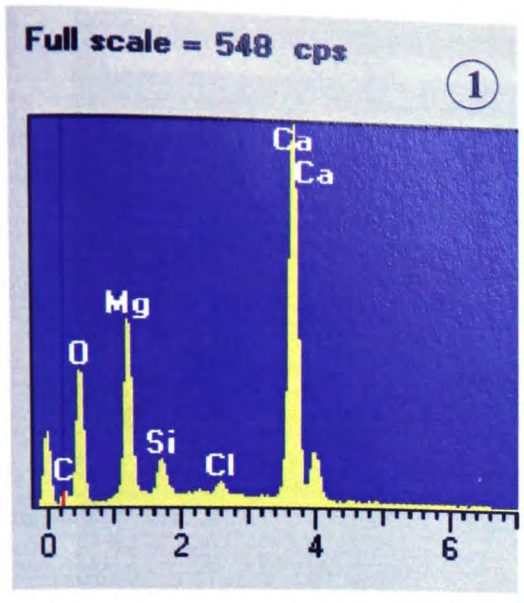
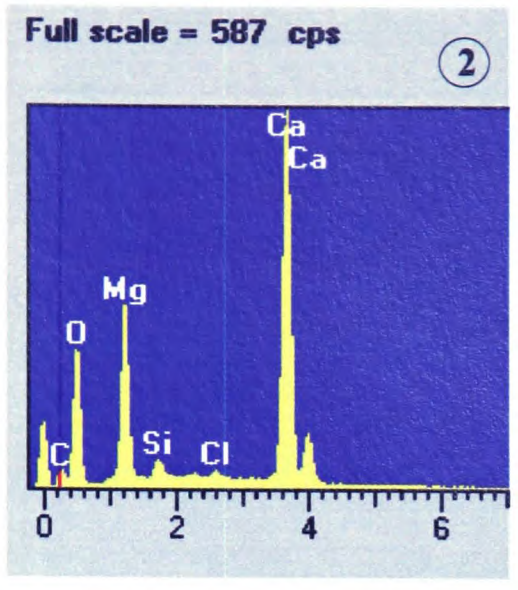
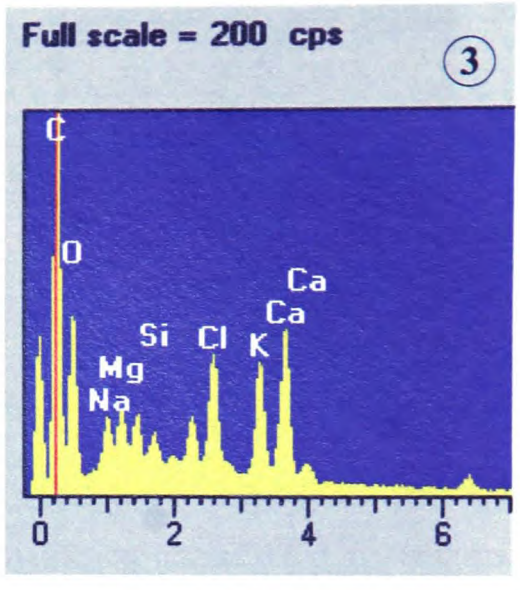
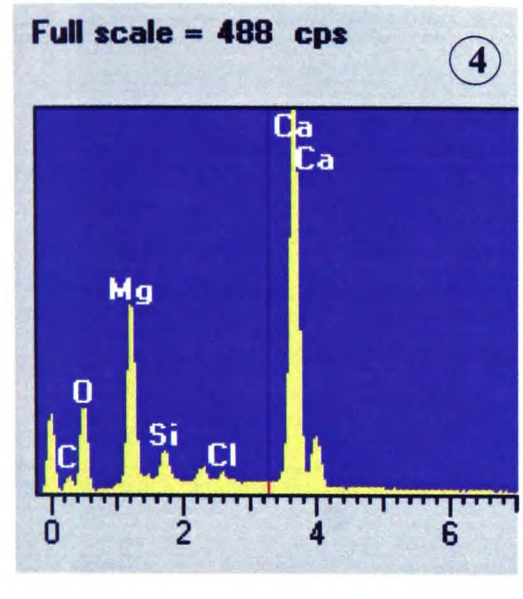


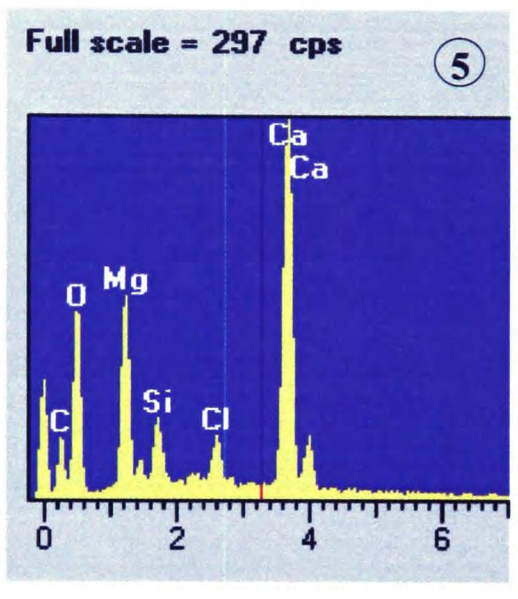
Figure A2.7. Back-scattered electron images of the sediment from McFaiden Lake showing points of compositional analysis. Numbers refer to the spectra number in Fig. A2.8 and Table A2.1.

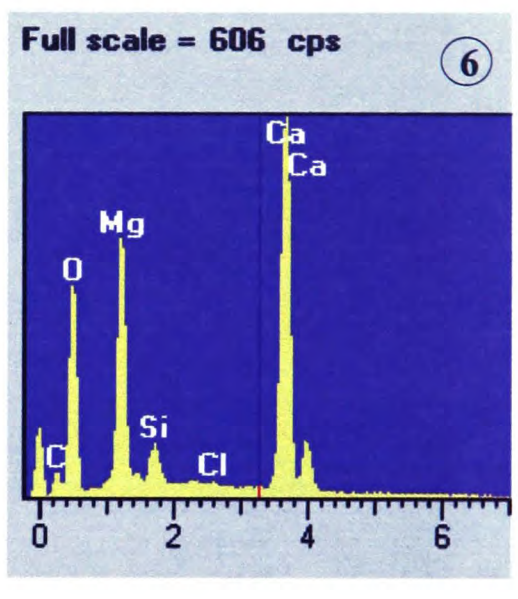


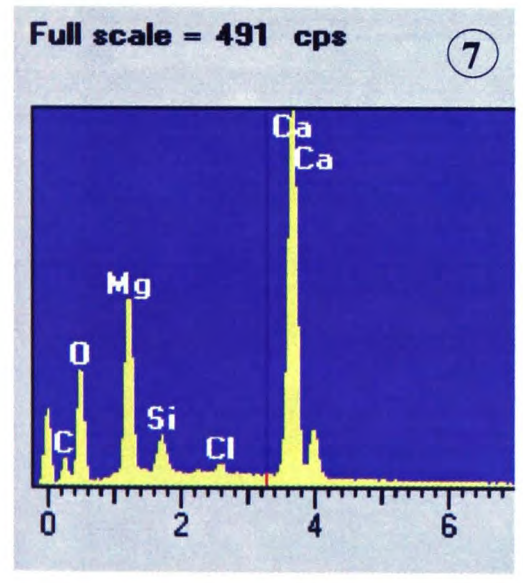


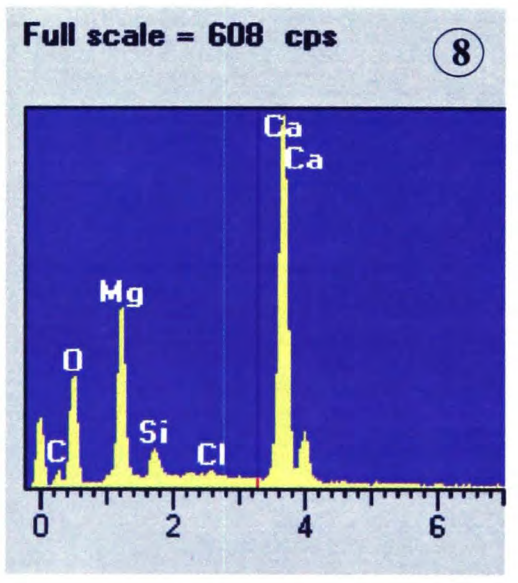


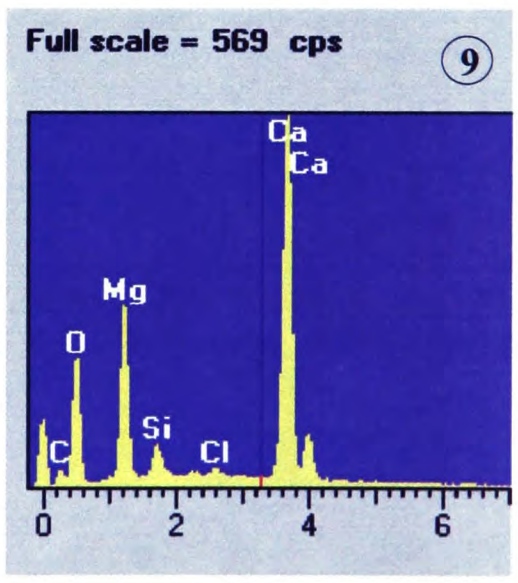


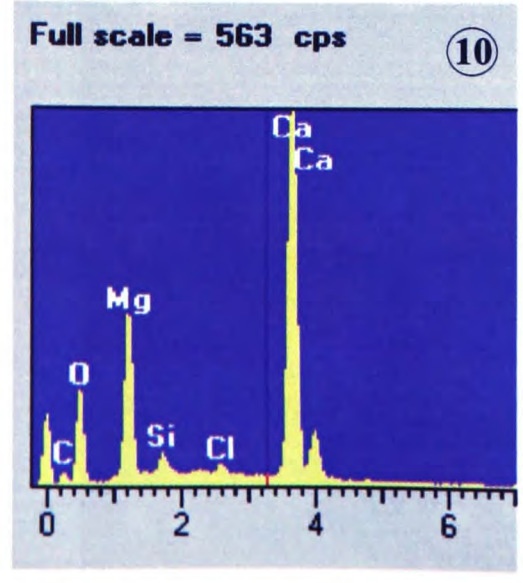












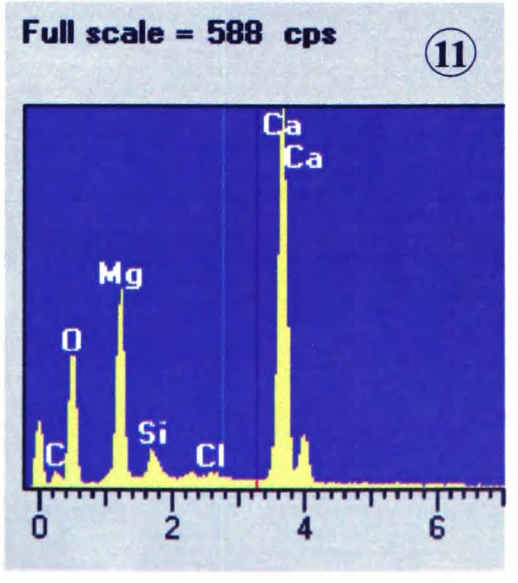
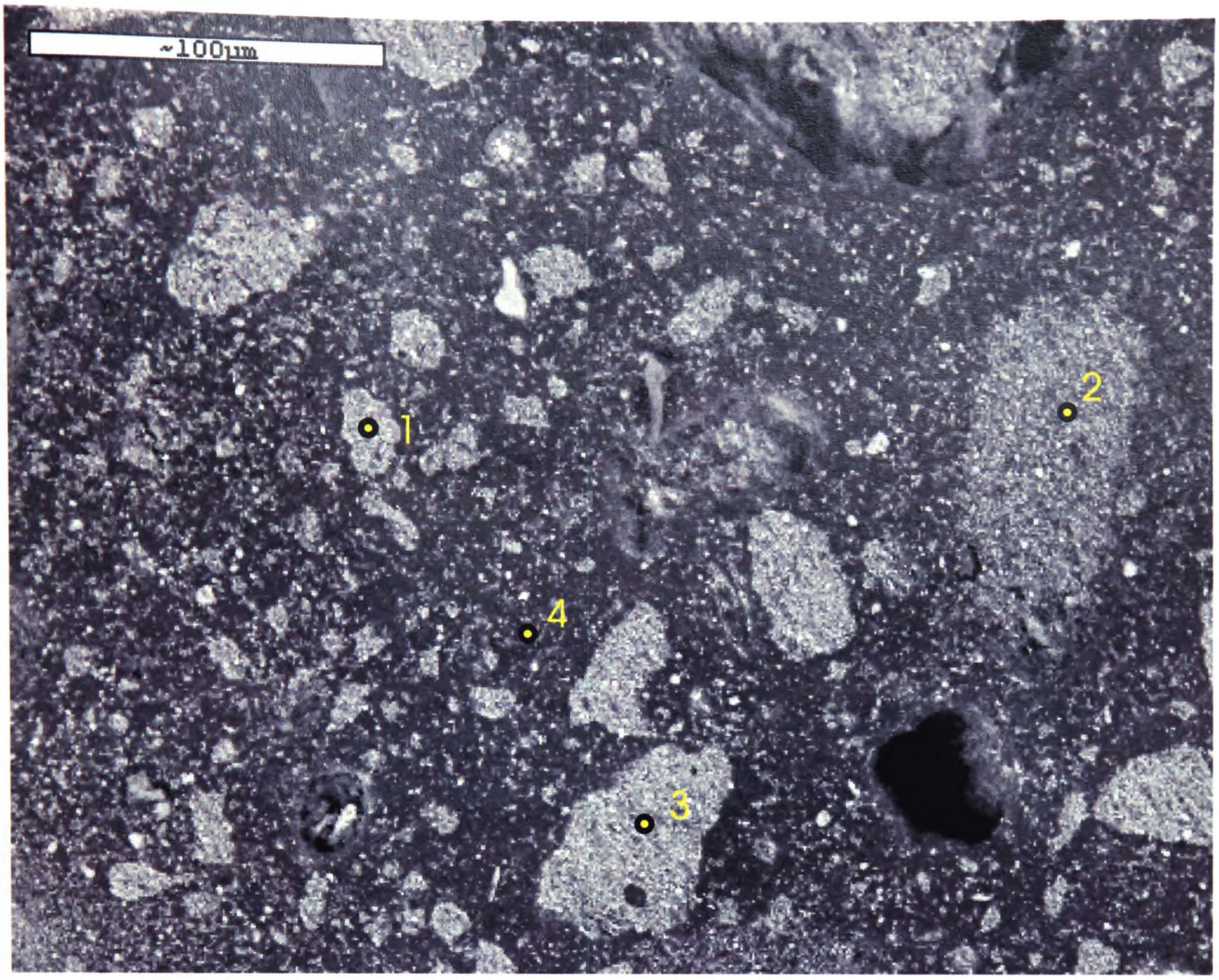


Figure A2.8. McFaiden Lake. Atomic spectra for the sediment shown in Fig. A2.7.



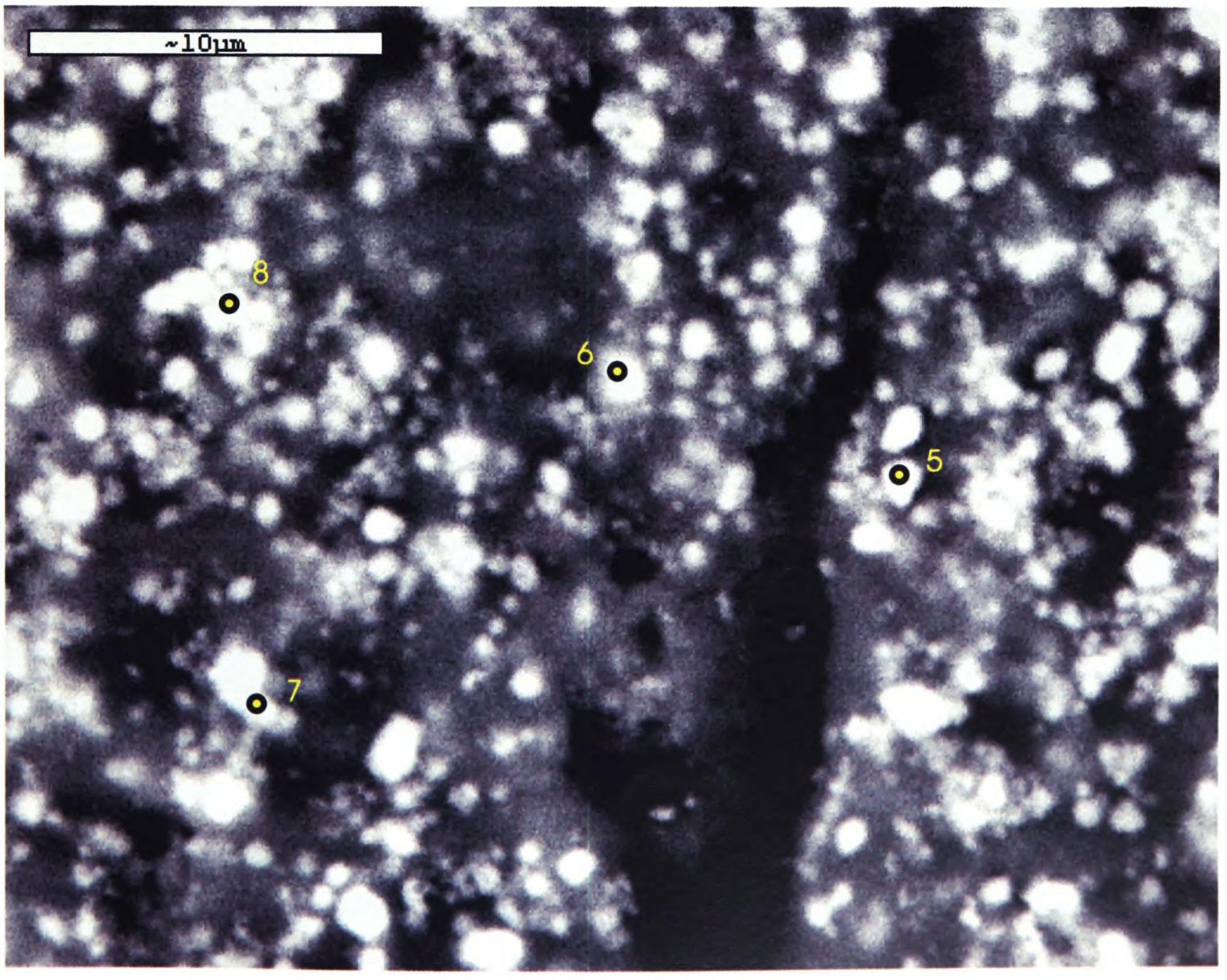


Figure A2.9. Back-scattered electron images of the sediment from Dolomite Lake showing points of compositional analysis. Numbers refer to the spectra number in Fig. A2.10 and Table A2.1.

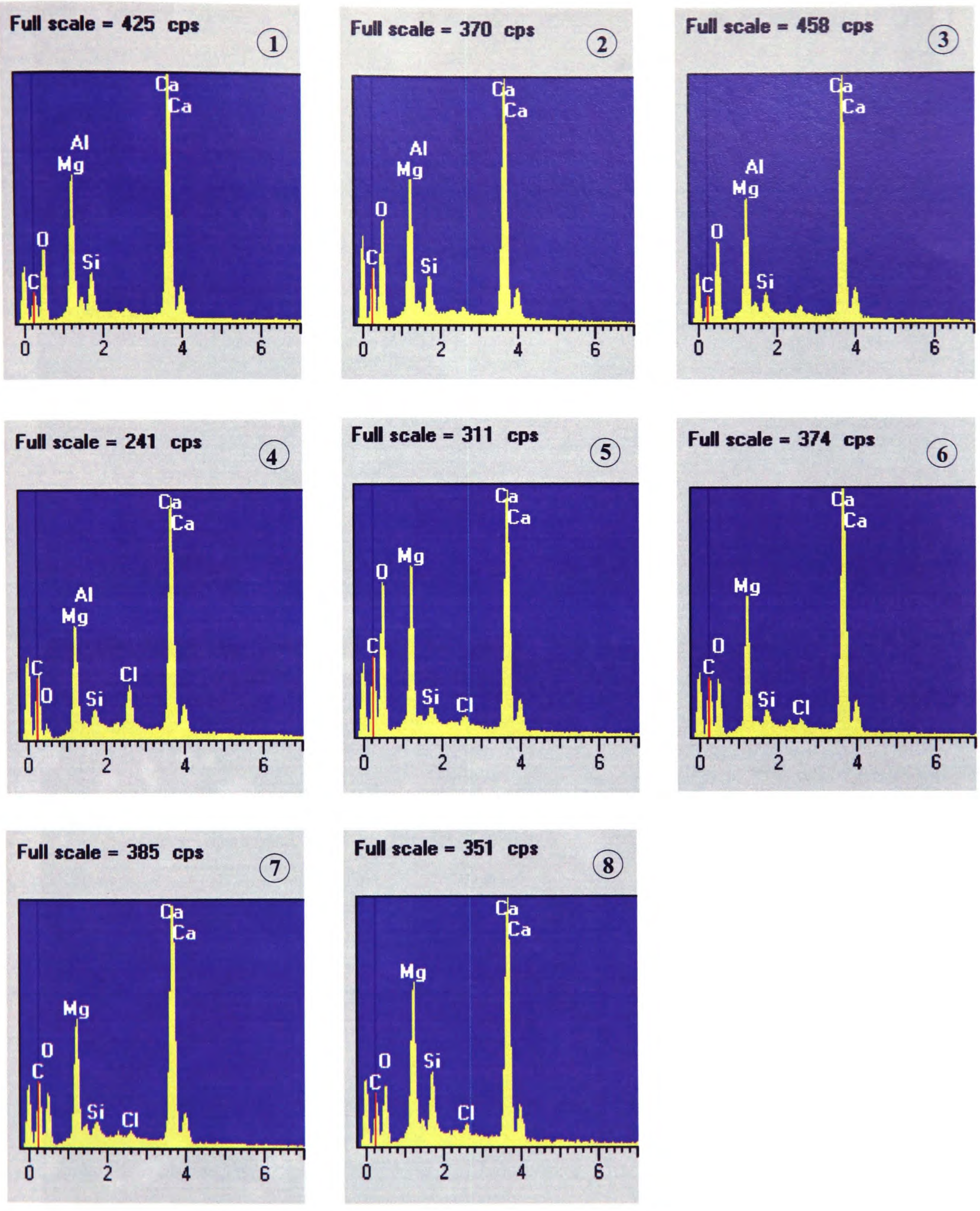
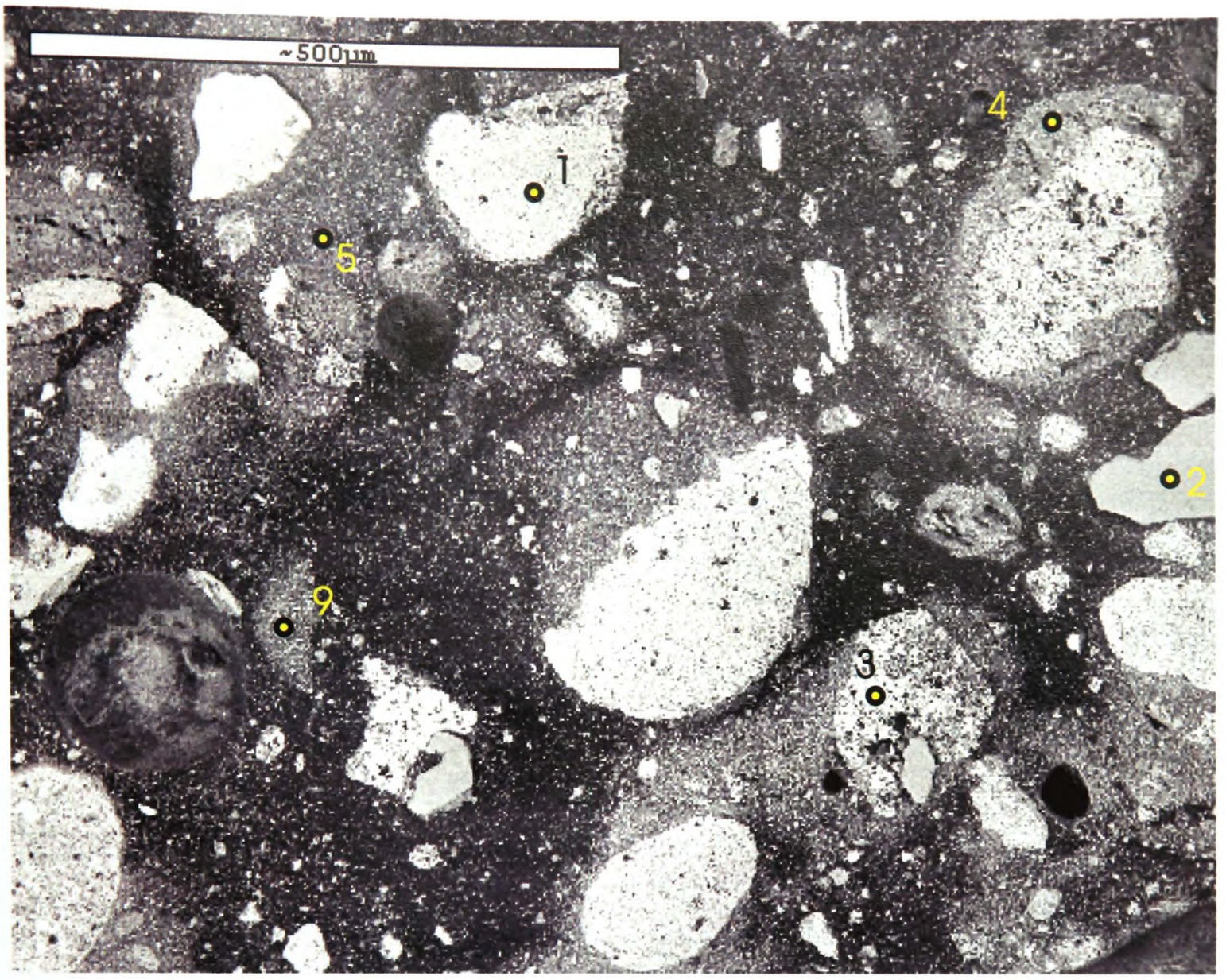


Figure A2.10. Dolomite Lake. Atomic spectra for the sediment shown in Fig. A2.9.



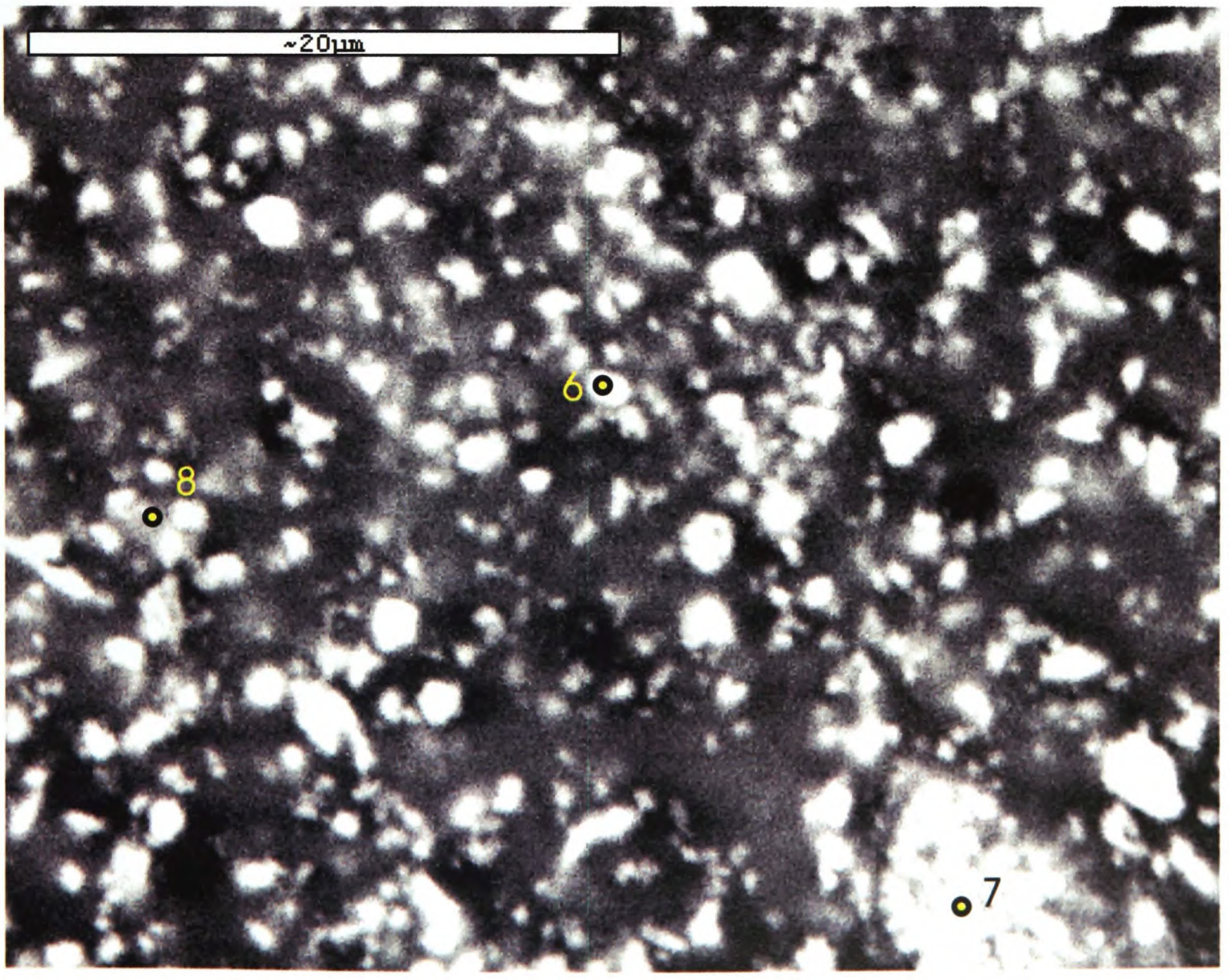


Figure A2.11. Back-scattered electron images of the sediment from Halite Lake showing points of compositional analysis. Numbers refer to the spectra number in Fig. A2.12 and Table A2.1.

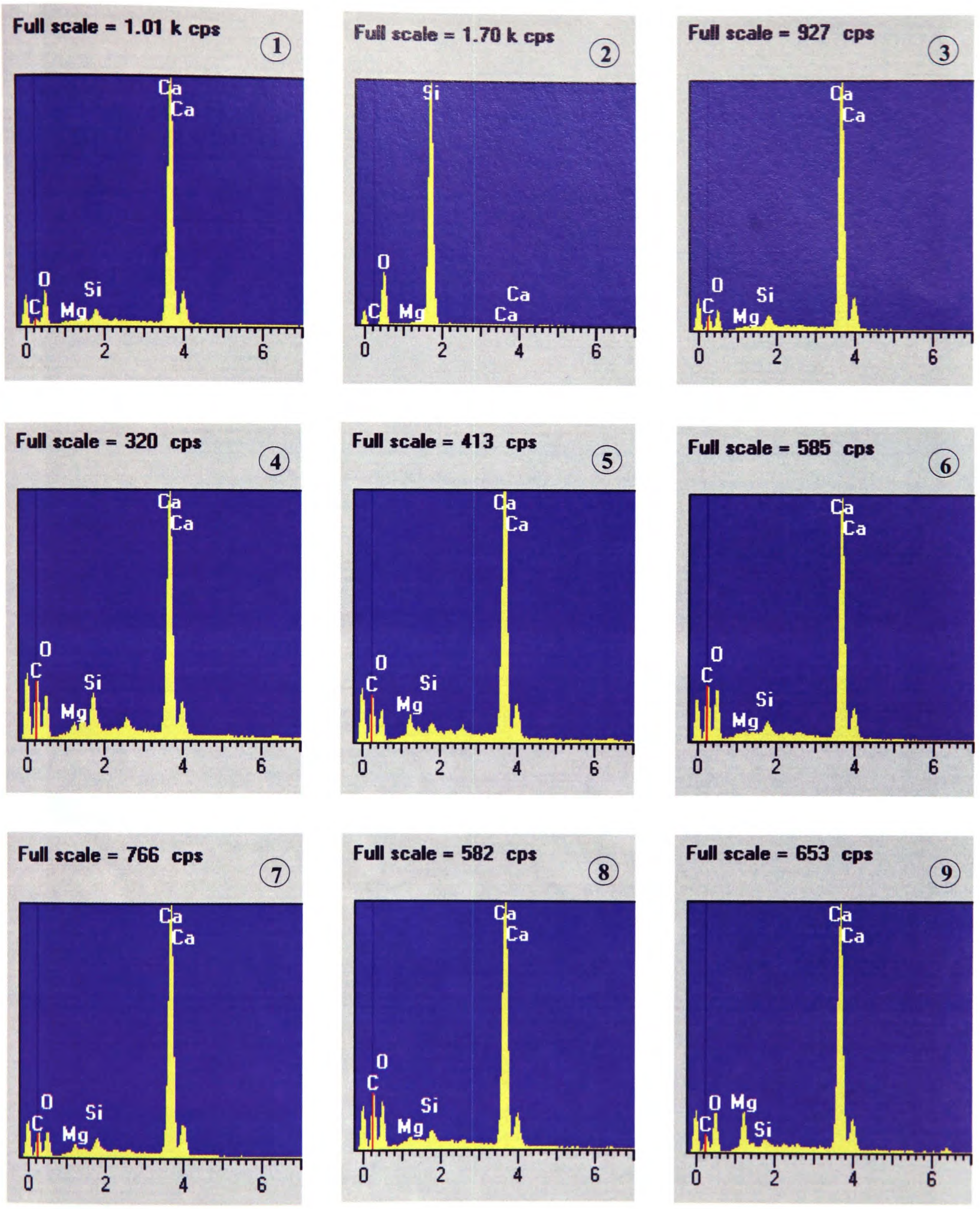
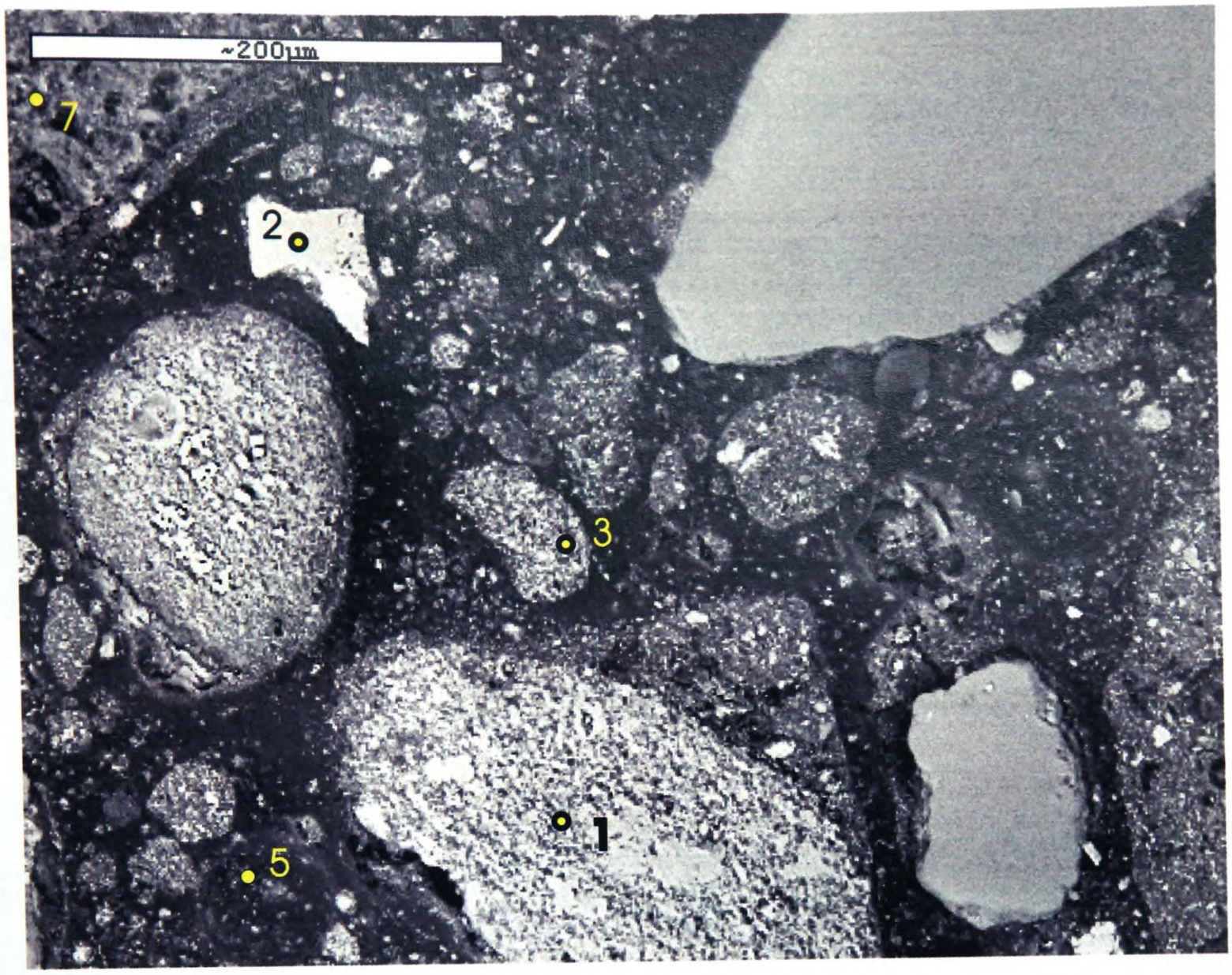


Figure A2.12. Halite Lake. Atomic spectra for the sediment shown in Fig. A2.11.



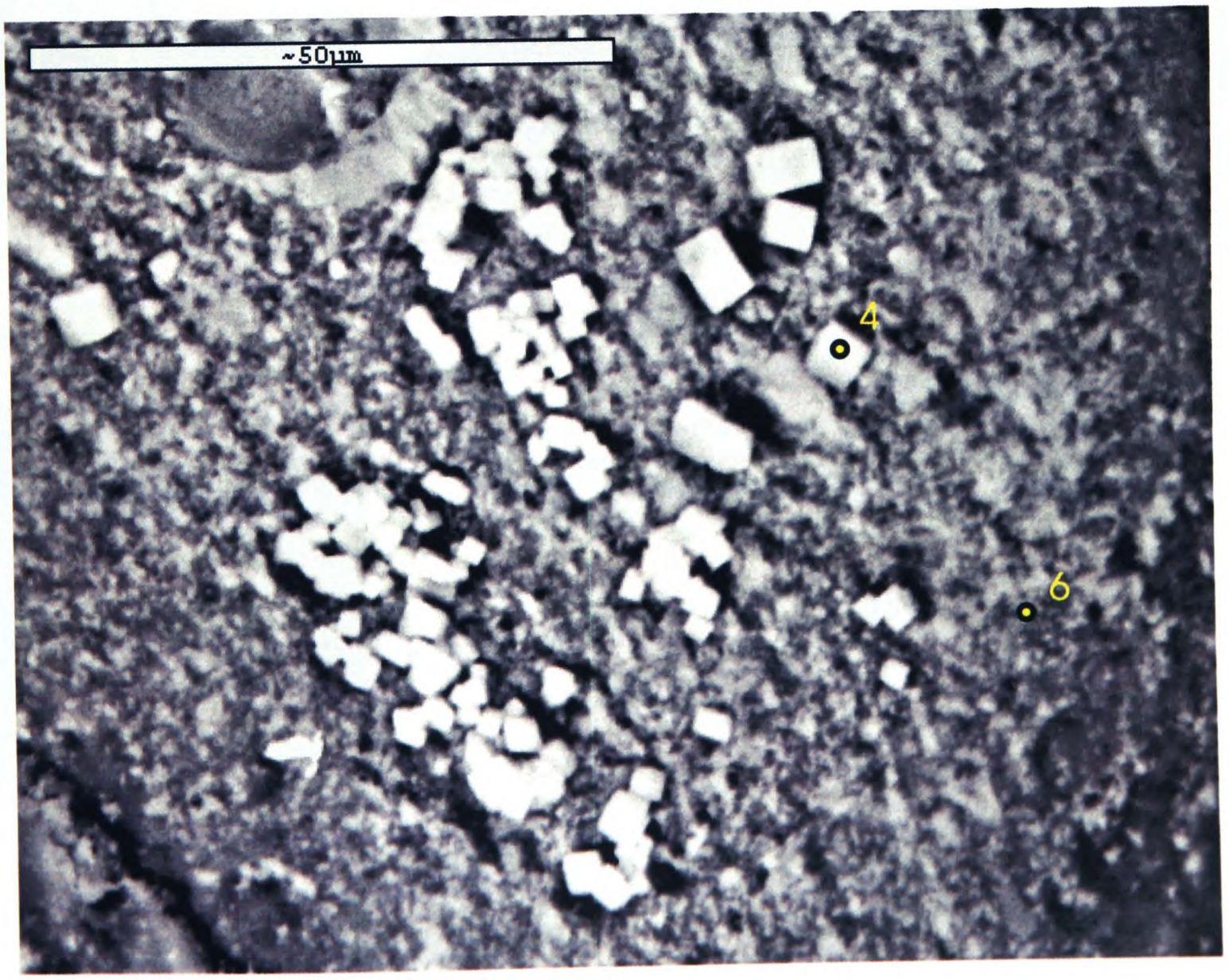
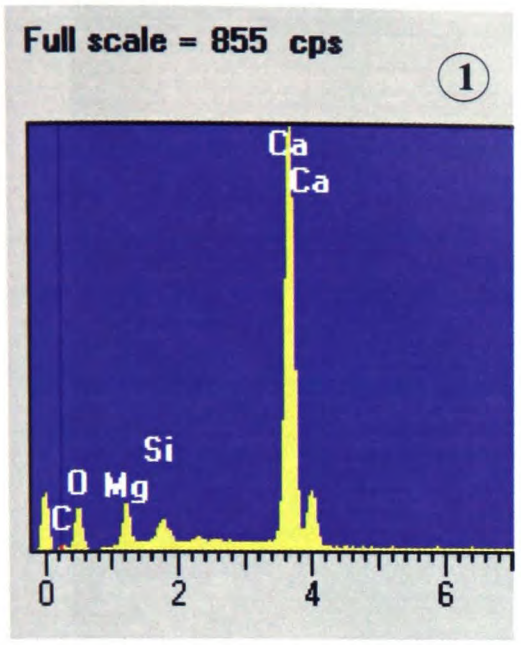
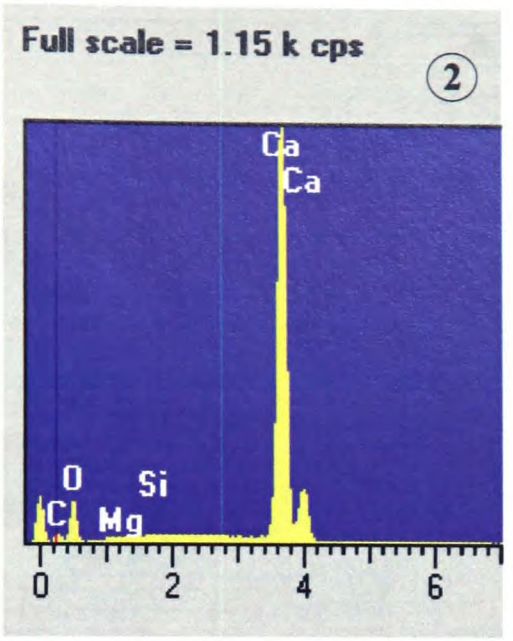
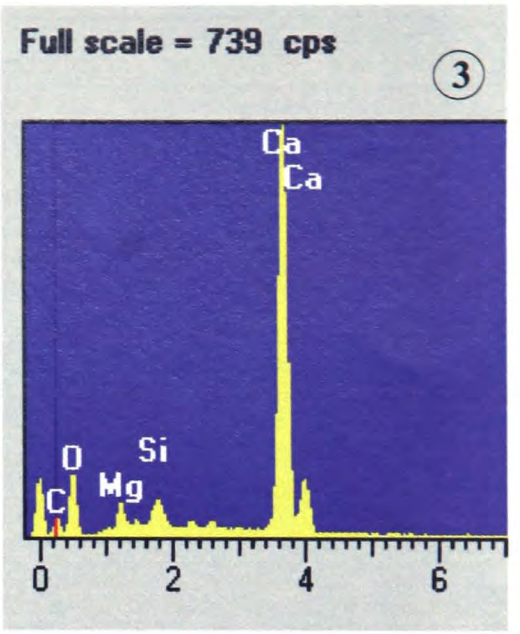
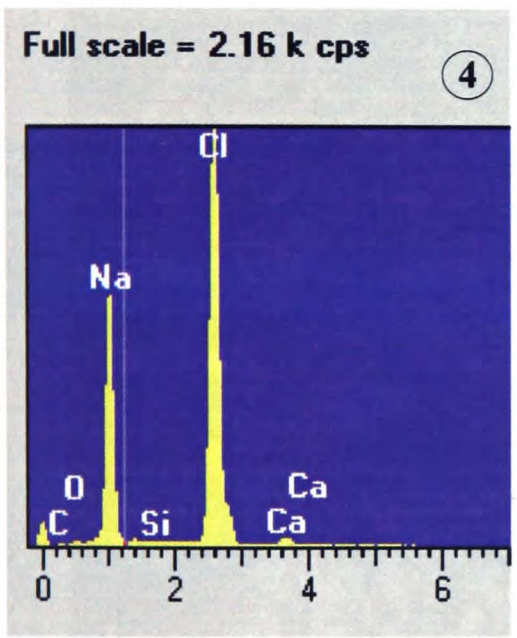


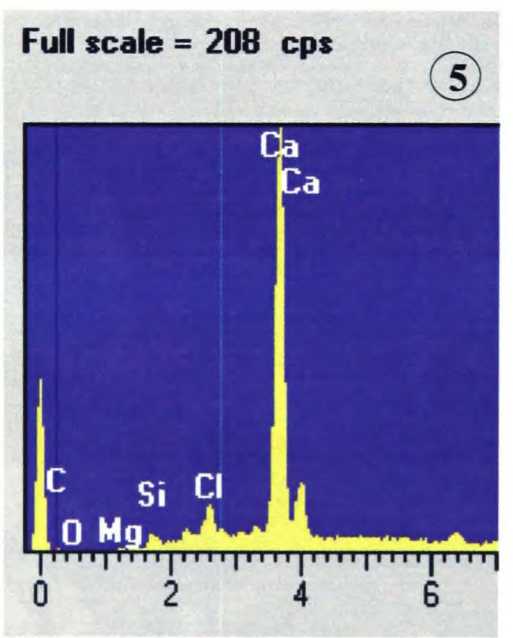
Figure A2.13. Back-scattered electron images of the sediment from North Stromatolite Lake showing points of compositional analysis. Numbers refer to the spectra number in Fig. A2.14 and Table A2.1.

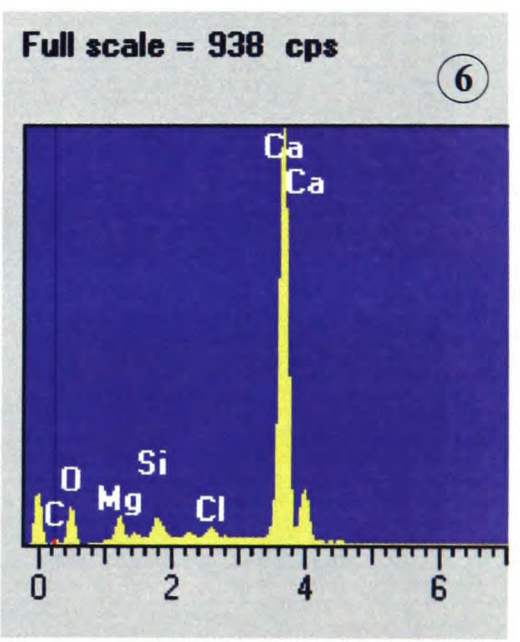












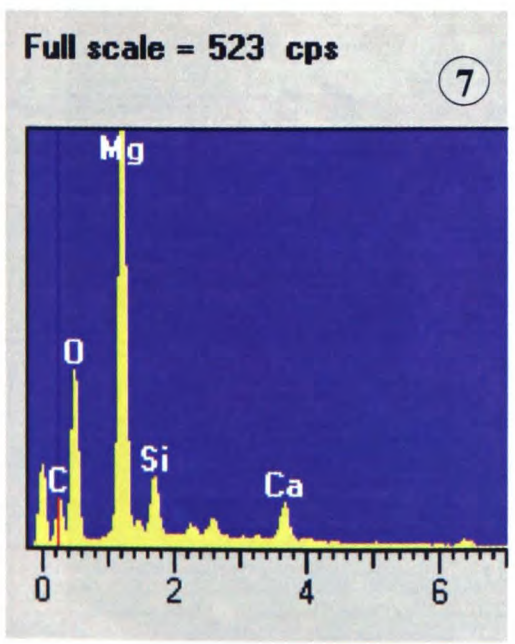


Figure A2.14. North Stromatolite Lake.
Atomic spectra for the sediment shown in Fig. A2.13.

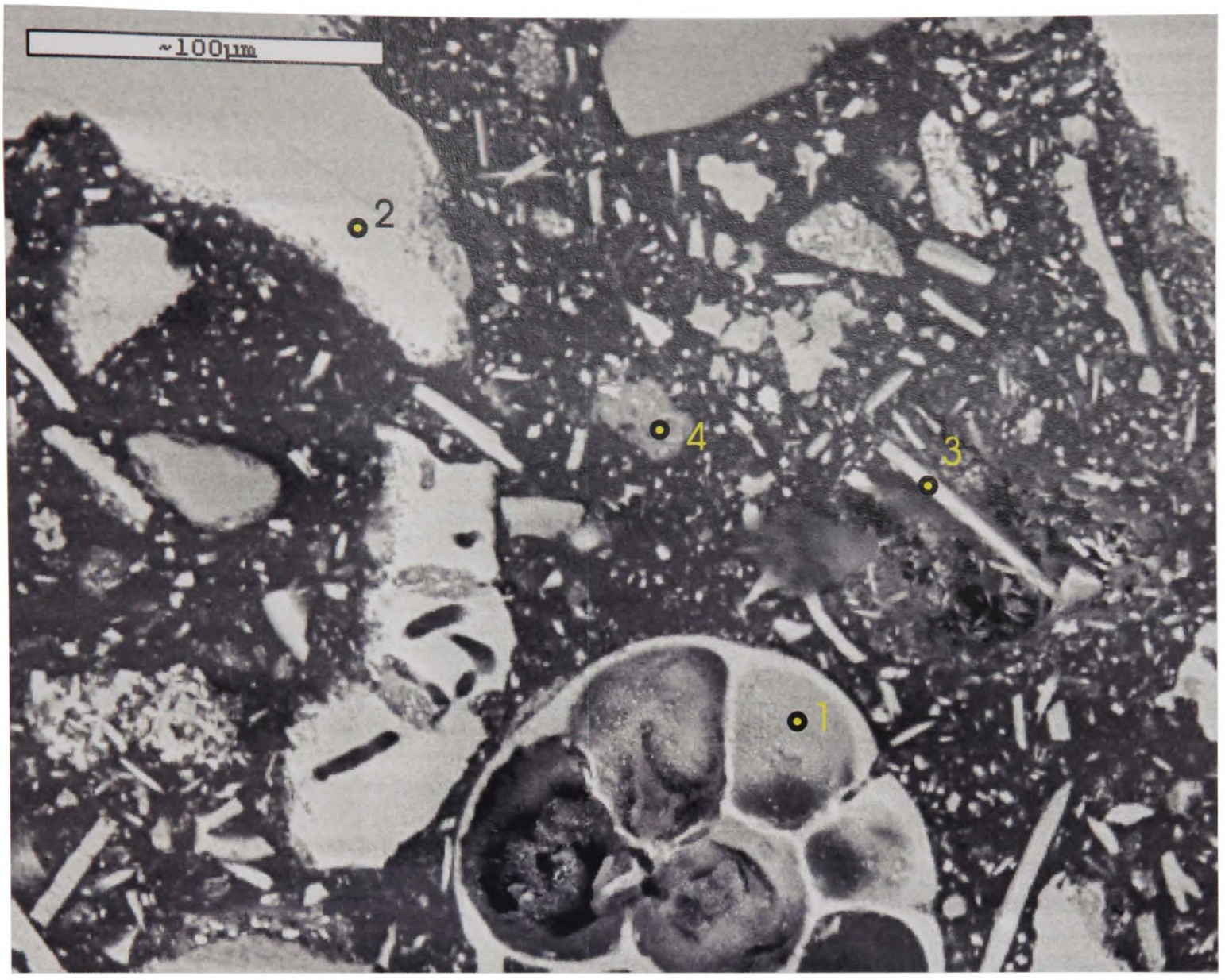


Figure A2.15. Back-scattered electron images of the sediment from South Stromatolite Lake showing points of compositional analysis. Numbers refer to the spectra number in Fig. A2.16 and Table A2.1.

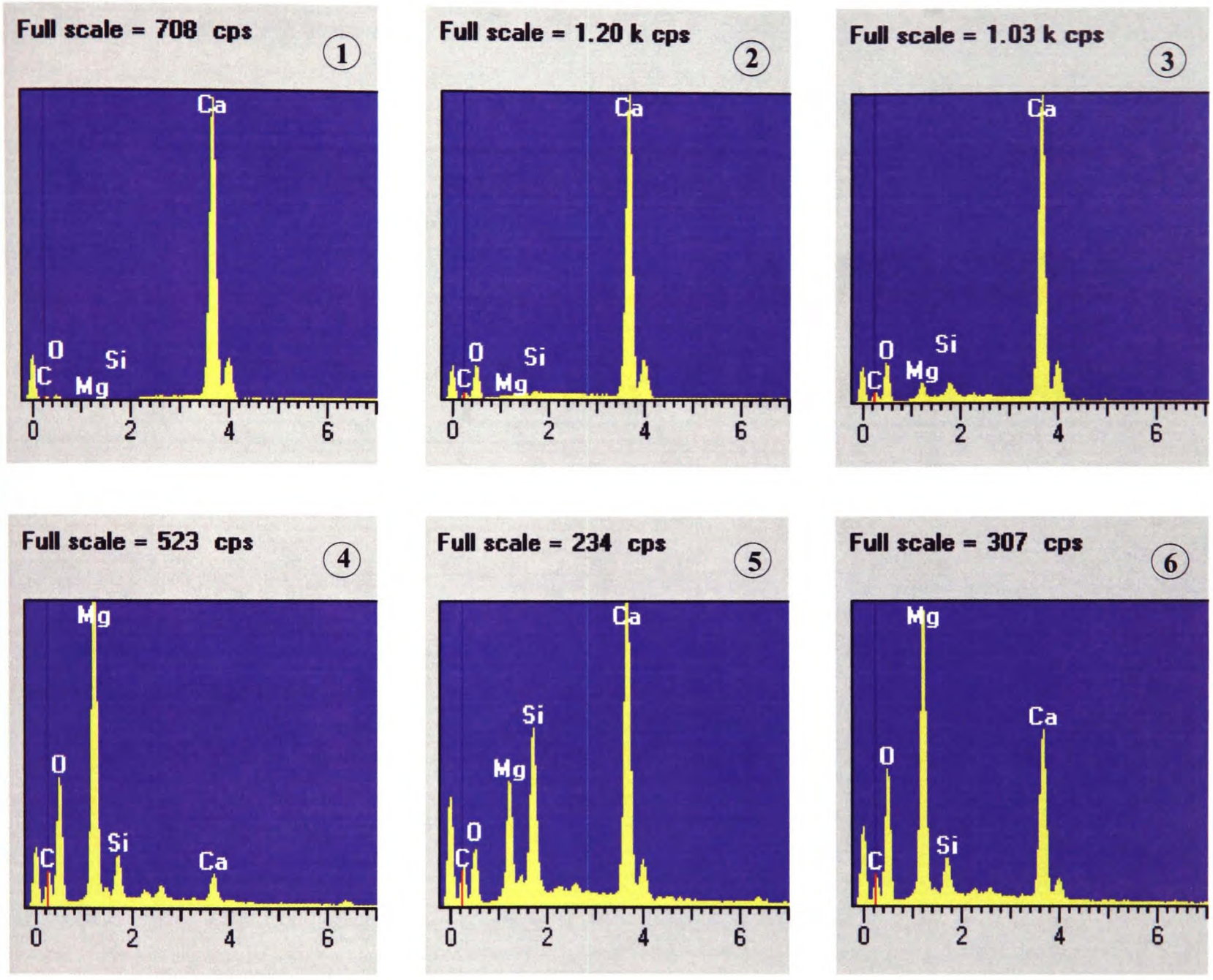


Figure A2.16. South Stromatolite Lake. Atomic spectra for the sediment shown in Fig. A2.15.

APPENDIX 3

pH and Carbonate Data

Table A3.1. Milne Lake Carbonate Data 1999

Depth (mm)	Date	pH	CO_3^{2-} (mg/l)	HCO_3^- (mg/l)
Lakewater	10/11/99	8.56	517	78
10				
20				
30				
45				
Lakewater	13/11/99	7.65	132	67
10		6.79	882	598
20		7.03	1446	1256
30		7.06	1734	504
45		7.23	1260	534
Lakewater	04/12/99	8.68	495	106
10		8	308	251

Table A3.2. Pellet Lake Carbonate Data 1999

Depth (mm)	Date	pH	CO_3^{2-} (mg/l)	HCO_3^- (mg/l)
Lakewater	16/11/99	8.37	635	108
10		8.1		
20		8.14	1231	107
30		8.14	1418	88
45		8.21	1406	268
Lakewater	23/11/99	8.38	1184	309
10		7.96	614	208
20		8.04	159	278
30		8.11	739	172
45		8.31	878	298
Lakewater	01/12/99	7.78	1455	
10		7.35	373	218
20		7.39		
30		7.66	727	456
45		7.94	908	431
Lakewater	07/12/99	7.3	563	337
10		6.9	1372	883
20		7.28	1116	683
30		7.39	832	972

Table A3.3. Mini Dolomite Lake Carbonate Data 1999

Depth (mm)	Date	pH	CO_3^{2-} (mg/l)	HCO_3^- (mg/l)
Lakewater	11/11/99	9.11	63	2
10		7.8	189	31
20		7.66	234	207
30		7.7	547	352
45		7.69	1043	272
Lakewater	14/11/99	8.25	125	13
10		7.21	105	34
20		7.05	722	212
30		7.03	761	129
45		6.98	749	142
Lakewater	19/11/99	6.82	135	81
10		6.71	520	377
20		6.74		
30		6.77	840	504
45		6.79	870	476
Lakewater	05/12/99	8.39	32	2
10		7.86	439	81
20		7.04	992	504
30		7.1	488	254

Table A3.4. McFaiden Lake Carbonate Data 1999

Depth (mm)	Date	pH	CO_3^{2-} (mg/l)	HCO_3^- (mg/l)
Lakewater	10/11/99	7.45	188	107
10		6.9	360	85
20		6.91	765	576
30		6.93	893	287
45		6.88	270	174
Lakewater	15/11/99	7.46	84	15
10		6.76	343	103
20		6.71	586	350
30		6.71	397	48
45		6.73	307	434
Lakewater	19/11/99	7.05	29	25
10		6.45	91	54
20		6.43		
30		6.46	168	124
45		6.68	156	136
Lakewater	04/12/99	8.69	174	11
10		7.49	233	52
20		7.53	490	249

Table A3.5. Halite Lake Carbonate Data 1999

Depth (mm)	Date	pH	CO_3^{2-} (mg/l)	HCO_3^- (mg/l)
Lakewater	12/11/99	7.82	48	15
10		7.13		
20		7.29	362	295
30		7.25	379	292
45		7.28	164	277
Lakewater	20/11/99	7.51	108	33
10		7.31	803	90
20		7.31	820	71
30		7.29	999	119
45		7.28	921	312
Lakewater	26/11/99	6.94	43	20
10		6.13	991	242
20		6.3	578	204
30		6.33	575	207
45		6.61	564	218
Lakewater	03/12/99	6.97	220	76
10		6.61	774	117
20		6.79	633	263
30		6.61	451	215
45		6.58	259	176

Table A3.6. North Stromatolite Lake Carbonate Data 1999

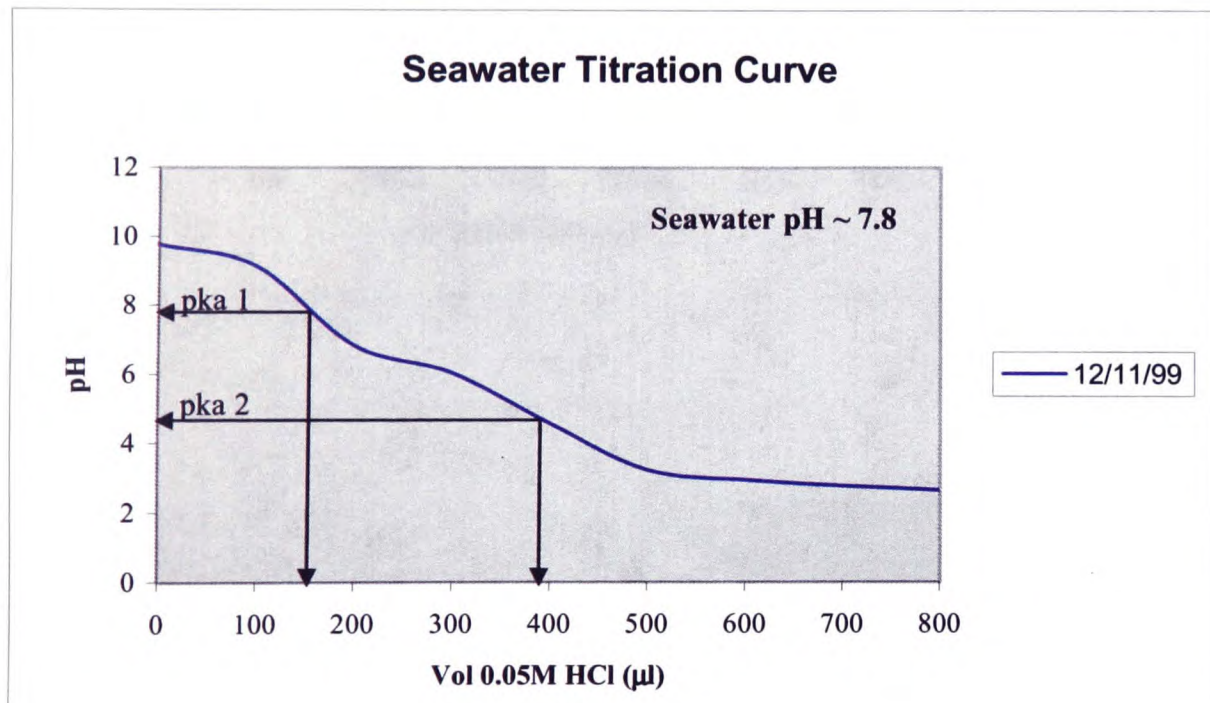
Depth (mm)	Date	pH	CO_3^{2-} (mg/l)	HCO_3^- (mg/l)
Lakewater	16/11/99	7.75	282	63
10		6.14	209	154
20		6.19	262	140
30		6.26	670	368
45		6.18	871	628
Lakewater	24/11/99	6.87	942	1244
10		6.54	593	763
20		6.68	1053	1019
30		6.84		
45		6.94	1604	877
Lakewater	02/12/99	6.62	510	375
10		6.46	89	275
20		6.75	427	611
30		6.84	738	463
45		6.8	861	492
Lakewater	08/12/99	7.76	413	109
10		7.06	274	249
20		7.16	472	276
30		7.34		
45		7.13	622	494

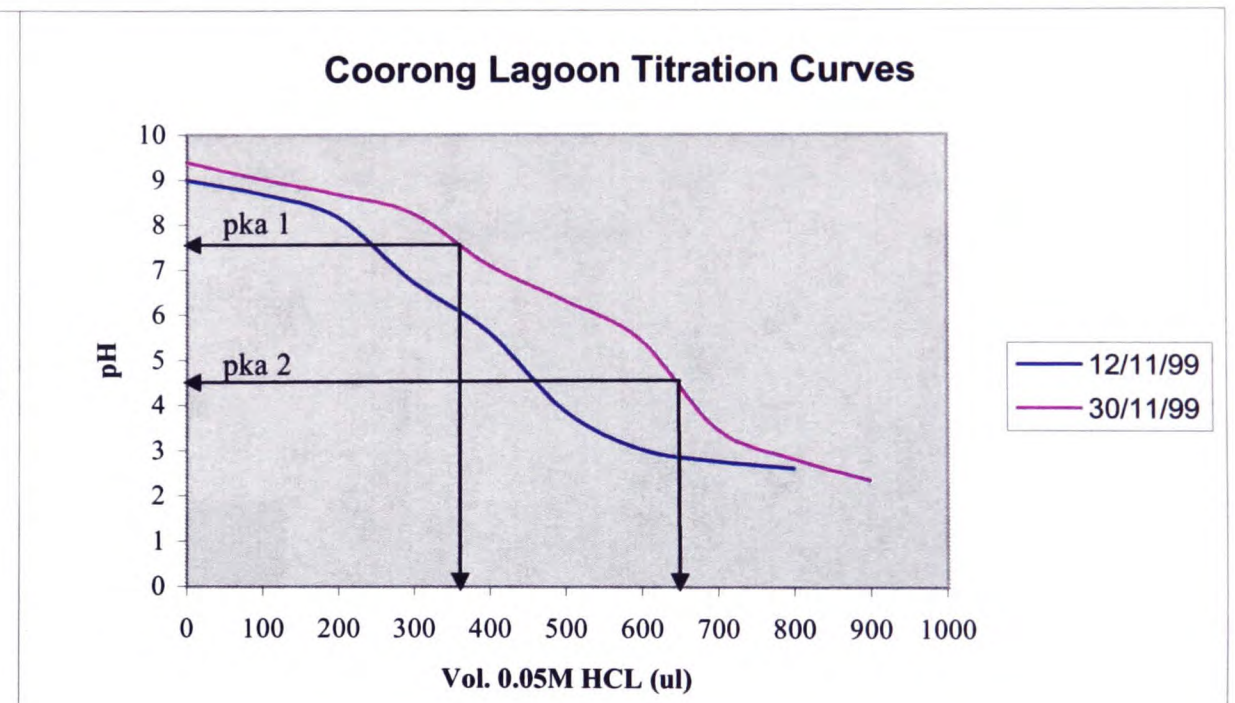
Table A3.7. South Stromatolite Lake Carbonate Data 1999

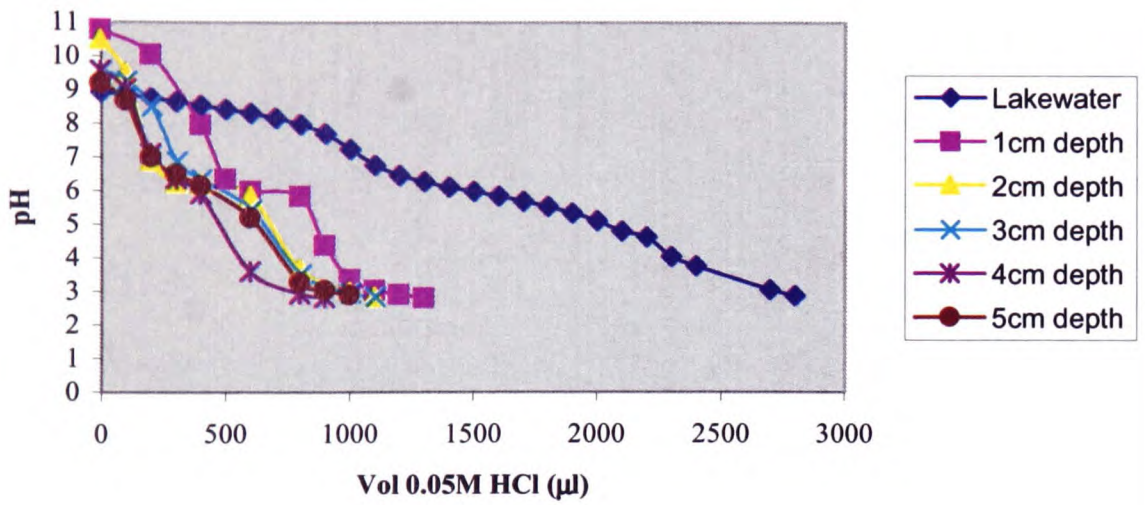
Depth (mm)	Date	pH	CO_3^{2-} (mg/l)	HCO_3^- (mg/l)
Lakewater	15/11/99	8.34	611	130
10		7.7	511	237
20		7.81	1402	392
30		7.79	1826	409
45		7.81	1769	473
Lakewater	22/11/99	8.42	767	205
10		7.92	1034	139
20		7.98	733	578
30		8	868	441
45		8.05	812	498
Lakewater	30/11/99	6.85	389	282
10		6.55	204	165
20		6.88	187	179
30		7.09	418	478
45		7.21	425	1234
Lakewater	05/12/99	8.42		
10		6.96		
20		7.03	803	86
30		7.13	138	138
45		7.29	584	297

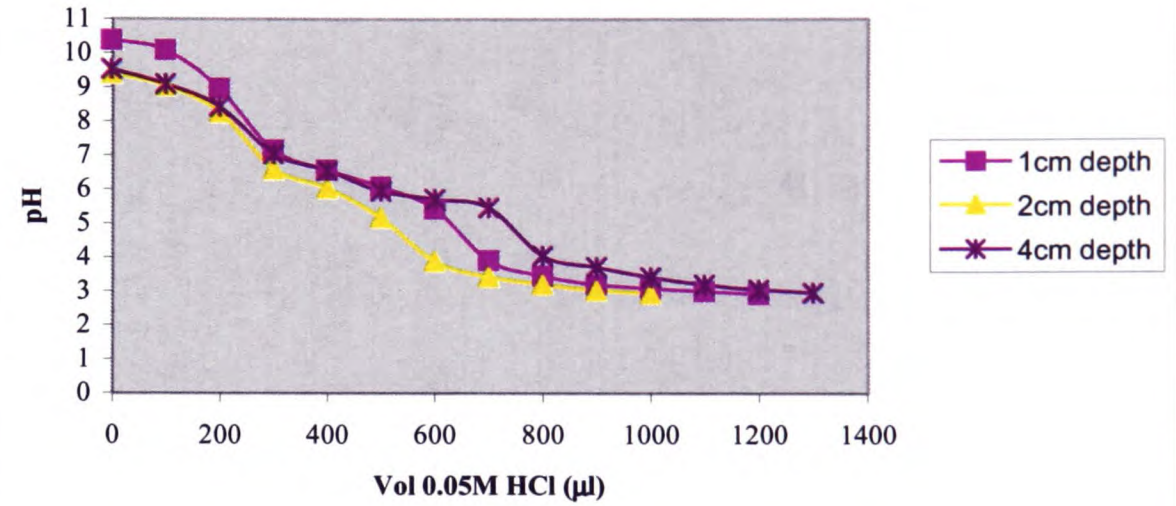
APPENDIX 4
Titration Curves

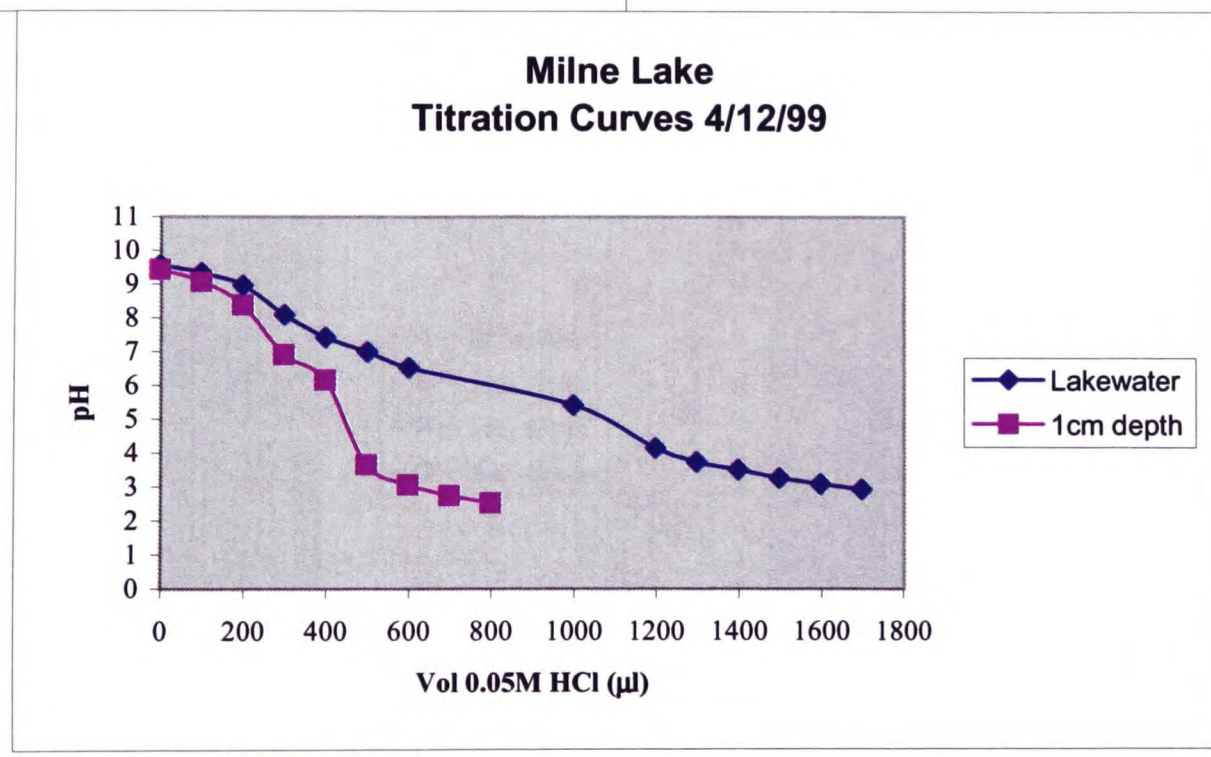
This Appendix contains the titration curves for lakewater and porewater from each of the study lakes. Data from these curves was subsequently used to calculate carbonate ion concentrations.


Seawater Titration Curve
Seawater pH ~ 7.8
pka 1
pka 2
pH
Vol 0.05M HCl (µl)
12/11/99
0
2
4
6
8
10
12
0
100
200
300
400
500
600
700
800

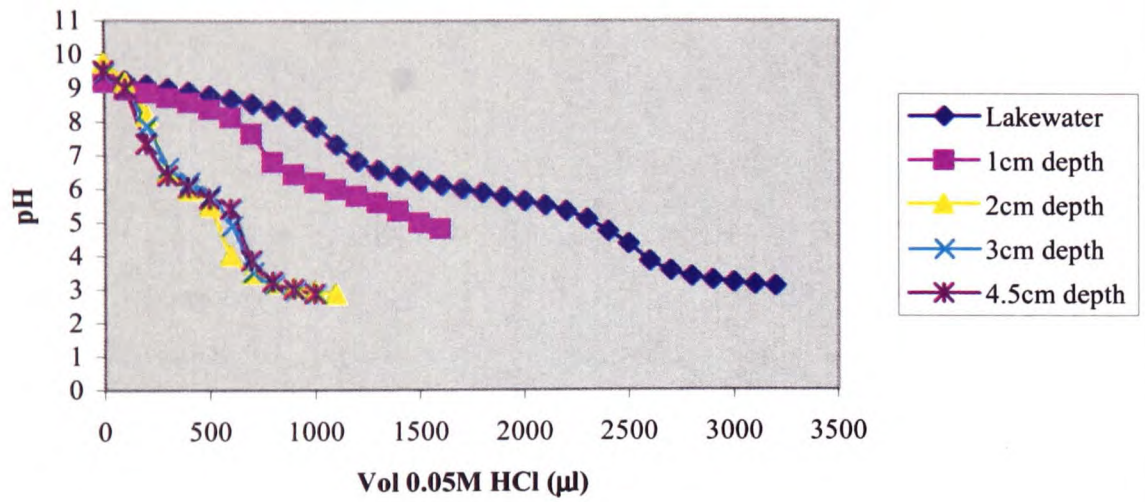

Coorong Lagoon Titration Curves
pka 1
pka 2
pH
Vol. 0.05M HCL (ul)
12/11/99
30/11/99
0
1
2
3
4
5
6
7
8
9
10
0
100
200
300
400
500
600
700
800
900
1000


Milne Lake
Titration Curves 13/11/99
pH
Vol 0.05M HCl (µl)
Lakewater
1cm depth
2cm depth
3cm depth
4cm depth
5cm depth

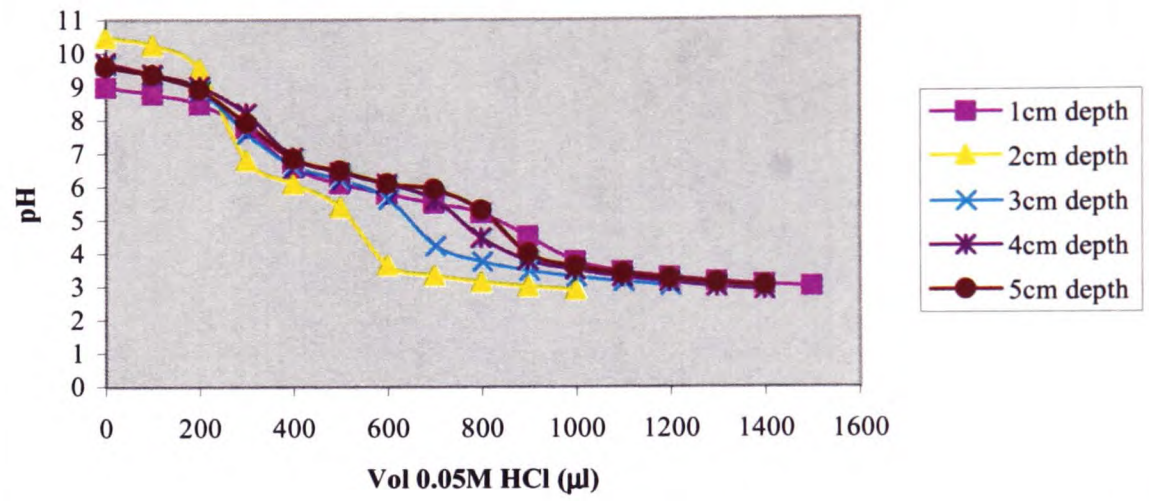

Milne Lake
Titration Curves 18/11/99
pH
Vol 0.05M HCl (µl)
1cm depth
2cm depth
4cm depth


Milne Lake
Titration Curves 4/12/99
pH
Vol 0.05M HCl (µl)
Lakewater
1cm depth

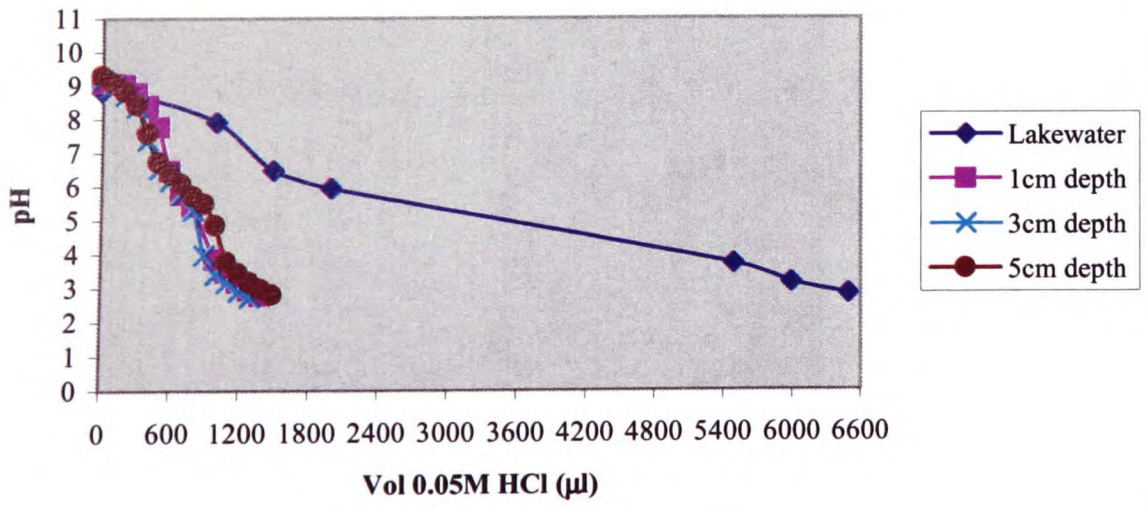
Pellet Lake
Titration Curves 16/11/99



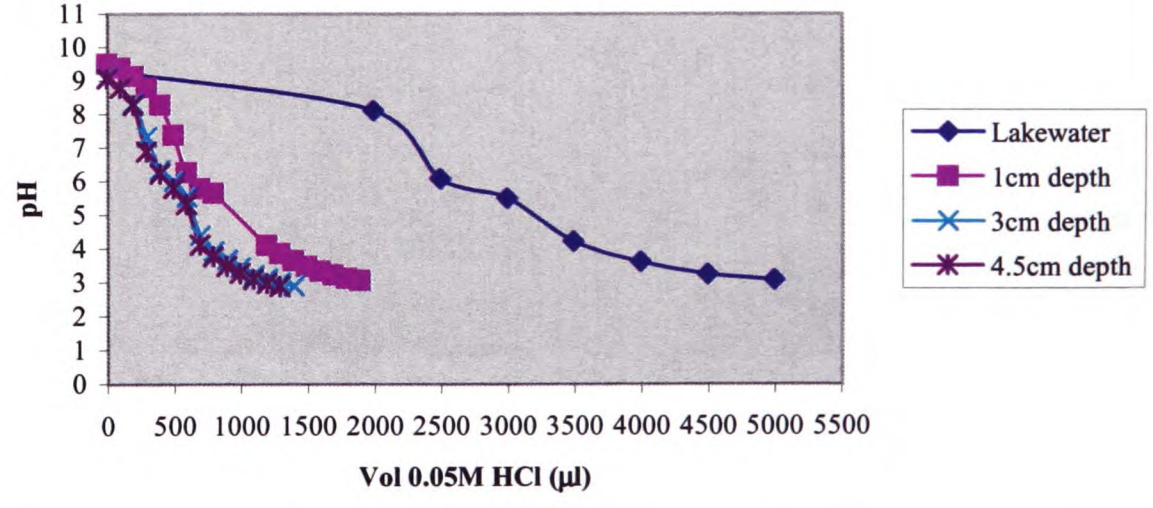
Pellet Lake
Titration Curves 23/11/99



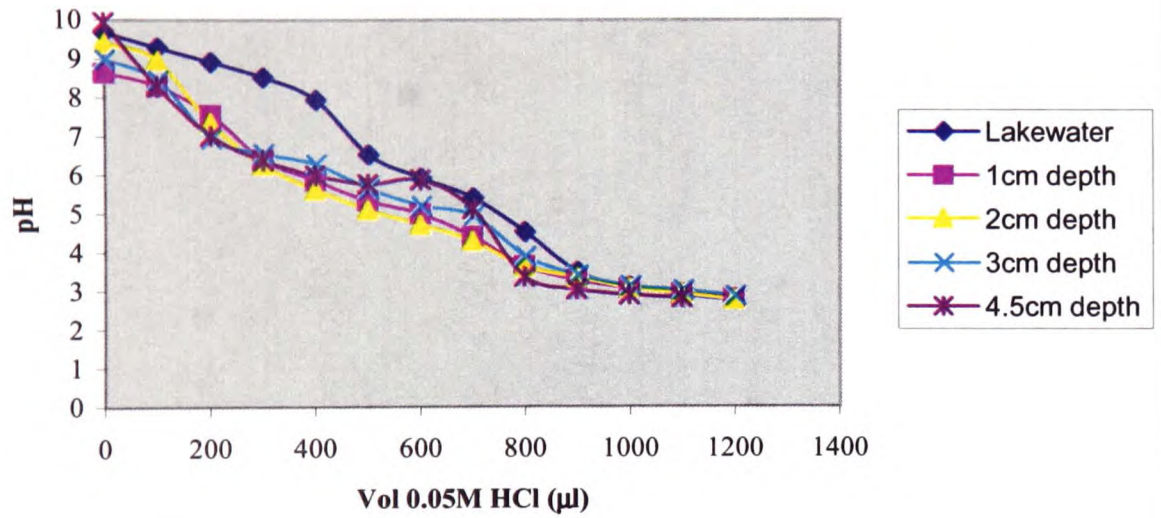
Pellet Lake
Titration Curves 1/12/99



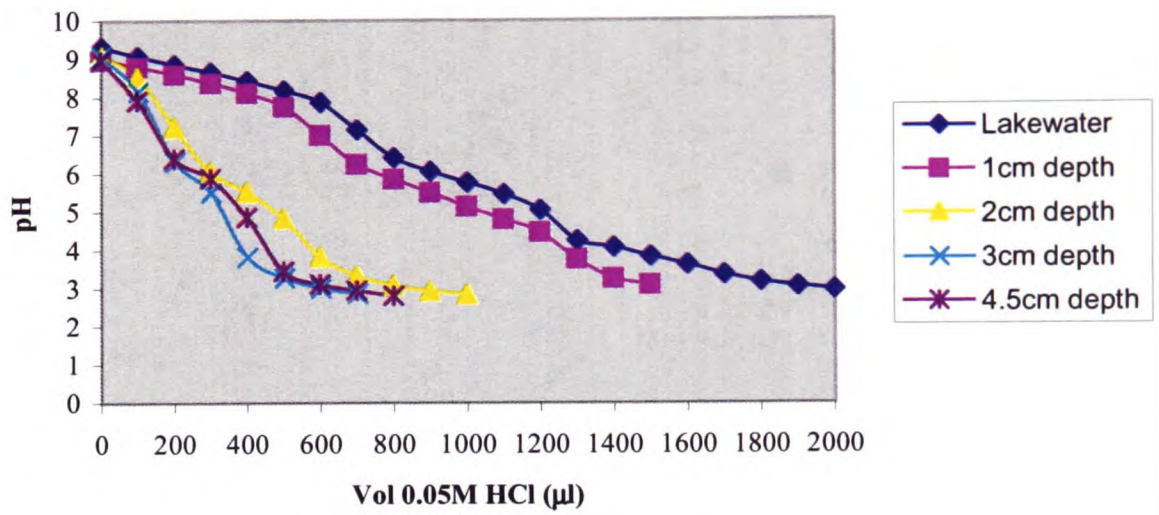
Pellet Lake
Titration Curves 8/12/99



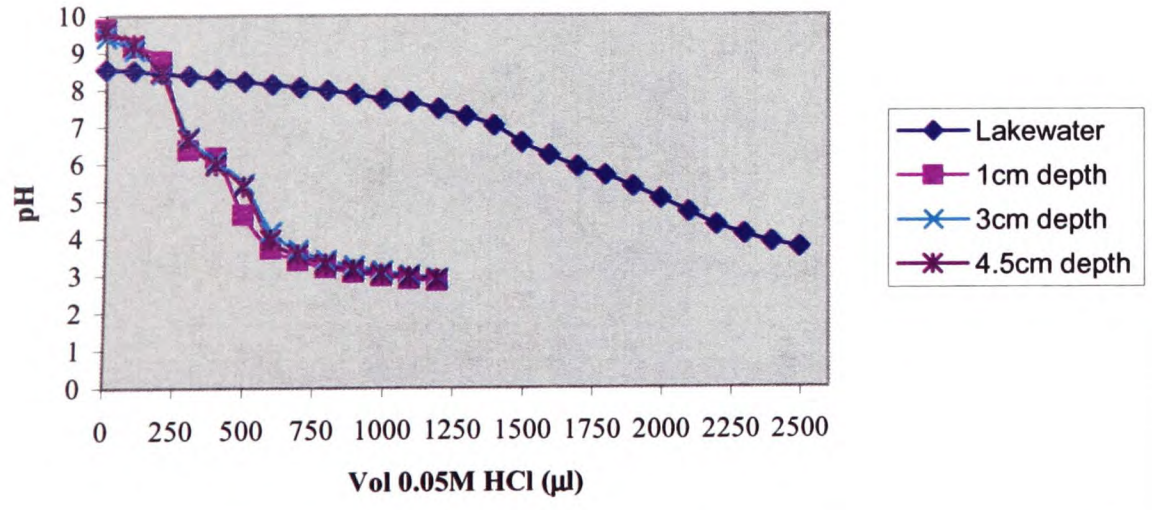
Mini Dolomite Lake
Titration Curves 11/11/99



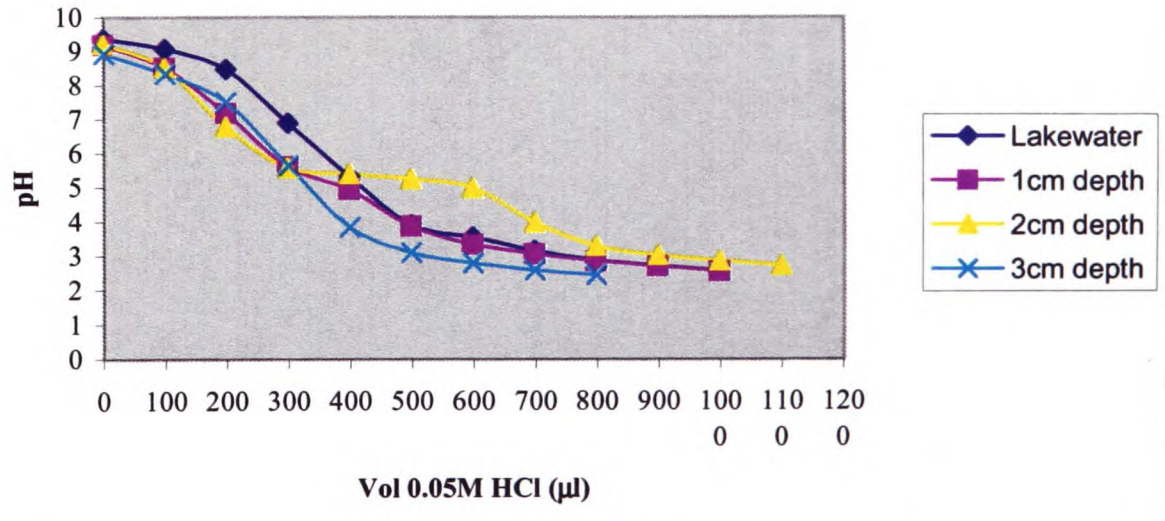
Mini Dolomite Lake
Titration Curves 14/11/99



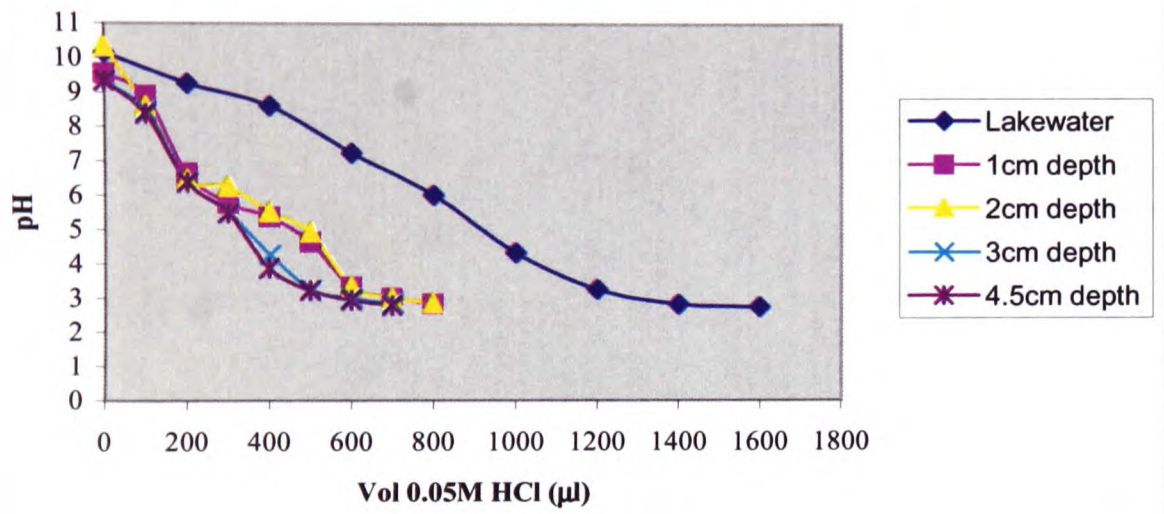
Mini Dolomite Lake
Titration Curves 19/11/99



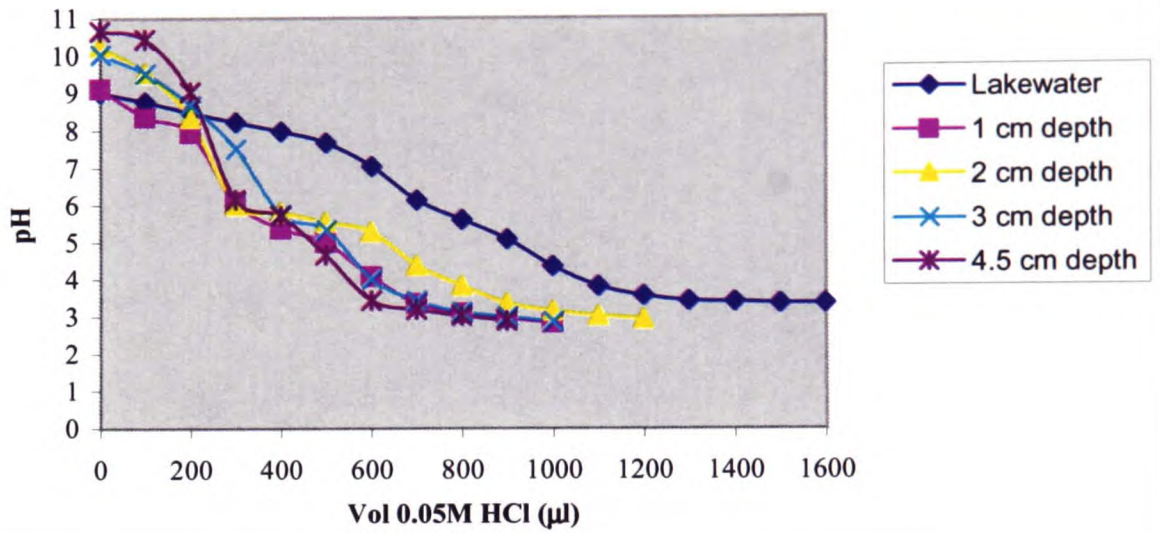
Mini Dolomite Lake
Titration Curves 5/12/99



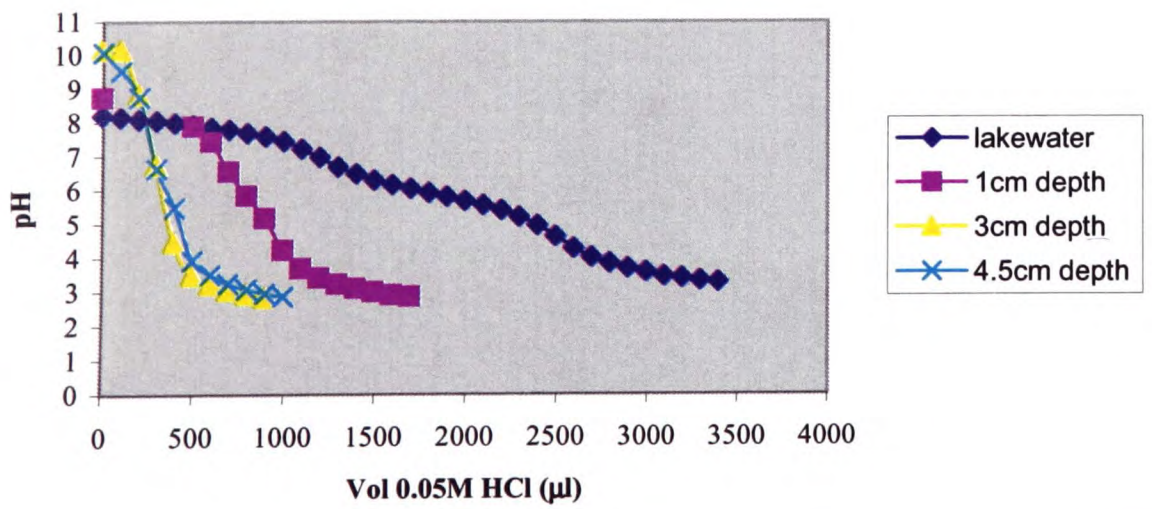
McFaiden Lake
Titration Curves 10/11/99



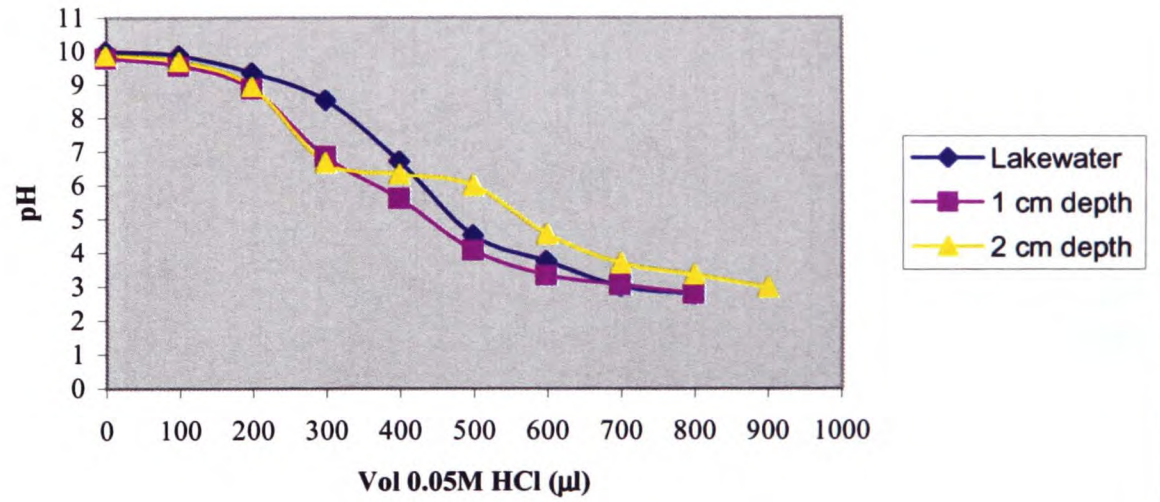
McFaiden Lake
Titration Curves 15/11/99



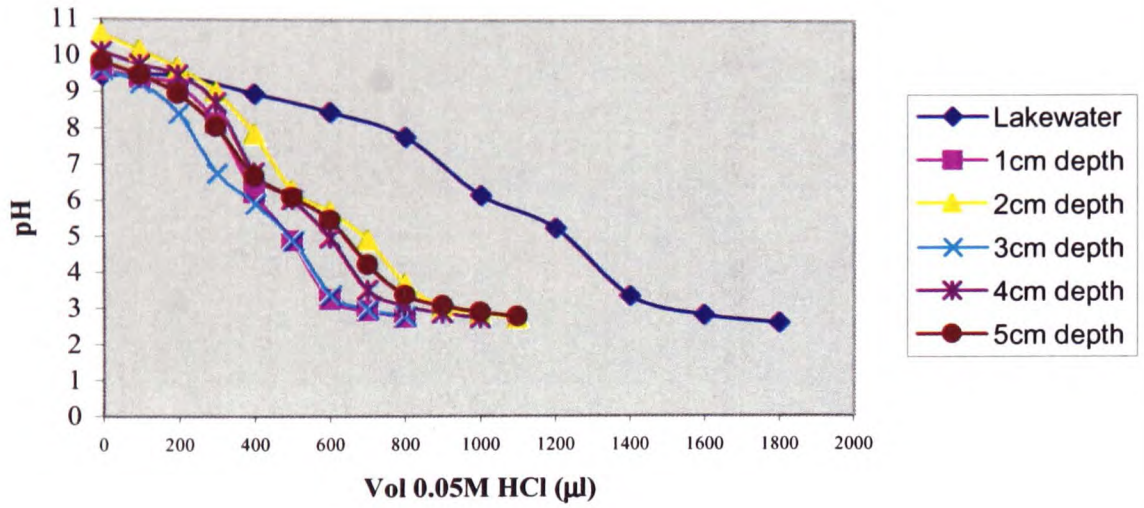
McFaiden Lake
Titration Curves 19/11/99



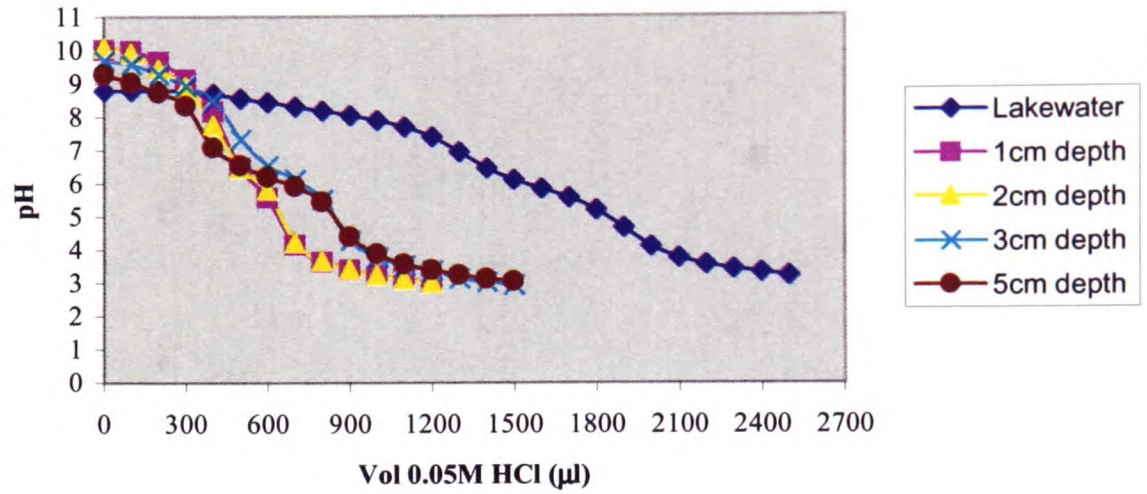
McFaiden Lake
Titration Curves 4/12/99



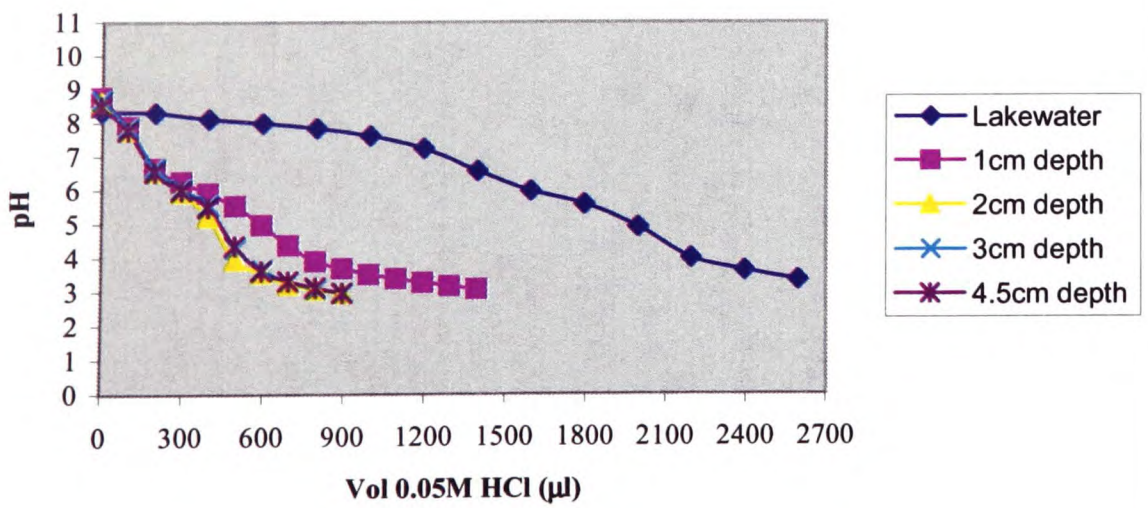
Halite Lake
Titration Curves 12/11/99



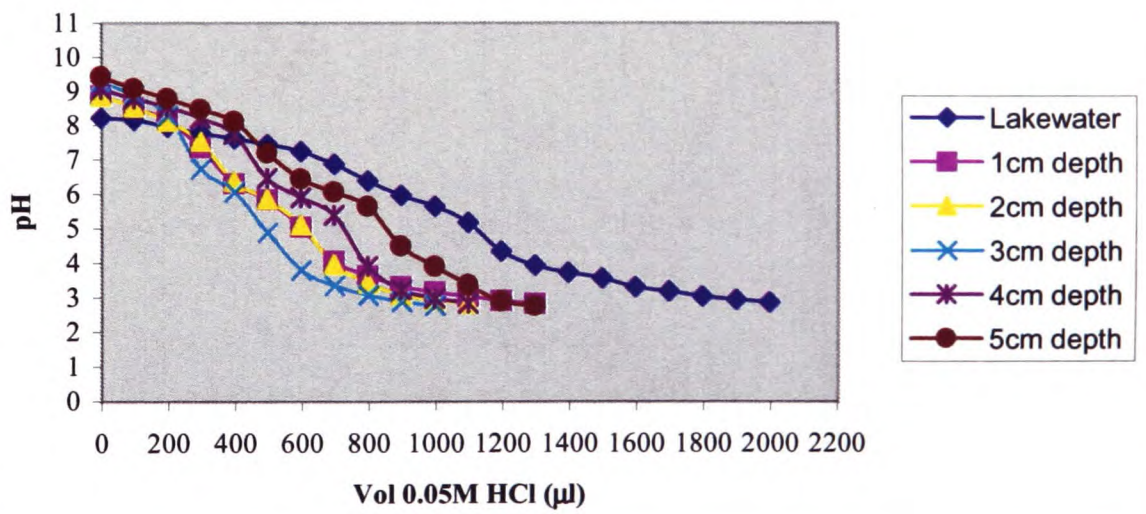
Halite Lake
Titration Curves 20/11/99



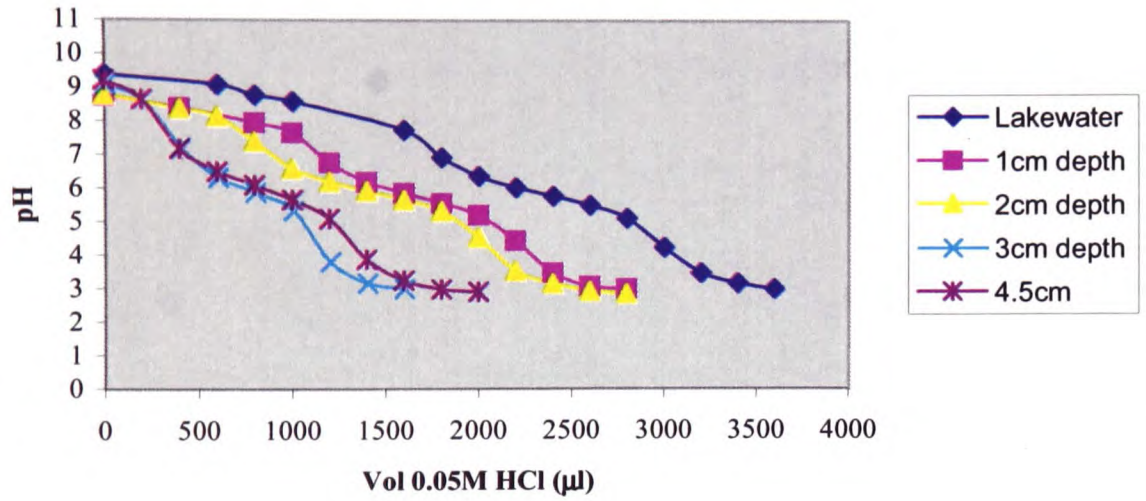
Halite Lake
Titration Curves 26/11/99



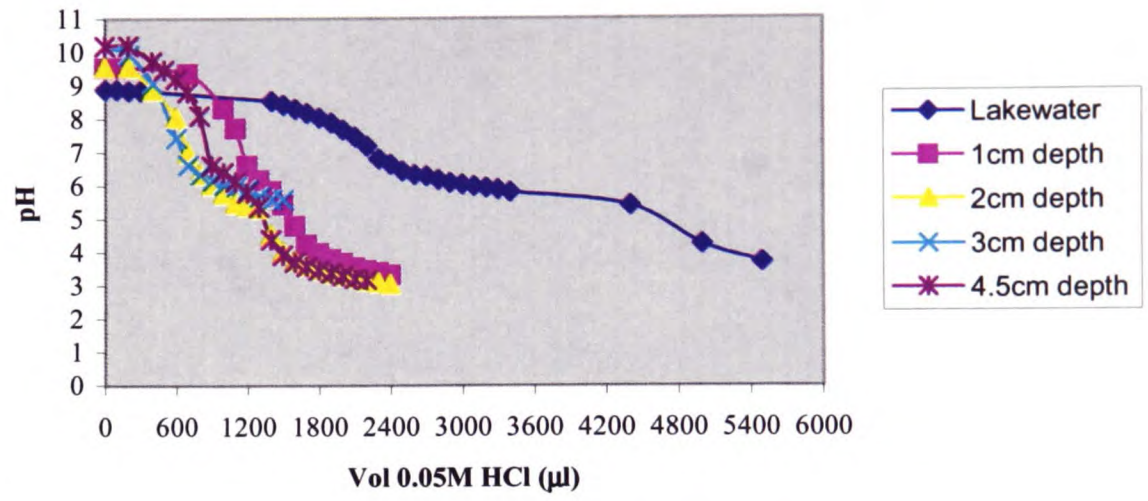
Halite Lake
Titration Curves 3/12/99



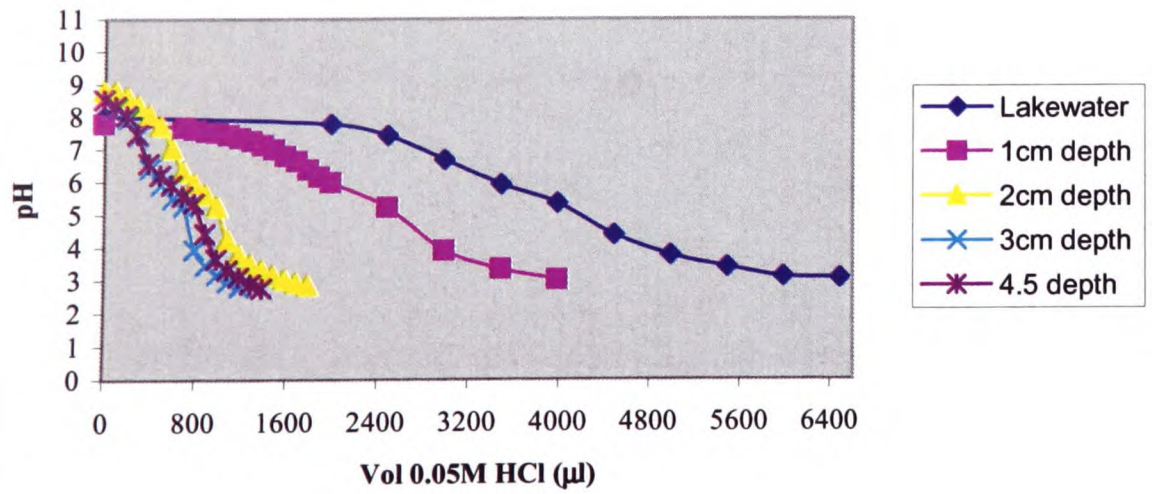
North Stromatolite Lake
Titration Curves 16/11/99



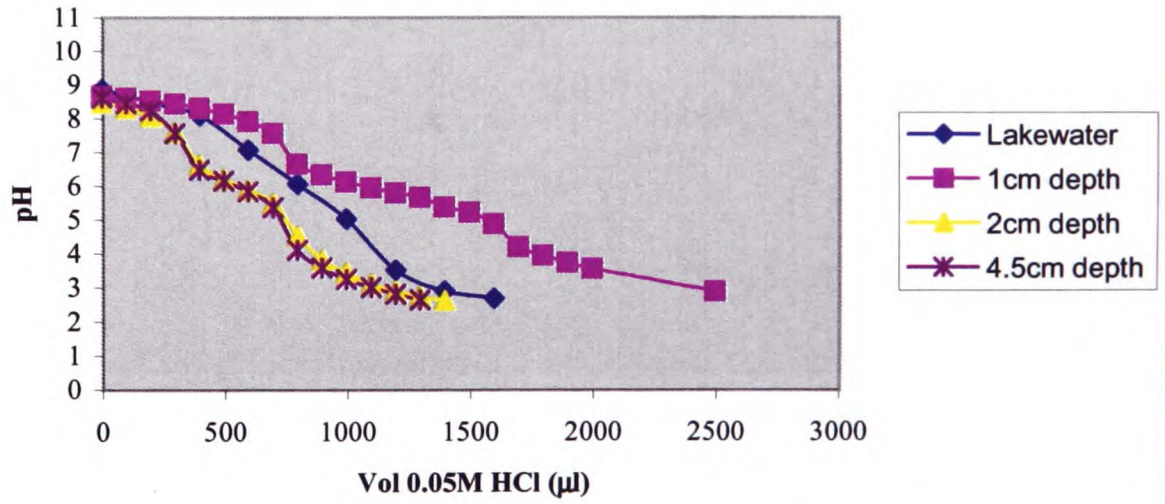
North Stromatolite Lake
Titration Curves 24/11/99



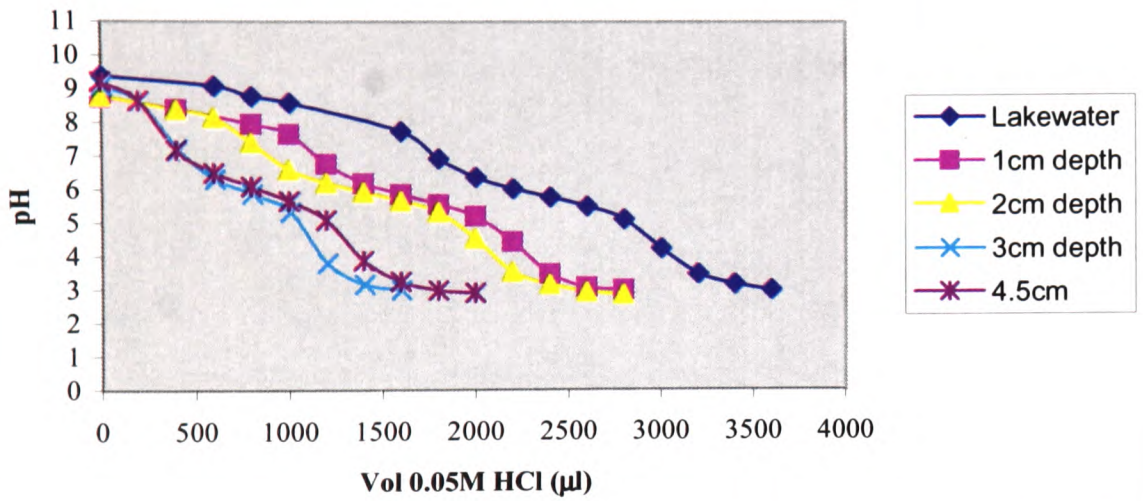
North Stromatolite Lake
Titration Curves 2/12/99



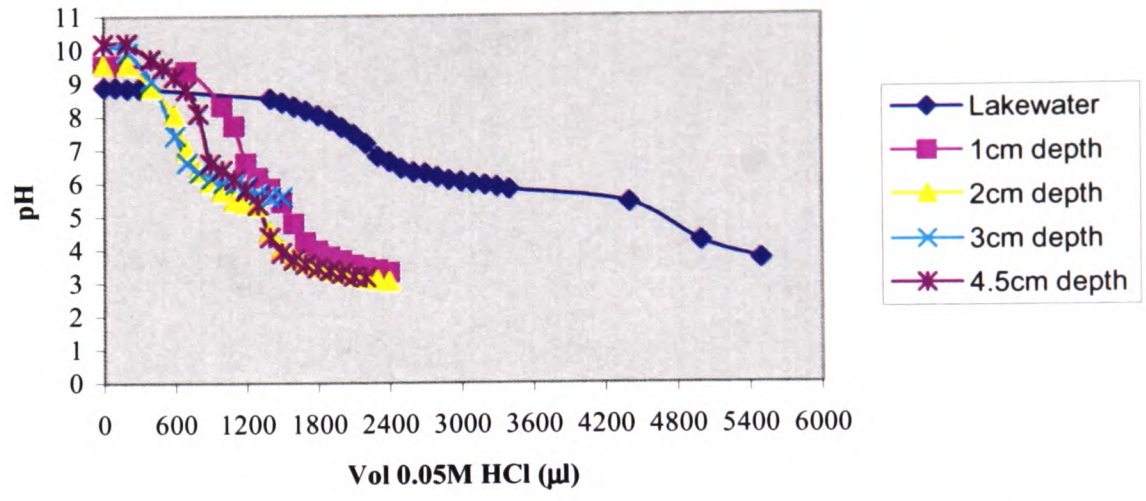
North Stromatolite Lake
Titration Curves 8/12/99



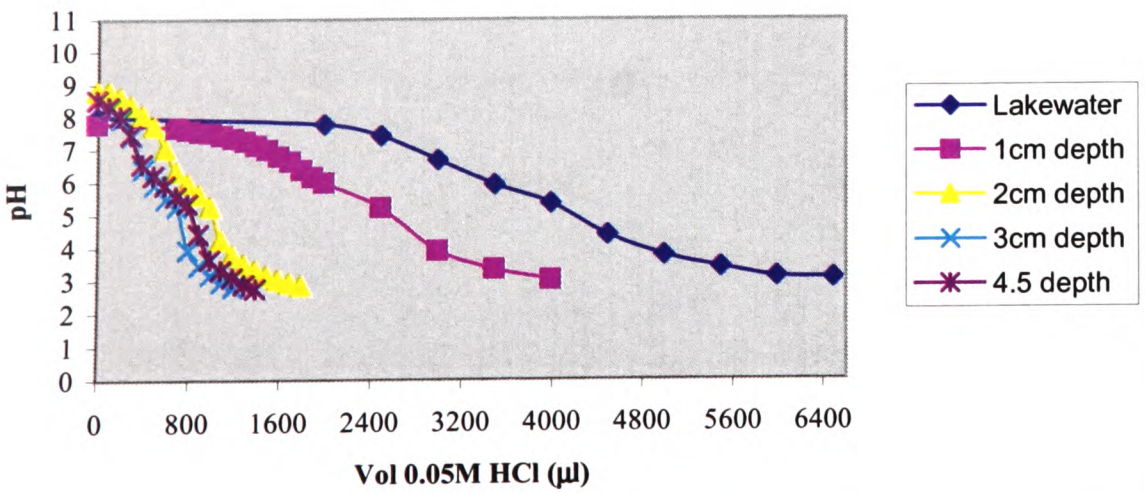
North Stromatolite Lake
Titration Curves 16/11/99



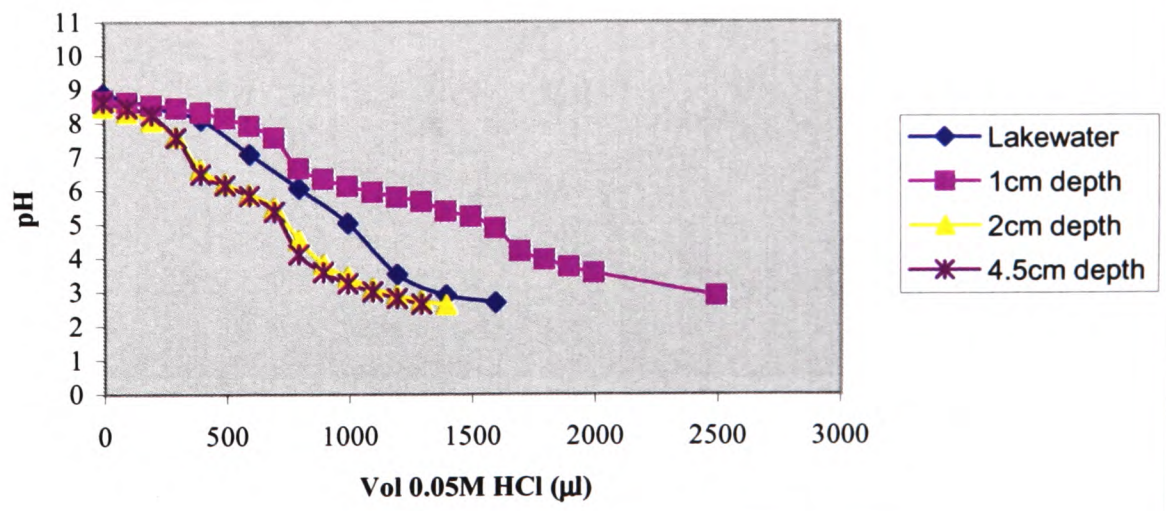
North Stromatolite Lake
Titration Curves 24/11/99



North Stromatolite Lake
Titration Curves 2/12/99



North Stromatolite Lake
Titration Curves 8/12/99



APPENDIX 5

Stable Isotope Data Sets

This Appendix contains detailed methodology for the preparation of barite samples for sulphur and oxygen isotope analysis, together with the methodology for carbon and oxygen isotopic analysis of carbonate and oxygen isotope analysis of water.

The complete set of sulphur and oxygen stable isotope data analysed from residual sulphate isolated from the lake and porewater of each of the study lakes is presented. It also contains oxygen and carbon stable isotope analyses from the carbonate sediments in each of the lakes, together with a summary of analyses by previous authors.

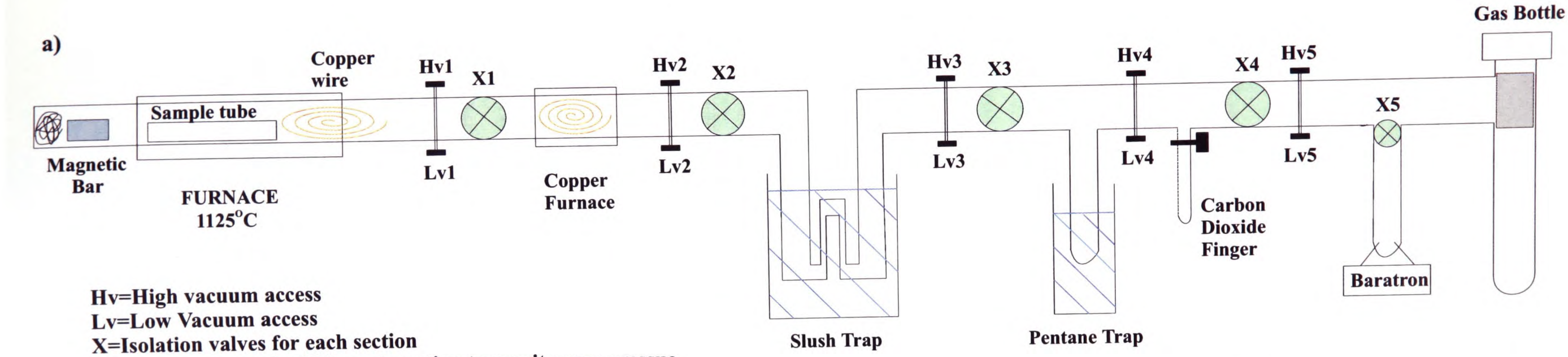


Figure A5.1. Vacuum line apparatus to combust barite in order to carry out isotopic analysis. a) To obtain So_2 for sulphur isotope work. b) To obtain CO_2 for oxygen isotope work.

Procedure for the preparation of a barite sample for sulphur isotope analysis:
(The letters and numbers refer to Figure A5.1).

- Ensure main furnace and copper furnace are both on and main furnace is set at 1125°C. Also ensure 'slush trap' (solid CO_2 + acetone) is placed around apparatus to dry product gases.
- Weigh out 10-15mg of barite sample, together with 200-250mg of copper oxide and 600-700mg of clean sand. Grind together using mortar and pestle and insert into small quartz tube sealing the ends with quartz wool.
- Transfer this glass tube into the ignition tube, together with a 5cm length of wound up copper wire. The copper wire should be half in and half out of the furnace.
- Ensure HV1, HV2, LV1, LV2 and X2 valves are all closed, then open X1. Slide sample into the furnace using the magnet and leave to combust for 15 minutes in this state.
- Close HV3 and HV4 (LV3 and LV4 should already be closed). Ensure X4 is closed. Open X3, ensure there is a good vacuum, then open X2. Place liquid nitrogen around the 'pentane trap' and leave for a further 15 minutes. At this stage SO_2 and CO_2 are collecting in the 'pentane trap'.
- Turn off the furnace and close X3 and X1. Open LV2 and LV3 until gauge 2 hits 4, then close and open HV2 and HV3 instead.
- Open LV4 and then HV4 until gauge 4 has recovered to around 8 – then close.
- Remove liquid nitrogen from the pentane trap and thaw out using a heat gun. Thawing results in gauge 4 falling. When fully thawed replace liquid nitrogen and refreeze – gauge 4 will recover to about 8. This takes up to about 5 minutes and in this time a new sample can be prepared.
- Open HV4 for a few seconds to pump off any residual non-condensable gases.
- This stage is a critical one. It separates the CO_2 that can be discarded, from the SO_2 to be analysed. The liquid nitrogen is transferred to the CO_2 finger and then gauge 4 is monitored. After around 90 seconds it drops to around 1-2; within 3 minutes it should recover to around 7 or 8. This is caused by the CO_2 escaping from the pentane trap into the finger. The CO_2 finger must be closed by about 3 minutes 15 seconds to prevent the SO_2 escaping. Now the gases are separated.
- Fully thaw out the pentane trap again. The SO_2 is now present between X3 and X4.

- Move the liquid nitrogen to the manometer gauge finger. Close HV5 and then open X4. The gas collects in the manometer finger. This is isolated by closing X4 and X5. The finger is then heated and the reading is noted – later this reading is used to calculate the yield.
- Next the gas is collected in the sample bottle. This is done by placing the liquid nitrogen around the sample bottle. Ensure LV5 and HV5 are shut and then open X5. The gas now transfers from the manometer finger to the sample bottle. Once gauge 5 is stable HV5 can be opened to pump away any non-condensables. Carefully support and close the sample bottle.
- Put a new bottle on, empty the CO_2 finger and leave the apparatus pumping for the next sample.

The sample bottle is directly attached to a SIRA II mass spectrometer to analyse the sulphur isotope composition of the gas.

Procedure for the preparation of a barite sample for oxygen isotope analysis:

(The letters and numbers refer to Figure A5.2).

- Weigh out 10-15mg of barite sample with an equal amount of carbon.
- Close LV1, HV1 and X1 to isolate the sample tube. Place the sample and carbon in a pre-cleaned platinum crucible in the sample tube and then reconnect the tube.
- Close the isolation valve and open LV1 and X1. When gauge 1 reaches 4, open the isolation valve, close LV1 and open HV1.
- Turn Radyne (induction heat source) on and leave at low power for 15 minutes to let the sample degas.
- Close all vacuum pumps up to HV3 and all valves up to X4 should be open. At this point the liquid nitrogen should be in place around the tubes indicated in the diagram and the 2Kv discharge box (RS 223-219) should be on. From now on the discharge box must be on whenever the liquid nitrogen is around the tube with the platinum electrodes in, and off otherwise.
- The Radyne can now be turned up to 25% and then, ideally, every 5 minutes turned up by 5%. On a good sample the Radyne can go as high as 60% but on a poor one only about 35% may be obtained. The signal to stop increasing the heat is seeing plasma form in the

sample tube – this leads to anomalous isotope results and should be avoided whenever possible. Generally the higher the Radyne can be turned up the better the yield obtained.

- During this period of heating gauges 1 and 2 should be observed and the reading noted every 10 minutes. After about 90 minutes the sample has usually heated enough to give a good yield, and the Radyne can be turned off.
- Remove liquid nitrogen from around barite sample tube and heat with heat gun. Two phases of gas will come off which can be observed by the fall and recovery of gauge 1. Then close X3 to prevent gas escaping backwards.
- Remove liquid nitrogen from tubes 2 and 3, then put it around the manometer gauge finger. Close X5 and then open X4 to freeze gas into the finger.
- Isolate the finger by ensuring X4 and X5 are both closed, then heat the finger and record the manometer reading.
- Transfer liquid nitrogen to gas sample bottle. Ensure X6 is open and LV4 and HV3 are closed. Then open X5 and freeze gas into the sample bottle. When gauge 3 has recovered close X6 and remove the bottle.
- Change the bottle and then leave the apparatus pumping.

Again the sample bottle is directly attached to a SIRA 10 mass spectrometer to analyse the isotopic composition of the gas. Note: in this process it is the oxygen in the carbon dioxide that is analysed.

Preparation and processing of carbonate samples for carbon and oxygen isotope analysis:

The sample preparation module:

1 mg of the sample was placed in a 6ml Vacutainer, which in turn was placed in a rack in a water bath. The water bath was set at 70°C (this is the reaction temperature, and must be carefully controlled to within 0.1°C) and, once the rack had been inserted, it was left for 15 minutes to equilibrate. The remainder of the preparation process is fully automated and all that was required was to input the number of samples and the start position into the computer. Helium at 6psi was injected into each tube in turn. Injection lasted for 2 minutes and ensured all the air was flushed out of the tube. 200 µl of 105% phosphoric acid was then

injected into each tube individually and the samples were left to react. Reaction time for calcites and aragonites was a minimum of 8 hours, whereas dolomites were left for 24 hours.

The sample processing module:

Once the reaction was complete the rack of tubes was transferred from the water bath to the mass spectrometer module. The mass spectrometer was an AP2003, which is compact and fairly simple, designed especially for looking solely at CO_2 gas. It analyses approximately 4% CO_2 in helium. This is similar to the amount of CO_2 in breath samples, which is what this apparatus was initially invented to analyse.

Each sample was pressurised slightly above atmospheric pressure with helium gas and then allowed to de-pressurise through the sample injection loop, allowing the loop to fill with the sample gas to be measured. Water vapour was removed by a Nafion trap before the gas reached the sample loop. From the sample loop the gas passed into an isothermal gas chromatograph where the CO_2 was purified. The pure gas was then carried in a stream of helium to the ion source for the mass spectrometer via an open split interface. This process can be repeated several times from one sample tube, allowing replicate analyses and improved precision. Two pulses of reference gas bracket the sample peaks; the isotopic enrichment of the sample gas was calculated and converted to PDB by comparison to this reference gas. The process described above takes less than ten minutes for one complete sample.

Water samples:

A further logical step was to investigate the isotopic characteristics of each of the lakewaters and attempt to reconcile this with data obtained from the sediments themselves. Water samples were run directly on the processing module described in the previous section and the $\delta^{18}O$ measured rapidly and accurately. 1ml of water was placed in a sample tube then flushed with helium. CO_2 was then injected to around 4% as in the carbonate samples; processing and analysis was fully automated, as before. Approximately 200 samples can be processed in a day.

Sulphur Isotope Standards

1998

Standard	Yield	$\delta^{34}S$ CDT (‰)
CP1	94	-4.47
CP1	97	-4.64
CP1	98	-4.44
NBS 123	100	+17.40

1999

Standard	Yield	$\delta^{34}S$ CDT (‰)
IAEA-S-3	93	- 30.97
IAEA-S-3	98	- 30.92
IAEA-S-3	107	- 31.00
NBS 123	102	+ 17.67
NBS 123	100	+ 17.26
CP1	93	- 4.54
CP1	97	- 4.75

Seawater

1998

Date	Time	Yield	$\delta^{34}S$ CDT (‰)
30 Oct	Dusk	88	+ 22.12
16 Nov	Midday	91	+ 22.04

1999

Date	Type	Yield	$\delta^{34}S$ CDT (‰)
12 Nov	Coorong	92	+ 22.29
12 Nov	Ocean	81	+ 21.94

Milne Lake Sulphur Isotopes

1998 - Lakewater

Date	Time	Yield	$\delta^{34}S$ CDT (‰)
28 Oct	Midday	86	+ 29.58
4 Nov	Dusk	91	+ 29.51
5 Nov	Midday	96	+ 29.11
14 Nov	Midday	92	+ 30.38
15 Nov	Dusk	88	+ 30.43

1999

Date	Depth	Yield	$\delta^{34}S$ CDT (‰)
13 Nov	Lakewater	92	+ 29.70
13 Nov	2-3cm	67	+ 29.39
18 Nov	1-2cm	68	+ 28.70
18 Nov	4cm	64	+ 29.43
4 Dec	Lakewater	75	+ 28.86
4 Dec	0-1cm	68	+ 29.24

Pellet Lake Sulphur Isotope Results

1998 - Lakewater

Date	Time	Yield	$\delta^{34}S$ CDT (‰)
8 Nov	Midday	81	+ 26.37
8 Nov	Dusk	84	+ 26.52
18 Nov	Midday	94	+ 26.29
20 Nov	Dusk	98	+ 26.39

1999

Date	Depth	Yield	$\delta^{34}S$ CDT (‰)
23 Nov	Lakewater	90	+ 24.70
23 Nov	0-1cm	82	+ 25.99
23 Nov	1-2cm	Gas lost	
23 Nov	2-3cm	65	+ 25.94
23 Nov	4.5cm	61	+ 25.07
7 Dec	Lakewater	65	+ 25.46
7 Dec	2-3cm	78	+ 26.53

Mini Dolomite Lake Sulphur Isotope Results

1998 - Lakewater

Date	Time	Yield	$\delta^{34}S$ CDT (‰)
29 Oct	Midday	92	+ 27.41
5 Nov	Midday	101	+ 27.62
5 Nov	Dusk	98	+ 28.08
15 Nov	Midday	99	+ 27.66
16 Nov	Dusk	87	+ 26.89

1999

Date	Depth	Yield	$\delta^{34}S$ CDT (‰)
14 Nov	Lakewater	86	+ 27.37
14 Nov	0-1cm	73	+ 26.82
14 Nov	1-2cm	88	+ 27.15
14 Nov	2-3cm	48	+ 27.10
14 Nov	4.5cm	88	+ 27.55
5 Dec	Lakewater	77	+ 27.15
5 Dec	0-1cm	71	+ 26.55
5 Dec	2-3cm	73	+ 27.39
5 Dec	4.5cn	69	+ 27.33

McFaiden Lake Sulphur Isotope Results

1998 - Lakewater

Date	Time	Yield	$\delta^{34}S$ CDT (‰)
30 Oct	Midday	73	+ 25.49
4 Nov	Midday	94	+ 25.77
4 Nov	Dusk	90	+ 25.90
14 Nov	Midday	95	+ 25.51
14 Nov	Dusk	80	+ 25.27

1999

Date	Depth	Yield	$\delta^{34}S$ CDT (‰)
15 Nov	Lakewater	93	+ 24.88
15 Nov	0-1cm	86	+ 24.40
15 Nov	1-2cm	81	+ 24.68
15 Nov	2-3cm	93	+ 24.80
15 Nov	4.5cm	75	+ 25.47
4 Dec	Lakewater	72	+ 24.66
4 Dec	0-1cm	23	+ 25.18

Dolomite Lake

1998 - Lakewater

Date	Time	Yield	$\delta^{34}S$ CDT (‰)
30 Oct	Midday	80	+ 28.53

Lake was dry at all other times

Halite Lake Sulphur Isotope Results

1998 - Lakewater

Date	Time	Yield	$\delta^{34}S$ CDT (‰)
29 Oct	Midday	99.7	+ 28.35
6 Nov	Midday	99.7	+ 28.46
6 Nov	Dusk	88.1	+ 28.60
16 Nov	Midday	90	+ 28.32
17 Nov	Dusk	89	+ 28.59

1999

Date	Depth	Yield	$\delta^{34}S$ CDT (‰)
26 Nov	Lakewater	80	+ 26.99
26 Nov	0-1cm	Gas lost	
26 Nov	1-2cm	59	+ 26.87
26 Nov	2-3cm	49	+ 27.61
26 Nov	4.5cm	90	+ 28.31
3 Dec	Lakewater	81	+ 28.33
3 Dec	0-1cm	62	+ 28.35
3 Dec	4.5cm	69	+ 29.45

North Stromatolite Lake Sulphur Isotope Results

1998 - Lakewater

Date	Time	Yield	$\delta^{34}S$ CDT (‰)
1 Nov	Midday	100	+ 23.82
7 Nov	Midday	99	+ 23.78
7 Nov	Dusk	93	+ 23.56
17 Nov	Midday	85	+ 23.46
19 Nov	Dusk	92	+ 23.58

1999

Date	Depth	Yield	$\delta^{34}S$ CDT (‰)
16 Nov	Lakewater	87	+ 23.28
16 Nov	0-1cm	94	+ 22.66
16 Nov	1-2cm	79	+ 23.24
16 Nov	2-3cm	85	+ 23.?
16 Nov	4.5cm	80	+ 23.32
8 Dec	Lakewater	85	+ 23.11
8 Dec	0-1cm	69	+ 21.95
8 Dec	4.5cm	70	+ 23.67

South Stromatolite Lake Sulphur Isotope Results

1998 - Lakewater

Date	Time	Yield	$\delta^{34}S$ CDT (‰)
29 Oct	Midday	93	+ 26.74
5 Nov	Dusk	91	+ 26.13
6 Nov	Midday	91	+ 26.48
15 Nov	Midday	90	+ 26.63
22 Nov	Dusk	94	+ 26.63

1999

Date	Depth	Yield	$\delta^{34}S$ CDT (‰)
15 Nov	Lakewater	92	+ 26.04
15 Nov	0-1cm	60	+ 26.17
15 Nov	1-2cm	71	+ 26.07
15 Nov	2-3cm	53	+ 25.71
15 Nov	4.5cm	57	+ 26.14
5 Dec	Lakewater	67	+ 26.44
5 Dec	1-2cm	70	+ 26.51
5 Dec	4.5cm	74	+ 26.42

Oxygen Isotope Standards for Sulphates

Standard	Yield	$\delta^{18}O$ SMOW (‰)
NBS 127	66	+ 9.3
NBS 127	68	+ 11.3
NBS 127	83	+ 9.1
NBS 127	87	+ 11.9
NBS 127	87	+ 11.4
NBS 127	95	+ 10.6

Oxygen Isotope Results from Residual Sulphate

Sample	Date	Yield	$\delta^{18}O$ SMOW (‰)
Seawater	30 Oct '98	84	+ 10.4
Seawater (repeat)	30 Oct '98	89	+ 11.3
Mini Dolomite	5 Nov '98	44	+ 25.0
Mini Dolomite (repeat)	5 Nov '98	76	+ 28.1
Mini Dolomite	19 Nov '99	66	+ 23.7
Mini Dolomite	5 Dec '99	77	+ 26.3
McFaiden	4 Nov '98	46	+ 22.1
McFaiden	19 Nov '99	83	+ 21.7
Milne	5 Nov '98	74	+ 27.0
Milne (repeat)	5 Nov '98	102	+ 34.2
Milne	13 Nov '99	50	+ 32.3
Pellet	18 Nov '98	11	+ 23.9
Pellet	1 Dec '99	85	+ 23.2
Pellet (2-3cm)	23 Nov '99	83	+ 19.9
Halite	16 Nov '98	80	+ 21.9
Halite	26 Nov '99	79	+ 26.7
North Stromatolite	1 Nov '98	81	+ 22.7
North Strom (repeat)	1 Nov'98	81	+ 25.2
South Stromatolite	6 Nov '98	85	+ 22.5
South stromatolite	22 Nov '99	82	+ 25.9

Note: All samples are lakewater unless otherwise stated

Carbon Isotopes of Carbonate Sediment from the Study Lakes

Lake	Depth	Mineral	$\delta^{13}C$ PDB
Milne	Top cm	Dol	3.13
	5cm	Dol	N/A
Pellet	Top cm	Dol	3.22
	5cm	Dol	N/A
Mini Dolomite	Top cm	Dol	0.91
	5cm	Dol	1.32
McFaiden	Top cm	Dol	-1.19
	5cm	Dol	-1.09
Dolomite	Top cm	Dol	-0.31
	5cm	Dol	-0.04
Halite	Top cm	Arag	2.76
	5cm	Arag	3.07
N. Stromatolite	Top cm	Arag	1.12
	5cm	Arag	2.06
S. Stromatolite	Top cm	Arag	1.55
	5cm	Arag	1.67

Oxygen Isotopes of Carbonate Sediment from the Study Lakes

Lake	Depth	Mineral	$\delta^{18}O$ PDB	$\delta^{18}O$ SMOW
Milne	Top cm	Dol	5.36	36.38
	5cm	Dol	N/A	N/A
Pellet	Top cm	Dol	3.04	34.00
	5cm	Dol	N/A	N/A
Mini Dolomite	Top cm	Dol	4.62	35.62
	5cm	Dol	4.52	35.53
McFaiden	Top cm	Dol	3.77	34.75
	5cm	Dol	3.95	34.93
Dolomite	Top cm	Dol	3.74	34.72
	5cm	Dol	4.06	35.05
Halite	Top cm	Arag	3.65	34.62
	5cm	Arag	4.14	35.13
N. Stromatolite	Top cm	Arag	3.31	34.27
	5cm	Arag	4.15	35.13
S. Stromatolite	Top cm	Arag	3.25	34.21
	5cm	Arag	2.83	33.77

Carbon Isotopes of Carbonate Sediment from Coorong Lakes (previous authors)

Lake	Depth	Mineral	$\delta^{13}C$ PDB (Botz &Von der Borch, 1984)	$\delta^{13}C$ PDB (Rosen, 1989)
Milne	Top cm	50/50 Dol/Mag	3.4	~ 3.5
		33/67 Dol/Mag	2.3	
	5cm	Dol		~ 3.5
Pellet	Top cm	Dol	4.1	4.1
	5cm	Dol		3.7
Mini Dolomite	Top cm	Dol	1.3	
	5cm	Dol		
McFaiden	Top cm	Dol	-1.5	
	5cm	Dol	-1.1	
Dolomite	Top cm	Dol	0.3	-0.3
	5cm	Dol		~ -1.0
Halite	Top cm	Arag	3.3	2.6
	5cm	Arag	4.3	
N. Stromatolite	Top cm	Arag	2.5	
	5cm	Arag		
S. Stromatolite	Top cm	Arag +Dol +Hmg	3.7	
	5cm	Arag	2.5	

Oxygen Isotopes of Carbonate Sediment from Coorong Lakes (previous authors)

Lake	Depth	Mineral	$\delta^{18}O$ PDB (Botz & Von der Borch 1984)	$\delta^{18}O$ PDB (Rosen 1989)
Milne	Top cm	50/50 Dol/Mag	6.1	~ 7.6
		33/67 Dol/Mag	6.6	
	5cm	Dol		~ 7.6
Pellet	Top cm	Dol	5.4	7.4
	5cm	Dol		5.5
Mini Dolomite	Top cm	Dol	4.9	
	5cm	Dol		
McFaiden	Top cm	Dol	3.5	
	5cm	Dol	4.9	
Dolomite	Top cm	Dol	4.9	6.4
	5cm	Dol		6.8
Halite	Top cm	Arag	4.2	~ 3
	5cm	Arag	4.0	
N. Stromatolite	Top cm	Arag	4.3	
	5cm	Arag		
S. Stromatolite	Top cm	Arag +Dol +Hmg	5.8	
	5cm	Arag	3.4	

APPENDIX 6

16S rRNA Sequencing Data

This Appendix contains the results of 16S ribosomal RNA sequencing carried out on selected cultured bacterial samples from two of the study lakes. The sequencing was performed by Amodia Bioservice using the method of Schwieger & Tebbe (1998). The sequences were analysed using the Genbank database.

LOCUS AF148141 1519 bp DNA linear BCT 14-JAN-2002
DEFINITION Delta proteobacterium S2550 16S ribosomal RNA gene, partial sequence.
ACCESSION AF148141
VERSION AF148141.1 GI:8131861
SOURCE delta proteobacterium S2550.
ORGANISM **delta proteobacterium S2550 (Desulfostipes saporovans)**
Bacteria; Proteobacteria; delta subdivision.

REFERENCE 1 (bases 1 to 1519)
AUTHORS Myhr,S., Lilleboe,B.-L.P., Sunde,E., Beeder,J. and Torsvik,T.
TITLE Inhibition of microbial H2S production in an oil reservoir model column by nitrate injection
JOURNAL Appl. Microbiol. Biotechnol. (2002) In press

REFERENCE 2 (bases 1 to 1519)
AUTHORS Myhr,S., Lilleboe,B.-L.P., Sunde,E., Beeder,J. and Torsvik,T.
TITLE Direct Submission
JOURNAL Submitted (04-MAY-1999) Department of Microbiology, Universtity of Bergen, Jahnebakken 5, Bergen N-5020, Norway

FEATURES Location/Qualifiers
source 1..1519
/organism="delta proteobacterium S2550"
/strain="S2550"
/db_xref="taxon:118012"
/product="16S ribosomal RNA"

BASE COUNT 379 a 349 c 474 g 317 t

ORIGIN

```
   1 ggctcagaat gaacgctggc ggcgtgctta acacatgcaa gtcgtacgag aactcccttg
  61 cttgcaaggg atagtaaagt ggcgcacggg tgagtaacgc gtgggtaatc taccttggga
 121 ttcgggataa cattgcgaaa gcggtgctaa taccggataa cattcgcagg tcttaggatg
 181 tgcggatcaa agatggcctc tacatgtaag ctatcgtctg aggaggagct cgcgtaccat
 241 tagctagttg gtggggtaaa ggcccaccaa ggctccgatg gttagctggt ctgagaggat
 301 gatcagccac actggaactg acacacggtc cagactccta cgggaggcag cagtgaggaa
 361 tcttgcgcaa tgggcgaaag cctgacgcag caacgccgcg tgagtgatga aggccttcgg
 421 gtcgtaaagc tctgtcaagt gggaagaacc tgcttctgat taatactcag gagtactgac
 481 ggtaccactg aaggaagcac cggctaactc cgtgccagca gccgcggtaa tacggagggt
 541 gcaagcgtta ttcggaatta ttgggcgtaa agggcgcgca ggcggccgtt taagtcagat
 601 gtgaaatccc ggggcttaac cccggaagtg catttgatac tggatggctt gagtatggga
 661 gagggaagtg gaattcctgg tgtagaggtg aaattcgtag atatcaggag gaacaccggt
 721 ggcgaaggcg acttcctgga ccaatactga cgctgaggcg cgaaggcgtg gggagcaaac
 781 aggattagat accctggtag tccacgcagt aaacgttgat cactaggtgt agcgggtatt
 841 gacccctgct gtgccgcagc taacgcatta agtgatccgc ctggggagta cggccgcaag
 901 gttaaaactc aaaggaattg acgggggccc gcacaagcgg tggagcatgt ggtttaattc
 961 gacgcaacgc gcaaaacctt acctggattt gacatctcgg gaatctcttt gaaagaagag
1021 agtgcccttc ggggagcccg atgacaggtg ctgcatggct gtcgtcagct cgtgtcgtga
1081 gatgttgggt taagtcccgc aacgagcgca acccctatgt ttagttgcca tcattcagtt
1141 gggcactcta aatagactgc cccggttaac ggggaggaag gtggggatga cgtcaagtcc
1201 tcatggccct tatgtccagg gctacacacg tgctacaatg gatcgcacaa agggcagcga
1261 actcgcgaga gtaagccaat cccaaaaaac ggtcctcagt tcggattgga gtctgcaact
1321 cgactccatg aagttggaat cgctagtaat cgcggatcag catgccgcgg tgaatacgtt
1381 cccgggcctt gtacacaccg cccgtcacac catgagagtt ggctgtacca gaagtcgtcg
1441 ggctaacctt cgggaggcag gcgcctaagg tatggttgat aattggggtg aagtcgtaac
1501 aaggtagccg ttggggaac
```

LOCUS AF211258 600 bp DNA linear BCT 09-AUG-2000
DEFINITION Uncultured Desulfosarcina CE105 16S ribosomal RNA gene, partial sequence.
ACCESSION AF211258
VERSION AF211258.1 GI:6707498
SOURCE uncultured Desulfosarcina CE105.
ORGANISM **uncultured Desulfosarcina CE105**
Bacteria; Proteobacteria; delta subdivision; Desulfosarcina; environmental samples.

REFERENCE 1 (bases 1 to 600)
AUTHORS Tanner,M.A., Everett,C.L., Coleman,W.J., Yang,M.M. and Youvan,D.C.
TITLE Complex microbial consortia inhabiting hydrogen sulfide-rich black mud from marine coastal environments
JOURNAL Biotechnology et alia 8, 1-16 (2000)
REMARK http://www.et-al.com/searchable/abstracts/ComplexMicrobial.htm

REFERENCE 2 (bases 1 to 600)
AUTHORS Tanner,M.A., Everett,C.L., Coleman,W.J., Yang,M.M. and Youvan,D.C.
TITLE Direct Submission
JOURNAL Submitted (03-DEC-1999) Kairos Scientific Inc., Bldg. 62, 3350 Scott Blvd., Santa Clara, CA 95054, USA

FEATURES Location/Qualifiers
source 1..600
/organism="uncultured Desulfosarcina CE105"
/db_xref="taxon:111753"
/clone="CE105"
/note="from brackish water black mud"
/product="16S ribosomal RNA"

BASE COUNT 146 a 131 c 191 g 132 t

ORIGIN

```
        1 gtgcaagcgt tattcggaat cattgggcgt aaagagcacg taggcggctt ggtaagtcag
       61 atgtgaaagc ccggggctta accccggaag tgcatttgat actgccaggc ttgagtatgg
      121 gagagggaag tggaattcct ggtgtagagg tgaaattcgt agatatcagg aggaacaccg
      181 gtggcgaagg cgacttcctg gaccaatact gacgctgagg tgcgaaggcg tgggtagcaa
      241 acaggattag ataccctggt agtccacgca gtaaacgttg ttcactaggt gtagcgggta
      301 ttgacccctg ctgtgccgca gttaacgcat taagtgaacc gcctggggag tacggccgca
      361 aggttaaaac tcaaaggaat tgacgggggc ccgcacaagc ggtggagcat gtggtttaat
      421 tcgacgcaac gcgaagaacc ttacctggat tttgacatcc cgggaatcct atcgaaagac
      481 tggagtgccc ttcggggagc ccggagacag gtgctgcatg gctgtcgtca gctcgtgtcg
      541 tgagatgttg ggttaagtcc cgcaacgagc gcaacccctt gtctttagtt accatcattg
```

LOCUS AF141328 1473 bp DNA linear BCT 12-JUL-1999
DEFINITION Sulfate-reducing bacterium AK-01 16S ribosomal RNA gene, partial sequence.
ACCESSION AF141328
VERSION AF141328.1 GI:5070446
SOURCE sulfate-reducing bacterium AK-01.
ORGANISM **sulfate-reducing bacterium AK-01**
Bacteria; Proteobacteria; delta subdivision.

REFERENCE 1 (bases 1 to 1473)
AUTHORS So,C.M. and Young,L.Y.
TITLE Isolation and characterization of a sulfate-reducing bacterium that anaerobically degrades alkanes
JOURNAL Appl. Environ. Microbiol. 65 (7), 2969-2976 (1999)
MEDLINE 99318650
PUBMED 10388691
REFERENCE 2 (bases 1 to 1473)
AUTHORS So,C.M. and Young,L.Y.
TITLE Direct Submission
JOURNAL Submitted (07-APR-1999) Biotechnology Center for Agriculture and the Environment, Rutgers, The State University of New Jersey, Foran Hall, 59 Dudley Road, New Brunswick, NJ 08901-8520, USA
FEATURES Location/Qualifiers
source 1..1473
/organism="sulfate-reducing bacterium AK-01"
/strain="AK-01"
/db_xref="taxon:96506"
/note="a novel anaerobic alkane degrader isolated from a marine-estuarine sediment"
/product="16S ribosomal RNA"

BASE COUNT 367 a 342 c 455 g 309 t

ORIGIN

```
   1 aacgctggcc gcgtgcttaa cacatgcaag tcgtacgaga atcccttgct tgcaagggat
  61 agtaaagtgg cgcacgggtg agtaacgcgt gggtaatcta cccttggatt cgggataaca
 121 ttgcgaaagc ggtgctaata ccggataaca ttcgcaggtc ttaggatgtg cggatcaaag
 181 atggcctcta catgtaagct atcgtctgag gaggagctcg cgtaccatta gctagttggt
 241 ggggtaaagg cccaccaagg ctccgatggt tagctggtct gagaggatga tcagccacac
 301 tggaactgac acacggtcca gactcctacg ggaggcagca gtgaggaatc ttgcgcaatg
 361 ggcgaaagcc tgacgcagca acgccgcgtg agtgatgaag gccttcgggt cgtaaagctc
 421 tgtcaagtgg gaagaacctg cttctgatta atactcagga gtactgacgg taccactgaa
 481 ggaagcaccg gctaactccg tgccagcagc cgcggtaata cggagggtgc aagcgttatt
 541 cggaattatt gggcgtaaag ggcgcgcagg cggccgttta agtcagatgt gaaatcccgg
 601 ggcttaaccc cggaagtgca tttgatactg gatggcttga gtatgggaga gggaagtgga
 661 attcctggtg tagaggtgaa attcgtagat atcaggagga acaccggtgg cgaaggcgac
 721 ttcctggacc aatactgacg ctgaggcgcg aaggcgtggg gagcaaacag gattagatac
 781 cctggtagtc cacgcagtaa acgttgatca ctaggtgtag cgggtattga cccctgctgt
 841 gccgcagcta acgcattaag tgatccgcct gggagtacgg ccgcaaggtt aaaactcaaa
 901 ggaattgacg ggggcccgca caagcggtgg agcatgtggt ttaattcgac gcaacgcgca
 961 aaaccttacc tggatttgac atctcgggaa tctctttgaa agaagagagt gcccttcggg
1021 gagcccgatg acaggtgctg catggctgtc gtcagctcgt gtcgtgagat gttgggttaa
1081 gtcccgcaac gagcgcaacc cctatgttta gttgccatca ttcagttggg cactctaaat
1141 agactgcccc ggttaacggg gaggaaggtg gggatgacgt caagtcctca tggcccttat
1201 gtccagggct acacacgtgc tacaatggat cgcacaaagg gcagcgaact cgcgagagta
1261 agccaatccc aaaaaacggt cctcagttcg gattggagtc tgcaactcga ctccatgaag
1321 ttggaatcgc tagtaatcgc ggatcagcat gccgcggtga atacgttccc gggccttgta
1381 cacaccgccc gtcacaccat gagagttggc tgtaccagaa gtcgtcgggc taaccttcgg
1441 gaggcaggcg cctaaggtat ggttgataat tgg
```

LOCUS AF354164 1476 bp DNA linear BCT 06-APR-2001
DEFINITION Uncultured delta proteobacterium isolate Eel-36e1H1 16S ribosomal RNA gene, partial sequence.
ACCESSION AF354164
VERSION AF354164.1 GI:13398671
SOURCE uncultured delta proteobacterium.
ORGANISM **uncultured delta proteobacterium**
Bacteria; Proteobacteria; delta subdivision; environmental samples.

REFERENCE 1 (bases 1 to 1476)
AUTHORS Orphan,V.J., Hinrichs,K.U., Ussler,W. III, Paull,C.K., Taylor,L.T., Sylva,S.P., Hayes,J.M. and Delong,E.F.
TITLE Comparative analysis of methane-oxidizing archaea and sulfate-reducing bacteria in anoxic marine sediments
JOURNAL Appl. Environ. Microbiol. 67 (4), 1922-1934 (2001)
MEDLINE 21178549
PUBMED 11282650
REFERENCE 2 (bases 1 to 1476)
AUTHORS Orphan,V.J., Hinrichs,K.U., Ussler,W., Taylor,L.T., Sylva,S., Hayes,J.M., Paull,C.K. and DeLong,E.F.
TITLE Direct Submission
JOURNAL Submitted (28-FEB-2001) Research and Development, Monterey Bay Aquarium Research Institute, 7700 Sandholdt Rd., Moss Landing, CA 95039, USA
FEATURES Location/Qualifiers
source 1..1476
/organism="uncultured delta proteobacterium"
/isolate="Eel-36e1H1"
/db_xref="taxon:34034"
/clone="1476"
/note="isolated from marine methane seep"
/product="16S ribosomal RNA"
BASE COUNT 383 a 323 c 450 g 320 t
ORIGIN

```
   1 catgcaagtc gcacgagaac tcttctgctt gcagaagata gtaaagtggc gcacgggtga
  61 gtaacgcgtg ggtaatctac ctctgaattg gggataacat tgtgaaagcg atgctaatac
 121 cgaataatat cccgagaact taggtttttg ggatcaaagg tggcctctac atgtaagcta
 181 ctgtttagag atgagcccgc gtaccattag cttgttggta gggtaatggc ctaccaaggc
 241 aacgatggtt agctggtctg agaggatgat cagccacact ggaactgaca cacggtccag
 301 actcctacgg gaggcagcag tgaggaattt tgcgcaatgg gggaaaccct gacgcagcaa
 361 cgccgcgtga gtgatgaagg ctttcgagtc gtaaagctct gtcaagtgag aagaacctat
 421 cccgcgctaa taccgtggga tactgacggt atcactgaag gaagcaccgg ctaactccgt
 481 gccagcagcc gcggtaatac ggagggtgca agcgttattc ggaattattg ggcgtaaagg
 541 gcgcgtaggc ggtcttttaa gtcagatgtg aaagcccggg gctcaacccc ggaagtgcat
 601 ttgaaactaa gggacttgag tatgggagag ggaagtggaa ttcctggtgt agaggtgaaa
 661 ttcgtagata tcaggaggaa caccggtggc gaaggcgact tcctggacca atactgacgc
 721 tgaggcgcga aggcgtgggg agcaaacagg attagatacc ctggtagtcc acgcagtaaa
 781 cggtgaacac taggtgtagc gggtattgac ccctgctgtg ccgcagttaa cgcattaagt
 841 gttccgcctg gggagtacgg ccgcaaggtt aaaactcaaa ggaattgacg ggggcccgca
 901 caagcggtgg agcatgtggt ttaattcgac gcaacgcgaa gaaccttacc tggatttgac
 961 atcccgagaa gtttttttgaa agaaagatgt gcttcgggga actcggtgac aggtgctgca
1021 tggctgtcgt cagctcgtgt cgtgagatgt tgggttaagt cccgcaacga gcgcaacccc
1081 tatctttagt taccatcatt aagttgggga ctctaaagat actgccccgg ttaacgggga
1141 ggaaggtggg gatgacgtca agtcctcatg gcctttatat ccagggctac acacgtgcta
1201 caatgggctg tacaaagggt cgcaaactcg cgagggtgag ctaatcccat aaagcagctc
1261 taagttcgga ttggagtctg caactcgact ccatgaagct ggaatcgcta gtaatcgcgg
1321 atcagcatgc cgcggtgaat acgttcccgg gccttgtaca caccgcccgt cacaccatga
1381 gagttggttg taccagaagt tgttggacca acccgcaagg ggggtaggca cctaaggtat
1441 ggctgatgat tggggtgaag tcgtaacaag gtaacc
```

LOCUS AF058004 885 bp DNA linear BCT 26-SEP-1998
DEFINITION Unidentified eubacterium RFLP15 16S ribosomal RNA gene, partial sequence.
ACCESSION AF058004
VERSION AF058004.1 GI:3659680
SOURCE unidentified eubacterium RFLP15.
ORGANISM **unidentified eubacterium RFLP15**
Bacteria; environmental samples.

REFERENCE 1 (bases 1 to 885)
AUTHORS Pulliam Holoman,T.R., Elberson,M.A., Cutter,L.A., May,H.D. and Sowers,K.R.
TITLE Characterization of a defined 2,3,5, 6-tetrachlorobiphenyl-ortho-dechlorinating microbial community by comparative sequence analysis of genes coding for 16S rRNA
JOURNAL Appl. Environ. Microbiol. 64 (9), 3359-3367 (1998)
MEDLINE 98395007
REFERENCE 2 (bases 1 to 885)
AUTHORS Pulliam Holoman,T.R., Elberson,M.A., Cutter,L.A., May,H.D. and Sowers,K.R.
TITLE Direct Submission
JOURNAL Submitted (07-APR-1998) Center of Marine Biotechnology, University of Maryland Biotechnology Institute, 701 East Pratt Street, Baltimore, MD 21202, USA
FEATURES Location/Qualifiers
source 1..885
/organism="unidentified eubacterium RFLP15"
/db_xref="taxon:82548"
/note="PCB-dechlorinating enrichment culture"
/product="16S ribosomal RNA"

BASE COUNT 223 a 205 c 271 g 186 t

ORIGIN
1 cagcagccgc ggtaatacgt aggggcaag cgttatccgg aatcactggg cgtaaagggt
61 gcgtaggcgg ctgataaagt ccggggtgaa aggctacggc ttaaccgtag taagccttgg
121 aaacttatca gcttgagtac aggagaggaa agtggaattc ctagtgtagc ggtgaaatgc
181 gtagatatta ggaggaacac cagtggcgaa ggcgactttc tggactgtta ctgacgctga
241 ggcacgaaag cgtggggagc gaacaggatt agataccctg gtagtccacg ccgtaaacga
301 tgagtgctag gtgtcggggg tcgaacctcg gtgccgcagc taacgcatta agcactccgc
361 ctggggagta cgttcgcaag aataaaactc aaaggaattg acggggaccc gcacaagcag
421 cggagcatgt ggtttaattc gaagcaacgc gaagaacctt acctggactt gacatccctt
481 tgaccgcttc ttaaccgaaa ctttcccttc ggggacaaag gtgacaggtg gtgcatggtt
541 gtcgtcagct cgtgtcgtga gatgttgggt taagtcccgc aacgagcgca acccctgtct
601 ttagttgcca gcattaagtt gggcactcta gagagactgc cgaggataac tcggaggaag
661 gtggggatga cgtcaaatca tcatgcccct tatgttcagg gctacacacg tgctacaatg
721 ggcggtacaa cgggcagcga gctcgcgaga gcaagccaat cccttaaagc cgttctcagt
781 tcggattgta ggctgaaact cgcctacatg aagctggagt tgctagtaat cgcggatcag
841 aatgccgcgg tgaatgcgtt cccgggtctt gtacacaccg cccgt

LOCUS AF424414 995 bp DNA linear BCT 30-OCT-2001
DEFINITION Uncultured low G+C Gram-positive bacterium MERTZ_0CM_115 16S ribosomal RNA gene, partial sequence.
ACCESSION AF424414
VERSION AF424414.1 GI:16518258
SOURCE uncultured low G+C Gram-positive bacterium.
ORGANISM **uncultured low G+C Gram-positive bacterium**
Bacteria; Firmicutes; Bacillus/Clostridium group; environmental samples.

REFERENCE 1 (bases 1 to 995)
AUTHORS Bowman,J.P., McCammon,S.A., McCuaig,R.D., Gibson,J.A.E. and Nichols,P.D.
TITLE Characterization of continental shelf sediments collected off Antarctica: microbial metabolic activity, community structure and biogeography
JOURNAL Unpublished

REFERENCE 2 (bases 1 to 995)
AUTHORS Bowman,J.P., McCammon,S.A., McCuaig,R.D., Gibson,J.A.E. and Nichols,P.D.
TITLE Direct Submission
JOURNAL Submitted (26-SEP-2001) School of Agricultural Science, University of Tasmania, GPO Box 252-54, Hobart, Tasmania 7001, Australia
FEATURES Location/Qualifiers
source 1..995
/organism="uncultured low G+C Gram-positive bacterium"
/isolate="361"
/db_xref="taxon:152508" /clone="MERTZ_0CM_115"
/product="16S ribosomal RNA"

BASE COUNT 272 a 210 c 295 g 218 t

ORIGIN
```
   1 cagcagccgc ggtaatacgt aggggacaag cgttatccgg aatcactggg cgtaaagggt
  61 gcgtaggcgg tttaacaagt cagaagtgaa aggcattggc tcaaccaatg taagcttttg
 121 aaactgttag acttgagtgc aggagaggaa agtggaattc ctagtgtagc ggtgaaatgc
 181 gtagatatta ggaggaacac cagtggcgaa ggcgactttc tggactgtaa ctgacgctga
 241 ggcacgaaag cgtggggagc gaacaggatt agataccctg gtagtccacg ccgtaaacga
 301 tgaatactag gtgtcgggag tcgaatctcg gtgccgcagc taacgcatta agtattccgc
 361 ctggggagta cgcacgcaag tgtgaaactc aaaggaattg acggggaccc gcacaagcag
 421 cggagcatgt ggtttaattc gaagcaacgc gaagaacctt accaggtctt gacatccatt
 481 tgaccaattc ttaatcgaat ttttccttcg ggaacaaatg agacaggtgg tgcatggttg
 541 tcgtcagctc gtgtcgtgag atgttgggtt aagtcccgca acgagcgcaa ccccttatttt
 601 tagttgccat caggttatgc tgggcactct agaaagactg ccggtgacaa accggaggaa
 661 ggtggggatg acgtcaaatc atcatgcccc ttatgatctg ggctacacac gtgctacaat
 721 ggtcgataca aagggcagcg aaggagtgat ctggagcaaa tcctctaaag tcgatctcag
 781 ttcggattgt aggctgaaac tcgcctacat gaagttggag ttgctagtaa tcgcgaatca
 841 gaatgtcgcg gtgaatgcgt tcccgggtct tgtacacacc gcccgtcaca ccacggaagt
 901 tgggggcgcc cgaagtcagt gttccaacct gtaaaggagg aagctgccga aggtgaaatc
 961 aatgactggg gtgaagtcgt aacaaggtaa ccgta
```

LOCUS CP16SRRN 1527 bp DNA linear BCT 22-NOV-1994
DEFINITION C.propionicum (DSM 1682) 16S rRNA gene.
ACCESSION X77841
VERSION X77841.1 GI:572659
KEYWORDS 16S ribosomal RNA.
SOURCE Clostridium propionicum.
ORGANISM **Clostridium propionicum**
Bacteria; Firmicutes; Bacillus/Clostridium group; Clostridia; Clostridiales; Clostridiaceae; Clostridium.

REFERENCE 1 (bases 1 to 1527)
AUTHORS Lawson,P.A.
TITLE Direct Submission
JOURNAL Submitted (17-FEB-1994) P.A. Lawson, AFRC Institute of Food Research, Reading Laboratory, Microbiology Dept, Earley Gate, Whiteknights Road, Reading RG6 2EF, UK
REFERENCE 2 (bases 1 to 1527)
AUTHORS Collins,M.D., Lawson,P.A., Willems,A., Cordoba,J.J., Fernandez-Garayzabal,J., Garcia,P., Cai,J., Hippe,H. and Farrow,J.A.
TITLE The phylogeny of the genus Clostridium: proposal of five new genera and eleven new species combinations
JOURNAL Int. J. Syst. Bacteriol. 44 (4), 812-826 (1994)
MEDLINE 95071902
FEATURES Location/Qualifiers
source 1..1527
/organism="Clostridium propionicum"
/strain="DSM 1682"
/db_xref="taxon:28446"
/product="16S ribosomal RNA"

BASE COUNT 414 a 343 c 461 g 300 t 9 others
ORIGIN

```
   1 nnnnnngaga gtttgtcctg gctcaggtga ancgctggcg gcgtgcttaa cacatgcaag
  61 tcgagcggaa atatgcaatc ggagcttcgg caggaagatt acatatttta gcggcggacg
 121 ggtgagtaac gtgtgggcaa cctgccctgt actgtggaat aatcactgga aacggtgact
 181 aataccgcat gtcattgcga gagggcatcc tcttgcaaga aaaggattta ttcggtacag
 241 gatgggcccg catctgatta gctagttggt gagataacag cccaccaagg caacgatcag
 301 tagccgacct gagagggtga tcaggccacc attgggctga gacacggccc aaactcctac
 361 gggaggcagc agtggggaat attgcacaat gggcgaaagc ctgatgcagc aacgcgcgtg
 421 aaggaagaag ggtttcggct cgtaaacttc tatcaacagg gacgaaaaaa atgacggtac
 481 ctgaataaga agccccggct aactacgtgc cagcagccgc ggtaatacgt agggggcaag
 541 cgttatccgg aattactggg tgtaaaggga gagtaggcgg catggtaagt tagatgtgaa
 601 agcccgaggc ttaacctcgg gattgcattt aaaactatca agctagagta caggagaggt
 661 aagtggaatt cctagtgtag cggtgaaatg cgtagatatt aggaagaaca ccagtggcga
 721 aggcgactta ctggactgaa actgacgctg aggctcgaaa gcgtggggag cgaacaggat
 781 tagataccct ggtagtccac gccgtaaacg atgagtgcta ggtgtcgggg gggaaccctc
 841 ggtgccgcag ctaacgcaat aagcactcca cctggggagt acgatcgcaa gattgaaact
 901 caaaggaatt gacgggggcc cgcacaagcg tggagcatgt ggtttaattc gaagcaacgc
 961 gaagaacctt accaaggctt gacatccctc tgaccggtgt agagatacac cttctcttcg
1021 gagcagaggt gacaggtggt gcatggttgt cgtcagctcg tgtcgtgaga tgttgggtta
1081 agtcccgcaa cgagcgcaac ccctattctt agtagccatc attcagttgg gcactctagg
1141 gagactgccg tggataacac ggaggaaggt ggggatgacg tcaaatcatc atgcccctta
1201 tgtcttgggc tacacacgtg ctacaatggc tggtaacaaa gtgacgcaaa acggcgacgt
1261 cgagcaaatc acaaaaaccc agtcccagtt cggattgtag tctgcaactc gactacatga
1321 agctggaatc gctagtaatc gcgaatcaga atgtcgcggt gaatacgttc ccgggccttg
1381 tacacaccgc ccgtcacacc atgggagttg gaagcacccg aagtcggtga cctgaccgta
1441 agaaggagcc gccgaaggtg aagccagcga ctggggtgaa gtcgtaacaa ggtagccgta
1501 tcggaaggtg cggntgnatc acctcct
```

MILNE LAKE - Product 1 **98% Identity** **NCBI GenBank**

LOCUS AY046956 1465 bp DNA linear BCT 25-SEP-2001
DEFINITION Vibrio harveyi strain M4 16S ribosomal RNA gene, partial sequence.

ACCESSION AY046956
VERSION AY046956.1 GI:15777743
KEYWORDS .
SOURCE Vibrio harveyi.
ORGANISM **Vibrio harveyi**
Bacteria; Proteobacteria; gamma subdivision; Vibrionaceae; Vibrio.

REFERENCE 1 (bases 1 to 1465)
AUTHORS Mo,Z.L., Mao,Y.X., Chen,S.Y., Zhang,Z.D. and Zhang,P.J.
TITLE Identification and phylogenetic analysis of a pathogenic bacterium asociated with septicemia of cultured flounder, Paralichthys olivaceus
JOURNAL Unpublished

REFERENCE 2 (bases 1 to 1465)
AUTHORS Mo,Z.L., Mao,Y.X., Chen,S.Y., Zhang,Z.D. and Zhang,P.J.
TITLE Direct Submission
JOURNAL Submitted (19-JUL-2001) Experimental Marine Biology Laboratory, Institute of Oceanology, Chinese Academy of Science, 7 Nanhai Road, Qingdao, Shandong 266071, People's Republic of China
FEATURES Location/Qualifiers
source 1..1465
/organism="Vibrio harveyi"
/strain="M4"
/db_xref="taxon:669"
/note="synonym: Vibrio carchariae"
/product="16S ribosomal RNA"

BASE COUNT 370 a 327 c 463 g 305 t

ORIGIN

```
   1 ttagacagct ggcggcaggc ctaacacatg caagtcgagc ggaaacgagt tatctgaacc
  61 ttcgggggaa cgataacggc gtcgagcggc ggcgggtgag taatgcctag gaaattgccc
 121 tgatgtgggg gataaccatt ggaaacgatg gctaataccg cataatacct acgggtcaaa
 181 gaggggacc ttcgggcctc tcgcgtcagg atatgcctag gtgggattag ctagttggtg
 241 aggtaatggc tcaccaaggc gacgatccct agctggtctg agaggatgat cagccacact
 301 ggaactgaga cacggtccag actcctacgg gaggcagcag tggggaatat tgcacaatgg
 361 gcgcaagcct gatgcagcca tgccgcgtgt gtgaagaagg ccttcgggtt gtaaagcact
 421 ttcagtcgtg aggaaggtag tagagttaat agctctatca tttgacgtta gcgacagaag
 481 aagcaccggc taactccgtg ccagcagccg cggtaatacg gagggtgcga gcgttaatcg
 541 gaattactgg gcgtaaagcg catgcaggtg gtttgttaag tcagatgtga aagcccgggg
 601 ctcaacctcg gaatagcatt tgaaactggc agactagagt actgtagagg ggggtagaat
 661 ttcaggtgta gcggtgaaat gcgtagagat ctgaaggaat accggtggcg aaggcggccc
 721 cctggacaga tactgacact cagatgcgaa agcgtgggga gcaaacagga ttagataccc
 781 tggtagtcca cgccgtaaac gatgtctact tggaggttgt ggccttgagc cgtggctttc
 841 ggagctaacg cgttaagtag accgcctggg gagtacggtc gcaagattaa aactcaaatg
 901 aattgacggg ggcccgcaca agcggtggag catgtggttt aattcgatgc aacgcgaaga
 961 accttaccta ctcttgacat ccagagaact ttccagagat ggattggtgc cttcgggaac
1021 tctgagacag gtgctgcatg gctgtcgtca gctcgtgttg tgaaatgttg ggttaagtcc
1081 cgcaacgagc gcaaccctta tccttgtttg ccagcacttc gggtgggaac tccagggaga
1141 ctgccggtga taaaccggag gaaggtgggg acgacgtcaa gtcatcatgg cccttacgag
1201 tagggctaca cacgtgctac aatggcgcat acagagggcg gccaacttgc gagagtgagc
1261 gaatcccaaa aagtgcgtcg tagtccggat cggagtctgc aactcgactc cgtgaagtcg
1321 gaatcgctag taatcgtgga tcagaatgcc acggtgaata cgttcccggg ccttgtacac
1381 accgcccgtc acaccatggg agtgggctgc aaaagaagta ggtagtttaa ccttcgggag
1441 gacgcttacc atcttgtggt tcatg
```

LOCUS AF319769 1475 bp DNA linear BCT 02-MAR-2002
DEFINITION Vibrio sp. BV25Ex 16S ribosomal RNA gene, partial sequence.
ACCESSION AF319769
VERSION AF319769.1 GI:13183634
SOURCE Vibrio sp. BV25Ex.
ORGANISM **Vibrio sp. BV25Ex**
Bacteria; Proteobacteria; gamma subdivision; Vibrionaceae; Vibrio.

REFERENCE 1 (bases 1 to 1475)
AUTHORS Kendall,M., Longnecker,K. and Reysenbach,A.-L.

TITLE Enrichment culture from a deep-sea hydrothermal vent
JOURNAL Unpublished

REFERENCE 2 (bases 1 to 1475)
AUTHORS Kendall,M., Longnecker,K. and Reysenbach,A.-L.
TITLE Direct Submission
JOURNAL Submitted (07-NOV-2000) Biology, Portland State University, P.O. Box 751, Portland, OR 97207-0751, USA
FEATURES Location/Qualifiers
source 1..1475
/organism="Vibrio sp. BV25Ex"
/isolate="BV25Ex"
/db_xref="taxon:150340"
/note="enrichment culture"
/product="16S ribosomal RNA"

BASE COUNT 373 a 326 c 469 g 307 t

ORIGIN

```
   1 attgaacgct ggcggcaggc ctaacacatg caagtcgagc ggaaacgagt tatctgaacc
  61 ttcggggaac gataacggcg tcgagcggcg gacgggtgag taatgcctag gaaattgccc
 121 tgatgtgggg gataaccatt ggaaacgatg gctaataccg catgatgcct acgggccaaa
 181 gaggggacc ttcgggcctc tcgcgtcagg atatgcctag gtgggattag ctagttggtg
 241 aggtaagggc tcaccaaggc gacgatccct agctggtctg agaggatgat cagccacact
 301 ggaactgaga cacggtccag actcctacgg gaggcagcag tggggaatat tgcacaatgg
 361 gcgcaagcct gatgcagcca tgccgcgtgt gtgaagaagg ccttcgggtt gtaaagcact
 421 ttcagtcgtg aggaaggtag tgtagttaat agctgcatta tttgacgtta gcgacagaag
 481 aagcaccggc taactccgtg ccagcagccg cggtaatacg gagggtgcga gcgttaatcg
 541 gaattactgg gcgtaaagcg catgcaggtg gtttgttaag tcagatgtga aagcccgggg
 601 ctcaacctcg gaatagcatt tgaaactggc agactagagt actgtagagg ggggtagaat
 661 ttcaggtgta gcggtgaaat gcgtagagat ctgaaggaat accggtggcg aaggcggccc
 721 cctggacaga tactgacact cagatgcgaa agcgtgggga gcaaacagga ttagataccc
 781 tggtagtcca cgccgtaaac gatgtctact tggaggttgt ggccttgagc cgtggctttc
 841 ggagctaacg cgttaagtag accgcctggg gagtacggtc gcaagattaa aactcaaatg
 901 aattgacggg ggcccgcaca agcggtggag catgtggttt aattcgatgc aacgcgaaga
 961 accttaccta ctcttgacat ccagagaact ttccagagat ggattggtgc cttcgggaac
1021 tctgagacag gtgctgcatg gctgtcgtca gctcgtgttg tgaaatgttg ggttaagtcc
1081 cgcaacgagc gcaaccctta tccttgtttg ccagcgagta atgtcgggaa ctccagggag
1141 actgccggtg ataaaccgga ggaaggtggg gacgacgtca agtcatcatg gcccttacga
1201 gtagggctac acacgtgcta caatggcgca tacagagggc agccaacttg cgaaagtgag
1261 cgaatcccaa aaagtgcgtc gtagtccgga ttggagtctg caactcgact ccatgaagtc
1321 ggaatcgcta gtaatcgtgg atcagaatgc cacggtgaat acgttcccgg gccttgtaca
1381 caccgcccgt cacaccatgg gagtgggctg caaaagaagt aggtagttta accttcgggg
1441 ggacgcttac cactttgtgg ttcatgactg gggtg
```

MILNE LAKE - Product 2 **91% Identity** **NCBI GenBank**

```
LOCUS       CP16SRRN                1527 bp    DNA     linear   BCT 22-NOV-1994
DEFINITION  C.propionicum (DSM 1682) 16S rRNA gene.
ACCESSION   X77841
VERSION     X77841.1  GI:572659
KEYWORDS    16S ribosomal RNA.
SOURCE      Clostridium propionicum.
ORGANISM    Clostridium propionicum
            Bacteria; Firmicutes; Bacillus/Clostridium group; Clostridia;
            Clostridiales; Clostridiaceae; Clostridium.

REFERENCE   1  (bases 1 to 1527)
  AUTHORS   Lawson,P.A.
  TITLE     Direct Submission
  JOURNAL   Submitted (17-FEB-1994) P.A. Lawson, AFRC Institute of Food
            Research, Reading Laboratory, Microbiology Dept, Earley Gate,
            Whiteknights Road, Reading RG6 2EF, UK

REFERENCE   2  (bases 1 to 1527)
  AUTHORS   Collins,M.D., Lawson,P.A., Willems,A., Cordoba,J.J.,
            Fernandez-Garayzabal,J., Garcia,P., Cai,J., Hippe,H. and
            Farrow,J.A.
  TITLE     The phylogeny of the genus Clostridium: proposal of five new genera
            and eleven new species combinations
  JOURNAL   Int. J. Syst. Bacteriol. 44 (4), 812-826 (1994)
  MEDLINE   95071902
FEATURES    Location/Qualifiers
 source     1..1527/organism="Clostridium propionicum"
            /strain="DSM 1682"
             /db_xref="taxon:28446"
             /product="16S ribosomal RNA"
```

```
BASE COUNT      414 a    343 c    461 g    300 t      9 others

ORIGIN  1 nnnnnngaga gtttgtcctg gctcaggtga ancgctggcg gcgtgcttaa cacatgcaag
       61 tcgagcggaa atatgcaatc ggagcttcgg caggaagatt acatatttta gcggcggacg
      121 ggtgagtaac gtgtgggcaa cctgccctgt actgtggaat aatcactgga aacggtgact
      181 aataccgcat gtcattgcga gagggcatcc tcttgcaaga aaaggattta ttcggtacag
      241 gatgggcccg catctgatta gctagttggt gagataacag cccaccaagg caacgatcag
      301 tagccgacct gagagggtga tcaggccacc attgggctga gacacggccc aaactcctac
      361 gggaggcagc agtggggaat attgcacaat gggcgaaagc ctgatgcagc aacgcgcgtg
      421 aaggaagaag ggtttcggct cgtaaacttc tatcaacagg gacgaaaaaa atgacggtac
      481 ctgaataaga agccccggct aactacgtgc cagcagccgc ggtaatacgt aggggcaag
      541 cgttatccgg aattactggg tgtaaaggga gagtaggcgg catggtaagt tagatgtgaa
      601 agcccgaggc ttaacctcgg gattgcattt aaaactatca agctagagta caggagaggt
      661 aagtggaatt cctagtgtag cggtgaaatg cgtagatatt aggaagaaca ccagtggcga
      721 aggcgactta ctggactgaa actgacgctg aggctcgaaa gcgtggggag cgaacaggat
      781 tagataccct ggtagtccac gccgtaaacg atgagtgcta ggtgtcgggg gggaaccctc
      841 ggtgccgcag ctaacgcaat aagcactcca cctggggagt acgatcgcaa gattgaaact
      901 caaaggaatt gacgggggcc cgcacaagcg tggagcatgt ggtttaattc gaagcaacgc
      961 gaagaacctt accaaggctt gacatccctc tgaccggtgt agagatacac cttctcttcg
     1021 gagcagaggt gacaggtggt gcatggttgt cgtcagctcg tgtcgtgaga tgttgggtta
     1081 agtcccgcaa cgagcgcaac ccctattctt agtagccatc attcagttgg gcactctagg
     1141 gagactgccg tggataacac ggaggaaggt ggggatgacg tcaaatcatc atgcccctta
     1201 tgtcttgggc tacacacgtg ctacaatggc tggtaacaaa gtgacgcaaa acggcgacgt
     1261 cgagcaaatc acaaaaaccc agtcccagtt cggattgtag tctgcaactc gactacatga
     1321 agctggaatc gctagtaatc gcgaatcaga atgtcgcggt gaatacgttc ccgggccttg
     1381 tacacaccgc ccgtcacacc atgggagttg gaagcacccg aagtcggtga cctgaccgta
     1441 agaaggagcc gccgaaggtg aagccagcga ctggggtgaa gtcgtaacaa ggtagccgta
     1501 tcggaaggtg cggntgnatc acctcct
```

LOCUS AY050176 517 bp DNA linear BCT 04-NOV-2001
DEFINITION Uncultured Clostridiaceae bacterium clone SRB-1 16S ribosomal RNA gene, partial sequence.
ACCESSION AY050176
VERSION AY050176.1 GI:16648523
SOURCE uncultured Clostridiaceae bacterium.
ORGANISM **uncultured Clostridiaceae bacterium**
Bacteria; Firmicutes; Bacillus/Clostridium group; Clostridia; Clostridiales; environmental samples.

REFERENCE 1 (bases 1 to 517)
AUTHORS Sigler,W.V., Kleikemper,J. and Zeyer,J.
TITLE Identifying bacteria active under sulfate reducing conditions using DNA immunocapture and denaturing gradient gel electrophoresis
JOURNAL Unpublished

REFERENCE 2 (bases 1 to 517)
AUTHORS Sigler,W.V.
TITLE Direct Submission
JOURNAL Submitted (03-AUG-2001) Soil Biology, ITOe / ETH-Zurich, Grabenstrasse 3, Schlieren 8952, Switzerland
FEATURES Location/Qualifiers
source 1..517
/organism="uncultured Clostridiaceae bacterium"
/db_xref="taxon:172733"
/clone="SRB-1"
/note="isolated from a sulfate reducing sediment microcosm"
/product="16S ribosomal RNA"

BASE COUNT 147 a 105 c 163 g 102 t

ORIGIN

```
   1 cctgacgcag cgacgccgcg tgaaggaaga agtatttcgg tatgtaaact tctatcagca
  61 aggaagaaaa tgacggtact tgactaagaa gccccggcta actacgtgcc agcagccgcg
 121 gtaatacgta gggggcaagc gttatccgga tttactgggt gtaaagggag cgtaggtggc
 181 atggcaagtc agatgtgaaa gcccggggct caaccccggg attgcatttg aaactgccag
 241 gctagagtgc aggagaggta agtggaattc ctagtgtagc ggtgaaatgc gtagatatta
 301 ggaggaacac cagtggcgaa ggcggcttac tggactgtaa ctgacactga ggctcgaaag
 361 cgtggggagc aaacaggatt agataccctg gtagtccacg ctgtaaacga tgaatactag
 421 gtgtcggggt cgtcaagacc tcggtgccgc agctaacgca ataagtattc cacctgggga
 481 gtacgttcgc aagaatgaaa cttaaaggaa ttgacgg
```

APPENDIX 7

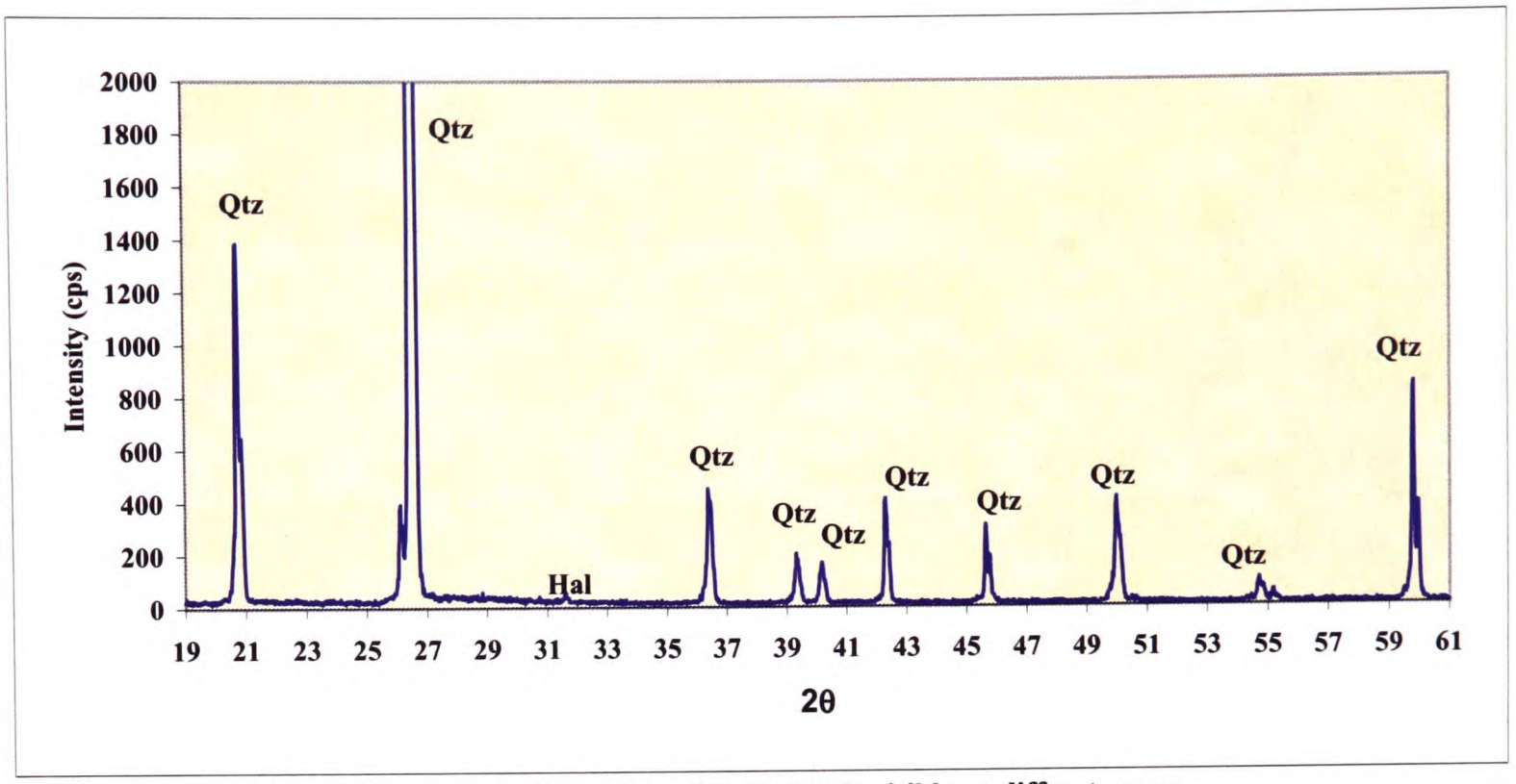
X-RAY DIFFRACTOMETRY AND ATOMIC SPECTRA FOR THE EXPERIMENTAL VIALS

The sediment extracted from each of the experimental vials was examined in an identical manner to the lake sediments (Appendix 1) using X-ray diffractometry. Dried and disaggregated sediment was mounted and run, as before, at the Department of Geology, University of Leicester on a Philips PW1716 diffractometer with a PW1729 generator and PW1050/25 detector.

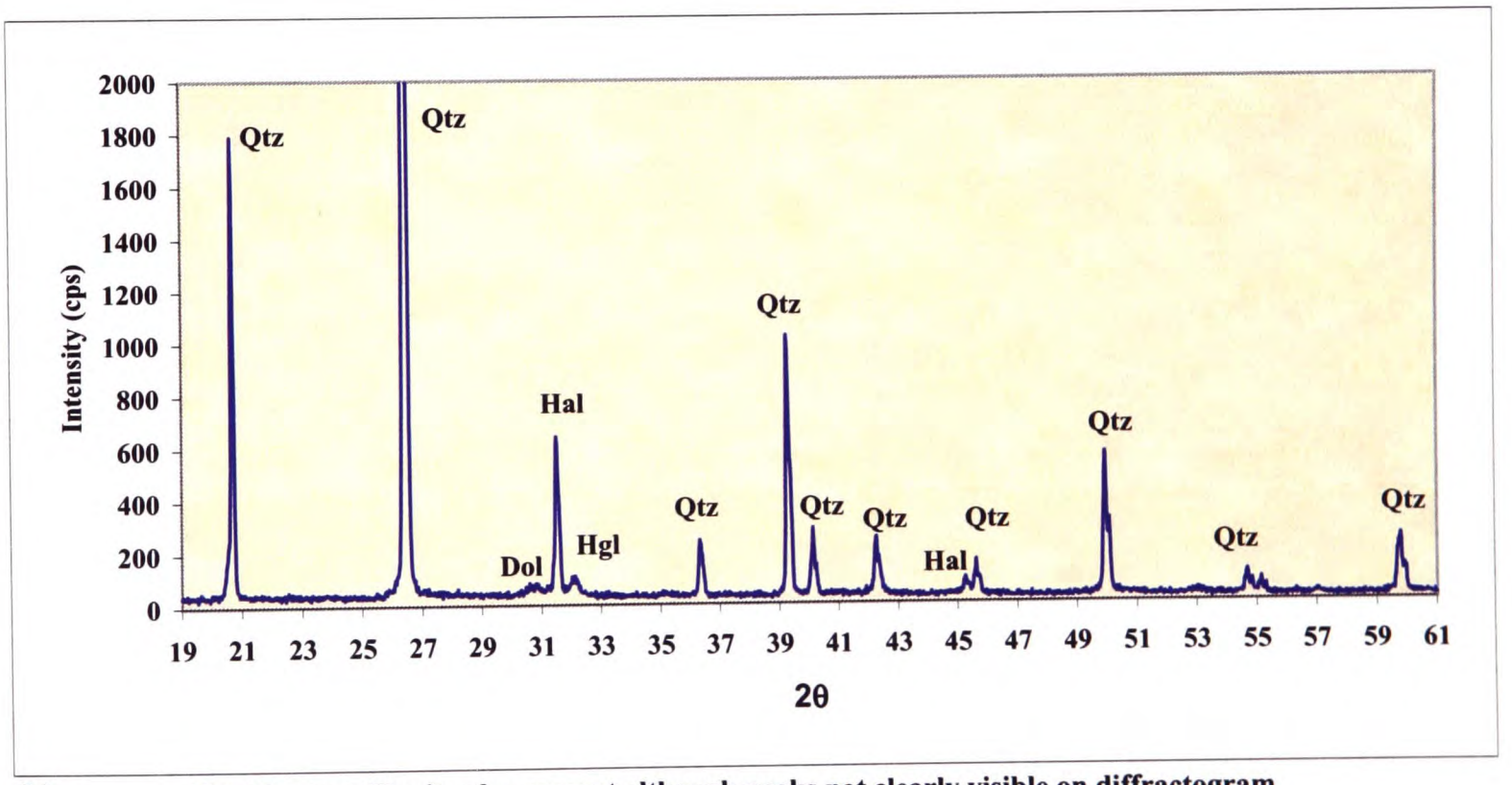
The results are summarised in Table A7.1, whilst the analyses are shown in Figures A7.1–A7.4. Atomic spectra from the SEM are presented in Figure A7.5.

Vial	Mineralogy	
	Substrate	**Precipitate**
1	Quartz	Halite, Smectite
6	Quartz	Dolomite, Halite, Hydro-glauberite, Montmorillonite
7	Quartz	Halite, Hydro-magnesite, Smectite
8	Quartz	Gypsum, Sauconite
10	Glass beads	-
15	Glass beads	Halite
21	Aragonite	Dolomite, Halite

Table A7.1. Mineralogy of the sediment recovered from experimental vials

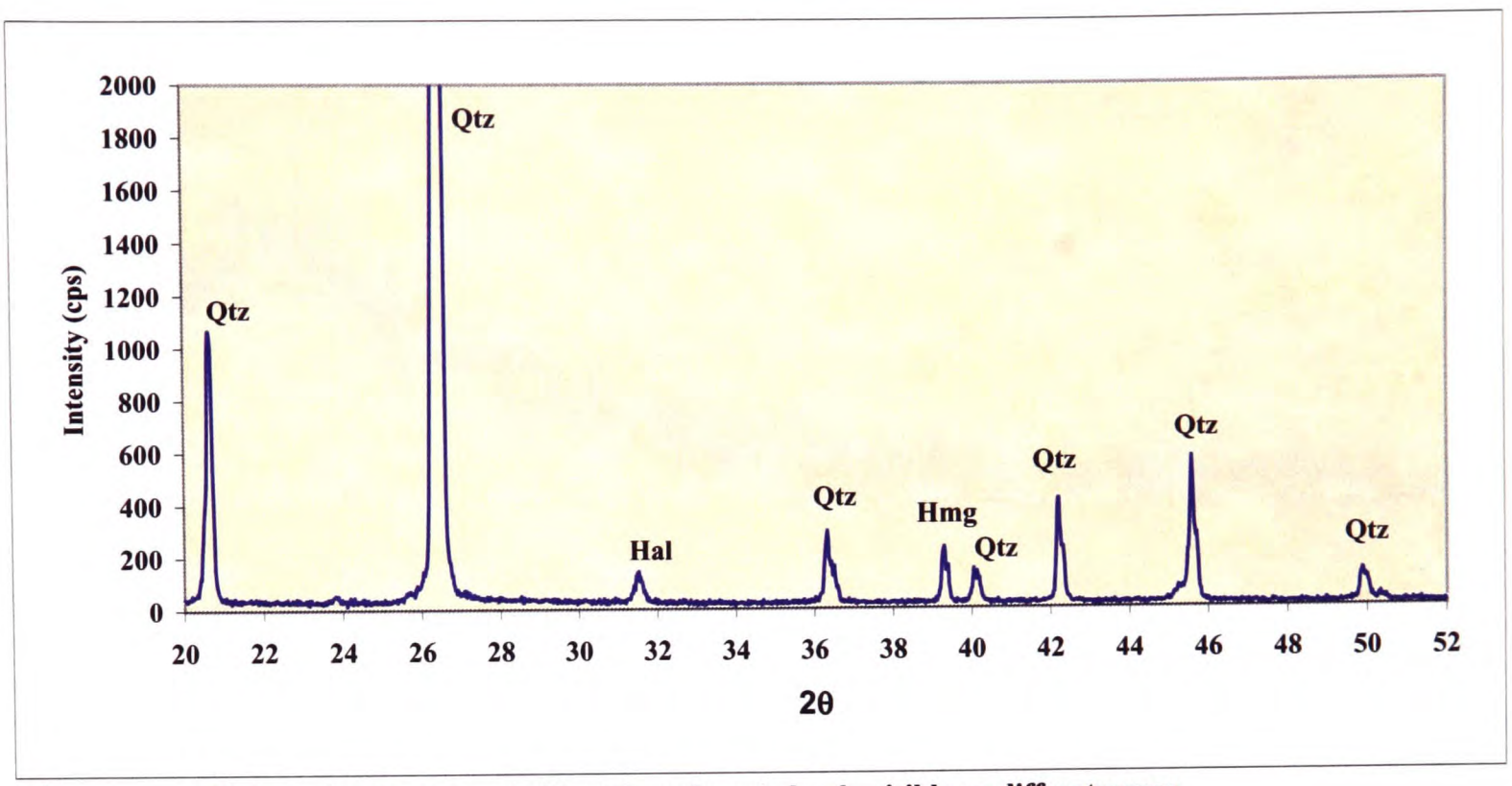


a) NB. Smectite also present although peaks not clearly visible on diffractogram

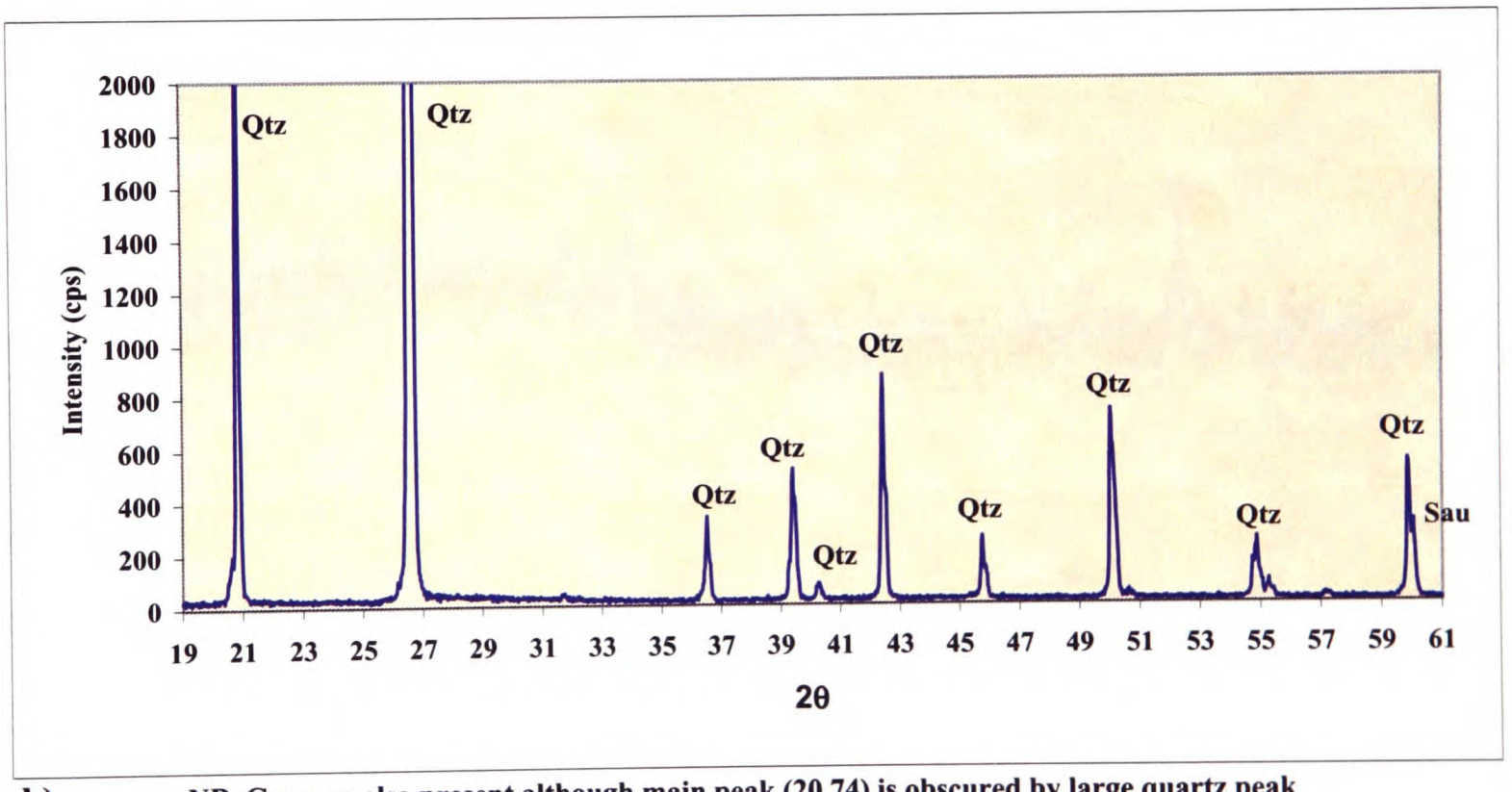


b) NB. Montmorillonite also present although peaks not clearly visible on diffractogram

Figure A7.1. X-ray diffractograms of sediment extracted from experimental vials a) Vial 1 b) Vial 6 - Note weak dolomite peak.

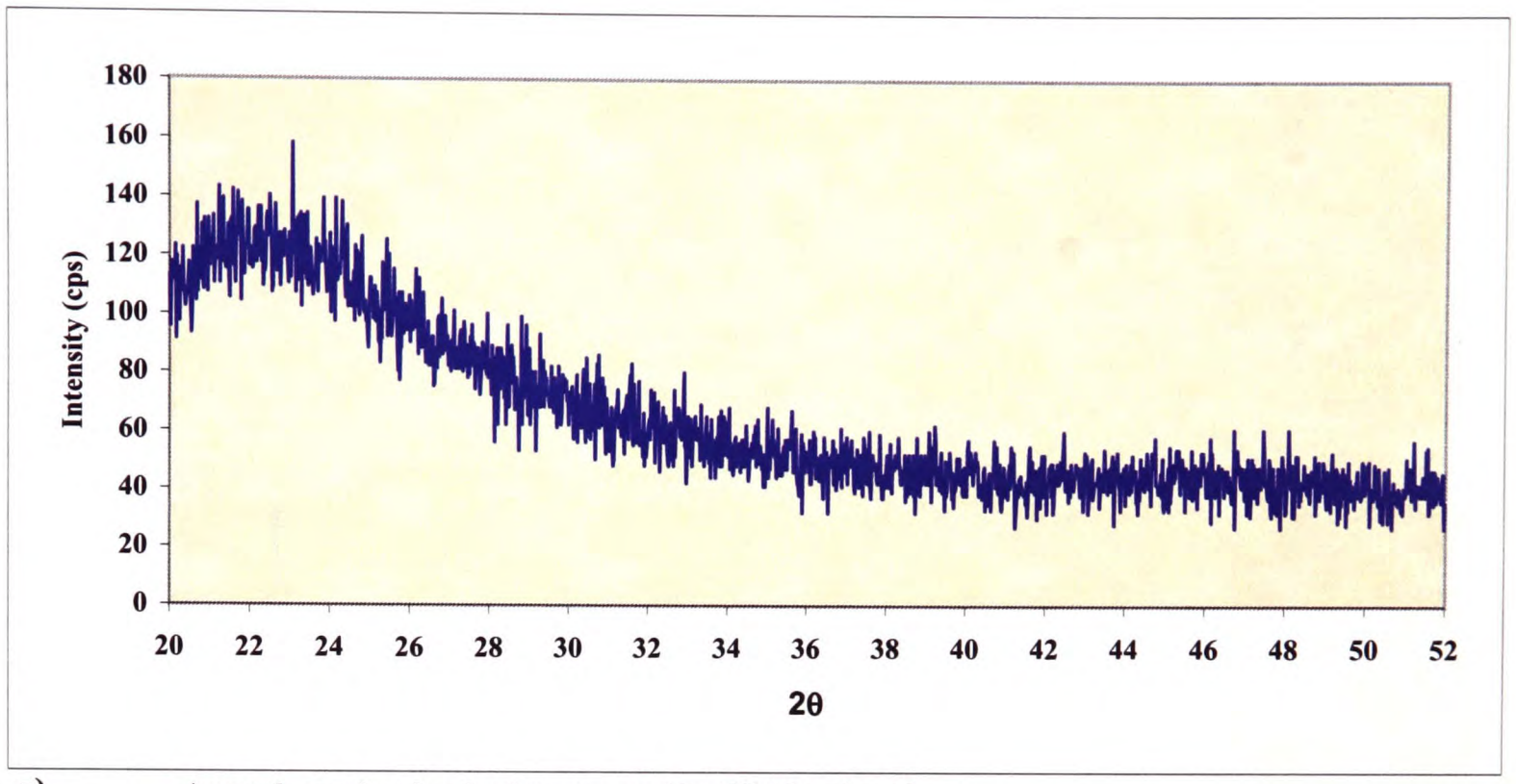


a) NB. Smectite also present although peaks not clearly visible on diffractogram

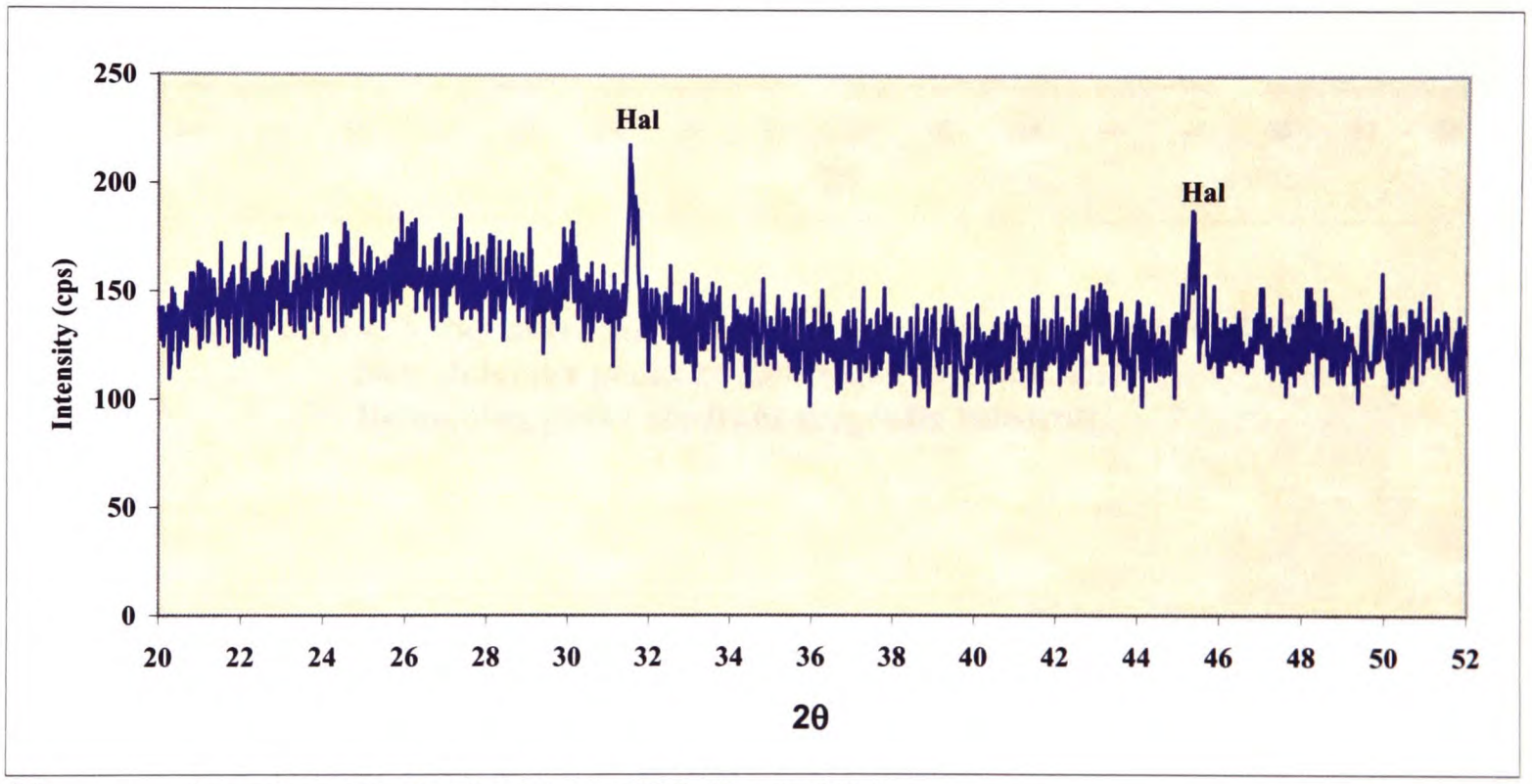


b) NB. Gypsum also present although main peak (20.74) is obscured by large quartz peak

Figure A7.2. X-ray diffractograms of sediment extracted from experimental vials a) Vial 7 b) Vial 8



a) Amorphous glass bead substrate - no identifiable minerals



b) Amorphous glass bead substrate with halite precipitate

Figure A7.3. X-ray diffractograms of sediment extracted from experimental vials a) Vial 10 b) Vial 15

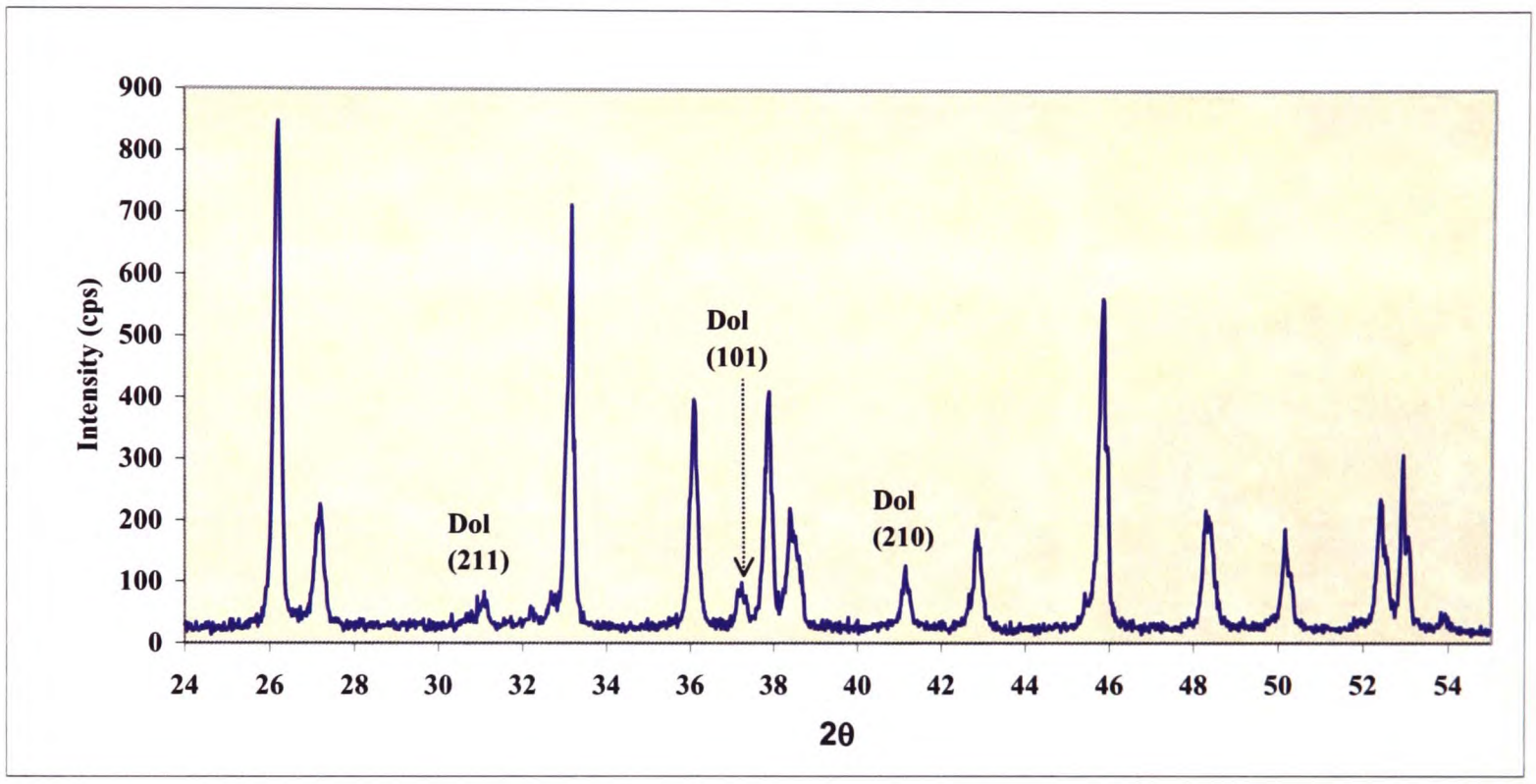


Figure A7.4. X-ray diffractogram of sediment extracted from Vial 21
Note dolomite peaks at 2θ = 30.98, 37.5 and 41.2.
Remaining peaks are from aragonite substrate.

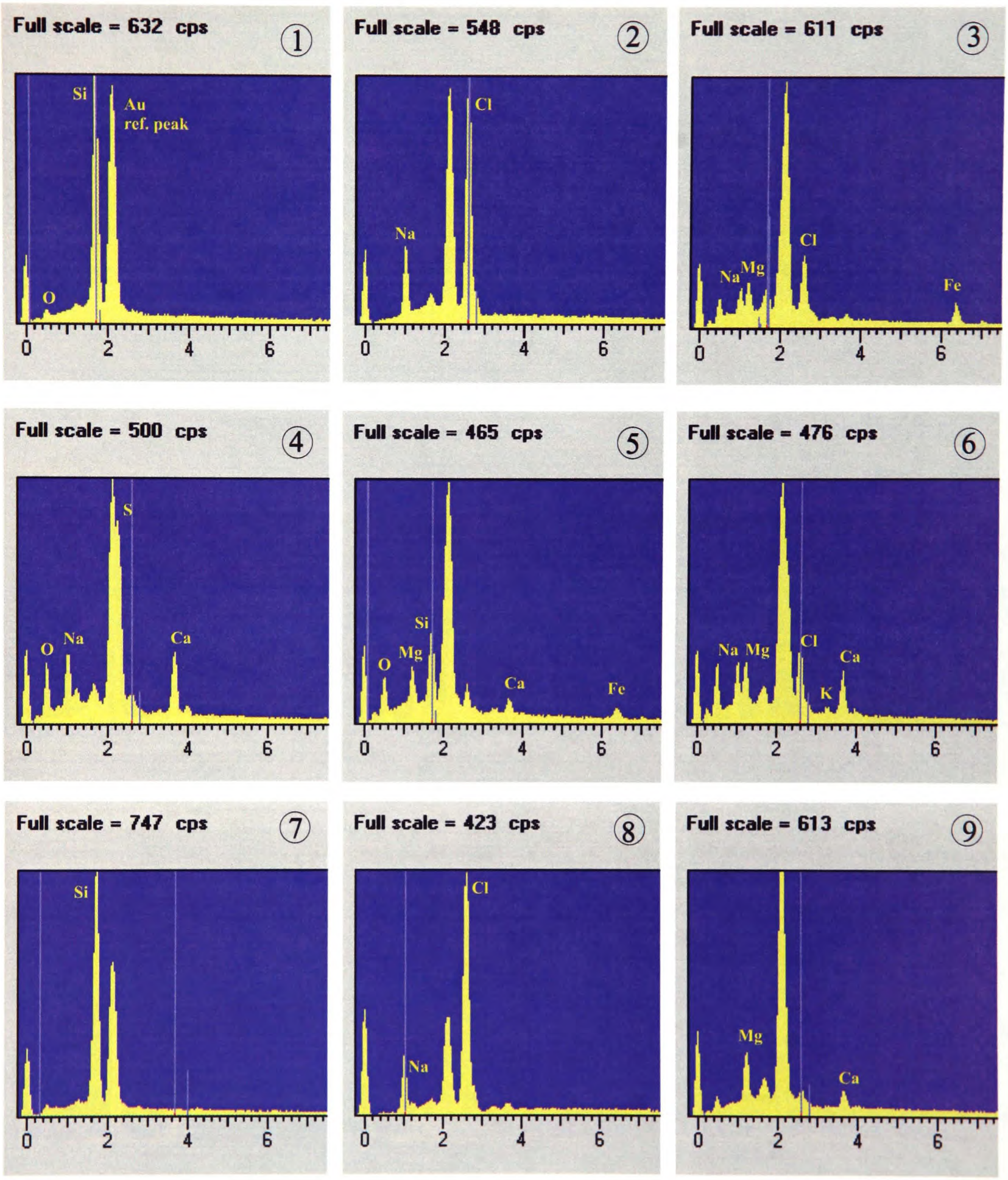


Figure A7.5. Atomic spectra from the experimental vials.
Numbers refer to labels on Figures 6.6-6.12.

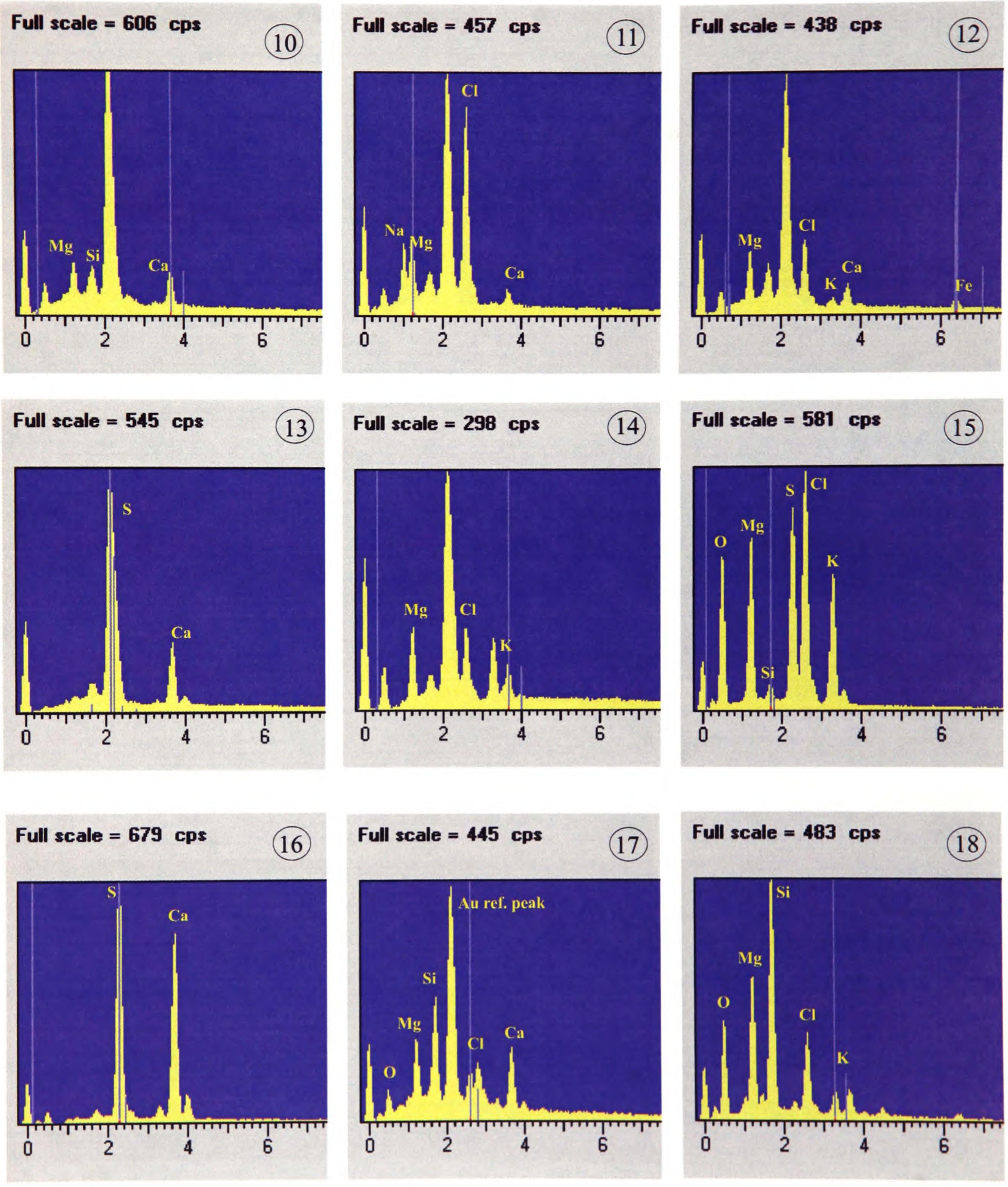


Figure A7.5. Atomic spectra from the experimental vials.
Numbers refer to labels on Figures 6.6-6.12.

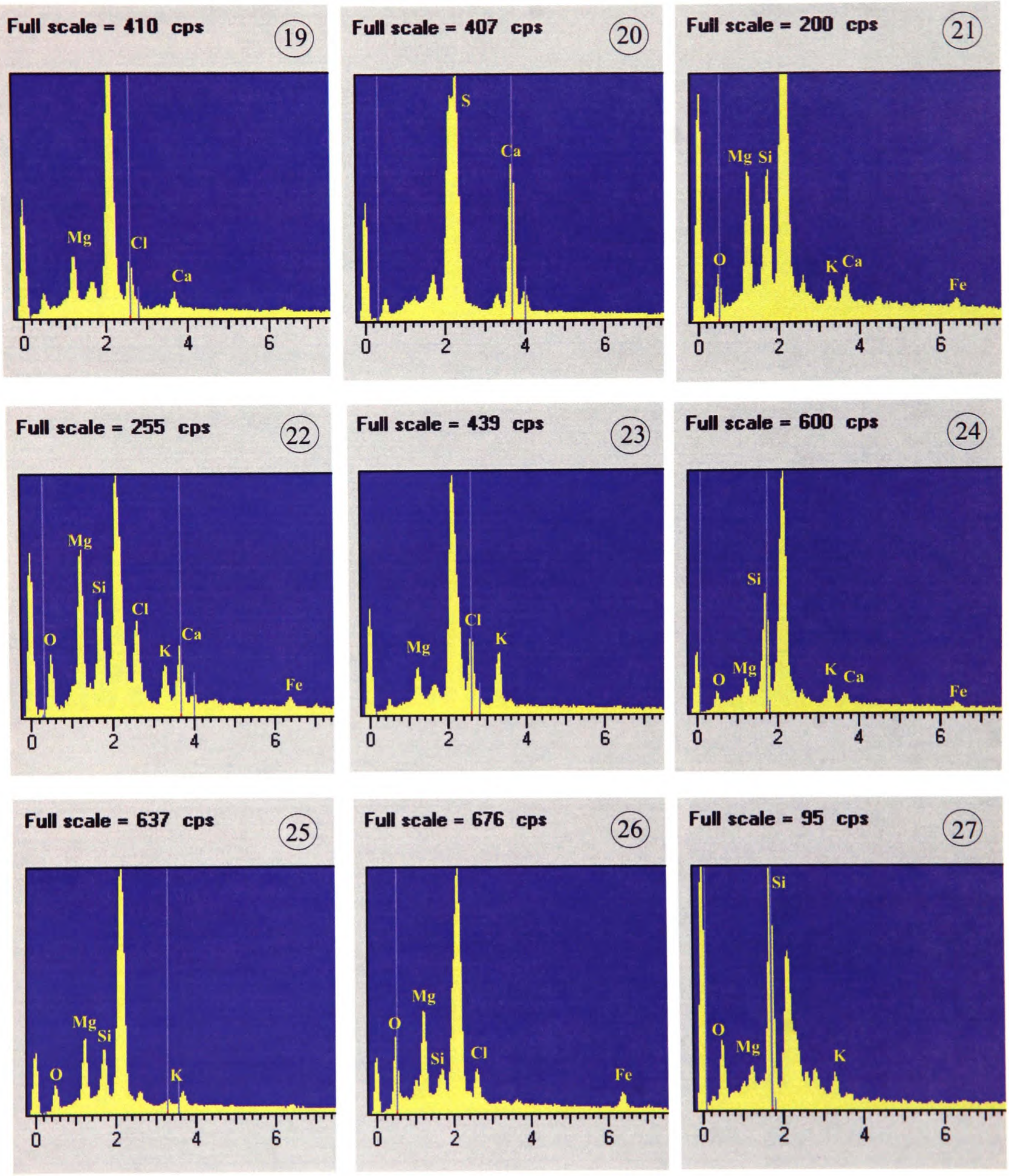


Figure A7.5. Atomic spectra from the experimental vials.
Numbers refer to labels on Figures 6.6-6.12.

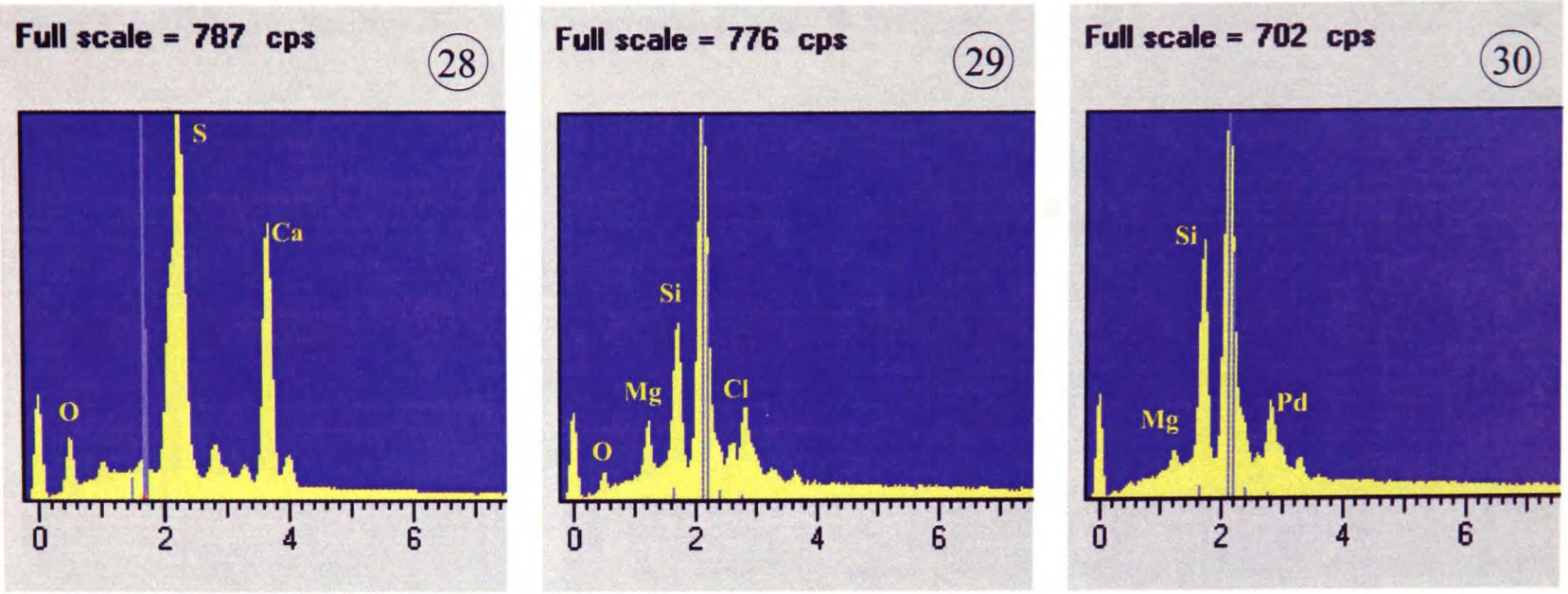


Figure A7.5. Atomic spectra from the experimental vials. Numbers refer to labels on Figures 6.6-6.12.